

Theory for the FCC-ee

Report on the 11th FCC-ee Workshop
Theory and Experiments
CERN, Geneva, 8–11 January 2019

Editors:

A. Blondel

DPNC University of Geneva, Switzerland

J. Gluza

Institute of Physics, University of Silesia, Katowice, Poland
Faculty of Science, University of Hradec Králové, Czech Republic

S. Jadach

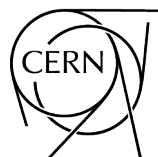
Institute of Nuclear Physics, PAN, 31-342 Kraków, Poland

P. Janot

CERN, CH-1211 Geneva 23, Switzerland

T. Riemann

Institute of Physics, University of Silesia, Katowice, Poland
Deutsches Elektronen-Synchrotron, DESY, 15738 Zeuthen, Germany



CERN Yellow Reports: Monographs
Published by CERN, CH-1211 Geneva 23, Switzerland

ISBN 978-92-9083-560-8 (paperback)

ISBN 978-92-9083-559-2 (PDF)

ISSN 2519-8068 (Print)

ISSN 2519-8076 (Online)

DOI <http://dx.doi.org/10.23731/CYRM-2020-003>

Accepted for publication by the CERN Reports Editorial Board (CREB) on 20 March 2020

Available online at <http://publishing.cern.ch/> and <http://cds.cern.ch/>

Copyright © CERN, 2020

© Creative Commons Attribution 4.0

Knowledge transfer is an integral part of CERN's mission.

CERN publishes this volume Open Access under the Creative Commons Attribution 4.0 license (<http://creativecommons.org/licenses/by/4.0/>) in order to permit its wide dissemination and use.

The submission of a contribution to a CERN Yellow Report series shall be deemed to constitute the contributor's agreement to this copyright and license statement. Contributors are requested to obtain any clearances that may be necessary for this purpose.

This volume is indexed in: INSPIRE and CERN Document Server (CDS)

This volume should be cited as:

Theory for the FCC-ee : Report on the 11th FCC-ee Workshop

Theory and Experiments, CERN, Geneva, 8–11 January 2019

Eds. A. Blondel, J. Gluza, S. Jadach, P. Janot and T. Riemann

CERN Yellow Reports: Monographs, CERN-2020-003 (CERN, Geneva, 2020),

<http://dx.doi.org/10.23731/CYRM-2020-003>

Theory for the FCC-ee

Report on the 11th FCC-ee Workshop*, CERN, Geneva, 8–11 January 2019

A. Blondel¹, J. Gluza^{†,2,3}, S. Jadach⁴, P. Janot⁵, T. Riemann^{2,6} (editors)

S. Abreu⁷, J.J. Aguilera-Verdugo⁸, A.B. Arbuzov⁹, J. Baglio¹⁰, S.D. Bakshi¹¹, S. Banerjee¹², M. Beneke¹³, C. Bobeth¹³, C. Bogner¹⁴, S.G. Bondarenko⁹, S. Borowka⁵, S. Braß¹⁵, C.M. Carloni Calame¹⁶, J. Chakraborty¹¹, M. Chiesa¹⁷, M. Chruszcz⁴, D. d’Enterria⁵, F. Domingo¹⁸, J. Dormans¹⁹, F. Driencourt-Mangin⁸, Y.V. Dydyshka²⁰, J. Erler^{21,22}, F. Febres Cordero^{19,23}, J.A. Gracey²⁴, Z.-G. He²⁵, S. Heinemeyer^{26,27,28}, G. Heinrich²⁹, I. Hönemann¹⁴, H. Ita¹⁹, S. Jahn²⁹, F. Jegerlehner^{6,30}, S.P. Jones⁵, L.V. Kalinovskaya²⁰, A. Kardos³¹, M. Kerner³², W. Kilian¹⁵, S. Kluth²⁶, B.A. Kniehl²⁵, A. Maier⁶, P. Maierhöfer¹⁹, G. Montagna^{16,33}, O. Nicrosini¹⁶, T. Ohl¹⁷, B. Page³⁴, S. Paßehr³⁵, S.K. Patra¹¹, F. Piccinini¹⁶, R. Pittau³⁶, W. Placzek³⁷, J. Plenter⁸, S. Ramírez-Uribe⁸, J. Reuter³⁸, G. Rodrigo⁸, V. Rothe³⁸, L.A. Rumyantsev^{20,39}, R.R. Sadykov²⁰, G.F.R. Sborlini⁸, J. Schlenk^{40,44}, M. Schott²¹, A. Schweitzer⁴¹, C. Schwinn⁴², M. Skrzypek⁴, G. Somogyi⁴³, M. Spira⁴⁴, P. Stenemeier³⁸, R. Szafron¹³, K. Tempest⁴⁵, W.J. Torres Bobadilla⁸, S. Tracz⁸, Z. Trócsányi^{43,46}, Z. Tulipánt⁴³, J. Usovitsch⁴⁷, A. Verbytskyi²⁶, B.F.L. Ward⁴⁸, Z. Was⁴, G. Weiglein³⁸, C. Weiland⁴⁹, S. Weinzierl²¹, V.L. Yermolchik²⁰, S.A. Yost⁵⁰, J. Zurita^{51,52}

¹ DPNC, University of Geneva, Switzerland

² Institute of Physics, University of Silesia, Katowice, Poland

³ Faculty of Science, University of Hradec Králové, Czech Republic

⁴ Institute of Nuclear Physics, PAN, 31-342 Kraków, Poland

⁵ CERN, CH-1211 Geneva 23, Switzerland

⁶ Deutsches Elektronen-Synchrotron, DESY, 15738 Zeuthen, Germany

⁷ Center for Cosmology, CP3, Université Catholique de Louvain, 1348 Louvain-La-Neuve, Belgium

⁸ IFIC, Universitat de València, E-46980 Paterna, Valencia, Spain

⁹ Bogoliubov Laboratory of Theoretical Physics, JINR, Dubna, 141980 Russia

¹⁰ Institut für Theoretische Physik, Eberhard Karls Universität, 72076 Tübingen, Germany

¹¹ Indian Institute of Technology, Kanpur, India

¹² University of Louisville, Louisville, KY 40292, USA

¹³ Physik Department T31, Technische Universität München, Garching, Germany

¹⁴ Institut für Physik, Johannes Gutenberg-Universität Mainz, D-55099 Mainz, Germany

¹⁵ Department Physik, Universität Siegen, 57068 Siegen, Germany

¹⁶ Istituto Nazionale di Fisica Nucleare, Sezione di Pavia, 27100 Pavia, Italy

¹⁷ Fakultät für Physik und Astronomie, Universität Würzburg, 97074 Würzburg, Germany

¹⁸ Bethe Center for Theoretical Physics & Physikalisches Institut der Universität Bonn, 53115 Bonn, Germany

¹⁹ Physikalisches Institut, Albert-Ludwigs-Universität Freiburg, 79104 Freiburg, Germany

²⁰ Dzhelapov Laboratory of Nuclear Problems, JINR, Dubna, 141980 Russia

²¹ PRISMA Cluster of Excellence, Institut für Physik, Johannes Gutenberg-Universität, 55099 Mainz, Germany

²² Departamento de Física Teórica, Instituto de Física, Universidad Nacional Autónoma de México, 04510 CDMX, Mexico

²³ Physics Department, Florida State University, Tallahassee, FL 32306, USA

*<https://indico.cern.ch/event/766859/>

†Corresponding editor, email: janusz.gluza@cern.ch

- ²⁴ *Theoretical Physics Division, Department of Mathematical Sciences, University of Liverpool, Liverpool, L69 3BX, United Kingdom*
- ²⁵ *Institut für Theoretische Physik, Universität Hamburg, 22761 Hamburg, Germany*
- ²⁶ *Instituto de Física Teórica (UAM/CSIC), Universidad Autónoma de Madrid, Cantoblanco, 28049 Madrid, Spain*
- ²⁷ *Instituto de Física de Cantabria (CSIC-UC), 39005 Santander, Spain*
- ²⁸ *Campus of International Excellence UAM+CSIC, Cantoblanco, 28049, Madrid, Spain*
- ²⁹ *Max Planck Institute for Physics, 80805 München, Germany*
- ³⁰ *Institut für Physik, Humboldt-Universität zu Berlin, 12489 Berlin, Germany*
- ³¹ *Institute of Physics, University of Debrecen, 4010 Debrecen, Hungary*
- ³² *Physik-Institut, Universität Zürich, 8057 Zürich, Switzerland*
- ³³ *Dipartimento di Fisica, Università di Pavia, 27100 Pavia, Italy*
- ³⁴ *Institut de Physique Théorique, CEA, CNRS, Université Paris-Saclay, F-91191 Gif-sur-Yvette, France*
- ³⁵ *Laboratoire de Physique Théorique et Hautes Énergies (LPTHE), Sorbonne Université, CNRS, 75252 Paris CEDEX 05, France*
- ³⁶ *Departamento de Física Teórica y del Cosmos and CAFPE, Universidad de Granada, 18071 Granada, Spain*
- ³⁷ *Marian Smoluchowski Institute of Physics, Jagiellonian University, Kraków, Poland*
- ³⁸ *Deutsches Elektronen-Synchrotron, DESY, 22607 Hamburg, Germany*
- ³⁹ *Institute of Physics, Southern Federal University, Rostov-on-Don, 344090 Russia*
- ⁴⁰ *Institute for Particle Physics Phenomenology, University of Durham, Durham DH1 3LE, UK*
- ⁴¹ *Institute for Theoretical Physics, ETH Zürich, 8093 Zürich, Switzerland*
- ⁴² *Institut für Theoretische Teilchenphysik und Kosmologie, RWTH Aachen University, 52056 Aachen, Germany*
- ⁴³ *MTA-DE Particle Physics Research Group, University of Debrecen, 4010 Debrecen, Hungary*
- ⁴⁴ *Paul Scherrer Institut, CH-5232 Villigen PSI, Switzerland*
- ⁴⁵ *Department of Physics, University of Toronto, Toronto, Ontario, M5S 1A7, Canada*
- ⁴⁶ *Institute for Theoretical Physics, Eötvös Loránd University, 1117 Budapest, Hungary*
- ⁴⁷ *School of Mathematics, Trinity College Dublin, University of Dublin, Ireland*
- ⁴⁸ *Baylor University, Waco, TX, USA*
- ⁴⁹ *Pittsburgh Particle Physics, Astrophysics, and Cosmology Center, Department of Physics and Astronomy, University of Pittsburgh, Pittsburgh, PA 15260, USA*
- ⁵⁰ *The Citadel, Charleston, SC, USA*
- ⁵¹ *Institute for Nuclear Physics (IKP), Karlsruhe Institute of Technology, 76344 Eggenstein-Leopoldshafen, Germany*
- ⁵² *Institute for Theoretical Particle Physics (TTP), Karlsruhe Institute of Technology, 76128 Karlsruhe, Germany*

Abstract

The Future Circular Collider (FCC) at CERN, a proposed 100 km circular facility with several colliders in succession, culminates in a 100 TeV proton–proton collider. It offers a vast new domain of exploration in particle physics, with orders-of-magnitude advances in terms of precision, sensitivity, and energy. The implementation plan published in 2018 foresees, as a first step, an electroweak factory electron–positron collider. This high-luminosity facility, operating at centre-of-mass energies between 90 and 365 GeV, will study the heavy particles of the Standard Model (SM), Z, W, and Higgs bosons, and top quarks with unprecedented accuracy. The physics programme offers great discovery potential: (i) through precision measurements, (ii) through sensitive searches for symmetry violations, forbidden, or extremely rare decays, and (iii) through the search for direct observation of new particles with extremely small couplings. The electroweak factory e^+e^- collider constitutes a real challenge to the theory and to precision calculations, triggering the need for the development of new mathematical methods and software tools. A first workshop in 2018 focused on the first FCC-ee stage, the Tera-Z, and confronted the theoretical status of precision Standard Model calculations on the Z boson resonance to the experimental demands.

The second workshop, in January 2019, extended the scope to the next stages, with the production of W bosons (FCC-ee-W), the Higgs boson (FCC-ee-H), and top quarks (FCC-ee-tt). In particular, the theoretical precision in the determination of the crucial input parameters, α_{QED} , α_{QCD} , M_W , and m_t , at the level of FCC-ee requirements was thoroughly discussed. The requirements on Standard Model theory calculations were spelt out, so as to meet the demanding accuracy of the FCC-ee experimental potential. The discussion of innovative methods and tools for multiloop calculations was deepened. Furthermore, phenomenological analyses beyond the Standard Model were discussed, including effective theory approaches. The reports of 2018 and 2019 serve as white papers of the workshop results and subsequent developments.

Editors' note

Understanding the origins of the Universe and how it works and evolves is the present mission of a large community of physicists of many nations and specialities. It calls for a large-scale vision, involving general relativity, astrophysics, and cosmology, together with the detailed basic understanding provided by particle physics; these disciplines work hand in hand, with the help of several other research fields. Presently, particle physics stands at an important moment in its history. With the discovery of the Higgs boson, the matrix of interactions and elementary particles that is called the ‘Standard Model’ (SM), is complete. Yet the Higgs boson itself, and how it breaks the electroweak symmetry, remains a fascinating subject requiring verification at the next order of precision, typically at percent, or even per-mille, accuracy. Furthermore, several experimental facts are not accounted for by the SM; let us mention: (i) the baryon asymmetry of the Universe, (ii) the nature and origin of dark matter, and (iii) the origin of neutrino masses. These have no unique, if any, explanation in the SM and yet will require answers from particle physics.

Particle physics exploration must continue... but we no longer have a guiding scale.

How can this exploration be carried out? Which next tool is needed? Going to higher and higher energies is an obvious idea. It has worked well for the Standard Model particles so far, because they all have roughly the same strong and electroweak couplings. It is far from evident, however, that the new phenomena or particles, required to explore these questions, will behave in the same way—the opportunity to explore much smaller couplings or much higher scales must be kept in mind. Here, the role of precision measurements, the search for extremely rare decays of known particles, for small violations of the SM symmetries, and for direct production of super-weakly coupled objects is in order. A broad search strategy is thus needed.

With this in mind, and armed with the recommendation of the European Strategy in 2013 that Europe should be in a position to “propose an ambitious post-LHC accelerator project at CERN”, the FCC collaboration has elaborated a strategy of circular colliders fitting in a new facility of 100 km circumference. It will start with a high-luminosity e^+e^- electroweak factory, FCC-ee, and culminate in a proton collider, FCC-hh, of more than 100 TeV collision energy. Additional options of heavy-ion collisions and $e-p$ scattering are foreseen and, possibly, muon collisions. This strategy offers, by way of synergy and complementarity, a thorough study of the Higgs boson, as well as unmatched capabilities of high-energy exploration, precision measurements, and sensitive rare process searches [1]. The FCC Conceptual Design Report (CDR) has been prepared and released [2–4]. This powerful exploratory project will, right from its first step as a Z factory, explore completely uncharted territory in terms of precision and sensitivity. Moreover, it constitutes an extraordinary challenge for theory. The theoretical community has responded with enthusiasm to the challenge; already several workshops have gathered an increasing number of contributions.

In this report, we collect theory contributions to the 11th FCC-ee meeting held in January 2019 at CERN [5], completed by a few invited guest contributions. The report is a kind of community white paper, rather than a conventional conference report. It collects, coherently, the contributions from 86 scientists, representing the state of the art in 2019 and envisioning the additional needs of future lepton colliders. We are grateful to Jens Vigen from CERN. Due to his efforts in the final productions, the document meets the highest editorial standards.

The collective interactions of all of us, in one way or another, at the meeting in January 2019 and for several months after, make the backbone of the final write-up. Nevertheless, for the convenience of the reader, we decided to retain a sectional structure for the bulk of the document, with individual bibliographies for the sections.

The volume follows the report [6] on the FCC-ee workshop in January 2018 [7], which focused on the theory needs for the Tera-Z, the first stage of the FCC-ee, working in the Z boson mass range. The purpose is to document existing studies and also to motivate future theoretical studies, enabling by their predictions a full exploration of the experimental potential of the FCC-ee.

It has become evident that a significant work must be accomplished, both in multiloop calculations in the Standard Model and also in projects beyond the Standard Model. Documentation of these requirements became highly desirable to complement the submitted Conceptual Design Report. The present report exemplifies both the well-advanced status of phenomenology for the FCC-ee and, at the same time, the need for further mathematically well-founded deepening of the technologies for precision measurements. In this respect, it is a necessary addition to the FCC CDR.

From a scientific point of view, the FCC is the most challenging collider project for the next few decades [8]. We see it as our duty and pleasure to prepare such a frontier project and to sustain CERN's leading role in basic research worldwide. The goals must be set as high as possible, i.e., at the level of the statistical uncertainties, because *this precision genuinely equates discovery potential*.

We thank all participants of the workshop for their engagement with presentations and in the discussions during the workshop, and the authors of the report for writing such excellent contributions. The exploratory potential of the FCC-ee can be fully exploited only if the talent and efforts of accelerator builders and experimenters is met by theory. The message is: we are working on it.

From this quest for the unknown, driven by curiosity, history shows that there is a return for all of us, scientists or not [9–11].

The editors.

References

- [1] <https://fcc.web.cern.ch>, last accessed 15 January 2020.
- [2] <https://fcc-cdr.web.cern.ch/>, last accessed 15 January 2020.
- [3] A. Abada *et al.*, *Eur. Phys. J. Spec. Top.* **228** (2019) 261. doi:10.1140/epjst/e2019-900045-4
- [4] A. Abada *et al.*, *Eur. Phys. J.* **C79** (2019) 474. doi:10.1140/epjc/s10052-019-6904-3
- [5] A. Blondel *et al.*, 11th FCC-ee Workshop: Theory and Experiments, 2019, CERN, Geneva, Switzerland, <https://indico.cern.ch/event/766859/>
- [6] A. Blondel *et al.*, Standard Model theory for the FCC-ee Tera-Z stage, CERN Yellow Reports: Monographs Vol. 3 (2019), CERN-2019-003 (CERN, Geneva, 2019), [arXiv:1809.01830](https://arxiv.org/abs/1809.01830), doi:10.23731/CYRM-2019-003

- [7] A. Blondel *et al.*, Mini Workshop. Precision EW and QCD Calculations for the FCC Studies: Methods and Tools, 2018, CERN, Geneva, Switzerland, <https://indico.cern.ch/event/669224/>
- [8] A. Blondel *et al.*, Theory requirements and possibilities for the FCC-ee and other future high energy and precision frontier lepton colliders, Input 101 to the Update of the European Strategy for Particle Physics, <https://indico.cern.ch/event/765096/contributions/3295742/>. [arXiv:1901.02648](https://arxiv.org/abs/1901.02648)
- [9] Why fundamental science? <https://public-archive.web.cern.ch/en/About/Fundamental-en.html>, last accessed 29 April 2019.
- [10] *Nat. Rev. Phys.* **1** (2019) 231. <https://doi.org/10.1038/s42254-019-0052-4>
- [11] <https://home.cern/news/opinion/physics/case-future-colliders>, last accessed 15 January 2020.

Contents

Abstract	v
Editors' note	vii
Executive summary	1
A Introduction and overview	3
<i>A. Blondel, J. Gluza, S. Jadach, P. Janot, T. Riemann</i>	3
1 The FCC-ee electroweak factory	3
2 What this theory report brings: an overview	7
B Precision calculations in the Standard Model	9
1 $\alpha_{\text{QED,eff}}(s)$ for precision physics at the FCC-ee/ILC <i>F. Jegerlehner</i>	9
1.1 $\alpha(M_Z^2)$ in precision physics (precision physics limitations)	9
1.2 The ultimate motivation for high-precision SM parameters	13
1.3 R data evaluation of $\alpha(M_Z^2)$	14
1.4 Reducing uncertainties via the Euclidean split trick: Adler function controlled pQCD	19
1.5 Prospects for future improvements	23
1.6 The need for a space-like effective $\alpha(t)$	26
1.7 Conclusions	28
1.8 Addendum: the coupling α_2 , M_W , and $\sin^2 \Theta_f$	28
2 Precision quantum chromodynamics <i>D. d'Enterria</i>	38
2.1 Higher fixed-order pQCD corrections	39
2.2 Higher-order logarithmic resummations	40
2.3 Per-mille-precision α_s extraction	42
2.4 High-precision non-perturbative QCD	45
3 Inclusion of mixed QCD–QED resummation effects at higher orders <i>G.F.R. Sborlini</i>	51
3.1 Introduction and motivation	51
3.2 Splittings and PDF evolution	51
3.3 Fixed-order effects: application to diphoton production	52
3.4 Mixed resummation effects: Z boson production	53
3.5 Conclusions	54
4 CoLoRFulNNLO at work: a determination of α_s <i>A. Kardos, S. Kluth, G. Somogyi, Z. Trócsányi, Z. Tulipánt, A. Verbytskyi</i>	57
4.1 Introduction	57

4.2	Precision through higher orders	58
4.3	Precision through small power corrections	60
4.4	Conclusions	62
5	Theoretical luminosity precision for the FCC-ee: overview of the path to 0.01% <i>B.F.L. Ward, S. Jadach, W. Placzek, M. Skrzypek, S.A. Yost</i>	65
6	$e^+e^- \rightarrow \gamma\gamma$ at large angles for FCC-ee luminometry <i>C.M. Carloni, M. Chiesa, G. Montagna, O. Nicrosini, F. Piccinini</i>	71
6.1	Introduction	71
6.2	Theoretical approach and numerical results	72
6.3	Summary and outlook	73
7	Prospects for higher-order corrections to W pair production near threshold in the EFT approach <i>C. Schwinn</i>	77
7.1	Effective theory approach to W pair production	78
7.2	Estimate of NNLO ^{EFT} corrections and beyond	83
7.3	Summary and outlook	86
8	Perspectives of heavy quarkonium production at the FCC-ee <i>Z.-G. He, B.A. Kniehl</i>	89
8.1	Heavy quarkonium production through e^+e^- annihilation	90
8.2	Heavy quarkonium production in $\gamma\gamma$ collisions	91
8.3	Summary and outlook	94
9	Vertex functions in QCD—preparation for beyond two loops <i>J.A. Gracey</i>	97
9.1	Introduction	97
9.2	Current status	98
9.3	Three-loop strategy	101
9.4	Discussion	103
10	Effective field theory approach to QED corrections in flavour physics <i>M. Beneke, C. Bobeth, R. Szafron</i>	107
10.1	Introduction and motivation	107
10.2	QED corrections in $B_q \rightarrow \ell^+\ell^-$	108
10.3	Summary and outlook	113
11	Top pair production and mass determination <i>A. Maier</i>	117
11.1	Introduction	117
11.2	Effective theory framework	117
11.3	Higher-order corrections	117
11.4	Cross-section predictions	119
12	Higgs boson decays: theoretical status <i>M. Spira</i>	123

12.1	Introduction	123
12.2	SM Higgs boson decays	123
12.3	Uncertainties	126
C	Methods and tools	135
1	Heritage projects, preservation, and re-usability concerns <i>S. Banerjee, M. Chrzaszcz, Z. Was, J. Zaremba</i>	135
1.1	Common tools for all FCC design studies	136
2	Scalar one-loop Feynman integrals in arbitrary space–time dimension d – an update <i>T. Riemann, J. Usovitsch</i>	139
2.1	Introduction	139
2.2	Interests in the d -dependence of one-loop Feynman integrals	140
2.3	Mellin–Barnes representations for one-loop Feynman integrals	143
2.4	The basic scalar one-loop functions	149
2.5	The cases of vanishing Cayley determinant $\lambda_n = 0$ and of vanishing Gram determinant $G_n = 0$	154
2.6	A massive four-point function with vanishing Gram determinant	154
2.7	Calculation of Gauss hypergeometric function ${}_2F_1$, Appell function F_1 , and Saran function F_S at arbitrary kinematics	155
3	NNLO corrections in four dimensions <i>R. Pittau</i>	163
3.1	Introduction	163
3.2	FDR integration and loop integrals	163
3.3	Keeping unitarity in the virtual component	165
3.4	Keeping unitarity in the real component	167
3.5	Results and conclusions	167
4	Unsubtractions at NNLO <i>J.J. Aguilera-Verdugo, F. Driencourt-Mangin, J. Plenter, S. Ramírez-Uribe, G. Rodrigo, G.F.R. Sborlini, W.J. Torres Bobadilla, S. Tracz</i>	169
4.1	Introduction	169
4.2	Loop-tree duality	170
4.3	Four-dimensional unsubtraction	171
4.4	Unitarity thresholds and anomalous thresholds	172
4.5	Conclusions	173
5	Numerics for elliptic Feynman integrals <i>C. Bogner, I. Hönemann, K. Tempest, A. Schweitzer, S. Weinzierl</i>	177
6	Numerical multiloop calculations: sector decomposition and QMC integration in pySECDEC <i>S. Borowka, G. Heinrich, S. Jahn, S.P. Jones, M. Kerner, J. Schlenk</i>	185
6.1	Feynman integrals and sector decomposition	185
6.2	Quasi-Monte Carlo integration	187

6.3	Summary and outlook	188
7	Analytics from numerics: five-point QCD amplitudes at two loops <i>S. Abreu, J. Dormans, F. Febres Cordero, H. Ita, B. Page</i>	193
7.1	Introduction	193
7.2	Amplitudes	194
7.3	Simplifications for functional reconstruction	195
7.4	Implementation and results	197
7.5	Conclusion	198
8	Recent developments in Kira <i>P. Maierhöfer, J. Usovitsch</i>	201
8.1	Introduction	201
8.2	Improved symmetrization	201
8.3	Parallel simplification algorithms for coefficients	201
8.4	Basis choice	203
8.5	Conclusions	203
9	Precision Monte Carlo simulations with WHIZARD <i>S. Braß, W. Kilian, T. Ohl, J. Reuter, V. Rothe, P. Stienemeier</i>	205
10	FCC tau polarisation <i>S. Banerjee, Z. Was</i>	211
11	Electron–positron annihilation processes in MCSANcEE <i>A. Arbuzov, S. Bondarenko, Y. Dydyshka, L. Kalinovskaya, L. Rumyantsev, R. Sadykov, V. Yermolchuk</i>	213
11.1	Introduction	213
11.2	Cross-section structure	213
11.3	Numerical results and comparison	214
11.4	Conclusion	214
12	Global electroweak fit in the FCC-ee era <i>J. Erler, M. Schott</i>	217
D	SMEFT	221
1	CoDEx: BSM physics being realised as SMEFT <i>S.D. Bakshi, J. Chakraborty, S.K. Patra</i>	221
1.1	Introduction	221
1.2	The package in detail	222
E	Beyond the Standard Model (BSM)	231
1	(Triple) Higgs coupling imprints at future lepton colliders <i>J. Baglio, C. Weiland</i>	231
1.1	Triple Higgs coupling studies in an EFT framework	231
1.2	Probing heavy neutral leptons via Higgs couplings	232
1.3	Conclusions	236

2	Exotic Higgs decays (and long-lived particles) at future colliders <i>J.F. Zurita</i>	241
2.1	Exotic Higgs decays: motivations and signatures	241
2.2	Long-lived particles (LLPs)	241
2.3	Exotic Higgs decays vis-à-vis current LHC data	242
2.4	Future experiments: HL-LHC, FCC, CEPC, LHeC	243
2.5	Conclusions	244
3	Precision predictions for Higgs decays in the (N)MSSM <i>F. Domingo, S. Heinemeyer, S. Paßehr, G. Weiglein</i>	247
3.1	Introduction	247
3.2	Higgs decays to SM particles in the \mathcal{CP} -violating NMSSM	248
3.3	Discussion concerning the remaining theoretical uncertainties	258
	Acknowledgements	267

Executive summary

The main theoretical issues of the FCC-ee studies discussed in this report may be summarised as follows.

1. To adjust the precision of theory predictions to the experimental demands from the FCC-ee, an update of existing software and the development of new, independent software will be needed. This should include, in the first instance, solutions to the following issues:
 - (a) factorisation to infinite order of multiphoton soft-virtual QED contributions;
 - (b) resummations in Monte Carlo generators;
 - (c) disentangling of QED and EW corrections beyond one loop, with soft-photon factorisation or resummation;
 - (d) proper implementation of higher-loop effects, such as Laurent series around the Z peak;
 - (e) further progress in methods and tools for multiloop calculations and Monte Carlo generators.

Some discussions have been initiated in the 2018 report [1]; here, they are extended in the Introduction and Chapters B and C.

2. To meet the experimental precision of the FCC-ee Tera-Z for electroweak precision observables (EWPOs), even three-loop EW calculations of the $Z\bar{f}f$ vertex will be needed, comprising the loop orders $\mathcal{O}(\alpha\alpha_s^2)$, $\mathcal{O}(N_f\alpha^2\alpha_s)$, $\mathcal{O}(N_f^2\alpha^3)$, and also the corresponding QCD four-loop terms. This was mainly a subject of the 2018 report [1].
3. To decrease the α_{QED} uncertainty by a factor of five to ten, to the level $(3\text{--}5) \times 10^{-5}$, will require improvements in low-energy experiments. Alongside this, the perturbative QCD (pQCD) prediction of the Adler function must be improved by a factor of two, accomplished with better uncertainty estimates for m_c and m_b . The next mandatory improvements required are:
 - (a) four-loop massive pQCD calculation of the Adler function;
 - (b) improved α_s in the low Q^2 region above the τ mass;
 - (c) a better control and understanding of $\Delta\alpha_{\text{had}}^{(5)}(M_Z^2)$, in terms of R data;
 - (d) different methods for directly accessing $\alpha(M_Z^2)$, e.g., the muon forward-backward asymmetry, or for calculating α_{QED} , either based on a radiative return experiment, e.g., at the FCC-ee Tera-Z, or using lattice QCD methods.

This is discussed in Chapter B.

4. FCC-ee precision measurements require many improvements on the theoretical QCD side. These include: (i) higher-order pQCD fixed-order calculations; (ii) higher-order logarithmic resummations; (iii) per-mille-precision extractions of the α_s coupling; and (iv) an accurate control of non-perturbative QCD effects (such as, e.g., colour reconnection, hadronization), both analytically and as implemented in the Monte Carlo generators. These issues are discussed in Chapter B.

-
5. The reduction of the theoretical uncertainty of the total W pair production cross-section to the level of $\sim 0.01\%$ at the FCC-ee-W requires at least the calculation of $\mathcal{O}(\alpha^2)$ and dominant $\mathcal{O}(\alpha^3)$ corrections to double-resonant diagrams. Estimates within an effective field theory (EFT) approach show that the theory-induced systematic uncertainty of the mass measurement from a threshold scan can be at the level of $\Delta M_W = (0.15 - 0.60)$ MeV. The lower value results from assuming that the non-resonant corrections are under control. In addition, it is also essential to reduce the uncertainty from initial-state radiation (ISR) corrections and QCD corrections for hadronic final states to the required accuracy. This is discussed in Chapter B.
 6. Predictions for H decay widths and branching ratios are known with sufficient accuracy for the LHC. At the FCC-ee, the Higgs mass can be measured with a precision below 0.05 GeV. The dependence of EWPOs on M_H is mild, $\propto \alpha \log(M_H/M_W)$, and an accuracy of 0.05 GeV of M_H will not affect their determination. The main improvements in Higgs boson studies will be connected with a better determination of branching ratios and self-couplings. More on related issues is discussed in the Introduction and in Chapter B.
 7. The top pair line shape for centre-of-mass energies close to the $t\bar{t}$ production threshold is highly sensitive to the mass of the top quark, allowing its determination with unprecedented precision. The statistical uncertainty of the measurement (~ 20 MeV) is projected to be significantly less than the current theoretical uncertainty. It is crucial to continuously improve the theoretical prediction. The most sensitive observable is the total production cross-section for $b\bar{b}W^+W^-X$ final states near the top pair production threshold. A very precise knowledge of the strong coupling constant from other sources will be crucial in order to meaningfully constrain the top Yukawa coupling. These issues are discussed in Chapter B.
 8. Proper truncation of the ultraviolet scale Λ depends on the experimental precision of the observables and Standard Model effective field theories (SMEFTs) must be adjusted to FCC-ee experimental conditions, e.g., in construction of appropriate complete operator bases and Wilson coefficients (WCs) for Beyond the Standard Model (BSM) theories. This issue is discussed in Chapter D.
 9. The FCC-ee and the FCC-hh will both be sensitive to BSM physics and exotic massive states reaching tens of TeV or very weak couplings. It is proposed to use the SMEFT framework and constrain the Higgs triple coupling by analysing precision measurements. For these studies, but also exotic Higgs decays, it will be important to combine the LHC and HL-LHC data with an analysis at the FCC-ee. These issues are discussed in Chapter E.

Reference

- [1] A. Blondel *et al.*, Standard Model theory for the FCC-ee Tera-Z stage, CERN (CERN Yellow Rep. Monogr. 3, Geneva, Switzerland),
[arXiv:1809.01830](https://arxiv.org/abs/1809.01830), [doi:10.23731/CYRM-2019-003](https://doi.org/10.23731/CYRM-2019-003)

Chapter A

Introduction and overview

Contribution* by: **A. Blondel, J. Gluza, S. Jadach, P. Janot, T. Riemann**

Corresponding author: J. Gluza [janusz.gluza@cern.ch]

This report includes a collection of studies devoted to a discussion of (i) the status of theoretical efforts towards the calculation of higher-order Standard Model (SM) corrections needed for the FCC-ee precision measurement programme, (ii) the possibility of making discoveries in physics by means of these precision measurements, and (iii) methods and tools that must be developed to guarantee precision calculations of the observables to be measured. This report originates from presentations at the 11th FCC-ee Workshop: Theory and Experiments, 8–11 January 2019, CERN, Geneva [1], with 117 registered participants and 42 talks on theory.

1 The FCC-ee electroweak factory

In the 2018 report [2], we focused on theoretical issues of the FCC-ee Tera-Z, which will be a e^+e^- collider working at the Z resonance energy region. However, the FCC-ee collider project will work in several energy regions, making it a complete *electroweak factory*, covering the direct production of all massive bosons of the SM and the top quark. This plan is summarised in Table A.1.1.

Table A.1.1: Run plan for FCC-ee in its baseline configuration with two experiments. The WW event numbers are given for the entirety of the FCC-ee running at and above the WW threshold.

Phase	Run duration (years)	Centre-of-mass energies (GeV)	Integrated luminosity (ab^{-1})	Event statistics
FCC-ee-Z	4	88–95	150	3×10^{12} visible Z decays
FCC-ee-W	2	158–162	12	10^8 WW events
FCC-ee-H	3	240	5	10^6 ZH events
FCC-ee-tt	5	345–365	1.7	10^6 $t\bar{t}$ events

The exceptional precision of the FCC-ee comes from several features of the programme.

1. Extremely high statistics of 5×10^{12} Z decays, 10^8 WW, 10^6 ZH, and 10^6 $t\bar{t}$ events.

*This contribution should be cited as:

A. Blondel, J. Gluza, S. Jadach, P. Janot, T. Riemann, Introduction and overview, DOI: [10.23731/CYRM-2020-003.3](https://doi.org/10.23731/CYRM-2020-003.3), in: Theory for the FCC-ee, Eds. A. Blondel, J. Gluza, S. Jadach, P. Janot and T. Riemann, CERN Yellow Reports: Monographs, CERN-2020-003, DOI: [10.23731/CYRM-2020-003](https://doi.org/10.23731/CYRM-2020-003), p. 3.
© CERN, 2020. Published by CERN under the [Creative Commons Attribution 4.0 license](https://creativecommons.org/licenses/by/4.0/).

2. High-precision (better than 100 keV) absolute determination of the centre-of mass energies at the Z pole and WW threshold, thanks to the availability of transverse polarisation and the resonant depolarisation. This is a unique feature of the circular lepton colliders, e^+e^- and $\mu^+\mu^-$. At higher energies, WW, ZZ, and $Z\gamma$ production can be used to constrain the centre-of-mass energy with precisions of 2 and 5 MeV, at the ZH cross-section maximum and at the $t\bar{t}$ threshold, respectively. At all energies, $e^+e^- \rightarrow \mu^+\mu^-$ events, which occur at a rate in excess of 3 kHz at the Z pole, provide, by themselves, in a matter of minutes, the determination of the centre-of mass energy spread, the residual difference between the energies of e^+ and e^- beams and (relative) centre-of-mass energy monitoring with a precision that is more than sufficient for the precision needs of the programme.
3. The clean environmental conditions and an optimised run plan allow a complete programme of ancillary measurements of currently precision-limiting input quantities for the precision EW tests. This is the case for the top quark mass from the scan of the $t\bar{t}$ production threshold; of the unique, direct, measurement of the QED running coupling constant at the Z mass from the $Z-\gamma$ interference; of the strong coupling constant by measurements of the hadronic-to-leptonic branching fractions of the Z, the W, and the τ lepton; and, of course, of the Higgs and Z masses themselves.

For the reader's convenience, we also include Table A.1.2 from the CDR, showing some of the most significant FCC-ee experimental accuracies compared with those of the current measurements. More on the experimental precision of the FCC-ee can be found in volumes 1 and 2 of the CDR documents [3, 4]. The experimenters are working hard to reduce systematic uncertainties by devising dedicated methods and ancillary measurements; the task of the theoretical community will be to ensure that the SM predictions will be precise enough so as not to spoil the best foreseeable experimental accuracies, i.e., the statistical uncertainties.

If future theory uncertainties match the FCC-ee experimental precision, the many different measurements from the FCC-ee will provide the capability of exhibiting and deciphering signs of new physics. Here are two examples: the EFT analysis searching for signs of heavy particles physics with SM couplings shows the potential to exhibit signs of new particles up to around 70 TeV; with a very different but characteristic pattern, observables involving neutrinos would show a significant deviation if these neutrinos were mixed with a heavy counterpart at the level of one part in 100 000, even if those were too heavy to be directly produced.

Table A.1.2 shows that the FCC-ee has the potential to achieve (at least) a 20–100 times higher precision or better in electroweak precision measurements over the present state-of-the-art situation. This includes such input quantities as the Z, Higgs, and top masses, and the strong and QED coupling constants at the Z scale. This extremely favourable situation will require leap-jumps in the precision of the theoretical computations for Standard Model phenomena, for all quantities given in Table A.1.2. The theory calculation must also be able to include the improved input parameters [2, 5], which, in the particular case of the FCC-ee, will be measured within the experimental programme.

The quantities listed in Table A.1.2 are called *electroweak precision observables* (EWPO) and encapsulate experimental data after extraction of well-known and controllable QED and QCD effects, in a model-independent manner. They provide a convenient bridge between real data and the predictions of the SM, or of the SM plus new physics. Contrary to raw experimental data (like differential cross-sections), EWPOs are also well-suited for archiving and long-term use. Archived EWPOs can be exploited over long periods of time for comparisons with steadily

Table A.1.2: Measurement of selected electroweak precision observables (EWPOs) at the FCC-ee, compared with the current precision. The systematic uncertainties are initial estimates and might improve on further examination. This set of measurements, together with those of the Higgs properties, achieves indirect sensitivity to new physics up to a scale Λ of 70 TeV in a description with dimension-6 operators, and possibly much higher in some specific new physics models.

Observable	Current value	\pm Error	FCC-ee stat.	FCC-ee syst.	Comment, dominant experimental error
m_Z (keV)	91186700	± 2200	4	100	From Z line shape scan, beam energy calibration
Γ_Z (keV)	2495200	± 2300	7	100	From Z line shape scan, beam energy calibration
R_ℓ^Z ($\times 10^3$)	20767	± 25	0.06	0.2–1	Ratio of hadrons to leptons, acceptance for leptons
$\alpha_s(m_Z)$ ($\times 10^4$)	1196	± 30	0.1	0.4–1.6	From R_ℓ^Z
R_b ($\times 10^6$)	216290	± 660	0.3	<60	Ratio of $b\bar{b}$ to hadrons, stat. extrapolated from SLD
σ_{had}^0 ($\times 10^3$) (nb)	41541	± 37	0.1	4	Peak hadronic cross-section, luminosity measurement
N_ν ($\times 10^3$)	2991	± 7	0.005	1	Z peak cross-sections, luminosity measurement
$\sin^2\theta_W^{\text{eff}}$ ($\times 10^6$)	231480	± 160	3	2–5	From $A_{\text{FB}}^{\mu\mu}$ from $A_{\text{FB}}^{\mu\mu}$ at Z peak, beam energy calibration
$1/\alpha_{\text{QED}}(m_Z)$ ($\times 10^3$)	128952	± 14	4	Small	From $A_{\text{FB}}^{\mu\mu}$ off peak
$A_{\text{FB},0}^b$ ($\times 10^4$)	992	± 16	0.02	1-3	b quark asymmetry at Z pole, from jet charge
$A_{\text{FB}}^{\text{pol},\tau}$ ($\times 10^4$)	1498	± 49	0.15	<2	τ polarisation and charge asymmetry, τ decay physics
m_W (MeV)	80350	± 15	0.5	0.3	From WW threshold scan, beam energy calibration
Γ_W (MeV)	2085	± 42	1.2	0.3	From WW threshold scan, beam energy calibration
$\alpha_s(m_W)$ ($\times 10^4$)	1170	± 420	3	Small	From R_ℓ^W
N_ν ($\times 10^3$)	2920	± 50	0.8	Small	Ratio of invisible to leptonic, in radiative Z returns
m_{top} (MeV/ c^2)	172740	± 500	17	Small	From $t\bar{t}$ threshold scan, QCD errors dominate
Γ_{top} (MeV/ c^2)	1410	± 190	45	Small	From $t\bar{t}$ threshold scan, QCD errors dominate
$\lambda_{\text{top}}/\lambda_{\text{top}}^{\text{SM}}$	1.2	± 0.3	0.10	Small	From $t\bar{t}$ threshold scan, QCD errors dominate
ttZ couplings		$\pm 30\%$	0.5 – 1.5%	Small	From $E_{\text{CM}} = 365$ GeV run

improving theoretical calculations of the SM predictions, and for validations of the new physics models beyond the SM. They are also useful for the comparison and combination of results from different experiments. However, removing trivial but sizeable QED or QCD effects from EWPOs might induce additional sources of uncertainty. The work needed is well-known concerning QED, more significant conceptual work may need to be done for QCD.

Let us summarise briefly the mandatory improvements of the calculations of QED effects in EWPOs according to recent work [6]:

1. improved calculation of the additional light fermion pair emissions (for Z boson mass and width);
2. better calculation of the final-state radiation effects in the presence of cut-offs (for R_ℓ^Z);
3. implementation of a new QED matrix element in the Monte Carlo (MC) event generator for low-angle Bhabha processes (for the luminosity determination in view of the measurement of σ_{had}^0 and other cross-sections);
4. $\mathcal{O}(\alpha^2)$ calculation for $e^+e^- \rightarrow Z\gamma$ (for the determination of N_ν);
5. improved MC simulation of τ decays (for the effective weak mixing angle and tau branching ratio measurements);
6. QED effects at the W pair production threshold (for measurement of the W mass and width);
7. initial–final-state interference (e.g., for the forward–backward charge asymmetry of lepton pairs around the Z peak).

For more on the related subject of the separation of QED effects from weak quantities at the FCC-ee precision and generally on the improvements in the definition of EWPOs, see recent discussions in Ref. [2]. A similar systematic discussion of the QCD effects in EWPOs is in progress, see Ref. [2] and Section B.2 in this report.

For the FCC-ee data analysis, owing to the rise of non-factorisable QED effects above the experimental uncertainties, direct use of MC programs might become the standard for fitting EWPOs to the data, even at the Tera-Z stage [2, 6, 7]. New MC event generators will have to provide built-in provisions for an efficient direct fitting of EWPOs to data, which are not present in the LEP legacy MCs. Section C.3 of Ref. [2] describes possible forms of future EWPOs at FCC-ee experiments and specifies the new required MC software. It is emphasized there that, owing to non-factorisable QED contributions, the multiphoton QED effects will have to be factorised at the amplitude level. Additional quantities available in tau and heavy flavour physics will reach 10^{-5} precision and are likely to need similar attention.

Very precise determinations of M_W at the FCC-ee will rely on the precise measurement of the cross-section of the $e^+e^- \rightarrow W^+W^-$ process near the threshold. A statistical precision of 0.04% of this cross-section translates into 0.6 MeV experimental uncertainty on M_W , compared with the current 3 MeV theoretical uncertainty for M_W . Therefore, improved theoretical calculations are required for the generic $e^+e^- \rightarrow 4f$ process near the WW threshold with an improvement of one order of magnitude. The most economical solution will be to combine the $\mathcal{O}(\alpha^1)$ calculation for the $e^+e^- \rightarrow 4f$ process with the $\mathcal{O}(\alpha^2)$ calculation for the doubly resonant $e^+e^- \rightarrow W^+W^-$ subprocess. The former calculation is already available [8]. The latter will need

to be developed; inclusion of the resummed QED corrections will be mandatory. For details, see Chapter B and Ref. [9].

In the case of the FCC-ee-H, M_H will be obtained from the $e^+e^- \rightarrow HZ$ process with a precision better than 10 MeV [3,10]. Theory uncertainties (mainly owing to final-state radiation effects) will be subdominant. The main focus will be on calculations of Higgs boson branching ratios and self-couplings. See Chapters B and E.

The anticipated experimental uncertainty on the m_t measurement at FCC-ee-tt [2] is $\mathcal{O}(20)$ MeV. On the theory side, there are several sources of uncertainties: (i) the perturbative uncertainty for the calculation of the threshold shape with higher-order QCD corrections; (ii) the threshold mass definition translated into the $\overline{\text{MS}}$ scheme; and (iii) the precision of α_s . Combining these three sources of uncertainty, a theoretical uncertainty close to the experimental one and less than 50 MeV for m_t appears feasible.* In addition, a very accurate determination of the efficiency of experimental acceptances and selection cuts is needed. This task will require the inclusion of higher-order corrections and resummation results in a Monte Carlo event generator; next-to-leading-order (NLO) QCD corrections for off-shell $t\bar{t}$ production, and matching between these contributions, complement previous semi-analytic results.

In this report, we are especially interested in the discussion of input parameters and of EWPOs connected with W, H, and top production physics. These are masses of heavy SM particles, their couplings, and also α_{QED} and α_{QCD} , which, as running quantities, must be adjusted carefully at the considered high-energy regions. These issues will be discussed in this report.

2 What this theory report brings: an overview

The report is divided into four basic chapters. Both the workshop and this report are mainly devoted to precision theoretical calculations. It is a most important subject because the value of most of the FCC-ee experimental analyses relies on the precision of the Standard Model and BSM predictions.

In Chapter B, the status and prospects for measurements and determination of α_{QED} and α_s at the FCC-ee are given, but also issues of QED and QCD resummations, an EFT radiative correction approach to W boson production, heavy quarkonia, analysis of the weak mixing angle from data (important, as it definitely has non-perturbative effects different from those in α), QCD vertex functions beyond two loops, EFT and QED in flavour physics, top pair production and mass determination, and a summary of SM precision predictions for partial Higgs decay widths.

In Chapter C, numerical and analytical methods for precision multiloop calculations are presented and recent advances in the field are discussed. The chapter is an addition to the 2018 report [2]. We mentioned already that Monte Carlo generators are very important, as they link pure experimental data with theory. Generators for precision e^+e^- simulations, τ , top, and W boson physics, heritage projects, and the need for proper software preservation with Monte Carlo generators are also discussed in Chapter C.

Chapter D consists of only one contribution. SMEFT theory is a bridge between SM physics and the analysis of extended gauge models. The chapter is connected with this issue and a specific code is presented. For another discussion, see the talk by J. de Blas [12].

*Examples show that estimations of higher-order corrections can differ from actual calculations by factors of three to five [7,11].

In Chapter E, finally, three contributions are collected, about Higgs models that go beyond the Standard Model theory.

References

- [1] A. Blondel *et al.*, 11th FCC-ee Workshop: Theory and Experiments, 2019, CERN, Geneva, Switzerland, <https://indico.cern.ch/event/766859/>
- [2] A. Blondel *et al.*, Standard Model theory for the FCC-ee Tera-Z stage, CERN (CERN Yellow Rep. Monogr. 3, Geneva, Switzerland), [arXiv:1809.01830](https://arxiv.org/abs/1809.01830), [doi:10.23731/CYRM-2019-003](https://doi.org/10.23731/CYRM-2019-003)
- [3] A. Abada *et al.*, *Eur. Phys. J. Spec. Top.* **228** (2019) 261. [doi:10.1140/epjst/e2019-900045-4](https://doi.org/10.1140/epjst/e2019-900045-4)
- [4] A. Abada *et al.*, *Eur. Phys. J.* **C79** (2019) 474. [doi:10.1140/epjc/s10052-019-6904-3](https://doi.org/10.1140/epjc/s10052-019-6904-3)
- [5] S. Schael *et al.* (ALEPH, DELPHI, L3, OPAL, SLD Collaborations, LEP Electroweak Working Group, SLD Electroweak Group, SLD Heavy Flavour Group, *Phys. Rep.* **427** (2006) 257. [arXiv:hep-ex/0509008](https://arxiv.org/abs/hep-ex/0509008), [doi:10.1016/j.physrep.2005.12.006](https://doi.org/10.1016/j.physrep.2005.12.006)
- [6] S. Jadach and M. Skrzypek, *Eur. Phys. J.* **C79** (2019) 756. [arXiv:1903.09895](https://arxiv.org/abs/1903.09895), [doi:10.1140/epjc/s10052-019-7255-9](https://doi.org/10.1140/epjc/s10052-019-7255-9)
- [7] A. Blondel *et al.*, Theory requirements and possibilities for the FCC-ee and other future high energy and precision frontier lepton colliders, Input 101 to the Update of the European Strategy for Particle Physics, <https://indico.cern.ch/event/765096/contributions/3295742/>. [arXiv:1901.02648](https://arxiv.org/abs/1901.02648)
- [8] A. Denner *et al.*, *Nucl. Phys.* **B724** (2005) 247 [Erratum: **B854** (2012) 504]. [arXiv:hep-ph/0505042](https://arxiv.org/abs/hep-ph/0505042), [doi:10.1016/j.nuclphysb.2005.06.033](https://doi.org/10.1016/j.nuclphysb.2005.06.033), [doi:10.1016/j.nuclphysb.2011.09.001](https://doi.org/10.1016/j.nuclphysb.2011.09.001),
- [9] M. Skrzypek and S. Jadach. KoralW and YFSWW3—lessons from LEP2 for FCC-ee, 11th FCC-ee Workshop: Theory and Experiments, 2019, CERN, Geneva, Switzerland, https://indico.cern.ch/event/766859/contributions/3252674/attachments/1775305/2970123/FCCeeKoralW_CERN2019_MS.pdf
- [10] <https://fcc-cdr.web.cern.ch/>, last accessed 15 January 15 2020.
- [11] I. Dubovyk *et al.*, *Phys. Lett.* **B783** (2018) 86. [arXiv:1804.10236](https://arxiv.org/abs/1804.10236), [doi:10.1016/j.physletb.2018.06.037](https://doi.org/10.1016/j.physletb.2018.06.037)
- [12] J. de Blas, SM effective field theory fits at the FCC, 11th FCC-ee Workshop: Theory and Experiments, 2019, CERN, Geneva, Switzerland, https://indico.cern.ch/event/766859/contributions/3252636/attachments/1776607/2888696/SMEFT_fits_at_FCC_deBlas.pdf

Chapter B

Precision calculations in the Standard Model

1 $\alpha_{\text{QED, eff}}(s)$ for precision physics at the FCC-ee/ILC

Contribution* by: F. Jegerlehner [fjeger@physik.hu-berlin.de]

Discovering the ‘physics behind precision’ at future linear or circular colliders (ILC or FCC projects) requires improved SM predictions based on more precise input parameters. I will review the role of $\alpha_{\text{QED, eff}}$ at future collider energies and report on possible progress based on results from low-energy machines.

1.1 $\alpha(M_Z^2)$ in precision physics (precision physics limitations)

Uncertainties of hadronic contributions to the effective fine structure constant $\alpha \equiv \alpha_{\text{QED}}$ are a problem for electroweak (EW) precision physics. Presently, we have α , G_μ , and M_Z as the most precise input parameters, which, together with the top Yukawa coupling y_t , the Higgs self-coupling λ , and the strong interaction coupling α_s allow us to make precision predictions for the particle reaction cross-sections encompassed by the Standard Model (SM). The cross-section data unfolded from detector and photon radiation resolution effects are often conveniently representable in terms of so-called pseudo-observables, such as $\sin^2 \Theta_f$, v_f , a_f , M_W , Γ_Z , Γ_W , \dots , as illustrated in Fig. B.1.1.

Because of the large 6% relative correction between α in the classical limit and the effective value $\alpha(M_Z^2)$ at the Z mass scale, where 50% of the shift is due to non-perturbative hadronic effects, one is losing about a factor of five orders of magnitude in precision. Nevertheless, for the vector boson Z and W, top quark, and Higgs boson precision physics possible at future e^+e^- colliders, the best effective input parameters are given by $\alpha(M_Z)$, G_μ , and M_Z . The effective $\alpha(s)$ at a process scale \sqrt{s} is given in terms of the photon vacuum polarisation (VP) self-energy correction $\Delta\alpha(s)$ by

$$\alpha(s) = \frac{\alpha}{1 - \Delta\alpha(s)} ; \quad \Delta\alpha(s) = \Delta\alpha_{\text{lep}}(s) + \Delta\alpha_{\text{had}}^{(5)}(s) + \Delta\alpha_{\text{top}}(s). \quad (1.1)$$

To be included are the perturbative lepton and top quark contributions, in addition to the non-perturbative hadronic VP shift $\Delta\alpha_{\text{had}}^{(5)}(s)$ from the five light quarks and the hadrons they form.

*This contribution should be cited as:

F. Jegerlehner, $\alpha_{\text{QED, eff}}(s)$ for precision physics at the FCC-ee/ILC, DOI: [10.23731/CYRM-2020-003.9](https://doi.org/10.23731/CYRM-2020-003.9), in: Theory for the FCC-ee, Eds. A. Blondel, J. Gluza, S. Jadach, P. Janot and T. Riemann, CERN Yellow Reports: Monographs, CERN-2020-003, DOI: [10.23731/CYRM-2020-003](https://doi.org/10.23731/CYRM-2020-003), p. 9.
© CERN, 2020. Published by CERN under the [Creative Commons Attribution 4.0 license](https://creativecommons.org/licenses/by/4.0/).

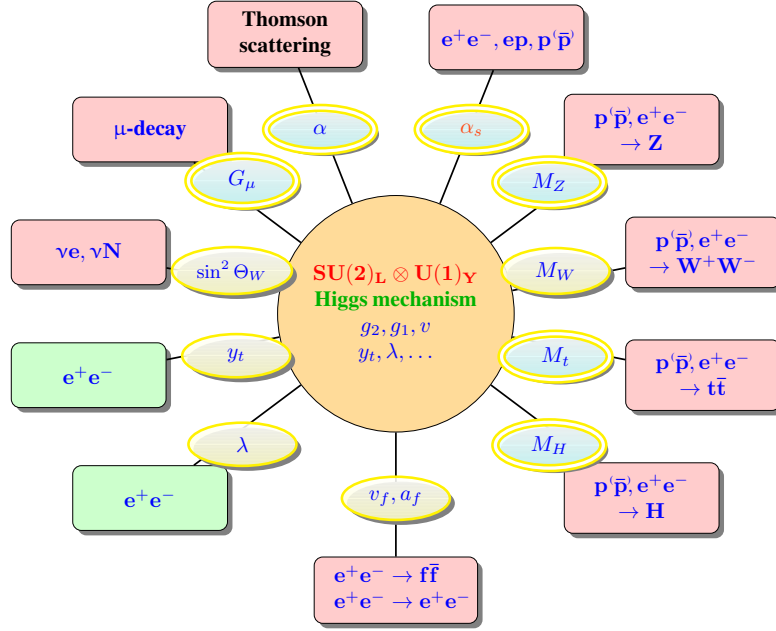


Fig. B.1.1: Many precisely measurable pseudo-observables associated with scattering-, production-, and decay processes are interrelated and predictable in terms of a few independent input parameters.

The current accuracies of the corresponding SM input parameter are:

$$\begin{aligned}
 \frac{\delta\alpha}{\alpha} &\sim 3.6 \times 10^{-9}, \\
 \frac{\delta G_\mu}{G_\mu} &\sim 8.6 \times 10^{-6}, \\
 \frac{\delta M_Z}{M_Z} &\sim 2.4 \times 10^{-5}, \\
 \frac{\delta\alpha(M_Z)}{\alpha(M_Z)} &\sim 0.9 \div 1.6 \times 10^{-4} \quad (\text{present : lost } 10^5 \text{ in precision!}), \\
 \frac{\delta\alpha(M_Z)}{\alpha(M_Z)} &\sim 5 \times 10^{-5} \quad (\text{FCC-ee/ILC requirement}).
 \end{aligned} \tag{1.2}$$

We further note that $\delta M_W/M_W \sim 1.5 \times 10^{-4}$, $\delta M_H/M_H \sim 1.3 \times 10^{-3}$, $\delta M_t/M_t \sim 2.3 \times 10^{-3}$, at present. Evidently, $\alpha(M_Z)$ is the least precise among the basic input parameters $\alpha(M_Z)$, G_μ , and M_Z , and requires a major effort of improvement. As an example, one of the most precisely measured derived observables, the leptonic weak mixing parameter $\sin^2 \Theta_{\ell\text{eff}} = (1 - v_\ell/a_\ell)/4 = 0.23148 \pm 0.00017$ and also the related W mass $M_W = 80.379 \pm 0.012 \text{ GeV}$ are affected by the present hadronic uncertainty $\delta\Delta\alpha(M_Z) = 0.00020$ in predictions by $\delta\sin^2 \Theta_{\ell\text{eff}} = 0.00007$ and $\delta M_W/M_W \sim 4.3 \times 10^{-5}$, respectively.

Here, one has to keep in mind that, besides $\Delta\alpha$, there is a second substantial leading one-loop correction, which enters the neutral to charged current effective Fermi-couplings ratio $\rho = G_{\text{NC}}(0)/G_{\text{CC}}(0) = 1 + \Delta\rho$, where $\Delta\rho = 3\sqrt{2}M_t^2 G_\mu/16\pi^2$ is quadratic in the top quark mass. The mentioned $\delta M_t/M_t$ uncertainty affects the M_W and $\sin^2 \Theta_{\ell\text{eff}}$ predictions, as given by

$$\frac{\delta M_W}{M_W} \sim M_W^2/(2M_W^2 - M_Z^2) \cdot \Delta\rho \frac{\delta M_t}{M_t} \sim 1.3 \times 10^{-2} \frac{\delta M_t}{M_t} \simeq 3.0 \times 10^{-5}, \tag{1.3}$$

$$\frac{\delta \sin^2 \Theta_f}{\sin^2 \Theta_f} \sim \frac{2 \cos^2 \Theta_f}{\cos^2 \Theta_f - \sin^2 \Theta_f} \Delta\rho \frac{\delta M_t}{M_t} \sim 2.7 \times 10^{-2} \frac{\delta M_t}{M_t} \simeq 6.2 \times 10^{-5}, \quad (1.4)$$

which are comparable to the current uncertainties from $\delta\Delta\alpha$. Thus, an improvement of δM_t by a factor of five appears to be as important as an improvement of $\alpha(M_Z)$. We are reminded that the dependence on M_H is very much weaker because of the custodial symmetry, which implies the absence of M_H^2 corrections, such that only relatively weak $\log M_H$ effects are remaining.

The input parameter uncertainties affect most future precision tests and may obscure new physics searches! To reduce hadronic uncertainties for perturbative QCD (pQCD) contributions, last but not least, it is also very crucial to improve the precision of QCD parameters α_s , m_c , m_b , m_t , which is also a big challenge for lattice QCD.

1.1.1 The relevance of $\alpha(M_Z^2)$

Understanding precisely even the simplest four-fermion, vector boson, and Higgs boson production and decay processes, requires very precise input parameters.

Unlike in QED and QCD in the SM, a spontaneously broken non-Abelian gauge theory, there are intricate parameter inter-dependences, all masses are related to couplings, and only six quantities (besides $f \neq t$ fermion masses and mixing parameters), α , G_μ , and M_Z , in addition to the QCD coupling α_s , the top quark Yukawa coupling y , and the Higgs boson self-coupling λ_H , are independent. The effective $\alpha(M_Z^2)$ exhibits large hadronic correction that affects prediction-like versions of the weak mixing parameter via

$$\sin^2 \Theta_i \cos^2 \Theta_i = \frac{\pi \alpha}{\sqrt{2} G_\mu M_Z^2} \frac{1}{1 - \Delta r_i}; \quad \Delta r_i = \Delta r_i(\alpha, G_\mu, M_Z, m_H, m_{f \neq t}, m_t), \quad (1.5)$$

with quantum corrections from gauge-boson self-energies and vertex and box corrections, where Δr_i depends on the definition of $\sin^2 \Theta_i$. The various definitions coincide at tree level and hence only differ by quantum effects. From the weak gauge-boson masses, the electroweak gauge couplings, and the neutral current couplings of the charged fermions, we obtain

$$\sin^2 \Theta_W = 1 - \frac{M_W^2}{M_Z^2}, \quad (1.6)$$

$$\sin^2 \Theta_g = e^2/g^2 = \frac{\pi \alpha}{\sqrt{2} G_\mu M_W^2}, \quad (1.7)$$

$$\sin^2 \Theta_f = \frac{1}{4|Q_f|} \left(1 - \frac{v_f}{a_f} \right), \quad f \neq \nu, \quad (1.8)$$

for the most important cases and the general form of Δr_i reads

$$\Delta r_i = \Delta\alpha - f_i(\sin^2 \Theta_i) \Delta\rho + \Delta r_{i \text{ reminder}}, \quad (1.9)$$

with a universal term $\Delta\alpha$, which affects the predictions of M_W , A_{LR} , A_{FB}^f , Γ_f , etc. The leading corrections are $\Delta\alpha(M_Z^2) = \Pi'_\gamma(0) - \text{Re} \Pi'_\gamma(M_Z^2)$ from the running fine structure constant and

$$\Delta\rho = \frac{\Pi_Z(0)}{M_Z^2} - \frac{\Pi_W(0)}{M_W^2} + 2 \frac{\sin \Theta_W}{\cos \Theta_W} \frac{\Pi_{\gamma Z}(0)}{M_Z^2},$$

which is proportional to $G_\mu M_t^2$ and therefore large, dominated by the heavy top quark mass effect, or by the large top Yukawa coupling.

The uncertainty $\delta\Delta\alpha$ implies uncertainties δM_W , $\delta \sin^2 \Theta_i$ given by

$$\frac{\delta M_W}{M_W} \sim \frac{1}{2} \frac{\sin^2 \Theta_W}{\cos^2 \Theta_W - \sin^2 \Theta_W} \delta\Delta\alpha \sim 0.23 \delta\Delta\alpha, \quad (1.10)$$

$$\frac{\delta \sin^2 \Theta_f}{\sin^2 \Theta_f} \sim \frac{\cos^2 \Theta_f}{\cos^2 \Theta_f - \sin^2 \Theta_f} \delta\Delta\alpha \sim 1.54 \delta\Delta\alpha. \quad (1.11)$$

Also affected are the important relationships between couplings and masses, such as

$$\lambda = 3 \sqrt{2} G_\mu M_H^2 (1 + \delta_H(\alpha, \dots)); \quad y_t^2 = 2 \sqrt{2} G_\mu M_t^2 (1 + \delta_t(\alpha, \dots)), \quad (1.12)$$

which currently offer the only way to determine λ and y_t via the experimentally accessible masses M_H and M_t . Direct measurement of λ and y_t will probably be possible only at future lepton colliders, such as the FCC-ee.

The *parameter relationships* between very precisely measurable quantities provide stringent precision tests and, at high enough precision, would reveal the physics missing within the SM. Currently, the non-perturbative hadronic contribution $\Delta\alpha_{\text{had}}^{(5)}(M_Z^2)$ limits the precision predictions. Concerning the relevance of quantum corrections and their precision, one should keep in mind that a 30 SD disagreement between some SM prediction and experiment is obtained when subleading SM corrections are neglected, and only the leading corrections $\Delta\alpha(M_Z^2)$ and $\Delta\rho$ in Eq. (1.9) are accounted for.

Calculate, for example, the W and Z mass from $\alpha(M_Z)$, G_μ and $\sin^2 \Theta_{\ell\text{eff}}$: first $\sin^2 \Theta_W = 1 - M_W^2/M_Z^2$ is related to $\sin^2 \theta_{\ell\text{eff}}(M_Z)$ via

$$\sin^2 \theta_{\ell\text{eff}}(M_Z) = \left(1 + \frac{\cos^2 \Theta_W}{\sin^2 \Theta_W} \Delta\rho \right) \sin^2 \Theta_W,$$

where the leading top quark mass square correction is

$$\Delta\rho = \frac{3 M_t^2 \sqrt{2} G_\mu}{16 \pi^2}; \quad M_t = 173 \pm 0.4 \text{ GeV}.$$

The iterative solution with input $\sin^2 \theta_{\ell\text{eff}}(M_Z) = 0.23148$ is $\sin^2 \Theta_W = 0.22426$ while $1 - M_W^2/M_Z^2 = 0.22263$ is what one gets using PDG:

$$M_W^{\text{exp}} = 80.379 \pm 0.012 \text{ GeV}; \quad M_Z^{\text{exp}} = 91.1876 \pm 0.0021 \text{ GeV}.$$

Predicting, then, the masses, we have

$$M_W = \frac{A_0}{\sin^2 \Theta_W}; \quad A_0 = \sqrt{\frac{\pi\alpha}{\sqrt{2} G_\mu}}; \quad M_Z = \frac{M_W}{\cos \Theta_W}$$

where, including photon VP correction $\alpha^{-1}(M_Z) = 128.953 \pm 0.016$. For the W and Z masses, we then get

$$M_W^{\text{the}} = 81.1636 \pm 0.0346 \text{ GeV}; \quad M_Z^{\text{the}} = 92.1484 \pm 0.0264 \text{ GeV}.$$

This gives the following SD values:

$$\text{W: } 23 \sigma; \quad \text{Z: } 36 \sigma$$

Uncertainties from $\sin^2 \theta$, $\alpha(M_Z)$, and M_t , as well as experimental uncertainties, are added in quadrature. The result is, of course, scheme-dependent, but illustrates well the sensitivity to taking into account the proper radiative corrections. Actually, including full one-loop and leading two-loop corrections reduces the disagreement below the 2σ level.

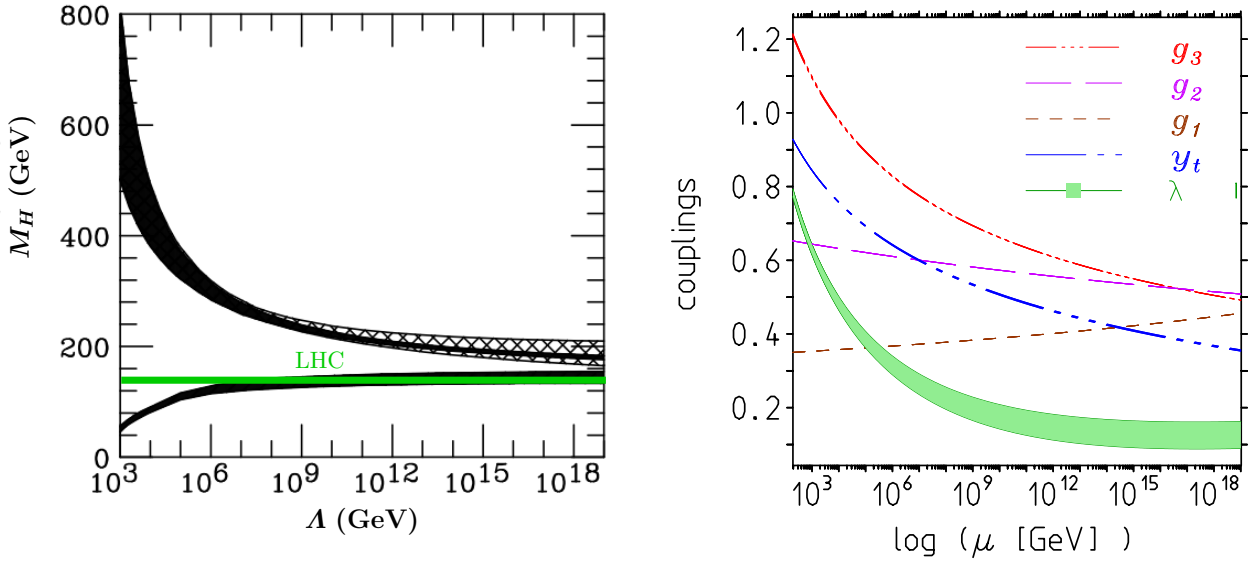


Fig. B.1.2: Left: Plot by Riesselmann and Hambye in 1996, the first two-loop analysis after knowing M_t from CDF [2]. Right: the SM dimensionless couplings in the $\overline{\text{MS}}$ scheme as a function of the renormalization scale for $M_H = 124\text{--}126$ GeV, which were obtained in Refs. [1, 3–5].

1.2 The ultimate motivation for high-precision SM parameters

After the ATLAS and CMS Higgs discovery at the LHC, the Higgs vacuum stability issue is one of the most interesting to be clarified at future e^+e^- facilities. Much more surprising than the discovery of its true existence is the fact that the Higgs boson turned out to exhibit a mass very close to what has been expected from vacuum stability extending up to the Planck scale Λ_{Pl} (see Fig. B.1.2). There appears to be a very tricky conspiracy with other couplings to achieve this ‘purpose’. Related is the question of whether the SM allows us to extrapolate up to the Planck scale. Thus, the central issue for the future is the very delicate ‘acting together’ between SM couplings, which makes the precision determination of SM parameters more important than ever. Therefore, higher-precision SM parameters g' , g , g_s , y_t , and λ are mandatory for progress in this direction. Actually, the vacuum stability is controversial at present at the 1.5σ level between a metastable and a stable EW vacuum, which depends on whether λ stays positive up to Λ_{Pl} or not. This is illustrated in Fig. B.1.3. If the SM extrapolates stable to Λ_{Pl} , obviously the resulting effective parameters affect early cosmology, Higgs inflation, Higgs reheating, etc. [1]. The sharp dependence of the Higgs vacuum stability on the SM input parameters, as well as on possible SM extensions and the vastly different scenarios that can result as a consequence of minor shifts in parameter space, makes the stable vacuum case a particularly interesting one and it could reveal the Higgs particle as ‘the master of the Universe’. After all, it is commonly accepted that dark energy provided by some scalar field is the ‘stuff’ shaping the Universe both at very early (inflation) as well as at late times (accelerated expansion).

It is highly conceivable that perturbation expansion works up to the Planck scale without a Landau pole or other singularities and that the Higgs potential remains (meta)stable! The discovery of the Higgs boson has supplied us, for the first time, with the complete set of SM parameters and, for the peculiar SM configuration, revealed that all SM couplings, with the exception of the hypercharge g_1 , are decreasing with energy. Very surprisingly, this implies

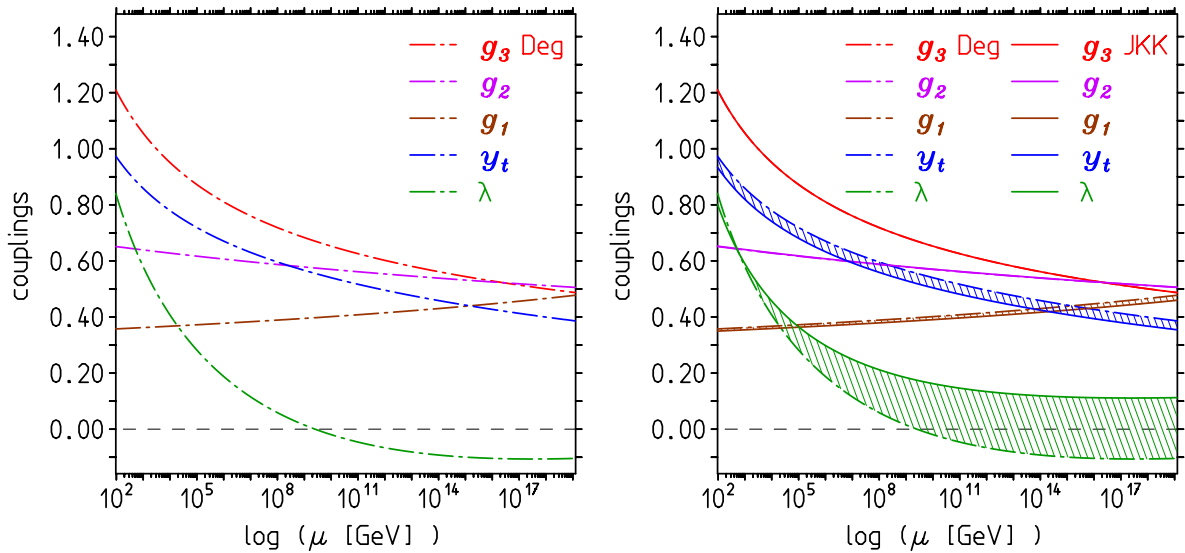


Fig. B.1.3: Left: Shaposhnikov *et al.* and Degrassi *et al.* matching [6, 7]. Right: The shaded bands show the difference in the SM parameter extrapolation using the central values of the $\overline{\text{MS}}$ parameters obtained from differences in the matching procedures.

that perturbative SM predictions improve at higher energies. More specifically, the pattern now looks as follows: the gauge coupling related to $U(1)_Y$ is screening (IR-free), the couplings associated with $SU(2)_L$ and $SU(3)_c$ are antiscreening (UV-free). Thus g_1 , g_2 , and g_3 behave as expected (standard wisdom). By contrast, the top Yukawa coupling y_t and Higgs self-coupling λ , while screening if stand-alone (IR-free, like QED), as part of the SM are transmuted from IR-free to UV-free. The SM reveals an amazing parameter conspiracy, which reminds us of phenomena often observed in condensed matter systems: “*There is a sudden rapid passage to a totally new and more comprehensive type of order or organisation, with quite new emergent properties*” [8], i.e., there must be reasons that couplings are as they are. This manifests itself in the QCD dominance within the renormalization group (RG) of the top Yukawa coupling, which requires $g_3 > 3 y_t/4$, and in the top Yukawa dominance within the RG of the Higgs boson coupling, which requires $\lambda < 3(\sqrt{5} - 1) y_t^2/2$ in the gaugeless ($g_1, g_2 = 0$) limit. Under focus is the Higgs self-coupling. Does it stay positive $\lambda > 0$ up to Λ_{Pl} ? A zero-valued λ would be an essential singularity. The key problem concerns the precise size of the top Yukawa coupling y_t , which decides the stability of our world! The metastability vs. stability controversy will be decided by obtaining more precise input parameters and by better-established EW matching conditions. Most important in this context is the direct measurement of y_t and λ at future e^+e^- colliders, but also the important role that the running gauge couplings are playing requires substantial progress in obtaining more precise hadronic cross-sections in order to reduce hadronic uncertainties in $\alpha(M_Z)$ and $\alpha_2(M_Z)$. This is a big challenge for low-energy hadron facilities. Complementary, progress in lattice QCD simulations of two-point correlators will be important to pin down hadronic effects from first principles. Such improvement in SM precision physics could open a new gateway to precision cosmology of the early Universe!

1.3 R data evaluation of $\alpha(M_Z^2)$

What we need is a precise calculation of the hadronic photon vacuum polarisation function. The non-perturbative hadronic piece from the five light quarks $\Delta\alpha_{\text{had}}^{(5)}(s) = -(\Pi'_\gamma(s) - \Pi'_\gamma(0))_{\text{had}}^{(5)}$

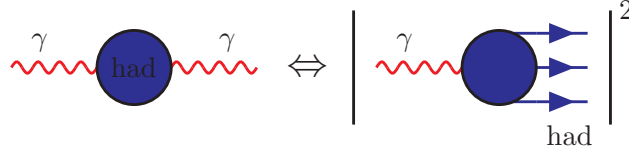


Fig. B.1.4: The master equation (1.13), relating $\Pi_\gamma^{\text{had}}(q^2)$ and $\sigma_{\text{tot}}^{\text{had}}(q^2)$, is based on analyticity and the optical theorem.

can be evaluated in terms of $\sigma(e^+e^- \rightarrow \text{hadrons})$ data via the dispersion integral

$$\Delta\alpha_{\text{had}}^{(5)}(s) = -\frac{\alpha s}{3\pi} \left(\int_{m_{\pi_0}^2}^{E_{\text{cut}}^2} ds' \frac{R_\gamma^{\text{data}}(s')}{s'(s'-s)} + \int_{E_{\text{cut}}^2}^{\infty} ds' \frac{R_\gamma^{\text{pQCD}}(s')}{s'(s'-s)} \right), \quad (1.13)$$

where $R_\gamma(s) \equiv \sigma^{(0)}(e^+e^- \rightarrow \gamma^* \rightarrow \text{hadrons})/(4\pi\alpha^2/3s)$ measures the hadronic cross-section in units of the tree-level $e^+e^- \rightarrow \mu^+\mu^-$ cross-section sufficiently above the muon pair production threshold ($s \gg 4m_\mu^2$). The master equation (Eq. (1.13)) is based on analyticity and the optical theorem, as shown in Fig. B.1.4.

A compilation of the available R data is shown in Fig. B.1.5 for the low-energy $\pi\pi$ channel and in Fig. B.1.6 for $R(s)$ above the ρ resonance peak. Since the mid 1990s [9], enormous progress has been achieved, also because the new initial-state radiation (ISR) radiative return approach[†] provided good statistics data from ϕ and B meson factories (see Refs. [10–53]). Still, an issue in hadronic vacuum polarisation (HVP) is the region 1.2–2 GeV, where we have a test ground for exclusive (more than 30 channels) versus inclusive R measurements, where data taking or data analysis is ongoing with CMD-3 and SND detectors (scan) and BaBar and BESIII detector data (radiative return). The region still contributes about 50% to the uncertainty of the hadronic contribution to the muon $g-2$, as we may learn from Fig. B.1.9, in the next section. Above 2 GeV, fairly accurate BES II data [49–51] are available. Recently, a new inclusive determination of $R_\gamma(s)$ in the range 1.84–3.72 GeV has been obtained with the KEDR detector at Novosibirsk [52, 53] (see Fig. B.1.7). At present, the results from the direct and the Adler function improved approach, to be discussed in Section 1.4, reads

$$\begin{aligned} \Delta\alpha_{\text{hadrons}}^{(5)}(M_Z^2) &= 0.0277\,56 \pm 0.000\,157 \\ &0.027563 \pm 0.000120 && \text{Adler} \\ \alpha^{-1}(M_Z^2) &= 128.916 \pm 0.022 \\ &128.953 \pm 0.016 && \text{Adler} \end{aligned} \quad (1.14)$$

In Fig. B.1.8, we show the effective fine structure constant as a function of the c.m. energy $E = \sqrt{s}$, for the time-like and space-like regions. The question now is: what are the possible improvements?

1. Evidently, a direct improvement of the dispersion integral involves reducing the uncertainty of $R(s)$ to 1% up to above the Υ resonances; probably, nobody will do that. One may rely on pQCD above 1.8 GeV and refer to quark–hadron duality, as in Ref. [57]. Then experimental input above 1.8 GeV is not required. But then we are left with questions

[†]This was pioneered by the KLOE Collaboration, followed by BaBar and BESIII experiments.

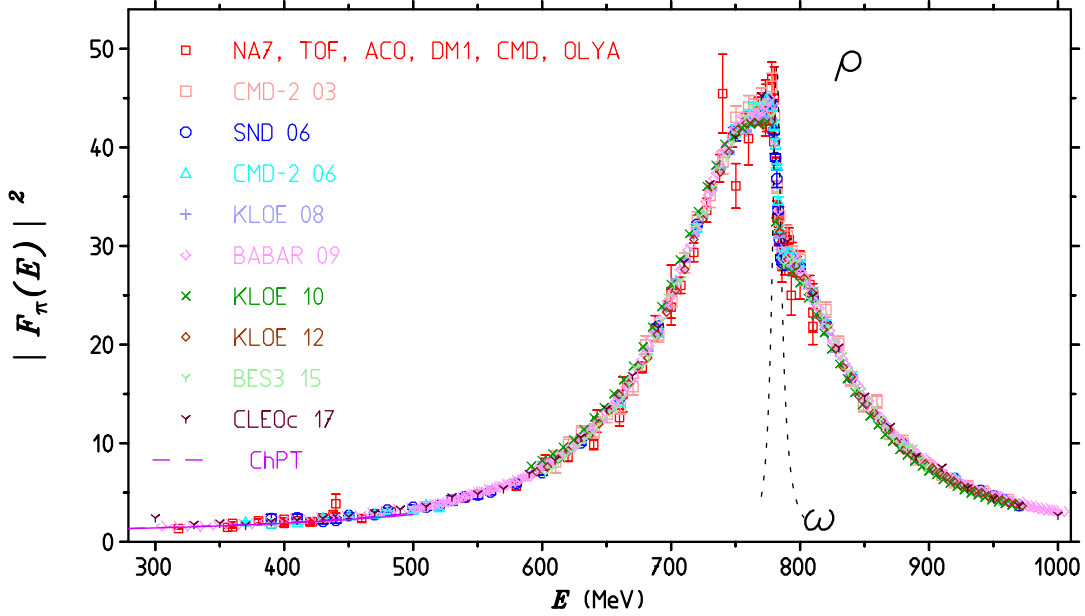


Fig. B.1.5: The low-energy tail of R is provided by $\pi^+\pi^-$ production data. Shown is a compilation of the modulus square of the pion form factor in the ρ meson region. The corresponding $R(s)$ is given by $R(s) = \frac{1}{4} \beta_\pi^3 |F_\pi^{(0)}(s)|^2$, $\beta_\pi = (1 - 4m_\pi^2/s)^{1/2}$ is the pion velocity ($s = E^2$). Data from CMD-2, SND, KLOE, BaBar, BESIII, and CLEOc [10–24] besides some older sets.

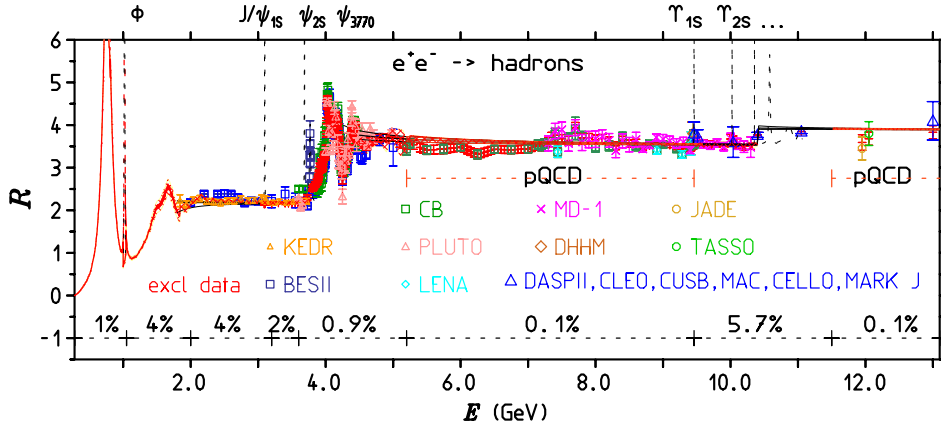


Fig. B.1.6: The compilation of $R(s)$ data utilised in the evaluation of $\Delta\alpha_{\text{had}}$. The bottom line shows the relative systematic uncertainties within the split regions. Different regions are assumed to have uncorrelated systematics. Data from Refs. [25–53] and others. We apply pQCD from 5.2 GeV to 9.46 GeV and above 11.5 GeV using the code of Ref. [54].

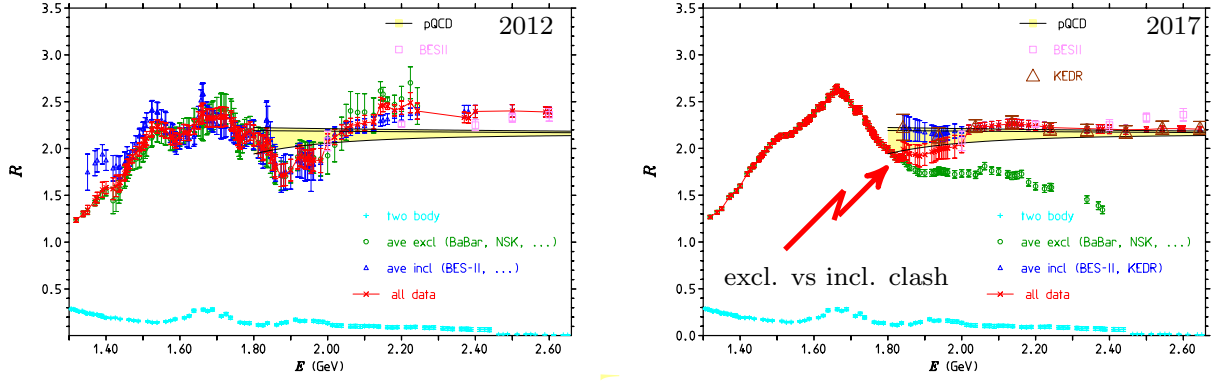


Fig. B.1.7: Illustrating progress by BaBar and NSK exclusive channel data vs. new inclusive data by KEDR. Why is the point at 1.84 GeV so high?

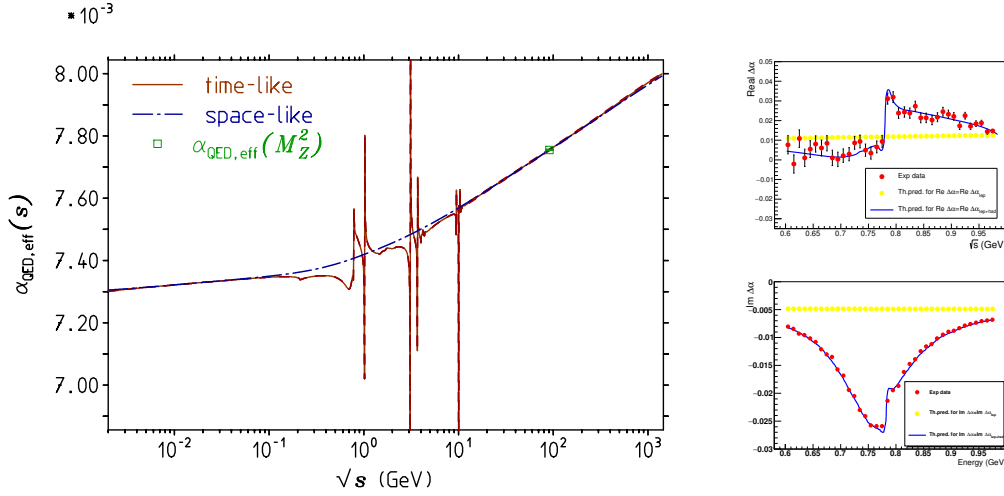


Fig. B.1.8: Left: The effective $\alpha(s)$ at time-like vs. space-like momentum transfer, showing quark–hadron duality at work. In the time-like region, the effective charge varies dramatically near resonances but agrees quite well on average with the space-like version. Locally, it is ill-defined near OZI suppressed meson decays J/ψ , ψ_1 , $\Upsilon_{1,2,3}$ where Dyson series of self-energy insertions do not converge (see Section 5 of Ref. [55]). Right: A first experimental determination of the effective charge in the ρ resonance region by KLOE-2 [56], which demonstrates the pronounced variation of the vacuum polarisation (charge screening) across a resonance.

about where precisely to assume thresholds and what are the mass effects near thresholds. Commonly, pQCD is applied, taking into account uncertainties in α_s only. This certainly does not provide a result that can be fully trusted, although the R data integral in this range is much less precise at present. The problem is that, in this theory-driven approach, 70% of $\Delta\alpha_{\text{had}}^{(5)}(M_Z^2)$ comes from pQCD. Thereby, one has to assume that, in the time-like region above 1.8 GeV, pQCD, on average, is as precise as the usually adopted $\overline{\text{MS}}$ parametrization suggests. Locally, pQCD does not work near thresholds and resonances, obviously.

Table B.1.1: $\Delta\alpha_{\text{had}}^{(5)}(M_Z)$ in terms of e^+e^- data and pQCD. The last two columns list the relative accuracy and the percentage contribution of the total. The systematic uncertainties (syst) are assumed to be independent among the different energy ranges listed in the table.

Final state	Range (GeV)	$\Delta\alpha_{\text{had}}^{(5)} \times 10^4$ (stat) (syst) [tot]	Rel (%)	Abs (%)
ρ	(0.28, 1.05)	34.14 (0.03) (0.28) [0.28]	0.8	3.1
ω	(0.42, 0.81)	3.10 (0.03) (0.06) [0.07]	2.1	0.2
ϕ	(1.00, 1.04)	4.76 (0.04) (0.05) [0.06]	1.4	0.2
J/ψ		12.38 (0.60) (0.67) [0.90]	7.2	31.9
Υ		1.30 (0.05) (0.07) [0.09]	6.9	0.3
Had	(1.05, 2.00)	16.91 (0.04) (0.82) [0.82]	4.9	26.7
Had	(2.00, 3.20)	15.34 (0.08) (0.61) [0.62]	4.0	15.1
Had	(3.20, 3.60)	4.98 (0.03) (0.09) [0.10]	1.9	0.4
Had	(3.60, 5.20)	16.84 (0.12) (0.21) [0.25]	0.0	2.4
pQCD	(5.20, 9.46)	33.84 (0.12) (0.25) [0.03]	0.1	0.0
Had	(9.46, 11.50)	11.12 (0.07) (0.69) [0.69]	6.2	19.1
pQCD	(11.50, ∞)	123.29 (0.00) (0.05) [0.05]	0.0	0.1
Data	(0.3, ∞)	120.85 (0.63) (1.46) [1.58]	1.0	0.0
Total		277.99 (0.63) (1.46) [1.59]	0.6	100.0

- The more promising approach discussed in the following relies on the Euclidean split method (Adler function controlled pQCD), which only requires improved R measurements in the exclusive region from 1 to 2 GeV. Here, NSK, BESIII, and Belle II can top what BaBar has achieved. However, in this rearrangement, a substantially more precise calculation of the pQCD Adler function is as important. Required is an essentially exact massive four-loop result, which is equivalent to sufficiently high-order low- and high-energy expansions, of which a few terms are available already [58].

Because of the high sensitivity to the precise charm and bottom quark values, one also needs better parameters m_c and m_b besides α_s . Here one can profit from activities going on anyway and the FCC-ee and ILC projects pose further strong motivation to attempt to reach higher precision for QCD parameters.

1.3.1 $\Delta\alpha_{\text{had}}(M_Z^2)$ results from ranges

Table B.1.1 shows the contributions and uncertainties to $\Delta\alpha_{\text{had}}^{(5)}(M_Z)$ for $M_Z = 91.1876$ GeV in units 10^{-4} from different regions. Typically, depending on cuts applied, the direct evaluation of the dispersion integral of R yields 43% from data and 57% from perturbative QCD. Here, pQCD is used between 5.2 GeV and 9.5 GeV and above 11.5 GeV. Systematic uncertainties are taken to be correlated within the different ranges, but taken as independent between the different ranges.

In Fig. B.1.9, we illustrate the relevance of different energy ranges by comparing the hadronic contribution to the muon $g - 2$ with that to the hadronic shift of the effective charge at M_Z . The point is that the new muon $g - 2$ experiments strongly motivate efforts the measure $R(s)$ in the low-energy region more precisely. From Fig. B.1.9, we learn that low-energy data alone are not able to substantially improve a direct evaluation of the dispersion integral

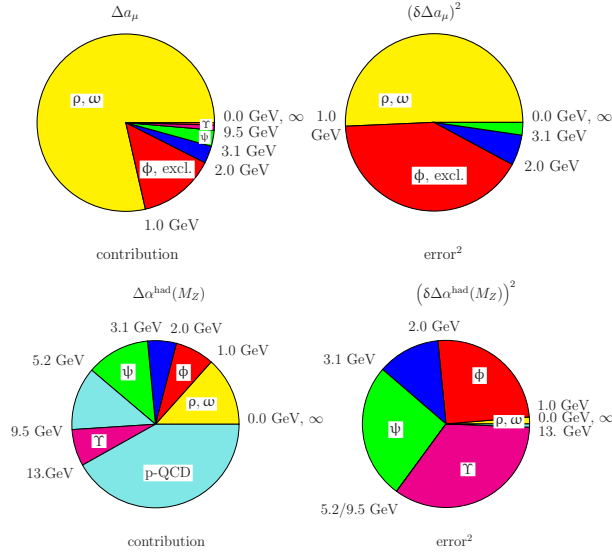


Fig. B.1.9: A comparison of the weights and square uncertainties between a_μ^{had} and $\Delta\alpha_{\text{had}}^{(5)}(M_Z^2)$ of contributions from different regions. It reveals the importance of the different energy regions. In contrast to the low-energy dominated a_μ^{had} , $\Delta\alpha_{\text{had}}^{(5)}(M_Z^2)$ is sensitive to data from much higher energies.

(Eq. (1.13)). Therefore, to achieve the required factor of five improvement, alternative methods to determine $\Delta\alpha_{\text{had}}^{(5)}(s)$ at high energies must be developed.

1.4 Reducing uncertainties via the Euclidean split trick: Adler function controlled pQCD

As we learn from Fig. B.1.6, it is difficult, if not impossible, to tell at what precision pQCD can replace data. This especially concerns resonance and threshold effects and to what extent quark–hadron duality can be made precise. This is much simpler to accommodate by comparison in the Euclidean (space-like) region, as suggested by Adler [59] a long time ago and successfully tested [60]. As the data pool has been improving greatly, the ‘experimental’ Adler function is now known with remarkable precision. Actually, on the experimental side, new more precise measurements of $R(s)$ are being made, primarily in the low-energy range. On the theory side, pQCD calculations for Euclidean two-point current correlators are expected to be pushed further. Advances are also expected from lattice QCD, which can also produce data for the Adler function. As suggested in Refs. [61–63], in the Euclidean region, a split into a non-perturbative and a pQCD part is self-evident. One may write

$$\alpha(M_Z^2) = \alpha^{\text{data}}(-M_0^2) + [\alpha(-M_Z^2) - \alpha(-M_0^2)]^{\text{pQCD}} + [\alpha(M_Z^2) - \alpha(-M_Z^2)]^{\text{pQCD}}, \quad (1.15)$$

where the space-like offset M_0 is chosen such that pQCD is well under control for $-s < -M_0^2$. The non-perturbative offset $\alpha^{\text{data}}(-M_0^2)$ may be obtained by integrating $R(s)$ data, by choosing $s = -M_0^2$ in Eq. (1.13).

The crucial point is that the contribution from different energy ranges to $\alpha^{\text{data}}(-M_0^2)$ is very different from those to $\alpha^{\text{data}}(M_Z^2)$. Table B.1.1 now is replaced by Table B.1.2, where $\alpha^{\text{data}}(-M_0^2)$ is listed for $M_0 = 2 \text{ GeV}$ in units 10^{-4} . Here 94% results using data and only

Table B.1.2: $\Delta\alpha_{\text{had}}^{(5)}(-M_0^2)$ at $M_0 = 2 \text{ GeV}$ in terms of e^+e^- data and pQCD. Labels as in Table B.1.1.

Final state	Range (GeV)	$\Delta\alpha_{\text{had}}^{(5)}(-M_0^2) \times 10^4$ (stat) (syst) [tot]	Rel (%)	Abs (%)
ρ	(0.28, 1.05)	29.97 (0.03) (0.24) [0.24]	0.8	14.3
ω	(0.42, 0.81)	2.69 (0.02) (0.05) [0.06]	2.1	0.8
ϕ	(1.00, 1.04)	3.78 (0.03) (0.04) [0.05]	1.4	0.6
J/ψ		3.21 (0.15) (0.15) [0.21]	6.7	11.2
Υ		0.05 (0.00) (0.00) [0.00]	6.8	0.0
Had	(1.05, 2.00)	10.56 (0.02) (0.48) [0.48]	4.6	56.9
Had	(2.00, 3.20)	6.06 (0.03) (0.25) [0.25]	4.2	15.7
Had	(3.20, 3.60)	1.31 (0.01) (0.02) [0.03]	1.9	0.2
Had	(3.60, 5.20)	2.90 (0.02) (0.02) [0.03]	0.0	0.2
pQCD	(5.20, 9.46)	2.66 (0.02) (0.02) [0.00]	0.1	0.0
Had	(9.46, 11.50)	0.39 (0.00) (0.02) [0.02]	5.7	0.1
pQCD	(1.50, 0.00)	0.90 (0.00) (0.00) [0.00]	0.0	0.0
Data	(0.3, ∞)	60.92 (0.16) (0.62) [0.64]	1.0	0.0
Total		64.47 (0.16) (0.62) [0.64]	1.0	100.0

6% pQCD, applied again between 5.2 GeV and 9.5 GeV and above 11.5 GeV. Of $\Delta\alpha_{\text{had}}^{(5)}(M_Z^2)$ 22% data, 78% pQCD! The split point, M_0 , may be shifted to optimise the uncertainty contributed from the pQCD part and the data based offset value. A reliable estimate of the latter is mandatory and we have also crosschecked its evaluation using the phenomenological effective Lagrangian global fit approach [64, 65], specifically, within the broken hidden local symmetry implementation.

In Fig. B.1.10, we illustrate the relevance of different energy ranges by comparing the hadronic shift of the effective charge as evaluated at space-like low-energy scale $M_0 = 2 \text{ GeV}$ with those at the time-like M_Z scale. The crucial point is that the profile of the offset α at M_0 much more closely resembles the profile found for the hadronic contribution to a_μ and improving a_μ^{had} automatically leads to an improvement of $\Delta\alpha_{\text{had}}^{(5)}(-M_0^2)$; this is the profit gained from the Euclidean split trick.

What does this have to do with the Adler function? (i) The Adler function is the monitor to control the applicability of pQCD and (ii) the pQCD part $[\alpha(-M_Z^2) - \alpha(-M_0^2)]^{\text{pQCD}}$ is favourably calculated by integrating the Adler function $D(Q^2)$. The small remainder $[\alpha(M_Z^2) - \alpha(-M_Z^2)]^{\text{pQCD}}$ can be obtained in terms of the VP function $\Pi'_\gamma(s)$. In fact, the Adler function is the ideal monitor for comparing theory and data. The Adler function is defined as the derivative of the VP function:

$$D(-s) \doteq \frac{3\pi}{\alpha} s \frac{d}{ds} \Delta\alpha_{\text{had}}(s) = - \left(12\pi^2\right) s \frac{d\Pi'_\gamma(s)}{ds} \quad (1.16)$$

and can be evaluated in terms of e^+e^- annihilation data by the dispersion integral

$$D(Q^2) = Q^2 \left(\int_{4m_\pi^2}^{E_{\text{cut}}^2} ds \frac{R(s)^{\text{data}}}{(s+Q^2)^2} + \int_{E_{\text{cut}}^2}^{\infty} ds \frac{R^{\text{pQCD}}(s)}{(s+Q^2)^2} \right). \quad (1.17)$$

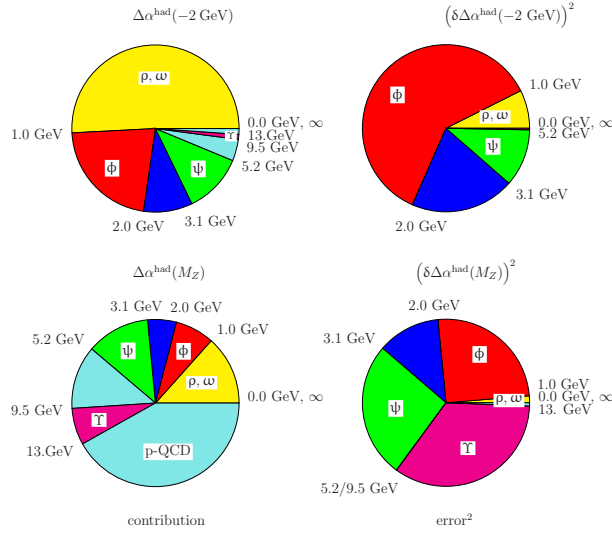


Fig. B.1.10: Contributions and square errors from e^+e^- data ranges and from pQCD to $\Delta\alpha_{\text{had}}^{(5)}(-M_0^2)$ vs. $\Delta\alpha_{\text{had}}^{(5)}(M_Z^2)$.

It is a finite object not subject to renormalization and it tends to a constant in the high-energy limit, where it is perfectly perturbative. Comparing the direct $R(s)$ -based and the $D(Q^2)$ -based methods

pQCD $\leftrightarrow R(s)$ Very difficult to obtain in theory	pQCD $\leftrightarrow D(Q^2)$ Smooth simple function in <i>Euclidean</i> region
--	---

we note that in the time-like approach pQCD only works well in ‘perturbative windows’ roughly in the ranges 3.00–3.73 GeV, 5.00–10.52 GeV and 11.50 GeV to ∞ [54], while in the space-like approach pQCD works well for $Q > 2.0$ GeV, a clear advantage.

In Fig. B.1.11, the ‘experimental’ Adler function is confronted with theory (pQCD + NP). Note that, in contrast to most xfR plots, like Fig. B.1.6, showing statistical errors only, in Fig. B.1.11. the total error is displayed as the shaded band. We see that while one-loop and two-loop predictions clearly fail to follow the data band, a full massive three-loop QCD prediction in the gauge-invariant background field MOM scheme [66] reproduces the experimental Adler function surprisingly well. This has been worked out [60] by Padé improvement of the moment expansions provided in Refs. [67–69]. Figure B.1.11 also shows that non-perturbative (NP) contributions from the quark and gluon condensates [70, 71][‡] start to contribute substantially only at energies where pQCD fails to converge because one is approaching the Landau pole in $\overline{\text{MS}}$ parametrized QCD. Strong coupling constant freezing, as in analytic perturbation theory, advocated in Ref. [72] or similar schemes, is not actually able to improve the agreement in the low-energy regime. Coupling constant freezing also contradicts lattice QCD results [73].

From the three terms of Eq. (1.15), we already know the low-energy offset $\Delta\alpha_{\text{had}}(-M_0^2)$ for $M_0 = 2.0$ GeV. We obtain the second term by integrating the pQCD predicted Adler function

$$\Delta_1 = \Delta\alpha_{\text{had}}(-M_Z^2) - \Delta\alpha_{\text{had}}(-M_0^2) = \frac{\alpha}{3\pi} \int_{M_0^2}^{M_Z^2} dQ'^2 \frac{D(Q'^2)}{Q'^2}, \quad (1.18)$$

[‡]These are evaluated by means of operator product expansions; the explicit expressions may be found in Ref. [60].

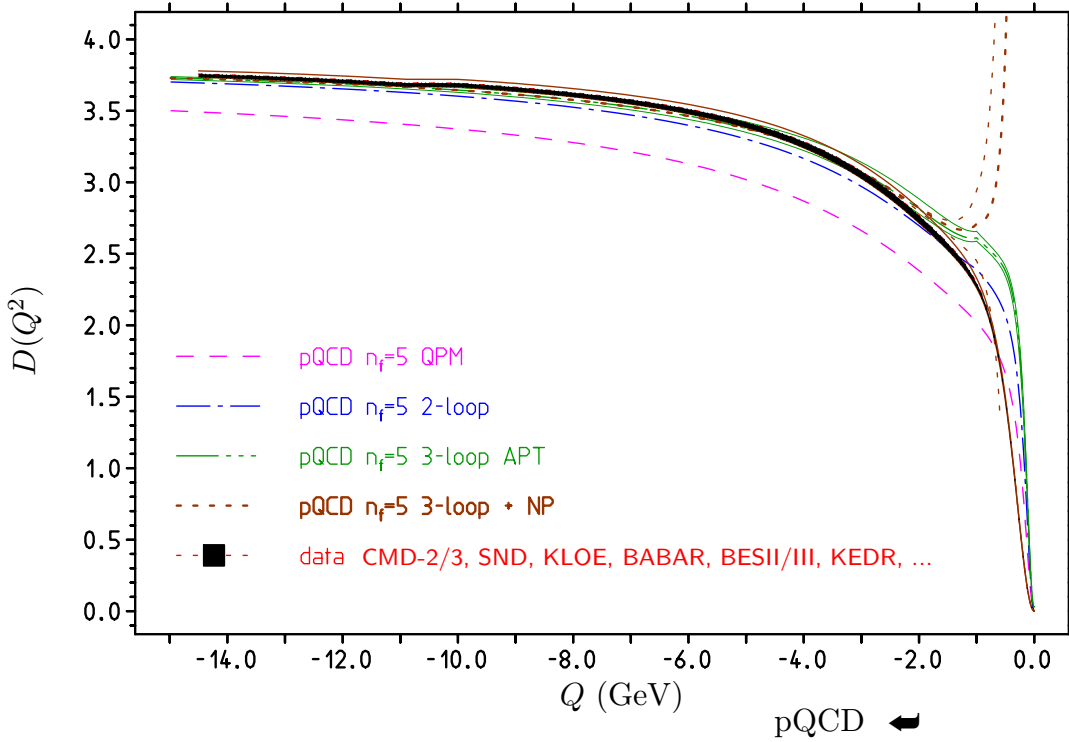


Fig. B.1.11: Monitoring pQCD vs. data: the pQCD prediction of $D(Q^2)$ works well down to $M_0 = 2.0$ GeV, provided full massive QCD at three-loop order or higher is employed.

based on a complete three-loop massive QCD analysis. The QCD parameters used are $\alpha_s(M_Z) = 0.1189(20)$, $m_c(m_c) = 1.286(13)[M_c = 1.666(17)]$ GeV, $m_b(m_c) = 4.164(25)[M_b = 4.800(29)]$ GeV. The result obtained is

$$\Delta_1 = \Delta\alpha_{\text{had}}(-M_Z^2) - \Delta\alpha_{\text{had}}(-M_0^2) = 0.021\,074 \pm 0.000\,100.$$

This includes a shift $+0.000\,008$ from the massless four-loop contribution included in the high-energy tail. The error $\pm 0.000\,100$ will be added in quadrature. Up to three loops, all contributions have the same sign and are substantial. Four-loop and higher orders could still add up to non-negligible contributions. An error for missing higher-order terms is not included.

The remaining term concerns the link between the space-like and the time-like region at the Z boson mass scale and is given by the difference

$$\Delta_2 = \Delta\alpha_{\text{had}}^{(5)}(M_Z^2) - \Delta\alpha_{\text{had}}^{(5)}(-M_Z^2) = 0.000\,045 \pm 0.000\,002,$$

which can be calculated in pQCD. It accounts for the $i\pi$ -terms from the logs $\ln(-q^2/\mu^2) = \ln(|q^2/\mu^2|) + i\pi$. Since the term is small, we can also get it from direct data integration based on our data compilation. We obtain $\Delta\alpha_{\text{had}}(-M_Z^2) = 276.44 \pm 0.64 \pm 1.78$ and $\Delta\alpha_{\text{had}}(+M_Z^2) = 276.84 \pm 0.64 \pm 1.90$, and taking into account that errors are almost 100% correlated, we have $\Delta\alpha_{\text{had}}(M_Z^2) - \Delta\alpha_{\text{had}}(-M_Z^2) = 0.40 \pm 0.12$ less precise but in agreement with the pQCD result. We then have

$$\begin{aligned} \Delta\alpha_{\text{had}}^{(5)}(-M_0^2)^{\text{data}} &= 0.006\,409 \pm 0.000\,063 \\ \Delta\alpha_{\text{had}}^{(5)}(-M_Z^2) &= 0.027\,483 \pm 0.000\,118 \end{aligned}$$

$$\Delta\alpha_{\text{had}}^{(5)}(M_Z^2) = 0.027\,523 \pm 0.000\,119 .$$

To get $\alpha^{-1}(M_Z^2)$, we also have to include the leptonic piece [74]

$$\Delta\alpha_{\text{lep}}(M_Z^2) \simeq 0.031\,419\,187\,418 , \quad (1.19)$$

and the top quark contribution. A very heavy top quark decouples as

$$\Delta\alpha_{\text{top}} \simeq -\frac{\alpha}{3\pi} \frac{4}{15} \frac{s}{m_t^2} \rightarrow 0$$

when $m_t \gg s$. At $s = M_Z^2$, the top quark contributes

$$\Delta\alpha_{\text{top}}(M_Z^2) = -0.76 \times 10^{-4} . \quad (1.20)$$

Collecting terms, this leads to the result presented in Eq. (1.14). One should note that the Adler function controlled Euclidean data vs. pQCD split approach is only moderately more pQCD-driven than the time-like approach adopted by Davier *et al.* [57] and others, as follows from the collection of results shown in Fig. B.1.12. The point is that the Adler function driven method only uses pQCD where reliable predictions are possible and direct cross checks against lattice QCD data may be carried out. Similarly, possible future direct measurements of $\alpha(-Q^2)$ in μ -e scattering [75] can provide Euclidean HVP data, in particular, also for the offset $\Delta\alpha_{\text{had}}(-M_0^2)$.

1.5 Prospects for future improvements

The new muon $g - 2$ experiments at Fermilab and at JPARC in Japan (expected to go into operation later) trigger the continuation of $e^+e^- \rightarrow$ hadrons cross-section measurements in the low-energy region by CMD-3 and SND at BINP Novosibirsk, by BES III at IHEP Beijing and soon by Belle II at KEK Tsukuba. This automatically helps to improve $\Delta\alpha(-M_0^2)$ and hence $\alpha(M_Z^2)$ via the Adler function controlled split-trick approach. Equally important are the results from lattice QCD, which come closer to being competitive with the data-driven dispersive method.

The improvement by a factor of five to ten in this case largely relies on improving the QCD prediction of the two-point vector correlator above the 2 GeV scale, which is a well-defined and comparably simple task. The mandatory pQCD improvements required are as follows.

- (a) Four-loop massive pQCD calculation of Adler function. In practice, this requires the calculation of a sufficient number of terms in the low- and high-momentum series expansions, such that an accurate Padé improvement is possible.
- (b) m_c, m_b improvements by sum rule or lattice QCD evaluation.
- (c) Improved α_s in low Q^2 region above the τ mass.

Note that the direct dispersion relations (DR) approach requires precise data up to much higher energies or a heavy reliance on the pQCD calculation of the time-like $R(s)$! The virtues of the Adler function approach are obvious:

- (a) no problems with physical threshold and resonances;
- (b) pQCD is used only where we can check it to work accurately (Euclidean $Q \gtrsim 2.0$ GeV);
- (c) no manipulation of data, no assumptions about global or local duality;

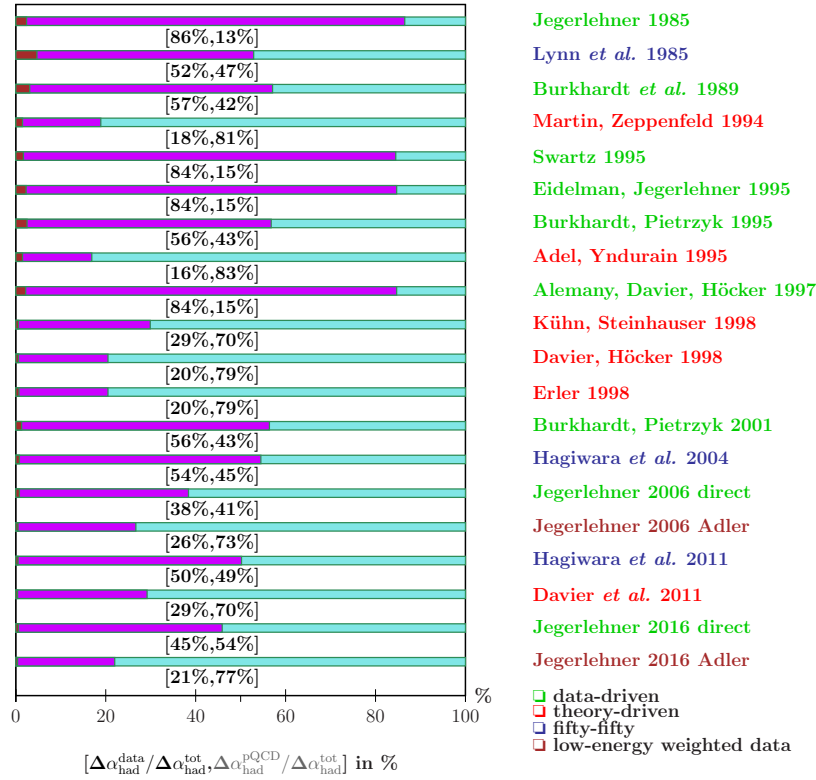


Fig. B.1.12: How much pQCD? Here a history of results by different authors. It shows that the Adler function controlled approach to $\Delta\alpha_{\text{had}}^{(5)}(M_Z^2)$ is barely more pQCD-driven than many of the standard evaluations. The pQCD piece is 70% in Davier *et al.* [57] and 77% in our Adler-driven case, with an important difference: in the Adler-controlled case, the major part of 71% is based on pQCD in the space-like region and only 6% contributing to the non-perturbative offset value is evaluated in the time-like region, while in the standard theory-driven, as well as in the more data-driven approaches, pQCD is applied in the time-like region, where it is much harder to be tested against data.

- (d) the non-perturbative ‘remainder’ $\Delta\alpha(-M_0^2)$ is mainly sensitive to low-energy data;
- (e) $\Delta\alpha(-M_0^2)$ would be directly accessible in a MUonE experiment (project) [75] or in lattice QCD.

In the direct approach, e.g., Davier *et al.* [57] use pQCD above 1.8 GeV, which means that no error reduction follows from remeasuring cross-sections above 1.8 GeV. Also, there is no proof that pQCD is valid at 0.04% precision as adopted. This is a general problem when utilising pQCD at time-like momenta exhibiting non-perturbative features.

What we can achieve is illustrated in Fig. B.1.13 and Table B.1.3. Our analysis shows that the Adler function inspired method is competitive with Patrick Janot’s [76] direct near- Z pole determination via a measurement of the forward–backward asymmetry $A_{\text{FB}}^{\mu\mu}$ in $e^+e^- \rightarrow \mu^+\mu^-$. The modulus square of the sum of the two tree-level diagrams has three terms: the Z exchange alone, $\mathcal{Z} \propto (M_Z^2 G_\mu)^2$, the γ – Z interference, $\mathcal{I} \propto \alpha(s) M_Z^2 G_\mu$, and the γ -exchange only, $\mathcal{G} \propto \alpha^2(s)$. The interference term determines the forward–backward (FB) asymmetry, which is linear in $\alpha(s)$; v denotes the vector $Z\mu\mu$ coupling that depends on $\sin^2 \Theta_{\ell\text{eff}}(s)$, while a denotes the axial $Z\mu\mu$ coupling that is sensitive to the ρ -parameter (strong M_t dependence). In extracting $\alpha(M_Z^2)$,

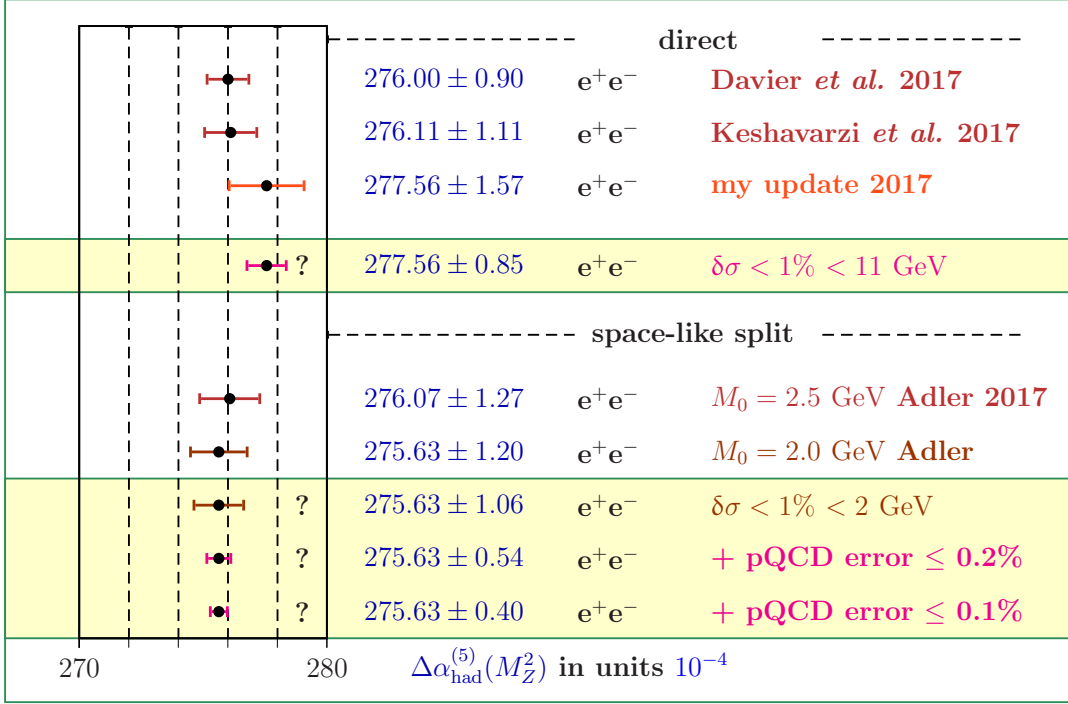


Fig. B.1.13: Comparison of possible improvements. My ‘direct’ analysis is data-driven, adopting pQCD in the window 5.2–9.5 GeV and above 11.5 GeV. The Adler-driven results under ‘space-like split’ show the current status for the two offset energies, $M_0 = 2.5$ GeV and 2 GeV. The improvement potential is displayed for three options: reducing the error of the data offset by a factor of two, improving pQCD to a 0.2% precision Adler function in addition and the same by improving pQCD to a 0.1% precision Adler function. The direct results are from Refs. [57,77,78].

one is using the v and a couplings as measured at the Z peak directly. At tree level, one then has

$$A_{\text{FB}}^{\mu\mu} = A_{\text{FB},0}^{\mu\mu} + \frac{3a^2}{4v^2} \frac{\mathcal{I}}{\mathcal{Z} + \mathcal{G}}; \quad A_{\text{FB},0}^{\mu\mu} = \frac{3}{4} \frac{4v^2a^2}{(v^2 + a^2)^2}, \quad (1.21)$$

where

$$\mathcal{G} = \frac{c_\gamma^2}{s}, \quad \mathcal{I} = \frac{2c_\gamma c_Z v^2 (s - M_Z^2)}{(s - M_Z^2)^2 + M_Z^2 \Gamma_Z^2}, \quad \mathcal{Z} = \frac{c_Z^2 (v^2 + a^2) s}{(s - M_Z^2)^2 + M_Z^2 \Gamma_Z^2}$$

$$c_\gamma = \sqrt{\frac{4\pi}{3}} \alpha(s), \quad c_Z = \sqrt{\frac{4\pi}{3}} \frac{M_Z^2}{2\pi} \frac{G_\mu}{\sqrt{2}}, \quad v = (1 - 4 \sin^2 \Theta_\ell) a, \quad a = -\frac{1}{2}.$$

Note that $M_Z^2 G_\mu = M_W^2 G_\mu / \cos^2 \Theta_W = \pi(\alpha_2(s)) / \sqrt{2}(\cos^2 \Theta_g(s))$ and $\sin^2 \Theta_g(s) = \alpha(s) / \alpha_2(s)$. i.e., all parameters vary more or less with energy, depending on the renormalization scheme utilised. The challenges for this direct measurement are precise radiative corrections (see Refs. [79, 80] and references therein) and the required dedicated off-Z peak running. Short accounts of the methods proposed for improving $\alpha(M_Z^2)$ may be found in Sections 8 and 9 of Ref. [81].

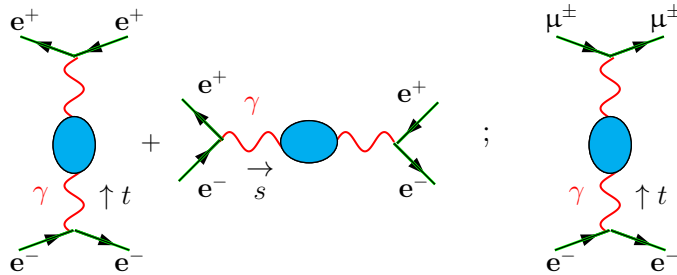
The Adler function based method is much cheaper, I think, and does not depend on understanding the Z peak region with unprecedented precision. Another very crucial point may

Table B.1.3: Precision in $\alpha(M_Z^2)$

Present	Direct	1.7×10^{-4}
	Adler	1.2×10^{-4}
Future	Adler QCD 0.2%	5.4×10^{-5}
	Adler QCD 0.1%	3.9×10^{-5}
Future	Via $A_{\text{FB}}^{\mu\mu}$ off-Z	3×10^{-5} [76]

Table B.1.4: Possible achievements for the FCC-ee project

\sqrt{s}	\sqrt{t} (GeV)	1996 [83, 84]	Present	FCC-ee expected [82]
M_Z	3.5	0.040%	0.013%	0.6×10^{-4}
350 GeV	13		1.2×10^{-4}	2.4×10^{-4}


 Fig. B.1.14: t-channel dominated QED processes. Left: VP dressed tree-level Bhabha scattering at small scattering angles. Right: the leading VP effect in μe scattering.

be that the dispersive method and the Adler function modified version provide the effective $\alpha(s)$ for arbitrary c.m. energies, not at $s = M_Z^2$ only; although, given a very precise $\alpha(M_Z^2)$, one can reliably calculate $\alpha(s) - \alpha(M_Z^2)$ via pQCD for values of s in the perturbative regime, i.e., especially going to higher energies. In any case, the requirements specified here that must be satisfied in order to reach a factor of five improvement appears to be achievable.

1.6 The need for a space-like effective $\alpha(t)$

As a normalization in measurements of cross-sections in e^+e^- collider experiments, small-angle Bhabha scattering is the standard choice. This reference process is dominated by the t-channel diagram of the Bhabha scattering process shown in the left of Fig. B.1.14. In small-angle Bhabha scattering, we have $\delta_{\text{HVP}}\sigma/\sigma = 2\delta\alpha(\bar{t})/\alpha(\bar{t})$, and for the FCC-ee luminometer $\sqrt{t} \simeq 3.5$ GeV near the Z peak and $\simeq 13$ GeV at 350 GeV [82]. The progress achieved after LEP times is displayed in Fig. B.1.15. What can be achieved for the FCC-ee project is listed in Table B.1.4. The estimates are based on expected improvements possible for $\Delta\alpha_{\text{had}}(-Q^2)$ in the appropriate energy ranges, centred at \sqrt{t} .

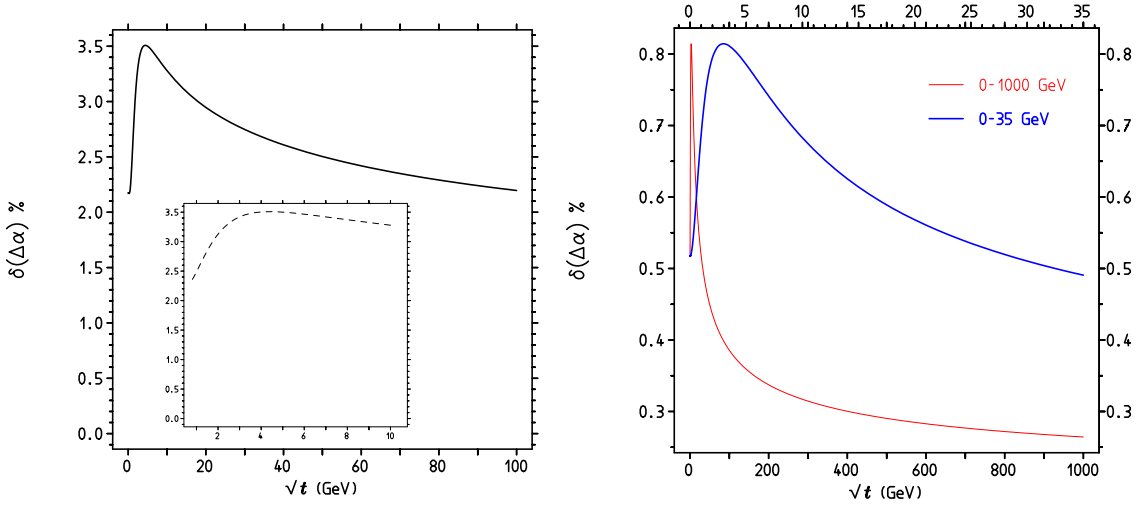


Fig. B.1.15: Hadronic uncertainty $\delta\Delta\alpha_{\text{had}}(\sqrt{t})$. The progress since LEP times, from 1996 (left) to now (right) is remarkable. A great deal of much more precise low-energy data, $\pi\pi$, etc., are now available.

1.6.1 A new project: measuring the low-energy $\alpha(t)$ directly

The possible direct measurement of $\Delta\alpha_{\text{had}}(-Q^2)$ follows a very different strategy of evaluating the HVP contribution to the muon $g - 2$. There is no VP subtraction issue, there is no exclusive channel separation and recombination, no issue of combining data from very different experiments and controlling correlations. Even a 1% level measurement can provide invaluable independent information. The recent proposal [75] to measure $\alpha(-Q^2)$ via μ^-e^- -scattering (see right part of Fig. B.1.15) in the MUonE projects at CERN is very important for future precision physics. It is based on a cross-section measurement

$$\frac{d\sigma_{\mu^-e^- \rightarrow \mu^-e^-}^{\text{unpol.}}}{dt} = 4\pi\alpha(t)^2 \frac{1}{\lambda(s, m_e^2, m_\mu^2)} \left\{ \frac{(s - m_\mu^2 - m_e^2)^2}{t^2} + \frac{s}{t} + \frac{1}{2} \right\}. \quad (1.22)$$

The primary goal of the project concerns the determination of a_μ^{had} in an alternative way

$$a_\mu^{\text{had}} = \frac{\alpha}{\pi} \int_0^1 dx (1-x) \Delta\alpha_{\text{had}}(-Q^2(x)), \quad (1.23)$$

where $Q^2(x) \equiv x^2 m_\mu^2 / (1-x)$ is the space-like square momentum transfer and

$$\Delta\alpha_{\text{had}}(-Q^2) = \frac{\alpha}{\alpha(-Q^2)} + \Delta\alpha_{\text{lep}}(-Q^2) - 1 \quad (1.24)$$

directly compares with lattice QCD data and the offset $\alpha(-M_0^2)$ discussed before. We propose to determine, very accurately, $\Delta\alpha_{\text{had}}(-Q^2)$ at $Q \approx 2.5$ GeV by this method (one single number!) as the non-perturbative part of $\Delta\alpha_{\text{had}}(M_Z^2)$, as needed in the ‘Adler function approach’. It would also be of direct use for a precise small-angle Bhabha luminometer! Because of the high precision required, accurate radiative corrections are mandatory and corresponding calculations are in progress [85–88].

1.7 Conclusions

Reducing the muon $g - 2$ prediction uncertainty remains the key issue of high-precision physics and strongly motivates more precise measurements of low-energy $e^+e^- \rightarrow$ hadrons cross-sections. Progress is expected from Novosibirsk (VEPP 2000/CMD3,SND), Beijing (BEPCL-I/BESIII), and Tsukuba (SuperKEKB/BelleII). This helps to improve $\alpha(t)$ in the region relevant for small-angle Bhabha scattering and in calculating $\alpha(s)$ at FCC-ee/ILC energies using the Euclidean split-trick method. The latter method requires pQCD prediction of the Adler function to improve by a factor of two. This also means that we need improved parameters, in particular, m_c and m_b .

One question remains to be asked. Are presently estimated and essentially agreed-on evaluations of $\Delta\alpha_{\text{had}}^{(5)}(M_Z^2)$ in terms of R data reliable? One has to keep in mind that the handling of systematic errors is rather an art than a science. Therefore, alternative methods are very important and, fortunately, are under consideration.

Patrick Janot's approach is certainly an important alternative method, directly accessing $\alpha(M_Z^2)$ with very different systematics. This is a challenging project.

Another interesting option is an improved radiative return measurement of $\sigma(e^+e^- \rightarrow$ hadrons) at the GigaZ, allowing for directly improved dispersion integral input, which would include all resonances and thresholds in one experiment!

In any case, on paper, $e^-\mu^+ \rightarrow e^-\mu^+$ appears to be the ideal process to perform an unambiguous measurement of $\alpha(-Q^2)$, which determines the leading-order (LO) HVP to a_μ , as well as the non-perturbative part of $\alpha(s)$!

Lattice QCD results are very close to becoming competitive here as well. Thus, in the end, we will have alternatives, allowing for important improvements and crosschecks.

The improvement obtained by reducing the experimental error to 1% in the range from ϕ to 3 GeV would allow one to choose a higher cut point, e.g., for $\sqrt{M_0} = 3.0$ GeV. One can then balance the importance of data against pQCD differently. This would provide further important consolidation of results. For a 3 GeV cut, one gets $\Delta\alpha_{\text{had}}(-M_0^2) = 82.21 \pm 0.88[0.38]$ in 10^{-4} . The QCD contribution is then smaller, as well as safer, because the mass effects that are responsible for the larger uncertainty of the pQCD prediction are also substantially reduced. Taking the view that a massive four-loop QCD calculation is a challenge, the possibility of optimising the choice of split scale M_0 would be very useful. Therefore, the ILC/FCC-ee community should actively support these activities as an integral part of the e^+e^- -collider precision physics programme!

1.8 Addendum: the coupling α_2 , M_W , and $\sin^2 \Theta_f$

Besides α , the $SU(2)$ gauge coupling $\alpha_2 = g^2/(4\pi)$ is also running and thereby affected by non-perturbative hadronic effects [78,89,90]. Related with the $U_Y(1) \otimes SU_L(2)$ gauge couplings is the running of the weak mixing parameter $\sin^2 \Theta_f$, which is actually defined by the ratio α/α_2 . In Refs. [78,89,90], the hadronic effects have been evaluated by means of DRs in terms of e^+e^- data with appropriate flavour separation and reweighting. Commonly, a much simpler approach is adopted in studies of the running of $\sin^2 \Theta_f$, namely using pQCD with effective quark masses [91–94], which have been determined elsewhere.

Given $g \equiv g_2$ and the Higgs vacuum expectation value (VEV) v , then

$$M_{\text{W}}^2 = \frac{g^2 v^2}{4} = \frac{\pi \alpha_2}{\sqrt{2} G_{\mu}}.$$

The running $\sin^2 \Theta_f(s)$ relates electromagnetic to weak neutral channel mixing at the LEP scale to low-energy $\nu_e e$ scattering as

$$\sin^2 \Theta_{\text{lep}}(M_Z^2) = \left\{ \frac{1 - \Delta\alpha_2}{1 - \Delta\alpha} + \Delta_{\nu_e, \text{vertex+box}} + \Delta\kappa_{e, \text{vertex}} \right\} \sin^2 \Theta_{\nu_e e}(0). \quad (1.25)$$

The first correction from the running coupling ratio is largely compensated for by the ν_{μ} charge radius, which dominates the second term. The ratio $\sin^2 \Theta_{\nu_{\mu} e} / \sin^2 \Theta_{\text{lep}}$ is close to 1.002, independent of the top and Higgs masses. Note that errors in the ratio $(1 - \Delta\alpha_2)/(1 - \Delta\alpha)$ can be taken to be 100% correlated and thus largely cancel. A similar relation between $\sin^2 \Theta_{\text{lep}}(M_Z^2)$ and the weak mixing angle appearing in polarised Møller scattering asymmetries has been worked out [91, 92]. It includes specific bosonic contribution $\Delta\kappa_b(Q^2)$, such that

$$\kappa(s = -Q^2) = \frac{1 - \Delta\alpha_2(s)}{1 - \Delta\alpha(s)} + \Delta\kappa_b(Q^2) - \Delta\kappa_b(0), \quad (1.26)$$

where, in our low-energy scheme, we require $\kappa(Q^2) = 1$ at $Q^2 = 0$. Explicitly [91, 92], at one-loop order

$$\Delta\kappa_b(Q^2) = -\frac{\alpha}{2\pi s_{\text{W}}} \left\{ -\frac{42 c_{\text{W}} + 1}{12} \ln c_{\text{W}} + \frac{1}{18} - \left(\frac{r}{2} \ln \xi - 1\right) \left[(7 - 4z) c_{\text{W}} + \frac{1}{6} (1 + 4z) \right] - z \left[\frac{3}{4} - z + \left(z - \frac{2}{3}\right) r \ln \xi + z(2 - z) \ln^2 \xi \right] \right\}, \quad (1.27)$$

$$\Delta\kappa_b(0) = -\frac{\alpha}{2\pi s_{\text{W}}} \left\{ -\frac{42 c_{\text{W}} + 1}{12} \ln c_{\text{W}} + \frac{1}{18} + \frac{6 c_{\text{W}} + 7}{18} \right\}, \quad (1.28)$$

with $z = M_{\text{W}}^2/Q^2$, $r = \sqrt{1 + 4z}$, $\xi = (r + 1)/(r - 1)$, $s_{\text{W}} = \sin^2 \Theta_{\text{W}}$, and $c_{\text{W}} = \cos^2 \Theta_{\text{W}}$. Results obtained in Refs. [91, 92] based on one-loop perturbation theory using light quark masses $m_{\text{u}} = m_{\text{d}} = m_{\text{s}} = 100$ MeV are compared with results obtained in our non-perturbative approach in Fig. B.1.16.

How can we evaluate the leading non-perturbative hadronic corrections to α_2 ? As in the case of α , they are related to quark-loop contributions to gauge-boson self-energies (SE) $\gamma\gamma$, γZ , ZZ , and WW , in particular, those involving the photon, which exhibit large leading logarithms. To disentangle the leading corrections, decompose the self-energy functions as follows ($s_{\Theta}^2 = e^2/g^2$; $c_{\Theta}^2 = 1 - s_{\Theta}^2$):

$$\begin{aligned} \Pi^{\gamma} &= e^2 \hat{\Pi}^{\gamma}, \\ \Pi^{Z\gamma} &= \frac{eg}{c_{\Theta}} \hat{\Pi}_V^{3\gamma} - \frac{e^2 s_{\Theta}}{c_{\Theta}} \hat{\Pi}_V^{\gamma}, \\ \Pi^{ZZ} &= \frac{g^2}{c_{\Theta}^2} \hat{\Pi}_{V-A}^{33} - 2 \frac{e^2}{c_{\Theta}^2} \hat{\Pi}_V^{3\gamma} + \frac{e^2 s_{\Theta}^2}{c_{\Theta}^2} \hat{\Pi}_V^{\gamma}, \\ \Pi^{\text{WW}} &= g^2 \hat{\Pi}_{V-A}^{+-}. \end{aligned} \quad (1.29)$$

With $\hat{\Pi}(s) = \hat{\Pi}(0) + s \Pi'(s)$, we find the leading hadronic corrections

$$\Delta\alpha_{\text{had}}^{(5)}(s) = -e^2 \left[\text{Re} \Pi'^{\gamma}(s) - \Pi'^{\gamma}(0) \right], \quad (1.30)$$

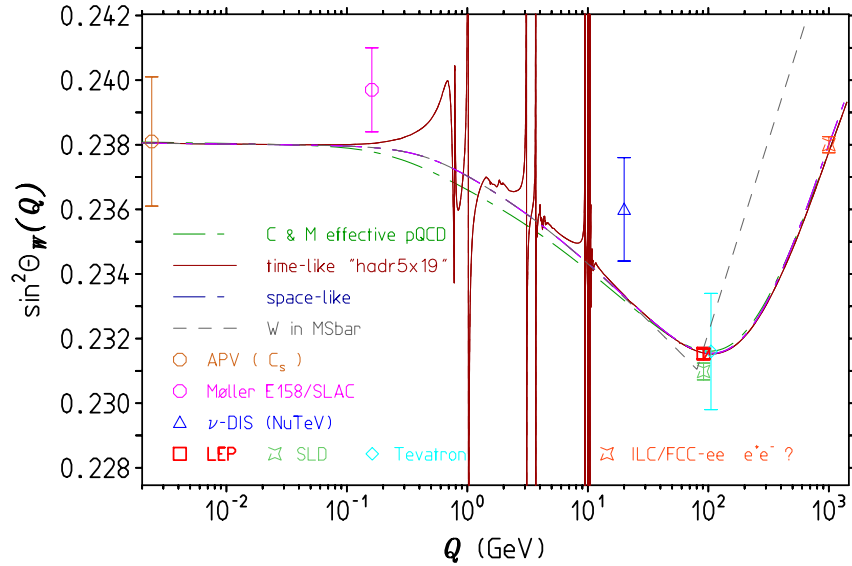


Fig. B.1.16: $\sin^2 \Theta_W(Q)$ as a function of Q in the time-like and space-like region. Hadronic uncertainties are included but barely visible in this plot. Uncertainties from the input parameter $\sin^2 \Theta_W(0) = 0.238\,22(100)$ or $\sin^2 \Theta_W(M_Z^2) = 0.231\,53(16)$ are not shown. Note the substantial difference from applying pQCD with effective quark masses. Future FCC-ee/ILC measurements at 1 TeV would be sensitive to Z' , H^{--} , etc.

$$\Delta\alpha_{2\text{had}}^{(5)}(s) = -\frac{e^2}{s_\Theta^2} \left[\text{Re} \Pi'^{3\gamma}(s) - \Pi'^{3\gamma}(0) \right], \quad (1.31)$$

which exhibit the leading hadronic non-perturbative parts, i.e., the ones involving the photon field via mixing. Besides $\Delta\alpha_{\text{had}}^{(5)}(s)$, $\Delta\alpha_{2\text{had}}^{(5)}(s)$ can also then be obtained in terms of e^+e^- data, together with isospin flavour separation of (u, d) and s components

$$\Pi_{\text{ud}}^{3\gamma} = \frac{1}{2} \Pi_{\text{ud}}^\gamma; \quad \Pi_{\text{s}}^{3\gamma} = \frac{3}{4} \Pi_{\text{s}}^\gamma \quad (1.32)$$

and for resonance contributions

$$\begin{aligned} \Pi^\gamma &= \Pi^{(\rho)} + \Pi^{(\omega)} + \Pi^{(\phi)} + \dots \\ \Pi^{3\gamma} &= \frac{1}{2} \Pi^{(\rho)} + \frac{3}{4} \Pi^{(\phi)} + \dots \end{aligned} \quad (1.33)$$

We are reminded that gauge-boson self-energies are potentially very sensitive to new physics (oblique corrections) and the discovery of what is missing in the SM may be obscured by non-perturbative hadronic effects. Therefore, it is important to reduce the related uncertainties. Interestingly, flavour separation assuming OZI violating terms to be small implies a perturbative reweighting, which, however, has been shown to disagree with lattice QCD results [95–98]! Indeed, the ‘wrong’ perturbative flavour weighting

$$\Pi_{\text{ud}}^{3\gamma} = \frac{9}{20} \Pi_{\text{ud}}^\gamma; \quad \Pi_{\text{s}}^{3\gamma} = \frac{3}{4} \Pi_{\text{s}}^\gamma$$

clearly mismatch lattice results, while the replacement $9/20 \Rightarrow 10/20$ is in good agreement. This also means that the OZI suppressed contributions should be at the 5% level and not negligibly

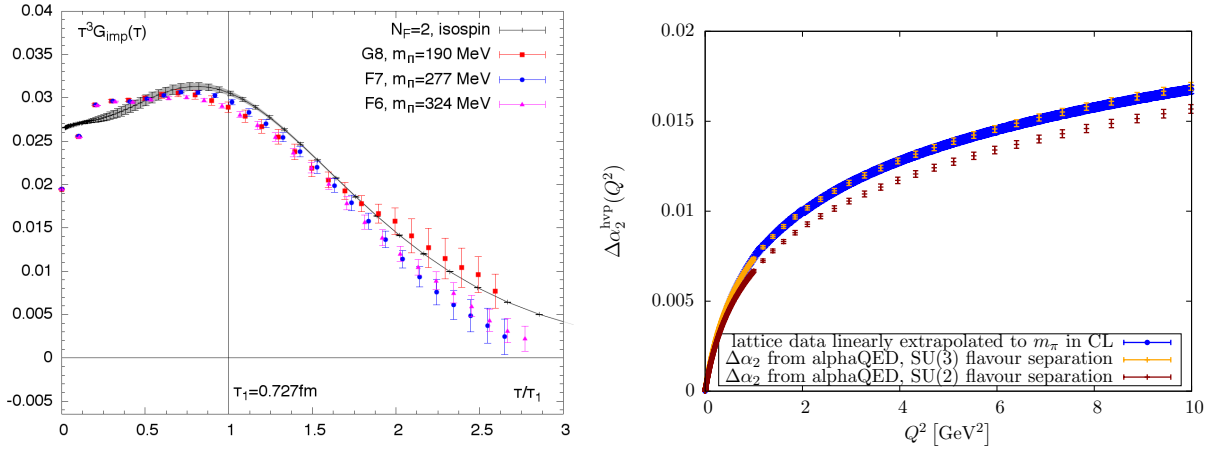


Fig. B.1.17: Testing flavour separation in lattice QCD. Left: a rough test by checking the Euclidean time correlators clearly favours the flavour separation of Eq. (1.33) [95–97], while the pQCD reweighting (not displayed) badly fails. Right: the renormalised photon self-energy at Euclidean Q^2 [98] is in good agreement with the flavour $SU(3)$ limit, while again it fails with the $SU(2)$ case, which coincides with perturbative reweighting.

small. Actually, if we assume flavour $SU(3)$ symmetry to be an acceptable approximation, we obtain

$$\Pi_{\text{uds}}^{3\gamma} = \frac{1}{2} \Pi_{\text{uds}}^{\gamma},$$

which does not require any flavour separation in the uds-sector, i.e., up to the charm threshold at about 3.1 GeV. Figure B.1.17 shows a lattice QCD test of two flavour separation schemes. One, labelled ‘ $SU(2)$ ’, denotes the perturbative reweighting advocated in Refs. [91–94] and the other, labelled ‘ $SU(3)$ ’, represents that proposed in Ref. [89]. Lattice data clearly disprove pQCD reweighting for the uds-sector! This also shows that pQCD-type predictions based on effective quark masses cannot be accurate. This criticism also applies in cases where the effective quark masses have been obtained by fitting $\Delta\alpha_{\text{had}}^{(5)}(s)$, even more so, when constituent quark masses are used.

The effective $SU(2)$ coupling $\Delta\alpha_2(E)$ in comparison with $\Delta\alpha_{\text{QED}}(E)$ is displayed in Fig. B.1.18, and the updated $\sin^2 \Theta_W(s)$ is shown in Fig. B.1.16 for time-like as well as for space-like momentum transfer. Note that $\sin^2 \Theta_W(0)/\sin^2 \Theta_W(M_Z^2) = 1.02876$; a 3% correction is established at 6.5σ . Except for the LEP and SLD points (which deviate by 1.8σ), all existing measurements are of rather limited accuracy, unfortunately. Upcoming experiments will substantially improve results at low space-like Q . We are reminded that $\sin^2 \Theta_{\ell\text{eff}}$, exhibiting a specific dependence on the gauge-boson self-energies, is an excellent monitor for new physics. At pre-LHC times, it was the predestined monitor for virtual Higgs particle effects and a corresponding limiter for the Higgs boson mass.

Acknowledgements

I would like to thank Janusz Gluza and the organising committee for the invitation to this workshop and for support. Thanks also to Maurice Benayoun, Simon Eidelman, and Graziano Venanzoni for collaboration and many useful discussions on the topics presented here.

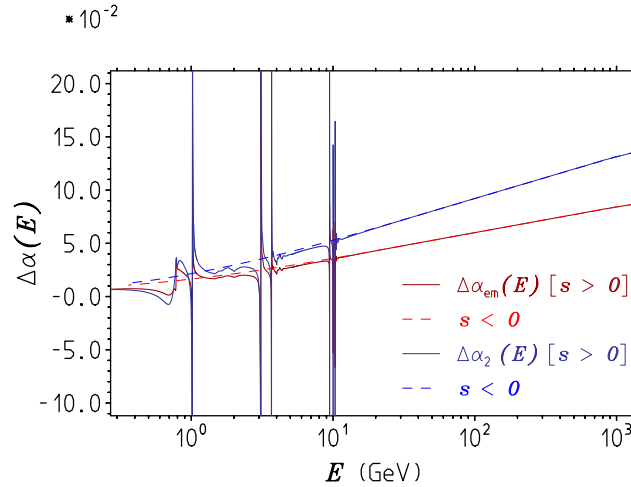


Fig. B.1.18: $\Delta\alpha_{\text{QED}}(E)$ and $\Delta\alpha_2(E)$ as functions of energy E in the time-like and space-like domain. The smooth space-like correction (dashed line) agrees rather well with the non-resonant ‘background’ above the ϕ resonance (a kind of duality). In resonance regions, as expected, ‘agreement’ is observed in the mean, with huge local deviations.

References

- [1] F. Jegerlehner, *Acta Phys. Pol.* **B45** (2014) 1167. [arXiv:1304.7813](#), [doi:10.5506/APhysPolB.45.1167](#)
- [2] T. Hambye and K. Riesselmann, *Phys. Rev.* **D55** (1997) 7255. [arXiv:hep-ph/9610272](#), [doi:10.1103/PhysRevD.55.7255](#)
- [3] F. Jegerlehner *et al.*, *Phys. Lett.* **B722** (2013) 123. [arXiv:1212.4319](#), [doi:10.1016/j.physletb.2013.04.012](#)
- [4] F. Jegerlehner, *Acta Phys. Pol.* **B45** (2014) 1215. [arXiv:1402.3738](#), [doi:10.5506/APhysPolB.45.1215](#)
- [5] F. Jegerlehner *et al.*, *J. Phys. Conf. Ser.* **608** (2015) 012074. [arXiv:1412.4215](#), [doi:10.1088/1742-6596/608/1/012074](#)
- [6] F. Bezrukov *et al.*, *JHEP* **10** (2012) 140, [[275\(2012\)](#)]. [arXiv:1205.2893](#), [doi:10.1007/JHEP10\(2012\)140](#)
- [7] G. Degrossi *et al.*, *JHEP* **08** (2012) 098. [arXiv:1205.6497](#), [doi:10.1007/JHEP08\(2012\)098](#)
- [8] J.S. Mackenzie, *Int. J. Ethics* **4** (1893) 126. [doi:10.1086/intejethi.4.1.2375721](#)
- [9] S. Eidelman and F. Jegerlehner, *Z. Phys.* **C67** (1995) 585. [arXiv:hep-ph/9502298](#), [doi:10.1007/BF01553984](#)
- [10] R.R. Akhmetshin *et al.*, *Phys. Lett.* **B578** (2004) 285. [arXiv:hep-ex/0308008](#), [doi:10.1016/j.physletb.2003.10.108](#)
- [11] V.M. Aul’chenko *et al.*, *JETP Lett.* **82** (2005) 743 [*Pisma Zh. Eksp. Teor. Fiz.* **82** (2005) 841.] [arXiv:hep-ex/0603021](#), [doi:10.1134/1.2175241](#)
- [12] V.M. Aul’chenko *et al.*, *JETP Lett.* **84** (2006) 413 [*Pisma Zh. Eksp. Teor. Fiz.* **84** (2006) 491]. [arXiv:hep-ex/0610016](#), [doi:10.1134/S0021364006200021](#)

- [13] R.R. Akhmetshin *et al.*, *Phys. Lett.* **B648** (2007) 28. [arXiv:hep-ex/0610021](#),
[doi:10.1016/j.physletb.2007.01.073](#)
- [14] M.N. Achasov *et al.*, *J. Exp. Theor. Phys.* **103** (2006) 380 [*Zh. Eksp. Teor. Fiz.* 130 (2006) 437]. [arXiv:hep-ex/0605013](#), [doi:10.1134/S106377610609007X](#)
- [15] A. Aloisio *et al.*, *Phys. Lett.* **B606** (2005) 12. [arXiv:hep-ex/0407048](#),
[doi:10.1016/j.physletb.2004.11.068](#)
- [16] F. Ambrosino *et al.*, *Phys. Lett.* **B670** (2009) 285. [arXiv:0809.3950](#),
[doi:10.1016/j.physletb.2008.10.060](#)
- [17] F. Ambrosino *et al.*, *Phys. Lett.* **B700** (2011) 102. [arXiv:1006.5313](#),
[doi:10.1016/j.physletb.2011.04.055](#)
- [18] D. Babusci *et al.*, *Phys. Lett.* **B720** (2013) 336. [arXiv:1212.4524](#),
[doi:10.1016/j.physletb.2013.02.029](#)
- [19] A. Anastasi *et al.*, *JHEP* **03** (2018) 173. [arXiv:1711.03085](#),
[doi:10.1007/JHEP03\(2018\)173](#)
- [20] G. Venanzoni, *EPJ Web Conf.* **166** (2018) 00021. [arXiv:1705.10365](#),
[doi:10.1051/epjconf/201816600021](#)
- [21] B. Aubert *et al.*, *Phys. Rev. Lett.* **103** (2009) 231801. [arXiv:0908.3589](#),
[doi:10.1103/PhysRevLett.103.231801](#)
- [22] J.P. Lees *et al.*, *Phys. Rev.* **D86** (2012) 032013. [arXiv:1205.2228](#),
[doi:10.1103/PhysRevD.86.032013](#)
- [23] M. Ablikim *et al.*, *Phys. Lett.* **B753** (2016) 629. [arXiv:1507.08188](#),
[doi:10.1016/j.physletb.2015.11.043](#)
- [24] T. Xiao *et al.*, *Phys. Rev.* **D97** (2018) 032012. [arXiv:1712.04530](#),
[doi:10.1103/PhysRevD.97.032012](#)
- [25] B. Aubert *et al.*, *Phys. Rev.* **D70** (2004) 072004. [arXiv:hep-ex/0408078](#),
[doi:10.1103/PhysRevD.70.072004](#)
- [26] B. Aubert *et al.*, *Phys. Rev.* **D71** (2005) 052001. [arXiv:hep-ex/0502025](#),
[doi:10.1103/PhysRevD.71.052001](#)
- [27] B. Aubert *et al.*, *Phys. Rev.* **D73** (2006) 012005. [arXiv:hep-ex/0512023](#),
[doi:10.1103/PhysRevD.73.012005](#)
- [28] B. Aubert *et al.*, *Phys. Rev.* **D73** (2006) 052003. [arXiv:hep-ex/0602006](#),
[doi:10.1103/PhysRevD.73.052003](#)
- [29] B. Aubert *et al.*, *Phys. Rev.* **D76** (2007) 092005 [Erratum: **D77** (2008) 119902].
[arXiv:0708.2461](#),
[doi:10.1103/PhysRevD.76.092005](#), [doi:10.1103/PhysRevD.77.119902](#)
- [30] B. Aubert *et al.*, *Phys. Rev.* **D77** (2008) 092002. [arXiv:0710.4451](#),
[doi:10.1103/PhysRevD.77.092002](#)
- [31] J.P. Lees *et al.*, *Phys. Rev.* **D85** (2012) 112009. [arXiv:1201.5677](#),
[doi:10.1103/PhysRevD.85.112009](#)
- [32] J.P. Lees *et al.*, *Phys. Rev.* **D86** (2012) 012008. [arXiv:1103.3001](#),
[doi:10.1103/PhysRevD.86.012008](#)

- [33] J.P. Lees *et al.*, *Phys. Rev.* **D87** (2013) 092005. [arXiv:1302.0055](#),
[doi:10.1103/PhysRevD.87.092005](#)
- [34] J.P. Lees *et al.*, *Phys. Rev.* **D88** (2013) 032013. [arXiv:1306.3600](#),
[doi:10.1103/PhysRevD.88.032013](#)
- [35] J.P. Lees *et al.*, *Phys. Rev.* **D89** (2014) 092002. [arXiv:1403.7593](#),
[doi:10.1103/PhysRevD.89.092002](#)
- [36] J.P. Lees *et al.*, *Phys. Rev.* **D98** (2018) 112015. [arXiv:1810.11962](#),
[doi:10.1103/PhysRevD.98.112015](#)
- [37] M. Davier, *Nucl. Part. Phys. Proc.* **260** (2015) 102.
[doi:10.1016/j.nuclphysbps.2015.02.021](#)
- [38] M. Davier *et al.*, in *The Standard Theory of Particle Physics*, Eds. L. Maiani and L. Rolandi
(World Scientific, Singapore, 2016), Chap. 7, pp. 129–144.
[doi:10.1142/9789814733519_0007](#)
- [39] R.R. Akhmetshin *et al.*, *Phys. Lett.* **B723** (2013) 82. [arXiv:1302.0053](#),
[doi:10.1016/j.physletb.2013.04.065](#)
- [40] R.R. Akhmetshin *et al.*, *Phys. Lett.* **B759** (2016) 634. [arXiv:1507.08013](#),
[doi:10.1016/j.physletb.2016.04.048](#)
- [41] E.A. Kozyrev *et al.*, *Phys. Lett.* **B760** (2016) 314. [arXiv:1604.02981](#),
[doi:10.1016/j.physletb.2016.07.003](#)
- [42] M.N. Achasov *et al.*, *Phys. Rev.* **D90** (2014) 112007. [arXiv:1410.3188](#),
[doi:10.1103/PhysRevD.90.112007](#)
- [43] V.M. Aulchenko *et al.*, *Phys. Rev.* **D91** (2015) 052013. [arXiv:1412.1971](#),
[doi:10.1103/PhysRevD.91.052013](#)
- [44] M.N. Achasov *et al.*, *Phys. Rev.* **D93** (2016) 092001. [arXiv:1601.08061](#),
[doi:10.1103/PhysRevD.93.092001](#)
- [45] M.N. Achasov *et al.*, *Phys. Rev.* **D94** (2016) 032010. [arXiv:1606.06481](#),
[doi:10.1103/PhysRevD.94.032010](#)
- [46] M.N. Achasov *et al.*, *Phys. Rev.* **D94** (2016) 092002. [arXiv:1607.00371](#),
[doi:10.1103/PhysRevD.94.092002](#)
- [47] M.N. Achasov *et al.*, *Phys. Rev.* **D94** (2016) 112006. [arXiv:1608.08757](#),
[doi:10.1103/PhysRevD.94.112006](#)
- [48] M.N. Achasov *et al.*, *Phys. Rev.* **D94** (2016) 112001. [arXiv:1610.00235](#),
[doi:10.1103/PhysRevD.94.112001](#)
- [49] J.Z. Bai *et al.*, *Phys. Rev. Lett.* **84** (2000) 594. [arXiv:hep-ex/9908046](#),
[doi:10.1103/PhysRevLett.84.594](#)
- [50] J.Z. Bai *et al.*, *Phys. Rev. Lett.* **88** (2002) 101802. [arXiv:hep-ex/0102003](#),
[doi:10.1103/PhysRevLett.88.101802](#)
- [51] M. Ablikim *et al.*, *Phys. Lett.* **B677** (2009) 239. [arXiv:0903.0900](#),
[doi:10.1016/j.physletb.2009.05.055](#)
- [52] V.V. Anashin *et al.*, *Phys. Lett.* **B753** (2016) 533. [arXiv:1510.02667](#),
[doi:10.1016/j.physletb.2015.12.059](#)

- [53] V.V. Anashin *et al.*, *Phys. Lett.* **B770** (2017) 174. [arXiv:1610.02827](#),
[doi:10.1016/j.physletb.2017.04.073](#)
- [54] R.V. Harlander and M. Steinhauser, *Comput. Phys. Commun.* **153** (2003) 244. [arXiv:hep-ph/0212294](#),
[doi:10.1016/S0010-4655\(03\)00204-2](#)
- [55] F. Jegerlehner, *EPJ Web Conf.* **118** (2016) 01016. [arXiv:1511.04473](#),
[doi:10.1051/epjconf/201611801016](#)
- [56] A. Anastasi *et al.*, *Phys. Lett.* **B767** (2017) 485. [arXiv:1609.06631](#),
[doi:10.1016/j.physletb.2016.12.016](#)
- [57] M. Davier *et al.*, *Eur. Phys. J.* **C77** (2017) 827. [arXiv:1706.09436](#),
[doi:10.1140/epjc/s10052-017-5161-6](#)
- [58] A. Maier and P. Marquard, *Phys. Rev.* **D97** (2018) 056016. [arXiv:1710.03724](#),
[doi:10.1103/PhysRevD.97.056016](#)
- [59] S.L. Adler, *Phys. Rev.* **D10** (1974) 3714. [doi:10.1103/PhysRevD.10.3714](#)
- [60] S. Eidelman *et al.*, *Phys. Lett.* **B454** (1999) 369. [arXiv:hep-ph/9812521](#),
[doi:10.1016/S0370-2693\(99\)00389-5](#)
- [61] F. Jegerlehner, Hadronic effects in $(g - 2)_\mu$ and $\alpha_{\text{QED}}(M_Z^2)$: status and perspectives, Radiative Corrections: Application of Quantum Field Theory to Phenomenology. Proc. 4th Int. Symp., RADCOR'98, Barcelona, Spain, 1998, pp. 75–89, [arXiv:hep-ph/9901386](#)
- [62] F. Jegerlehner, Hadronic vacuum polarisation effects in $\alpha_{\text{em}}(M_Z^2)$, Electroweak Precision Data and the Higgs Mass. Proc. Workshop, Zeuthen, Germany, 2003, pp. 97–112, [arXiv:hep-ph/0308117](#)
- [63] F. Jegerlehner, *Nucl. Phys. Proc. Suppl.* **181–182** (2008) 135. [arXiv:0807.4206](#),
[doi:10.1016/j.nuclphysbps.2008.09.010](#)
- [64] M. Benayoun *et al.*, *Eur. Phys. J.* **C75** (2015) 613. [arXiv:1507.02943](#),
[doi:10.1140/epjc/s10052-015-3830-x](#)
- [65] M. Benayoun *et al.*, *Eur. Phys. J.* **C80** (2020), 81 [Erratum: **C80** (2020), 224].
[arXiv:1903.11034](#),
[doi:10.1140/epjc/s10052-020-7611-9](#), [doi:10.1140/epjc/s10052-020-7724-1](#)
- [66] F. Jegerlehner and O.V. Tarasov, *Nucl. Phys.* **B549** (1999) 481. [arXiv:hep-ph/9809485](#),
[doi:10.1016/S0550-3213\(99\)00141-8](#)
- [67] K.G. Chetyrkin *et al.*, *Nucl. Phys.* **B482** (1996) 213. [arXiv:hep-ph/9606230](#),
[doi:10.1016/S0550-3213\(96\)00534-2](#)
- [68] K.G. Chetyrkin *et al.*, *Nucl. Phys.* **B503** (1997) 339. [arXiv:hep-ph/9704222](#),
[doi:10.1016/S0550-3213\(97\)00383-0](#)
- [69] K.G. Chetyrkin *et al.*, *Nucl. Phys.* **B505** (1997) 40. [arXiv:hep-ph/9705254](#),
[doi:10.1016/S0550-3213\(97\)00481-1](#)
- [70] M.A. Shifman *et al.*, *Nucl. Phys.* **B147** (1979) 385. [doi:10.1016/0550-3213\(79\)90022-1](#)
- [71] M.A. Shifman *et al.*, *Nucl. Phys.* **B147** (1979) 448. [doi:10.1016/0550-3213\(79\)90023-3](#)
- [72] D.V. Shirkov and I.L. Solovtsov, *Phys. Rev. Lett.* **79** (1997) 1209. [arXiv:hep-ph/9704333](#),
[doi:10.1103/PhysRevLett.79.1209](#)

- [73] M. Bruno *et al.*, *Phys. Rev. Lett.* **119** (2017) 102001. [arXiv:1706.03821](#), [doi:10.1103/PhysRevLett.119.102001](#)
- [74] M. Steinhauser, *Phys. Lett.* **B429** (1998) 158. [arXiv:hep-ph/9803313](#), [doi:10.1016/S0370-2693\(98\)00503-6](#)
- [75] G. Abbiendi *et al.*, *Eur. Phys. J.* **C77** (2017) 139. [arXiv:1609.08987](#), [doi:10.1140/epjc/s10052-017-4633-z](#)
- [76] P. Janot, *JHEP* **02** (2016) 053 [Erratum: **11** (2017) 164]. [arXiv:1512.05544](#), [doi:10.1007/JHEP02\(2016\)053](#), [doi:10.1007/JHEP11\(2017\)164](#)
- [77] A. Keshavarzi *et al.*, *Phys. Rev.* **D97** (2018) 114025. [arXiv:1802.02995](#), [doi:10.1103/PhysRevD.97.114025](#)
- [78] F. Jegerlehner, Variations on photon vacuum polarisation, , *EPJ Web Conf.* **218** (2019), 01003 [arXiv:1711.06089](#) [doi:10.1051/epjconf/201921801003](#)
- [79] A. Blondel *et al.*, Standard Model theory for the FCC-ee Tera-Z stage, CERN (CERN Yellow Rep. Monogr. 3, Geneva, Switzerland), [arXiv:1809.01830](#), [doi:10.23731/CYRM-2019-003](#)
- [80] I. Dubovyk *et al.*, *Phys. Lett.* **B783** (2018) 86. [arXiv:1804.10236](#), [doi:10.1016/j.physletb.2018.06.037](#)
- [81] P. Azzurri *et al.*, Physics behind precision, [arXiv:1703.01626](#)
- [82] S. Jadach *et al.*, *Phys. Lett.* **B790** (2019) 314. [arXiv:1812.01004](#), [doi:10.1016/j.physletb.2019.01.012](#)
- [83] S. Jadach *et al.*, Event generators for Bhabha scattering, CERN Workshop on LEP2 Physics, (CERN, Geneva, Switzerland, 1995), pp. 229–298, [arXiv:hep-ph/9602393](#)
- [84] A. Arbuzov *et al.*, *Phys. Lett.* **B383** (1996) 238. [arXiv:hep-ph/9605239](#), [doi:10.1016/0370-2693\(96\)00733-2](#)
- [85] P. Mastrolia *et al.*, *JHEP* **11** (2017) 198. [arXiv:1709.07435](#), [doi:10.1007/JHEP11\(2017\)198](#)
- [86] S. Di Vita *et al.*, *JHEP* **09** (2018) 016. [arXiv:1806.08241](#), [doi:10.1007/JHEP09\(2018\)016](#)
- [87] M. Fael, *JHEP* **02** (2019) 027. [arXiv:1808.08233](#), [doi:10.1007/JHEP02\(2019\)027](#)
- [88] M. Alacevich *et al.*, *JHEP* **02** (2019) 155. [arXiv:1811.06743](#), [doi:10.1007/JHEP02\(2019\)155](#)
- [89] F. Jegerlehner, *Z. Phys.* **C32** (1986) 195. [doi:10.1007/BF01552495](#)
- [90] F. Jegerlehner, *Nuovo Cim.* **C034S1** (2011) 31. [arXiv:1107.4683](#), [doi:10.1393/ncc/i2011-11011-0](#)
- [91] A. Czarnecki and W.J. Marciano, *Phys. Rev.* **D53** (1996) 1066. [arXiv:hep-ph/9507420](#), [doi:10.1103/PhysRevD.53.1066](#)
- [92] A. Czarnecki and W.J. Marciano, *Int. J. Mod. Phys.* **A15** (2000) 2365. [arXiv:hep-ph/0003049](#), [doi:10.1142/S0217751X00002433](#)
- [93] J. Erler and M.J. Ramsey-Musolf, *Phys. Rev.* **D72** (2005) 073003. [arXiv:hep-ph/0409169](#), [doi:10.1103/PhysRevD.72.073003](#)

- [94] J. Erler and R. Ferro-Hernández, *JHEP* **03** (2018) 196. [arXiv:1712.09146](#), [doi:10.1007/JHEP03\(2018\)196](#)
- [95] D. Bernecker and H.B. Meyer, *Eur. Phys. J.* **A47** (2011) 148. [arXiv:1107.4388](#), [doi:10.1140/epja/i2011-11148-6](#)
- [96] A. Francis *et al.*, Vector correlator and scale determination in lattice QCD, PoS LATTICE 2013, Mainz 2013, paper 320. [arXiv:1312.0035](#), [doi:10.22323/1.187.0320](#)
- [97] M. Cè *et al.*, The leading hadronic contribution to the running of the Weinberg angle using covariant coordinate-space methods, 36th Ann. Int. Symp. Lattice Field Theory, 2018, East Lansing, MI, USA, 2018, paper 137. [arXiv:1811.08669](#)
- [98] F. Burger *et al.*, *JHEP* **11** (2015) 215. [arXiv:1505.03283](#), [doi:10.1007/JHEP11\(2015\)215](#)

2 Precision quantum chromodynamics

Contribution* by: D. d’Enterria [dde@cern.ch]

The unprecedentedly small experimental uncertainties expected in the electron–positron measurements at the FCC-ee, key to searches for physics beyond the SM up to $\Lambda \approx 50$ TeV, impose precise calculations for the corresponding theoretical observables. At the level of theoretical precision required to match that of the FCC-ee experimental measurements, the current relevant QCD uncertainties have to be reduced at at least four different levels.

1. Purely theoretical perturbative uncertainties from missing higher-order (HO) corrections in perturbative QCD (pQCD) calculations of e^+e^- scattering amplitudes and decay processes involving multiple real emissions or virtual exchanges of quarks and gluons. Such fixed-order (FO) corrections include pure QCD and mixed QCD–QED or QCD–weak terms. Reducing such uncertainties requires pQCD calculations beyond the current state of the art, often given by next-to-next-to-leading-order (NNLO) accuracy, pure, or mixed with higher-order electroweak terms.
2. Theoretical uncertainties due to incomplete logarithmic resummations of different energy scales potentially appearing in the theoretical calculations. Examples include resummations of (i) soft and collinear logs in final states dominated by jets—either in analytical calculations or (only partially) incorporated into matched parton shower Monte Carlo generators—and (ii) logarithmic terms in the velocity of the produced top quarks in $e^+e^- \rightarrow t\bar{t}$ cross-sections. Reducing such uncertainties requires calculations beyond the current state of the art, often given by the next-to-next-to-leading-log (NNLL) accuracy.
3. Parametric uncertainties propagated into the final theoretical result, owing to the dependence of the calculation on the input values of (i) the QCD coupling at the Z pole scale, $\alpha_s(m_Z)$, known today with a relatively poor $\pm 0.9\%$ precision, and (ii) the heavy quark (charm and bottom) masses m_c and m_b . Theoretical progress in lattice QCD determinations of α_s and $m_{c,b}$ is needed, complemented with much more precise experimental measurements. A per-mille extraction of $\alpha_s(m_Z)$ is thereby also a key axis of the FCC-ee physics programme [1].
4. Non-perturbative uncertainties from final-state hadronic effects linked to power-suppressed infrared phenomena, such as colour reconnection, hadronization, and multiparticle correlations (in spin, colour, space, momenta), that cannot be currently computed from first-principles QCD theory, and that often rely on phenomenological Monte Carlo models. The high-precision study of parton hadronization and other non-pQCD phenomena is also an intrinsic part of the FCC-ee physics programme [2].

*This contribution should be cited as:

D. d’Enterria, Precision quantum chromodynamics, DOI: [10.23731/CYRM-2020-003.38](https://doi.org/10.23731/CYRM-2020-003.38), in: Theory for the FCC-ee, Eds. A. Blondel, J. Gluza, S. Jadach, P. Janot and T. Riemann, CERN Yellow Reports: Monographs, CERN-2020-003, DOI: [10.23731/CYRM-2020-003](https://doi.org/10.23731/CYRM-2020-003), p. 38.
 © CERN, 2020. Published by CERN under the [Creative Commons Attribution 4.0 license](https://creativecommons.org/licenses/by/4.0/).

Examples of key observables where such four sources of QCD uncertainty will have an impact at the FCC-ee are numerous.

1. Uncertainties from missing HO terms are non-negligible in theoretical predictions for electroweak precision observables (EWPOs) at the Z pole, WW and $t\bar{t}$ cross-sections, (N)MSSM Higgs cross-sections and decays, etc.
2. Uncertainties from missing soft and collinear log resummations, in analytical calculations or in parton shower MC generators, impact all e^+e^- final states with jets—e.g., the accurate extraction of forward–backward quark asymmetries at the Z pole—as well as precision flavour physics studies via B meson decays. Similarly, the size of the NNLL corrections (in the $\ln v$ top quark velocity) appears to be as large as that from the FO N³LO terms in $e^+e^- \rightarrow t\bar{t}$ cross-section calculations.
3. The $\alpha_s(m_Z)$ parametric uncertainty has a significant effect on the determination of all top properties (m_{top} , λ_{top} , Γ_{top}), all hadronic Higgs decay widths ($H \rightarrow c\bar{c}, b\bar{b}, q\bar{q}, gg$) and associated Yukawa couplings, as well as on the extraction of other similarly crucial SM parameters ($m_c, m_b, \alpha_{\text{QED}}$).
4. Non-perturbative uncertainties, in particular colour reconnection and hadronization effects, impact hadronic final states in $e^+e^- \rightarrow WW$ and $e^+e^- \rightarrow t\bar{t}$, and forward–backward angular asymmetries of quarks at the Z pole.

In the following sections, the current status and FCC-ee prospects for these four axes of QCD studies are summarised.

2.1 Higher fixed-order pQCD corrections

Computations of pQCD corrections beyond the N^{2,3}LO accuracy are required for many theoretical FCC-ee observables, in order to match their expected experimental precision. New analytical, algorithmic, and numerical concepts and tools are needed to be able to compute HO QCD and mixed QCD+electroweak multiloop, -legs, and -scales corrections for processes involving the heaviest SM particles (W, Z, H, t) to be carefully scrutinised at the FCC-ee. Concrete developments are covered in more detail in various other sections of this report, and are summarised here.

1. EWPOs: Mixed QCD-electroweak calculations of the $Zf\bar{f}$ vertex will be needed at the FCC-ee at higher order than known today, including the $\mathcal{O}(\alpha\alpha_s^2)$, $\mathcal{O}(N_f\alpha^2\alpha_s)$, $\mathcal{O}(N_f^2\alpha^3)$ loop orders, where N_f^n denotes n or more closed internal fermion loops, plus the corresponding QCD four-loop terms [3]. The number of QCD diagrams for $Z \rightarrow b\bar{b}$ decays at two (three) loops is 98 (10 386) [3]. Section 9 provides, e.g., details on the extension of calculations beyond the two-loop QCD off-shell vertex functions, noting that for the triple-gluon vertex there are 2382 (63 992) three- (four-) loop graphs to evaluate. Including massive quarks in three- and four-point functions is a further requirement in order to reduce the FO theoretical uncertainties.
2. W bosons (Section 7): The resonant $e^+e^- \rightarrow WW$ cross-section contains soft corrections to the Coulomb function, analogous to ultrasoft ($m_{\text{top}}v^2$) QCD corrections in $t\bar{t}$ production [4]. For the W hadronic decay modes, QCD corrections to the partial decay

widths have to be included beyond NNLO to match the corresponding theoretical QED precision given by the counting $\mathcal{O}(\alpha_s^2) \sim \mathcal{O}(\alpha_{\text{QED}})$. QCD corrections to W self-energies and decay widths up to $\mathcal{O}(\alpha_{\text{QED}} \alpha_s^2)$ and $\mathcal{O}(\alpha_s^4)$ are required. Currently, $\mathcal{O}(\alpha_s^4)$ corrections for inclusive hadronic vector boson decays are known [5], while mixed QCD-EW corrections are known up to $\mathcal{O}(\alpha_{\text{QED}} \alpha_s)$ [6].

3. Higgs bosons (Section 12): The pure QCD corrections to Higgs boson decays into quarks, gluons, and photons are known up to N⁴LO (no mass effects), N³LO (heavy top limit), and NLO, respectively. Those translate into approximately 0.2%, 1%, and <3% scale uncertainties from missing HO corrections. In the case of the (N)MSSM Higgs sector (Section 3), HO pQCD corrections to the Higgs bosons decays are mostly known at NLO accuracy; thereby, their uncertainty is larger than for the SM Higgs case.
4. Top quarks (Section 11): The total cross-section for inclusive $e^+e^- \rightarrow b\bar{b}W^+W^-X$ production can be computed in a non-relativistic effective field theory with local effective vertices and matching corrections known up to N³LO in pQCD [7]. Those translate into about 3% theoretical scale uncertainties of the threshold $t\bar{t}$ cross-sections that propagate into an uncertainty of ± 60 MeV in the position of the resonant peak. Although the uncertainty has been reduced by a factor of two going from NNLO to N³LO, perturbative progress is still needed, in particular in the threshold top mass definition translated into the $\overline{\text{MS}}$ scheme.
5. The extraction of α_{QED} from the R ratio requires the calculation of the four-loop massive pQCD calculation of the Adler function (together with better estimates of α_s in the low- Q^2 region above the τ mass, as well as of the m_c and m_b masses).

2.2 Higher-order logarithmic resummations

Improvements in the resummations of all-order logarithmic terms from different energy scales, appearing in the theoretical calculations for certain processes, are needed in various directions.

1. Soft and collinear parton radiation impacts many e^+e^- observables with jets in the final state. Such uncertainties enter through incomplete NNLL resummations in analytical calculations (e.g., based on soft-collinear effective theory, SCET), or through approximate models of the coherent branching implemented in the parton shower MC generators used to unfold and interpret the experimental data. Among those experimental observables, the measured forward–backward (FB) angular asymmetries of charm and bottom quarks in e^+e^- collisions around the Z pole, directly connected to the weak mixing angle, will need a careful study. The asymmetry value measured at LEP, $(A_{\text{FB}}^{0,b})_{\text{exp}} = 0.0992 \pm 0.0016$, remains today the electroweak precision observable with the largest disagreement (2.9σ) with respect to the SM prediction, $(A_{\text{FB}}^{0,b})_{\text{th}} = 0.1038$ [8,9]. Consequently, so also does the effective weak mixing angle derived from it, $\sin^2 \theta_{\text{eff}}^f = 0.232\,21 \pm 0.000\,29$, compared with the $\sin^2 \theta_{\text{eff}}^f = 0.231\,54 \pm 0.000\,03$ world-average [10]. The dominant systematic uncertainties on $(A_{\text{FB}}^{0,b})_{\text{exp}}$ arise from angular decorrelations induced in the thrust axis by soft and collinear parton radiation or parton-to-hadron b quark hadronization, and were estimated using MC simulations 20 years ago [11]. A recent reanalysis of the QCD corrections to $A_{\text{FB}}^{0,b}$ [12], with different modern parton shower models [13–15], indicates propagated uncertainties of about 1% (0.4%) for the lepton (jet) charge-based measurements, slightly

smaller but still consistent with the original measurements derived at LEP. The measurement of $A_{\text{FB}}^{0,b}$ at the FCC-ee will feature insignificant statistical uncertainties, and improvements in the modelling of parton radiation will be required for any high-precision extraction of the associated $\sin^2 \theta_{\text{eff}}^f$ value.

2. Another field of e^+e^- measurements where progress in logarithmic resummations is needed is in the studies of event shapes—such as the thrust T , C parameter, and jet broadening. All those observables are commonly used to extract the QCD coupling [1]. Theoretical studies of event shapes supplement FO perturbation theory with the resummation of enhanced logarithmic contributions, specifically accounting for terms ranging from $\alpha_s^n \ln^{n+1}$ down to $\alpha_s^n \ln^{n-2}$, i.e., N³LL [16]. However, the $\alpha_s(m_Z)$ values derived from the T and C measurements differ and their combination has thereby a final 2.9% systematic uncertainty [10]. This result points to limits in the resummation formalism that (i) hold only for $C, 1 - T \ll 1$, where every emission is so soft and collinear that one can effectively neglect the kinematic cross-talk (e.g., energy–momentum conservation) that arises when there are a number of emissions, and (ii) use a power correction valid only in the two-jet limit, $1 - T \ll 1$ [16].
3. High-precision studies of n -jet rates at the FCC-ee will also benefit from a reduction of resummation uncertainties. Jet rates in e^+e^- rely on an algorithm to reconstruct them that comes with a parameter ($y_{\text{cut}} = k_{\text{T}}^2/s$, in the k_{T} Durham [17] and Cambridge [18] cases) to define how energetic the emission should be in order to be considered a jet. For $\ln y_{\text{cut}} > -4$, the extracted α_s value from three-jet rates is fairly independent of y_{cut} , whereas the result depends substantially on the choice of y_{cut} below that [19]. This feature points to a breakdown of FO perturbation theory, owing to logarithmically enhanced $(\alpha_s \ln^2 y_{\text{cut}})^n$ terms. Jet rates at the one-in-a-million level in e^+e^- at the Z pole will be available at the FCC-ee, including: four-jet events up to $k_{\text{T}} \approx 30$ GeV (corresponding to $|\ln y_{\text{cut}}| \approx 2$), five-jet events at $k_{\text{T}} \approx 20$ GeV ($|\ln y_{\text{cut}}| \approx 3$), six-jet events at $k_{\text{T}} \approx 12$ GeV ($|\ln y_{\text{cut}}| \approx 4$), and seven-jet events at $k_{\text{T}} \approx 7.5$ GeV ($|\ln y_{\text{cut}}| \approx 5$). Such results will be compared with theoretical calculations with an accuracy beyond the NNLO + NNLL provided today by the EERAD3 [20], MERCUTIO 2 [21], and CoLoRFulNNLO [22] (NNLO), and ARES [23] (NNLL) codes, thereby leading to α_s extractions with uncertainties well below the current few-percent level. In general, with the envisioned FCC-ee luminosities, jet measurements will extend along the six axes of higher accuracy, finer binning, higher jet resolution scales, larger numbers of resolved final-state objects, more differential distributions, and possibility placing stringent additional cuts to isolate specific interesting regions of the n -jet phase spaces not strongly constrained by LEP measurements [24].
4. In top physics studies, the size of the NNLL corrections (in top quark velocity, $\ln v$) in $e^+e^- \rightarrow t\bar{t}$ cross-section calculations appears to be as large as that from the FO N³LO terms [7], calling for improved resummation studies for such an observable.
5. In the sector of flavour physics (Section 10), new tools based on SCET, developed to study processes with energetic quarks and gluons, can be applied after certain modifications to improve the accuracy of theoretical corrections for B-physics studies at the FCC-ee, in particular for regions of phase space where the perturbative approach breaks down, owing to the presence of large logarithmic enhancements, and where the next-to-soft effects become more important.

2.3 Per-mille-precision α_s extraction

The strong coupling, α_s , is one of the fundamental parameters of the Standard Model, and its value not only directly affects the stability of the electroweak vacuum [25] but it chiefly impacts all theoretical calculations of e^+e^- scattering and decay processes involving real or virtual quarks and gluons [1]. Known today with a 0.9% precision, making it the worst known of all fundamental interaction couplings in nature [10], the input value of $\alpha_s(m_Z)$ propagates as a parametric uncertainty into many of the FCC-ee physics observables, chiefly in the Z, Higgs, and top quark sectors.

1. The leading source of uncertainty in the calculation of crucial EWPOs at the Z pole, such as Γ_Z , σ_{had}^0 , and R_ℓ , is the propagated $\delta\alpha_s$ parametric source [3].
2. In the Higgs sector (Section 12), the current $\alpha_s(m_Z)$ parametric uncertainty (combined with uncertainties arising from our imperfect knowledge of m_c and m_b) propagates into total final uncertainties of $\sim 2\%$ for the $\text{BR}(H \rightarrow WW, ZZ)$ and $\text{BR}(H \rightarrow \tau^+\tau^-, \mu^+\mu^-)$ branching ratios, of $\sim 6\text{--}7\%$ for $\text{BR}(H \rightarrow gg)$ and $\text{BR}(H \rightarrow c\bar{c})$, $\sim 3\%$ for $\text{BR}(H \rightarrow \gamma\gamma)$, and $\sim 7\%$ for $\text{BR}(H \rightarrow Z\gamma)$.
3. Precise studies of the $e^+e^- \rightarrow t\bar{t}$ cross-section (Section 11) indicate that it should be possible to extract the top quark width and mass with an uncertainty of around 50 MeV, provided that a precise independent extraction of the strong coupling is available. Such a requirement is, in particular, crucial to meaningfully constrain the top Yukawa coupling.

The current world-average value, $\alpha_s(m_Z) = 0.1181 \pm 0.0011$, is derived from a combination of six subclasses of approximately independent observables [10] measured in e^+e^- (hadronic Z boson and τ decays, and event shapes and jet rates), DIS (structure functions and global fits of parton distributions functions), and p–p collisions (top pair cross-sections), as well as from lattice QCD computations constrained by the empirical values of hadron masses and decay constants. To enter into the $\alpha_s(m_Z)$ world-average, the experimental (or lattice) results need to have a counterpart pQCD theoretical prediction at NNLO (or beyond) accuracy.

Of the current six $\alpha_s(m_Z)$ extractions entering in the PDG average, that derived from comparisons of NNLO pQCD predictions with lattice QCD results (Wilson loops, $q\bar{q}$ potentials, hadronic vacuum polarisation, QCD static energy) [26] today provides the most precise result: $\alpha_s(m_Z) = 0.1188 \pm 0.0011$. The current $\sim 0.9\%$ uncertainty is dominated by finite lattice spacing, truncations of the pQCD expansion up to NNLO, and hadron extrapolations. Over the next 10 years, reduction of the statistical uncertainties, at least by a factor of two, can be anticipated with increased computing power, while reaching the $\sim 0.1\%$ uncertainty level will also require the computation of fourth-order pQCD corrections [1].

After the lattice result, the most theoretically and experimentally ‘clean’ extractions of α_s are those based on the hadronic decays of the τ lepton, and W and Z bosons that will be measured with unparalleled accuracies at the FCC-ee. To derive $\alpha_s(m_Z)$, the experimental ratios of hadronic-to-leptonic decays are compared with the corresponding pQCD theoretical prediction, known today up to $\mathcal{O}(\alpha_s^4)$ [5, 27]:

$$\begin{aligned}
R_\ell^{\tau, W, Z}(Q = m_\tau, m_W, m_Z) &= \frac{\sigma(e^+e^- \rightarrow (\tau, W, Z) \rightarrow \text{hadrons})}{\sigma(e^+e^- \rightarrow (\tau, W, Z) \rightarrow \ell^+\ell^-)} \\
&= R_{\text{EW}}(Q) \left(1 + \sum_{i=1}^{N=4} c_i(Q) \left(\frac{\alpha_s(Q)}{\pi} \right)^i + \mathcal{O}(\alpha_s^5) + \delta_m + \delta_{\text{np}} \right). \quad (2.1)
\end{aligned}$$

In this equation, Q is the typical momentum transfer in the process used for measuring R_ℓ , c_n are coefficients of the perturbative series that can, in practice, be calculated up to some finite order $n = N$, and the terms δ_m and δ_{np} correspond, respectively, to mixed QCD+EW higher-order and power-suppressed $\mathcal{O}(\Lambda^p/Q^p)$ non-perturbative corrections, which affect, differently, the tau lepton and electroweak boson decays. For $\alpha_s(m_Z) = 0.118$, the size of the QCD term in Eq. (2.1) amounts to a 4% effect, so at least per-mille measurement accuracies for the R_ℓ ratios are required for a competitive $\alpha_s(m_Z)$ determination [8]. Such an experimental precision has been reached in measurements of τ and Z boson decays, but not for the W boson and that is why the latter still does not provide a precise α_s extraction [28]. Reaching per-mille uncertainties in α_s determinations based on Eq. (2.1) requires 100 times smaller uncertainties in the experimental τ , W, and Z measurements, a situation only reachable at the FCC-ee.

The ratio of hadronic to leptonic tau decays, known experimentally to within $\pm 0.23\%$ ($R_\ell^{\tau, \text{exp}} = 3.4697 \pm 0.0080$), compared with next-to-NNLO (N³LO) calculations, yields $\alpha_s(m_Z) = 0.1192 \pm 0.0018$, i.e., a 1.5% uncertainty, through a combination of results from different theoretical approaches (contour-improved perturbation theory (CIPT) and fixed-order perturbation theory (FOPT)) with different treatments of non-pQCD corrections [29,30]. The current α_s uncertainty is shared roughly equally between experimental and theoretical systematics. The latter are driven by differences in the CIPT and FOPT results, although the power-suppressed non-perturbative δ_{np} term in Eq. (2.1), which is of $\mathcal{O}(\Lambda^2/m_\tau^2) \approx 10^{-2}$, is not negligible for the tau, at variance with the much heavier W and Z bosons. High-statistics τ spectral functions (e.g., from B factories now, and the FCC-ee in the future), and solving CIPT–FOPT discrepancies (extending the calculations to N⁴LO accuracy and controlling the non-pQCD uncertainties) are required to reduce the relative α_s uncertainty below the $\sim 1\%$ level.

The current state-of-the-art N³LO calculations of W boson decays [6] would allow a theoretical extraction of α_s with a $\sim 0.7\%$ uncertainty, provided that one would have experimental measurements of sufficient precision. Unfortunately, the relevant LEP W^+W^- data are poor, based on 5×10^4 W bosons alone, and result in a QCD coupling extraction, $\alpha_s(m_Z) = 0.117 \pm 0.040$, with a huge $\sim 37\%$ uncertainty today [28]. A determination of α_s with per-mille uncertainty from W boson decays can only be achieved through the combination of two developments: (i) data samples commensurate with those expected at the FCC-ee (10^8 W bosons) and (ii) a significantly reduced uncertainty of the V_{cs} CKM element, which directly enters into the leading $R_{EW}(Q)$ prefactor of Eq. (2.1) and propagates into a significant parametric uncertainty on the extracted α_s . Figure B.2.1 (left) shows the expected $\alpha_s(m_Z)$ value derived from the R_ℓ^W ratio with 10^8 W bosons at the FCC-ee, assuming that V_{cs} has a negligible uncertainty (or, identical, assuming Cabibbo–Kobayashi–Maskawa (CKM) matrix unitarity). The extracted QCD coupling would have $\sim 0.2\%$ propagated experimental uncertainties.

The current QCD coupling extraction based on Z boson hadron decays uses three closely related pseudo-observables measured at the LEP: $R_\ell^0 = \Gamma_{\text{had}}/\Gamma_\ell$, $\sigma_{\text{had}}^0 = 12\pi/m_Z \cdot \Gamma_e \Gamma_{\text{had}}/\Gamma_Z^2$, and Γ_Z , combined with N³LO calculations, to give $\alpha_s(m_Z) = 0.1203 \pm 0.0028$ with a 2.5% uncertainty [10]. Alternatively, fixing all SM parameters to their measured values and letting free α_s in the electroweak fit yields $\alpha_s = 0.1194 \pm 0.0029$ ($\sim 2.4\%$ uncertainty, shallow blue curve in Fig. B.2.1 (right)) [31]. At the FCC-ee, with 10^{12} Z bosons providing high-precision measurements with $\Delta m_Z = 0.1$ MeV, and $\Delta \Gamma_Z = 0.1$ MeV, $\Delta R_\ell^0 = 10^{-3}$ (achievable thanks to the possibility of performing a threshold scan including energy self-calibration with resonant depolarisation) reduces the uncertainty on $\alpha_s(m_Z)$ to $\sim 0.15\%$. Figure B.2.1 (right) shows the expected α_s extractions from R_ℓ^Z and Γ^Z at the FCC-ee (yellow band) with the experimental

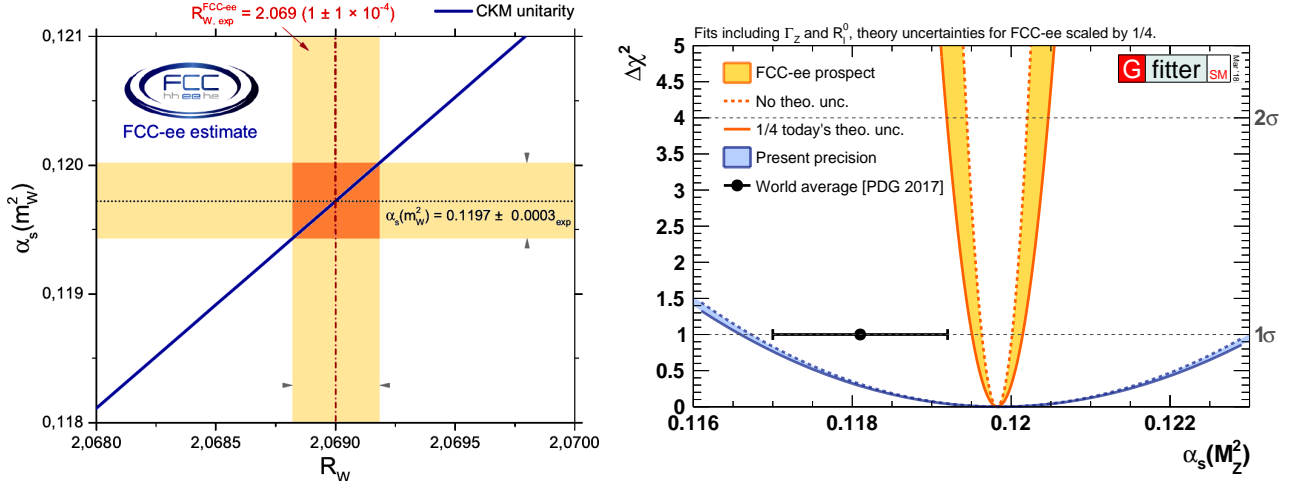


Fig. B.2.1: Left: Expected α_s determination from the W hadronic-to-leptonic decay ratio (R_ℓ^W) at the FCC-ee (the diagonal blue line assumes CKM matrix unitarity) [28]. Right: Precision on α_s derived from the electroweak fit today (blue band) [31] and expected at the FCC-ee (yellow band, without theoretical uncertainties and with the current theoretical uncertainties divided by a factor of four).

uncertainties listed in Table (A.1.2), without theoretical uncertainties (dotted red curve) and with the theoretical uncertainties reduced to one-quarter of their current values (solid red curve) [31].

The FCC-ee will not only provide an unprecedented amount of electroweak boson data, but also many orders of magnitude more jets than collected at LEP. The large and clean set of accurately reconstructed (and flavour-tagged) e^+e^- hadronic final states will provide additional high-precision α_s determinations from studies of event shapes, jet rates, and parton-to-hadron fragmentation functions (FFs) [1]. The existing measurements of e^+e^- event shapes (thrust T , C parameter) [23, 32–34] and n -jet rates [19, 35, 36], analysed with $N^{2,3}$ LO calculations matched, in some cases, to soft and collinear $N^{(2)}$ LL resummations, yield $\alpha_s(m_Z) = 0.1169 \pm 0.0034$, with a 2.9% uncertainty [10]. This relatively large uncertainty is mostly driven by the span of individual extractions that use different (Monte Carlo or analytical) approaches to account for soft and collinear radiation as well as to correct for hadronization effects. Modern jet substructure techniques [37] can help mitigate the latter corrections. In terms of event shapes, the recent combination of the CoLoRFulNNLO subtraction method [38] with NNLL corrections in the back-to-back region [39] has led to a precise calculation of the energy–energy correlation (EEC) observable in electron–positron collisions, and thereby an accurate NNLO+NNLL extraction of $\alpha_s(m_Z) = 0.1175 \pm 0.0029$ ($\sim 2.5\%$ uncertainty) [40], as discussed in detail in Section 4. Moreover, a very recent analysis of two-jet rates in e^+e^- collisions at N^3 LO+NNLL accuracy [41] has provided a new QCD coupling determination with $\sim 1\%$ uncertainty: $\alpha_s(m_Z) = 0.11881 \pm 0.00132$. In addition, other sets of observables computed today with a lower degree of accuracy (NLO, or approximately NNLO, bottom part of Fig. B.2.2), and thereby not now included in the PDG average, will provide additional constraints [1]. The energy dependence of the low- z FFs today provides $\alpha_s(m_Z) = 0.1205 \pm 0.0022$ ($\sim 2\%$ uncertainty) at NNLO*+NNLL [42, 43], whereas NLO scaling violations of the high- z FFs yield $\alpha_s(m_Z) = 0.1176 \pm 0.0055$ ($\sim 5\%$ uncertainty, mostly of experimental origin) [44]. In addition, measurements of the photon structure function $F_2^\gamma(x, Q^2)$, via $e^+e^- \rightarrow \gamma\gamma \rightarrow \text{hadrons}$, have been employed to derive $\alpha_s(m_Z) = 0.1198 \pm 0.0054$ ($\sim 4.5\%$

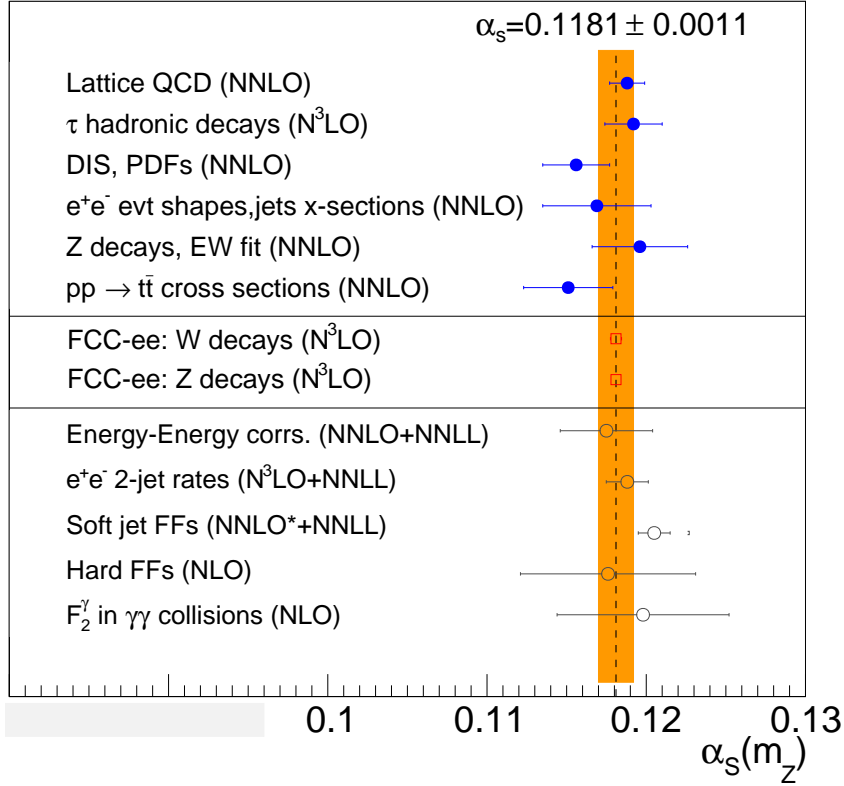


Fig. B.2.2: Summary of the $\alpha_s(m_z)$ determinations discussed here. Top: Subclasses entering in the current PDG world-average (solid dots, orange band) whose numerical value is listed on top [10]. Middle: Expected FCC-ee values via W, Z hadronic decays (open squares). Bottom: Other methods based on e^+e^- data not (yet) in the $\alpha_s(m_z)$ world-average: recent EEC [40] and two-jet rates [41], plus other extractions at a (currently) lower level of theoretical accuracy.

uncertainty) at NLO [45]. Extension to full-NNLO accuracy of the FFs and $F_2^\gamma(x, Q^2)$ fits using the much larger e^+e^- datasets available at various centre-of-mass energies at the FCC-ee will enable subpercentage precision in $\alpha_s(m_z)$ to be attained. Figure B.2.2 presents a comparison of the current $\alpha_s(m_z)$ results (top), the expected FCC-ee extractions (middle), and the other aforementioned methods based on e^+e^- data not currently included in the world-average.

2.4 High-precision non-perturbative QCD

All e^+e^- processes with quarks and gluons in the final state have an intrinsic uncertainty linked to the final non-perturbative conversion of the partons, present in the last stage of the QCD shower, into hadrons. Such a process cannot be computed using first-principles QCD calculations and is described using phenomenological models, such as the Lund string [46], as implemented in the PYTHIA MC generator [13], or the cluster hadronization approach [47] typical of the HERWIG event generator [48]. The analysis and unfolding of any e^+e^- experimental measurement of hadronic final states relies on these very same Monte Carlo generators; therefore, the final results are sensitive to their particular implementation of soft and collinear parton radiation (whose MC modelling is equivalent to an approximate next-to-leading-log (NLL) accuracy [49]) and of the hadronization process. Examples of such propagated uncertainties have been discussed already in the context of α_s extractions from various experimental e^+e^- observables. An improved MC reproduction of the experimental hadron data can, e.g., help in enabling

advanced light quark and gluon jet tagging in constraints of the Higgs Yukawa couplings to the first and second family of quarks. Controlling the uncertainties linked to hadronization and other final-state partonic effects, such as colour reconnection and multiparticle (spin, momenta, space, etc.) correlations, is, therefore, basic for many high-precision SM studies. Such effects are optimally studied in the clean environment provided by e^+e^- collisions, without coloured objects in the initial state. An FCC-ee goal, therefore, is to produce truly precise QCD measurements to constrain many aspects of non-perturbative dynamics to the 1% level or better, leaving an important legacy for MC generators for the FCC-eh and FCC-hh physics programme, much as those from LEP proved crucial for the parton shower models used today at the LHC [2]. In particular, the FCC-ee operating at different c.m. energies will enormously help to control resummation and hadronization effects in event shape distributions, reducing, in particular, non-perturbative uncertainties from a 9% effect at $\sqrt{s} = 91.2$ GeV to a 2% at 400 GeV [2, 50].

The modelling of parton hadronization in the current MC event generators has achieved a moderate success, and the LHC data have only further complicated the situation. First, the production of baryons (in particular containing strange quarks) remains poorly understood and is hard to measure in the complicated hadron–hadron environment. Second, and most importantly, the LHC measurements have challenged the standard assumption of parton hadronization universality, i.e., that models developed from e^+e^- data can be directly applied to hadron–hadron collisions. Strong final-state effects, more commonly associated with heavy-ion physics and quark–gluon–plasma formation, such as the ‘ridge’ [51] or the increase of strangeness production in high-multiplicity pp events [52], cannot be accommodated within the standard MC generators. The large statistical samples available at the FCC-ee will allow parton hadronization to be controlled in the QCD vacuum with subpercentage uncertainties, and thereby provide a better understanding of any collective final-state effects present in hadron–hadron collisions, starting with multistrange baryons, whose total production rates could only be determined with 5–20% accuracy at the LEP [53, 54], and going further to excited [54, 55], exotic, or multiple heavy hadrons, with implications for more advanced fragmentation models. For Λ – Λ correlation distributions, where MC generator programs today fail to describe the LEP [56] and LHC data, the huge FCC-ee samples of hadronic Z decays will have statistical uncertainties matching the best LEP systematic uncertainties, corresponding to a total errors reduction by a factor of ten or more.

In $e^+e^- \rightarrow t\bar{t}$, when the top and antitop quarks decay and hadronize close to each other, interactions and interferences between them, the decay bottoms, and any radiated gluons affect the rearrangement of the colour flow and thereby the kinematic distributions of the final hadronic state. Whereas the perturbative radiation in the process can, in principle, be theoretically controlled, there is a ‘cross-talk’ among the produced hadronic strings, also known as colour reconnection (CR), that can only be modelled phenomenologically [57]. In the pp case, such CR effects can decrease the precision that can be achieved in the extraction of the top mass, and constitute 20–40% of its uncertainty [58]. Colour reconnection can also impact limits for CP-violation searches in $H \rightarrow W^+W^- \rightarrow q_1\bar{q}_2q_3\bar{q}_4$ decays [59]. Searches for such effects can be optimally studied in the process $e^+e^- \rightarrow W^+W^- \rightarrow q_1\bar{q}_2q_3\bar{q}_4$ [59], where CR could lead to the formation of alternative ‘flipped’ singlets $q_1\bar{q}_4$ and $q_3\bar{q}_2$, and correspondingly more complicated string topologies [60]. The combination of results from all four LEP collaborations excluded the no-CR null hypothesis at 99.5% CL [61], but the size of the WW data sample was too small for any quantitative studies. At the FCC-ee, with the W mass determined to better than 1 MeV by a threshold scan, the semileptonic WW measurements (unaffected by

CR) can be used to probe the impact of CR in the hadronic WW events [2,62]. Alternative CR constraints at the FCC-ee have been proposed through the study of event shape observables sensitive to string overlap, such as sphericity for different hadron flavours, as described in ‘rope hadronization’ approaches [63,64].

References

- [1] D. d’Enterria and P.Z. Skands (Eds.), *Proc. High-Precision α_s Measurements from LHC to FCC-ee*, CERN (CERN, Geneva, 2015), [arXiv:1512.05194](#),
- [2] D. d’Enterria and P.Z. Skands (Eds.), *Proc. Parton Radiation and Fragmentation from LHC to FCC-ee*, 2017. [arXiv:1702.01329](#)
- [3] A. Blondel *et al.*, *Standard Model theory for the FCC-ee Tera-Z stage*, CERN (CERN Yellow Rep. Monogr. 3, Geneva, Switzerland), [arXiv:1809.01830](#), [doi:10.23731/CYRM-2019-003](#)
- [4] M. Beneke and Y. Kiyo, *Phys. Lett.* **B668** (2008) 143. [arXiv:0804.4004](#), [doi:10.1016/j.physletb.2008.08.031](#)
- [5] P.A. Baikov *et al.*, *Phys. Rev. Lett.* **101** (2008) 012002. [arXiv:0801.1821](#), [doi:10.1103/PhysRevLett.101.012002](#)
- [6] D. Kara, *Nucl. Phys.* **B877** (2013) 683. [arXiv:1307.7190](#), [doi:10.1016/j.nuclphysb.2013.10.024](#)
- [7] M. Beneke *et al.*, *Phys. Rev. Lett.* **115** (2015) 192001. [arXiv:1506.06864](#), [doi:10.1103/PhysRevLett.115.192001](#)
- [8] S. Schael *et al.*, *Phys. Rep.* **427** (2006) 257. [arXiv:hep-ex/0509008](#), [doi:10.1016/j.physrep.2005.12.006](#)
- [9] LEP Electroweak Working Group, *Precision electroweak measurements and constraints on the Standard Model*, [arXiv:1012.2367](#)
- [10] C. Patrignani *et al.*, *Chin. Phys.* **C40** (2016) 100001. [doi:10.1088/1674-1137/40/10/100001](#)
- [11] D. Abbaneo *et al.*, *Eur. Phys. J.* **C4** (1998) 185. [doi:10.1007/s100520050196](#)
- [12] D. d’Enterria and C. Yan, *Forward–backward b-quark asymmetry at the Z pole: QCD uncertainties redux*, 53rd Rencontres de Moriond on QCD and High Energy Interactions (Moriond QCD 2018) La Thuile, Italy, 2018, [arXiv:1806.00141](#)
- [13] T. Sjöstrand *et al.*, *Comput. Phys. Commun.* **191** (2015) 159. [arXiv:1410.3012](#), [doi:10.1016/j.cpc.2015.01.024](#)
- [14] W.T. Giele *et al.*, *Phys. Rev.* **D84** (2011) 054003. [arXiv:1102.2126](#), [doi:10.1103/PhysRevD.84.054003](#)
- [15] N. Fischer *et al.*, *Eur. Phys. J.* **C76** (2016) 589. [arXiv:1605.06142](#), [doi:10.1140/epjc/s10052-016-4429-6](#)
- [16] G.P. Salam, in *From My Vast Repertoire...: Guido Altarelli’s Legacy*, Eds. S. Forte *et al.* (World Scientific, Singapore, 2019), Chap. 7, pp. 101–121. [arXiv:1712.05165](#), [doi:10.1142/9789813238053_0007](#)
- [17] S. Catani *et al.*, *Phys. Lett.* **B269** (1991) 432. [doi:10.1016/0370-2693\(91\)90196-W](#)

-
- [18] Y. L. Dokshitzer *et al.*, *JHEP* **08** (1997) 001. [arXiv:hep-ph/9707323](#), [doi:10.1088/1126-6708/1997/08/001](#)
- [19] G. Dissertori *et al.*, *Phys. Rev. Lett.* **104** (2010) 072002. [arXiv:0910.4283](#), [doi:10.1103/PhysRevLett.104.072002](#)
- [20] A. Gehrmann-De Ridder *et al.*, *Comput. Phys. Commun.* **185** (2014) 3331. [arXiv:1402.4140](#), [doi:10.1016/j.cpc.2014.07.024](#)
- [21] S. Weinzierl, *Eur. Phys. J.* **C71** (2011) 1565 [Erratum: **C71** (2011) 1717]. [arXiv:1011.6247](#), [doi:10.1140/epjc/s10052-011-1565-x](#), [doi:10.1140/epjc/s10052-011-1717-z](#)
- [22] V. Del Duca *et al.*, *Phys. Rev. Lett.* **117** (2016) 152004. [arXiv:1603.08927](#), [doi:10.1103/PhysRevLett.117.152004](#)
- [23] A. Banf *et al.*, *JHEP* **05** (2015) 102. [arXiv:1412.2126](#), [doi:10.1007/JHEP05\(2015\)102](#)
- [24] N. Fischer *et al.*, *Eur. Phys. J.* **C75** (2015) 571. [arXiv:1505.01636](#), [doi:10.1140/epjc/s10052-015-3766-1](#)
- [25] D. Buttazzo *et al.*, *JHEP* **12** (2013) 089. [arXiv:1307.3536](#), [doi:10.1007/JHEP12\(2013\)089](#)
- [26] S. Aoki *et al.*, FLAG review 2019, [arXiv:1902.08191](#)
- [27] P.A. Baikov *et al.*, *Phys. Lett.* **B714** (2012) 62. [arXiv:1206.1288](#), [doi:10.1016/j.physletb.2012.06.052](#)
- [28] D. d'Enterria and M. Srebre, *Phys. Lett.* **B763** (2016) 465. [arXiv:1603.06501](#), [doi:10.1016/j.physletb.2016.10.012](#)
- [29] A. Pich and A. Rodríguez-Sánchez, *Phys. Rev.* **D94** (2016) 034027. [arXiv:1605.06830](#), [doi:10.1103/PhysRevD.94.034027](#)
- [30] D. Boito *et al.*, *Phys. Rev.* **D95** (2017) 034024. [arXiv:1611.03457](#), [doi:10.1103/PhysRevD.95.034024](#)
- [31] J. Haller *et al.*, *Eur. Phys. J.* **C78** (2018) 675. [arXiv:1803.01853](#), [doi:10.1140/epjc/s10052-018-6131-3](#)
- [32] S. Bethke *et al.*, *Eur. Phys. J.* **C64** (2009) 351. [arXiv:0810.1389](#), [doi:10.1140/epjc/s10052-009-1149-1](#)
- [33] R. Abbate *et al.*, *Phys. Rev.* **D86** (2012) 094002. [arXiv:1204.5746](#), [doi:10.1103/PhysRevD.86.094002](#)
- [34] A.H. Hoang *et al.*, *Phys. Rev.* **D91** (2015) 094018. [arXiv:1501.04111](#), [doi:10.1103/PhysRevD.91.094018](#)
- [35] S. Weinzierl, *Phys. Rev. Lett.* **101** (2008) 162001. [arXiv:0807.3241](#), [doi:10.1103/PhysRevLett.101.162001](#)
- [36] J. Schieck *et al.*, *Eur. Phys. J.* **C73** (2013) 2332. [arXiv:1205.3714](#), [doi:10.1140/epjc/s10052-013-2332-y](#)
- [37] Les Houches 2017: Physics at TeV colliders Standard Model working group report. [arXiv:1803.07977](#).
- [38] V. Del Duca *et al.*, *Phys. Rev.* **D94** (2016) 074019. [arXiv:1606.03453](#), [doi:10.1103/PhysRevD.94.074019](#)

- [39] D. de Florian and M. Grazzini, *Nucl. Phys.* **B704** (2005) 387. [arXiv:hep-ph/0407241](#), [doi:10.1016/j.nuclphysb.2004.10.051](#)
- [40] A. Kardos *et al.*, *Eur. Phys. J.* **C78** (2018) 498. [arXiv:1804.09146](#), [doi:10.1140/epjc/s10052-018-5963-1](#)
- [41] A. Verbytskyi *et al.*, *JHEP* **2019** (2019) 129. [arXiv:1902.08158](#) [doi:10.1007/JHEP08\(2019\)129](#)
- [42] R. Pérez-Ramos and D. d’Enterria, *JHEP* **08** (2014) 068. [arXiv:1310.8534](#), [doi:10.1007/JHEP08\(2014\)068](#)
- [43] D. d’Enterria and R. Pérez-Ramos, α_s determination at NNLO*+NNLL accuracy from the energy evolution of jet fragmentation functions at low z , Proc. 50th Rencontres de Moriond, QCD and high energy interactions: La Thuile, Italy (2015), p. 117. [arXiv:1505.02624](#)
- [44] S. Albino *et al.*, *Nucl. Phys.* **B725** (2005) 181. [arXiv:hep-ph/0502188](#), [doi:10.1016/j.nuclphysb.2005.07.010](#)
- [45] S. Albino *et al.*, *Phys. Rev. Lett.* **89** (2002) 122004. [arXiv:hep-ph/0205069](#), [doi:10.1103/PhysRevLett.89.122004](#)
- [46] B. Andersson *et al.*, *Z. Phys.* **C20** (1983) 317. [doi:10.1007/BF01407824](#)
- [47] B.R. Webber, *Nucl. Phys.* **B238** (1984) 492. [doi:10.1016/0550-3213\(84\)90333-X](#)
- [48] G. Corcella *et al.*, *JHEP* **01** (2001) 010. [arXiv:hep-ph/0011363](#), [doi:10.1088/1126-6708/2001/01/010](#)
- [49] M. Dasgupta *et al.*, *JHEP* **09** (2018) 033. [arXiv:1805.09327](#), [doi:10.1007/JHEP09\(2018\)033](#)
- [50] G. Bell *et al.*, *JHEP* **01** (2019) 147. [arXiv:1808.07867](#), [doi:10.1007/JHEP01\(2019\)147](#)
- [51] V. Khachatryan *et al.*, *JHEP* **09** (2010) 091. [arXiv:1009.4122](#), [doi:10.1007/JHEP09\(2010\)091](#)
- [52] J. Adam *et al.*, *Nat. Phys.* **13** (2017) 535. [arXiv:1606.07424](#), [doi:10.1038/nphys4111](#)
- [53] P. Abreu *et al.*, *Z. Phys.* **C67** (1995) 543. [doi:10.1007/BF01553980](#)
- [54] G. Alexander *et al.*, *Z. Phys.* **C73** (1997) 569. [doi:10.1007/s002880050349](#)
- [55] R. Akers *et al.*, *Z. Phys.* **C68** (1995) 1. [doi:10.1007/BF01579799](#)
- [56] G. Abbiendi *et al.*, *Eur. Phys. J.* **C13** (2000) 185. [arXiv:hep-ex/9808031](#), [doi:10.1007/s100520000207](#), [doi:10.1007/s100520050685](#)
- [57] V.A. Khoze and T. Sjöstrand, *Phys. Lett.* **B328** (1994) 466. [arXiv:hep-ph/9403394](#), [doi:10.1016/0370-2693\(94\)91506-7](#)
- [58] S. Argyropoulos and T. Sjöstrand, *JHEP* **11** (2014) 043. [arXiv:1407.6653](#), [doi:10.1007/JHEP11\(2014\)043](#)
- [59] J.R. Christiansen and T. Sjöstrand, *Eur. Phys. J.* **C75** (2015) 441. [arXiv:1506.09085](#), [doi:10.1140/epjc/s10052-015-3674-4](#)
- [60] T. Sjöstrand and V.A. Khoze, *Z. Phys.* **C62** (1994) 281. [arXiv:hep-ph/9310242](#), [doi:10.1007/BF01560244](#)
- [61] S. Schael *et al.*, *Phys. Rep.* **532** (2013) 119. [arXiv:1302.3415](#), [doi:10.1016/j.physrep.2013.07.004](#)

- [62] A. Abada *et al.*, *Eur. Phys. J.* **C79** (2019), 474, [doi:10.1140/epjc/s10052-019-6904-3](https://doi.org/10.1140/epjc/s10052-019-6904-3)
- [63] C. Bierlich *et al.* A shoving model for collectivity in hadronic collisions, [arXiv:1612.05132](https://arxiv.org/abs/1612.05132)
- [64] C. Bierlich, *EPJ Web Conf.* **171** (2018) 14003. [arXiv:1710.04464](https://arxiv.org/abs/1710.04464),
[doi:10.1051/epjconf/201817114003](https://doi.org/10.1051/epjconf/201817114003)

3 Inclusion of mixed QCD–QED resummation effects at higher orders

Contribution* by: G.F.R. Sborlini [german.sborlini@ific.uv.es]

In this section, we review some recent results concerning the inclusion of mixed QCD–QED corrections in the computation of physical observables. First, we comment on the extension of the Dokshitzer–Gribov–Lipatov–Altarelli–Parisi (DGLAP) equations to deal with the presence of mixed QCD–QED interactions. We describe the calculation of the full set of higher-order corrections to the splitting kernels, through the Abelianization algorithm. This procedure allows us to build the functional form of the QCD–QED corrections, starting from pure QCD terms. As a practical application of this technique, we also explore the computation of fixed-order corrections to diphoton production, and the inclusion of higher-order mixed QCD–QED resummation effects to Z production. In both cases, we directly apply the Abelianization to the q_T subtraction or resummation formalism, obtaining the universal ingredients that allow us to compute the aforementioned corrections to any process involving colourless and neutral particles in the final state.

3.1 Introduction and motivation

The large amount of data that high-energy experiments are collecting allows the precision of several measurements to be increased. In consequence, theoretical predictions must be pushed forward by including previously neglected small effects. This is the case for electroweak (EW) or QED corrections, which are subdominating for collider physics. However, from naïve power counting, it is easy to notice that $\mathcal{O}(\alpha) \approx \mathcal{O}(\alpha_S^2)$. In addition, QED interactions (as well as the full set of EW calculations) lead to novel effects that could interfere with the well-known QCD signals. Moreover, these effects might play a crucial role in the context of future lepton colliders, such as the FCC-ee. For these reasons, EW and QED higher-order corrections must be seriously studied in a fully consistent framework.

The aim of this brief section is to present some results related to the impact of QED corrections on the calculation of physical observables for colliders. In Section 3.2, we recall the computation of the full set of QCD–QED splitting functions at $\mathcal{O}(\alpha\alpha_S)$ and $\mathcal{O}(\alpha^2)$, centring into the Abelianization algorithm and the relevance of the corrections to achieve a better determination of the photon PDF. Then, we apply the Abelianization to the well-established q_T subtraction or resummation [1,2] framework. In Section 3.3, we show the impact of the NLO QED corrections to diphoton production. After that, we characterize the mixed QCD–QED resummation of soft gluons or photons for Z boson production in Section 3.4. Conclusions are drawn and future research directions are discussed in Section 3.5.

3.2 Splittings and PDF evolution

Splitting functions are crucial in describing the singular collinear behaviour of scattering amplitudes. On the one hand, they are used to build the counterterms to subtract infrared (IR)

*This contribution should be cited as:

G.F.R. Sborlini, Inclusion of mixed QCD–QED resummation effects at higher orders, DOI: [10.23731/CYRM-2020-003.51](https://doi.org/10.23731/CYRM-2020-003.51), in: Theory for the FCC-ee, Eds. A. Blondel, J. Gluza, S. Jadach, P. Janot and T. Riemann, CERN Yellow Reports: Monographs, CERN-2020-003, DOI: [10.23731/CYRM-2020-003](https://doi.org/10.23731/CYRM-2020-003), p. 51.
 © CERN, 2020. Published by CERN under the [Creative Commons Attribution 4.0 license](https://creativecommons.org/licenses/by/4.0/).

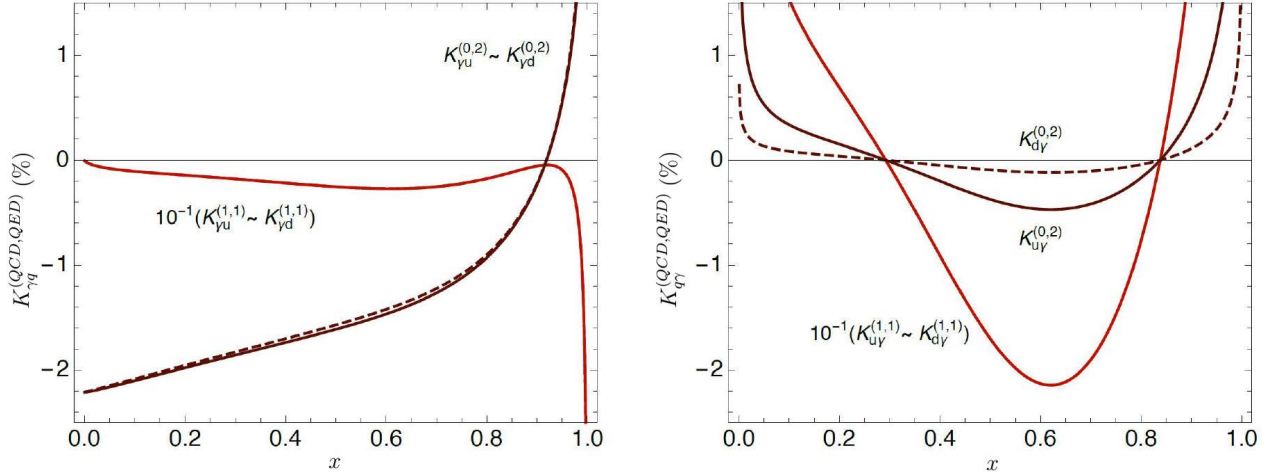


Fig. B.3.1: Corrections due to the inclusion of QED contributions in the $P_{q\gamma}$ (right) and $P_{\gamma q}$ (left) splitting kernels. We include both $\mathcal{O}(\alpha^2)$ (brown) and $\mathcal{O}(\alpha\alpha_S)$ (red) terms. The K ratio is defined using the leading order as normalization. To ease the visual presentation, we rescaled the $\mathcal{O}(\alpha\alpha_S)$ terms by a factor of 0.1.

singularities from cross-sections. On the other hand, they are the evolution kernels of the integro-differential DGLAP equations [3], which govern the perturbative evolution of PDFs. When taking QCD and EW or QED interactions into account, it is necessary to include photon and lepton PDFs, and this will lead to the presence of new splitting functions. In Refs. [4, 5], we computed the $\mathcal{O}(\alpha\alpha_S)$ and $\mathcal{O}(\alpha^2)$ corrections to the DGLAP equations, as well as the associated kernels. The strategy that we adopted was based on the implementation of a universal algorithm, called *Abelianization*, which aims to explode previously known pure QCD results to obtain the corresponding QCD–QED or QED expressions. Roughly speaking, the key idea behind this method is that of *transforming gluons into photons*: colour factors are replaced by suitable electric charges, as well as symmetry or counting factors.

With the purpose of exhibiting the quantitative effects that mixed QCD–QED or $\mathcal{O}(\alpha^2)$ corrections might have, we plot the K ratio for quark–photon and photon–quark splitting functions in Fig. B.3.1. It is important to notice that these contributions are not present in pure QCD, which implies that the evolution of photon PDF is noticeably affected by $\mathcal{O}(\alpha\alpha_S)$ splittings or even higher orders in the mixed QCD–QED perturbative expansion. We would like to point out that a precise determination of photon distributions is crucial to obtaining more accurate predictions for several physical observables.

3.3 Fixed-order effects: application to diphoton production

The q_T subtraction or resummation formalism [1, 2] is a powerful approach to computing higher-order corrections to physical observables. This formalism has been mainly applied to QCD calculations, and relies on the colour neutrality of the final-state particles.[†] Thus, we used the Abelianization algorithm to compute the universal coefficients required to implement NLO QED corrections to any process involving only neutral particles in the final state. In this way, we demonstrate that this extension can deal consistently with the cancellation of IR divergences

[†]An extension to deal with massive or coloured particles in the final state is presented in Refs. [6, 7].

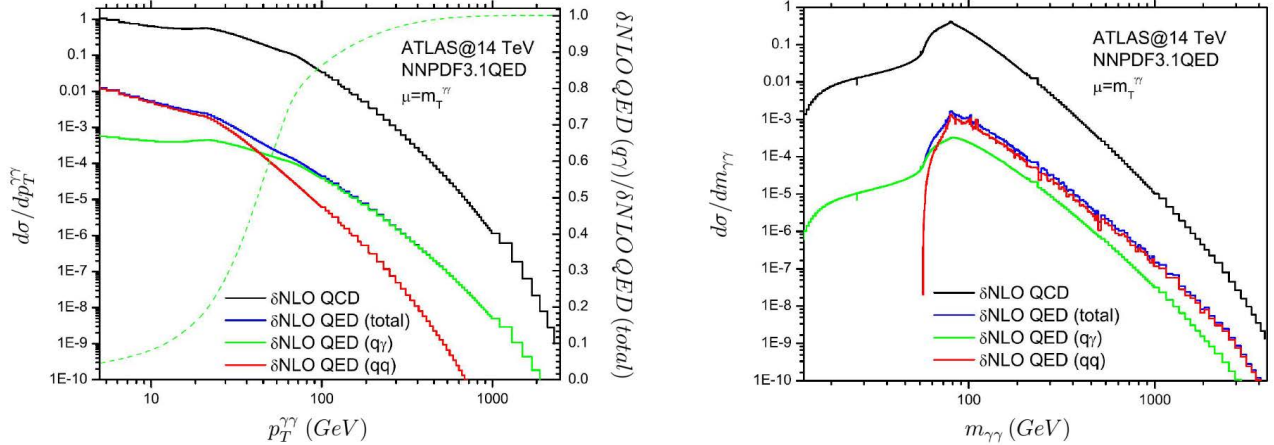


Fig. B.3.2: Impact of higher-order QED corrections on the transverse momentum (left) and invariant mass (right) distributions for diphoton production. The black (blue) curve shows the total NLO QCD (QED) prediction, without including the LO contribution. The dashed green line indicates the relative contribution of the $q\bar{q}$ -channel to the total NLO QED correction.

in the limit $q_T \rightarrow 0$.

As a practical example, we used the public code `2gNNLO` [8,9], which provides up to NNLO QCD corrections to diphoton production, and we implemented the corresponding NLO QED corrections [10,11]. We applied the default ATLAS cuts, with 14 TeV centre-of-mass energy, and the NNPDF3.1QED [12,13] PDF set. The transverse momentum and invariant mass spectra are shown in Fig. B.3.2. It is interesting to note that, even if the corrections are small compared with the QCD contributions, the QED interactions lead to novel features, such as a dynamic cut in the invariant mass spectrum. This is because real radiation in the $q\bar{q}$ channel contains three final-state photons, which must be ordered according to their transverse momenta before imposing the selection cuts. Moreover, introducing the QED corrections (or, even better, mixed NLO QCD–QED corrections) will allow us to reduce the scale uncertainties and produce more reliable theoretical predictions.

3.4 Mixed resummation effects: Z boson production

Finally, we studied the impact of including mixed QCD–QED terms within the q_T resummation formalism. This is equivalent to considering the simultaneous emission of soft or collinear gluons and photons. A detailed description of the formalism is presented in Ref. [14], which gives the computation of the modified Sudakov form factors as well as all the required universal coefficients to reach mixed NLL'+NLO accuracy in the double expansion in α and α_S . Explicitly, we obtained

$$\begin{aligned}
 \mathcal{G}'_N(\alpha_S, \alpha, L) = & \mathcal{G}_N(\alpha_S, L) + L g'^{(1)}(\alpha L) + g_N'^{(2)}(\alpha L) + \sum_{n=3}^{\infty} \left(\frac{\alpha}{\pi}\right)^{n-2} g_N'^{(n)}(\alpha L) \\
 & + g'^{(1,1)}(\alpha_S L, \alpha L) + \sum_{\substack{n,m=1 \\ n+m \neq 2}}^{\infty} \left(\frac{\alpha_S}{\pi}\right)^{n-1} \left(\frac{\alpha}{\pi}\right)^{m-1} g_N'^{(n,m)}(\alpha_S L, \alpha L) \quad (3.1)
 \end{aligned}$$

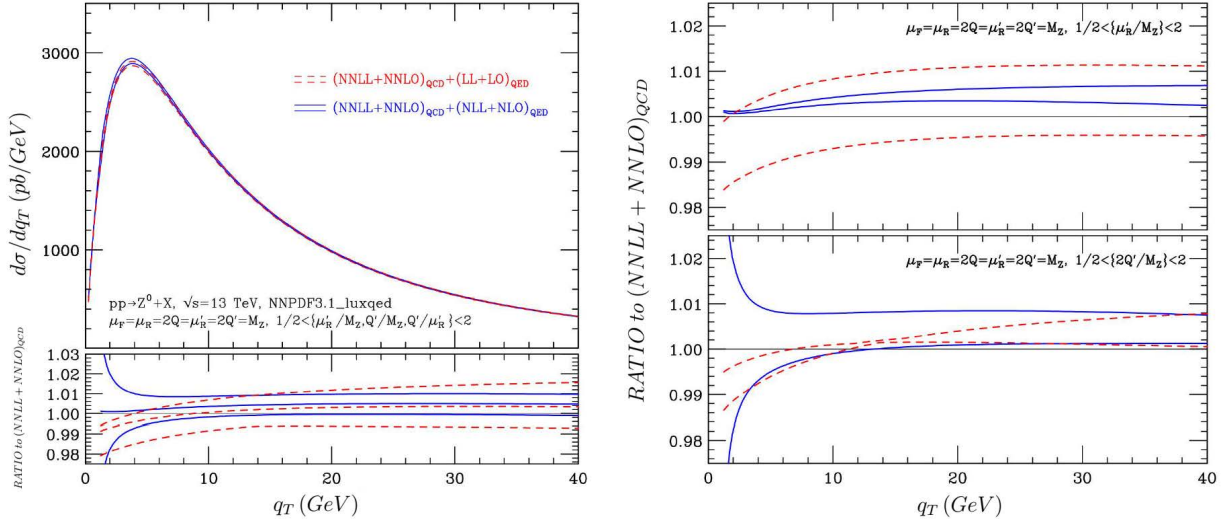


Fig. B.3.3: The q_T spectrum for Z boson production at the LHC with 13 TeV centre-of-mass energy. In the left panel, we show the combination of NNLL+NNLO QCD contributions together with the LL (red dashed curve) and NLL'+NLO (blue solid curve) QED effects. We include the uncertainty bands that result from the full scale variation by a factor of two (up and down). More details about scale uncertainties are shown in the right panel, where we independently modify the resummation (upper plot) and renormalization (lower plot) scales.

and

$$\mathcal{H}'_N{}^F(\alpha_S, \alpha) = \mathcal{H}'_N{}^F(\alpha_S) + \frac{\alpha}{\pi} \mathcal{H}'_N{}^F(1) + \sum_{n=2}^{\infty} \left(\frac{\alpha}{\pi}\right)^n \mathcal{H}'_N{}^F(n) + \sum_{n,m=1}^{\infty} \left(\frac{\alpha_S}{\pi}\right)^n \left(\frac{\alpha}{\pi}\right)^m \mathcal{H}'_N{}^F(n,m) \quad (3.2)$$

for the expansion of the Sudakov exponents and the hard-virtual coefficients, respectively. A similar expansion is available for the soft-collinear coefficients C_{ab} . Other important ingredients of the formalism are the mixed QCD–QED renormalization group equations, which include a double expansion of the corresponding β functions [14].

To test our formalism, we used Z boson production as a benchmark process. We started from the code `DYqT` [15] to compute the next-to-next-to-leading logarithmic QCD (NNLL) corrections properly matched to the fixed-order contribution (i.e., NNLO QCD in this case). In Fig. B.3.3, we show the combination of NNLL+NNLO QCD predictions for the q_T spectrum of the produced Z (in the narrow width approximation), together with the LL (red dashed curve) and mixed NLL'+NLO QED contributions (blue solid curve). The effects introduced by mixed QCD–QED terms reach the percentage level for $q_T \approx 20$ GeV, when considering LHC kinematics at 13 TeV centre-of-mass energy. However, the most noticeable consequence of introducing these corrections is the scale-dependence reduction. This means that our predictions are more stable when varying the electroweak parameters or the factorisation, renormalization, or resummation scales.

3.5 Conclusions

In this brief section, we reviewed some of our recent efforts towards more precise phenomenological predictions for colliders. We centred the discussion on the inclusion of QED and mixed

QCD–QED corrections to the evolution of PDFs (through the computation of novel splitting functions), QED fixed-order computations (using diphoton production as a benchmark), and mixed QCD–QED q_T resummation (applied to Z boson production). In all these cases, the corrections constitute percentage-level deviation from the dominant QCD correction, but this could still be detected through an increased precision of the forthcoming experimental measurements (such as those provided by the FCC-ee). Thus, understanding how to extend the exposed frameworks to deal with even higher perturbative orders is crucial to match the quality of the experimental data, allowing us to detect any possible deviation from the Standard Model and discover new physical phenomena.

Acknowledgements

The work was done in collaboration with D. de Florian, G. Rodrigo, L. Cieri, and G. Ferrera.

References

- [1] S. Catani and M. Grazzini, *Phys. Rev. Lett.* **98** (2007) 222002. [arXiv:hep-ph/0703012](#), [doi:10.1103/PhysRevLett.98.222002](#)
- [2] S. Catani *et al.*, *Nucl. Phys.* **B881** (2014) 414. [arXiv:1311.1654](#), [doi:10.1016/j.nuclphysb.2014.02.011](#)
- [3] G. Altarelli and G. Parisi, *Nucl. Phys.* **B126** (1977) 298. [doi:10.1016/0550-3213\(77\)90384-4](#)
- [4] D. de Florian *et al.*, *Eur. Phys. J.* **C76** (2016) 282. [arXiv:1512.00612](#), [doi:10.1140/epjc/s10052-016-4131-8](#)
- [5] D. de Florian *et al.*, *JHEP* **10** (2016) 056. [arXiv:1606.02887](#), [doi:10.1007/JHEP10\(2016\)056](#)
- [6] S. Catani *et al.*, *Nucl. Phys.* **B890** (2014) 518. [arXiv:1408.4564](#), [doi:10.1016/j.nuclphysb.2014.11.019](#)
- [7] R. Bonciani *et al.*, *Eur. Phys. J.* **C75** (2015) 581. [arXiv:1508.03585](#), [doi:10.1140/epjc/s10052-015-3793-y](#)
- [8] S. Catani *et al.*, *Phys. Rev. Lett.* **108** (2012) 072001 [Erratum: **117** (2016) 089901]. [arXiv:1110.2375](#), [doi:10.1103/PhysRevLett.108.072001](#), [doi:10.1103/PhysRevLett.117.089901](#)
- [9] S. Catani *et al.*, *JHEP* **04** (2018) 142. [arXiv:1802.02095](#), [doi:10.1007/JHEP04\(2018\)142](#)
- [10] G.F.R. Sborlini, Higher-order QED effects in hadronic processes, PoS EPS-HEP 2017, Venice, 2017, paper 398. [arXiv:1709.09596](#), [doi:10.22323/1.314.0398](#)
- [11] G.F.R. Sborlini, Including higher-order mixed QCD–QED effects in hadronic calculations, 53rd Rencontres de Moriond on QCD and High Energy Interactions (Moriond QCD 2018), La Thuile, Italy, 2018. [arXiv:1805.06192](#)
- [12] R.D. Ball *et al.*, *Eur. Phys. J.* **C77** (2017) 663. [arXiv:1706.00428](#), [doi:10.1140/epjc/s10052-017-5199-5](#)
- [13] V. Bertone *et al.*, *SciPost Phys.* **5** (2018) 008. [arXiv:1712.07053](#), [doi:10.21468/SciPostPhys.5.1.008](#)

- [14] L. Cieri *et al.*, *JHEP* **08** (2018) 165. [arXiv:1805.11948](#),
[doi:10.1007/JHEP08\(2018\)165](#)
- [15] G. Bozzi *et al.*, *Nucl. Phys.* **B815** (2009) 1747. [arXiv:0812.2862](#),
[doi:10.1016/j.nuclphysb.2009.02.014](#)

4 CoLoRFulNNLO at work: a determination of α_S

Contribution* by: A. Kardos, S. Kluth, G. Somogyi, Z. Trócsányi, Z. Tulipánt, A. Verbytskyi

Corresponding author: A. Kardos [kardos.adam@science.unideb.hu]

4.1 Introduction

The most precise determination of fundamental parameters of the Standard Model is very important. One such fundamental parameter is the strong coupling of QCD. Its importance can be gauged by taking a look at the various experiments and configurations where it was measured; for an up-to-date summary, see Ref. [1]. The precise measurement of such a parameter is difficult for two reasons. First, high-quality data with small and well-controlled uncertainties are needed. Second, high-precision calculations are needed from the theory side, such that theoretical uncertainties are small as well.

In a theoretical prediction based on calculation in perturbation theory, the uncertainty has two main sources: the omission of higher-order terms, which are estimated by the renormalization scale, and the numerical stability of the integrations. While the dependence on unphysical scales can, in principle, be decreased by including more and more higher-order contributions in the prediction, the numerical uncertainty can be intrinsic to the method used to obtain the theoretical prediction. Moreover, the method of comparing experiment with theory is also affected by another uncertainty. While an experiment measures colour singlet objects, hadrons, the predictions are made in QCD for colourful ones, partons. The assumption of local parton-hadron duality ensures a correspondence between these two up to non-perturbative effects. Non-perturbative effects are power corrections in nature, going with some negative power of the collision energy. This means that, for an accurate comparison, either (i) these effects should be estimated and taken into account, or (ii) the experiment should have a high enough energy that these contributions become negligible compared with other effects, or (iii) an observable must be chosen that is not sensitive to these effects.

To take these non-perturbative effects into account, we must choose from phenomenological [2, 3] or analytical models [4]. It is worth noting that none of these models is derived from first principles; hence, there is still room for improvement. Non-perturbative effects derived from first principles would also be favoured because these corrections are to be used in comparisons of predictions with experimental measurements. Currently, phenomenological models use several parameters fitted to experimental data; thus, bias is introduced in the measurement of physical parameters. The calculation of non-perturbative corrections from first principles is also advocated because the only available analytical model seems to be ill-suited for the current precision of theoretical calculations, as shown in Ref. [5].

In this report, we show two approaches to how the measurement of a physical parameter, the strong coupling, can be carried out with high precision. Because the used observables allow for such measurements, these can be considered as interesting subjects to study in a future

*This contribution should be cited as:

A. Kardos, S. Kluth, G. Somogyi, Z. Trócsányi, Z. Tulipánt, A. Verbytskyi, CoLoRFulNNLO at work: a determination of α_S , DOI: [10.23731/CYRM-2020-003.57](https://doi.org/10.23731/CYRM-2020-003.57), in: Theory for the FCC-ee, Eds. A. Blondel, J. Gluza, S. Jadach, P. Janot and T. Riemann,

CERN Yellow Reports: Monographs, CERN-2020-003, DOI: [10.23731/CYRM-2020-003](https://doi.org/10.23731/CYRM-2020-003), p. 57.

© CERN, 2020. Published by CERN under the [Creative Commons Attribution 4.0 license](https://creativecommons.org/licenses/by/4.0/).

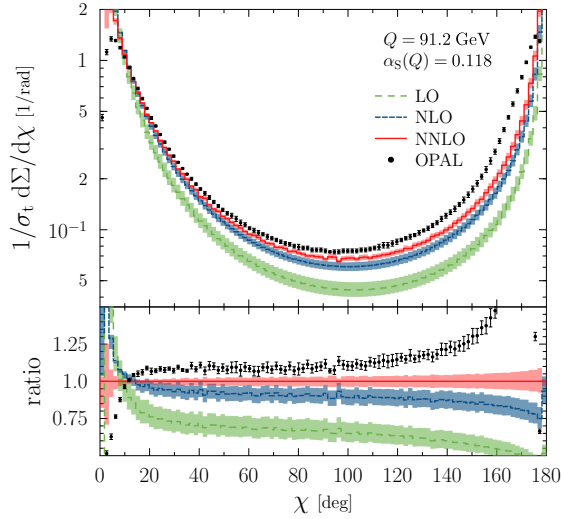


Fig. B.4.1: Top: Fixed-order prediction for EEC in the first three orders of perturbation theory with theoretical uncertainties. The dots show the measurement by the OPAL collaboration [11]. Bottom: Comparison of the predictions and the measurement with the NNLO result.

electron–positron collider.

4.2 Precision through higher orders

A possible approach to increasing the precision of a measurement from the theoretical perspective is to select an observable and refine its prediction by including higher-order contributions in fixed-order perturbation theory or by means of resummation. With the completion of the CoLoRFulNNLO subtraction method [6–8] for electron–positron collisions, the next-to-next-to-leading-order (NNLO) QCD prediction for energy–energy correlation (EEC) recently became available [9] for the first time. Matching this with predictions obtained by resumming leading (LL), next-to-leading (NLL), and next-to-next-to-leading logarithms (NNLL) in the back-to-back region [10], it was possible, by matching the two calculations, to arrive at the most precise theoretical prediction for this observable at NNLO+NNLL accuracy in QCD [5]. The energy–energy correlation is defined as a normalised energy-weighted sum of two-particle correlations:

$$\frac{1}{\sigma_t} \frac{d\Sigma(\chi)}{d \cos \chi} \equiv \frac{1}{\sigma_t} \int \sum_{i,j} \frac{E_i E_j}{Q^2} d\sigma_{e^+e^- \rightarrow ij+X} \delta(\cos \chi + \cos \theta_{ij}), \quad (4.1)$$

where Q is the centre-of mass energy of the collision, σ_t is the corresponding total cross-section, E_i is the energy of the i th particle, and $\cos \theta_{ij}$ is the enclosed angle between particles i and j . The theoretical prediction for EEC in the first three orders of perturbation theory is depicted in Fig. B.4.1. The theoretical uncertainties were obtained by varying the renormalization scale between $m_Z/2$ and $2m_Z$. As can be seen from the lower panel, even when using the highest-precision prediction, the difference between measurement and theory is sizeable. This can be attributed to missing higher-order terms becoming important at the edge of phase space and missing hadronization corrections.

The behaviour near $\chi = 0$ can be improved by including all-order results through resummation. As described in Ref. [12], we used modern Monte Carlo (MC) tools to extract such

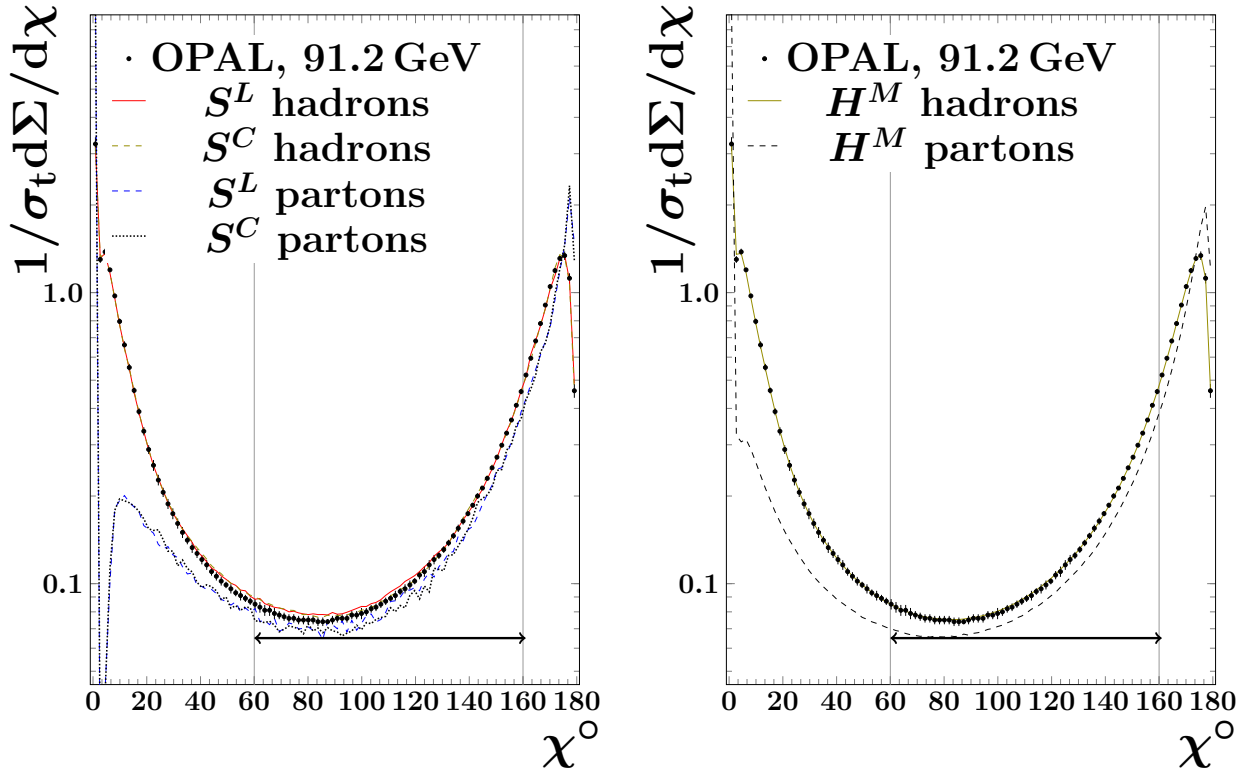


Fig. B.4.2: EEC distributions obtained with the two MC tools at the parton and hadron level at 91.2 GeV, with corresponding OPAL data. Note that for these two plots a different definition of χ was used: this time, the back-to-back region corresponds to $\chi \rightarrow 180^\circ$.

corrections for EEC. To do this, we generated event samples at both the hadron and the parton level and the ratio of these provided the hadron-to-parton ratio or H/P . Using this ratio and multiplying our parton-level predictions bin by bin, we obtained our theoretical prediction at the hadron level. As MC tools, we used `SHERPA2.2.4` [13] and `Herwig7.1.1` [14]. The exact set-up of the MC tools is presented in Ref. [12].

The value for the strong coupling was determined by fitting the predictions to 20 different datasets (for details, see Table 1 of Ref. [12]). For illustrative purposes, Fig. B.4.2 shows the predictions obtained with `SHERPA` and `Herwig` at the parton and hadron level. For `SHERPA`, we used both the Lund (S^L) [3] and cluster (S^C) [2] hadronization models, while in `Herwig` we used the built-in cluster model. The figure also indicates the range used in the actual fitting procedure.

For the fitting, the `MINUIT2` program [15] was used to minimize the quantity:

$$\chi^2(\alpha_S) = \sum_{\text{datasets}} \chi_{\text{dataset}}^2(\alpha_S) \quad (4.2)$$

with the $\chi^2(\alpha_S)^\dagger$ quantity calculated as:

$$\chi^2(\alpha_S) = (\mathbf{D} - \mathbf{P}(\alpha_S))^T \underline{\underline{V}}^{-1} (\mathbf{D} - \mathbf{P}(\alpha_S)), \quad (4.3)$$

where \mathbf{D} is the vector of data points, \mathbf{P} is the vector of predictions as functions of α_S and $\underline{\underline{V}}$ is the covariance matrix.

[†]Not to be confused with the angle χ .

With the fitting procedure performed in the range between 60° and 160° . The resulting strong coupling NNLL+NNLO prediction is

$$\alpha_S(m_Z) = 0.117\,50 \pm 0.002\,87 \quad (4.4)$$

and at NNLL+NLO accuracy is

$$\alpha_S(m_Z) = 0.122\,00 \pm 0.005\,35. \quad (4.5)$$

Notice the reduction in uncertainty as we go from NNLL+NLO to NNLL+NNLO.

4.3 Precision through small power corrections

As outlined in the introduction, the current methods of taking the effect of non-perturbative contributions into account can raise concerns, mainly because only phenomenological models are present for them. The other big concern is that these models rely on experimental results through tuned parameters. The best option, without any model derived from first principles, is to decrease these effects as much as possible. The idea is simple: if the non-perturbative contribution can be shrunk, its large uncertainties will make a smaller contribution to the final uncertainty of the extracted value of the strong coupling.

In this section, we focus on altering the definitions of existing observables to decrease the non-perturbative corrections. The most basic and most used observables in electron–positron collisions are the thrust (T) and the various jet masses. In their original definitions, these all incorporate all registered hadronic objects of the event or a given, well-defined region. Hence, a natural way to modify them is to filter the tracks contributing to their value in an event. One possible way to remove tracks is by means of grooming [16–21]. In particular, the soft drop [21] is a grooming when a part of the soft content of the event is removed according to some criteria.

In Ref. [22], soft-drop variants were defined for thrust, $\tau'_{\text{SD}} = 1 - T'_{\text{SD}}$, hemisphere jet mass, $e_2^{(2)}$ and narrow jet mass, ρ . As showed in that paper, the non-perturbative corrections can be drastically decreased if soft drop is applied. The effect of soft drop turns out to be the most significant in the peak region of the distributions, where the contribution from all-order resummation and non-perturbative effects is the greatest. This makes these observables promising candidates for strong coupling measurements at a future electron–positron collider. The application of these observables—although very interesting—is limited at LEP measurements, owing to the limited amount of data taken and because the soft-drop procedure inherently results in a decrease of cross-section.

In our recent paper [23], we analysed the proposed observables from the standpoint of perturbative behaviour by calculating the NNLO QCD corrections to the observables and analysing their dependence on the non-physical renormalization scale as an indicator of the size of neglected higher-order terms. The soft-drop versions of the observables listed have two parameters related to soft drop: z_c and β [22]. This allows for optimisation in order to minimize the decrease in cross-section when the soft-drop procedure is applied.

Figure B.4.3 shows the soft-dropped thrust distribution in the first three orders of QCD perturbation theory for a specific choice of the two soft-drop related parameters. On the right-hand side of the figure, the K factors are depicted for various parameter choices to illustrate the stability of the result. We found that the most stable perturbation prediction and moderate drop in cross-section can be achieved when $(z_c, \beta) = (0.1, 0)$.

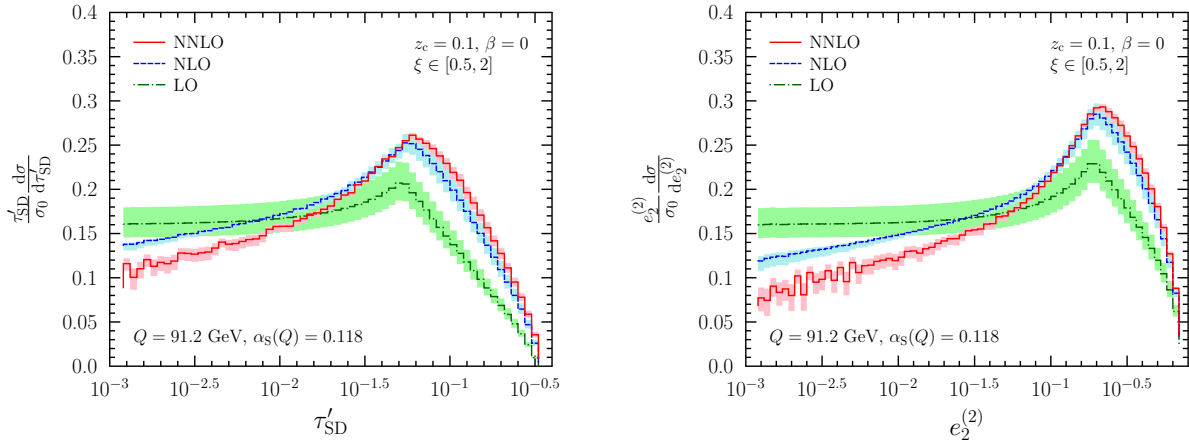


Fig. B.4.3: Left: Soft-dropped thrust distribution at the Z peak in the first three orders of perturbation theory; the bands represent the uncertainty coming from the variation of the renormalization scale between $Q/2$ and $2Q$. Right: The K factors for the soft-dropped thrust distribution for various choices of the soft-drop parameters.

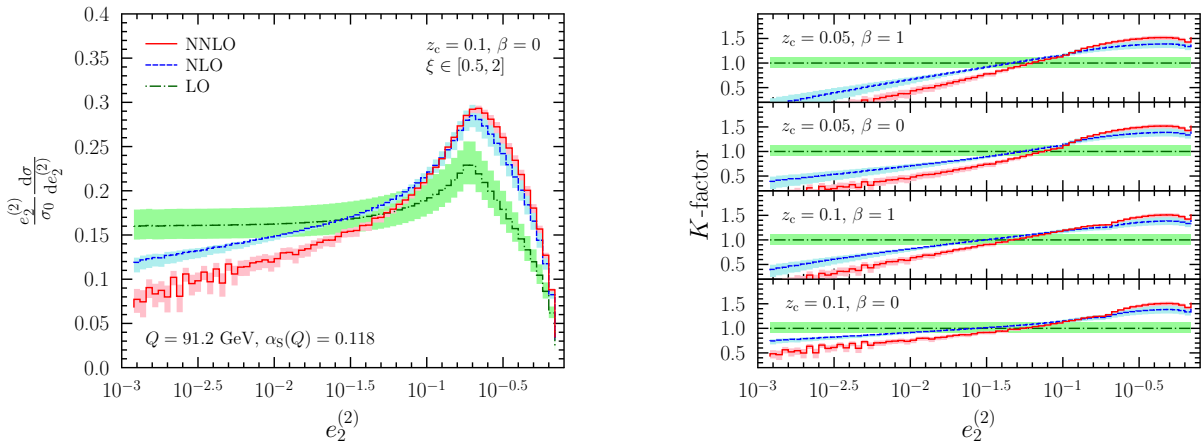


Fig. B.4.4: The same as Fig. B.4.3 but for the hemisphere jet mass

Figure B.4.4 depicts the soft-dropped hemisphere jet mass in exactly the same way as the soft-dropped thrust shown in Fig. B.4.3. In this case, it can be seen once more that the perturbative behaviour stabilizes on going to higher orders in perturbation theory. This is most pronounced at the left-hand side of the peak, where the NLO and NNLO predictions coincide. For this observable, we found that the best choice for the soft-drop parameters is also $(z_c, \beta) = (0.1, 0)$. For the traditional versions of these observables, the peak region is the one where the all-order resummed results and non-perturbative corrections must have agreement with the experiment, but for the soft-dropped versions neither the higher-order contributions nor the non-perturbative corrections are drastic. The minimal role of higher orders in perturbation theory can be seen from the perturbative stability of our results, while the small size of non-perturbative corrections has been shown in Ref. [22]. These properties make the soft-dropped event shapes attractive observables for the extraction of the strong coupling.

4.4 Conclusions

A future electron–positron collider would be considered a dream machine for many reasons. A machine of this type would allow for a precise tuning of collision energy; it would have no annoying underlying event and it would have coloured partons in the initial state. Several possible measurements could be envisioned at such a machine but from the QCD point of view, determination of the strong coupling stands out. The strong coupling is a fundamental parameter of the Standard Model of particle physics, so knowing its value is of key importance.

In this report, we showed two possible ways to conduct such a measurement. First, it can be achieved by including higher-order corrections in the theoretical prediction and comparing this with the experimental result modelling non-perturbative effects with modern MC tools. Second, we showed modified versions of well-known observables defined in electron–positron collisions where non-perturbative corrections can be minimized, hence diminishing the effects of their uncertainties on theoretical predictions. These observables seem to be promising candidates, not just for strong coupling measurements but also for the purpose of testing the Standard Model further. Thus, they should be seriously considered as important measurements at a future electron–positron facility.

Acknowledgements

A.K. is grateful to the organisers of the CERN FCC-ee 2019 workshop for the invitation to give a talk about recent advancements in QCD related to e^+e^- colliders and for the warm atmosphere they created.

References

- [1] S. Bethke, *Nucl. Part. Phys. Proc.* **282–284** (2017) 149. [doi:10.1016/j.nuclphysbps.2016.12.028](https://doi.org/10.1016/j.nuclphysbps.2016.12.028)
- [2] B.R. Webber, *Nucl. Phys.* **B238** (1984) 492. [doi:10.1016/0550-3213\(84\)90333-X](https://doi.org/10.1016/0550-3213(84)90333-X)
- [3] B. Andersson *et al.*, *Phys. Rep.* **97** (1983) 31. [doi:10.1016/0370-1573\(83\)90080-7](https://doi.org/10.1016/0370-1573(83)90080-7)
- [4] Y.L. Dokshitzer *et al.*, *JHEP* **07** (1999) 012. [arXiv:hep-ph/9905339](https://arxiv.org/abs/hep-ph/9905339), [doi:10.1088/1126-6708/1999/07/012](https://doi.org/10.1088/1126-6708/1999/07/012)
- [5] Z. Tulipánt *et al.*, *Eur. Phys. J.* **C77** (2017) 749. [arXiv:1708.04093](https://arxiv.org/abs/1708.04093), [doi:10.1140/epjc/s10052-017-5320-9](https://doi.org/10.1140/epjc/s10052-017-5320-9)
- [6] G. Somogyi *et al.*, *JHEP* **01** (2007) 070. [arXiv:hep-ph/0609042](https://arxiv.org/abs/hep-ph/0609042), [doi:10.1088/1126-6708/2007/01/070](https://doi.org/10.1088/1126-6708/2007/01/070)
- [7] G. Somogyi and Z. Trócsányi, *JHEP* **01** (2007) 052. [arXiv:hep-ph/0609043](https://arxiv.org/abs/hep-ph/0609043), [doi:10.1088/1126-6708/2007/01/052](https://doi.org/10.1088/1126-6708/2007/01/052)
- [8] V. Del Duca *et al.*, *Phys. Rev.* **D94** (2016) 074019. [arXiv:1606.03453](https://arxiv.org/abs/1606.03453), [doi:10.1103/PhysRevD.94.074019](https://doi.org/10.1103/PhysRevD.94.074019)
- [9] V. Del Duca *et al.*, *Phys. Rev. Lett.* **117** (2016) 152004. [arXiv:1603.08927](https://arxiv.org/abs/1603.08927), [doi:10.1103/PhysRevLett.117.152004](https://doi.org/10.1103/PhysRevLett.117.152004)
- [10] D. de Florian and M. Grazzini, *Nucl. Phys.* **B704** (2005) 387. [arXiv:hep-ph/0407241](https://arxiv.org/abs/hep-ph/0407241), [doi:10.1016/j.nuclphysb.2004.10.051](https://doi.org/10.1016/j.nuclphysb.2004.10.051)
- [11] P.D. Acton *et al.*, *Z. Phys.* **C59** (1993) 1. [doi:10.1007/BF01555834](https://doi.org/10.1007/BF01555834)

- [12] A. Kardos *et al.*, *Eur. Phys. J.* **C78** (2018) 498. [arXiv:1804.09146](#),
[doi:10.1140/epjc/s10052-018-5963-1](#)
- [13] T. Gleisberg *et al.*, *JHEP* **02** (2009) 007. [arXiv:0811.4622](#),
[doi:10.1088/1126-6708/2009/02/007](#)
- [14] J. Bellm *et al.*, *Eur. Phys. J.* **C76** (2016) 196. [arXiv:1512.01178](#),
[doi:10.1140/epjc/s10052-016-4018-8](#)
- [15] F. James and M. Roos, *Comput. Phys. Commun.* **10** (1975) 343.
[doi:10.1016/0010-4655\(75\)90039-9](#)
- [16] J.M. Butterworth *et al.*, *Phys. Rev. Lett.* **100** (2008) 242001. [arXiv:0802.2470](#),
[doi:10.1103/PhysRevLett.100.242001](#)
- [17] D. Krohn *et al.*, *JHEP* **02** (2010) 084. [arXiv:0912.1342](#),
[doi:10.1007/JHEP02\(2010\)084](#)
- [18] S.D. Ellis *et al.*, *Phys. Rev.* **D81** (2010) 094023. [arXiv:0912.0033](#),
[doi:10.1103/PhysRevD.81.094023](#)
- [19] S.D. Ellis *et al.*, *Phys. Rev.* **D80** (2009) 051501. [arXiv:0903.5081](#),
[doi:10.1103/PhysRevD.80.051501](#)
- [20] M. Dasgupta *et al.*, *JHEP* **09** (2013) 029. [arXiv:1307.0007](#),
[doi:10.1007/JHEP09\(2013\)029](#)
- [21] A.J. Larkoski *et al.*, *JHEP* **05** (2014) 146. [arXiv:1402.2657](#),
[doi:10.1007/JHEP05\(2014\)146](#)
- [22] J. Baron *et al.*, *JHEP* **08** (2018) 105. [arXiv:1803.04719](#),
[doi:10.1007/JHEP08\(2018\)105](#)
- [23] A. Kardos *et al.*, *Phys. Lett.* **B786** (2018) 313. [arXiv:1807.11472](#),
[doi:10.1016/j.physletb.2018.10.014](#)

5 Theoretical luminosity precision for the FCC-ee: overview of the path to 0.01%

Contribution* by: B.F.L. Ward, S. Jadach, W. Płaczek, M. Skrzypek, S.A. Yost
Corresponding author: B.F.L. Ward [BFL_Ward@baylor.edu]

We present an overview of the pathways to the required theoretical precision for the luminosity targeted by the FCC-ee precision studies. We put the discussion in context with a brief review of the situation at the time of the LEP. We then present the current status and an overview of routes to the desired 0.01% targeted by the FCC-ee (as well as by the ILC).

We use the situation that existed at the end of the LEP as our starting point. At the end of the LEP, the error budget for the BHLUMI4.04 MC used by all LEP collaborations to simulate the luminosity process was that calculated in Ref. [1]. For reference, we reproduce this result here in Table B.5.1. In this table, we show the published works on which the various error estimates are based, as discussed in Ref. [1].

Table B.5.1: Summary of the total (physical + technical) theoretical uncertainty for a typical calorimetric detector. For LEP1, this estimate is valid for a generic angular range of 1° – 3° (18–52 mrad), and for LEP2 it is valid for energies up to 176 GeV and an angular range of 3° – 6° . Total uncertainty is taken in quadrature. Technical precision is included in (a).

Type of correction or error	LEP1		LEP2	
	1996 (%)	1999 (%)	1996 (%)	1999 (%)
(a) Missing photonic $\mathcal{O}(\alpha^2)$ [2, 3]	0.10	0.027	0.20	0.04
(b) Missing photonic $\mathcal{O}(\alpha^3 L_e^3)$ [4]	0.015	0.015	0.03	0.03
(c) Vacuum polarisation [5, 6]	0.04	0.04	0.10	0.10
(d) Light pairs [7, 8]	0.03	0.03	0.05	0.05
(e) Z and s-channel γ [9, 10]	0.015	0.015	0.0	0.0
Total	0.11 [10]	0.061 [1]	0.25 [10]	0.12 [1]

One way to address the 0.01% precision tag needed for the luminosity theory error for the FCC-ee is to develop the corresponding improved version of the BHLUMI. This problem is addressed in Ref. [11], wherein the path to 0.01% theory precision for the FCC-ee luminosity is presented in some detail. The results of this latter reference are shown in Table B.5.2, wherein we also present the current state of the art for completeness, as discussed in more detail in Ref. [11].

The key steps in arriving at Table B.5.2 are as follows. The errors associated with the photonic corrections in lines (a) and (b) in the LEP results in Table B.5.1 are due to effects that are known from Refs. [2–4] but were not implemented into BHLUMI. In Table B.5.2, we show what these errors will become after these known results are included in BHLUMI, as discussed in

*This contribution should be cited as:

B.F.L. Ward, S. Jadach, W. Płaczek, M. Skrzypek, S.A. Yost, Theoretical luminosity precision for the FCC-ee: overview of the path to 0.01%, DOI: [10.23731/CYRM-2020-003.65](https://doi.org/10.23731/CYRM-2020-003.65), in: Theory for the FCC-ee, Eds. A. Blondel, J. Gluza, S. Jadach, P. Janot and T. Riemann, CERN Yellow Reports: Monographs, CERN-2020-003, DOI: [10.23731/CYRM-2020-003](https://doi.org/10.23731/CYRM-2020-003), p. 65.
 © CERN, 2020. Published by CERN under the [Creative Commons Attribution 4.0 license](https://creativecommons.org/licenses/by/4.0/).

Table B.5.2: Anticipated total (physical + technical) theoretical uncertainty for a FCC-ee luminosity calorimetric detector with angular range 64–86 mrad (narrow), near the Z peak. Description of photonic corrections in square brackets is related to the second column. The total error is summed in quadrature.

Type of correction or error	Update 2018 (%)	FCC-ee forecast
(a) Photonic [$\mathcal{O}(L_e\alpha^2)$] $\mathcal{O}(L_e^2\alpha^3)$	0.027	0.1×10^{-4}
(b) Photonic [$\mathcal{O}(L_e^3\alpha^3)$] $\mathcal{O}(L_e^4\alpha^4)$	0.015	0.6×10^{-5}
(c) Vacuum polarisation	0.014 [12]	0.6×10^{-4}
(d) Light pairs	0.010 [13, 14]	0.5×10^{-4}
(e) Z and s-channel γ exchange	0.090 [9]	0.1×10^{-4}
(f) Up–down interference	0.009 [15]	0.1×10^{-4}
(f) Technical precision	(0.027)	0.1×10^{-4}
Total	0.097	1.0×10^{-4}

Ref. [11]. Similarly, in line (c) of Table B.5.1, the error is due to the uncertainty at the time of LEP on the hadronic contribution to the vacuum polarisation for the photon at the respective momentum transfers for the luminosity process; in Table B.5.2, we show the improvement of this error that is expected for the FCC-ee, as discussed in Refs. [12, 16].

Continuing in this way, in line (d) in Table B.5.2, we show the expected improvement [11], with reference to the LEP time for Table B.5.1, in the light pairs error for the FCC-ee. As explained in Ref. [11], the complete matrix element for the additional real e^+e^- pair radiation should be used, because non-photonic graphs can contribute as much as 0.01% for the cut-off, $z_{\text{cut}} \sim 0.7$. This can be done with the MC generators developed for the $e^+e^- \rightarrow 4f$ processes for LEP2 physics—see Ref. [11] for further discussion. With known methods [11], the contributions of light quark pairs, muon pairs, and non-leading, non-soft additional $e^+e^- + n\gamma$ corrections can be controlled such that the error on the pairs contribution is as given in line (d) for the FCC-ee. As noted, we also show the current state of the art [11] for this error in line (d) of Table B.5.2.

Turning to line (e) in Table B.5.2, we show the improvement of the error for the Z and s-channel γ exchange for the FCC-ee as well as its current state of the art. In Ref. [11], a detailed discussion is presented of all of the six interference and three additional squared modulus terms that result from the s-channel γ , s-channel Z, and t-channel Z exchange contributions to the amplitude for the luminosity process. It is shown that, if the predictions of BHLUMI for the luminosity measurement at FCC-ee are combined with those from Bhwide [17] for this Z and s-channel γ exchange contribution, then the error in the second column of line (e) of Table B.5.2 could be reduced to 0.01%. To reduce the uncertainty of this contribution practically to zero we would include these Z and γ_s exchanges within the CEEX-type matrix element at $\mathcal{O}(\alpha^1)$ in BHLUMI [18]. Here, CEEX stands for coherent exclusive exponentiation, which acts at the level of the amplitudes, as compared with the original Yennie–Frautschi–Suura [19] (YFS) exclusive exponentiation (EEX), which is used in BHLUMI4.04 and which acts at the level of the squared amplitudes. It is expected to be enough to add the EW corrections to the large angle Bhabha (LABH) process in the form of effective couplings in the Born amplitudes. This leads to the error estimate shown in Table B.5.2 in line (e) for the FCC-ee.

For completeness, we note that for our discussion of the Z- and s-channel γ exchanges we made [11] a numerical study using Bhwide for the the calorimetric LCAL-type detector,

Table B.5.3: Results from **Bhwide** for the Z and γ_s exchange contributions to the FCC-ee luminosity with respect to the $\gamma_t \otimes \gamma_t$ process for the calorimetric LCAL-type detector [20] with the symmetric angular range 64–86 mrad; no acoplanarity cut was applied. MC errors are marked in brackets.

E_{CM} (GeV)	Δ_{tot} (%)	$\delta_{\mathcal{O}(\alpha)}^{\text{QED}}$ (%)	$\delta_{\text{h.o.}}^{\text{QED}}$ (%)	$\delta_{\text{tot}}^{\text{weak}}$ (%)
90.1876	+0.642 (12)	-0.152 (59)	+0.034 (38)	-0.005 (12)
91.1876	+0.041 (11)	+0.148 (59)	-0.035 (38)	+0.009 (12)
92.1876	-0.719 (13)	+0.348 (59)	-0.081 (38)	+0.039 (13)

as described in Ref. [20], for the symmetric angular range 64–86 mrad without any cut in acoplanarity. The pure weak corrections were calculated with the **ALIBABA** EW library [21, 22]. The results, shown in Table B.5.3, were obtained for three values of the centre-of-mass (CM) energy: $E_{\text{CM}} = M_Z$, $M_Z \pm 1$ GeV, where the latter two values have Z contributions that are close to maximal in size. The results in the second column for the total size of the Z and γ_s exchanges are consistent with our expectations, as explained in Ref. [11]: the contribution is positive below the Z peak, where it reaches a size $\sim 0.64\%$, is close to zero near the peak, and changes sign above the peak, where it reaches a size $\sim -0.72\%$. The third column features the fixed-order (non-exponentiated) $\mathcal{O}(\alpha)$ QED correction and shows that it is sizeable and up to a half of the size of the Born level effect, with a sign that is opposite to that of the latter effect. The fourth column shows the size of the higher-order QED effects from YFS exponentiation, which also change their sign near the Z peak, in opposition to the corresponding change of the $\mathcal{O}(\alpha)$ corrections. We see that the size of the former effects is about a quarter of that of the latter. The effects in the fourth column allow us to make a conservative estimate of the size of the missing higher-order QED effects in **Bhwide** using the big log factor $\gamma = \alpha \ln(|\vec{t}|/m_e^2)/\pi = 0.042$ from Section 4 of Ref. [11] and the safety factor of 2 from Ref. [9], together with the largest higher-order effect in Table B.5.3, 0.081%, as $0.081\% \times \gamma \times 2 \simeq 0.007\%$. The last column shows that the size of the pure weak corrections, as implemented within the $\mathcal{O}(\alpha)$ YFS exponentiation scheme, is at a level of 0.01% below and at M_Z and increases up to $\sim 0.04\%$ above M_Z . We may use the same factor as we did for the higher-order corrections to estimate the size of the missing higher-order pure weak corrections in **Bhwide** as $\sim 0.003\%$. Altogether, by adding the two estimates of its massing effects, we obtain a conservative estimate of 0.01% for the physical precision of **Bhwide** to justify our remarks concerning the error in line (e) of Table B.5.2 that would result from the combination of the prediction of **BHLUMI** and that of **Bhwide** for this contribution.

In line (f) in Table B.5.2, we show the estimate of the error in the up–down interference between radiation from the e^- and e^+ lines. Unlike in LEP1, where it was negligible, for the FCC-ee, this effect, calculated in Ref. [15] at $\mathcal{O}(\alpha^1)$, is ten times larger and must be included in the upgraded **BHLUMI**. Once this is done, the error estimate shown in line (f) for the FCC-ee is obtained [11].

This brings us to the issue of the technical precision. In an ideal situation, to get the upgraded **BHLUMI**'s technical precision at a level of 10^{-5} for the total cross-section and 10^{-4} for single differential distributions, one would need to compare it with another MC program developed independently, which properly implements the soft-photon resummation, LO corrections up to $\mathcal{O}(\alpha^3 L_e^3)$, and the second-order corrections with the complete $\mathcal{O}(\alpha^2 L_e)$. In principle, an

extension of a program like *BabaYaga* [23–25], which is currently exact at NLO with a matched QED shower, to the level of NNLO for the hard process, while keeping the correct soft-photon resummation, would provide the best comparison with the upgraded *BHLUMI* to establish the technical precision of both programs at the 10^{-5} precision level.[†] During the intervening time period, a very good test of the technical precision of the upgraded *BHLUMI* would follow from the comparison of its results with EEX and CEEEX matrix elements; the basic multiphoton phase space integration module of *BHLUMI* was already well tested in Ref. [27] and such a test can be repeated at an even higher precision level.

In summary, we conclude that, with the appropriate resources, the path to 0.01% precision for the FCC-ee luminosity (and the ILC luminosity) at the Z peak is open via an upgraded version of *BHLUMI*.

References

- [1] B.F.L. Ward *et al.*, *Phys. Lett.* **B450** (1999) 262. [arXiv:hep-ph/9811245](#), [doi:10.1016/S0370-2693\(99\)00104-5](#)
- [2] S. Jadach *et al.*, *Phys. Lett.* **B377** (1996) 168. [arXiv:hep-ph/9603248](#), [doi:10.1016/0370-2693\(96\)00354-1](#)
- [3] S. Jadach *et al.*, *Acta Phys. Pol.* **B30** (1999) 1745. <https://inspirehep.net/record/507675>
- [4] S. Jadach *et al.*, *Phys. Lett.* **B389** (1996) 129. [doi:10.1016/S0370-2693\(96\)01242-7](#)
- [5] H. Burkhardt and B. Pietrzyk, *Phys. Lett.* **B356** (1995) 398. [doi:10.1016/0370-2693\(95\)00820-B](#)
- [6] S. Eidelman and F. Jegerlehner, *Z. Phys.* **C67** (1995) 585. [arXiv:hep-ph/9502298](#), [doi:10.1007/BF01553984](#)
- [7] S. Jadach *et al.*, *Phys. Rev.* **D47** (1993) 3733. [doi:10.1103/PhysRevD.47.3733](#)
- [8] S. Jadach *et al.*, *Phys. Rev.* **D55** (1997) 1206. [doi:10.1103/PhysRevD.55.1206](#)
- [9] S. Jadach *et al.*, *Phys. Lett.* **B353** (1995) 349. [doi:10.1016/0370-2693\(95\)00576-7](#)
- [10] A. Arbuzov *et al.*, *Phys. Lett.* **B383** (1996) 238. [arXiv:hep-ph/9605239](#), [doi:10.1016/0370-2693\(96\)00733-2](#)
- [11] S. Jadach *et al.*, *Phys. Lett.* **B790** (2019) 314. [arXiv:1812.01004](#), [doi:10.1016/j.physletb.2019.01.012](#)
- [12] F. Jegerlehner, $\alpha_{\text{QED}}(M_Z)$ and future prospects with low energy e^+e^- collider data, FCC-ee Mini-Workshop: Physics Behind Precision, <https://indico.cern.ch/event/469561/>
- [13] G. Montagna *et al.*, *Nucl. Phys.* **B547** (1999) 39. [arXiv:hep-ph/9811436](#), [doi:10.1016/S0550-3213\(99\)00064-4](#)
- [14] G. Montagna *et al.*, *Phys. Lett.* **B459** (1999) 649. [arXiv:hep-ph/9905235](#), [doi:10.1016/S0370-2693\(99\)00729-7](#)
- [15] S. Jadach *et al.*, *Phys. Lett.* **B253** (1991) 469. [doi:10.1016/0370-2693\(91\)91754-J](#)
- [16] F. Jegerlehner, *EPJ Web Conf.* **218** (2019), 01003. [arXiv:1711.06089](#) [doi:10.1051/epjconf/201921801003](#)

[†]The upgrade of the *BHLUMI* distributions will be relatively straightforward because its multiphoton phase space is exact [26] for any number of photons.

- [17] S. Jadach *et al.*, *Phys. Lett.* **B390** (1997) 298. [arXiv:hep-ph/9608412](#),
[doi:10.1016/S0370-2693\(96\)01382-2](#)
- [18] S. Jadach *et al.*, *Phys. Rev.* **D63** (2001) 113009. [arXiv:hep-ph/0006359](#),
[doi:10.1103/PhysRevD.63.113009](#)
- [19] D.R. Yennie *et al.*, *Ann. Phys.* **13** (1961) 379. [doi:10.1016/0003-4916\(61\)90151-8](#)
- [20] S. Jadach *et al.*, *Phys. Lett.* **B268** (1991) 253. [doi:10.1016/0370-2693\(91\)90813-6](#)
- [21] W. Beenakker *et al.*, *Nucl. Phys.* **B349** (1991) 323. [doi:10.1016/0550-3213\(91\)90328-U](#)
- [22] W. Beenakker *et al.*, *Nucl. Phys.* **B355** (1991) 281. [doi:10.1016/0550-3213\(91\)90114-D](#)
- [23] C.M. Carloni Calame *et al.*, *Nucl. Phys.* **B584** (2000) 459. [arXiv:hep-ph/0003268](#),
[doi:10.1016/S0550-3213\(00\)00356-4](#)
- [24] C.M. Carloni Calame, *Phys. Lett.* **B520** (2001) 16. [arXiv:hep-ph/0103117](#),
[doi:10.1016/S0370-2693\(01\)01108-X](#)
- [25] G. Balossini *et al.*, *Nucl. Phys.* **B758** (2006) 227. [arXiv:hep-ph/0607181](#),
[doi:10.1016/j.nuclphysb.2006.09.022](#)
- [26] S. Jadach *et al.*, *Comput. Phys. Commun.* **130** (2000) 260 [Program source available from
<http://jadach.web.cern.ch/>]. [arXiv:hep-ph/9912214](#)
- [27] S. Jadach and B.F.L. Ward, *Acta Phys. Pol.* **B28** (1997) 1907.
<https://inspirehep.net/record/428472>

6 $e^+e^- \rightarrow \gamma\gamma$ at large angles for FCC-ee luminometry

Contribution* by: C.M. Carloni, M. Chiesa, G. Montagna, O. Nicrosini, F. Piccinini
Corresponding author: C.M. Carloni [carlo.carloni.calame@pv.infn.it]

Abstract

We examine large-angle two-photon production in e^+e^- annihilation as a possible process to monitor the luminosity of the FCC-ee. We review the current status of the theoretical predictions and perform an exploratory phenomenological study of the next-to-leading and higher-order QED corrections using the Monte Carlo event generator `BabaYaga@NLO`. We also consider the one-loop weak corrections, which are necessary to meet the high-precision requirements of the FCC-ee. Possible ways to approach the target theoretical accuracy are sketched.

6.1 Introduction

The successful accomplishment of the FCC-ee physics goals requires a detailed knowledge of the collider luminosity. The ambitious FCC-ee target is a luminosity measurement with a total error of the order of 10^{-4} (or even better) and calls for a major effort by both the experimental and theoretical community.

At the FCC-ee, the standard luminosity process is expected to be small-angle Bhabha scattering, likewise at the LEP. However, the process of large-angle two-photon production, i.e., $e^+e^- \rightarrow \gamma\gamma$, has also been recently proposed as a possible alternative normalization process for FCC-ee operation [1–3]. Actually, this is a purely QED process at leading order at any energy; it receives QED corrections from the initial state only and does not contain at order α the contribution due to the vacuum polarisation (in particular, hadronic loops), which enters at next-to-next-to-leading-order (NNLO) only. Conversely, the cross-section of $e^+e^- \rightarrow \gamma\gamma$ is significantly smaller than that of small-angle Bhabha scattering but adequate everywhere at the FCC-ee, with the exception of the running at the Z resonance. Moreover, the process is affected by a large background, owing to large-angle Bhabha scattering.

In spite of these limitations, the possibility of using photon-pair production as a luminosity process at the FCC-ee is an interesting option to be pursued. Contrarily to Bhabha scattering, which received a lot of attention over the past decades, there is rather scant theoretical literature about $e^+e^- \rightarrow \gamma\gamma$ annihilation and the most recent phenomenological results refer to e^+e^- colliders of moderate energies [4–7]. Moreover, the few available Monte Carlo (MC) generators [5, 7] are tailored for low-energy accelerators and need to be improved for the high-energy, high-precision requirements of the FCC-ee.

In this contribution, we provide a first assessment of the current status of the theoretical accuracy for large-angle two-photon production at FCC-ee energies. For this purpose, we use the MC program `BABAYAGA@NLO` [5, 8–11], which includes next-to-leading-order (NLO) QED corrections matched to a QED parton shower, and compute the one-loop weak corrections

*This contribution should be cited as:

C.M. Carloni, M. Chiesa, G. Montagna, O. Nicrosini, F. Piccinini, $e^+e^- \rightarrow \gamma\gamma$ at large angles for FCC-ee luminometry, DOI: [10.23731/CYRM-2020-003.71](https://doi.org/10.23731/CYRM-2020-003.71), in: Theory for the FCC-ee, Eds. A. Blondel, J. Gluza, S. Jadach, P. Janot and T. Riemann, CERN Yellow Reports: Monographs, CERN-2020-003, DOI: [10.23731/CYRM-2020-003](https://doi.org/10.23731/CYRM-2020-003), p. 71.
 © CERN, 2020. Published by CERN under the [Creative Commons Attribution 4.0 license](https://creativecommons.org/licenses/by/4.0/).

Table B.6.1: Two-photon production cross-section at LO, NLO, and higher-order QED corrections for four FCC-ee c.m. energies. Numbers in parentheses are the relative contributions of NLO and higher-order QED corrections.

\sqrt{s} (GeV)	LO (pb)	NLO (pb)	Higher-order (pb)
91	39.821	41.043 [+3.07%]	40.868(3) [-0.44%]
160	12.881	13.291 [+3.18%]	13.228(1) [-0.49%]
240	5.7250	5.9120 [+3.26%]	5.884(2) [-0.49%]
365	2.4752	2.5582 [+3.35%]	2.5436(2) [-0.59%]

from heavy boson exchange. The QED corrections to $e^+e^- \rightarrow \gamma\gamma$ at order α were previously calculated some time ago [12–14] and NLO electroweak corrections are reported in Refs. [15–17]. A generator based on Ref. [14] was used at LEP for the analysis of photon-pair production at energies above the Z [18]. Here, we perform an exploratory phenomenological study of the QED corrections at NLO and evaluate the impact of higher-order contributions due to multiple photon emission, by considering typical values for the c.m. energies of the FCC-ee. Possible perspectives to achieve the target theoretical accuracy are briefly outlined.

6.2 Theoretical approach and numerical results

According to the theoretical formulation implemented in BABAYAGA@NLO, the photonic corrections are computed using a fully exclusive QED parton shower matched to QED contributions at NLO. The matching of the parton shower ingredients with the NLO QED corrections is realised in such a way that its $O(\alpha)$ expansion reproduces the NLO cross-section, and exponentiation of the leading contributions owing to soft and collinear radiation is preserved, as in a pure parton shower algorithm. Various studies and comparisons with independent calculations [6, 11, 19] showed that this formulation enables a theoretical accuracy at a level of 0.1% (or slightly better) for the calculation of integrated cross-sections.

To meet the high-precision requirements of FCC-ee, we also computed the one-loop weak corrections due to heavy boson exchange. The calculation was performed by treating the ultra-violet divergencies in dimensional regularisation and using the computer program RECOLA [20], which internally adopts the COLLIER [21] library for the evaluation of one-loop scalar and tensor integrals. In our calculation, we used the on-shell renormalization scheme, with complex mass values for the heavy boson masses [22].

In the following, we show a sample of numerical results obtained using the code BABAYAGA@NLO. They refer to four canonical c.m. energy values, which are representative of the expected FCC-ee operation programme (Z pole, WW, ZH, and $t\bar{t}$ thresholds)

$$\sqrt{s} = 91, 160, 240, 365 \text{ GeV} \tag{6.1}$$

To study the effects due to the QED corrections, we consider a simulation set-up, in which we require at least two photons within the angular acceptance $20^\circ \leq \theta_\gamma \leq 160^\circ$ with energy $E_\gamma \geq 0.25 \times \sqrt{s}$. In Table B.6.1, we examine the impact of the QED radiative corrections on the integrated cross-sections, when considering these kinematic cuts.

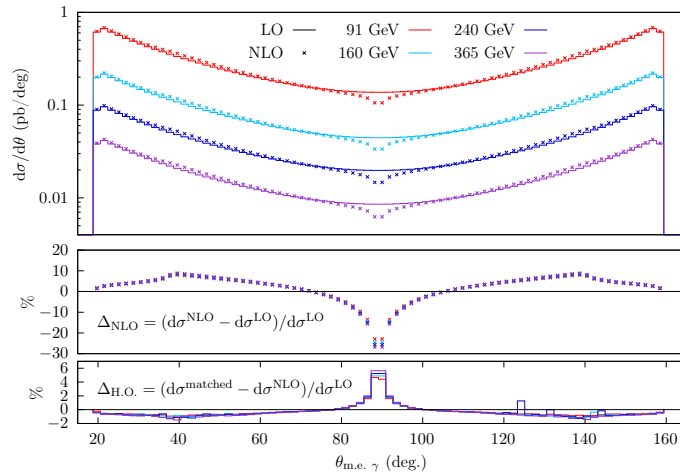


Fig. B.6.1: Top: Angular distribution of the most energetic photon, for four FCC-ee c.m. energies. Bottom: Relative contributions of NLO and higher-order QED corrections.

The photon-pair production cross-section is shown for different accuracy levels, i.e., at LO, NLO QED, and including higher-order contributions due to multiphoton radiation. The numbers in parentheses are the relative contributions due to NLO and higher-order QED corrections, respectively. It can be observed that the NLO corrections are at the level of a few percent, while the higher-order contributions amount to about 5% and reduce the effect due to $O(\alpha)$ corrections.

A representative example of the effects due to QED corrections on the differential cross-sections is given in Fig. B.6.1, which shows the angular distribution of the most energetic photon for the four energy points. One can see that the NLO corrections are particularly important in the central region, where they reach the 20–30% level, being mainly due to soft-photon radiation. This effect is partially compensated for by the higher-order corrections, which amount to some percent in the same region.

We also preliminarily explored the contribution of one-loop weak corrections, to conclude that their size is at the percentage level, i.e., roughly as large as QED contributions beyond NLO. A more detailed investigation of their effects is being made.

6.3 Summary and outlook

We have examined large-angle two-photon production in e^+e^- annihilation as a possible process to monitor the luminosity at the FCC-ee. We have assessed the present status of the theoretical accuracy through an exploratory phenomenological study of the radiative corrections to $e^+e^- \rightarrow \gamma\gamma$ annihilation at the c.m. energies of main interest. To this end, we have improved the theoretical content of the code BABAYAGA@NLO, which includes exact NLO QED corrections matched to parton shower, by computing the weak corrections due to the presence of heavy bosons in the internal loops.

The accuracy of the present calculation can be estimated to be at the 0.1% level or slightly better. A first way to improve it is given by the calculation of NNLO fermion loop contributions, accompanied by the computation of the same-order real pair corrections, along the lines described in Refs. [19, 23]. This should be sufficient to get close to an accuracy at the 10^{-4} level. Beyond that, a full calculation of NNLO QED corrections and, eventually, of

two-loop weak contributions will ultimately be needed to reach the challenging frontier of the 10 ppm theoretical accuracy. These developments are now under consideration.

References

- [1] P. Janot, Determination of $\alpha_{\text{QED}}(M_Z)$ @ FCC-ee, FCC-ee Physics Meeting (CERN, Geneva, Switzerland, 2015), <https://indico.cern.ch/event/401698/contributions/952678/attachments/804695/1102847/alphaQEDFCCee.pdf>
- [2] M. Dam, Luminosity measurements at FCC-ee, FCC Week, Rome, 2016, <https://indico.cern.ch/event/438866/contributions/1085101/attachments1258125/1858155/RomaLumi.pdf>
- [3] C.M.C. Calame, $e^+e^- \rightarrow \gamma\gamma$ at large angle for FCC-ee luminometry, 11th FCC-ee Workshop: Theory and Experiments (CERN, Geneva, Switzerland, 2010), <https://indico.cern.ch/event/766859/contributions/3252694/attachments/1776892/2889350/carloni.pdf>
- [4] A.B. Arbuzov *et al.*, *JHEP* **10** (1997) 001. [arXiv:hep-ph/9702262](https://arxiv.org/abs/hep-ph/9702262), [doi:10.1088/1126-6708/1997/10/001](https://doi.org/10.1088/1126-6708/1997/10/001)
- [5] G. Balossini *et al.*, *Phys. Lett.* **B663** (2008) 209. [arXiv:0801.3360](https://arxiv.org/abs/0801.3360), [doi:10.1016/j.physletb.2008.04.007](https://doi.org/10.1016/j.physletb.2008.04.007)
- [6] S. Actis *et al.*, *Eur. Phys. J.* **C66** (2010) 585. [arXiv:0912.0749](https://arxiv.org/abs/0912.0749), [doi:10.1140/epjc/s10052-010-1251-4](https://doi.org/10.1140/epjc/s10052-010-1251-4)
- [7] S.I. Eidelman *et al.*, *Eur. Phys. J.* **C71** (2011) 1597. [arXiv:1009.3390](https://arxiv.org/abs/1009.3390), [doi:10.1140/epjc/s10052-011-1597-2](https://doi.org/10.1140/epjc/s10052-011-1597-2)
- [8] C.M.C. Calame *et al.*, *Nucl. Phys.* **B584** (2000) 459. [arXiv:hep-ph/0003268](https://arxiv.org/abs/hep-ph/0003268), [doi:10.1016/S0550-3213\(00\)00356-4](https://doi.org/10.1016/S0550-3213(00)00356-4)
- [9] C.M.C. Calame, *Phys. Lett.* **B520** (2001) 16. [arXiv:hep-ph/0103117](https://arxiv.org/abs/hep-ph/0103117), [doi:10.1016/S0370-2693\(01\)01108-X](https://doi.org/10.1016/S0370-2693(01)01108-X)
- [10] C.M.C. Calame *et al.*, *Nucl. Phys. Proc. Suppl.* **131** (2004) 48. [arXiv:hep-ph/0312014](https://arxiv.org/abs/hep-ph/0312014), [doi:10.1016/j.nuclphysbps.2004.02.008](https://doi.org/10.1016/j.nuclphysbps.2004.02.008)
- [11] G. Balossini *et al.*, *Nucl. Phys.* **B758** (2006) 227. [arXiv:hep-ph/0607181](https://arxiv.org/abs/hep-ph/0607181), [doi:10.1016/j.nuclphysb.2006.09.022](https://doi.org/10.1016/j.nuclphysb.2006.09.022)
- [12] F.A. Berends and R. Gastmans, *Nucl. Phys.* **B61** (1973) 414. [doi:10.1016/0550-3213\(73\)90372-6](https://doi.org/10.1016/0550-3213(73)90372-6)
- [13] S.I. Eidelman and E.A. Kuraev, *Nucl. Phys.* **B143** (1978) 353. [doi:10.1016/0550-3213\(78\)90030-5](https://doi.org/10.1016/0550-3213(78)90030-5)
- [14] F.A. Berends and R. Kleiss, *Nucl. Phys.* **B186** (1981) 22. [doi:10.1016/0550-3213\(81\)90090-0](https://doi.org/10.1016/0550-3213(81)90090-0)
- [15] M. Capdequi-Peyranere *et al.*, *Nucl. Phys.* **B149** (1979) 243. [doi:10.1016/0550-3213\(79\)90240-2](https://doi.org/10.1016/0550-3213(79)90240-2)
- [16] M. Böhm and T. Sack, *Z. Phys.* **C33** (1986) 157. [doi:10.1007/BF01410463](https://doi.org/10.1007/BF01410463)
- [17] J. Fujimoto *et al.*, *Prog. Theor. Phys.* **77** (1987) 118. [doi:10.1143/PTP.77.118](https://doi.org/10.1143/PTP.77.118)
- [18] J. Alcaraz *et al.*, A combination of preliminary electroweak measurements and constraints on the Standard Model, [arXiv:hep-ex/0612034](https://arxiv.org/abs/hep-ex/0612034)

- [19] C.C. Calame *et al.*, *J. High Energy P.* **07** (2011) 126. [arXiv:1106.3178](#),
[doi:10.1007/JHEP07\(2011\)126](#)
- [20] S. Actis *et al.*, *Comput. Phys. Commun.* **214** (2017) 140. [arXiv:1605.01090](#),
[doi:10.1016/j.cpc.2017.01.004](#)
- [21] A. Denner *et al.*, *Comput. Phys. Commun.* **212** (2017) 220. [arXiv:1604.06792](#),
[doi:10.1016/j.cpc.2016.10.013](#)
- [22] A. Denner and S. Dittmaier, *Nucl. Phys. Proc. Suppl.* **160** (2006) 22.
[arXiv:hep-ph/0605312](#), [doi:10.1016/j.nuclphysbps.2006.09.025](#)
- [23] G. Montagna *et al.*, *Nucl. Phys.* **B547** (1999) 39. [arXiv:hep-ph/9811436](#),
[doi:10.1016/S0550-3213\(99\)00064-4](#)

7 Prospects for higher-order corrections to W pair production near threshold in the EFT approach

Contribution* by: C. Schwinn [schwinn@physik.rwth-aachen.de]

The precise measurement of the mass of the W boson plays an essential role for precision tests of the Standard Model (SM) and indirect searches for new physics through global fits to electroweak observables. Cross-section measurements near the W pair production threshold at a possible future e^-e^+ collider promise to reduce the experimental uncertainty to the level of 3 MeV at an International Linear Collider (ILC) [1,2], while a high-luminosity circular collider offers a potential improvement to 0.5 MeV in the case of the FCC-ee [3,4] or 1 MeV at the CEPC [5]. At the point of highest sensitivity, an uncertainty in the cross-section measurement of 0.1% translates to an uncertainty of ~ 1.5 MeV on M_W [3]. Therefore, a theoretical prediction for the cross-section with an accuracy of $\Delta\sigma \sim 0.01\%$ at threshold is required to fully exploit the potential of a future circular e^-e^+ collider. Theory predictions using the double-pole approximation (DPA) [6] at next-to-leading order (NLO) [7–11] successfully described LEP2 results with an accuracy of better than 1% above threshold. An extension of the DPA to NNLO appears to be appropriate for a future e^-e^+ collider operating above the W pair threshold, e.g., for the interpretation of anomalous triple-gauge-coupling measurements at $\sqrt{s} = 240$ GeV. However, the accuracy of the DPA at NLO degrades to 2–3% near the threshold. In this region, the combination of a full NLO calculation of four-fermion production [12,13] with leading NNLO effects obtained using effective field theory (EFT) methods [14,15] reduces the theory uncertainty of the total cross-section to below 0.3%; sufficient for the ILC target uncertainty but far above that of the FCC-ee. This raises the question of the methods required to reach a theory accuracy $\sim 0.01\%$. In this contribution, this issue is addressed from the EFT point of view. The discussion is limited to the total cross-section, where the EFT approach is best developed so far, although cuts on the W decay products can also be incorporated [15]. To reach the target accuracy, it will also be essential to have theoretical control of effects beyond the pure electroweak effects considered here. In particular, it is assumed that next-to-leading logarithmic corrections $(\alpha/\pi)^2 \ln(m_e^2/s)$ from collinear initial-state photon radiation (ISR), which have been estimated to be $\lesssim 0.1\%$ [12], will be resummed to all orders. The QCD effects, which are particularly important for the fully hadronic decay modes, are only briefly considered. In Section 7.1, aspects of the EFT approach are reviewed from an updated perspective using insight into the factorisation of soft, hard, and Coulomb corrections [16]. The NLO and leading NNLO results are summarised and compared with the NLO^{ee4f} calculation [12]. In Section 7.2, the structure of the EFT expansion and calculations of subsets of corrections are used to estimate the magnitude of the NNLO and leading N³LO corrections and to determine whether such calculations are sufficient to meet the FCC-ee target accuracy.

*This contribution should be cited as:

C. Schwinn, Prospects for higher-order corrections to W pair production near threshold in the EFT approach, DOI: [10.23731/CYRM-2020-003.77](https://doi.org/10.23731/CYRM-2020-003.77), in: Theory for the FCC-ee, Eds. A. Blondel, J. Gluza, S. Jadach, P. Janot and T. Riemann,

CERN Yellow Reports: Monographs, CERN-2020-003, DOI: [10.23731/CYRM-2020-003](https://doi.org/10.23731/CYRM-2020-003), p. 77.

© CERN, 2020. Published by CERN under the [Creative Commons Attribution 4.0 license](https://creativecommons.org/licenses/by/4.0/).

7.1 Effective theory approach to W pair production

In the EFT approach to four-fermion production near the W pair production threshold [14], the cross-section is expanded simultaneously in the coupling, the W decay width, and the energy relative to the production threshold, which are taken to be of similar order and are denoted collectively by

$$\delta \sim v^2 \equiv \frac{(s - 4M_W^2)}{M_W^2} \sim \frac{\Gamma_W}{M_W} \sim \alpha. \quad (7.1)$$

An NNLO^{EFT} calculation includes corrections up to $\mathcal{O}(\delta^n)$, whereas, as usual, NNLO refers to the $\mathcal{O}(\alpha^n)$ corrections. As discussed in Sections 7.1.1 and 7.1.2, non-resonant and Coulomb corrections lead to odd powers of v , so that the expansion proceeds in half-integer powers of δ . The current state of the art in the EFT is the calculation of the total cross-section for the semi-leptonic final state $\mu^- \bar{\nu}_\mu \bar{u} d$ up to NLO^{EFT} [14], which includes corrections of the order

$$\text{NLO}^{\text{EFT}} : v^2, \alpha, \alpha^2/v^2, \quad (7.2)$$

supplemented with the genuine $\mathcal{O}(\alpha^2, \alpha^3)$ corrections at the next order, $\delta^{3/2}$, in the δ -expansion [15],

$$\text{N}^{3/2}\text{LO}^{\text{EFT}} : \alpha v, \alpha^2/v, \alpha^3/v^3. \quad (7.3)$$

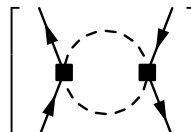
In the following, aspects of these results and the EFT method are reviewed that are useful for the estimate of NNLO^{EFT} corrections and the remaining uncertainty.

7.1.1 Expansion of the Born cross-section

The total cross-section $e^-e^+ \rightarrow 4f$ can be obtained from the imaginary part of the forward-scattering amplitude $e^-e^+ \rightarrow e^-e^+$, where the Cutkosky cuts are restricted to those with four-fermion final states. Flavour-specific final states can be selected accordingly. The expansion of the forward-scattering amplitude in δ can be formulated in terms of an EFT [14, 17, 18], where the initial-state leptons are described by soft-collinear effective theory [19], and the W bosons by a non-relativistic EFT. Similarly to the DPA [6], the cross-section is decomposed into resonant and non-resonant contributions:

$$\sigma^{ee4f}(s \approx 4M_W^2) = \sigma_{\text{res}}(s) + \sigma_{\text{non-res}}(s). \quad (7.4)$$

The EFT method enables computation of the Born cross-section as an expansion according to the counting (Eq. (7.1)), $\sigma_{\text{Born}}^{ee4f} = \sigma_{\text{Born}}^{(0)} + \sigma_{\text{Born}}^{(1/2)} + \dots$. This is not necessary in practice since the full $e^-e^+ \rightarrow 4f$ Born cross-section for arbitrary kinematics can be computed using automated Monte Carlo programs. However, the expansion serves as a test-case of the EFT method and provides useful input for estimating the accuracy of a future NNLO^{EFT} calculation. The leading-order resonant contribution to the cross-section is given by the imaginary part of a one-loop EFT diagram with non-relativistic W propagators, denoted by dashed lines,

$$\sigma_{\text{Born}}^{(0)}(s) = \sigma_{\text{res}}^{(0)}(s) = \frac{1}{s} \text{Im} \left[\text{Diagram} \right] = \frac{\pi \alpha^2}{s_W^4 s} \text{Im} \left[-\sqrt{-\frac{\mathcal{E}_W}{M_W}} \right]. \quad (7.5)$$


Here, the complex energy variable $\mathcal{E}_W \equiv \sqrt{s} - 2M_W + i\Gamma_W \sim M_W v^2$ has been introduced and $s_W = \sin \theta_W$ with the weak mixing angle θ_W . A specific final state is selected by multiplying Eq. (7.5) by the LO branching ratios,

$$\sigma_{f_1 \bar{f}_2 f_3 \bar{f}_4}^{(0)} = \frac{\Gamma_{W^- \rightarrow f_1 \bar{f}_2}^{(0)} \Gamma_{W^+ \rightarrow f_3 \bar{f}_4}^{(0)}}{\Gamma_W^2} \sigma_{\text{res}}^{(0)}. \quad (7.6)$$

The non-resonant contribution to the cross-section arises from local four-electron operators,

$$\sigma_{\text{non-res}}(s) = \frac{1}{s} \text{Im} \left[\text{Diagram} \right] = \frac{\alpha^3}{s_W^6 s} \mathcal{K}, \quad (7.7)$$

where the dimensionless constant $\mathcal{K} = \mathcal{K}^{(0)} + \alpha \mathcal{K}^{(1)}/s_W^2 + \dots$ is computed from the forward-scattering amplitude in the full SM without self-energy resummation in the W propagators. The first contribution is of order α^3 and arises from cut two-loop diagrams corresponding to squared tree diagrams of the $e^-e^+ \rightarrow W^\pm \bar{f}f$ processes. Hence, the leading non-resonant contribution $\sigma_{\text{non-res}}^{(1/2)} \equiv \sigma_{\text{Born}}^{(1/2)}$ is suppressed by $\alpha/v \sim \delta^{1/2}$ compared with the resonant LO cross-section (Eq. (7.5)). For the final state, $\mu^- \bar{\nu}_\mu u \bar{d}$, the explicit result is [14]*

$$\mathcal{K}^{(0)} = -4.25698. \quad (7.8)$$

The $\mathcal{O}(v^2)$ corrections in Eq. (7.2) originate from higher-order terms in the EFT expansion of the resonant Born cross-section, $\sigma_{\text{Born}}^{(1)}$, and depend strongly on the centre-of-mass energy [14],

$$\sigma_{\text{Born}}^{(1)}(\sqrt{s} = 161 \text{ GeV}) = 8\% \times \sigma_{\text{Born}}^{\text{ee4f}}, \quad \sigma_{\text{Born}}^{(1)}(\sqrt{s} = 170 \text{ GeV}) = -8\% \times \sigma_{\text{Born}}^{\text{ee4f}}. \quad (7.9)$$

7.1.2 Radiative corrections

Including radiative corrections, the resonant cross-section factorises into hard, soft, and Coulomb functions [16]. (This formula holds for the leading term in the expansion in v . Subleading terms result in a sum over Wilson coefficients and Green functions related to higher partial waves. In higher orders, there are also soft corrections to the Coulomb function analogous to ultrasoft QCD corrections in $t\bar{t}$ production [20].)

$$\sigma_{\text{res}}(s) = \text{Im} \left[\text{Diagram} \right] = \frac{4\pi^2 \alpha^2}{s M_W^2 s_W^4} \text{Im} \left[C^2 \int d\omega W(\omega) G_C(0, 0, \mathcal{E}_W - \omega) \right]. \quad (7.10)$$

Here, curly lines depict soft photons with momenta $(q^0, \vec{q}) \sim (\delta, \delta)$, while dotted lines denote potential (Coulomb) photons with $(q^0, \vec{q}) \sim (\delta, \sqrt{\delta})$. The Wilson coefficient $C = 1 + \alpha C^{(1)}/2\pi \dots$ is related to contributions of hard loop momenta $q \sim M_W$ to the on-shell amplitudes $e^-e^+ \rightarrow W^-W^+$ evaluated at the production threshold. For the input parameters used in Ref. [14], the explicit value of the one-loop coefficient is

$$C^{(1)} = \text{Re } c_{p,\text{LR}}^{(1,\text{fin})} = -10.076. \quad (7.11)$$

The function $W(\omega)$ includes soft-photon effects, which decouple from the W bosons [21, 22] for the total cross-section, since soft radiation is only sensitive to the total (i.e., vanishing) electric charge of the produced system. This function is the QED analogue of the soft function for Drell–Yan production near the partonic threshold [23, 24]. The leading Coulomb Green function at the origin,

$$G_C^{(0)}(0, 0; \mathcal{E}_W) = -\frac{M_W^2}{4\pi} \left\{ \sqrt{-\frac{\mathcal{E}_W}{M_W}} + \frac{\alpha}{2} \ln \left(-\frac{\mathcal{E}_W}{M_W} \right) - \frac{\alpha^2 \pi^2}{12} \sqrt{-\frac{M_W}{\mathcal{E}_W}} + \alpha^3 \frac{\zeta(3)}{4} \frac{M_W}{\mathcal{E}_W} + \dots \right\}, \quad (7.12)$$

*Equation (7.8) is obtained by setting $s = 4M_W^2$ in Eq. (37) in Ref. [14], where an additional s -dependence of \mathcal{K} has been kept.

sums Coulomb exchange and is known to all orders (see, e.g., Ref. [14]). At each order, the Coulomb corrections $\sim(\alpha/v)^n \sim \delta^{n/2}$ are parametrically enhanced over the remaining $\mathcal{O}(\alpha^n)$ corrections but do not have to be resummed to all orders, owing to the screening of the Coulomb singularity by Γ_W [25]. The convolution of the soft and Coulomb functions results in logarithms of $\mathcal{E}_W \sim M_W v^2$, which can be resummed in analogy to threshold resummation at hadron colliders [24, 26, 27]. However, for QED corrections, $\alpha \log v$ is not enhanced, so this resummation is formally not necessary.[†] Higher-order corrections to the non-resonant cross-section (Eq. (7.7)) only arise through hard corrections to \mathcal{K} , while loop corrections in the EFT vanish.

These ingredients provide results for massless initial-state electrons and could be used, in analogy to QCD predictions at hadron colliders, to define appropriate ‘partonic’ cross-sections that are convoluted with corresponding electron structure functions resumming large mass logarithms. Structure functions in such a scheme are known up to NNLO [29]. In the NLO^{EFT} calculation of Ref. [14], however, electron mass effects have been treated by including collinear corrections and matching to the commonly used resummed structure functions [30] by subtracting double-counting contributions.[‡]

A useful result [15] for computing a class of higher-order effects of the form α^{n+1}/v^n is obtained from Eq. (7.10) by combining the all-order Coulomb Green function with one-loop hard and soft corrections and matching to ISR structure functions, as in the NLO^{EFT} calculation:

$$\Delta\sigma^{\text{C}\times[\text{S+H}]_1}(s) = \frac{4\pi^2\alpha^2}{sM_W^2s_W^4} \frac{\alpha}{\pi} \left\{ \left(\frac{7}{2} + \frac{\pi^2}{4} + C^{(1)} \right) \text{Im} G_C(0, 0; \mathcal{E}_W) \right\}. \quad (7.13)$$

Corrections of the same order, α^{n+1}/v^n , result from the NLO Green function [31] $G_C^{(1)}$, which includes the $\mathcal{O}(\alpha)$ correction to the Coulomb potential. In the G_μ input parameter scheme, the $\mathcal{O}(\alpha^2/v)$ correction reads [15]

$$\Delta G_C^{(1)}(0, 0, \mathcal{E}_W) = -\frac{M_W^2}{4\pi} \frac{\alpha^2}{8\pi} \ln\left(-\frac{\mathcal{E}_W}{M_W}\right) \left\{ -\frac{\beta_0}{2} \left[\ln\left(-\frac{\mathcal{E}_W}{M_W}\right) \right] + \Delta_{G_\mu} \right\} + \mathcal{O}(\alpha^3) \quad (7.14)$$

with the QED beta function with five quark flavours, $\beta_0 = -4(\sum_{f \neq t} N_{C_f} Q_f^2)/3 = -80/9$, and where the scheme-dependent constant $\Delta_{G_\mu} = 61.634$ is related to the quantity

$$\delta_{\alpha(M_Z) \rightarrow G_\mu} = \frac{\alpha}{4\pi} \left(\Delta_{G_\mu} + 2\beta_0 \ln\left(\frac{2M_W}{M_Z}\right) \right)$$

used in Ref. [15]. Equations (7.13) and (7.14) are the basis for computing examples of leading N³LO corrections in Section 7.2.

7.1.3 NLO^{EFT} result

The genuine radiative corrections at NLO^{EFT} can be obtained by expanding Eq. (7.13) to $\mathcal{O}(\alpha)$ relative to the leading order and adding the second-order Coulomb correction from Eq. (7.12).

[†]An initial study obtained NLL effects of 0.1% [28], so the relevance for the FCC-ee may have to be revisited.

[‡]In the process of finalizing this report, we have noted that NLL contributions arising from the combination of numerator factors of m_e and integrals with negative powers of m_e have been inadvertently omitted in the computation of the collinear corrections. The expressions and numerical predictions in this report are preliminary results including the missing contributions. A more complete discussion will be given elsewhere.

A specific four-fermion final state is selected by multiplying the NLO correction with the LO branching ratios (Eq. (7.6)) and adding NLO decay corrections,

$$\Delta\sigma_{\text{decay}}^{(1)} = \left(\frac{\Gamma_{f_1\bar{f}_2}^{(1,\text{ew})}}{\Gamma_{f_1\bar{f}_2}^{(0)}} + \frac{\Gamma_{f_3\bar{f}_4}^{(1,\text{ew})}}{\Gamma_{f_3\bar{f}_4}^{(0)}} \right) \sigma_{\text{res}}^{(0)}, \quad (7.15)$$

with the one-loop electroweak corrections to the partial decay widths, $\Gamma_{f_i\bar{f}_j}^{(1,\text{ew})}$. For hadronic decay modes, QCD corrections to the partial decay widths must also be included up to NNLO, using the counting $\alpha_s^2 \sim \alpha$. In Table B.7.1, the $\mathcal{O}(\alpha)$ -contributions of the NLO^{EFT} result are compared with the NLO^{ee4f} calculation in the full SM [12].[§] The differences are of the order

$$\Delta\sigma_{4f}^{(1)}(s) \equiv \sigma_{\text{NLO}}^{\text{ee4f}}(s) - \sigma_{\text{EFT}}^{(1)}(s) = \sigma_{\text{Born}}^{\text{ee4f}}(s) \times (0.7 - 0.1)\% \quad (7.16)$$

for $\sqrt{s} = 161\text{--}170$ GeV. Near the threshold, the dominant source of this discrepancy is expected to be the $\mathcal{O}(\delta^{3/2})$ contribution from the $\mathcal{O}(\alpha)$ correction to the non-resonant cross-section (Eq. (7.7)), which has not been computed in the EFT approach.[¶] Attributing the difference at $\sqrt{s} = 161$ GeV to this correction, one obtains

$$\mathcal{K}^{(1)} \approx 1.4, \quad (7.17)$$

indicating that the $\mathcal{O}(\alpha)$ corrections to the non-resonant contribution (Eq. (7.8)) are moderate, $|\mathcal{K}^{(1)}/\mathcal{K}^{(0)}| \approx 0.3$. Above the threshold, $\mathcal{O}(\delta^{3/2})$ and $\mathcal{O}(\delta^2)$ corrections to the resonant cross-section are expected to be important; these arise from the combination of $\mathcal{O}(\alpha/v, \alpha)$ corrections in the EFT with $\mathcal{O}(v^2)$ kinematic corrections and from $\mathcal{O}(\alpha)$ corrections to the Wilson coefficients of subleading production operators. Naive estimates using the $\mathcal{O}(v^2)$ expansion of the Born amplitude and the first Coulomb correction,

$$\sigma_{\alpha v}^{(3/2)}(s) \sim |\sigma_{\text{Born}}^{(1)}(s)|\sigma_{\text{C}}^{(1/2)}(s)/\sigma_{\text{Born}}^{(0)}(s), \quad \sigma_{\alpha v^2}^{(2)}(s) \sim \frac{\alpha}{s_{\text{W}}^2} |\sigma_{\text{Born}}^{(1)}(s)|, \quad (7.18)$$

indicate that both corrections are $\sim 0.3\% \times \sigma_{\text{Born}}^{\text{ee4f}}$ at $\sqrt{s} = 170$ GeV, overestimating the discrepancy to the NLO^{ee4f} calculation. To assess the accuracy of the EFT expansion, it would be interesting to calculate these corrections exactly and investigate whether the difference to the NLO^{ee4f} calculation could be reduced, e.g., by resumming relativistic corrections to the W propagators.

7.1.4 Leading NNLO corrections

In Ref. [15], those $\mathcal{O}(\delta^{3/2})$ corrections according to Eq. (7.3) have been computed that originate from genuine NNLO corrections in the usual counting in α . These consist of several classes: (a) interference of one-loop Coulomb corrections with soft and hard corrections (Eq. (7.13)); (b) interference of one-loop Coulomb corrections with corrections to W decay, obtained from Eq. (7.15) by replacing the LO cross-section with the first Coulomb correction; (c) interference of one-loop Coulomb corrections with NLO corrections to residues of W propagators; and (d) radiative NLO corrections to the Coulomb potential (Eq. (7.14)). The third Coulomb correction

[§]Note that here the updated results in the erratum to Ref. [12] are used. The EFT results here and in Table B.7.2 differ from those of Refs. [14, 15] because of the corrected collinear contributions.

[¶]For $e^-e^+ \rightarrow t\bar{t}$, a related calculation has been performed recently [32].

Table B.7.1: Comparison of the strict electroweak NLO results (without QCD corrections, second Coulomb correction and ISR resummation) in the EFT approach to the full NLO^{ee4f} calculation and the DPA implementation of Ref. [11].

\sqrt{s} (GeV)	$\sigma(e^-e^+ \rightarrow \mu^- \bar{\nu}_\mu \text{ud} X)(\text{fb})$			
	Born	NLO(EFT) [14]	ee4f [12]	DPA [12]
161	150.05(6)	107.34(6)	106.33(7)	103.15(7)
170	481.2(2)	379.03(2)	379.5(2)	376.9(2)

Table B.7.2: Leading $\mathcal{O}(\alpha^2)$ corrections [15] (second and third column) and contributions to leading $\mathcal{O}(\alpha^3)$ corrections from triple-Coulomb exchange [15] (fourth column), interference of double-Coulomb exchange with soft and hard corrections (Eq. (7.26)) (fifth column), and double-Coulomb exchange with the NLO Coulomb potential (Eq. (7.27)) (sixth column). The relative correction is given with respect to the Born cross-section without ISR improvement, as quoted in Ref. [15].

\sqrt{s} (GeV)	$\sigma(e^-e^+ \rightarrow \mu^- \bar{\nu}_\mu \text{ud} X)(\text{fb})$				
	$\mathcal{O}(\alpha^2/v^2)$	$\mathcal{O}(\alpha^2/v)$	$\mathcal{O}(\alpha^3/v^3)$	$\mathcal{O}(\alpha^3/v^2) _{\text{C}_2 \times [\text{S+H}]_1}$	$\mathcal{O}(\alpha^3/v^2) _{\text{C}_2^{\text{NLO}}}$
158	0.151 [+0.245%]	0.061 [+0.099%]	3.82×10^{-3} [+0.006%]	-1.50×10^{-3} [-0.002%]	5.38×10^{-3} [+0.009%]
161	0.437 [+0.284%]	0.331 [+0.215%]	9.92×10^{-3} [+0.006%]	-0.433×10^{-2} [-0.003%]	1.52×10^{-2} [+0.010%]
164	0.399 [+0.132%]	1.038 [+0.342%]	2.84×10^{-3} [+0.001%]	-3.95×10^{-3} [-0.001%]	1.97×10^{-2} [+0.007%]
167	0.303 [+0.074%]	1.479 [+0.362%]	9.43×10^{-4} [+0.000%]	-3.00×10^{-3} [-0.001%]	1.77×10^{-2} [+0.004%]
170	0.246 [+0.051%]	1.734 [+0.360%]	4.39×10^{-4} [+0.000%]	-2.43×10^{-3} [-0.001%]	1.56×10^{-2} [+0.003%]

from Eq. (7.12) contributes at the same order, $\delta^{3/2}$. Care has been taken to avoid double-counting corrections already included in the NLO^{ee4f} calculation, so the two results can be added to obtain the current best prediction for the total cross-section near the threshold. The numerical results are reproduced in Table B.7.2, together with the second Coulomb correction included in the NLO^{EFT} calculation. The results show that the leading Coulomb-enhanced two-loop corrections are of the order of 0.3%. The uncertainty due to the remaining non-Coulomb-enhanced NNLO corrections was estimated to be below the ILC target accuracy of $\Delta M_W = 3$ MeV [15] but not sufficient for the FCC-ee.

7.2 Estimate of NNLO^{EFT} corrections and beyond

In this section, the structure of the EFT expansion of the cross-section and the ingredients for higher-order corrections reviewed in Section 7.1 are used to estimate the possible effects of a future NNLO^{EFT} calculation. Owing to the counting (Eq. (7.1)), this also includes leading corrections beyond NNLO in the conventional perturbative expansion:

$$\text{NNLO}^{\text{EFT}} : v^4, \quad \alpha v^2, \quad \alpha^2 \alpha^3/v^2, \quad \alpha^4/v^4. \quad (7.19)$$

The contributions of $\mathcal{O}(v^4, \alpha v^2)$ in Eq. (7.19) arise from kinematic corrections to the Born and NLO cross-section in the full SM, as discussed in Sections 7.1.1 and 7.1.3, respectively. The genuine $\mathcal{O}(\alpha^2)$ corrections are estimated in Section 7.2.1. A representative subset of the $\mathcal{O}(\alpha^3/v^2)$ corrections is computed in Section 7.2.2 and serves as an estimate of effects beyond a conventional NNLO calculation. The quadruple-Coulomb correction α^4/v^4 follows from the expansion of the known Coulomb Green function and is smaller than 0.001% and therefore negligible. Counting $\alpha \sim \alpha_s^2$, QCD corrections to W self-energies and decay widths up to

$$\alpha\alpha_s^2, \quad \alpha_s^4 \quad (7.20)$$

are also required. Currently, the required $\mathcal{O}(\alpha_s^4)$ corrections for inclusive hadronic vector boson decays are known [33], while mixed QCD-EW corrections are known up to $\mathcal{O}(\alpha\alpha_s)$ [34]. The uncertainty of a future NNLO^{EFT} calculation can be estimated by considering the impact of corrections at the next order in the δ -expansion, i.e.,

$$\text{N}^{5/2}\text{LO}^{\text{EFT}} : \alpha v^3, \quad \alpha^2 v, \quad \alpha^3/v, \quad \alpha^4/v^3, \quad \alpha^5/v^5. \quad (7.21)$$

The contributions $\sim \alpha v^3$ are already included in the NLO^{ee4f} calculation. The fifth Coulomb correction $\sim \alpha^5/v^5$ is known but negligibly small. The corrections $\sim \alpha^4/v^3$ arise from the combination of $\mathcal{O}(\alpha)$ corrections with triple-Coulomb exchange and are also expected to be negligible, since the latter is $<0.01\%$. Therefore, the dominant genuine radiative corrections beyond NNLO^{EFT} are expected to be of order α^3/v . These arise from a combination of single Coulomb exchange and various sources of $\mathcal{O}(\alpha^2)$ corrections and are estimated in Section 7.2.3. Further contributions from triple-Coulomb exchange combined with $\sim v^2$ kinematic corrections are again expected to be negligible. The $\mathcal{O}(\alpha^2)$ corrections to the non-resonant cross-section (Eq. (7.7)) also provide $\sim \alpha^3/v$ corrections relative to the LO cross-section, while corrections $\sim \alpha^2 v$ arise from a combination of single Coulomb exchange with kinematic corrections $\sim \alpha v^2$. Such non-resonant and kinematic corrections are estimated in Section 7.2.4. It is assumed throughout that large logarithms of m_e are absorbed in electron structure functions and only the uncertainty due to non-universal $\mathcal{O}(\alpha^2, \alpha^3)$ corrections is considered.

7.2.1 $\mathcal{O}(\alpha^2)$ corrections in the EFT

The most involved corrections of order α^2 in the EFT arise from hard two-loop corrections to the Wilson coefficients of production operators and to decay rates and from soft two-loop corrections to the forward-scattering amplitude. Additional corrections from higher-order potentials or the combination of double-Coulomb exchange with kinematic corrections $\sim v^2$ are anticipated to be subdominant. The soft corrections for massless initial-state electrons can be extracted from the two-loop Drell–Yan soft function [23, 24] and converted to the electron mass regulator scheme using the NNLO structure functions computed in Ref. [29]. We make no attempt here to estimate these soft corrections, which are formally of the same order as the hard corrections.

This is supported by the NLO result, where hard corrections alone provide a reasonable order-of-magnitude estimate and soft corrections contribute less than 50% of the NLO corrections for $\sqrt{s} = 158\text{--}170$ GeV. The contribution of the NNLO Wilson coefficient of the production operator to the cross-section reads

$$\sigma_{\text{hard}}^{(2)}(s) = \frac{\pi\alpha^2}{s_W^4 s} \text{Im} \left[-\sqrt{-\frac{\mathcal{E}_W}{M_W}} \left(\frac{\alpha}{\pi}\right)^2 C^{(2)} \right], \quad (7.22)$$

where the NNLO hard coefficient is defined in terms of the squared Wilson coefficient,

$$C^2 = 1 + \frac{\alpha}{\pi} C^{(1)} + \left(\frac{\alpha}{\pi}\right)^2 C^{(2)} + \dots$$

The computation of $C^{(2)}$ involves the two-loop amplitude for $e^-e^+ \rightarrow W^-W^+$, evaluated directly at the threshold. Such a computation is beyond the current state of the art, which includes two-loop EW corrections to three-point functions [35–37], but will presumably be feasible before the operation of the FCC-ee. A naive estimate of the NNLO coefficient in terms of the one-loop result (Eq. (7.11)),

$$C^{(2)} \sim (C^{(1)})^2, \quad (7.23)$$

suggests an effect on the cross-section of

$$\Delta\sigma_{\text{hard}}^{(2)} \approx \sigma_{\text{res}}^{(0)} \times 0.06\%. \quad (7.24)$$

The NNLO corrections to W boson decay give rise to the correction

$$\Delta\sigma_{\text{decay}}^{(2)} = \left(\frac{\Gamma_{\mu^- \bar{\nu}_\mu}^{(2,\text{ew})}}{\Gamma_{\mu^- \bar{\nu}_\mu}^{(0)}} + \frac{\Gamma_{\text{u}\bar{\text{d}}}^{(2,\text{ew})}}{\Gamma_{\text{u}\bar{\text{d}}}^{(0)}} + \frac{\Gamma_{\mu^- \bar{\nu}_\mu}^{(1,\text{ew})} \Gamma_{\text{u}\bar{\text{d}}}^{(1,\text{ew})}}{\Gamma_{\mu^- \bar{\nu}_\mu}^{(0)} \Gamma_{\text{u}\bar{\text{d}}}^{(0,\text{ew})}} \right) \sigma_{\text{res}}^{(0)}. \quad (7.25)$$

The product of NLO corrections in the last term contributes a negligible 0.001% to the G_μ input parameter scheme. A naive estimate of the currently unknown $\mathcal{O}(\alpha^2)$ corrections to W decay suggests

$$\Gamma_{f_i \bar{f}_j}^{(2,\text{ew})} \approx \frac{\alpha}{s_W^2} \Gamma_{f_i \bar{f}_j}^{(1,\text{ew})} \sim 0.01\% \times \Gamma_{f_i \bar{f}_j}^{(0)},$$

consistent with the size of the $\mathcal{O}(\alpha^2)$ corrections to Z decay [36, 37]. The estimates given in this subsection indicate that the combined non-Coulomb-enhanced corrections of $\mathcal{O}(\alpha^2)$ are of the order of 0.1% and are therefore mandatory to reduce the uncertainty below $\Delta M_W \lesssim 1.5$ MeV.

7.2.2 Corrections of $\mathcal{O}(\alpha^3/v^2)$

The corrections of $\mathcal{O}(\alpha^3/v^2)$ involve a double-Coulomb exchange in combination with an $\mathcal{O}(\alpha)$ correction and arise from similar sources to those of the $\mathcal{O}(\alpha^2/v)$ corrections discussed in Section 7.1.4. The subclass of contributions arising from the combination of double-Coulomb exchange with soft and hard corrections is obtained by inserting the $\mathcal{O}(\alpha^2)$ term in the expansion of the Coulomb Green function (Eq. (7.12)) into Eq. (7.13), resulting in the contribution to the cross-section

$$\Delta\sigma^{\text{C}_2 \times [\text{S}+\text{H}]_1} = \frac{\alpha^2}{s_W^4 s} \frac{\alpha^3 \pi^2}{12} \text{Im} \left\{ \sqrt{-\frac{M_W}{\mathcal{E}_W}} \left[\left(\frac{7}{2} + \frac{\pi^2}{4} + C^{(1)} \right) \right] \right\} \quad (7.26)$$

Corrections from the NLO Coulomb potential to double-Coulomb exchange can be obtained by expanding the expression for the NLO Coulomb Green function [31] quoted in Ref. [38] and using the result for the Coulomb potential in the G_μ input parameter scheme [15], resulting in

$$\Delta\sigma^{\text{C}_2^{\text{NLO}}}(s) = \frac{\alpha^2}{s_W^4 s} \frac{\alpha^3}{24} \text{Im} \left\{ \sqrt{-\frac{M_W}{\mathcal{E}_W}} \left[\pi^2 \left(-\beta_0 \ln\left(-\frac{\mathcal{E}_W}{M_W}\right) + \Delta_{G_\mu}\right) - 12\beta_0\zeta_3 \right] \right\}. \quad (7.27)$$

The combination of double-Coulomb exchange with NLO corrections to W decay is obtained from Eq. (7.15) by replacing $\sigma_{\text{res}}^{(0)}$ with the second Coulomb correction. The resulting effect is, at most, 0.002%. Further corrections arise from corrections to the propagator residues and can be computed with current methods, but are beyond the scope of the present simple estimates. At $\mathcal{O}(\alpha^2/v)$, the corresponding corrections are of a similar size to the mixed soft+hard Coulomb corrections [15]. Therefore, the predictions from Eqs. (7.26) and (7.27), which are shown in Table B.7.2 together with the known two- and three-loop corrections [15], are expected to be representative of the the $\mathcal{O}(\alpha^3/v^2)$ corrections. They are of a similar order as the third Coulomb correction, and individually of the order $\lesssim 0.01\%$ near the threshold. The sum of all $\mathcal{O}(\alpha^3/v^2)$ corrections may, therefore, be of the order of 0.01%, indicating the need to go beyond a strict $\mathcal{O}(\alpha^2)$ calculation to reach the FCC-ee accuracy goal.

7.2.3 Radiative corrections of $\mathcal{O}(\alpha^3/v)$

Genuine three-loop corrections at $\mathcal{O}(\alpha^3/v)$ can arise from a combination of the first Coulomb correction and soft or hard $\mathcal{O}(\alpha^2)$ corrections, corrections from higher-order potentials to the Coulomb Green function or a combination of $\mathcal{O}(\alpha)$ hard or soft and potential corrections. One contribution in the latter class can be computed by inserting the NLO Green function (Eq. (7.14)) into the product with the $\mathcal{O}(\alpha)$ hard and soft corrections (Eq. (7.13)),

$$\hat{\sigma}^{\text{C}^{\text{NLO}} \times [\text{S+H}]_1}(s) = \frac{\alpha^2}{s s_W^4} \frac{\alpha^3}{8\pi} \text{Im} \left\{ \left(\frac{7}{2} + \frac{\pi^2}{4} + C^{(1)} \right) \left(-\frac{\beta_0}{2} \ln\left(-\frac{\mathcal{E}_W}{M_W}\right) + \Delta_{G_\mu} \right) \ln\left(-\frac{\mathcal{E}_W}{M_W}\right) \right\}. \quad (7.28)$$

The corrections to the cross-section for $\sqrt{s} = 161\text{--}170$ GeV are given by

$$\Delta\sigma^{\text{C}^{\text{NLO}} \times [\text{S+H}]_1} = -0.001\% \times \sigma_{\text{LO}}. \quad (7.29)$$

A further indication for the magnitude of corrections at this order can be obtained from the combination of the NNLO hard coefficient with the first Coulomb correction,

$$\Delta\sigma^{\text{C}_1 \times \text{H}_2} = -\frac{\pi\alpha^2}{s_W^4 s} \frac{\alpha^3 C^{(2)}}{2\pi} \text{Im} \left[\ln\left(-\frac{\mathcal{E}_W}{M_W}\right) \right], \quad (7.30)$$

and using the estimate (Eq. (7.23)) for the hard two-loop coefficient, which results in

$$\Delta\sigma^{\text{C}_1 \times \text{H}_2}(161 \text{ GeV}) \approx 0.005\% \times \sigma_{\text{LO}}, \quad \Delta\sigma^{\text{C}_1 \times \text{H}_2}(170 \text{ GeV}) \approx 0.002\% \times \sigma_{\text{LO}}. \quad (7.31)$$

These results indicate that the $\mathcal{O}(\alpha^3)$ corrections beyond NNLO^{EFT} are $\lesssim 0.01\%$. It is expected that the factorisation (Eq. (7.10)) and the N³LO Coulomb Green function [39] enable the computation of all $\mathcal{O}(\alpha^3/v)$ corrections once the NNLO^{EFT} result is known, as for a related calculation for hadronic $t\bar{t}$ production [40].

7.2.4 Non-resonant and kinematic $\mathcal{O}(\alpha^2)$ corrections

Kinematic $\mathcal{O}(\alpha^2 v)$ corrections and $\mathcal{O}(\alpha^2)$ corrections to the non-resonant cross-section in Eq. (7.21) would be included in a full NNLO^{ee4f} calculation, which is far beyond current calculational methods. The comparison of the NLO^{EFT} and NLO^{ee4f} results in Section 7.1.3 indicate a well-behaved perturbative expansion of the non-resonant corrections (Eq. (7.7)), with coefficients $\mathcal{K}^{(i)}$ of order one. This suggests that the non-resonant and kinematic NNLO corrections are reasonably estimated by scaling the corresponding NLO corrections,

$$\Delta\sigma_{4f}^{(2)}(s) = \sigma_{\text{NNLO}}^{\text{ee4f}}(s) - \sigma_{\text{EFT}}^{(2)}(s) \approx \frac{\alpha}{s_W^2} \left(\sigma_{\text{NLO}}^{\text{ee4f}}(s) - \sigma_{\text{EFT}}^{(1)}(s) \right) = \sigma_{\text{Born}}^{\text{ee4f}}(s) \times 0.02\% \quad (7.32)$$

for $\sqrt{s} = 161\text{--}170$ GeV. Therefore, these effects must be under control to reach the desired accuracy for the FCC-ee. A calculation of the $\mathcal{O}(\alpha^2)$ non-resonant correction in the EFT involves a combination of $\mathcal{O}(\alpha^2)$ corrections to the processes $e^-e^+ \rightarrow W^\pm f\bar{f}$ with $\mathcal{O}(\alpha)$ corrections for $e^-e^+ \rightarrow 4f$. Such a computation is beyond current capabilities, but may be possible before a full NNLO^{ee4f} calculation is available. A comparison of future NNLO calculations in the EFT and the conventional DPA may also enable these corrections to be constrained.

7.3 Summary and outlook

The prospects of reducing the theoretical uncertainty of the total W pair production cross-section near the threshold to the level of $\sim 0.01\%$ required to fully exploit the high statistics at a future circular e^-e^+ collider have been investigated within the EFT approach, building on results for the NLO and dominant NNLO corrections. The estimates in Section 7.2.1 suggest that $\mathcal{O}(\alpha^2)$ corrections beyond the leading Coulomb effects [15] are of the order

$$\Delta\sigma_{\text{NNLO}} \approx 0.1\% \times \sigma_{\text{Born}} \quad (7.33)$$

at the threshold and are therefore mandatory to reach FCC-ee precision. In Sections 7.2.2 and 7.2.3, the dominant, Coulomb-enhanced three-loop effects have been estimated to be of the order

$$\Delta\sigma_{\text{N}^3\text{LO}} \approx \text{few} \times 0.01\% \times \sigma_{\text{Born}}, \quad (7.34)$$

based on computations or estimates of representative examples of $\mathcal{O}(\alpha^3/v^2, \alpha^3/v)$ effects. These corrections are either part of the NNLO^{EFT} result or can be computed once this result is available. The effect of the remaining $\mathcal{O}(\alpha^3)$ corrections without Coulomb enhancement is expected to be below the FCC-ee target accuracy. However, the accuracy of the NNLO^{EFT} calculation is limited by non-resonant and kinematic corrections. An extrapolation of the difference of the NLO^{EFT} and NLO^{ee4f} calculations suggests the magnitude

$$\Delta\sigma_{4f}^{(2)} \approx 0.02\% \times \sigma_{\text{Born}}. \quad (7.35)$$

Related estimates, $\Delta\sigma_{\text{N}^3\text{LO}} \approx 0.02\%$ and $\Delta\sigma_{\text{NNLO}}^{(\text{non-res})} \approx 0.016\%$, have been obtained using scaling arguments and an extrapolation of the accuracy of the DPA [41]. Our results suggest that a theory-induced systematic error of the mass measurement from a threshold scan of

$$\Delta M_W = (0.15 - 0.45) \text{ MeV} \quad (7.36)$$

should be achievable, where the lower value results from assuming that the non-resonant corrections are under control. In addition to the corrections considered here, it is also essential to reduce the uncertainty from ISR corrections and QCD corrections for hadronic final states to the required accuracy. It would also be desirable to bring the precision for differential cross-sections to a similar level to that of the total cross-section.

Acknowledgements

I would like to thank M. Beneke for useful comments.

References

- [1] H. Baer *et al.*, The international linear collider technical design report, vol. 2: physics (2013), [arXiv:1306.6352](#)
- [2] M. Baak *et al.*, Working group report: precision study of electroweak interactions, APS DPF Community Summer Study (Snowmass 2013), [arXiv:1310.6708](#)
- [3] P. Azzurri *et al.*, Physics behind precision (2017). [arXiv:1703.01626](#)
- [4] A. Abada *et al.*, *Eur. Phys. J.* **C79** (2019) 474. [doi:10.1140/epjc/s10052-019-6904-3](#)
- [5] M. Dong and G. Li, CEPC Conceptual Design Report, vol. 2: physics & detector (2018), [arXiv:1811.10545](#)
- [6] A. Aeppli *et al.*, *Nucl. Phys.* **B428** (1994) 126. [arXiv:hep-ph/9312212](#), [doi:10.1016/0550-3213\(94\)90195-3](#)
- [7] S. Jadach *et al.*, *Phys. Lett.* **B417** (1998) 326. [arXiv:hep-ph/9705429](#), [doi:10.1016/S0370-2693\(97\)01253-7](#)
- [8] S. Jadach *et al.*, *Comput. Phys. Commun.* **140** (2001) 432. [arXiv:hep-ph/0103163](#), [doi:10.1016/S0010-4655\(01\)00288-0](#)
- [9] W. Beenakker *et al.*, *Nucl. Phys.* **B548** (1999) 3. [arXiv:hep-ph/9811481](#), [doi:10.1016/S0550-3213\(99\)00110-8](#)
- [10] A. Denner *et al.*, *Phys. Lett.* **B475** (2000) 127. [arXiv:hep-ph/9912261](#), [doi:10.1016/S0370-2693\(00\)00059-9](#)
- [11] A. Denner *et al.*, *Nucl. Phys.* **B587** (2000) 67. [arXiv:hep-ph/0006307](#), [doi:10.1016/S0550-3213\(00\)00511-3](#)
- [12] A. Denner *et al.*, *Phys. Lett.* **B612** (2005) 223. [arXiv:hep-ph/0502063](#), [doi:10.1016/j.physletb.2005.03.007](#)
- [13] A. Denner *et al.*, *Nucl. Phys.* **B724** (2005) 247. [arXiv:hep-ph/0505042](#), [doi:10.1016/j.nuclphysb.2005.06.033](#)
- [14] M. Beneke *et al.*, *Nucl. Phys.* **B792** (2008) 89. [arXiv:0707.0773](#), [doi:10.1016/j.nuclphysb.2007.09.030](#)
- [15] S. Actis *et al.*, *Nucl. Phys.* **B807** (2009) 1. [arXiv:0807.0102](#), [doi:10.1016/j.nuclphysb.2008.08.006](#)
- [16] M. Beneke *et al.*, *Nucl. Phys.* **B842** (2011) 414. [arXiv:1007.5414](#), [doi:10.1016/j.nuclphysb.2010.09.009](#)
- [17] M. Beneke *et al.*, *Phys. Rev. Lett.* **93** (2004) 011602. [arXiv:hep-ph/0312331](#), [doi:10.1103/PhysRevLett.93.011602](#)
- [18] M. Beneke *et al.*, *Nucl. Phys.* **B686** (2004) 205. [arXiv:hep-ph/0401002](#), [doi:10.1016/j.nuclphysb.2004.03.016](#)
- [19] C.W. Bauer *et al.*, *Phys. Rev.* **D63** (2001) 114020. [arXiv:hep-ph/0011336](#), [doi:10.1103/PhysRevD.63.114020](#)
- [20] M. Beneke and Y. Kiyo, *Phys. Lett.* **B668** (2008) 143. [arXiv:0804.4004](#), [doi:10.1016/j.physletb.2008.08.031](#)

-
- [21] V.S. Fadin *et al.*, *Phys. Rev.* **D49** (1994) 2247. [doi:10.1103/PhysRevD.49.2247](https://doi.org/10.1103/PhysRevD.49.2247)
- [22] K. Melnikov and O.I. Yakovlev, *Phys. Lett.* **B324** (1994) 217. [arXiv:hep-ph/9302311](https://arxiv.org/abs/hep-ph/9302311)
[doi:10.1016/0370-2693\(94\)90410-3](https://doi.org/10.1016/0370-2693(94)90410-3)
- [23] A.V. Belitsky, *Phys. Lett.* **B442** (1998) 307. [arXiv:hep-ph/9808389](https://arxiv.org/abs/hep-ph/9808389)
[doi:10.1016/S0370-2693\(98\)01249-0](https://doi.org/10.1016/S0370-2693(98)01249-0)
- [24] T. Becher *et al.*, *J High Energy Phys.* **07** (2008) 030. [arXiv:0710.0680](https://arxiv.org/abs/0710.0680),
[doi:10.1088/1126-6708/2008/07/030](https://doi.org/10.1088/1126-6708/2008/07/030)
- [25] V.S. Fadin *et al.*, *Phys. Rev.* **D52** (1995) 1377. [arXiv:hep-ph/9501214](https://arxiv.org/abs/hep-ph/9501214),
[doi:10.1103/PhysRevD.52.1377](https://doi.org/10.1103/PhysRevD.52.1377)
- [26] G. Sterman, *Nucl. Phys.* **B281** (1987) 310. [doi:10.1016/0550-3213\(87\)90258-6](https://doi.org/10.1016/0550-3213(87)90258-6)
- [27] S. Catani and L. Trentadue, *Nucl. Phys.* **B327** (1989) 323.
[doi:10.1016/0550-3213\(89\)90273-3](https://doi.org/10.1016/0550-3213(89)90273-3)
- [28] P. Falgari, Ph.D. thesis, RWTH Aachen University, 2008.
<http://darwin.bth.rwth-aachen.de/opus3/volltexte/2009/2682/>
- [29] J. Blümlein *et al.*, *Nucl. Phys.* **B855** (2012) 508. [arXiv:1107.4638](https://arxiv.org/abs/1107.4638),
[doi:10.1016/j.nuclphysb.2011.10.009](https://doi.org/10.1016/j.nuclphysb.2011.10.009)
- [30] M. Skrzypek, *Acta Phys. Pol.* **B23** (1992) 135.
<https://inspirehep.net/literature/335990>
- [31] M. Beneke *et al.*, *Phys. Lett.* **B454** (1999) 137. [arXiv:hep-ph/9903260](https://arxiv.org/abs/hep-ph/9903260),
[doi:10.1016/S0370-2693\(99\)00343-3](https://doi.org/10.1016/S0370-2693(99)00343-3)
- [32] M. Beneke *et al.*, *JHEP* **02** (2018) 125. [arXiv:1711.10429](https://arxiv.org/abs/1711.10429),
[doi:10.1007/JHEP02\(2018\)125](https://doi.org/10.1007/JHEP02(2018)125)
- [33] P.A. Baikov *et al.*, *Phys. Rev. Lett.* **101** (2008) 012002. [arXiv:0801.1821](https://arxiv.org/abs/0801.1821),
[doi:10.1103/PhysRevLett.101.012002](https://doi.org/10.1103/PhysRevLett.101.012002)
- [34] D. Kara, *Nucl. Phys.* **B877** (2013) 683. [arXiv:1307.7190](https://arxiv.org/abs/1307.7190),
[doi:10.1016/j.nuclphysb.2013.10.024](https://doi.org/10.1016/j.nuclphysb.2013.10.024)
- [35] S. Actis *et al.*, *Nucl. Phys.* **B811** (2009) 182. [arXiv:0809.3667](https://arxiv.org/abs/0809.3667),
[doi:10.1016/j.nuclphysb.2008.11.024](https://doi.org/10.1016/j.nuclphysb.2008.11.024)
- [36] A. Freitas, *JHEP* **04** (2014) 070. [arXiv:1401.2447](https://arxiv.org/abs/1401.2447),
[doi:10.1007/JHEP04\(2014\)070](https://doi.org/10.1007/JHEP04(2014)070)
- [37] I. Dubovyk *et al.*, *Phys. Lett.* **B783** (2018) 86. [arXiv:1804.10236](https://arxiv.org/abs/1804.10236),
[doi:10.1016/j.physletb.2018.06.037](https://doi.org/10.1016/j.physletb.2018.06.037)
- [38] M. Beneke *et al.*, *Nucl. Phys.* **B855** (2012) 695. [arXiv:1109.1536](https://arxiv.org/abs/1109.1536),
[doi:10.1016/j.nuclphysb.2011.10.021](https://doi.org/10.1016/j.nuclphysb.2011.10.021)
- [39] M. Beneke, *et al.*, *Phys. Rev. Lett.* **115** (2015) 192001. [arXiv:1506.06864](https://arxiv.org/abs/1506.06864),
[doi:10.1103/PhysRevLett.115.192001](https://doi.org/10.1103/PhysRevLett.115.192001)
- [40] J. Piclum and C. Schwinn, *JHEP* **03** (2018) 164. [arXiv:1801.05788](https://arxiv.org/abs/1801.05788), [doi:10.1007/JHEP03\(2018\)164](https://doi.org/10.1007/JHEP03(2018)164)
- [41] S. Jadach and M. Skrzypek, *Eur. Phys. J.* **C79** (2019) 756. [arXiv:1903.09895](https://arxiv.org/abs/1903.09895),
[doi:10.1140/epjc/s10052-019-7255-9](https://doi.org/10.1140/epjc/s10052-019-7255-9)

8 Perspectives of heavy quarkonium production at the FCC-ee

Contribution* by: Z.-G. He, B.A. Kniehl

Corresponding author: B.A. Kniehl [kniehl@desy.de]

Owing to its non-relativistic nature, heavy quarkonium, constituting heavy quark–antiquark pairs ($Q\bar{Q} = b\bar{b}$ or $c\bar{c}$) is an ideal object to investigate both perturbative and non-perturbative aspects of QCD. The non-relativistic QCD factorisation formalism [1], built on rigorous effective field theory [2], provides a powerful tool to calculate heavy quarkonium production and decay systematically. In this formalism, the production of heavy quarkonium is factorised into the process-dependent short-distance coefficients (SDCs) multiplied by supposedly universal long-distance matrix elements (LDMEs). The SDC describing the production of a $Q\bar{Q}$ pair in Fock state $n = {}^{2S+1}L_J^{[a]}$ with total spin S , orbital angular momentum L , and total angular momentum J can be calculated perturbatively as an expansion in α_s . The LDMEs related to the probability that Fock state n will evolve into the heavy meson are organised by the velocity scaling rules [3] of non-relativistic QCD (NRQCD), and their values can be determined by fitting to experimental data. Here, the velocity, v_Q , refers to the motion of a heavy quark, Q , in the rest frame of the heavy meson. Although NRQCD has greatly improved our understanding of the heavy quarkonium production mechanism, the long-standing ‘ J/ψ polarisation puzzle’ has not yet been resolved. The SDCs for the relevant colour singlet (CS) channel (${}^3S_1^{[1]}$) and the three colour octet (CO) (${}^3S_1^{[8]}$, ${}^1S_0^{[8]}$, ${}^3P_J^{[8]}$) channels have been obtained by three groups independently, while the corresponding LDMEs were fitted to different sets of experimental data, based on different considerations [4–6]. However, none of these predictions can explain both the J/ψ yield and polarisation data at hadron colliders simultaneously. Recently, the universality of the NRQCD LDMEs was challenged by η_c hadroproduction data [7].

Compared with hadron colliders, in e^+e^- colliders, the production mechanism is simpler, the uncertainties in the theoretical calculations are smaller, and the convergence of perturbative calculations is faster. Moreover, on the experimental side, the much cleaner background makes it possible to study the production of other heavy quarkonia besides the J/ψ and Υ mesons, such as $\eta_{c,b}$ and $\chi_{c,b}$, and to study more production processes, such as the associated production of heavy quarkonium with a photon or a heavy quark pair, in detail. Therefore, heavy quarkonium production in e^+e^- colliders plays an important role in testing NRQCD factorisation, so as to help resolving the ‘ J/ψ polarisation puzzle’. There are two ways to produce heavy quarkonium directly.* One is in e^+e^- annihilation and the other is in $\gamma\gamma$ collisions. We review heavy quarkonium production, concentrating on the J/ψ case, by these two processes in Sections 8.1 and 8.2, respectively, and discuss the prospects of heavy quarkonium production at the FCC-ee beyond the current measurements made at B factories and CERN LEP-II. Section 8.3 contains a summary and an outlook.

*This contribution should be cited as:

Z.-G. He, B.A. Kniehl, Perspectives of heavy quarkonium production at the FCC-ee, DOI: [10.23731/CYRM-2020-003.89](https://doi.org/10.23731/CYRM-2020-003.89), in: Theory for the FCC-ee, Eds. A. Blondel, J. Gluza, S. Jadach, P. Janot and T. Riemann, CERN Yellow Reports: Monographs, CERN-2020-003, DOI: [10.23731/CYRM-2020-003](https://doi.org/10.23731/CYRM-2020-003), p. 89.
 © CERN, 2020. Published by CERN under the [Creative Commons Attribution 4.0 license](https://creativecommons.org/licenses/by/4.0/).

*Here, we mean production other than through the decay of other heavy particles, like the Z boson, Higgs boson, or top quark.

8.1 Heavy quarkonium production through e^+e^- annihilation

The total cross-section for inclusive J/ψ production in e^+e^- annihilation was measured by the Babar [8], Belle [9], and CLEO [10] collaborations at $\sqrt{s} = 10.6$ GeV, yielding

$$\sigma(e^+e^- \rightarrow J/\psi + X) = \begin{cases} 2.5 \pm 0.21 \pm 0.21 \text{ pb} & \text{Babar} \\ 1.47 \pm 0.10 \pm 0.13 \text{ pb} & \text{Belle} \\ 1.9 \pm 0.2 \text{ pb} & \text{CLEO} \end{cases}$$

The NRQCD prediction at leading order (LO) is in the wide range of 0.8-1.7 pb [11–14], including 0.3 pb from the CS mechanism. The Belle collaboration further managed to discriminate the contributions due to the final states $J/\psi + c\bar{c} + X$ and $J/\psi + X_{\text{non-}c\bar{c}}$, and found that $\sigma(e^+e^- \rightarrow J/\psi + c\bar{c} + X) = 0.74 \pm 0.08_{-0.08}^{+0.09}$ pb and $\sigma(e^+e^- \rightarrow J/\psi + X_{\text{non-}c\bar{c}}) = 0.43 \pm 0.09 \pm 0.09$ pb [15]. Neither of these results is compatible with LO NRQCD predictions.

The LO NRQCD prediction for $\sigma(e^+e^- \rightarrow J/\psi + c\bar{c} + X)$ is about 0.15 pb, in which the CO contribution is negligible [16]. To solve the problem, both the next-to-leading-order (NLO) QCD [17] and relativistic corrections [18] were calculated. The relativistic correction was found to be less than one percent of the LO contribution. The effect of the NLO QCD correction is large. Its K factor is about 1.8 for $m_c = 1.5$ GeV and $\alpha_s = 0.26$. After including the feed-down contribution from $\psi(2S)$, the NRQCD prediction at NLO becomes $0.53_{-0.23}^{+0.59}$ pb and largely removes the discrepancy [17]. However, the theoretical prediction depends strongly on the chosen values of m_c and α_s . According to the design [19], the FCC-ee will run at several beam energies. Measuring $J/\psi + c\bar{c}$ production at different energies will definitely help to improve our understanding of the parameter setting in the theoretical calculation.

At high energies, the predominant contribution to $J/\psi + c\bar{c}$ production comes from the fragmentation process. For heavy quarkonium production, it is found that there are two types of fragmentation [20], (1) single-parton fragmentation (SPF) and (2) double-parton fragmentation (DPF). At hadron colliders, experimentally, the $J/\psi + c\bar{c}$ final state is hard to detect and, theoretically, both SPF and DPF contribute, so that it is very difficult to study their properties separately.

In the e^+e^- annihilation process, only SPF contributes. Thus, the differential cross-section in the fragmentation limit can be expressed as

$$d\sigma(e^+e^- \rightarrow J/\psi + c\bar{c}) = 2 \int d\sigma(e^+e^- \rightarrow c\bar{c}) D_{c \rightarrow J/\psi}(z) dz, \quad (8.1)$$

where

$$D_{c \rightarrow J/\psi}(z) = \frac{8\alpha_s^2}{27\pi} \frac{z(1-z)^2(5z^4 - 32z^3 + 72z^2 - 32z + 16)}{(2-z)^6} \frac{|R(0)|^2}{m_c^3}, \quad (8.2)$$

with $z = E_{J/\psi}/\sqrt{s}$, where $|R(0)|$ is the wave function of J/ψ at the origin [21].

At $\sqrt{s} = 10.6$ GeV, the fragmentation contribution can only account for 58% of the complete calculation [16]. The comparison between the complete calculation and the fragmentation approximation is shown in Fig. B.8.1. We observe that, only in the energy range of the FCC-ee or even beyond, the fragmentation contribution provides a good approximation. Conversely, the differential cross-section of $e^+e^- \rightarrow Q\bar{Q}$ is known at $\mathcal{O}(\alpha_s^2)$ [22, 23]. By comparing experimental measurements with higher-order theoretical calculations, the fragmentation function at higher orders can also be extracted.

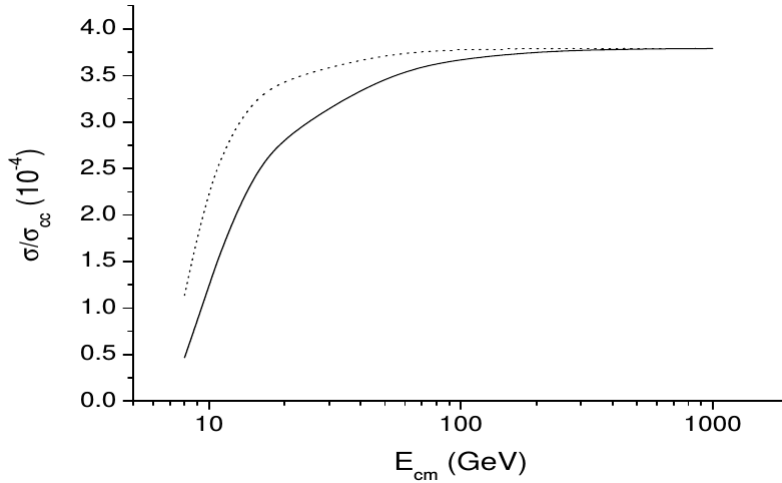


Fig. B.8.1: Cross-section of $\sigma(e^+e^- \rightarrow J/\psi + c\bar{c} + X)$ normalised to $\sigma(e^+e^- \rightarrow c\bar{c} + X)$ at LO in NRQCD as a function of the centre-of-mass energy. The dotted line denotes the complete result, and the solid line denotes the fragmentation calculation. Figure courtesy ref. [16].

For $J/\psi + X_{\text{non-}c\bar{c}}$ production, in the CS contribution, the NLO QCD corrections [24] and relativistic corrections [25] are equally important. Their K factors are both around 1.2 [24, 25], and the cross-section through NLO in QCD and v^2 becomes $\sigma(e^+e^- \rightarrow J/\psi + gg) \simeq 437$ fb for $\mu = \sqrt{s}/2$ and $m_c = 1.5$ GeV, which almost saturates the Belle measurement and leaves little room for the CO contribution [25]. The NLO QCD corrections to the CO channels $^1S_0^{[8]}$ and $^3P_J^{[8]}$ were also computed [26]. A lower bound on the CO contribution is obtained by using the LDMEs from Ref. [4], yielding 0.3 pb. Therefore, the total NRQCD prediction is larger than the Belle measurements, but does not conflict with the Babar and CLEO measurements if we assume that $\sigma(e^+e^- \rightarrow J/\psi + c\bar{c} + X)$ is similar in these three experiments. To understand the CO mechanism in e^+e^- annihilation, further analysis of $J/\psi + X_{\text{non-}c\bar{c}}$ production at 10.6 GeV and in the future at the FCC-ee is necessary.

Besides charmonium, the production of bottomonium in e^+e^- annihilation is also of great interest. However, the collision energy at B factories is so close to the Υ production threshold that perturbative calculations are no longer reliable. Moreover, such a low energy is not sufficient to enable $\Upsilon + b\bar{b}$ production. At the FCC-ee, the collision energy is of the order of 10^2 GeV and, therefore, provides a unique opportunity to study $\Upsilon + X_{\text{non-}b\bar{b}}$ and $\Upsilon + b\bar{b}$ production in e^+e^- annihilation. Theoretically, the NRQCD prediction through NLO can easily be obtained from the known J/ψ calculation by changing the value of \sqrt{s} and replacing m_c with m_b and the LDMEs of J/ψ by those of Υ .

8.2 Heavy quarkonium production in $\gamma\gamma$ collisions

J/ψ photoproduction in $\gamma\gamma$ collisions ($e^+e^- \rightarrow e^+e^- J/\psi + X$) was measured by the DELPHI collaboration at LEP-II [27, 28]. The total cross-section was found to be $\sigma(e^+e^- \rightarrow e^+e^- J/\psi + X) = (45 \pm 9 \pm 17)$ pb [28]. The DELPHI collaboration also measured the transverse momentum (p_T) distribution of the cross-section. Since the higher excited states χ_{cJ} and ψ' can decay into J/ψ via radiative decays or hadronic transitions, their feed-down contributions should also be considered. In such processes, the $c\bar{c}$ pair can either be produced by photons directly (direct photoproduction) or via the light quark and gluon content of the photons (resolved

photoproduction), so that there are three channels: direct, single resolved, and double resolved, all of which contribute formally at the same order in the perturbative expansion and should be included.

Working in the Weizsäcker–Williams approximation to describe the bremsstrahlung photons radiated off the e^\pm beams and using the factorisation theorems of the QCD parton model and NRQCD, the general formula for the differential cross-section for the production of the heavy quarkonium state H can be written as

$$\frac{d\sigma(e^+e^- \rightarrow e^+e^-H + X)}{dx_1 dx_2 dx_a dx_b} = \sum_{a,b,n} f_\gamma(x_1) f_\gamma(x_2) f_{a/\gamma}(x_a) f_{b/\gamma}(x_b) \times d\hat{\sigma}(a + b \rightarrow Q\bar{Q}(n) + X) \langle \mathcal{O}^H(n) \rangle, \quad (8.3)$$

where $f_\gamma(x)$ is the flux function of the photon in the e^\pm beam, $f_{j/\gamma}(x)$ is $\delta(1-x)$ if $j = \gamma$ and otherwise the parton distribution function of parton j in the resolved photon, $d\hat{\sigma}(a + b \rightarrow Q\bar{Q}(n) + X)$ is the partonic cross-section, and $\langle \mathcal{O}^H(n) \rangle$ is the NRQCD LDME.

In the LO calculation, both direct J/ψ production and the feed-down from χ_{cJ} for $J = 0, 1, 2$ and ψ' are included [29]. For J/ψ (ψ') production through relative order $\mathcal{O}(v^4)$, the Fock states include $n = {}^3S_1^{[1,8]}, {}^1S_0^{[8]}, {}^3P_J^{[8]}$, and for χ_{cJ} production at LO in v^2 one needs $n = {}^3P_J^{[1]}, {}^3S_1^{[8]}$. As shown in Fig. B.8.2, the LO NRQCD prediction of $d\sigma/dp_T^2$, evaluated with the LDMEs from the LO fit to Tevatron data [30], agree very well with the DELPHI data, while the CS contribution itself lies far below the data, as the central values are about 16 times smaller. The total cross-section in the range $1 \leq p_T^2 \leq 10 \text{ GeV}^2$ measured by DELPHI is $6.4 \pm 2.0 \text{ pb}$ [27]. The NRQCD prediction is $4.7_{-1.2}^{+1.9} \text{ pb}$ [29], which is also consistent with the DELPHI result, within errors. However, the CS contribution is only $0.39_{-0.09}^{+0.16} \text{ pb}$ [29]. The nice agreement between the NRQCD calculation and the experimental measurement for J/ψ photoproduction is one of the earliest pieces of evidence for the CO mechanism predicted by NRQCD.

In 2011, two groups independently obtained complete NLO QCD corrections to J/ψ direct hadroproduction for the first time [31, 32]. However, their LDMEs are different because they fitted to data in different p_T ranges. To eliminate such problems and further check the universality of the NRQCD LDMEs at NLO, a global analysis to worldwide data including $\gamma\gamma$ collisions was conducted. The resulting three CO LDMEs, $\langle \mathcal{O}^{J/\psi}({}^1S_0^{[8]}) \rangle = (4.97 \pm 0.44) \times 10^{-2} \text{ GeV}^3$, $\langle \mathcal{O}^{J/\psi}({}^3S_1^{[8]}) \rangle = (2.24 \pm 0.59) \times 10^{-3} \text{ GeV}^3$, and $\langle \mathcal{O}^{J/\psi}({}^3P_0^{[8]}) \rangle = (-1.61 \pm 0.20) \times 10^{-2} \text{ GeV}^5$, which obey the velocity scaling rules, were found to explain all the J/ψ yield data fairly well, except for the case of $\gamma\gamma$ collisions [4]. In contrast to the situation at LO, the DELPHI data systematically overshoot the NLO NRQCD prediction, as may be seen in Fig. B.8.3. However, Figs. B.8.2 and B.8.3 indicate that the uncertainties in the experimental measurements are very large. There are only 36 ± 7 $J/\psi \rightarrow \mu^+\mu^-$ events in total (and 16 thereof in the region $p_T > 1 \text{ GeV}$), collected with an integrated luminosity of 617 pb^{-1} . The integrated luminosity at the FCC-ee will reach the ab^{-1} level, which is more than three orders of magnitude larger than that of LEP-II. Measuring J/ψ production in $\gamma\gamma$ collisions at the FCC-ee would not only serve as a cross-check of the LEP-II results, but also provide results with high accuracy. Such a study could surely clarify the current conflict and deepen our understanding of the heavy quarkonium production mechanism in $\gamma\gamma$ collisions.

Unlike the case of e^+e^- annihilation, $J/\psi + c\bar{c} + X$ production in $\gamma\gamma$ collisions is predicted to have a smaller cross-section than $J/\psi + X_{\text{non-}c\bar{c}}$ production. While $\gamma\gamma \rightarrow J/\psi + X_{\text{non-}c\bar{c}}$ proceeds dominantly via single resolved photoproduction, $\gamma\gamma \rightarrow J/\psi + c\bar{c} + X$ proceeds dominantly via

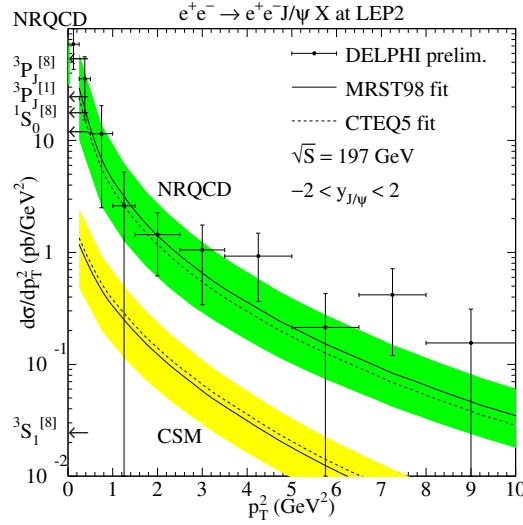


Fig. B.8.2: Comparison between NRQCD and CS model predictions of $d\sigma/dp_T^2$ as functions of p_T^2 for $\gamma\gamma \rightarrow J/\psi$ at LO and DELPHI measurement at LEP-II. The solid and dashed lines are calculated with the MRST98 LO and CTEQ5 parton distribution functions, respectively. The bands indicate the theoretical uncertainties. Figure courtesy ref. [29].

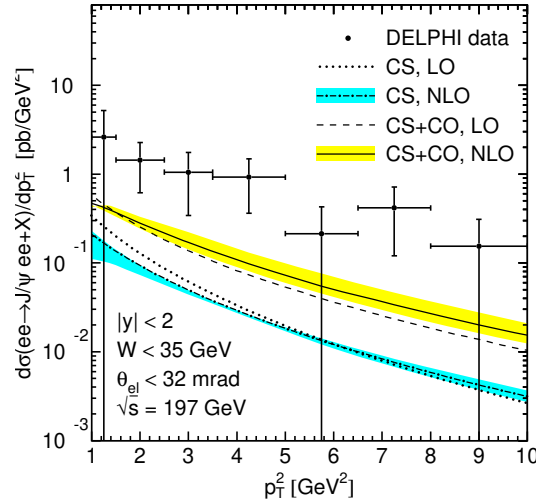


Fig. B.8.3: Comparison of LEP-II data on $\gamma\gamma \rightarrow J/\psi$ with NLO NRQCD predictions evaluated with LDMEs obtained via a global data analysis. Figure courtesy ref. [4].

direct photoproduction [33]. The total cross-section in the region $p_T^{J/\psi} > 1$ GeV is predicted to be about 0.16–0.20 pb, depending on the chosen values of α_s and the CS LDME [33, 34]. Its NLO NRQCD correction has also been calculated, and the K factor is found to be 1.46, enhancing the total cross-section in the region $p_T^{J/\psi} > 1$ GeV to become around 0.23–0.29 pb, which is too small to be analysed at LEP-II [34]. The cross-section becomes larger as the e^+e^- collision energy increases. Based on the results given in Ref. [34], we estimate the numbers of $J\psi + c\bar{c}$ events accumulated with the FCC-ee at the ZZ and ZH thresholds to be around 2×10^6 each, assuming the kinematic-cut conditions for the FCC-ee to be the same as for LEP-II. Such large data samples should be enough to usefully study $J/\psi + c\bar{c} + X$ production in $\gamma\gamma$ collisions.

8.3 Summary and outlook

The production mechanisms of heavy quarkonium, especially of the J/ψ meson, have not yet been fully understood within the framework of NRQCD factorisation. We have discussed here two modes of J/ψ production at e^+e^- colliders, through e^+e^- annihilation and $\gamma\gamma$ collisions. In the e^+e^- annihilation case, for $J/\psi + c\bar{c} + X$ production, the NRQCD prediction and the Belle measurement agree within errors; however, for $J/\psi + X_{\text{non-}c\bar{c}}$ production, the Belle result favours the CS model prediction and is overshoot by NRQCD predictions evaluated using any of the available LDME sets, although the latter are mutually inconsistent. We note that the NRQCD predictions seem to be compatible with the Babar and CLEO results. As for J/ψ production in $\gamma\gamma$ collisions, the NRQCD prediction can explain the LEP-II data, whose uncertainties are large, at LO, but fails once the NLO correction is included.

The FCC-ee will run at different energy points with considerable integrated luminosity, of $\mathcal{O}(\text{ab}^{-1})$ or even $\mathcal{O}(10^2 \text{ ab}^{-1})$ at the Z boson peak [19], which will provide a perfect environment to judge the disagreements independently. Moreover, it can significantly enrich our knowledge of heavy quarkonium production in e^+e^- collisions, especially by studying bottomonium production, the fragmentation function of $c \rightarrow J/\psi$, and $J/\psi + c\bar{c}$ production in $\gamma\gamma$ collisions.

References

- [1] G.T. Bodwin *et al.*, *Phys. Rev.* **D51** (1995) 1125 [Erratum: **D55** (1997) 5853].
[arXiv:hep-ph/9407339](#), [10.1103/PhysRevD.51.1125](#), [doi:10.1103/PhysRevD.55.5853](#)
- [2] W.E. Caswell and G.P. Lepage, *Phys. Lett.* **167B** (1986) 437.
[doi:10.1016/0370-2693\(86\)91297-9](#)
- [3] G.P. Lepage *et al.*, *Phys. Rev.* **D46** (1992) 4052. [arXiv:hep-lat/9205007](#),
[doi:10.1103/PhysRevD.46.4052](#)
- [4] M. Butenschoen and B.A. Kniehl, *Phys. Rev.* **D84** (2011) 051501. [arXiv:1105.0820](#),
[doi:10.1103/PhysRevD.84.051501](#)
- [5] K.-T. Chao *et al.*, *Phys. Rev. Lett.* **108** (2012) 242004. [arXiv:1201.2675](#),
[doi:10.1103/PhysRevLett.108.242004](#)
- [6] B. Gong *et al.*, *Phys. Rev. Lett.* **110** (2013) 042002. [arXiv:1205.6682](#),
[doi:10.1103/PhysRevLett.110.042002](#)
- [7] M. Butenschoen *et al.*, *Phys. Rev. Lett.* **114** (2015) 092004. [arXiv:1411.5287](#),
[doi:10.1103/PhysRevLett.114.092004](#)
- [8] B. Aubert *et al.*, *Phys. Rev. Lett.* **87** (2001) 162002. [arXiv:hep-ex/0106044](#),
[doi:10.1103/PhysRevLett.87.162002](#)
- [9] K. Abe *et al.*, *Phys. Rev. Lett.* **88** (2002) 052001. [arXiv:hep-ex/0110012](#),
[doi:10.1103/PhysRevLett.88.052001](#)
- [10] R.A. Briere *et al.*, *Phys. Rev.* **D70** (2004) 072001. [arXiv:hep-ex/0407030](#),
[doi:10.1103/PhysRevD.70.072001](#)
- [11] F. Yuan *et al.*, *Phys. Rev.* **D56** (1997) 321. [arXiv:hep-ph/9703438](#),
[doi:10.1103/PhysRevD.56.321](#)
- [12] F. Yuan *et al.*, *Phys. Rev.* **D56** (1997) 1663. [arXiv:hep-ph/9701361](#),
[doi:10.1103/PhysRevD.56.1663](#)
- [13] S. Baek *et al.*, *J. Korean Phys. Soc.* **33** (1998) 97. [arXiv:hep-ph/9804455](#).

- [14] G.A. Schuler, *Eur. Phys. J.* **C8** (1999) 273. [arXiv:hep-ph/9804349](#),
[doi:10.1007/s100529900948](#)
- [15] P. Pakhlov *et al.*, *Phys. Rev.* **D79** (2009) 071101. [arXiv:0901.2775](#),
[doi:10.1103/PhysRevD.79.071101](#)
- [16] K.-Y. Liu *et al.*, *Phys. Rev.* **D69** (2004) 094027. [arXiv:hep-ph/0301218](#),
[doi:10.1103/PhysRevD.69.094027](#)
- [17] Y.-J. Zhang and K.-T. Chao, *Phys. Rev. Lett.* **98** (2007) 092003. [arXiv:hep-ph/0611086](#),
[doi:10.1103/PhysRevLett.98.092003](#)
- [18] Z.-G. He *et al.*, *Phys. Rev.* **D75** (2007) 074011. [arXiv:hep-ph/0702239](#),
[doi:10.1103/PhysRevD.75.074011](#)
- [19] M. Benedikt *et al.*, *Eur. Phys. J. ST* **228** (2019), 261-623.
[doi:10.1140/epjst/e2019-900045-4](#)
- [20] Z.-B. Kang *et al.*, *Phys. Rev. Lett.* **108** (2012) 102002. [arXiv:1109.1520](#),
[doi:10.1103/PhysRevLett.108.102002](#)
- [21] E. Braaten *et al.*, *Phys. Rev.* **D48** (1993) 4230. [arXiv:hep-ph/9302307](#),
[doi:10.1103/PhysRevD.48.4230](#)
- [22] J. Gao and H.X. Zhu, *Phys. Rev.* **D90** (2014) 114022. [arXiv:1408.5150](#),
[doi:10.1103/PhysRevD.90.114022](#)
- [23] J. Gao and H.X. Zhu, *Phys. Rev. Lett.* **113** (2014) 262001. [arXiv:1410.3165](#),
[doi:10.1103/PhysRevLett.113.262001](#)
- [24] Y.-Q. Ma *et al.*, *Phys. Rev. Lett.* **102** (2009) 162002. [arXiv:0812.5106](#),
[doi:10.1103/PhysRevLett.102.162002](#)
- [25] Z.-G. He *et al.*, *Phys. Rev.* **D81** (2010) 054036. [arXiv:0910.3636](#),
[doi:10.1103/PhysRevD.81.054036](#)
- [26] Y.-J. Zhang *et al.*, *Phys. Rev.* **D81** (2010) 034015. [arXiv:0911.2166](#),
[doi:10.1103/PhysRevD.81.034015](#)
- [27] S. Todorova-Nova, (Some of) recent gamma gamma measurements from LEP, Multiparticle Dynamics. Proc. 31st Int. Symposium, ISMD 2001, Datong, China, 2001, pp. 62–67.
[arXiv:hep-ph/0112050](#), [doi:10.1142/9789812778048_0010](#).
URL: <http://www.slac.stanford.edu/econf/C010901>
- [28] J. Abdallah *et al.*, *Phys. Lett.* **B565** (2003) 76. [arXiv:hep-ex/0307049](#),
[doi:10.1016/S0370-2693\(03\)00660-9](#)
- [29] M. Klasen *et al.*, *Phys. Rev. Lett.* **89** (2002) 032001. [arXiv:hep-ph/0112259](#),
[doi:10.1103/PhysRevLett.89.032001](#)
- [30] E. Braaten *et al.*, *Phys. Rev.* **D62** (2000) 094005. [arXiv:hep-ph/9911436](#),
[doi:10.1103/PhysRevD.62.094005](#)
- [31] M. Butenschoen and B.A. Kniehl, *Phys. Rev. Lett.* **106** (2011) 022003. [arXiv:1009.5662](#),
[doi:10.1103/PhysRevLett.106.022003](#)
- [32] Y.-Q. Ma *et al.*, *Phys. Rev. Lett.* **106** (2011) 042002. [arXiv:1009.3655](#),
[doi:10.1103/PhysRevLett.106.042002](#)
- [33] R. Li and K.-T. Chao, *Phys. Rev.* **D79** (2009) 114020. [arXiv:0904.1643](#),
[doi:10.1103/PhysRevD.79.114020](#)

- [34] Z.-Q. Chen *et al.*, *Phys. Rev.* **D95** (2017) 036001. [arXiv:1608.06231](#),
[doi:10.1103/PhysRevD.95.036001](#)

9 Vertex functions in QCD—preparation for beyond two loops

Contribution* by: J.A. Gracey [gracey@liverpool.ac.uk]

Abstract

We summarise the algorithm to determine the two-loop off-shell three-point vertex functions of QCD before outlining the steps required to extend the results to three and more loops.

9.1 Introduction

In our current generation of high-energy particle accelerators involving hadron collisions, a major source of background is radiation derived from the strong sector. As this is governed by quantum chromodynamics (QCD), to quantify the background effects one must carry out high loop order computations. There has been remarkable activity and progress in this direction since around the turn of the millennium. The primary focus has been with the evaluation of on-shell n -point gluonic and fermionic amplitudes to several loop orders, both analytically and numerically. Indeed, such results have been crucial in ensuring that the Higgs particle was observed at CERN's LHC. However, having information on the off-shell Green's functions, such as the three-point vertices of QCD, is also important for theory as well as experiment. For instance, various articles in this direction have appeared over the years. A non-exhaustive literature for this status of three- and four-point functions at various external momenta configurations is given by Refs. [1–11]. There are various theoretical reasons for having such off-shell Green's functions. One is that knowing, say, the two-loop off-shell vertex functions enables higher-loop n -point on-shell amplitudes to be modelled numerically. This could be an interim position in the absence of the technology to compute them fully explicitly. Such an approach is not uncommon. Equally, in solving QCD beyond the perturbative limit analytically to probe deep infrared properties using the Schwinger–Dyson formalism, approximations must be made in order to solve the infinite tower of Green's functions. Until recent years, the validity of such approximations could not be fully quantified. However, with explicit perturbative results, for instance, such error analyses have been made possible. For instance, one approximation in solving two- and three-point Schwinger–Dyson equations is to neglect the summed graphs deriving from the quartic gluon vertex. Work in this direction over a period of time [12–16] has confirmed that such a step does not affect final results by more than a few percent. Equally, the Schwinger–Dyson method has been applied to finding the behaviour of the vertex functions. While similar approximations have been made, such analyses must be consistent with explicit perturbative results where *no* approximation is made at a particular loop order to drop a subset of contributing graphs. As an aside, lattice gauge theory calculations of vertex functions equally have to match on to perturbative results. Therefore, in light of these different areas of activity, there is a clear need to compute QCD n -point, and specifically vertex functions, off-shell as well as on-shell. For the former, which is the focus of this article, we will review the status of the two-loop evaluation of the three-point vertices as well as outline the algorithm to extend this to higher-

*This contribution should be cited as:

J.A. Gracey, Vertex functions in QCD—preparation for beyond two loops, DOI: [10.23731/CYRM-2020-003.97](https://doi.org/10.23731/CYRM-2020-003.97), in: Theory for the FCC-ee, Eds. A. Blondel, J. Gluza, S. Jadach, P. Janot and T. Riemann, CERN Yellow Reports: Monographs, CERN-2020-003, DOI: [10.23731/CYRM-2020-003](https://doi.org/10.23731/CYRM-2020-003), p. 97.
© CERN, 2020. Published by CERN under the [Creative Commons Attribution 4.0 license](https://creativecommons.org/licenses/by/4.0/).

loop order. While the discussion will be technical in nature, we will pool together all the necessary ingredients for the goal to be obtained at three loops.

While it is not immediately obvious, it is the case that the route to achieve this will involve higher-level mathematics extracted, for instance, from an algebraic geometry approach. Indeed, this also lies at the heart of on-shell amplitude computations. This technology has revolutionized the programme of loop calculations. An example of this can be seen in the results for two-loop off-shell vertex results of Ref. [17], where harmonic polylogarithms based on a specific type of polynomials, known as cyclotomic, [18], appeared. One corollary of such results is the possibility of effecting renormalization schemes other than the canonical $\overline{\text{MS}}$ one, which is universally accepted as the default scheme. Although this is the scheme with which one can carry out very high loop order calculations, it is not a kinematic one and retains no data within the β function, for instance, of the information on the subtraction point. In Ref. [19], the momentum subtraction scheme, denoted MOM, was introduced and the R ratio studied [20]. Extending Ref. [19] to the next order in Ref. [21] produced the three-loop MOM renormalization group functions. This allowed for studies of physical quantities at a loop order where scheme effects were apparent [22]. One consequence is that choosing alternative renormalization schemes could lead to a different way of estimating theory errors in measurements. In other words, similar to an experiment estimating a measured quantity in different schemes, the average of the result could be a more sound way of assessing truncation errors as an alternative to using values at different scales. With fully off-shell vertex functions, for instance, this idea can be extended beyond the symmetric point subtraction of the MOM case to have a region bounding the central value.

This section is organised as follows. The method used to evaluate three-point off-shell vertex functions is discussed next, with reference to the triple-gluon vertex. This forms the basis for higher-loop computations, with the algorithm being outlined in Section 9.3. Concluding remarks are made in Section 9.4.

9.2 Current status

At the outset, it is worth reviewing aspects of the early QCD vertex evaluations. By this we mean that our focus will be on cases where there is *no* nullification of an external momentum. This is important, since, in the computation of the QCD β -function to very high loop order, the extraction of the $\overline{\text{MS}}$ coupling constant renormalization constant can be facilitated by setting the momentum of one of the external fields of the vertex function to zero. This is a mathematical shortcut, since the ultraviolet divergence is not contaminated by any infrared ones. By contrast, this infrared-safe procedure does not produce the *correct* finite part of the vertex functions, so it is not an appropriate method for gaining insight into any aspect of the kinematic properties of the vertex functions themselves. To be more concrete in the discussion, we will focus on the triple-gluon vertex function of Fig. B.9.1, which represents

$$\langle A_\mu^a(p_1) A_\nu^b(p_2) A_\sigma^c(-p_1 - p_2) \rangle = f^{abc} \Sigma_{\mu\nu\sigma}^{\text{ggg}}(p_1, p_2) = f^{abc} \sum_{k=1}^{14} \mathcal{P}_{(k)\mu\nu\sigma}^{\text{ggg}}(p_1, p_2) \Sigma_{(k)}^{\text{ggg}}(p_1, p_2), \quad (9.1)$$

where f^{abc} are the colour group structure constants. The momenta p_i satisfy energy–momentum conservation

$$\sum_{n=1}^3 p_n = 0 \quad (9.2)$$

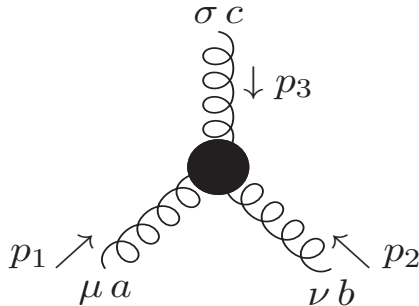


Fig. B.9.1: Triple-gluon vertex function

and the underlying Lorentz invariants that the three-point functions depend on are expressed in terms of two dimensionless variables, x and y , and one mass scale, μ , which are defined by

$$x = \frac{p_1^2}{p_3^2}, \quad y = \frac{p_2^2}{p_3^2}, \quad p_3^2 = -\mu^2, \quad (9.3)$$

and we assume that none of p_i^2 vanishes. In Eq. (9.1), we have decomposed the vertex into its 14 scalar amplitudes $\Sigma_{(k)}^{\text{ggg}}(p_1, p_2)$ with respect to a basis of Lorentz tensors $\mathcal{P}_{(k)\mu\nu\sigma}^{\text{ggg}}(p_1, p_2)$. With this structure in mind for the other two three-point vertices, the full one-loop vertex functions were studied in Ref. [19] in the early years following the discovery of asymptotic freedom.

Two important main early papers that stand out are Refs. [19, 23]. The former focused on the vertex functions at the fully symmetric subtraction point defined by $x = y = 1$ and introduced the MOM kinematic renormalization scheme known as MOM for momentum subtraction. Unlike the $\overline{\text{MS}}$ scheme, the renormalization is carried out at this specific symmetric point and the finite part of the vertex functions is absorbed into the renormalization constants. Therefore, the β -functions contain kinematic data. The motivation of Ref. [19] was to study whether the convergence of the perturbative series could be improved in this new scheme. The other article [23] reported a systematic study of each fully off-shell three-point vertex with a view to writing each in terms of amplitudes dictated by external gluons being transverse. As such, it has served as the default vertex function convention, where Schwinger–Dyson techniques are used to approximate other Green’s functions. Consequently, there have been a large number of one-loop studies of the three three-point vertices for different external momentum configurations, as noted earlier. In some cases, these studies have been at two loops, but for the most part one or more external gluon legs were on-shell and quarks have been massless, except in the case of Refs. [3, 7]. In the main, the evaluation has been by standard quantum field theory techniques via Feynman graphs. However, modern string-inspired methods have been used [11, 24] for off-shell one-loop vertex functions. The case where a gluon, for example, is on-shell must be treated separately from the configuration introduced in Eq. (9.3), owing to potential infrared singularities in taking the on-shell limit from the fully off-shell results.

Studies of the vertex functions for the special cases where one or more external lines are on-shell has direct applications to experimental set-ups. One of the reasons why these were computed was, in the main, that the calculational tools for the off-shell case were not developed until much later. Several main components were necessary for this, with the main breakthrough arriving in the form of the Laporta algorithm [25]. This is a procedure of relating scalar Feynman integrals of a particular n -point function at a specified loop order to core or master integrals of r -point functions with $r \leq n$ and the same loop order, the connection between integrals

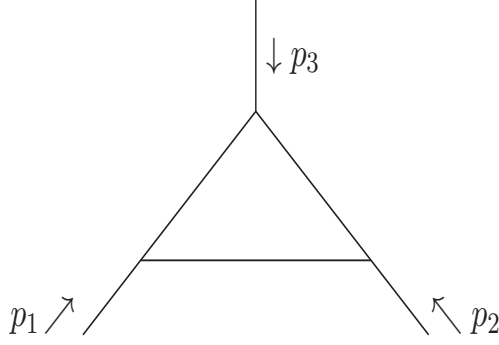


Fig. B.9.2: One-loop three-point master integral $I_1(x, y)$

being made via integration by parts. Then, starting with the most complicated integral, the relations derived from integration by parts could be solved algebraically. While such a large set of equations clearly contains a degree of redundancy, the whole process can be encoded for a computer to handle and several packages to do so are publicly available [26–32]. The second breakthrough necessary to complete this task was the determination of the master integrals. For three-point functions, these had to be constructed by specialised methods [33–36] to two loops, as integration by parts had been exhausted by the Laporta algorithm. To give a flavour of the resultant mathematical structure, the one-loop master integral of Fig. B.9.2 is, for instance, given by [33–35]

$$I_1(x, y) = -\frac{1}{\mu^2} \left[\Phi_1(x, y) + \Psi_1(x, y)\epsilon + \left[\frac{\zeta(2)}{2}\Phi_1(x, y) + \chi_1(x, y) \right] \epsilon^2 + O(\epsilon^3) \right] \quad (9.4)$$

in $d = 4 - 2\epsilon$ dimensions, where $\zeta(z)$ is the Riemann zeta function. Here, the functions are related to polylogarithms $\text{Li}_n(z)$. For instance

$$\Phi_1(x, y) = \frac{1}{\lambda} \left[2\text{Li}_2(-\rho x) + 2\text{Li}_2(-\rho y) + \ln\left(\frac{y}{x}\right) \ln\left(\frac{(1 + \rho y)}{(1 + \rho x)}\right) + \ln(\rho x) \ln(\rho y) + \frac{\pi^2}{3} \right], \quad (9.5)$$

with

$$\rho(x, y) = \frac{2}{[1 - x - y + \lambda(x, y)]}, \quad \lambda(x, y) = [1 - 2x - 2y + x^2 - 2xy + y^2]^{\frac{1}{2}}, \quad (9.6)$$

with the other functions of Eq. (9.4) given in [33–35] too. While the $O(\epsilon)$ terms may not, at first sight, appear to be necessary, they are required for various reasons. One is that, at higher loops, these one-loop expressions are multiplied by the counterterms. Thus, when a pole in ϵ multiplies a term that is $O(\epsilon)$, then that will contribute to the finite part of the vertex function at the next loop order. Accordingly, one needs the master integrals to at least $O(\epsilon^2)$ at one loop for a three-loop evaluation. We have indicated this since it could be the case that, in the reduction using the Laporta algorithm, a spurious pole in ϵ arises, which we discuss later. This is not an uncommon occurrence but the latest Laporta algorithm packages now have tools to circumvent this possibility. These technical issues aside, the full off-shell three-point QCD vertex functions are available to two loops with more details provided in Ref. [17].

9.3 Three-loop strategy

One reason for detailing the formalism to carry out the two-loop computations is that it points the way for higher-loop corrections. On that basis, we outline the next parts of the jigsaw to construct the three-loop extension of Ref. [17]. First, we assume that the procedure of the general algorithm for the Green's functions is applied to obtain the three-loop scalar amplitudes, as illustrated in Eq. (9.1). From these, the large set of scalar Feynman integrals is assembled; these must be reduced to the master integrals. The Laporta algorithm can, in principle, be applied in the three-loop case, using one of the latest packages that have the built-in improvements, such as the refined algebraic reduction of the KIRA package [32]. However, to speed the integration by parts procedure, it is not inconceivable that a faster algorithm could be developed. For instance, for many years, the MINCER package served the multiloop community well for three-loop massless two-point graphs in four dimensions [37,38]. It implemented the star-triangle rule to produce an efficient code to evaluate even the heaviest fully gluonic three-loop graphs. With the need for more precision experimentally, the four-loop FORCER package [39,40] has superseded MINCER in the journey to hit the latest precision benchmark. Each has been encoded in the symbolic manipulation language FORM [41,42]. With increasing loop order, the evaluation time for a Green's function increases. However, the FORCER algorithm implements a *new* integration rule to handle an internal topology that has no three-loop antecedents and hence is a purely four-loop feature. We have mentioned this since FORCER, like MINCER, applies only to two-point functions. However, the same new rule should be applicable or adaptable to three-loop three-point functions, since such a configuration emerges when one slices the vertex off a two-point function, where that vertex contains one of the external legs. The remaining graph would retain the internal topology of the two-point four-loop case. Therefore, an adaptation of the new feature of FORCER could, in principle, be transferred to the three-point case to provide an efficient alternative to the application of the Laporta algorithm for massless three-point functions.

While such technology is already in effect in situ, the main obstacle to the full implementation of a three-loop evaluation is the determination of the required three-loop master integrals. In recent years, this field has advanced, with progress made in understanding the mathematical properties of high-order Feynman integrals. Examples of such articles include Refs. [43,44], which provide novel procedures to compute Feynman graphs. The background to this is that there is a wide range of tools to evaluate a graph. One method is to introduce the Schwinger parameter representation of each propagator and convert the L -loop d -dimensional space-time integral into an integral over Schwinger parameters. The resulting integral has a large number of parameter integrations to be carried out and there is no guarantee that this can be achieved analytically. This is to be preferred over a numerical approach, as the latter, if a Monte Carlo approach is used, could require a sizeable amount of computer resources to obtain reasonable accuracy. In certain instances, an analytical evaluation is possible and, in essence, uses algebraic geometry to produce an integration strategy. Such higher mathematics is relevant, since the integrand contains polynomials of the parameters, which represent higher-dimensional geometries. Established mathematical theorems are then effected, which determine which parameter integration order is to be used, with the guiding principle being linear reducibility. By this, we mean that after each parameter integration the polynomial degree reduces but the key to achieve this is to have the polynomial factor off a smaller polynomial involving only factors linear in the next variable to be integrated. It is this linearity that is key, as it allows one to use the machinery of hyperlogarithms to carry out the integration over that Schwinger parameter.

What was not immediately evident is whether this procedure could be iterated without obstruction and that when it terminates the value of the integral is found. It has now been shown that, if an integral is linearly reducible [45,46], in this sense there is at least one choice of integration order that allows the integral to be determined. While this is, in essence, the general current position, it is known that, to three loops, the three-point vertex master integrals are all linearly reducible. Thus, in principle, the required master integrals can be determined.

The actual practicalities of this have yet to be carried out. However, several packages are available to assist with this task. For instance, converting a scalar Feynman integral into Schwinger parameter representation via the underlying graph polynomials is now a standard feature of integration packages, such as HYPERINT [47]. This package is appropriate for an analytical determination, since any evaluation can be written in various hyperlogarithm representations. It has features that allow one to find the order of integration over the parameter variables to ensure that there is no obstruction to the linear reducibility. In principle, one can expand to several orders in the ϵ expansion in $d = 4 - 2\epsilon$ dimensions. However, for terms beyond the leading few, the parameter integration can become tedious, especially for high loop orders. Therefore, a more appropriate strategy would be one where only the first term of the ϵ expansion of a master integral was required, which would then require the Laporta reduction to be constrained to producing a basis of masters that is finite. There is a caveat with this because one is using dimensional regularisation, which means that the reduction produces factors of rational polynomials in d . Such functions can include poles in $(d - 4)$, which are termed spurious poles. This is in the sense that while they correspond to a divergence it is not necessarily one due to the divergence of an actual graph. There are now ways to circumvent this, which work hand in hand with another property of the beauty of computing in d dimensions. This was analysed in depth in Refs. [48,49], where it was shown that d -dimensional integrals can be related to the corresponding topology in $(d + 2)$ dimensions plus a sum of others that have the same core topology but with propagators missing. Such higher-dimensional integrals can be incorporated in the Laporta reduction process and have been implemented in version 2.11 of the REDUZE package [27]. The advantage is that, with the increase in dimensionality in the higher-dimensional integral, it is not as ultraviolet divergent as its lower-dimensional counterpart. Thereby, in principle, one reduces the evaluation of the more difficult master integrals to finite higher-dimensional ones, which should therefore be more accessible to the HYPERINT package.

In summarising the algorithm to extend the two-loop QCD off-shell vertex functions, it is worth noting that, for the triple-gluon vertex, there will be 2382 three-loop graphs to evaluate and 63 992 at four loops. For both the other three-point vertices, the numbers of graphs in each case are the same and are 688 and 17 311, respectively, at three and four loops. Thus, the evaluation of even just the three-loop vertex functions will require a substantial amount of work and computing time. This would especially be the case at four loops without access to appropriate computers to build the necessary databases of integral relations. In the interim, there is a potential alternative to gain some insight into or estimate of the three-loop contributions. In the period between the early work of Celmaster and Gonsalves [19] and its extension to the next order in Ref. [21], a method was developed [9] where the vertex functions were computed, at the fully symmetric point, numerically at two loops in QCD. The approach was to apply a large momentum expansion of the vertex functions to very high order. This produced a set of two-point integrals, which were evaluated using MINCER [37,38]. Provided that enough terms were computed, the approximate value of the contributing graphs could

be accurately estimated numerically. The stability and accuracy of the expansion could be checked by choosing different external momenta to play the role of the large momentum. What was remarkable when the analytic two-loop expressions became available [21] was how accurate the large-momentum MINCER-based expansion values were. The only major difference was for a colour group Casimir coefficient in one three-loop MOM β function, which turned out to be of the order 0.01 [9]. The numerical coefficient was small and the expansion needed to a higher accuracy than was computationally available at the time [9]. With advances in symbolic manipulation, such as the provision of the FORCER program, which is significantly more efficient than MINCER, such an interim numerical evaluation of the vertex functions would at least give information on the magnitude of the next-order corrections. As a corollary, it would provide the four-loop MOM β functions numerically.

9.4 Discussion

To recap, we have reviewed recent results in the determination of the three-point vertex functions of QCD at two loops. We have for the most part concentrated on the off-shell case; it would not have been possible to achieve this without the earlier work on different external momentum configurations. While the two-loop off-shell results followed a long time after the one-loop case, the main reason for this was lack of the required computational technology. The last decade has seen a revolution in this direction with the Laporta algorithm [25], as well as a systematic way of computing master integrals from high-level mathematics. Consequently, the road to achieve the extension to three loops is, in principle, possible. One useful corollary of such a computation would be the extension of the renormalization group functions to four loops in kinematic schemes such as MOM. To go to higher orders beyond three, this depends on whether the linear reducibility of four-loop masters can be established. One case that we have not touched on is that of the four-point functions. The technology to compute the full off-shell one-loop amplitudes is already available. However, the current situation is that the relevant two-loop off-shell masters have not been computed. Moreover, it has not been established whether they are linearly reducible in order that the hyperlogarithm approach can be applied. This at present appears to be an open question for future work. Finally, including massive quarks in three- and four-point functions is another direction that needs consideration. However, this is not straightforward at two loops, since the three-point masters with one mass scale and off-shell momentum configuration are not yet known.

References

- [1] P. Pascual and R. Tarrach, *Nucl. Phys.* **B174** (1980) 123 [Erratum: **B181** (1981) 546]. [doi:10.1016/0550-3213\(80\)90193-5](https://doi.org/10.1016/0550-3213(80)90193-5), [doi:10.1016/0550-3213\(81\)90540-X](https://doi.org/10.1016/0550-3213(81)90540-X)
- [2] A.I. Davydychev *et al.*, *Phys. Rev.* **D54** (1996) 4087 [Erratum: **D59** (1999) 109901]. [arXiv:hep-ph/9605348](https://arxiv.org/abs/hep-ph/9605348), [doi:10.1103/PhysRevD.54.4087](https://doi.org/10.1103/PhysRevD.54.4087), [doi:10.1103/PhysRevD.59.109901](https://doi.org/10.1103/PhysRevD.59.109901)
- [3] A.I. Davydychev *et al.*, *JHEP* **08** (2001) 050. [arXiv:hep-ph/0105072](https://arxiv.org/abs/hep-ph/0105072), [doi:10.1088/1126-6708/2001/08/050](https://doi.org/10.1088/1126-6708/2001/08/050)
- [4] M. Binger and S.J. Brodsky, *Phys. Rev.* **D74** (2006) 054016. [arXiv:hep-ph/0602199](https://arxiv.org/abs/hep-ph/0602199), [doi:10.1103/PhysRevD.74.054016](https://doi.org/10.1103/PhysRevD.74.054016)
- [5] A.I. Davydychev *et al.*, *Phys. Rev.* **D58** (1998) 036007. [arXiv:hep-ph/9801380](https://arxiv.org/abs/hep-ph/9801380), [doi:10.1103/PhysRevD.58.036007](https://doi.org/10.1103/PhysRevD.58.036007)

-
- [6] A.I. Davydychev and P. Osland, *Phys. Rev.* **D59** (1999) 014006. [arXiv:hep-ph/9806522](#), [doi:10.1103/PhysRevD.59.014006](#)
- [7] A.I. Davydychev *et al.*, *Phys. Rev.* **D63** (2001) 014022. [arXiv:hep-ph/0008171](#), [doi:10.1103/PhysRevD.63.014022](#)
- [8] K.G. Chetyrkin and A. Retey, Three loop three linear vertices and four loop similar to MOM beta functions in massless QCD. [arXiv:hep-ph/0007088](#)
- [9] K.G. Chetyrkin and T. Seidensticker, *Phys. Lett.* **B495** (2000) 74. [arXiv:hep-ph/0008094](#), [doi:10.1016/S0370-2693\(00\)01217-X](#)
- [10] C. Kellermann and C.S. Fischer, *Phys. Rev.* **D78** (2008) 025015. [arXiv:0801.2697](#), [doi:10.1103/PhysRevD.78.025015](#)
- [11] N. Ahmadiaz and C. Schubert, *Nucl. Phys.* **B869** (2013) 417. [arXiv:1210.2331](#), [doi:10.1016/j.nuclphysb.2012.12.019](#)
- [12] A. Blum *et al.*, *Phys. Rev.* **D89** (2014) 061703. [arXiv:1401.0713](#), [doi:10.1103/PhysRevD.89.061703](#)
- [13] A.L. Blum *et al.*, *EPJ Web Conf.* **137** (2017) 03001. [arXiv:1611.04827](#), [doi:10.1051/epjconf/201713703001](#)
- [14] M. Mitter *et al.*, *Phys. Rev.* **D91** (2015) 054035. [arXiv:1411.7978](#), [doi:10.1103/PhysRevD.91.054035](#)
- [15] R. Alkofer *et al.*, *Ann. Phys.* **324** (2009) 106. [arXiv:0804.3042](#), [doi:10.1016/j.aop.2008.07.001](#)
- [16] R. Alkofer and M. Mitter, *PoS ConfinementX* (2012) 061. [arXiv:1302.0307](#), [doi:10.22323/1.171.0061](#)
- [17] J.A. Gracey, *Phys. Rev.* **D90** (2014) 025014. [arXiv:1406.0649](#), [doi:10.1103/PhysRevD.90.025014](#)
- [18] J. Ablinger *et al.*, *J. Math. Phys.* **52** (2011) 102301. [arXiv:1105.6063](#), [doi:10.1063/1.3629472](#)
- [19] W. Celmaster and R.J. Gonsalves, *Phys. Rev.* **D20** (1979) 1420. [doi:10.1103/PhysRevD.20.1420](#)
- [20] W. Celmaster and R.J. Gonsalves, *Phys. Rev.* **D21** (1980) 3112. [doi:10.1103/PhysRevD.21.3112](#)
- [21] J.A. Gracey, *Phys. Rev.* **D84** (2011) 085011. [arXiv:1108.4806](#), [doi:10.1103/PhysRevD.84.085011](#)
- [22] J.A. Gracey, *Phys. Rev.* **D90** (2014) 094026. [arXiv:1410.6715](#), [doi:10.1103/PhysRevD.90.094026](#)
- [23] J.S. Ball and T.-W. Chiu, *Phys. Rev.* **D22** (1980) 2550, [Erratum: **D23**,3085(1981)]. [doi:10.1103/PhysRevD.22.2550](#), [doi:10.1103/PhysRevD.23.3085.2](#)
- [24] N. Ahmadiaz, C. Schubert, *PoS QCD-TNT-III* (2013) 002. [arXiv:1311.6829](#), [doi:10.22323/1.193.0002](#)
- [25] S. Laporta, *Int. J. Mod. Phys.* **A15** (2000) 5087. [arXiv:hep-ph/0102033](#), [doi:10.1142/S0217751X00002157](#)
- [26] C. Studerus, *Comput. Phys. Commun.* **181** (2010) 1293. [arXiv:0912.2546](#), [doi:10.1016/j.cpc.2010.03.012](#)

- [27] A. von Manteuffel and C. Studerus, Reduze 2—distributed Feynman integral reduction. [arXiv:1201.4330](#)
- [28] A.V. Smirnov, *JHEP* **10** (2008) 107. [arXiv:0807.3243](#),
[doi:10.1088/1126-6708/2008/10/107](#)
- [29] R.N. Lee, Presenting LiteRed: a tool for the Loop InTEgrals REDuction. [arXiv:1212.2685](#)
- [30] R.N. Lee, *J. Phys. Conf. Ser.* **523** (2014) 012059. [arXiv:1310.1145](#),
[doi:10.1088/1742-6596/523/1/012059](#)
- [31] C. Anastasiou and A. Lazopoulos, *JHEP* **07** (2004) 046.
[arXiv:hep-ph/0404258](#), [doi:10.1088/1126-6708/2004/07/046](#)
- [32] P. Maierhofer *et al.*, *Comput. Phys. Commun.* **230** (2018) 99. [arXiv:1705.05610](#),
[doi:10.1016/j.cpc.2018.04.012](#)
- [33] A.I. Davydychev, *J. Phys.* **A25** (1992) 5587. [doi:10.1088/0305-4470/25/21/017](#)
- [34] N.I. Usyukina and A.I. Davydychev, *Phys. Atom. Nucl.* **56** (1993) 1553 [*Yad. Fiz.* **56N11** (1993) 172]. [arXiv:hep-ph/9307327](#)
- [35] N.I. Usyukina and A.I. Davydychev, *Phys. Lett.* **B332** (1994) 159.
[arXiv:hep-ph/9402223](#), [doi:10.1016/0370-2693\(94\)90874-5](#)
- [36] T.G. Birthwright *et al.*, *JHEP* **09** (2004) 042. [arXiv:hep-ph/0407343](#), [doi:10.1088/1126-6708/2004/09/042](#)
- [37] S.G. Gorishnii *et al.*, *Comput. Phys. Commun.* **55** (1989) 381.
[doi:10.1016/0010-4655\(89\)90134-3](#)
- [38] S.A. Larin *et al.*, The FORM version of MINCER, NIKHEF-H-91-18.
- [39] T. Ueda *et al.*, *PoS LL2016* (2016) 070. [arXiv:1607.07318](#), [doi:10.22323/1.260.0070](#)
- [40] B. Ruijl *et al.*, Forcer, a FORM program for the parametric reduction of four-loop massless propagator diagrams. [arXiv:1704.06650](#)
- [41] J.A.M. Vermaseren, New features of FORM, [arXiv:math-ph/0010025](#)
- [42] M. Tentyukov and J.A.M. Vermaseren, *Comput. Phys. Commun.* **181** (2010) 1419.
[arXiv:hep-ph/0702279](#), [doi:10.1016/j.cpc.2010.04.009](#)
- [43] F. Brown, On the decomposition of motivic multiple zeta values. [arXiv:1102.1310](#)
- [44] O. Schnetz, *Phys. Rev.* **D97** (2018) 085018. [arXiv:1606.08598](#),
[doi:10.1103/PhysRevD.97.085018](#)
- [45] F. Brown, *Commun. Math. Phys.* **287** (2009) 925. [arXiv:0804.1660](#),
[doi:10.1007/s00220-009-0740-5](#)
- [46] F.C.S. Brown, On the periods of some Feynman integrals. [arXiv:0910.0114](#)
- [47] E. Panzer, *Comput. Phys. Commun.* **188** (2015) 148. [arXiv:1403.3385](#),
[doi:10.1016/j.cpc.2014.10.019](#)
- [48] O.V. Tarasov, *Phys. Rev.* **D54** (1996) 6479. [arXiv:hep-th/9606018](#),
[doi:10.1103/PhysRevD.54.6479](#)
- [49] O.V. Tarasov, *Nucl. Phys.* **B502** (1997) 455. [arXiv:hep-ph/9703319](#),
[doi:10.1016/S0550-3213\(97\)00376-3](#)

10 Effective field theory approach to QED corrections in flavour physics

Contribution* by: M. Beneke, C. Bobeth, R. Szafron

Corresponding author: R. Szafron [robert.szafron@tum.de]

10.1 Introduction and motivation

Thanks to the accurate measurements performed at the low-energy facilities [1] and the LHC, flavour physics of light quarks, especially the bottom quark, emerged on the precision frontier for tests of the Standard Model (SM) and in searches for new physics effects. On the theoretical side, short-distance perturbative higher-order QCD and electroweak corrections are under good control for many processes. Moreover, tremendous progress in lattice computations [2] allows percentage to even subpercentage accuracy to be achieved for long-distance non-perturbative quantities. This allows for the prediction of some key observables with unprecedented accuracy and, in turn, the determination of short-distance parameters, such as the elements of the quark-mixing matrix (CKM) in the framework of the SM. Given these prospects, it is also desirable to improve the understanding and treatment of QED corrections, which are generally assumed to be small. Unfortunately, not much new development has taken place in the evaluation of such corrections.

For the future e^+e^- machines, the proper computation of QED corrections will be particularly important because the large data samples allow for precision measurements that require their inclusion in theoretical predictions. We would like to advocate a framework for a proper and systematic treatment of QED effects based on the effective field theory (EFT) approach, which exploits scale hierarchies present in processes involving mesons. In this spirit, QED corrections to $B_s \rightarrow \mu^+\mu^-$ have recently been analysed [3], revealing an unexpectedly large contribution owing to power enhancement. Such an effect cannot be found in the standard approach based on soft-photon approximation [4–6], as it requires a helicity flip induced by the photon. Further, the common assumption that hadrons are point-like objects neglects effects related to the structure of hadrons. It implies implicitly that the soft-photon approximation itself is performed in the framework of an EFT in which photons have virtuality below a typical hadronic binding scale $\Lambda_{\text{QCD}} \sim \mathcal{O}(100 \text{ MeV})$ of partons in hadrons, below which they do not resolve the partonic structure of the hadrons. In consequence, this approach cannot address QED corrections, owing to virtualities above the scale Λ_{QCD} . These observations are a motivation to scrutinise further QED corrections in flavour physics in the light of upcoming precise measurements and existing tensions in flavour measurements, in particular, related to tests of lepton flavour universality.

In addition to a systematic power counting, the EFT treatment offers the possibility of the all-order resummation of the corrections. This is particularly important for the mixed QCD–QED corrections, owing to the size of the QCD coupling constant and the presence of large logarithmic corrections. While the soft-exponentiation theorem allows resumming leading QED

*This contribution should be cited as:

M. Beneke, C. Bobeth, R. Szafron, Effective field theory approach to QED corrections in flavour physics, DOI: [10.23731/CYRM-2020-003.107](https://doi.org/10.23731/CYRM-2020-003.107), in: Theory for the FCC-ee, Eds. A. Blondel, J. Gluza, S. Jadach, P. Janot and T. Riemann,

CERN Yellow Reports: Monographs, CERN-2020-003, DOI: [10.23731/CYRM-2020-003](https://doi.org/10.23731/CYRM-2020-003), p. 107.

© CERN, 2020. Published by CERN under the [Creative Commons Attribution 4.0 license](https://creativecommons.org/licenses/by/4.0/).

effects related to ultrasoft photons that do not resolve the partonic structure of hadrons, not much is known about the resummation of the subleading logarithms in QED for photons with larger virtuality. Standard factorisation theorems derived in QCD cannot be directly translated to QED, for, in the QCD case, the mass effects related to light degrees of freedom are typically neglected. This is not the case in QED, where the lepton mass provides a cut-off for collinear divergences. Moreover, the fact that in QCD one can observe only colour singlet states additionally simplifies the computations, while in QED, and more generally in the electroweak sector of the SM [7,8], it is necessary to account for charged particles in both the final and initial states. As a result, the QED factorisation theorems have not been explored intensively in the literature so far, but this gap should be filled before a precise e^+e^- collider becomes operational.

Power corrections to the standard soft approximation may also play an important role in certain processes. Studies of power corrections in the QCD case recently gained much attention [9–15]. New tools based on soft-collinear EFT (SCET) developed to study processes with energetic quarks and gluons can, after certain modifications, be applied to improve the accuracy of electroweak corrections in future lepton colliders. This is particularly important in collider physics for regions of phase space where the perturbative approach breaks down, owing to the presence of large logarithmic enhancements, and the next-to-soft effects become more important. Particularly interesting are mass-suppressed effects related to soft fermion exchange [16–18], whose consistent treatment in the SCET language is not yet fully known. Beyond applications to precision SM physics, the SCET framework may be necessary after possible discovery of new physics at the LHC [19,20].

10.2 QED corrections in $B_q \rightarrow \ell^+\ell^-$

The decay of a neutral meson $B_q \rightarrow \ell^+\ell^-$ ($\ell = e, \mu, \tau$) is the first step in an investigation of QED effects in QCD bound states. Its purely leptonic final state and neutral initial state keep complications related to the non-perturbative nature of QCD to the necessary minimum. Yet, as we shall see, even this simple example requires investigation of power corrections in SCET. The importance of this decay derives from the fact that it depends, at leading order (LO) in QED, only on the B_q meson decay constant, which can nowadays be calculated with subpercentage precision on the lattice [21], necessitating the inclusion of higher-order QED corrections from all scales at this level. This decay has been observed for $\ell = \mu$ by LHCb [22,23], CMS [24], and ATLAS [25]. The currently measured branching fraction for B_s decays of about 3×10^{-9} is compatible with the latest SM predictions [3,26,27] and it is expected that the LHCb experiment will be able to measure the branching fraction with 5% accuracy with 50/fb (Run 4) around the year 2030 [28]. The FCC-ee running on the Z resonance is expected to provide, with about $\mathcal{O}(10^3)$ reconstructed events [29], an even higher event yield compared with LHCb Run 4. This, together with the cleaner hadronic environment at the FCC-ee, should allow better control of backgrounds and also systematic uncertainties, such that one can expect improved accuracy. However, the gain in accuracy cannot be quantified without a dedicated study.

On the theory side, electroweak and QCD corrections above the scale $\mu_b \sim 5$ GeV of the order of the b quark mass m_b are treated in the standard framework of weak EFT of the SM [30]. The effective Lagrangian is a sum of four-fermion and dipole operators

$$\mathcal{L}_{\Delta B=1} = \mathcal{N}_{\Delta B=1} \left[\sum_{i=1}^{10} C_i(\mu_b) Q_i \right] + \text{h.c.}, \quad (10.1)$$

with $\mathcal{N}_{\Delta B=1} \equiv 2\sqrt{2}G_F V_{tb} V_{tq}^*$ and covers, in principle, all weak decays of b hadrons. The perti-

relevant operators for $B_q \rightarrow \ell^+ \ell^-$ ($q = d, s$) are

$$\begin{aligned} Q_7 &= \frac{e}{(4\pi)^2} [\bar{q} \sigma^{\mu\nu} (m_b P_R + m_q P_L) b] F_{\mu\nu}, \\ Q_9 &= \frac{\alpha_{\text{em}}}{4\pi} [\bar{q} \gamma^\mu P_L b] \sum_\ell [\bar{\ell} \gamma_\mu \ell], \\ Q_{10} &= \frac{\alpha_{\text{em}}}{4\pi} [\bar{q} \gamma^\mu P_L b] \sum_\ell [\bar{\ell} \gamma_\mu \gamma_5 \ell]. \end{aligned} \quad (10.2)$$

The matching $C_i(\mu_b)$ coefficients are computed at the electroweak scale $\mu_W \sim \mathcal{O}(100 \text{ GeV})$ and evolved to the scale of $\mu_b \sim m_b$ with the renormalization group equation of the weak EFT.

Because the neutral B_q meson is a pseudo-scalar and the SM interactions are mediated by axial and vector currents, the decay rate must vanish in the limit $m_\ell \rightarrow 0$, and therefore the decay amplitude is proportional to the lepton mass. The hadronic matrix element at LO in QED is parametrized by a single decay constant f_{B_q} , defined by $\langle 0 | \bar{q} \gamma^\mu \gamma_5 b | \bar{B}_q(p) \rangle = i f_{B_q} p^\mu$. The leading amplitude for $B_q \rightarrow \ell^+ \ell^-$ is

$$i\mathcal{A} = m_\ell f_{B_q} \mathcal{N} C_{10}(\mu_b) [\bar{\ell} \gamma_5 \ell], \quad \left(\mathcal{N} \equiv \mathcal{N}_{\Delta B=1} \frac{\alpha_{\text{em}}}{4\pi} \right) \quad (10.3)$$

and the branching fraction is

$$\text{Br}_{q\ell}^{(0)} \equiv \text{Br}^{(0)}[B_q \rightarrow \ell^+ \ell^-] = \frac{\tau_{B_q} m_{B_q}^3 f_{B_q}^2}{8\pi} |\mathcal{N}|^2 \frac{m_\ell^2}{m_{B_q}^2} \sqrt{1 - \frac{4m_\ell^2}{m_{B_q}^2}} |C_{10}|^2, \quad (10.4)$$

with m_{B_q} denoting the mass of the meson and τ_{B_q} its total lifetime. For neutral B_s mesons, the mixing needs to be accounted for [31], thereby allowing for the measurement of related CP asymmetries, to be discussed next. In this case, Eq. (10.4) refers to the ‘instantaneous’ branching fraction at time $t = 0$, which differs from the measured untagged time-integrated branching fraction by the factor $(1 - y_s^2)/(1 + y_s \mathcal{A}_{\Delta\Gamma})$, where $y_s = \Delta\Gamma_s/(2\Gamma_s)$ is related to the lifetime difference and $\mathcal{A}_{\Delta\Gamma}$ denotes the mass-eigenstate rate asymmetry. Concerning QED corrections, this branching fraction refers to the ‘non-radiative’ one prior to the inclusion of photon bremsstrahlung effects.

If one takes into account soft-photon radiation (both real and virtual) with energies smaller than the lepton mass, the decay amplitude is dressed by the standard Yennie–Frautschi–Suura exponent [4, 32]

$$\text{Br}[B_q \rightarrow \ell^+ \ell^- + n\gamma] = \text{Br}_{q\ell}^{(0)} \times \left(\frac{2E_{\text{max}}}{m_{B_q}} \right)^{2\frac{\alpha_{\text{em}}}{\pi} \left(\ln \frac{m_{B_q}^2}{m_\ell^2} - 1 \right) + \mathcal{O}(m_\ell)}. \quad (10.5)$$

This ‘photon-inclusive’ branching fraction is based on eikonal approximation, in the limit when the total energy carried away by the n photons, E_{max} , is much smaller than the lepton mass. The QED corrections in the initial state are entirely neglected and photons are assumed to couple to leptons through eikonal currents

$$J^\mu(q) = e \sum_i Q_i \eta_i \frac{p_i^\mu}{p_i \cdot q}, \quad (10.6)$$

where $\eta = -1$ for incoming particles and $\eta = +1$ for outgoing particles. The sum runs over all charged particles with momenta p_i and charges Q_i . Eikonal currents are spin-independent and thus they do not change the helicity of the leptons.

From this point, we focus only on the case of muons in the final state, $\ell = \mu$. In the experimental analysis [23–25], the signal is simulated fully inclusive of final-state radiation off the muons by applying PHOTOS [33] corresponding to a convolution of the E_{\max} -dependent exponential factor in the determination of the signal efficiency. Conversely, photon emission from the quarks (initial state) vanishes in the limit of small photon energies because it is infrared-safe, since the decaying meson is electrically neutral. Hence, it can be neglected as long as the signal window is sufficiently small, in practice of $\mathcal{O}(60 \text{ MeV})$ [34], and is effectively treated as negligible background on both experimental and theory sides. In consequence, the experimental analyses currently provide the non-radiative branching fraction relying on the simulation with PHOTOS.

The limitations of the conventional approximation had missed the important effect responsible for the power enhancement of QED corrections to the $B_s \rightarrow \mu^+ \mu^-$ decay. Indeed, even when the cut on the real photon emission is much smaller than the muon mass, virtual photons with virtualities of the order of the muon mass or larger can resolve the structure of the meson, whose typical size is of the order of $1/\Lambda_{\text{QCD}}$. In this case, the meson cannot be treated as a point-like object. Moreover, the eikonal approximation is not suitable for such photons, as they can induce a helicity flip of the leptons. However, straightforward computation of the QED corrections is not possible, as it requires the evaluation of non-local time-ordered products of the $\mathcal{L}_{\Delta B=1}(0)$ Lagrangian with the electromagnetic current $j_{\text{QED}} = Q_q \bar{q} \gamma^\mu q$, such as

$$\langle 0 | \int d^4x T \{ j_{\text{QED}}(x), \mathcal{L}_{\Delta B=1}(0) \} | \bar{B}_q \rangle. \quad (10.7)$$

Currently, this object is beyond the reach of lattice QCD, while the SCET approach allows one to systematically expand this matrix element and reduce the non-perturbative quantities to universal ones at leading order.

Let us consider Fig. B.10.1, where the photon is exchanged between the light quark and the lepton. There are two low-energy scales in the diagram, set by the external kinematics of the process $B_q \rightarrow \mu^+ \mu^-$. One is the muon mass m_μ , which is related to the collinear scale. We parametrize the lepton momentum in terms of the light-cone co-ordinates as $p_\ell = (n_+ p_\ell, n_- p_\ell, p_\ell^\perp) \sim m_b (1, \lambda_c^2, \lambda_c)$, where we introduced the small counting parameter $\lambda_c \sim m_\mu/m_b$. The second low-energy scale is related to the typical size of the soft light quark momentum $l_q \sim \Lambda_{\text{QCD}}$ and for counting purposes we introduce $\lambda_s \sim \Lambda_{\text{QCD}}/m_b$. In the case of muons, it happens that numerically $\lambda_c \approx \lambda_s$ and in the following we equate them and do not distinguish between them. It turns out that there also exists a hard-collinear invariant constructed from the lepton and quark momentum $p_\ell \cdot l_q \sim \lambda m_b^2$, thus in addition to the collinear and soft regions we must also consider a hard-collinear region, where momenta scale as $k \sim m_b (1, \lambda, \lambda^{1/2})$. This non-trivial hierarchy of intermediate scales must be properly accounted to evaluate the leading QED corrections, which can be done by subsequent matching on SCET_I and SCET_{II} [35] at the hard ($\sim m_b$) and hard-collinear scales, respectively.

The power enhancement is directly related to the interplay of collinear and hard-collinear scales. When the hard-collinear or collinear photon interacts with the soft quark, momentum conservation forces the quark to become hard-collinear. These modes can be integrated out perturbatively with the help of the EFT methods. In this case, we must first match the operators

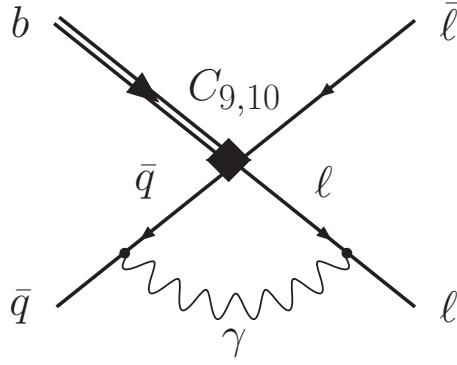


Fig. B.10.1: Example diagram that gives rise to the power-enhanced QED correction. A photon can be either collinear with virtuality $k^2 \sim m_\mu^2$ or hard-collinear, $k^2 \sim m_\mu m_b$.

in Eq. (10.2) on SCET_I currents [36]. In SCET_I, we retain soft, collinear, and hard-collinear modes; only the hard modes are integrated out. The leading SCET_I operator contains a hard-collinear quark field, which scales as $\lambda^{1/2}$ instead of the soft quark field with scaling $\lambda^{3/2}$. When we integrate out the hard-collinear modes, we must convert the hard-collinear quark field $\xi_C(x)$ to the soft quark field q_s . This is done with the help of power-suppressed Lagrangian [37]

$$\mathcal{L}_{\xi q}^{(1)} = \bar{q}_s(x_-) W_{\xi C}^\dagger i \not{D}_\perp \xi_C(x) - \bar{\xi}_C(x) i \overleftarrow{\not{D}}_\perp W_{\xi C} q_s(x_-),$$

where $W_{\xi C}$ is a collinear Wilson line carrying charge of the collinear field ξ_C . This Lagrangian insertion costs an additional power of $\lambda^{1/2}$, but the resulting SCET_{II} operators are still power-enhanced, as compared with the operators obtained without an intermediate hard-collinear scale. The power-enhanced correction to the amplitude is [3]

$$i\Delta\mathcal{A} = \frac{\alpha_{\text{em}}}{4\pi} Q_\ell Q_q m_\ell m_{B_q} f_{B_q} \mathcal{N} \left[\bar{\ell}(1 + \gamma_5)\ell \right] \\ \times \left\{ \int_0^1 du (1-u) C_9^{\text{eff}}(um_b^2) \int_0^\infty \frac{d\omega}{\omega} \phi_{B^+}(\omega) \left[\ln \frac{m_b \omega}{m_\ell^2} + \ln \frac{u}{1-u} \right] \right. \\ \left. - Q_\ell C_7^{\text{eff}} \int_0^\infty \frac{d\omega}{\omega} \phi_{B^+}(\omega) \left[\ln^2 \frac{m_b \omega}{m_\ell^2} - 2 \ln \frac{m_b \omega}{m_\ell^2} + \frac{2\pi^2}{3} \right] \right\}, \quad (10.8)$$

where $\phi_{B^+}(\omega)$ is the B_q meson light-cone distribution amplitude (LCDA), which contains information about the non-perturbative structure of the meson. This virtual correction is, by itself, infrared-finite, as it modifies the exclusive decay rate. The power enhancement manifests itself in Eq. (10.8) as the inverse power of the ω variable that results from the decoupling of the hard-collinear quark modes

$$m_{B_q} \int_0^\infty \frac{d\omega}{\omega} \phi_{B^+}(\omega) \ln^k \omega \sim \frac{m_{B_q}}{\Lambda_{\text{QCD}}} \sim \frac{1}{\lambda}. \quad (10.9)$$

The ω may be interpreted as a momentum of the soft quark along the light-cone direction of the lepton, and thus $\omega \sim \Lambda_{\text{QCD}}$. The annihilation of the quark into leptons is a non-local process in the presence of the QED interactions and the virtual leptons with the wrong helicity can propagate over distances of the order of the meson size. Thus, the helicity flip costs a

factor $m_\ell/\Lambda_{\text{QCD}}$ instead of the typical suppression factor of m_ℓ/m_b present in the leading-order amplitude.

The terms proportional to C_{10} cancel after the collinear and anticollinear contributions are added, such that only C_9 contributes out of the semileptonic operators. The term $\propto C_7$ requires separate treatment since the convolution integral containing the hard matching coefficient exhibits an endpoint singularity. In addition, the collinear contribution has a rapidity-type divergence. There exists an additional contribution related to the soft region, which, after a suitable rapidity regularisation, can be combined with the collinear contribution. When the convolution integral is performed in dimensional regularisation before taking the limit $d \rightarrow 4$, the total correction is finite and exhibits the double-logarithmic enhancement.

The numerical evaluation [3] of the power-enhanced correction (Eq. (10.8)) shows a partial cancellation of the terms $\propto C_9^{\text{eff}}$ and $\propto C_7^{\text{eff}}$. The final impact on the branching fraction $\text{Br}_{\text{qu}}^{(0)}$ is a decrease in the range (0.3–1.1)%, with a central value of 0.7%. Despite the cancellation, the overall correction is still sizeable compared with the natural size of a QED correction of $\alpha_{\text{em}}/\pi \sim 0.3\%$. The large uncertainties of the power-enhanced QED correction are due to the poorly known inverse moment λ_B and almost unknown inverse-logarithmic moments σ_1 and σ_2 of the B meson LCDA.* The prediction for the muonic modes for the untagged time-integrated branching fractions for $B_s \rightarrow \mu^+\mu^-$ and $B_d \rightarrow \mu^+\mu^-$ are

$$\overline{\text{Br}}_{\text{s}\mu}^{(0)} = \begin{pmatrix} 3.59 \\ 3.65 \end{pmatrix} \left[1 \pm \begin{pmatrix} 0.032 \\ 0.011 \end{pmatrix}_{f_{B_s}} \pm 0.031|_{\text{CKM}} \pm 0.011|_{m_t} \pm 0.012|_{\text{non-pmr}} \pm 0.006|_{\text{pmr}} \pm \begin{matrix} +0.003 \\ -0.005 \end{matrix}|_{\text{QED}} \right] \times 10^{-9}, \quad (10.10)$$

$$\overline{\text{Br}}_{\text{d}\mu}^{(0)} = \begin{pmatrix} 1.05 \\ 1.02 \end{pmatrix} \left[1 \pm \begin{pmatrix} 0.045 \\ 0.014 \end{pmatrix}_{f_{B_d}} \pm 0.046|_{\text{CKM}} \pm 0.011|_{m_t} \pm 0.012|_{\text{non-pmr}} \pm 0.003|_{\text{pmr}} \pm \begin{matrix} +0.003 \\ -0.005 \end{matrix}|_{\text{QED}} \right] \times 10^{-10}, \quad (10.11)$$

where we group uncertainties: (i) main parametric long-distance (f_{B_q}) and short-distance (CKM and m_t), (ii) remaining non-QED parametric (τ_{B_q} , α_s) and non-QED non-parametric (μ_W , μ_b , higher order, see Ref. [26]), and (iii) from the QED correction (λ_B and $\sigma_{1,2}$, see Ref. [3]). We provide here two values, depending on the choice of the lattice calculation of f_{B_q} for $N_f = 2 + 1$ (upper) and $N_f = 2 + 1 + 1$ (lower), with averages from FLAG 2019 [2]. Note that the small uncertainties of the $N_f = 2 + 1 + 1$ results are currently dominated by a single group [21] and confirmation by other lattice groups in the future is desirable. It can be observed that, in this case, the largest uncertainties are due to CKM parameters, such that they can be determined provided the accuracy of the measurements at the FCC-ee is at the 1% level. Still fairly large errors are due to the top quark mass $m_t = (173.1 \pm 0.6)$ GeV, here assumed to be in the pole scheme, where an additional non-parametric uncertainty of 0.2% is included (in ‘non-pmr’) for the conversion to the $\overline{\text{MS}}$ scheme. Further ‘non-pmr’ contains a 0.4% uncertainty from μ_W variation and 0.5% further higher-order uncertainty, all linearly added. For the CKM input, we use Refs. [3, 27].

As mentioned, for the B_s meson, the mixing provides the opportunity to measure CP asymmetries in a time-dependent analysis

$$\frac{\Gamma[B_s(t) \rightarrow \mu_\lambda^+ \mu_\lambda^-] - \Gamma[\bar{B}_s(t) \rightarrow \mu_\lambda^+ \mu_\lambda^-]}{\Gamma[B_s(t) \rightarrow \mu_\lambda^+ \mu_\lambda^-] + \Gamma[\bar{B}_s(t) \rightarrow \mu_\lambda^+ \mu_\lambda^-]} = \frac{C_\lambda \cos(\Delta m_{B_s} t) + S_\lambda \sin(\Delta m_{B_s} t)}{\cosh(y_s t / \tau_{B_s}) + \mathcal{A}_{\Delta\Gamma}^\lambda \sinh(y_s t / \tau_{B_s})}, \quad (10.12)$$

*Throughout, the same numerical values as in Ref. [3] are used for B_s and B_d , neglecting $SU(3)$ -flavour breaking effects.

where all quantities are defined in Ref. [31] and $|\mathcal{A}_{\Delta\Gamma}^\lambda|^2 + |C_\lambda|^2 + |S_\lambda|^2 = 1$ holds. For example, the mass-eigenstate rate asymmetry $\mathcal{A}_{\Delta\Gamma} = +1$ in the SM exactly, if only a pseudo-scalar amplitude exists, and is therefore assumed to be very sensitive to possible new flavour-changing interactions, with essentially no uncertainty from SM background. We now see that the QED correction of the SM itself generates small ‘contamination’ of the observable, given by Ref. [3]

$$\mathcal{A}_{\Delta\Gamma}^\lambda \approx 1 - 1.0 \cdot 10^{-5}, \quad S_\lambda \approx -0.1\%, \quad C_\lambda \approx \eta_\lambda 0.6\%, \quad (10.13)$$

where $\eta_{L/R} = \pm 1$. Present measurements [23] set only very weak constraints on the deviations of $\mathcal{A}_{\Delta\Gamma}^\lambda$ from unity, and C_λ , S_λ have not yet been measured,[†] but the uncertainty in the B meson LCDA is, in principle, a limiting factor for the precision with which new physics can be constrained from these observables. Also, S_λ and C_λ deviate marginally from the leading-order SM prediction of zero, but signals from new physics should be substantially larger to distinguish them from the SM QED correction.

A similar framework can be used to analyse QED corrections to $B^\pm \rightarrow \ell^\pm \nu_\ell$. In this case, power enhancement does not arise, owing to the different chirality structure of the current and the presence of only one charged lepton in the final state [3]. QED corrections that depend on the meson structure are subleading in this case. The leading QED corrections for this process can be obtained from the usual soft-photon approximation, where the charged meson is treated as a point-like charge.

10.3 Summary and outlook

The proper treatment of QED corrections in theoretical predictions is essential to the success of future e^+e^- colliders. We have shown how this goal could be achieved in flavour physics for the example of a power-enhanced leading QED correction to the leptonic decays $B_q \rightarrow \mu^+ \mu^-$ with $q = d, s$ [3] and provided updated predictions. A systematic expansion based on the appropriate EFTs must be implemented to cover dynamics from the hard scale $\mu_b \sim 5$ GeV over hard-collinear (SCET_I) and collinear scales (SCET_{II}) down to the ultrasoft scales $\mathcal{O}(10$ MeV). Further, the EFTs allow for a systematic resummation of the leading logarithmic corrections and they provide a field-theoretical definition of non-perturbative objects in the presence of QED, as, for example, generalised light-cone distribution amplitudes of the B meson dressed by process-dependent Wilson lines [36]. The consistent evaluation of the QED corrections is thus a challenging task, but it can be accomplished with the help of effective field theory.

In the example at hand, the special numerical value of the muon mass and its proximity to the typical size of hadronic binding energies Λ_{QCD} gave rise to a special tower of EFTs. The application to the cases of electrons and taus requires additional considerations. Full theoretical control of QED corrections is also desirable for other decays that will allow future precision determination of short-distance parameters. For example, an important class is that of exclusive $b \rightarrow u \bar{\nu}_\ell$ and $b \rightarrow c \bar{\nu}_\ell$ decays for the determination of CKM elements V_{ub} and V_{cb} , respectively. Owing to the absence of resonant hadronic contributions, the only hadronic uncertainties from $B \rightarrow M$ form factors could become controllable with high accuracy in lattice calculations for large dilepton invariant masses, i.e., energetic leptons, which is also the preferred kinematic region for the tower of EFTs discussed here. Other interesting applications are observables that are predicted in the SM to vanish when restricting to the leading order in the weak

[†]Note that C^λ requires the measurement of the muon helicity, whereas $\mathcal{A}_{\Delta\Gamma}^\lambda$ and S_λ can also be determined as averages over the muon helicity; furthermore, $\mathcal{A}_{\Delta\Gamma}^\lambda$ can be measured without flavour-tagging, whereas it is required for S_λ and C_λ .

operator product expansion but might be sensitive to non-standard interactions. Then the QED corrections in the SM provide a background to the new physics searches, as in the example of $\mathcal{A}_{\Delta\Gamma}$ in $B_s \rightarrow \mu^+\mu^-$ given here. This concerns observables in the angular distributions of $B \rightarrow K^{(*)}\ell^+\ell^-$ as, for example, discussed in Refs. [38, 39].

References

- [1] A.J. Bevan *et al.*, *Eur. Phys. J.* **C74** (2014) 3026. [arXiv:1406.6311](#),
[doi:10.1140/epjc/s10052-014-3026-9](#)
- [2] S. Aoki *et al.*, FLAG review 2019. [arXiv:1902.08191](#)
- [3] M. Beneke *et al.*, *Phys. Rev. Lett.* **120** (2018) 011801. [arXiv:1708.09152](#),
[doi:10.1103/PhysRevLett.120.011801](#)
- [4] D.R. Yennie *et al.*, *Ann. Phys.* **13** (1961) 379. [doi:10.1016/0003-4916\(61\)90151-8](#)
- [5] S. Weinberg, *Phys. Rev.* **140** (1965) B516. [doi:10.1103/PhysRev.140.B516](#)
- [6] G. Isidori, *Eur. Phys. J.* **C53** (2008) 567. [arXiv:0709.2439](#),
[doi:10.1140/epjc/s10052-007-0487-0](#)
- [7] A.V. Manohar and W.J. Waalewijn, *JHEP* **08** (2018) 137.
[arXiv:1802.08687](#), [doi:10.1007/JHEP08\(2018\)137](#)
- [8] B. Fornal *et al.*, *JHEP* **05** (2018) 106. [arXiv:1803.06347](#),
[doi:10.1007/JHEP05\(2018\)106](#)
- [9] D. Bonocore *et al.*, *JHEP* **12** (2016) 121. [arXiv:1610.06842](#),
[doi:10.1007/JHEP12\(2016\)121](#)
- [10] I. Moult *et al.*, *Phys. Rev.* **D95** (2017) 074023. [arXiv:1612.00450](#),
[doi:10.1103/PhysRevD.95.074023](#)
- [11] I. Moult *et al.*, *Phys. Rev.* **D97** (2018) 014013. [arXiv:1710.03227](#),
[doi:10.1103/PhysRevD.97.014013](#)
- [12] M. Beneke *et al.*, *JHEP* **03** (2018) 001. [arXiv:1712.04416](#),
[doi:10.1007/JHEP03\(2018\)001](#)
- [13] M. Beneke *et al.*, *JHEP* **11** (2018) 112. [arXiv:1808.04742](#),
[doi:10.1007/JHEP11\(2018\)112](#)
- [14] I. Moult *et al.*, *JHEP* **08** (2018) 013. [arXiv:1804.04665](#),
[doi:10.1007/JHEP08\(2018\)013](#)
- [15] M. Beneke *et al.*, *JHEP* **03** (2019) 043. [arXiv:1809.10631](#),
[doi:10.1007/JHEP03\(2019\)043](#)
- [16] T. Liu and A.A. Penin, *Phys. Rev. Lett.* **119** (2017) 262001. [arXiv:1709.01092](#),
[doi:10.1103/PhysRevLett.119.262001](#)
- [17] T. Liu and A. Penin, *JHEP* **11** (2018) 158. [arXiv:1809.04950](#),
[doi:10.1007/JHEP11\(2018\)158](#)
- [18] A.A. Penin, *Phys. Lett.* **B745** (2015) 69 [Corrigenda: **B751** (2015) 596, **B771** (2017) 633].
[arXiv:1412.0671](#), [doi:10.1016/j.physletb.2015.04.036](#),
[10.1016/j.physletb.2015.10.035](#), [doi:10.1016/j.physletb.2017.05.069](#)
- [19] S. Alte *et al.*, *JHEP* **08** (2018) 095. [arXiv:1806.01278](#),
[doi:10.1007/JHEP08\(2018\)095](#)

- [20] S. Alte *et al.*, Effective theory for a heavy scalar coupled to the SM via vector-like quarks. [arXiv:1902.04593](#)
- [21] A. Bazavov *et al.*, *Phys. Rev.* **D98** (2018) 074512. [arXiv:1712.09262](#), [doi:10.1103/PhysRevD.98.074512](#)
- [22] R. Aaij *et al.*, *Phys. Rev. Lett.* **111** (2013) 101805. [arXiv:1307.5024](#), [doi:10.1103/PhysRevLett.111.101805](#)
- [23] R. Aaij *et al.*, *Phys. Rev. Lett.* **118** (2017) 191801. [arXiv:1703.05747](#), [doi:10.1103/PhysRevLett.118.191801](#)
- [24] S. Chatrchyan *et al.*, *Phys. Rev. Lett.* **111** (2013) 101804. [arXiv:1307.5025](#), [doi:10.1103/PhysRevLett.111.101804](#)
- [25] M. Aaboud *et al.*, *Eur. Phys. J.* **C76** (2016) 513. [arXiv:1604.04263](#), [doi:10.1140/epjc/s10052-016-4338-8](#)
- [26] C. Bobeth *et al.*, *Phys. Rev. Lett.* **112** (2014) 101801. [arXiv:1311.0903](#), [doi:10.1103/PhysRevLett.112.101801](#)
- [27] A. Crivellin *et al.*, PSI/UZH Workshop: Impact of $B \rightarrow \mu^+\mu^-$ on New Physics Searches, [arXiv:1803.10097](#)
- [28] R. Aaij *et al.*, *Eur. Phys. J.* **C73** (2013) 2373. [arXiv:1208.3355](#), [doi:10.1140/epjc/s10052-013-2373-2](#)
- [29] A. Abada *et al.*, *Eur. Phys. J.* **C79** (2019), 474. [doi:10.1140/epjc/s10052-019-6904-3](#)
- [30] A.J. Buras, Weak Hamiltonian, CP violation and rare decays, Probing the Standard Model of Particle Interactions. Proc. Summer School in Theoretical Physics, NATO Advanced Study Institute, 68th session, Les Houches, France, 1997. part. 1, 2, 1998, pp. 281–539, [arXiv:hep-ph/9806471](#)
- [31] K. De Bruyn *et al.*, *Phys. Rev. Lett.* **109** (2012) 041801. [arXiv:1204.1737](#), [doi:10.1103/PhysRevLett.109.041801](#)
- [32] A.J. Buras *et al.*, *Eur. Phys. J.* **C72** (2012) 2172. [arXiv:1208.0934](#), [doi:10.1140/epjc/s10052-012-2172-1](#)
- [33] P. Golonka and Z. Was, *Eur. Phys. J.* **C45** (2006) 97. [arXiv:hep-ph/0506026](#), [doi:10.1140/epjc/s2005-02396-4](#)
- [34] Y.G. Aditya *et al.*, *Phys. Rev.* **D87** (2013) 074028. [arXiv:1212.4166](#), [doi:10.1103/PhysRevD.87.074028](#)
- [35] M. Beneke and T. Feldmann, *Nucl. Phys.* **B685** (2004) 249. [arXiv:hep-ph/0311335](#), [doi:10.1016/j.nuclphysb.2004.02.033](#)
- [36] M. Beneke *et al.*, *JHEP* **10** (2019) 232. [arXiv:1908.07011](#), [doi:10.1007/JHEP10\(2019\)232](#)
- [37] M. Beneke and T. Feldmann, *Phys. Lett.* **B553** (2003) 267. [arXiv:hep-ph/0211358](#), [doi:10.1016/S0370-2693\(02\)03204-5](#)
- [38] C. Bobeth *et al.*, *JHEP* **12** (2007) 040. [arXiv:0709.4174](#), [doi:10.1088/1126-6708/2007/12/040](#)
- [39] F. Beaujean *et al.*, *Eur. Phys. J.* **C75** (2015) 456. [arXiv:1508.01526](#), [doi:10.1140/epjc/s10052-015-3676-2](#)

11 Top pair production and mass determination

Contribution* by: A. Maier [[andreas.martin.maier@desy](mailto:andreas.martin.maier@desy.it)]

The mass of the top quark can be measured in a well-defined scheme and with unrivalled precision at a future electron–positron collider, like the FCC-ee. The most sensitive observable is the total production cross-section for $b\bar{b}W^+W^-X$ final states near the top pair production threshold. I review the state of the art in theory predictions for this quantity.

11.1 Introduction

The total cross-section for inclusive $b\bar{b}W^+W^-X$ production can be measured with very high precision at a future high-energy electron–positron collider. Owing to the potential for large integrated luminosity, the FCC-ee is especially well-suited for such a measurement. The line shape for centre-of-mass energies close to the top–antitop production threshold is highly sensitive to the mass of the top quark, which allows its determination with unprecedented precision. Since the statistical uncertainty of the measurement is projected to be significantly below the current theory error [1, 2], it is crucial to continuously improve the theoretical prediction.

11.2 Effective theory framework

The $b\bar{b}W^+W^-X$ final state is mostly produced through the creation and decay of non-relativistic top–antitop pairs, interacting predominantly via a colour Coulomb potential. The dynamics of this system are described by potential non-relativistic effective field theory (PNREFT) [3–5], combined with unstable particle effective field theory [6, 7]. Within this framework, higher-order corrections can be treated systematically through a simultaneous expansion in the non-relativistic velocity v and the strong, electromagnetic, and top Yukawa couplings α_s , α , and y_t . We adopt the power counting $v \sim \alpha_s \sim \sqrt{\alpha} \sim y_t$ with the top quark width $\Gamma_t \sim m_t \alpha$. Powers of α_s/v from the bound-state interaction are resummed to all orders in perturbation theory.

At leading order, the PNREFT Lagrangian is given by

$$\mathcal{L}_{\text{PNREFT, LO}} = \psi^\dagger \left(i\partial_0 + \frac{\vec{\partial}^2 + im_t \Gamma_t}{2m_t} \right) \psi + \mathcal{L}_{\text{anti-quark}} - \int d^3\vec{r} [\psi^\dagger \psi](\vec{x} + \vec{r}) \frac{C_F \alpha_s}{r} [\chi^\dagger \chi](\vec{x}), \quad (11.1)$$

where ψ is the quark field and χ the antiquark field. The resulting top pair propagator is the Green function of the Schrödinger equation with the colour Coulomb potential interaction. Its imaginary part is closely related to the resonant top pair production cross-section via the optical theorem.

11.3 Higher-order corrections

Higher-order corrections to the PNREFT Lagrangian are obtained by matching to the full Standard Model. In the first step, hard modes with large four-momenta $k \sim m_t$ are integrated out. This gives rise to a non-relativistic effective field theory with local effective vertices. These

*This contribution should be cited as:

A. Maier, Top pair production and mass determination, DOI: [10.23731/CYRM-2020-003.117](https://doi.org/10.23731/CYRM-2020-003.117), in: Theory for the FCC-ee, Eds. A. Blondel, J. Gluza, S. Jadach, P. Janot and T. Riemann, CERN Yellow Reports: Monographs, CERN-2020-003, DOI: [10.23731/CYRM-2020-003](https://doi.org/10.23731/CYRM-2020-003), p. 117. © CERN, 2020. Published by CERN under the [Creative Commons Attribution 4.0 license](https://creativecommons.org/licenses/by/4.0/).

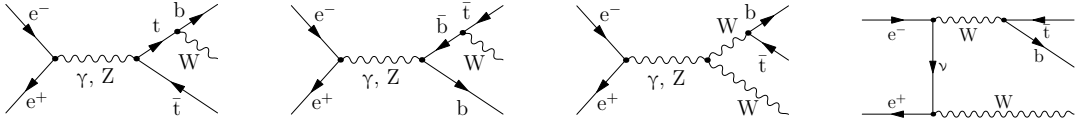


Fig. B.11.1: Non-resonant diagrams contributing to the $W^+b\bar{t}$ final state at NLO. The final state $W^-b\bar{t}$ follows from charge conjugation.

matching corrections are known to NNNLO in the QCD and Higgs sector [8–11] and to NNLO in the electroweak sector [12–16].

In the second matching step, soft modes $k \sim m_t v$ and potential modes $k_0 \sim m_t v^2, \vec{k} \sim m_t v$ for gluons and light quarks are also eliminated from the theory. The most challenging part is the calculation of the corrections to the static colour Coulomb potential to NNNLO, which is reported in Refs. [17–19].

11.3.1 Resonant production

With the matched PNREFT Lagrangian, the resonant top pair production cross-section can be calculated, including NNNLO QCD and Higgs effects and NNLO electroweak effects, by computing corrections to the Green function to this order. The complete result for the QCD corrections was first presented for the S-wave contribution in Ref. [20] and for the P-wave contribution in Ref. [9] (see also Ref. [21]). Schematically, the known contributions to the top pair production cross-section can be written as

$$\sigma_{\text{res}} \sim \alpha^2 v \sum_{k=0}^{\infty} \left(\frac{\alpha_s}{v} \right)^k \times \begin{cases} 1 & \text{LO} \\ \alpha_s, v, \frac{\alpha}{v} & \text{NLO} \\ \alpha_s^2, \alpha_s v, v^2, \frac{\alpha}{v} \times \left\{ \frac{\alpha}{v}, \alpha_s s, v \right\}, y_t \sqrt{\alpha}, y_t^2 & \text{NNLO} \\ \alpha_s^{3-i} v^i, y_t^2 \times \left\{ \frac{\alpha}{v}, \alpha_s, v \right\} & \text{NNNLO} \end{cases} \quad (11.2)$$

11.3.2 Non-resonant production

Top quarks are unstable and the final state $b\bar{b}W^+W^-X$ can also be produced in non-resonant channels that do not involve the creation of a top–antitop pair near the mass shell. According to unstable particle effective field theory, the full cross-section is given by the sum of the resonant and non-resonant contributions:

$$\sigma = \sigma_{\text{res}} + \sigma_{\text{non-res}} \quad (11.3)$$

While non-resonant production is suppressed by one power of α , it does not suffer from the same phase space suppression as resonant production and therefore contributes with a factor of α/v relative to the leading-order cross-section, i.e., at NLO. The diagrams at this order are shown in Fig. B.11.1; their contribution was first detailed in Ref. [22]. The NNLO non-resonant cross-section was later detailed in Ref. [16].

Virtual top quarks in the non-resonant channels are formally far off-shell with squared momenta $p_t^2 - m_t^2 \sim m_t^2 \gg m_t \Gamma_t$, so the width must not be resummed in the propagators. Since we integrate over the full phase space, endpoint divergences occur whenever $p_t^2 - m_t^2$ vanishes. At NNLO, this leads to poles proportional to Γ_t/ϵ in $4 - 2\epsilon$ dimensions. As usual in asymptotic expansions, these cancel against poles in a different expansion region. In this case, the corresponding poles appear in the form of finite-width divergences in the resonant

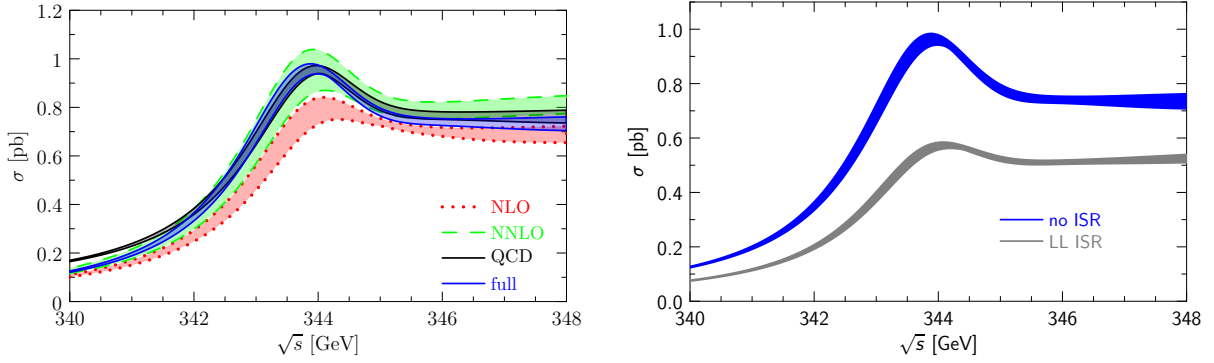


Fig. B.11.2: Total cross-section for the process $e^+e^- \rightarrow t\bar{t}$ at various orders in perturbation theory. Left: Cross-section without ISR from NLO to NNNLO with the pure NNNLO QCD result as comparison. Right: Effect of ISR on the cross-section.

cross-section. A detailed account of the NNLO calculation including the arrangement of pole cancellations is given in Ref. [16].

11.3.3 Initial-state radiation

Formally, photonic corrections in the initial state are suppressed by one order in α and therefore contribute at NNLO according to our power counting. However, it is well-known that these corrections are enhanced by logarithms of m_t over m_e , which have to be resummed to all orders. The resummed cross-section is given by [23, 24]

$$\sigma(s) = \int_0^1 dx_1 \int_0^1 dx_2 \Gamma_{ee}^{\text{LL}}(x_1) \Gamma_{ee}^{\text{LL}}(x_2) \hat{\sigma}(x_1 x_2 s) + \sigma_{\text{const}}^{\text{ISR}}(s), \quad (11.4)$$

where $\Gamma_{ee}^{\text{LL}}(x)$ is a leading logarithmic structure function, $\hat{\sigma}$ is the ‘partonic’ cross-section without ISR resummation and $\sigma_{\text{const}}^{\text{ISR}}$ accounts for the non-logarithmic NNLO contribution.

11.4 Cross-section predictions

The formulae for the cross-section can be evaluated numerically with the code `QQbar_threshold` [25], which includes all aforementioned corrections. Figure B.11.2 shows the behaviour of the total cross-section near threshold for a top quark mass of $m_t(20 \text{ GeV}) = 171.5 \text{ GeV}$ in the potential-subtracted scheme [26] and input parameters $\Gamma_t = 1.33 \text{ GeV}$, $m_H = 125 \text{ GeV}$, $\alpha_s(m_Z) = 0.1177$, $\alpha(m_Z) = 1/128.944$. The uncertainty bands originate from a variation of the renormalization scale between 50 and 350 GeV.

Figure B.11.3 shows the effect of changing various parameters. The variation suggests that it should be possible to extract the top quark width and mass in the potential-subtracted scheme with an uncertainty of better than 100 MeV. The sensitivity to the top Yukawa coupling and the strong coupling is less pronounced and there is a considerable degeneracy between the two parameters. A precise knowledge of the strong coupling constant from other sources will be crucial to meaningfully constrain the Yukawa coupling. In any case, a dedicated experimental analysis will be needed to determine the exact precision with which the various top quark properties can be extracted from a measurement of the cross-section.

Acknowledgements

I thank the CERN Theory Department for their hospitality and support during the workshop.

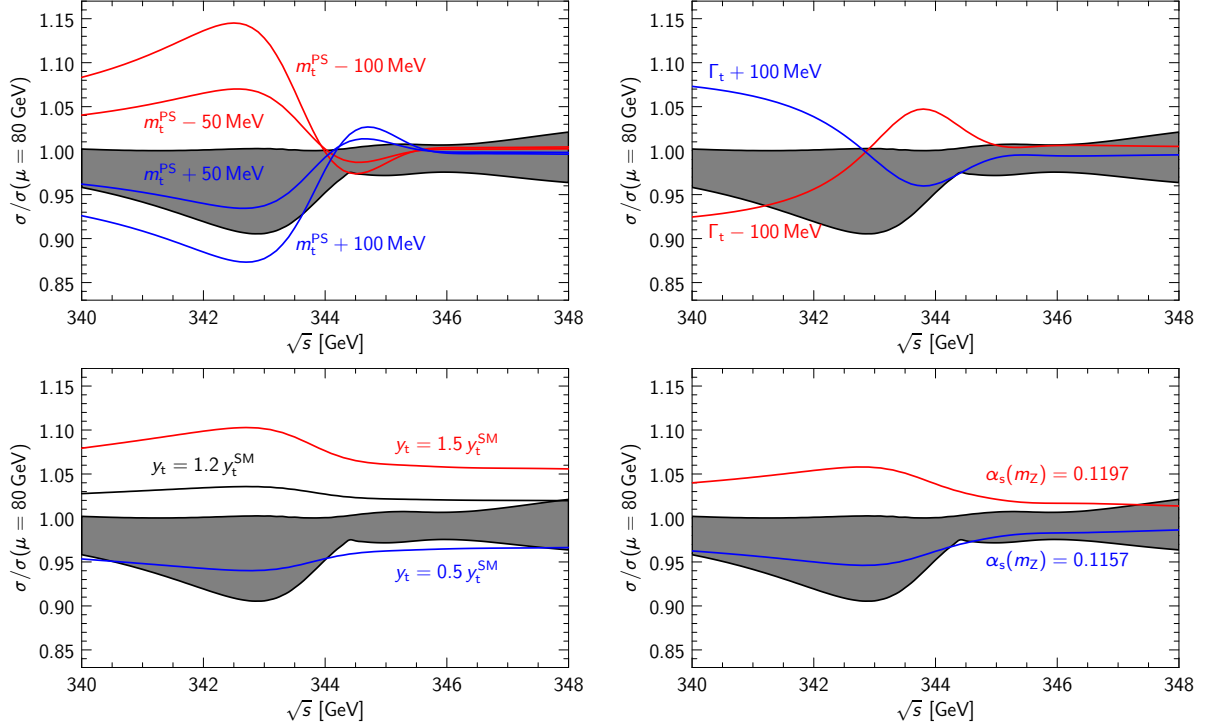


Fig. B.11.3: Sensitivity of the cross-section to parameter variation. Top left: Variation of the top quark mass by up to ± 100 MeV. Top right: Variation of the top quark width by up ± 100 MeV. Bottom left: Variation of the top Yukawa coupling. Bottom right: Variation of the strong coupling constant.

References

- [1] K. Seidel *et al.*, *Eur. Phys. J.* **C73** (2013) 2530. [arXiv:1303.3758](#), [doi:10.1140/epjc/s10052-013-2530-7](#)
- [2] F. Simon, *PoS ICHEP2016* (2017) 872. [arXiv:1611.03399](#), [doi:10.22323/1.282.0872](#)
- [3] A. Pineda and J. Soto, *Nucl. Phys. Proc. Suppl.* **64** (1998) 428. [arXiv:hep-ph/9707481](#), [doi:10.1016/S0920-5632\(97\)01102-X](#)
- [4] M. Beneke and V.A. Smirnov, *Nucl. Phys.* **B522** (1998) 321. [arXiv:hep-ph/9711391](#), [doi:10.1016/S0550-3213\(98\)00138-2](#)
- [5] N. Brambilla *et al.*, *Nucl. Phys.* **B566** (2000) 275. [arXiv:hep-ph/9907240](#), [doi:10.1016/S0550-3213\(99\)00693-8](#)
- [6] M. Beneke *et al.*, *Phys. Rev. Lett.* **93** (2004) 011602. [arXiv:hep-ph/0312331](#), [doi:10.1103/PhysRevLett.93.011602](#)
- [7] M. Beneke *et al.*, *Nucl. Phys.* **B686** (2004) 205. [arXiv:hep-ph/0401002](#), [doi:10.1016/j.nuclphysb.2004.03.016](#)
- [8] D. Eiras and M. Steinhauser, *Nucl. Phys.* **B757** (2006) 197. [arXiv:hep-ph/0605227](#), [doi:10.1016/j.nuclphysb.2006.09.010](#)
- [9] M. Beneke *et al.*, *Nucl. Phys.* **B880** (2014) 414. [arXiv:1312.4792](#), [doi:10.1016/j.nuclphysb.2014.01.015](#)

- [10] P. Marquard *et al.*, *Phys. Rev.* **D89** (2014) 034027. [arXiv:1401.3004](#),
[doi:10.1103/PhysRevD.89.034027](#)
- [11] M. Beneke *et al.*, *Nucl. Phys.* **B899** (2015) 180. [arXiv:1506.06865](#),
[doi:10.1016/j.nuclphysb.2015.07.034](#)
- [12] B. Grzadkowski *et al.*, *Nucl. Phys.* **B281** (1987) 18. [doi:10.1016/0550-3213\(87\)90245-8](#)
- [13] R.J. Guth and J.H. Kühn, *Nucl. Phys.* **B368** (1992) 38.
[doi:10.1016/0550-3213\(92\)90196-I](#)
- [14] A.H. Hoang and C.J. Reisser, *Phys. Rev.* **D71** (2005) 074022. [arXiv:hep-ph/0412258](#),
[doi:10.1103/PhysRevD.71.074022](#)
- [15] A.H. Hoang and C.J. Reisser, *Phys. Rev.* **D74** (2006) 034002. [arXiv:hep-ph/0604104](#),
[doi:10.1103/PhysRevD.74.034002](#)
- [16] M. Beneke *et al.*, *JHEP* **02** (2018) 125. [arXiv:1711.10429](#),
[doi:10.1007/JHEP02\(2018\)125](#)
- [17] C. Anzai *et al.*, *Phys. Rev. Lett.* **104** (2010) 112003. [arXiv:0911.4335](#), [doi:10.1103/PhysRevLett.104.112003](#)
- [18] A.V. Smirnov *et al.*, *Phys. Rev. Lett.* **104** (2010) 112002. [arXiv:0911.4742](#), [doi:10.1103/PhysRevLett.104.112002](#)
- [19] R.N. Lee *et al.*, *Phys. Rev.* **D94** (2016) 054029. [arXiv:1608.02603](#), [doi:10.1103/PhysRevD.94.054029](#)
- [20] M. Beneke *et al.*, *Phys. Rev. Lett.* **115** (2015) 192001. [arXiv:1506.06864](#),
[doi:10.1103/PhysRevLett.115.192001](#)
- [21] A.A. Penin and A.A. Pivovarov, *Phys. At. Nucl.* **64** (2001) 275, [*Yad. Fiz.* **64** (2001) 323].
[arXiv:hep-ph/9904278](#), [doi:10.1134/1.1349450](#)
- [22] M. Beneke *et al.*, *Nucl. Phys.* **B840** (2010) 186. [arXiv:1004.2188](#),
[doi:10.1016/j.nuclphysb.2010.07.006](#)
- [23] E.A. Kuraev and V.S. Fadin, *Sov. J. Nucl. Phys.* **41** (1985) 466 [*Yad. Fiz.* **41** (1985) 733].
- [24] V.S. Fadin and V.A. Khoze, *JETP Lett.* **46** (1987) 525 [*Pisma Zh. Eksp. Teor. Fiz.* **46** (1987) 417]. http://www.jetpletters.ac.ru/ps/1234/article_18631.shtml
- [25] M. Beneke *et al.*, *Comput. Phys. Commun.* **209** (2016) 96. [arXiv:1605.03010](#),
[doi:10.1016/j.cpc.2016.07.026](#)
- [26] M. Beneke, *Phys. Lett.* **B434** (1998) 115. [arXiv:hep-ph/9804241](#),
[doi:10.1016/S0370-2693\(98\)00741-2](#)

12 Higgs boson decays: theoretical status

Contribution* by: M. Spira [Michael.Spira@psi.ch]

12.1 Introduction

The discovery of a Standard-Model-like Higgs boson at the LHC [1, 2] completed the theory of electroweak and strong interactions. The measured Higgs mass of (125.09 ± 0.24) GeV [3] ranges at the order of the weak scale. The existence of the Higgs boson [4–9] allows the Standard Model (SM) particles to be weakly interacting up to high-energy scales. This, however, is only possible for particular Higgs boson couplings to all other particles so that with the knowledge of the Higgs boson mass all its properties are uniquely fixed. The massive gauge bosons and fermions acquire mass through their interaction with the Higgs field, which develops a finite vacuum expectation value in its ground state. The minimal model requires the introduction of one isospin doublet of the Higgs field and leads after spontaneous symmetry breaking to the existence of one scalar Higgs boson.

Since all Higgs couplings are fixed within the SM, any meaningful approach to introduce variations requires the introduction of effects beyond the SM (BSM). Two major branches are being pursued for this purpose: (i) the introduction of higher-dimension operators in terms of a general effective Lagrangian with dimension-6 operators providing the leading contributions for energy scales sufficiently below the novel cut-off scale of these operators and (ii) the introduction of specific BSM models with extended Higgs, gauge, and fermion sectors. The extraction of BSM effects, however, strongly relies on the accuracy of the SM part as, e.g., sketched in the basic decomposition of the SM-like Higgs boson decay widths as

$$\Gamma = \Gamma_{\text{SM}} + \Delta\Gamma_{\text{BSM}} \quad (12.1)$$

Any potential to extract the BSM effects $\Delta\Gamma_{\text{BSM}}$ is limited by the uncertainties $\delta\Gamma_{\text{SM}}$ of the SM part.

12.2 SM Higgs boson decays

The determination of the branching ratios of Higgs boson decays thus necessitates the inclusion of the available higher-order corrections (for a recent overview see, e.g., Ref. [10]) and a sophisticated estimate of the theoretical and parametric uncertainties.

12.2.1 $\text{H} \rightarrow \text{f}\bar{\text{f}}$

The Higgs decay $\text{H} \rightarrow \text{b}\bar{\text{b}}$ is the dominant Higgs boson decay with a branching ratio of about 58%. The subleading fermionic decays $\text{H} \rightarrow \tau^+\tau^-$ and $\text{H} \rightarrow \text{c}\bar{\text{c}}$ reach branching ratios of about 6% and 3%, respectively. The rare decay $\text{H} \rightarrow \mu^+\mu^-$ will become visible at the HL-LHC and happens with about 0.02% probability [11]. The present status of the partial decay widths can be summarised in terms of the (factorised) expression

$$\Gamma(\text{H} \rightarrow \text{f}\bar{\text{f}}) = \frac{N_c G_F M_{\text{H}}}{4\sqrt{2}\pi} m_{\text{f}}^2 (1 + \delta_{\text{QCD}} + \delta_{\text{t}} + \delta_{\text{mixed}}) (1 + \delta_{\text{elw}}) , \quad (12.2)$$

*This contribution should be cited as:

M. Spira, Higgs boson decays: theoretical status, DOI: [10.23731/CYRM-2020-003.123](https://doi.org/10.23731/CYRM-2020-003.123), in: Theory for the FCC-ee, Eds. A. Blondel, J. Gluza, S. Jadach, P. Janot and T. Riemann, CERN Yellow Reports: Monographs, CERN-2020-003, DOI: [10.23731/CYRM-2020-003](https://doi.org/10.23731/CYRM-2020-003), p. 123.
 © CERN, 2020. Published by CERN under the [Creative Commons Attribution 4.0 license](https://creativecommons.org/licenses/by/4.0/).

where $N_c = 3(1)$ for quarks (leptons), G_F denotes the Fermi constant, M_H denotes the Higgs mass, and m_f denotes the fermion mass. In general, the pure QCD corrections δ_{QCD} to the Higgs boson decays into quarks are known up to NLO including the full quark mass dependence [12–16] and up to N⁴LO for the leading corrections with the leading mass effects [17–23]. The dominant part of the QCD corrections can be absorbed in the running quark mass evaluated at the scale of the Higgs mass. The top-induced QCD corrections, which are related to interference effects between $H \rightarrow gg$ and $H \rightarrow q\bar{q}$, are known at NNLO in the limit of heavy top quarks and light bottom quarks [24–26]. In the case of leptons, there are no QCD corrections ($\delta_{\text{QCD}} = \delta_t = \delta_{\text{mixed}} = 0$). The electroweak corrections δ_{elw} are known at NLO exactly [27–30]. In addition, the mixed QCD-elw corrections range at the per-mille level if the factorised expression with respect to QCD and elw corrections is used [31–36]. The public tool `Hdecay` [37, 38] neglects these mixed QCD-elw corrections but includes all other corrections. The partial decay width of $H \rightarrow b\bar{b}$ is also known fully differential at N³LO QCD [39–42].

12.2.2 $H \rightarrow W^{(*)}W^{(*)}, Z^{(*)}Z^{(*)}$

The branching ratios of SM Higgs boson decays into (off-shell) W and Z bosons amount to about 21% and 3%, respectively. Off-shell effects of the W and Z bosons are important [43–45] and lead to the $H \rightarrow Z^*Z^{(*)} \rightarrow 4\ell^\pm$ decay as one of the discovery modes of the SM Higgs boson [1, 2]. The electroweak corrections to the full decay modes $H \rightarrow V^{(*)}V^{(*)} \rightarrow 4f$ ($V = W, Z$) have been calculated [27, 46–49]. The public tool `Prophecy4f` [48, 49] for calculating the exclusive decay processes has been used in the experimental analyses. An improvement beyond the pure elw corrections has been made by the proper matching to parton showers at NLO [50]. However, shower effects have not been relevant for the analyses performed so far.

12.2.3 $H \rightarrow gg$

The loop-induced Higgs decay into gluons reaches a branching ratio of about 8%. The decay is dominantly mediated by top and bottom quark loops, with the latter providing a 10% contribution. The charm quark contributes at the level of about 2%. The two-loop QCD corrections are known, including the exact quark mass dependences [51–53]. They enhance the partial decay width by about 70% and thus cannot be neglected in the decay profile of the Higgs boson. The NNLO, N³LO, and, recently, the N⁴LO QCD corrections have been obtained for the top loops in the limit of heavy top quarks, i.e., the leading term of a heavy top mass expansion [54–56]. The QCD corrections beyond NLO amount to less than 20% of the NLO QCD-corrected partial decay width, thus signalling perturbative convergence in spite of the large NLO corrections. The residual theoretical uncertainties have been estimated at the level of about 3% from the scale dependence of the QCD-corrected partial decay width. The NLO elw corrections have been calculated for the top-loop contributions first in the limit of heavy top quarks [34, 57, 58], then the electroweak corrections involving light fermion loops exactly [59–61], and finally the full electroweak corrections involving W , Z , and top-loop contributions, including the full virtual mass dependences, by means of a numerical integration [62, 63]. They amount to about 5% for the SM Higgs mass value. The public tool `Hdecay` [37, 38] includes the NLO QCD results with the full quark mass dependences, the NNLO and N³LO QCD corrections in the heavy top limit, and the full NLO elw corrections in terms of a grid in the Higgs and top masses used for an interpolation.

12.2.4 $H \rightarrow \gamma\gamma$

The rare loop-induced Higgs decay into photons reaches a branching ratio of about 0.2%. The decay is dominantly mediated by W and top quark loops, with the W loops being dominant. The two-loop QCD corrections are known, including the exact top mass dependences [53, 64–73]. They correct the partial decay width by a small amount, about 2%. The QCD corrections beyond NLO have been estimated in the limit of heavy top quarks to be in the per-mille range [74–76]. The NLO elw corrections to the W and top-induced contributions have been obtained by a numerical integration of the corresponding two-loop diagrams [63, 77–79]. They decrease the partial photonic branching ratio of the SM Higgs boson by about 2%, thus nearly cancelling against the QCD corrections by accident. The public tool `Hdecay` [37, 38] includes the NLO QCD results with the full quark mass dependences and the full NLO elw corrections in terms of a grid in the Higgs and top masses used for an interpolation, but neglects all corrections beyond NLO.

12.2.5 $H \rightarrow Z\gamma$ and Dalitz decays

The rare loop-induced Higgs decay into a Z boson and a photon reaches a branching ratio of less than 0.2%. The decay is dominantly mediated by W and top quark loops, with the W loops being dominant. The two-loop QCD corrections are known, including the exact top mass dependences [80–82]. They correct the partial decay width by a small amount in the per-mille range and thus can safely be neglected. The electroweak corrections to this decay mode are unknown. However, the decay mode $H \rightarrow Z\gamma \rightarrow f\bar{f}\gamma$ is one of the more general Dalitz decays $H \rightarrow f\bar{f}\gamma$ [83–89]. The latter are described by the diagrams in Fig. B.12.1, where the Z boson exchange appears in a part of the triangle diagrams. The resonant Z boson exchange corresponds to the $H \rightarrow Z\gamma$ decay mode. The separation of this part, however, depends on the experimental strategy to reconstruct the Z boson in the final state. A first step for the reconstruction of the Z boson is to cut on the invariant mass of the final-state fermion pair. The corresponding distributions of the Dalitz decays are shown in Fig. B.12.2 for the three charged lepton final states normalised to the partial width into photons with a cut $E_\gamma > 1$ GeV on the photon energy. For small invariant masses, the photon conversion $H \rightarrow \gamma\gamma^* \rightarrow \gamma\ell^+\ell^-$ provides the dominant contribution, while for invariant masses around the Z boson mass the Z boson contribution $H \rightarrow \gamma Z^* \rightarrow \gamma f\bar{f}$ takes the dominant role. At the endpoint $q^2 \lesssim M_H^2$ of the spectrum, the direct contribution determines the distributions. This increases with growing Yukawa coupling, i.e., it is largest for $H \rightarrow \gamma\tau^+\tau^-$ (where it dominates in the whole q^2 range). (It should be noted that the endpoint in the $e^+e^-\gamma$ case is four or five orders of magnitude smaller than the photon and Z exchange contributions, thus making it impossible to determine the electron Yukawa coupling. The same conclusion is also valid for the reverse process $e^+e^- \rightarrow H\gamma$, so that the s-channel line shape measurement proposed in Ref. [90] will not be sensitive to the electron Yukawa coupling but dominated by the loop-induced contribution with an additional photon.) For a clean separation of the $H \rightarrow \gamma\gamma$, $H \rightarrow \gamma\gamma^* \rightarrow \gamma\ell^+\ell^-$, $H \rightarrow Z\gamma$, and $H \rightarrow \ell^+\ell^-$ contributions, appropriate cuts must be implemented for the Dalitz decays. The low- q^2 part must be attributed to $H \rightarrow \gamma\gamma$, the q^2 -part around M_Z^2 to $H \rightarrow Z\gamma$ and the endpoint region close to M_H^2 to the QED corrections to $H \rightarrow \ell^+\ell^-$. The public code `Hdecay` [37, 38] does not include the full Dalitz decays.

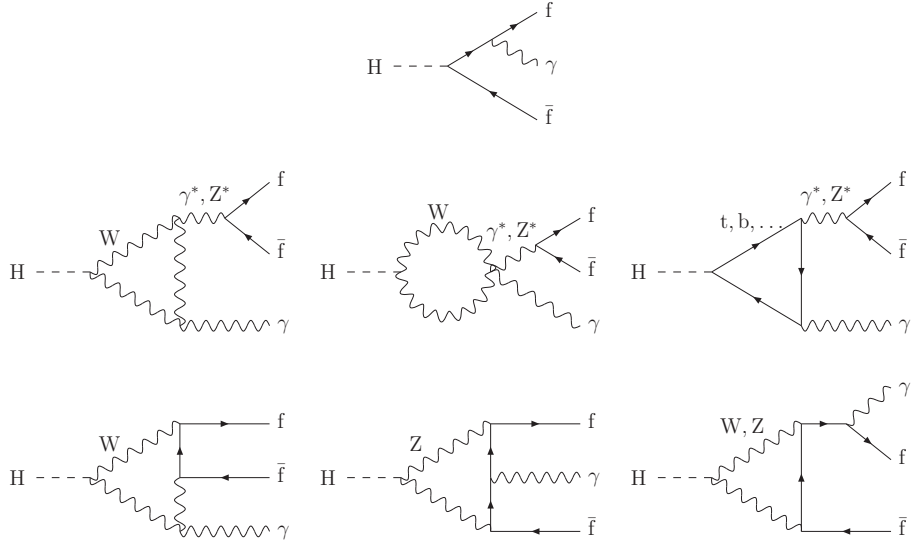


Fig. B.12.1: Generic diagrams contributing to the Dalitz decays $H \rightarrow \gamma f\bar{f}$

12.3 Uncertainties

The parametric errors are dominated by the uncertainties in the top, bottom, and charm quark masses, as well as the strong coupling α_s . We have used the $\overline{\text{MS}}$ masses for the bottom and charm quarks, $\overline{m}_b(\overline{m}_b) = (4.18 \pm 0.03)$ GeV and $\overline{m}_c(3 \text{ GeV}) = (0.986 \pm 0.026)$ GeV, and the top quark pole mass $m_t = (172.5 \pm 1)$ GeV, according to the conventions of the LHC Higgs cross-section WG (HXS WG) [11]. The $\overline{\text{MS}}$ bottom and charm masses are evolved from the input scale to the scale of the decay process with four-loop accuracy in QCD. The strong coupling α_s is fixed by the input value at the Z boson mass scale, $\alpha_s(M_Z) = 0.118 \pm 0.0015$. The total parametric uncertainty for each branching ratio has been derived from a quadratic sum of the individual impacts of the input parameters on the decay modes along the lines of the original analyses in Refs. [91, 92] and the later analysis in Ref. [93].

The theoretical uncertainties from missing higher orders in the perturbative expansion are summarised in Table B.12.1 for the individual partial decay processes, along with the perturbative orders of the included QCD or elw corrections [10, 11]. To be conservative, the total parametric uncertainties are added linearly to the theoretical uncertainties. The final result for the branching ratios is shown in Fig. B.12.3 for the leading Higgs decay modes with branching ratio larger than 10^{-4} for the Higgs mass range between 120 and 130 GeV. These have been obtained using `Prophecy4f` [48, 49] for the decays $H \rightarrow WW, ZZ$ and `Hdecay` [37, 38] for the other decay modes. The bands represent the total uncertainties of the individual branching ratios. For a Higgs mass $M_H = 125$ GeV, the total uncertainty of the leading decay mode $H \rightarrow b\bar{b}$ amounts to less than 2%, since the bulk of it cancels out within the branching ratio. The uncertainty of $\Gamma(H \rightarrow b\bar{b})$, however, generates a significant increase in the uncertainties of the subleading decay modes. The total uncertainties of $\text{BR}(H \rightarrow WW/ZZ)$ and $\text{BR}(H \rightarrow \tau^+\tau^-/\mu^+\mu^-)$ amount to $\sim 2\%$, while the uncertainties of $\text{BR}(H \rightarrow gg)$ and $\text{BR}(H \rightarrow c\bar{c})$ range at $\sim 6\text{--}7\%$, of $\text{BR}(H \rightarrow \gamma\gamma)$ at $\sim 3\%$ and of $\text{BR}(H \rightarrow Z\gamma)$ at $\sim 7\%$. The total decay width of ~ 4.1 MeV can be predicted with $\sim 2\%$ total uncertainty.

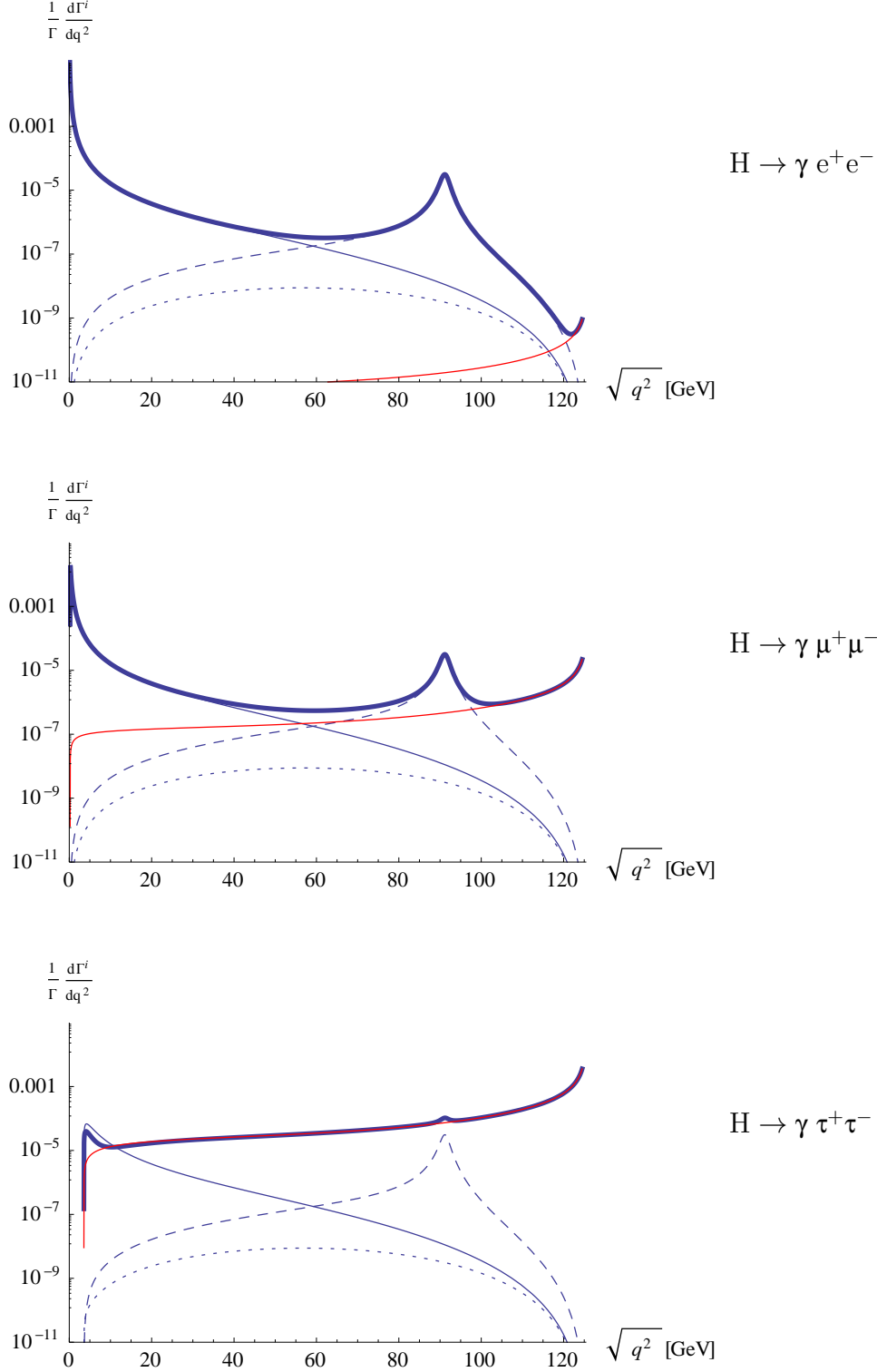


Fig. B.12.2: The invariant mass distributions in $\sqrt{q^2} = M_{\ell^+\ell^-}$ of the Dalitz decays $H \rightarrow \gamma + e^+e^-/\mu^+\mu^-/\tau^+\tau^-$ normalised to $\Gamma(H \rightarrow \gamma\gamma)$ with a cut $E_\gamma > 1$ GeV on the photon energy. The red lines show the contribution of the tree diagrams, the thin solid lines denote the contribution of the photon conversion $H \rightarrow \gamma\gamma^* \rightarrow \gamma\ell^+\ell^-$, and the dashed line the contribution from the Z^* exchange diagrams, while the thick lines present the total contributions. The dotted lines denote the contribution from the box diagrams (in 't Hooft–Feynman gauge). From Ref. [89].

Table B.12.1: Estimated theoretical uncertainties from missing higher orders and the perturbative orders (QCD/elw) of the results included in the analysis.

Partial width	QCD (%)	Electroweak (%)	Total (%)	On-shell Higgs
$H \rightarrow b\bar{b}/c\bar{c}$	~ 0.2	~ 0.5	~ 0.5	$N^4\text{LO} / \text{NLO}$
$H \rightarrow \tau^+\tau^-/\mu^+\mu^-$	—	~ 0.5	~ 0.5	— / NLO
$H \rightarrow gg$	~ 3	~ 1	~ 3	$N^3\text{LO} / \text{NLO}$
$H \rightarrow \gamma\gamma$	< 1	< 1	~ 1	NLO / NLO
$H \rightarrow Z\gamma$	< 1	~ 5	~ 5	LO / LO
$H \rightarrow WW/ZZ \rightarrow 4f$	< 0.5	~ 0.5	~ 0.5	NLO/NLO

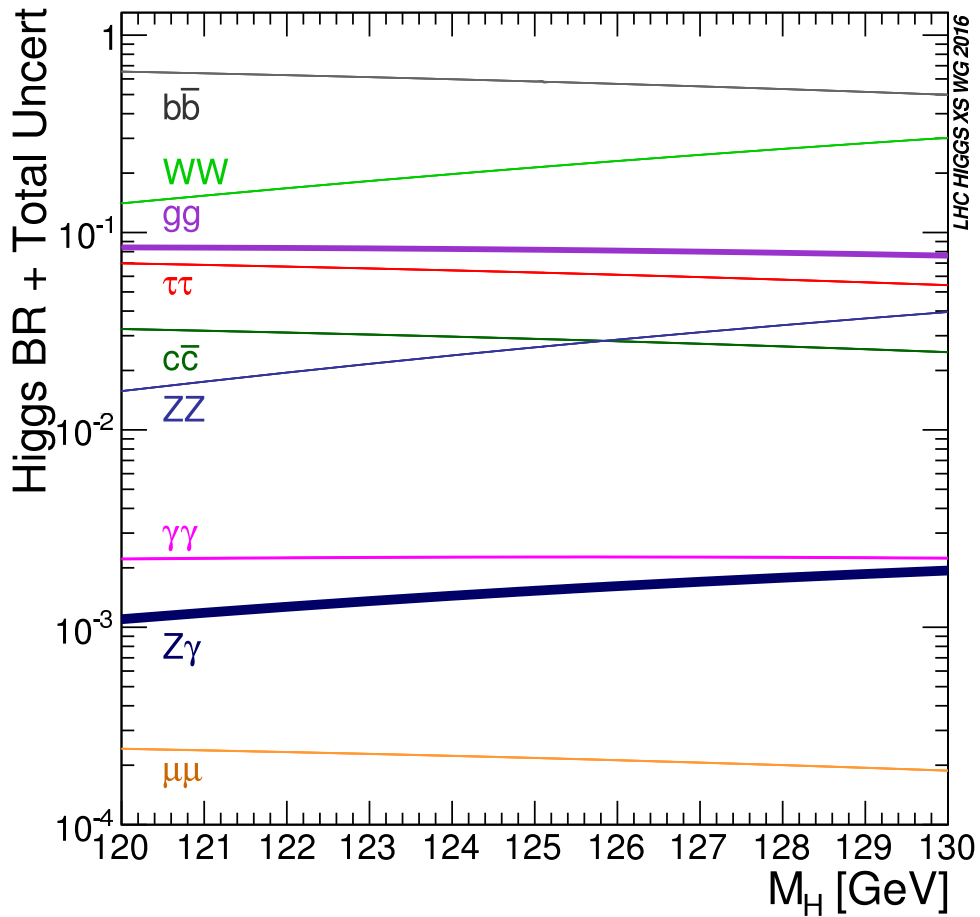


Fig. B.12.3: Higgs boson branching ratios and their uncertainties for Higgs masses around 125 GeV. Figure courtesy ref. [11].

References

- [1] G. Aad *et al.*, *Phys. Lett.* **B716** (2012) 1. [arXiv:1207.7214](#),
[doi:10.1016/j.physletb.2012.08.020](#)
- [2] S. Chatrchyan *et al.*, *Phys. Lett.* **B716** (2012) 30. [arXiv:1207.7235](#),
[doi:10.1016/j.physletb.2012.08.021](#)
- [3] G. Aad *et al.*, *JHEP* **08** (2016) 045. [arXiv:1606.02266](#),
[doi:10.1007/JHEP08\(2016\)045](#)
- [4] P.W. Higgs, *Phys. Lett.* **12** (1964) 132. [doi:10.1016/0031-9163\(64\)91136-9](#)
- [5] P.W. Higgs, *Phys. Rev. Lett.* **13** (1964) 508. [doi:10.1103/PhysRevLett.13.508](#)
- [6] F. Englert and R. Brout, *Phys. Rev. Lett.* **13** (1964) 321.
[doi:10.1103/PhysRevLett.13.321](#)
- [7] G.S. Guralnik *et al.*, *Phys. Rev. Lett.* **13** (1964) 585. [doi:10.1103/PhysRevLett.13.585](#)
- [8] P.W. Higgs, *Phys. Rev.* **145** (1966) 1156. [doi:10.1103/PhysRev.145.1156](#)
- [9] T.W.B. Kibble, *Phys. Rev.* **155** (1967) 1554. [doi:10.1103/PhysRev.155.1554](#)
- [10] M. Spira, *Prog. Part. Nucl. Phys.* **95** (2017) 98. [arXiv:1612.07651](#),
[doi:10.1016/j.pnpnp.2017.04.001](#)
- [11] D. de Florian *et al.*, Handbook of LHC Higgs cross sections: 4. Deciphering the nature of the Higgs sector, CERN-2017-002-M, (CERN, Geneva, 2017), [arXiv:1610.07922](#),
[doi:10.23731/CYRM-2017-002](#)
- [12] E. Braaten and J.P. Leveille, *Phys. Rev.* **D22** (1980) 715. [doi:10.1103/PhysRevD.22.715](#)
- [13] N. Sakai, *Phys. Rev.* **D22** (1980) 2220. [doi:10.1103/PhysRevD.22.2220](#)
- [14] T. Inami and T. Kubota, *Nucl. Phys.* **B179** (1981) 171.
[doi:10.1016/0550-3213\(81\)90253-4](#)
- [15] M. Drees and K.-I. Hikasa, *Phys. Lett.* **B240** (1990) 455 [Erratum: **B262** (1991) 497].
[doi:10.1016/0370-2693\(90\)91130-4](#), [doi:10.1016/0370-2693\(91\)90629-5](#)
- [16] M. Drees and K.-I. Hikasa, *Phys. Rev.* **D41** (1990) 1547. [doi:10.1103/PhysRevD.41.1547](#)
- [17] S.G. Gorishnii *et al.*, *Sov. J. Nucl. Phys.* **40** (1984) 329 [*Yad. Fiz.* **40** (1984) 517].
- [18] S.G. Gorishnii *et al.*, *Mod. Phys. Lett.* **A5** (1990) 2703. [doi:10.1142/S0217732390003152](#)
- [19] S.G. Gorishnii *et al.*, *Phys. Rev.* **D43** (1991) 1633. [doi:10.1103/PhysRevD.43.1633](#)
- [20] A.L. Kataev and V.T. Kim, *Mod. Phys. Lett.* **A9** (1994) 1309.
[doi:10.1142/S0217732394001131](#)
- [21] L.R. Surguladze, *Phys. Lett.* **B341** (1994) 60. [arXiv:hep-ph/9405325](#),
[doi:10.1016/0370-2693\(94\)01253-9](#)
- [22] K.G. Chetyrkin, *Phys. Lett.* **B390** (1997) 309. [arXiv:hep-ph/9608318](#),
[doi:10.1016/S0370-2693\(96\)01368-8](#)
- [23] K. Melnikov, *Phys. Rev.* **D53** (1996) 5020. [arXiv:hep-ph/9511310](#),
[doi:10.1103/PhysRevD.53.5020](#)
- [24] K.G. Chetyrkin and A. Kwiatkowski, *Nucl. Phys.* **B461** (1996) 3. [arXiv:hep-ph/9505358](#),
[doi:10.1016/0550-3213\(95\)00616-8](#)
- [25] S.A. Larin *et al.*, *Phys. Lett.* **B362** (1995) 134. [arXiv:hep-ph/9506465](#),
[doi:10.1016/0370-2693\(95\)01192-S](#)

-
- [26] A. Primo *et al.*, *Phys. Rev.* **D99** (2019) 054013. [arXiv:1812.07811](#),
[doi:10.1103/PhysRevD.99.054013](#)
- [27] J. Fleischer and F. Jegerlehner, *Phys. Rev.* **D23** (1981) 2001.
[doi:10.1103/PhysRevD.23.2001](#)
- [28] D.Y. Bardin *et al.*, *Sov. J. Nucl. Phys.* **53** (1991) 152 [*Yad. Fiz.* **53** (1991) 240].
- [29] A. Dabelstein and W. Hollik, *Z. Phys.* **C53** (1992) 507. [doi:10.1007/BF01625912](#)
- [30] B.A. Kniehl, *Nucl. Phys.* **B376** (1992) 3. [doi:10.1016/0550-3213\(92\)90065-J](#)
- [31] A.L. Kataev, *JETP Lett.* **66** (1997) 327. [arXiv:hep-ph/9708292](#), [doi:10.1134/1.567516](#)
- [32] B.A. Kniehl and M. Spira, *Nucl. Phys.* **B432** (1994) 39. [arXiv:hep-ph/9410319](#),
[doi:10.1016/0550-3213\(94\)90592-4](#)
- [33] A. Kwiatkowski and M. Steinhauser, *Phys. Lett.* **B338** (1994) 66 [Erratum: **B342** (1995) 455]. [arXiv:hep-ph/9405308](#), [doi:10.1016/0370-2693\(94\)91345-5](#),
[doi:10.1016/0370-2693\(94\)01527-J](#)
- [34] K.G. Chetyrkin *et al.*, *Phys. Rev. Lett.* **78** (1997) 594. [arXiv:hep-ph/9610456](#),
[doi:10.1103/PhysRevLett.78.594](#)
- [35] L. Mihaila *et al.*, *Phys. Lett.* **B751** (2015) 442. [arXiv:1509.02294](#),
[doi:10.1016/j.physletb.2015.10.078](#)
- [36] E. Chaubey and S. Weinzierl, *JHEP* **05** (2019) 185. [arXiv:1904.00382](#),
[doi:doi:10.1007/JHEP05\(2019\)185](#)
- [37] A. Djouadi *et al.*, *Comput. Phys. Commun.* **108** (1998) 56. [arXiv:hep-ph/9704448](#),
[doi:10.1016/S0010-4655\(97\)00123-9](#)
- [38] A. Djouadi *et al.*, *Comput. Phys. Commun.* **238** (2019) 214. [arXiv:1801.09506](#),
[doi:10.1016/j.cpc.2018.12.010](#)
- [39] C. Anastasiou *et al.*, *JHEP* **03** (2012) 035. [arXiv:1110.2368](#),
[doi:10.1007/JHEP03\(2012\)035](#)
- [40] V. Del Duca *et al.*, *JHEP* **04** (2015) 036. [arXiv:1501.07226](#),
[doi:10.1007/JHEP04\(2015\)036](#)
- [41] G. Ferrera *et al.*, *Phys. Lett.* **B780** (2018) 346. [arXiv:1705.10304](#),
[doi:10.1016/j.physletb.2018.03.021](#)
- [42] R. Mondini *et al.*, *JHEP* **06**, (2019) 079. [arXiv:1904.08960](#),
[doi:10.1007/JHEP06\(2019\)079](#)
- [43] T.G. Rizzo, *Phys. Rev.* **D22** (1980) 722. [doi:10.1103/PhysRevD.22.722](#)
- [44] W.-Y. Keung and W.J. Marciano, *Phys. Rev.* **D30** (1984) 248.
[doi:10.1103/PhysRevD.30.248](#)
- [45] R.N. Cahn, *Rep. Prog. Phys.* **52** (1989) 389. [doi:10.1088/0034-4885/52/4/001](#)
- [46] B.A. Kniehl, *Nucl. Phys.* **B352** (1991) 1. [doi:10.1016/0550-3213\(91\)90126-I](#)
- [47] D.Y. Bardin *et al.*, *Sov. J. Nucl. Phys.* **54** (1991) 833 [*Yad. Fiz.* **54** (1991) 1366].
- [48] A. Bredenstein *et al.*, *Phys. Rev.* **D74** (2006) 013004. [arXiv:hep-ph/0604011](#),
[doi:10.1103/PhysRevD.74.013004](#)
- [49] A. Bredenstein *et al.*, *JHEP* **02** (2007) 080. [arXiv:hep-ph/0611234](#),
[doi:10.1088/1126-6708/2007/02/080](#)

- [50] S. Boselli *et al.*, *JHEP* **06** (2015) 023. [arXiv:1503.07394](#),
[doi:10.1007/JHEP06\(2015\)023](#)
- [51] T. Inami *et al.*, *Z. Phys.* **C18** (1983) 69. [doi:10.1007/BF01571710](#)
- [52] A. Djouadi *et al.*, *Phys. Lett.* **B264** (1991) 440. [doi:10.1016/0370-2693\(91\)90375-Z](#)
- [53] M. Spira *et al.*, *Nucl. Phys.* **B453** (1995) 17. [arXiv:hep-ph/9504378](#),
[doi:10.1016/0550-3213\(95\)00379-7](#)
- [54] K.G. Chetyrkin *et al.*, *Phys. Rev. Lett.* **79** (1997) 353. [arXiv:hep-ph/9705240](#),
[doi:10.1103/PhysRevLett.79.353](#)
- [55] P.A. Baikov and K.G. Chetyrkin, *Phys. Rev. Lett.* **97** (2006) 061803.
[arXiv:hep-ph/0604194](#), [doi:10.1103/PhysRevLett.97.061803](#)
- [56] F. Herzog *et al.*, *JHEP* **08** (2017) 113. [arXiv:1707.01044](#),
[doi:10.1007/JHEP08\(2017\)113](#)
- [57] A. Djouadi and P. Gambino, *Phys. Rev. Lett.* **73** (1994) 2528. [arXiv:hep-ph/9406432](#),
[doi:10.1103/PhysRevLett.73.2528](#)
- [58] K.G. Chetyrkin *et al.*, *Nucl. Phys.* **B490** (1997) 19. [arXiv:hep-ph/9701277](#),
[doi:10.1016/S0550-3213\(97\)00051-5](#)
- [59] U. Aglietti *et al.*, *Phys. Lett.* **B595** (2004) 432. [arXiv:hep-ph/0404071](#),
[doi:10.1016/j.physletb.2004.06.063](#)
- [60] U. Aglietti *et al.*, Two-loop electroweak corrections to Higgs production in proton–proton collisions, TeV4LHC Workshop: 2nd Meeting, Brookhaven, Upton, New York, 2005, [arXiv:hep-ph/0610033](#)
- [61] G. Degrandi and F. Maltoni, *Phys. Lett.* **B600** (2004) 255. [arXiv:hep-ph/0407249](#),
[doi:10.1016/j.physletb.2004.09.008](#)
- [62] S. Actis *et al.*, *Phys. Lett.* **B670** (2008) 12. [arXiv:0809.1301](#),
[doi:10.1016/j.physletb.2008.10.018](#)
- [63] S. Actis *et al.*, *Nucl. Phys.* **B811** (2009) 182. [arXiv:0809.3667](#),
[doi:10.1016/j.nuclphysb.2008.11.024](#)
- [64] H.-Q. Zheng and D.-D. Wu, *Phys. Rev.* **D42** (1990) 3760.
[doi:10.1103/PhysRevD.42.3760](#)
- [65] A. Djouadi *et al.*, *Phys. Lett.* **B257** (1991) 187. [doi:10.1016/0370-2693\(91\)90879-U](#)
- [66] S. Dawson and R.P. Kauffman, *Phys. Rev.* **D47** (1993) 1264.
[doi:10.1103/PhysRevD.47.1264](#)
- [67] A. Djouadi *et al.*, *Phys. Lett.* **B311** (1993) 255.
[arXiv:hep-ph/9305335](#), [doi:10.1016/0370-2693\(93\)90564-X](#)
- [68] K. Melnikov and O.I. Yakovlev, *Phys. Lett.* **B312** (1993) 179. [arXiv:hep-ph/9302281](#),
[doi:10.1016/0370-2693\(93\)90507-E](#)
- [69] M. Inoue *et al.*, *Mod. Phys. Lett.* **A9** (1994) 1189. [doi:10.1142/S0217732394001003](#)
- [70] J. Fleischer *et al.*, *Phys. Lett.* **B584** (2004) 294. [arXiv:hep-ph/0401090](#),
[doi:10.1016/j.physletb.2004.01.063](#)
- [71] R. Harlander and P. Kant, *JHEP* **12** (2005) 015. [arXiv:hep-ph/0509189](#), [doi:10.1088/1126-6708/2005/12/015](#)

-
- [72] C. Anastasiou *et al.*, *JHEP* **01** (2007) 082. [arXiv:hep-ph/0611236](#),
[doi:10.1088/1126-6708/2007/01/082](#)
- [73] U. Aglietti *et al.*, *JHEP* **01** (2007) 021. [arXiv:hep-ph/0611266](#),
[doi:10.1088/1126-6708/2007/01/021](#)
- [74] M. Steinhauser, Corrections of $\mathcal{O}(\alpha_s^2)$ to the decay of an intermediate mass Higgs boson into two photons, The Higgs Puzzle—What Can We Learn from LEP-2, LHC, NLC and FMC? Proc. Ringberg Workshop, Tegernsee, Germany, 1996, pp. 177–185,
[arXiv:hep-ph/9612395](#)
- [75] C. Sturm, *Eur. Phys. J.* **C74** (2014) 2978. [arXiv:1404.3433](#),
[doi:10.1140/epjc/s10052-014-2978-0](#)
- [76] P. Maierhöfer and P. Marquard, *Phys. Lett.* **B721** (2013) 131. [arXiv:1212.6233](#),
[doi:10.1016/j.physletb.2013.02.040](#)
- [77] A. Djouadi *et al.*, *Nucl. Phys.* **B523** (1998) 17. [arXiv:hep-ph/9712330](#),
[doi:10.1016/S0550-3213\(98\)00147-3](#)
- [78] G. Degrossi and F. Maltoni, *Nucl. Phys.* **B724** (2005) 183. [arXiv:hep-ph/0504137](#),
[doi:10.1016/j.nuclphysb.2005.06.027](#)
- [79] G. Passarino *et al.*, *Phys. Lett.* **B655** (2007) 298. [arXiv:0707.1401](#),
[doi:10.1016/j.physletb.2007.09.002](#)
- [80] M. Spira *et al.*, *Phys. Lett.* **B276** (1992) 350. [doi:10.1016/0370-2693\(92\)90331-W](#)
- [81] R. Bonciani *et al.*, *JHEP* **08** (2015) 108. [arXiv:1505.00567](#),
[doi:10.1007/JHEP08\(2015\)108](#)
- [82] T. Gehrmann *et al.*, *JHEP* **09** (2015) 038. [arXiv:1505.00561](#),
[doi:10.1007/JHEP09\(2015\)038](#)
- [83] A. Abbasabadi *et al.*, *Phys. Rev.* **D55** (1997) 5647. [arXiv:hep-ph/9611209](#),
[doi:10.1103/PhysRevD.55.5647](#)
- [84] A. Abbasabadi *et al.*, *JHEP* **08** (2006) 048. [arXiv:hep-ph/0602087](#),
[doi:10.1088/1126-6708/2006/08/048](#)
- [85] A. Abbasabadi and W.W. Repko, *Phys. Rev.* **D71** (2005) 017304. [arXiv:hep-ph/0411152](#),
[doi:10.1103/PhysRevD.71.017304](#)
- [86] D.A. Dicus and W.W. Repko, *Phys. Rev.* **D87** (2013) 077301. [arXiv:1302.2159](#),
[doi:10.1103/PhysRevD.87.077301](#)
- [87] L.-B. Chen *et al.*, *Phys. Lett.* **B726** (2013) 306. [arXiv:1211.6058](#),
[doi:10.1016/j.physletb.2013.08.050](#)
- [88] G. Passarino, *Phys. Lett.* **B727** (2013) 424. [arXiv:1308.0422](#),
[doi:10.1016/j.physletb.2013.10.052](#)
- [89] Y. Sun *et al.*, *JHEP* **05** (2013) 061. [arXiv:1303.2230](#),
[doi:10.1007/JHEP05\(2013\)061](#)
- [90] S. Jadach and R.A. Kycia, *Phys. Lett.* **B755** (2016) 58. [arXiv:1509.02406](#),
[doi:10.1016/j.physletb.2016.01.065](#)
- [91] A. Djouadi *et al.*, *Z. Phys.* **C70** (1996) 427. [arXiv:hep-ph/9511344](#),
[doi:10.1007/s002880050120](#)

- [92] E. Gross *et al.*, *Z. Phys.* **C63** (1994) 417 [Erratum: **C66** (1995) 321].
[arXiv:hep-ph/9404220](#), [doi:10.1007/BF01580322](#), [doi:10.1007/BF01496607](#)
- [93] A. Denner *et al.*, *Eur. Phys. J.* **C71** (2011) 1753. [arXiv:1107.5909](#),
[doi:10.1140/epjc/s10052-011-1753-8](#)

Chapter C

Methods and tools

1 Heritage projects, preservation, and re-usability concerns

Contribution* by: S. Banerjee, M. Chrzaszcz, Z. Was, J. Zaremba

Corresponding author: Z. Was [z.was@cern.ch]

The FCC is a long-term project, novel in many respects, and new calculations, including simulation programs, will be appearing in the forthcoming years. However, many of the approaches developed for previous experiments, in particular LEP, will be useful, either directly as a tools or as a means to prepare substantial benchmarks. In addition, programs that will be prepared for Belle II, especially in the domain of τ , B, and D resonance physics, will continue to be valuable tools. Such programs and projects will undoubtedly evolve in the meantime, but one can expect that ready-to-use versions will be available when the need arises. Then only interfaces will need to be archived solely for the FCC. In some cases, the whole projects will require long-term preservation. Before we will explain some attempts on preservation of some example projects, such as τ decays, radiative corrections in decays, or electroweak corrections, let us mention possible general approaches.

There are many helpful tools for managing software projects, in both development and preservation. However, preservation-development tools become obsolete and code history, necessary for future extensions and validation, may become lost; therefore, it is important to ensure proper migration from one preservation-development tool to the next. In addition, very stable solutions belong to repositories beyond an author's responsibility, specifically targeting long-term preservation.

The CPC International Program Library [1] serves such a purpose; CERN web pages like that used for TAUOLA [2] or PHOTOS [3] may also offer the necessary facility.

Issues arise if parts of the code are prepared using automated code development tools. If those tools (i.e., other programs) are not published, the programs prepared with their help are of limited help for future applications, especially if extensions are needed.

The interfaces between segments of the code can be of a different type. The reassurance offered by solutions based on some tools is indisputable, but can be overshadowed if such a tool evolves over an unsuitable time. We have experienced minor, but at inconvenient moments for our project evolution, difficulties as a result of ROOT library [4] upgrades to new versions. Manual intervention on our part and changes to the work routine were necessary.[†] Because many software development projects of phenomenology represent a sizeable fraction of the total effort

*This contribution should be cited as:

S. Banerjee, M. Chrzaszcz, Z. Was, J. Zaremba, Heritage projects, preservation, and re-usability concerns, DOI: [10.23731/CYRM-2020-003.135](https://doi.org/10.23731/CYRM-2020-003.135), in: Theory for the FCC-ee, Eds. A. Blondel, J. Gluza, S. Jadach, P. Janot and T. Riemann, CERN Yellow Reports: Monographs, CERN-2020-003, DOI: [10.23731/CYRM-2020-003](https://doi.org/10.23731/CYRM-2020-003), p. 135.
© CERN, 2020. Published by CERN under the [Creative Commons Attribution 4.0 license](https://creativecommons.org/licenses/by/4.0/).

[†]We had to modify the code for our projects, owing to changes in the ROOT library, first in July 2002 and again for the changes introduced with ROOT release 6.

and the people involved may often not be immediately available, this may represent a major inconvenience.

1.1 Common tools for all FCC design studies

As already mentioned, it is of crucial importance to have a common software platform with all the repositories. In the FCC, this effort has begun with the creation of a twiki page [5], where different MC generators are available. This collection should be extended with documentation of programs, links to available original `git` repositories, etc. Everybody is welcome to link or put there related codes or results to be used in future software.

The twiki page [5] currently includes three sections.

1. *FccComputing*, in which the installation procedure of the FCC-ee software is described.
2. *FccGenerators*, containing different MC generators. Currently, Tauola, Higgsline, KKMC, and Bhabha generators are presented.
3. *FccSoftware*, containing various examples of simulations run in the FCC framework.

Next, we will briefly describe currently available generators and discuss their preservation.

1.1.1 *Tauola*

The τ decay phenomenology relies to a large degree on experimental data. This is because of the complexity of experimental analyses and the difficulty in phenomenology modelling decays where intermediate resonances used in hadronic currents are broad and perturbative QCD description is only partly suitable. Background analysis for multidimensional distributions is a problem. Collaborations are hesitant to enable outside use of their matrix element parametrizations, because they may be unsuitable for other, externally studied, distributions. Nevertheless, if they become available, it is worthwhile to store them in publicly available repositories. In Ref. [6], parametrizations developed for ALEPH and CLEO were archived, together with the original parametrization, useful for technical testing of the Tauola algorithm. In Ref. [7], thanks to discussions with the BaBar community, an extension of Tauola with multichannel capacity that is easy to manipulate by users was prepared. The resulting default parametrization equivalent to that work was archived in Ref. [8]. In that reference, a framework for work with C++ currents and for Belle II was prepared. Hopefully, this may provide a means to feed back code at the FCC. A smooth transition period for evolution from partly Fortran to fully C++ code is envisaged in this solution.

1.1.2 *Photos and Tauola Universal interface*

The code for these projects is currently in C++. Preservation of the up-to-date variants is assured, thanks to CERN special accounts and web pages [2, 3]. Some versions are archived in the CPC [9, 10]. The main issue for the project is the fast evolution of event format HepMC [11], and especially how other projects use that format to write down generated events. In addition, long-term preservation efforts may be impaired because of the evolution of configuration and make-file arrangements.

1.1.3 *EvtGen*

The decays of heavy flavoured hadrons provide huge constraints on Beyond Standard Model physics [12]. The FCC-ee is due to run on the Z pole, and will also be a heavy flavour factory. The decays of such mesons and hadrons are modelled with the `EvtGen` package [13]. The package consists of various models, which are constantly being updated with the theory predictions, such as form factors and amplitude calculations. Currently, the main developers of `EvtGen` are involved in LHCb collaboration; however, the package is made publicly available [14] via the git repository. It was recently extended to describe the decays of spin 1/2 particles. The project is written in C++ and interfaces with the HepMC format [11]. It is also possible to interface it with the `Tauola`, `Pythia`, and `Photos` packages.

1.1.4 *Electroweak corrections*

The `KKMC` code is published and archived in Ref. [15]. Its electroweak correction library, in use until today, is also published and archived: `Dizet` version 6.21 [16, 17]. At present, only `Dizet` version 6.42 [18, 19] is available for the `KKMC` electroweak sector upgrade. This version of `Dizet` is missing updates, owing to the photonic vacuum polarisation, e.g., as provided in Refs. [20, 21]. We could implement the updates ourselves because `Dizet` version 6.42 is well-documented. However, some versions of `Dizet` that still exist may become unavailable at a later date. In fact, it was difficult for us to obtain access and we decided to revert to version 6.42. This indicates the necessity for code maintenance, even if authors may at some time become unavailable.

In any case, `Dizet` version 6.42 [18, 19] with updates from Refs. [20, 21] is prepared as a facility for the electroweak tables used in `KKMC` [15].

Using tables prepared by one program in another program is not only the method to enhance the speed of the calculation. Interpolation of values enable technical regularisation of the functions. Technical instabilities at the phase space edges can be regulated.

The tables can be used by other programs that understand the format. In this way, for example, the `TauSpinner` package [10, 22] can be used for graphical presentation for different variants of `Dizet` and of its initialization as a natural continuation of work [23] for the LHC or similar activities for the FCC.

This limit is a substantial burden for interfaces. Preservation of projects is only partly assured by the CPC publications. The most up-to-date versions are available at user webpages, which sometimes are not available or may become unavailable.

References

- [1] <http://www.cpc.cs.qub.ac.uk/>, last accessed 22 January 2020.
- [2] <http://taulapp.web.cern.ch/taulapp/>, last accessed 22 January 2020.
- [3] <http://photospp.web.cern.ch/photospp/>, last accessed 22 January 2020.
- [4] R. Brun and F. Rademakers, *Nucl. Instrum. Meth.* **A389** (1997) 81.
[doi:10.1016/S0168-9002\(97\)00048-X](https://doi.org/10.1016/S0168-9002(97)00048-X)
- [5] <https://twiki.cern.ch/twiki/bin/view/FCC/CommonTools>, last accessed 22 January 2020.
- [6] P. Golonka *et al.*, *Comput. Phys. Commun.* **174** (2006) 818. [arXiv:hep-ph/0312240](https://arxiv.org/abs/hep-ph/0312240),
[doi:10.1016/j.cpc.2005.12.018](https://doi.org/10.1016/j.cpc.2005.12.018)

- [7] Z. Was and P. Golonka, *Nucl. Phys. Proc. Suppl.* **144** (2005) 88. [arXiv:hep-ph/0411377](#), [doi:10.1016/j.nuclphysbps.2005.02.012](#)
- [8] M. Chruszcz *et al.*, *Comput. Phys. Commun.* **232** (2018) 220. [arXiv:1609.04617](#), [doi:10.1016/j.cpc.2018.05.017](#)
- [9] N. Davidson *et al.*, *Comput. Phys. Commun.* **199** (2016) 86. [arXiv:1011.0937](#), [doi:10.1016/j.cpc.2015.09.013](#)
- [10] N. Davidson *et al.*, *Comput. Phys. Commun.* **183** (2012) 821. [arXiv:1002.0543](#), [doi:10.1016/j.cpc.2011.12.009](#)
- [11] M. Dobbs and J.B. Hansen, *Comput. Phys. Commun.* **134** (2001) 41. [doi:10.1016/S0010-4655\(00\)00189-2](#)
- [12] J. Aebischer *et al.*, *Eur. Phys. J.* **C80** (2020) 252. [arXiv:1903.10434](#), [doi:10.1140/epjc/s10052-020-7817-x](#)
- [13] <https://evtgen.hepforge.org/>, last accessed 22 January 2020.
- [14] <https://phab.hepforge.org/source/evtgen>, last accessed 22 January 2020.
- [15] S. Jadach *et al.*, *Comput. Phys. Commun.* **130** (2000) 260. [arXiv:hep-ph/9912214](#), [doi:10.1016/S0010-4655\(00\)00048-5](#)
- [16] D.Y. Bardin *et al.*, *Comput. Phys. Commun.* **59** (1990) 303. [doi:10.1016/0010-4655\(90\)90179-5](#)
- [17] D.Y. Bardin *et al.*, *Comput. Phys. Commun.* **133** (2001) 229. [arXiv:hep-ph/9908433](#), [doi:10.1016/S0010-4655\(00\)00152-1](#)
- [18] A. Andonov *et al.*, *Comput. Phys. Commun.* **181** (2010) 305. [arXiv:0812.4207](#), [doi:10.1016/j.cpc.2009.10.004](#)
- [19] A. Akhundov *et al.*, *Phys. Part. Nucl.* **45** (2014) 529. [arXiv:1302.1395](#), [doi:10.1134/S1063779614030022](#)
- [20] H. Burkhardt and B. Pietrzyk, *Phys. Rev.* **D72** (2005) 057501. [arXiv:hep-ph/0506323](#), [doi:10.1103/PhysRevD.72.057501](#)
- [21] F. Jegerlehner, *EPJ Web Conf.* **218** (2019), 01003. [arXiv:1711.06089](#), [doi:10.1051/epjconf/201921801003](#)
- [22] Z. Czynzula *et al.*, *Eur. Phys. J.* **C72** (2012) 1988. [arXiv:1201.0117](#), [doi:10.1140/epjc/s10052-012-1988-z](#)
- [23] E. Richter-Was and Z. Was, *Eur. Phys. J.* **C79** (2019) 480. [arXiv:1808.08616](#), [doi:10.1140/epjc/s10052-019-6987-x](#)

2 Scalar one-loop Feynman integrals in arbitrary space–time dimension d – an update

Contribution* by: T. Riemann, J. Usovitsch

Corresponding author: T. Riemann [tordriemann@gmail.com]

2.1 Introduction

The study and use of analyticity of scattering amplitudes was founded by R. Eden, P. Landshoff, D. Olive, and J. Polkinghorn in their famous book *The Analytic S-Matrix* in 1966 [1]. Indeed, as early as 1969, J. Schwinger quoted: “One of the most remarkable discoveries in elementary particle physics has been that of the complex plane, [...] the theory of functions of complex variables plays the role not of a mathematical tool, but of a fundamental description of nature inseparable from physics.” [2].

It took many years to make use of analyticity and unitarity, together with renormalizability and gauge invariance of quantum field theory, as a practical tool for the calculation of cross-sections at real colliders. When the analysis of LEP 1 data, around 1989, was prepared, it became evident that the S-matrix language helps to efficiently sort the various perturbative contributions of the Standard Model.

The scattering amplitude for the reaction $e^+e^- \rightarrow (Z, \gamma) \rightarrow f\bar{f}$ at LEP energies depends on two variables, s and $\cos\theta$, and the integrated cross-section may be described by an analytical function of s with a simple pole, describing mass and width of the Z resonance:

$$A = \frac{R}{s - M_Z^2 + iM_Z\Gamma_Z} + \sum_{i=0}^{\infty} a_i (s - M_Z^2 + iM_Z\Gamma_Z)^i. \quad (2.1)$$

Here, position $s_0 = M_Z^2 - iM_Z\Gamma_Z$ and residue R of the pole, as well as the background expansion, are of interest. The analytic form of Eq. (2.1) must be respected when deriving a Z amplitude at multiloop accuracy; see Ref. [3] and the references therein.

Shortly after the work by Eden *et al.* [1], physical amplitudes were also proposed for consideration as complex functions of space–time dimension d (dimensional regularisation) [4,5].

In perturbative calculations with dimensional regularisation, Feynman integrals I are complex functions of the space–time dimension $d = 4 - 2\epsilon$. In fact, they are meromorphic functions of d and may be expanded in Laurent series around poles at, e.g., $d_s = 4 + 2N_0$, $N_0 \geq 0$. Let J_n be an n -point one-loop Feynman integral, as shown in Fig. C.2.1:

$$J_n \equiv J_n(d; \{p_i p_j\}, \{m_i^2\}) = \int \frac{d^d k}{i\pi^{d/2}} \frac{1}{D_1^{\nu_1} D_2^{\nu_2} \dots D_n^{\nu_n}} \quad (2.2)$$

with

$$D_i = \frac{1}{(k + q_i)^2 - m_i^2 + i\epsilon} \quad (2.3)$$

*This contribution should be cited as:

T. Riemann, J. Usovitsch, Scalar one-loop Feynman integrals in arbitrary space-time dimension d – an update, DOI: [10.23731/CYRM-2020-003.139](https://doi.org/10.23731/CYRM-2020-003.139), in: Theory for the FCC-ee, Eds. A. Blondel, J. Gluza, S. Jadach, P. Janot and T. Riemann,

CERN Yellow Reports: Monographs, CERN-2020-003, DOI: [10.23731/CYRM-2020-003](https://doi.org/10.23731/CYRM-2020-003), p. 139.

© CERN, 2020. Published by CERN under the [Creative Commons Attribution 4.0 license](https://creativecommons.org/licenses/by/4.0/).

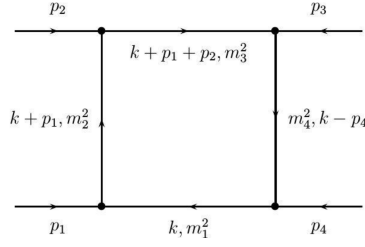


Fig. C.2.1: One-loop Feynman integral

and

$$\nu = \sum_{i=1}^n \nu_i, \quad \sum_{e=1}^n p_e = 0. \quad (2.4)$$

The Feynman integrals are analytical functions of d everywhere with exclusion of isolated singular points d_s , where they behave not worse than

$$\frac{A_s}{(d - d_s)^{N_s}}. \quad (2.5)$$

In physics applications, we need the Feynman integrals at a potentially singular point, $d = 4$, so that their general behaviour at non-singular points is not in the original focus. Nevertheless, the question arises:

Can we determine the general d -dependence of a Feynman integral?

For one-loop integrals, the question has been answered recently, in Ref. [6].

At the beginning of systematic cross-section calculations in d dimensions came two seminal papers on one-loop Feynman integrals in dimensional regularisation [7, 8]. Later, many improvements and generalisations were introduced in various respects.

We see several reasons to study the d -dependence of one-loop Feynman integrals and will discuss them briefly in the next subsection.

2.2 Interests in the d -dependence of one-loop Feynman integrals

2.2.1 Interest from mathematical physics

There is a general interest in the Feynman integrals as meromorphic functions of space–time dimension d ; the easiest case is that of one loop. Early attempts, for the massless case, trace back to Boos and Davydychev [9]. The general one-loop integrals were tackled systematically by Tarasov *et al.* since the 1990s; see, e.g., Refs. [10–13] and references therein. In Refs. [14, 15], the class of generalised hypergeometric functions for massive one-loop Feynman integrals with unit indices was determined and studied with a novel approach based on dimensional difference equations.

- (a) ${}_2F_1$ Gauss hypergeometric functions are needed for self-energies.
- (b) F_1 Appell functions are needed for vertices.
- (c) F_S Lauricella–Saran functions are needed for boxes.

Finally, the correct, general massive one-loop one- to four-point functions with unit indices at arbitrary kinematics were determined by Phan and Riemann [6], who also calculated the numerics of the generalised hypergeometric functions.

2.2.2 Interest from tensor reductions of n -point functions in higher space–time dimensions

For many-particle calculations, inverse Gram determinants $1/G(p_i)$ from tensor reductions appear at certain kinematic configurations p_i . These terms $1/G(p_i)$ may diverge, because Gram determinants can exactly vanish: $G(p_i) \equiv 0$. One may perform tensor reductions so that no inverse Gram determinants appear. But then one has to calculate scalar one-loop integrals in higher dimensions, $D = 4 + 2n - 2\epsilon, n > 0$ [16, 17]. In fact, one introduces new scalar integrals [16]. Let us take as an example a rank-5 tensor of an n -point function:

$$\begin{aligned}
 I_n^{\mu\nu\lambda\rho\sigma} &= \int \frac{d^d k}{i\pi^{d/2}} \frac{k^\mu k^\nu k^\lambda k^\rho k^\sigma}{\prod_{j=1}^n c_j} \\
 &= - \sum_{i,j,k,l,m=1}^n q_i^\mu q_j^\nu q_k^\lambda q_l^\rho q_m^\sigma n_{ijklm} I_{n,ijklm}^{[d+]^5} + \frac{1}{2} \sum_{i,j,k=1}^n g^{[\mu\nu} q_i^\lambda q_j^\rho q_k^\sigma] n_{ijk} I_{n,ijk}^{[d+]^4} \\
 &\quad - \frac{1}{4} \sum_{i=1}^n g^{[\mu\nu} g^{\lambda\rho} q_i^\sigma] I_{n,i}^{[d+]^3}.
 \end{aligned} \tag{2.6}$$

The integrals $I_{n,ab\dots}^{[d+]^l}$ are special cases of $I_{n,ab\dots}^{[d+]^l, s}$, defined in $[d+]^l = 4 - 2\epsilon + 2l$ dimensions, by shrinking line s and raising the powers of propagators (indices) a, b, \dots

At this step, the tensor integral is represented by scalar integrals with higher space–time dimensions and higher propagator powers. The publicly available Feynman integral libraries deliver, though, ordinary scalar integrals in $d = 4 - 2\epsilon$ dimensions, with unit propagator powers. With the usual integration by parts reduction technique [18, 19], one may shift indices, i.e., reduce propagator powers to unity:

$$\nu_j \mathbf{j}^+ I_5 = \frac{1}{\binom{0}{0}_5} \sum_{k=1}^5 \binom{0j}{0k}_5 \left[d - \sum_{i=1}^5 \nu_i (\mathbf{k}^- \mathbf{i}^+ + 1) \right] I_5. \tag{2.7}$$

The operators $\mathbf{i}^\pm, \mathbf{j}^\pm, \mathbf{k}^\pm$ act by shifting the indices ν_i, ν_j, ν_k by ± 1 .

After this step, one has yet to deal with scalar functions in $d = 4 - 2\epsilon + 2l$ dimensions. This may be further reduced by applying dimensional reduction formulae invented by Tarasov [10, 13]: shift of dimension and index,

$$\nu_j (\mathbf{j}^+ I_5^{[d+]}) = \frac{1}{\binom{0}{0}_5} \left[- \binom{j}{0}_5 + \sum_{k=1}^5 \binom{j}{k}_5 \mathbf{k}^- \right] I_5, \tag{2.8}$$

and shift only of dimension,

$$\left(d - \sum_{i=1}^5 \nu_i + 1 \right) I_5^{[d+]} = \frac{1}{\binom{0}{0}_5} \left[\binom{0}{0}_5 - \sum_{k=1}^5 \binom{0}{k}_5 \mathbf{k}^- \right] I_5. \tag{2.9}$$

The procedure is elegant, but it introduces inverse powers of potentially vanishing Gram determinants in both cases. As a consequence, one has finally to treat the numerical implications in sophisticated ways.

At this stage, one might try an alternative. Perform the reductions of tensor functions to scalar functions with unit indices, but allowing for the use of higher space–time dimensions. This avoids the vanishing inverse Gram problem, but introduces the need of a library of scalar

Feynman integrals in higher dimensions. This idea makes it attractive to derive an algorithm allowing the systematic calculation of scalar one- to n -point functions in arbitrary dimensions, and to implement a numerical solution for it.

To be a little more definite, we quote here some unpublished formulae from Refs. [17, 20]. The following reduction of a five-point tensor in terms of tensor coefficients E_{ijklm}^s , with line s skipped from the five-point integral, may be used as a starting point:

$$I_5^{\mu\nu\lambda\rho\sigma} = \sum_{s=1}^5 \left[\sum_{i,j,k,l,m=1}^5 q_i^\mu q_j^\nu q_k^\lambda q_l^\rho q_m^\sigma E_{ijklm}^s + \sum_{i,j,k=1}^5 g^{[\mu\nu} q_i^\lambda q_j^\rho q_k^{\sigma]} E_{00ijk}^s + \sum_{i=1}^5 g^{[\mu\nu} g^{\lambda\rho} q_i^{\sigma]} E_{0000i}^s \right]. \quad (2.10)$$

The tensor coefficients E_{ijklm}^s are expressed in terms of integrals $I_{4,i\dots}^{[d+]^l,s}$, e.g.:

$$E_{ijklm}^s = -\frac{1}{\binom{0}{0}_5} \left\{ \left[\binom{0l}{sm}_5 n_{ijk} I_{4,ijk}^{[d+]^4,s} + (i \leftrightarrow l) + (j \leftrightarrow l) + (k \leftrightarrow l) \right] + \binom{0s}{0m}_5 n_{ijkl} I_{4,ijkl}^{[d+]^4,s} \right\}. \quad (2.11)$$

No factors $1/G_5 = \binom{0}{0}_5$ appear. Now, in a next step, one may avoid the appearance of inverse sub-Gram determinants $\binom{0}{0}_4$. Further, the complete dependence on the indices i of the tensor coefficients can be shifted into the integral's pre-factors with signed minors. One can say that the indices *decouple* from the integrals. As an example, we reproduce the four-point part of $I_{4,ijkl}^{[d+]^4}$:

$$\begin{aligned} n_{ijkl} I_{4,ijkl}^{[d+]^4} &= \frac{\binom{0}{i} \binom{0}{j} \binom{0}{k} \binom{0}{l}}{\binom{0}{0} \binom{0}{0} \binom{0}{0} \binom{0}{0}} d(d+1)(d+2)(d+3) I_4^{[d+]^4} \\ &+ \frac{\binom{0i}{0j} \binom{0}{k} \binom{0}{l} + \binom{0i}{0k} \binom{0}{j} \binom{0}{l} + \binom{0j}{0k} \binom{0}{i} \binom{0}{l} + \binom{0i}{0l} \binom{0}{j} \binom{0}{k} + \binom{0j}{0l} \binom{0}{i} \binom{0}{k} + \binom{0k}{0l} \binom{0}{i} \binom{0}{j}}{\binom{0}{0}^3} \\ &\times d(d+1) I_4^{[d+]^3} + \frac{\binom{0i}{0l} \binom{0j}{0k} + \binom{0j}{0l} \binom{0i}{0k} + \binom{0k}{0l} \binom{0i}{0j}}{\binom{0}{0}^2} I_4^{[d+]^2} + \dots \end{aligned} \quad (2.12)$$

In Eq. (2.12), one has to understand the four-point integrals to carry the corresponding index s of Eq. (2.10) and that the signed minors are $\binom{0}{k} \rightarrow \binom{0s}{ks}_5$, etc. We arrived at:

- (a) no scalar five-point integrals in higher dimensions;
- (b) no inverse Gram determinants $\binom{0}{0}_5$;
- (c) four-point integrals without indices;
- (d) scalar four-point integrals in higher dimensions appearing as $I_4^{[d+]^2,s}$, etc.;
- (e) inverse four-point Gram determinants $\binom{0}{0}_5 \equiv \binom{0}{0}_4$.

2.2.3 Interest from multiloop calculations

Higher-order loop calculations need higher-order contributions from ϵ -expansions of one-loop terms, typically stemming from the expansions

$$\frac{1}{d-4} = -\frac{1}{2\epsilon} \quad (2.13)$$

and

$$\Gamma(\epsilon) = \frac{a_1}{\epsilon} + a_0 + a_1\epsilon + \dots \quad (2.14)$$

A seminal paper on the ϵ -terms of one-loop functions is Ref. [21]. A general analytical solution of the problem of determining the general ϵ -expansion of Feynman integrals is unsolved so far, even for the one-loop case, although see Refs. [22–25]. The determination of one-loop Feynman integrals as meromorphic functions of d might be a useful preparatory step for determining the pole expansion in d around, e.g., $d = 4$.

2.2.4 Interest from Mellin–Barnes representations

A powerful approach to arbitrary Feynman integrals is based on Mellin–Barnes representations [26, 27]. One-loop integrals with variable, in general non-integer, indices are needed in the context of the *loop-by-loop Mellin–Barnes approach* to multiloop integrals. Details may be found in the literature on the Mathematica package AMBRE [28–35], and in references therein.

A crucial technical problem of the Mellin–Barnes representations arises from the increasing number of dimensions of these representations with an increasing number of physical scales. We will detail this in Section 2.3.1. Thus, there is an unresolved need for low-dimensional one-loop Mellin–Barnes (MB) integrals, with arbitrary indices.

2.3 Mellin–Barnes representations for one-loop Feynman integrals

Two numerical MB approaches are advocated.

2.3.1 AMBRE

There are several ways to take advantage of Mellin–Barnes representations for the calculation of Feynman integrals. One approach is the replacement of massive propagators by Mellin–Barnes integrals over massless propagators, invented by Usyukina [36]. Another approach transforms the Feynman parameter representation with Mellin–Barnes representations into a number of complex path integrals, invented in 1999 by Smirnov for planar diagrams [26] and Tausk for non-planar diagrams [27]. This approach ‘automatically’ implies a general solution of the infrared problem and has been worked out in the AMBRE approach [28, 32, 34, 35, 37].

The general definitions for a multiloop Feynman integral are

$$J_n^L \equiv J_n^L(d; \{p_i p_j\}, \{m_i^2\}) = \int \prod_{j=1}^L \frac{d^d k_j}{i\pi^{d/2}} \frac{1}{D_1^{\nu_1} D_2^{\nu_2} \dots D_n^{\nu_n}} \quad (2.15)$$

with

$$D_i = \left(\sum_{l=1}^L a_{il} k_l + \sum_{e=1}^E b_{ie} p_e \right)^2 - m_i^2 + i\delta, \quad a_{il}, b_{ie} \in \{-1, 0, 1\}, \quad (2.16)$$

where m_i are the masses, p_e the external momenta, k_l the loop momenta, $i\delta$ the Feynman prescription, and, finally, ν_i the complex variables.

With the following Feynman trick, we get a really neat parametric representation:

$$\frac{(-1)^\nu}{\prod_{j=1}^n (-D_j^{\nu_j})} = \frac{(-1)^\nu \Gamma(\nu) \left(\prod_{j=1}^n \int_{\{x_j \geq 0\}} \frac{dx_j x_j^{\nu_j-1}}{\Gamma(\nu_j)} \right) \delta \left(1 - \sum_{j=1}^n x_j \right)}{(-k_l^\mu M_{l\nu} k_{l\nu} + 2k_l^\mu Q_{l\mu} + J - i\delta)^\nu}, \quad \nu = \sum_{j=1}^n \nu_j, \quad (2.17)$$

where

$$M_{ll'} = \sum_{j=1}^n a_{jl} a_{j l'} x_j \quad (2.18)$$

is an $L \times L$ symmetric matrix,

$$Q_l^\nu = - \sum_{j=1}^n x_j a_{jl} \sum_{e=1}^E b_{je} p_e^\nu \quad (2.19)$$

is a vector with L components, and

$$J = - \sum_{j=1}^n x_j \left(\sum_{e=1}^E b_{je} p_e^\mu \sum_{e'=1}^E p_{e'}^\nu b_{j e'} g_{\mu\nu} - m_j^2 \right), \quad (2.20)$$

where x_j are the Feynman parameters introduced using the Feynman trick. The metric tensor is $g_{\mu\nu} = \text{diag}(1, -1, \dots, -1)$.

The Feynman integral can now be written in the Feynman parameter integral representation:

$$J_n^L = (-1)^\nu \Gamma(\nu - LD/2) \left(\prod_{j=1}^n \int_{\{x_j \geq 0\}} \frac{dx_j x_j^{\nu_j - 1}}{\Gamma(\nu_j)} \right) \delta \left(1 - \sum_{j=1}^n x_j \right) \frac{U(x)^{\nu - (L+1)D/2}}{F(x)^{\nu - LD/2}}, \quad (2.21)$$

where

$$U(x) = \det M, \quad (2.22)$$

$$F(x) = U(x) \left(Q_l^\mu M_{ll'}^{-1} Q_{l'\mu} + J - i\delta \right). \quad (2.23)$$

From these definitions, it follows that the functions $F(x)$ and $U(x)$ are homogeneous in the Feynman parameters x_i . The function $U(x)$ is of degree L and the function $F(x)$ is of degree $L + 1$. The functions $U(x)$ and $F(x)$ are also known as Symanzik polynomials.

At one-loop level, the definition of the Feynman integral simplifies drastically and gives many insights straight away, which we will bring to light in this work:

$$J_n \equiv J_n(d; \{p_i p_j\}, \{m_i^2\}) = \int \frac{d^d k}{i\pi^{d/2}} \frac{1}{D_1^{\nu_1} D_2^{\nu_2} \dots D_n^{\nu_n}} \quad (2.24)$$

with propagators depending only on one-loop momenta:

$$D_i = \frac{1}{(k + q_i)^2 - m_i^2 + i\epsilon}, \quad (2.25)$$

with

$$q_i = \sum_{e=1}^i p_e. \quad (2.26)$$

We assume here, for brevity,

$$\nu_i = 1, \quad \sum_{e=1}^n p_e = 0. \quad (2.27)$$

If we take the argument of the Dirac delta function to be $1 - \sum_{j=1}^n x_j$, the Feynman parameter representation for one-loop Feynman integrals simplifies to

$$J_n = (-1)^n \Gamma(n - d/2) \int_0^1 \prod_{i=1}^n dx_i \delta\left(1 - \sum_{j=1}^n x_j\right) \frac{1}{F_n(x)^{n-d/2}}. \quad (2.28)$$

Here, the F function is the second Symanzik polynomial, which is just of second degree in the Feynman parameters:

$$F_n(x) = \frac{1}{2} \sum_{i,j} x_i Y_{ij} x_j - i\epsilon. \quad (2.29)$$

The Y_{ij} are elements of the Cayley matrix $Y = (Y_{ij})$,

$$Y_{ij} = Y_{ji} = m_i^2 + m_j^2 - (q_i - q_j)^2. \quad (2.30)$$

Gram and Cayley determinants were introduced by Melrose [38]; see also Ref. [13]. The $(n - 1) \times (n - 1)$ -dimensional Gram determinant $G_n \equiv G_{12\dots n}$ is

$$G_n = - \begin{vmatrix} (q_1 - q_n)^2 & (q_1 - q_n)(q_2 - q_n) & \dots & (q_1 - q_n)(q_{n-1} - q_n) \\ (q_1 - q_n)(q_2 - q_n) & (q_2 - q_n)^2 & \dots & (q_2 - q_n)(q_{n-1} - q_n) \\ \vdots & \vdots & \ddots & \vdots \\ (q_1 - q_n)(q_{n-1} - q_n) & (q_2 - q_n)(q_{n-1} - q_n) & \dots & (q_{n-1} - q_n)^2 \end{vmatrix}. \quad (2.31)$$

The $2^n G_n$ equals, notationally, the G_{n-1} of Ref. [13]. Evidently, the Gram determinant G_n is independent of the propagator masses.

The Cayley determinant $\Delta_n = \lambda_{12\dots n}$ is composed of the Y_{ij} introduced in Eq. (2.30):

$$\text{Cayley determinant : } \Delta_n = \lambda_n \equiv \lambda_{12\dots n} = \begin{vmatrix} Y_{11} & Y_{12} & \dots & Y_{1n} \\ Y_{12} & Y_{22} & \dots & Y_{2n} \\ \vdots & \vdots & \ddots & \vdots \\ Y_{1n} & Y_{2n} & \dots & Y_{nn} \end{vmatrix}. \quad (2.32)$$

We also define the modified Cayley determinant

$$\text{modified Cayley determinant : } ()_n = \begin{vmatrix} 0 & 1 & 1 & \dots & 1 \\ 1 & Y_{11} & Y_{12} & \dots & Y_{1n} \\ 1 & Y_{12} & Y_{22} & \dots & Y_{2n} \\ \vdots & \vdots & \vdots & \ddots & \vdots \\ 1 & Y_{1n} & Y_{2n} & \dots & Y_{nn} \end{vmatrix}. \quad (2.33)$$

The determinants Δ_n , $()_n$, and G_n are evidently independent of a common shifting of the momenta q_i .

One may use Mellin–Barnes integrals [39],

$$\frac{1}{(1+z)^\lambda} = \frac{1}{2\pi i} \int_{-i\infty}^{+i\infty} ds \frac{\Gamma(-s) \Gamma(\lambda + s)}{\Gamma(\lambda)} z^s = {}_2F_1\left[\begin{matrix} \lambda, b; \\ b; \end{matrix} -z\right], \quad (2.34)$$

to split the sum $F_n(x)$ in Eq. (2.29) into a product, enabling nested MB integrals to be calculated. For some mathematics behind the derivation, see the corollary at p. 289 in Ref. [40]. Equation (2.34) is valid if $|\text{Arg}(z)| < \pi$. The integration contour must be chosen such that the poles of $\Gamma(-s)$ and $\Gamma(\lambda + s)$ are well-separated. The right-hand side of Eq. (2.34) is identified as Gauss's hypergeometric function.

There are $N_n = n(n+1)/2$ different Y_{ij} for n -point functions, leading to $N_n = [n(n+1)/2 - 1]$ -dimensional Mellin–Barnes integrals when splitting the sum in Eq. (2.29) into a product:

- $N_3 = 5$ MB dimensions for the most general massive vertices;
- $N_4 = 9$ MB dimensions for the most general massive box integrals;
- $N_5 = 14$ MB dimensions for the most general massive pentagon integrals.

The introduction of N_n -dimensional MB integrals allows x integrations to be calculated. The MB integrations must be calculated afterwards, and this raises some mathematical problems with increasing integral dimensions. This is, for Mellin–Barnes integrals numerical applications, one of the most important limiting factors.

For further details of this approach, we refer to the quoted literature on AMBRE and MBnumerics.

2.3.2 MBOneLoop

A completely different approach was initiated in Refs. [6, 41]. The idea is based on rewriting the F function in Eq. (2.28) by exploring the factor $\delta(1 - \sum x_i)$, which makes the n -fold x -integration to be an integral over an $(n - 1)$ -simplex.

The δ function allows for the elimination of x_n , just one of the x_i , which creates linear terms in the remaining x_i variables in the F function:

$$F_n(x) = x^T G_n x + 2H_n^T x + K_n. \quad (2.35)$$

The $F_n(x)$ may be recast into a bilinear form by shifts $x \rightarrow (x - y)$,

$$F_n(x) = (x - y)^T G_n (x - y) + r_n - i\varepsilon = \Lambda_n(x) + r_n - i\varepsilon = \Lambda_n(x) + R_n. \quad (2.36)$$

As a result, there is a separation of F into a homogeneous part $\Lambda_n(x)$,

$$\Lambda_n(x) = (x - y)^T G_n (x - y), \quad (2.37)$$

and an inhomogeneity R_n ,

$$R_n = r_n - i\varepsilon = K_n - H_n^T G_n^{-1} H_n - i\varepsilon = -\frac{\lambda_n}{g_n} - i\varepsilon = -\frac{\begin{pmatrix} 0 \\ 0 \end{pmatrix}_n}{\binom{}{n}}. \quad (2.38)$$

It is only this inhomogeneity $R_n = r_n - i\varepsilon$ that carries the $i\varepsilon$ prescription. The $(n - 1)$ components y_i of the shift vector y appearing here in $F_n(x)$ are

$$y_i = -\left(G_n^{-1} K_n\right)_i, \quad i \neq n. \quad (2.39)$$

The following relations are also valid:

$$y_i = \frac{\partial r_n}{\partial m_i^2} = -\frac{1}{g_n} \frac{\partial \lambda_n}{\partial m_i^2} = -\frac{\partial_i \lambda_n}{g_n} = \frac{2}{g_n} \frac{\begin{pmatrix} 0 \\ i \end{pmatrix}_n}{\binom{}{n}}, \quad i = 1, \dots, n. \quad (2.40)$$

One further notation has been introduced in Eq. (2.40), namely that of *cofactors of the modified Cayley matrix*, also called signed minors in, e.g., [38, 42]

$$\begin{pmatrix} j_1 & j_2 & \cdots & j_m \\ k_1 & k_2 & \cdots & k_m \end{pmatrix}_n. \quad (2.41)$$

The signed minors are determinants, labelled by those rows j_1, j_2, \dots, j_m and columns k_1, k_2, \dots, k_m that have been discarded from the definition of the modified Cayley determinant $(\)_n$, with a sign convention:

$$\begin{aligned} & \text{sign} \begin{pmatrix} j_1 & j_2 & \cdots & j_m \\ k_1 & k_2 & \cdots & k_m \end{pmatrix}_n \\ &= (-1)^{j_1+j_2+\cdots+j_m+k_1+k_2+\cdots+k_m} \times \text{Signature}[j_1, j_2, \dots, j_m] \times \text{Signature}[k_1, k_2, \dots, k_m]. \end{aligned} \quad (2.42)$$

Here, **Signature** (defined like the Wolfram Mathematica command) gives the sign of permutations needed to place the indices in increasing order. The Cayley determinant is a signed minor of the modified Cayley determinant,

$$\Delta_n = \lambda_n = \begin{pmatrix} 0 \\ 0 \end{pmatrix}_n. \quad (2.43)$$

For later use, we also introduce

$$y_n = 1 - \sum_{i=1}^{n-1} y_i \equiv \frac{\partial r_n}{\partial m_n^2}. \quad (2.44)$$

The auxiliary condition $\sum_i^n y_i = 1$ is fulfilled. Further, the notations for the F function are finally independent of the choice of the variable that was eliminated by the use of the δ function in the integrand of Eq. (2.28). Moreover, the inhomogeneity R_n is the only variable carrying the causal $i\epsilon$ prescription, while, e.g., $\Lambda(x)$ and y_i are, by definition, real quantities. The R_n may be expressed by the ratio of the Cayley determinant (Eq. (2.32)) and the Gram determinant (Eq. (2.31)),

$$R_n = r_{1\dots n} - i\epsilon = -\frac{\lambda_{1\dots n}}{g_{1\dots n}} - i\epsilon. \quad (2.45)$$

One may use the Mellin–Barnes relation (Eq. (2.34)) to decompose the integrand of J_n given in Eq. (2.28), as follows:

$$\begin{aligned} J_n &\sim \int dx \frac{1}{[F(x)]^{n-\frac{d}{2}}} \equiv \int dx \frac{1}{[\Lambda_n(x) + R_n]^{n-\frac{d}{2}}} \equiv \int dx \frac{R_n^{-(n-\frac{d}{2})}}{\left[1 + \frac{\Lambda_n(x)}{R_n}\right]^{n-\frac{d}{2}}} \\ &= \int dx \frac{R_n^{-(n-\frac{d}{2})}}{2\pi i} \int_{-i\infty}^{+i\infty} ds \frac{\Gamma(-s) \Gamma\left(n - \frac{d}{2} + s\right)}{\Gamma\left(n - \frac{d}{2}\right)} \left[\frac{\Lambda_n(x)}{R_n}\right]^s, \end{aligned} \quad (2.46)$$

for $|\text{Arg}(\Lambda_n/R_n)| < \pi$. The condition always applies. Further, the integration path in the complex s -plane separates the poles of $\Gamma(-s)$ and $\Gamma(n - d/2 + s)$.

As a result of Eq. (2.46), the Feynman parameter integral of J_n becomes homogeneous:

$$\begin{aligned}\kappa_n &= \int dx \left[\frac{\Lambda_n(x)}{R_n} \right]^s \\ &= \prod_{j=1}^{n-1} \int_0^{1-\sum_{i=j+1}^{n-1} x_i} dx_j \left[\frac{\Lambda_n(x)}{R_n} \right]^s \equiv \int dS_{n-1} \left[\frac{\Lambda_n(x)}{R_n} \right]^s.\end{aligned}\quad (2.47)$$

To reformulate this integral, one may introduce the differential operator \hat{P}_n [43, 44],

$$\frac{\hat{P}_n}{s} \left[\frac{\Lambda_n(x)}{R_n} \right]^s \equiv \sum_{i=1}^{n-1} \frac{1}{2s} (x_i - y_i) \frac{\partial}{\partial x_i} \left[\frac{\Lambda_n(x)}{R_n} \right]^s = \left[\frac{\Lambda_n(x)}{R_n} \right]^s, \quad (2.48)$$

into Eq. (2.47):

$$K_n = \frac{1}{s} \int dS_{n-1} \hat{P}_n \left[\frac{\Lambda_n(x)}{R_n} \right]^s = \frac{1}{2s} \sum_{i=1}^{n-1} \prod_{k=1}^{n-1} \int_0^{u_k} dx'_k (x_i - y_i) \frac{\partial}{\partial x_i} \left[\frac{\Lambda_n(x)}{R_n} \right]^s. \quad (2.49)$$

After calculating one of the x integrations—by partial integration, eliminating in this way the corresponding differential, and applying a Barnes relation [39] (see Ref. [45]), one arrives at a recursion relation in the number of internal lines n :

$$\begin{aligned}J_n(d, \{q_i, m_i^2\}) \\ = \frac{-1}{2\pi i} \int_{-i\infty}^{+i\infty} ds \frac{\Gamma(-s)\Gamma(\frac{d-n+1}{2} + s)\Gamma(s+1)}{2\Gamma(\frac{d-n+1}{2})} \left(\frac{1}{R_n}\right)^s \times \sum_{k=1}^n \left(\frac{1}{R_n} \frac{\partial r_n}{\partial m_k^2}\right) \mathbf{k}^- J_n(d+2s; \{q_i, m_i^2\}).\end{aligned}\quad (2.50)$$

The operator \mathbf{k}^- , introduced in Eq. (2.7), will reduce an n -point Feynman integral J_n to a sum of $(n-1)$ -point integrals J_{n-1} by shrinking propagators D_k from the original n -point integral. The starting term is the one-point function, or tadpole,

$$J_1(d; m^2) = \int \frac{d^d k}{i\pi^{d/2}} \frac{1}{k^2 - m^2 + i\varepsilon} = -\frac{\Gamma(1-d/2)}{R_1^{1-d/2}}, \quad (2.51)$$

$$R_1 = m^2 - i\varepsilon. \quad (2.52)$$

The cases $G_n = 0$ and $\lambda_n = r_n = 0$ are discussed in Section 2.5.

Equation (2.50) is the master integral for one-loop n -point functions in space-time dimension d , representing them by n integrals over $(n-1)$ -point functions with a shifted dimension $d+2s$. The recursion was first published in Ref. [41]. This implies a series of Mellin–Barnes representations for arbitrary massive one-loop n -point integrals with $(n-1)$ Mellin–Barnes integral dimensions. This linear increase in the MB dimension is highly advantageous compared with the number of MB integral dimensions in the AMBRE approach (increasing as n^2 with the number n of scales).

Based on Eq. (2.50), one has now several opportunities to proceed.

- (i) Evaluate the MB integral in a direct numerical way.
- (ii) Derive ε -expansions for the Feynman integrals.

- (iii) Apply the Cauchy theorem for deriving sums and determine analytical expressions in terms of known special functions.

The first approach is based on AMBRE/MBOneLoop, the middle one is not yet finished, and the last approach was applied in Ref. [41] for massive vertex integrals and in Ref. [6] for massive box integrals.

A few comments are in order.

1. Any four-point integral, e.g., is, in the recursion, a three-fold Mellin–Barnes integral, whereas, with AMBRE, one gets for, e.g., box integrals up to nine-fold MB integrals.
2. Euclidean and Minkowskian integrals converge equally well; see Refs. [46, 47].
3. There appear to be no numerical problems due to vanishing Gram determinants. For a few details, see Table C.2.6 and Ref. [48].

2.4 The basic scalar one-loop functions

2.4.1 Massive two-point functions

From the recursion relation (Eq. (2.50)), taken at $n = 2$ and using Eq. (2.51) with $d \rightarrow d + 2s$ for the one-point functions under the integral, one gets the following Mellin–Barnes representation:

$$J_2(d; q_1, m_1^2, q_2, m_2^2) = \frac{e^{\epsilon\gamma_E}}{2\pi i} \int_{-i\infty}^{+i\infty} ds \frac{\Gamma(-s) \Gamma\left(\frac{d-1}{2} + s\right) \Gamma(s+1)}{2 \Gamma\left(\frac{d-1}{2}\right)} R_2^s \times \left[\frac{1}{r_2} \frac{\partial r_2}{\partial m_2^2} \frac{\Gamma\left(1 - \frac{d+2s}{2}\right)}{(m_1^2)^{1 - \frac{d+2s}{2}}} + (m_1^2 \leftrightarrow m_2^2) \right]. \quad (2.53)$$

One may close the integration contour of the MB integral in Eq. (2.53) to the right, apply the Cauchy theorem, and collect the residua originating from two series of zeros of arguments of Γ functions at $s = m$ and $s = m - d/2 - 1$ for $m \in \mathbb{N}$. The first series stems from the MB-integration kernel, the other one from the dimensionally shifted one-point functions. And then one may sum up analytically in terms of Gauss’ hypergeometric functions.

The two-point function, with $R_2 \equiv R_{12}$, becomes

$$J_2(d; Q^2, m_1^2, q_2, m_2^2) = -\frac{\Gamma\left(2 - \frac{d}{2}\right) \Gamma\left(\frac{d}{2} - 1\right)}{(d-2) \Gamma\left(\frac{d}{2}\right)} \frac{\partial_2 R_2}{R_2} \left[(m_1^2)^{\frac{d}{2}-1} {}_2F_1\left[1, \frac{d}{2} - \frac{1}{2}; \frac{m_1^2}{R_2}\right] + \frac{R_2^{\frac{d}{2}-1}}{\sqrt{1 - \frac{m_1^2}{R_2}}} \sqrt{\pi} \frac{\Gamma\left(\frac{d}{2}\right)}{\Gamma\left(\frac{d}{2} - \frac{1}{2}\right)} \right] + (m_1^2 \leftrightarrow m_2^2). \quad (2.54)$$

Equation (2.54) is valid for $|m_1^2/r_{12}| < 1$, $|m_2^2/r_{12}| < 1$ and $\mathcal{R}e((d-2)/2) > 0$. The result is in agreement with Eq. (53) of Ref. [15].

The iterative determination of higher-point functions proceeds analogously. Closing the integration contours to the right or to the left will cover different kinematic regions in the invariants R_n .

2.4.2 Massive three-point functions

The Mellin–Barnes integral for the massive vertex is a sum of three terms [49]:

$$J_3 = J_{123} + J_{231} + J_{312}, \quad (2.55)$$

using the representation for, e.g., J_{123} ,

$$J_{123}(d, \{q_i, m_i^2\}) = -\frac{e^{\epsilon_{VE}}}{2\pi i} \int_{-i\infty}^{+i\infty} ds \frac{\Gamma(-s) \Gamma(\frac{d-2+2s}{2}) \Gamma(s+1)}{2 \Gamma(\frac{d-2}{2})} R_3^{-s} \times \frac{1}{r_3} \frac{\partial r_3}{\partial m_3^2} J_2(d+2s; q_1, m_1^2, q_2, m_2^2). \quad (2.56)$$

After applying the Cauchy theorem and summing up, one gets an analytical representation. The integrated massive vertex has been published in Ref. [41]. We quote here the representation given in Ref [6]:

$$\begin{aligned} J_{123} = & \Gamma\left(2 - \frac{d}{2}\right) \frac{\partial_3 r_3}{r_3} \frac{\partial_2 r_2}{r_2} \frac{r_2}{2\sqrt{1 - m_1^2/r_2}} \\ & \left[-R_2^{d/2-2} \frac{\sqrt{\pi}}{2} \frac{\Gamma\left(\frac{d}{2} - 1\right)}{\Gamma\left(\frac{d}{2} - \frac{1}{2}\right)} {}_2F_1\left[\frac{d-2}{2}, 1; \frac{R_2}{R_3}\right] + R_3^{d/2-2} {}_2F_1\left[1, 1; \frac{R_2}{R_3}\right] \right] \\ & + \Gamma\left(2 - \frac{d}{2}\right) \frac{\partial_3 r_3}{r_3} \frac{\partial_2 r_2}{r_2} \frac{m_1^2}{4\sqrt{1 - m_1^2/r_2}} \\ & \left[+ \frac{2(m_1^2)^{d/2-2}}{d-2} F_1\left(\frac{d-2}{2}; 1, \frac{1}{2}; \frac{d}{2}; \frac{m_1^2}{R_3}, \frac{m_1^2}{R_2}\right) - R_3^{d/2-2} F_1\left(1; 1, \frac{1}{2}; 2; \frac{m_1^2}{R_3}, \frac{m_1^2}{R_2}\right) \right] \\ & + (m_1^2 \leftrightarrow m_2^2), \end{aligned}$$

with the short notation

$$R_3 = R_{123}, \quad R_2 = R_{12}, \quad (2.57)$$

etc. For $d \rightarrow 4$, the bracket expressions vanish so that their product with the prefactor $\Gamma(2-d/2)$ stays finite in this limit, as it must come out for a massive vertex function. For some numerics, see Tables C.2.1, C.2.2, C.2.3, and C.2.4.

2.4.3 Massive four-point functions

Finally, we reproduce the box integral, as a three-dimensional Mellin–Barnes representation:

$$\begin{aligned} J_4(d; \{p_i^2\}, s, t, \{m_i^2\}) = & \left(\frac{-1}{4\pi i}\right)^4 \frac{1}{\Gamma(\frac{d-3}{2})} \sum_{k_1, k_2, k_3, k_4=1}^4 D_{k_1 k_2 k_3 k_4} \left(\frac{1}{r_4} \frac{\partial r_4}{\partial m_{k_4}^2}\right) \\ & \left(\frac{1}{r_{k_3 k_2 k_1}} \frac{\partial r_{k_3 k_2 k_1}}{\partial m_{k_3}^2}\right) \left(\frac{1}{r_{k_2 k_1}} \frac{\partial r_{k_2 k_1}}{\partial m_{k_2}^2}\right) (m_{k_1}^2)^{d/2-1} \\ & \int_{-i\infty}^{+i\infty} dz_4 \int_{-i\infty}^{+i\infty} dz_3 \int_{-i\infty}^{+i\infty} dz_2 \left(\frac{m_{k_1}^2}{R_4}\right)^{z_4} \left(\frac{m_{k_1}^2}{R_{k_3 k_2 k_1}}\right)^{z_3} \left(\frac{m_{k_1}^2}{R_{k_2 k_1}}\right)^{z_2} \\ & \Gamma(-z_4) \Gamma(z_4 + 1) \frac{\Gamma(z_4 + \frac{d-3}{2})}{\Gamma(z_4 + \frac{d-2}{2})} \Gamma(-z_3) \Gamma(z_3 + 1) \frac{\Gamma(z_3 + z_4 + \frac{d-2}{2})}{\Gamma(z_3 + z_4 + \frac{d-1}{2})} \times \dots \end{aligned} \quad (2.58)$$

Table C.2.1: Numerics for a vertex, $d = 4 - 2\epsilon$. Input quantities suggest that, according to Eq. (73) in Ref. [15], one has to set $b_3 = 0$. Although b_3 of Ref. [15] deviates from our vanishing value, it has to be set to zero, $b_3 \rightarrow 0$. The results of both calculations for J_3 agree for this case.

$[p_i^2], [m_i^2]$	[+100, +200, +300], [10, 20, 30]	
G_{123}	-160 000	
λ_{123}	-8 860 000	
m_i^2/r_{123}	-0.180 587, -0.361 174, -0.541 761	
m_i^2/r_{12}	-0.975 61, -1.951 22, -2.926 83	
m_i^2/r_{23}	-0.398 01, -0.796 02, -1.194 03	
m_i^2/r_{31}	-0.180 723, -0.361 446, -0.542 169	
$\sum J$ terms [15]	(0.019 223 879 - 0.007 987 267 i)	
$\sum b_3$ terms (TR)	0	
J_3 (TR)	(0.019 223 879 - 0.007 987 267 i)	
b_3 term [15]	(-0.089 171 509 + 0.069 788 641 i)	(0.022 214 414)/eps
$b_3 + \sum J$ terms	(-0.012 307 377 - 0.009 301 346 i)	
J_3 (OT)	$\sum J$ terms, b_3 term $\rightarrow 0$, OK	
MB suite		
(-1)×fiesta3 [50]	(-0.012 307 + 0.009 301 i)	+ (8 × 10 ⁻⁶ + 0.000 01 i) ± (1 + i)10 ⁻⁴)
LoopTools [51]	0.019 223 88 - 0.007 987 267 i	

Table C.2.2: Numerics for a vertex, $d = 4 - 2\epsilon$. Input quantities suggest that, according to Eq. (73) in Ref. [15], one has to set $b_3 = 0$. Further, we have set in the numerics for Eq. (75) of Ref. [15] so that the root of the Gram determinant is $\sqrt{-g_{123} + i\epsilon}$, which seems counterintuitive for a ‘momentum’-like function. Both results agree if we *do not* set Tarasov’s $b_3 \rightarrow 0$. Table courtesy of Ref. [52].

$[p_i^2], [m_i^2]$	[-100, +200, -300], [10, 20, 30]	
G_{123}	480 000	
λ_3	-19 300 000	
m_i^2/r_3	0.248 705, 0.497 409, 0.746 114	
m_i^2/r_{12}	0.248 447, 0.496 894, 0.745 342	
m_i^2/r_{23}	-0.398 01, -0.796 02, -1.194 03	
m_i^2/r_{31}	0.104 895, 0.209 79, 0.314 685	
$\sum J$ terms	(-0.012 307 377 - 0.056 679 689 i)	(0.012 825 498 i)/eps
$\sum b_3$ terms	(0.047 378 343 i)	(-0.012 825 498 i)/eps
J_3 (TR)	(-0.012 307 377 - 0.009 301 346 i)	
b_3 term	(0.047 378 343 i)	(-0.012 825 498 i)/eps
$b_3 + \sum J$ terms	(-0.012 307 377 - 0.009 301 346 i)	
J_3 (OT)	$\sum J$ terms, b_3 term $\rightarrow 0$, gets wrong!	
MB suite		
(-1)*fiesta3	(-0.012 307 + 0.009 301 i)	(8 × 10 ⁻⁶ + 0.000 01 i) ± (1 + i)10 ⁻⁴)
LoopTools/FF, ϵ^0	-0.012 307 377 367 78 - 0.009 301 346 170 i	

Table C.2.3: Numerics for a vertex in space–time dimension $d = 4 - 2\epsilon$. Causal $\epsilon = 10^{-20}$. Agreement with Ref. [15]. Table courtesy Ref. [52].

p_i^2	-100, -200, -300	
m_i^2	10, 20, 30	
G_{123}	-160 000	
λ_{123}	15 260 000	
m_i^2/r_{123}	0.104 849, 0.209 699, 0.314 548	
m_i^2/r_{12}	0.248 447, 0.496 894, 0.745 342	
m_i^2/r_{23}	0.133 111, 0.266 223, 0.399 334	
m_i^2/r_{31}	0.104 895, 0.209 79, 0.314 685	
$\sum J$ terms	(0.093 387 7 - 0 i)	-(0.022 214 4 - 0 i)/eps
$\sum b$ terms	-0.101 249	+0.022 214 4/eps
$J_3(\text{TR})$	(-0.007 861 55 - 0 i)	
b_3	(-0.101 249 + 0 i)	(0.022 214 4 + 0 i)/eps
$b_3 + J$ terms	(-0.007 861 546 + 0 i)	
$J_3(\text{OT})$	$b_3 + J$ terms \rightarrow OK	
MB suite	-0.007 862 014, $5.002 549 159 \times 10^{-6}$, 0	
(-1)*fiesta3	-0.007 862	$6 \times 10^{-6} + 6 \times 10^{-6} i \pm (1 + i)10^{-10}$
LoopTools/FF, ϵ^0	-0.007 861 546 132 290 822 90	

Table C.2.4: Numerics for a vertex in space–time dimension $d = 4 - 2\epsilon$. Causal $\epsilon = 10^{-20}$. Input quantities suggest that, according to Eq. (73) in Ref. [15], one has to set $b_3 = 0$. Agreement, owing to setting $b_3 = 0$ there. Table courtesy Ref. [52].

p_i^2	+100, -200, +300	
m_i^2	10, 20, 30	
G_{123}	480 000	
λ_{123}	4 900 000	
m_i^2/r_{123}	-0.979 592, -1.959 18, -2.938 78	
m_i^2/r_{12}	-0.975 61, -1.951 22, -2.926 83	
m_i^2/r_{23}	0.133 111, 0.266 223, 0.399 334	
m_i^2/r_{31}	-0.180 723, -0.361 446, -0.542 169	
$\sum J$ terms	(0.006 243 624 - 0.018 272 524 i)	
$\sum b_3$ terms	0	
$J_3(\text{TR})$	(0.006 243 624 - 0.018 272 524 i)	
b_3 term	(0.040 292 491 + 0.029 796 253 i)	(-0.012 825 498 i)/eps
$b_3 + \sum J$ terms	(-0.012 307 377 - 0.009 301 346 i)	$(4 \times 10^{-18} - 6 \times 10^{-18} i)/\text{eps}$
$J_3(\text{OT})$	$\sum J$ terms, b_3 term \rightarrow 0, OK	
MB suite		
(-1)×fiesta3	$-(-0.006 322 + 0.014 701 i)$	$+(0.000 012 + 0.000 014 i) \pm (1 + i)10^{-2}$
LoopTools/FF, ϵ^0	0.006 243 624 78 - 0.018 272 524 0 i	

Table C.2.5: Comparison of the box integral J_4 defined in Eq. (2.60) with the LoopTools function $D0(p_1^2, p_2^2, p_3^2, p_4^2, (p_1 + p_2)^2, (p_2 + p_3)^2, m_1^2, m_2^2, m_3^2, m_4^2)$ [51, 55] at $m_2^2 = m_3^2 = m_4^2 = 0$. Further numerical references are from the packages K.H.P_D0 (PHK, unpublished) and MBOneLoop [56, 57]. External invariants: $(p_1^2 = \pm 1, p_2^2 = \pm 5, p_3^2 = \pm 2, p_4^2 = \pm 7, s = \pm 20, t = \pm 1)$. Table from Ref. [6], licence: <https://creativecommons.org/licenses/by/4.0/>.

$(p_1^2, p_2^2, p_3^2, p_4^2, s, t)$	Four-point integral
$(-, -, -, -, -, -)$	$d = 4, m_1^2 = 100$
J_4	0.009 178 67
LoopTools	0.009 178 670 7
MBOneLoop	0.009 178 670 7
$(+, +, +, +, +, +)$	$d = 4, m_1^2 = 100$
J_4	$-0.011 592 7 - 0.000 406 03 i$
LoopTools	$-0.011 591 7 - 0.000 406 02 i$
MBOneLoop	$-0.011 591 736 9 - 0.000 406 024 3 i$
$(-, -, -, -, -, -)$	$d = 5, m_1^2 = 100$
J_4	0.009 268 95
K.H.P_D0	0.009 268 88
MBOneLoop	0.009 268 948 8
$(+, +, +, +, +, +)$	$d = 5, m_1^2 = 100$
J_4	$-0.002 728 89 + 0.012 648 8 i$
K.H.P_D0	(-)
MBOneLoop	$-0.002 728 424 2 + 0.012 648 813 4 i$
$(-, -, -, -, -, -)$	$d = 5, m_1^2 = 100 - 10 i$
J_4	$0.009 200 65 + 0.000 782 308 i$
K.H.P_D0	$0.009 200 6 + 0.000 782 301 i$
MBOneLoop	$0.009 200 648 1 + 0.000 782 309 0 i$
$(+, +, +, +, +, +)$	$d = 5, m_1^2 = 100 - 10 i$
J_4	$-0.003 987 25 + 0.012 067 i$
K.H.P_D0	$-0.003 987 23 + 0.012 069 i$
MBOneLoop	$-0.003 986 770 2 + 0.012 067 038 8 i$

$$\cdots \times \Gamma\left(z_2 + z_3 + z_4 + \frac{d-1}{2}\right) \Gamma\left(-z_2 - z_3 - z_4 - \frac{d+2}{2}\right) \Gamma(-z_2)\Gamma(z_2 + 1).$$

Equation (2.58) can be treated using the Mathematica packages MB and MBnumerics of the MBsuite, replacing AMBRE with a derivative of MBnumerics: MBOneLoop [46, 53]. For numerical examples, see Table C.2.5.

After applying the Cauchy theorem and summing the residues, we get [6, 54]:

$$J_4 = J_{1234} + J_{2341} + J_{3412} + J_{4123}, \quad (2.59)$$

with $R_4 = R_{1234}$, $R_3 = R_{123}$, $R_2 = R_{12}$, etc.:

$$\begin{aligned}
 J_{1234} = & \Gamma\left(2 - \frac{d}{2}\right) \frac{\partial_4 r_4}{r_4} \left\{ \left[\frac{b_{123}}{2} \left(-R_3^{d/2-2} {}_2F_1\left[\frac{d-3}{2}, 1; R_2\right] + R_4^{d/2-2} \sqrt{\pi} \frac{\Gamma\left(\frac{d}{2}-1\right)}{\Gamma\left(\frac{d}{2}-\frac{3}{2}\right)} {}_2F_1(d \rightarrow 4) \right) \right] \right. \\
 & + \left[+ \frac{R_2^{d/2-2}}{d-3} F_1\left(\frac{d-3}{2}; 1, \frac{1}{2}; \frac{d-1}{2}; \frac{R_2}{R_4}, \frac{R_2}{R_3}\right) - R_4^{d/2-2} F_1(d \rightarrow 4) \right] \\
 & + \frac{m_1^2 \Gamma\left(\frac{d}{2}-1\right)}{8 \Gamma\left(\frac{d}{2}-\frac{3}{2}\right)} \frac{\partial_3 r_3}{r_3} \frac{\partial_2 r_2}{r_2} \frac{r_3}{r_3 - m_1^2} \frac{r_2}{r_2 - m_1^2} \\
 & \left[- (m_1^2)^{d/2-2} \frac{\Gamma\left(\frac{d}{2}-3/2\right)}{\Gamma\left(\frac{d}{2}\right)} F_S\left(\frac{d}{2}-\frac{3}{2}, 1, 1, 1, 1, \frac{d}{2}, \frac{d}{2}, \frac{d}{2}, \frac{d}{2}, \frac{m_1^2}{R_4}, \frac{m_1^2}{m_1^2 - R_3}, \frac{m_1^2}{m_1^2 - R_2}\right) \right. \\
 & \left. + R_4^{d/2-2} \sqrt{\pi} F_S(d \rightarrow 4) \right] + (m_1^2 \leftrightarrow m_2^2) \left. \right\}. \tag{2.60}
 \end{aligned}$$

For $d \rightarrow 4$, all three contributions in square brackets approach zero, so that the massive J_4 gets finite in this limit, as it should do. Table C.2.5 contains numerical examples.

2.5 The cases of vanishing Cayley determinant $\lambda_n = 0$ and of vanishing Gram determinant $G_n = 0$

We refer here to two important special cases, where the general derivations cannot be applied.

In the case of vanishing Cayley determinant, $\lambda_n = 0$, we cannot introduce the inhomogeneity $R_n = -\lambda_n/G_n$ into the Symanzik polynomial F_n . Let us assume that it is $G_n \neq 0$, so that $r_n = 0$. A useful alternative representation to Eq. (2.50) is known from the literature, see e.g., Eq. (3) in Ref. [15]:

$$J_n(d) = \frac{1}{d-n-1} \sum_{k=1}^n \frac{\partial_k \lambda_n}{G_n} \mathbf{k}^- J_n(d-2). \tag{2.61}$$

Another special case is a vanishing Gram determinant, $G_n = 0$. Here again, one may use Eq. (3) of Ref. [15] and the result is (for $\lambda_n \neq 0$):

$$J_n(d) = - \sum_{k=1}^n \frac{\partial_k \lambda_n}{2\lambda_n} \mathbf{k}^- J_n(d). \tag{2.62}$$

The representation was, for the special case of the vertex function, also given in Eq. (46) of Ref. [58].

For the vertex function, a general study of the special cases has been conducted, as reported in Ref. [59].

2.6 A massive four-point function with vanishing Gram determinant

As a very interesting non-trivial example, we have restudied the numerics of a massive four-point function with a small or vanishing Gram determinant [46, 48, 49, 53]. The original example has been taken from Appendix C of Ref. [17].

Table C.2.6: The Feynman integral $J_4(12 - 2\epsilon, 1, 5, 1, 1)$ compared with numbers from Ref. [17]. The $I_{4,2222}^{[d+]^4}$ is the scalar integral, where propagator 2 has index $\nu_2 = 1 + (1 + 1 + 1 + 1) = 5$, and the other propagators have index 1. The integral corresponds to D_{1111} in the notation of LoopTools [51]. For $x = 0$, the Gram determinant vanishes. We see an agreement of about 10 to 11 relevant digits. The deviations of the two calculations seem to stem from a limited accuracy of the Padé approximations used in Ref. [17]. Table courtesy Refs. [48, 53].

x	Value for $4! \times J_4(12 - 2\epsilon, 1, 5, 1, 1)$	
0	$(2.059\,692\,897\,30 + 1.555\,949\,101\,18\,i)10^{-10}$	[17]
0	$(2.059\,692\,897\,30 + 1.555\,949\,101\,18\,i)10^{-10}$	MBOneLoop+Kira+MBnumerics
10^{-8}	$(2.059\,692\,893\,42 + 1.555\,949\,091\,87\,i)10^{-10}$	[17]
10^{-8}	$(2.059\,692\,893\,63 + 1.555\,949\,091\,87\,i)10^{-10}$	MBOneLoop+Kira+MBnumerics
10^{-4}	$(2.059\,656\,094\,97 + 1.555\,856\,053\,43\,i)10^{-10}$	[17]
10^{-4}	$(2.059\,656\,094\,89 + 1.555\,856\,053\,43\,i)10^{-10}$	MBOneLoop+Kira+MBnumerics

The sample outcome is shown in Table C.2.6. The new iterative Mellin–Barnes representations deliver very precise numerical results for, e.g., box functions, including cases of small or vanishing Gram determinants. The software used is MBOneLoop [60]. The notational correspondences are, e.g.,

$$J_4(12 - 2\epsilon, 1, 5, 1, 1) \rightarrow I_{4,2222}^{[d+]^4} = D_{1111}.$$

2.7 Calculation of Gauss hypergeometric function ${}_2F_1$, Appell function F_1 , and Saran function F_S at arbitrary kinematics

Little is known about the precise numerical calculation of generalised hypergeometric functions at arbitrary arguments. Numerical calculations of specific Gauss hypergeometric functions ${}_2F_1$, Appell functions F_1 (Eq. (1) of Ref. [61]), and Lauricella–Saran functions F_S (Eq. (2.9) of Ref. [62]) are needed for the scalar one-loop Feynman integrals:

$${}_2F_1(a, b; c; x) = \sum_{k=0}^{\infty} \frac{(a)_k (b)_k}{k! (c)_k} x^k, \quad (2.63)$$

$$F_1(a; b, b'; c; y, z) = \sum_{m,n=0}^{\infty} \frac{(a)_{m+n} (b)_m (b')_n}{m! n! (c)_{m+n}} y^m z^n, \quad (2.64)$$

$$F_S(a_1, a_2, a_2; b_1, b_2, b_3; c, c, c; x, y, z) = \sum_{m,n,p=0}^{\infty} \frac{(a_1)_m (a_2)_{n+p} (b_1)_m (b_2)_n (b_3)_p}{m! n! p! (c)_{m+n+p}} x^m y^n z^p. \quad (2.65)$$

The $(a)_k$ is the Pochhammer symbol. The specific cases needed here are discussed in the appendices of Ref. [6]. Here, we repeat only few definitions.

One approach to the numerics of ${}_2F_1$, F_1 , and F_S may be based on Mellin–Barnes representations. For the Gauss function ${}_2F_1$ and the Appell function F_1 , Mellin–Barnes representations have been known for some time. See Eq. (1.6.1.6) in Ref. [63],

$${}_2F_1(a, b; c; z) = \frac{1}{2\pi i} \frac{\Gamma(c)}{\Gamma(a)\Gamma(b)} \int_{-i\infty}^{+i\infty} ds (-z)^s \frac{\Gamma(a+s)\Gamma(b+s)\Gamma(-s)}{\Gamma(c+s)}, \quad (2.66)$$

and Eq. (10) in Ref. [61], which is a two-dimensional MB integral:

$$F_1(a; b, b'; c; x, y) = \frac{1}{2\pi i} \frac{\Gamma(c)}{\Gamma(a)\Gamma(b')} \int_{-i\infty}^{+i\infty} dt (-y)^t {}_2F_1(a+t, b; c+t, x) \frac{\Gamma(a+t)\Gamma(b'+t)\Gamma(-t)}{\Gamma(c+t)}. \quad (2.67)$$

For the Lauricella–Saran function F_S , the following, new, three-dimensional MB integral was given in Ref. [6]:

$$F_S(a_1, a_2, a_2; b_1, b_2, b_3; c, c, c; x, y, z) = \frac{1}{2\pi i} \frac{\Gamma(c)}{\Gamma(a_1)\Gamma(b_1)} \int_{-i\infty}^{+i\infty} dt (-x)^t \frac{\Gamma(a_1+t)\Gamma(b_1+t)\Gamma(-t)}{\Gamma(c+t)} \times F_1(a_2; b_2, b_3; c+t; y, z). \quad (2.68)$$

The numerics of the Gauss hypergeometric function are generally known in all detail.

For the Appell function F_1 , the numerical mean value integration of the one-dimensional integral representation of Ref. [64] may be advocated, being quoted in Eq. (9) of Ref. [61]:

$$F_1(a; b, b'; c; x, y) = \frac{\Gamma(c)}{\Gamma(a)\Gamma(c-a)} \int_0^1 du \frac{u^{a-1}(1-u)^{c-a-1}}{(1-xu)^b(1-yu)^{b'}}. \quad (2.69)$$

We need three specific cases, taken at $d \geq 4$. For vertices, e.g.,

$$F_1^v(d) \equiv F_1\left(\frac{d-2}{2}; 1, \frac{1}{2}; \frac{d}{2}; x_c, y_c\right) = \frac{1}{2}(d-2) \int_0^1 \frac{du u^{\frac{d}{2}-2}}{(1-x_c u)\sqrt{1-y_c u}}. \quad (2.70)$$

Integrability is violated at $u = 0$ if not $\Re(d) > 2$. The stability of numerics is well-controlled, as exemplified in Table C.2.7.

For the calculation of the four-point Feynman integrals, one also needs the Lauricella–Saran function F_S [62]. Saran defines F_S as a three-fold sum (Eq. (2.65)), see Eq. (2.9) in Ref. [62]. Saran derives a three-fold integral representation in Eq. (2.15) and a two-fold integral in Eq. (2.16). We recommend use of the following representation, given on p. 304 of [62]:

$$F_S(a_1, a_2, a_2; b_1, b_2, b_3; c, c, c, x, y, z) = \frac{\Gamma(c)}{\Gamma(a_1)\Gamma(c-a_1)} \int_0^1 dt \frac{t^{c-a_1-1}(1-t)^{a_1-1}}{(1-x+tx)^{b_1}} F_1(a_2; b_2, b_3; c-a_1; ty, tz). \quad (2.71)$$

For the box integrals, one needs the specific case

$$F_S^b(d) = F_S\left(\frac{d-3}{2}, 1, 1; 1, 1, \frac{1}{2}; \frac{d}{2}, \frac{d}{2}, \frac{d}{2}, x_c, y_c, z_c\right) = \frac{\Gamma(\frac{d}{2})}{\Gamma(\frac{d-3}{2})\Gamma(\frac{3}{2})} \int_0^1 dt \frac{\sqrt{t}(1-t)^{\frac{d-5}{2}}}{(1-x_c+xt)} F_1(1; 1, \frac{1}{2}; \frac{3}{2}; y_c t, z_c t). \quad (2.72)$$

Equation (2.72) is valid if $\Re(d) > 3$.

Acknowledgement

We would like to thank J. Gluza for a careful reading of the manuscript.

Table C.2.7: The Appell function F_1 of the massive vertex integrals as defined in Eq. (2.70). As a proof of principle, only the constant term of the expansion in $d = 4 - 2\varepsilon$ is shown, $F_1(1; 1, \frac{1}{2}; 2; x, y)$. Upper values from general numerics of appendices of Ref. [6]; lower values from setting $d = 4$ and the use of analytical formulae. Table courtesy of Ref. [6] under licence <http://creativecommons.org/licenses/by/4.0/>.

$x - i\varepsilon_x$	$y - i\varepsilon_y$	$F_1(1; 1, \frac{1}{2}; 2; x, y)$
+11.1 - 10 ⁻¹² i	+12.1 - 10 ⁻¹² i	-0.175 044 248 073 5 -0.175 044 248 073 518 778 844 982 899 12
+11.1 - 10 ⁻¹² i	+12.1 + 10 ⁻¹² i	+1.710 854 529 324 4 +1.710 854 529 324 335 571 348 382 041 75
+11.1 + 10 ⁻¹² i	+12.1 - 10 ⁻¹² i	+1.710 854 530 411 4 +1.710 854 529 324 335 571 348 382 041 75
+11.1 + 10 ⁻¹² i	+12.1 + 10 ⁻¹² i	-0.175 044 248 073 5 -0.175 044 248 073 518 778 844 982 899 12
+12.1 - 10 ⁻¹⁵ i	+11.1 - 10 ⁻¹⁵ i	-0.170 082 716 648 4
+12.1 - 10 ⁻¹⁰ i	+11.1 - 10 ⁻¹⁵ i	-0.170 082 716 648 000 581 011 657 492 79
+12.1 - 10 ⁻¹⁵ i	+11.1 + 10 ⁻¹⁵ i	-0.170 082 716 648 4 -0.170 082 716 648 440 256 472 688 173 99
+12.1 + 10 ⁻¹⁵ i	+11.1 - 10 ⁻¹⁵ i	-0.170 082 716 648 4 -0.170 082 716 648 440 256 472 688 173 99
+12.1 + 10 ⁻¹⁵ i	+11.1 + 10 ⁻¹⁵ i	-0.170 082 716 648 4
+12.1 - 10 ⁻¹⁰ i	+11.1 - 10 ⁻¹⁵ i	-0.170 082 716 648 000 581 011 657 492 79
+11.1 - 10 ⁻¹⁵ i	-12.1	-0.053 370 514 651 8 -0.053 370 514 651 899 444 733 494 011 52
+11.1 + 10 ⁻¹⁵ i	-12.1	-0.053 370 514 651 8 -0.053 370 514 651 899 444 733 494 011 52
-11.1	+12.1 - 10 ⁻¹² i	+0.106 086 408 466 2 +0.106 086 408 476 510 642 871 335 275 99
-11.1	+12.1 + 10 ⁻¹² i	+0.106 086 408 466 2 +0.106 086 408 476 510 642 871 335 275 99
-12.1	-11.1	+0.122 456 767 687 224 028 +0.122 456 767 687 224 025 065 133 951 61

References

- [1] R.J. Eden *et al.*, *The Analytic S-Matrix* (Cambridge University Press, Cambridge, 1966).
- [2] J. Schwinger, *Particles, Sources, and Fields*, vol. 1 (CRC Press, Boca Raton, 1970).
- [3] A. Blondel *et al.*, Standard Model theory for the FCC-ee Tera-Z stage, CERN (CERN Yellow Rep. Monogr. 3, Geneva, Switzerland), [arXiv:1809.01830](https://arxiv.org/abs/1809.01830), [doi:10.23731/CYRM-2019-003](https://doi.org/10.23731/CYRM-2019-003)
- [4] C.G. Bollini and J.J. Giambiagi, *Nuovo Cim.* **B12** (1972) 20. [doi:10.1007/BF02895558](https://doi.org/10.1007/BF02895558)
- [5] G. 't Hooft and M.J.G. Veltman, *Nucl. Phys.* **B44** (1972) 189. [doi:10.1016/0550-3213\(72\)90279-9](https://doi.org/10.1016/0550-3213(72)90279-9)
- [6] K.H. Phan and T. Riemann, *Phys. Lett.* **B791** (2019) 257. [arXiv:1812.10975](https://arxiv.org/abs/1812.10975), [doi:10.1016/j.physletb.2019.02.044](https://doi.org/10.1016/j.physletb.2019.02.044)
- [7] G. Passarino and M. Veltman, *Nucl. Phys.* **B160** (1979) 151. [doi:10.1016/0550-3213\(79\)90234-7](https://doi.org/10.1016/0550-3213(79)90234-7)

- [8] G. 't Hooft and M. Veltman, *Nucl. Phys.* **B153** (1979) 365.
[doi:10.1016/0550-3213\(79\)90605-9](https://doi.org/10.1016/0550-3213(79)90605-9)
- [9] E.E. Boos and A.I. Davydychev, *Moscow Univ. Phys. Bull.* **42N3** (1987) 6 [*Vestn. Mosk. Univ. Fiz. Astron.* **28N3** (1987) 8].
http://www.higgs.de/~davyd/preprints/bd_vmu.pdf
- [10] O. Tarasov, *Phys. Rev.* **D54** (1996) 6479. [arXiv:hep-th/9606018](https://arxiv.org/abs/hep-th/9606018),
[doi:10.1103/PhysRevD.54.6479](https://doi.org/10.1103/PhysRevD.54.6479)
- [11] O. Tarasov, *Nucl. Phys.* **B502** (1997) 455. [arXiv:hep-ph/9703319](https://arxiv.org/abs/hep-ph/9703319),
[doi:10.1016/S0550-3213\(97\)00376-3](https://doi.org/10.1016/S0550-3213(97)00376-3)
- [12] O.V. Tarasov, *Acta Phys. Pol.* **B29** (1998) 2655. [arXiv:hep-ph/9812250](https://arxiv.org/abs/hep-ph/9812250),
<http://www.actaphys.uj.edu.pl/fulltext?series=Reg&vol=29&page=2655>
- [13] J. Fleischer *et al.*, *Nucl. Phys.* **B566** (2000) 423. [arXiv:hep-ph/9907327](https://arxiv.org/abs/hep-ph/9907327),
[doi:10.1016/S0550-3213\(99\)00678-1](https://doi.org/10.1016/S0550-3213(99)00678-1)
- [14] O. Tarasov, *Nucl. Phys. Proc. Suppl.* **89** (2000) 237. [arXiv:hep-ph/0102271](https://arxiv.org/abs/hep-ph/0102271),
[doi:10.1016/S0920-5632\(00\)00849-5](https://doi.org/10.1016/S0920-5632(00)00849-5)
- [15] J. Fleischer *et al.*, *Nucl. Phys.* **B672** (2003) 303. [arXiv:hep-ph/0307113](https://arxiv.org/abs/hep-ph/0307113),
[doi:10.1016/j.nuclphysb.2003.09.004](https://doi.org/10.1016/j.nuclphysb.2003.09.004)
- [16] A.I. Davydychev, *Phys. Lett.* **B263** (1991) 107.
<http://www.higgs.de/~davyd/preprints/tensor1.pdf>,
[doi:10.1016/0370-2693\(91\)91715-8](https://doi.org/10.1016/0370-2693(91)91715-8)
- [17] J. Fleischer and T. Riemann, *Phys. Rev.* **D83** (2011) 073004. [arXiv:1009.4436](https://arxiv.org/abs/1009.4436),
[doi:10.1103/PhysRevD.83.073004](https://doi.org/10.1103/PhysRevD.83.073004)
- [18] F.V. Tkachov, *Phys. Lett.* **100B** (1981) 65. [doi:10.1016/0370-2693\(81\)90288-4](https://doi.org/10.1016/0370-2693(81)90288-4)
- [19] K. Chetyrkin and F. Tkachov, *Nucl. Phys.* **B192** (1981) 159.
[doi:10.1016/0550-3213\(81\)90199-1](https://doi.org/10.1016/0550-3213(81)90199-1)
- [20] J. Fleischer *et al.*, Replacing 1-loop tensor reduction by contractions, 11th Int. Symposium on Radiative Corrections—Applications of Quantum Field Theory to Phenomenology—RADCOR, Lumley Castle, UK, 2013, <https://conference.ippp.dur.ac.uk/event/341/session/8/contribution/56/material/slides/0.pdf>
- [21] U. Nierste *et al.*, *Z. Phys.* **C57** (1993) 605. [doi:10.1007/BF01561479](https://doi.org/10.1007/BF01561479)
- [22] G. Passarino, *Nucl. Phys.* **B619** (2001) 257. [arXiv:hep-ph/0108252](https://arxiv.org/abs/hep-ph/0108252),
[doi:10.1016/S0550-3213\(01\)00528-4](https://doi.org/10.1016/S0550-3213(01)00528-4)
- [23] A. Ferroglia *et al.*, *Nucl. Phys. Proc. Suppl.* **117** (2003) 206.
[doi:10.1016/S0920-5632\(03\)90526-3](https://doi.org/10.1016/S0920-5632(03)90526-3)
- [24] A. Ferroglia *et al.*, *Nucl. Instrum. Meth.* **A502** (2003) 391.
[doi:10.1016/S0168-9002\(03\)00450-9](https://doi.org/10.1016/S0168-9002(03)00450-9)
- [25] A. Ferroglia *et al.*, *Nucl. Phys.* **B650** (2003) 162. [arXiv:hep-ph/0209219](https://arxiv.org/abs/hep-ph/0209219),
[doi:10.1016/S0550-3213\(02\)01070-2](https://doi.org/10.1016/S0550-3213(02)01070-2)
- [26] V.A. Smirnov, *Phys. Lett.* **B460** (1999) 397. [arXiv:hep-ph/9905323](https://arxiv.org/abs/hep-ph/9905323),
[doi:10.1016/S0370-2693\(99\)00777-7](https://doi.org/10.1016/S0370-2693(99)00777-7)
- [27] J. Tausk, *Phys. Lett.* **B469** (1999) 225. [arXiv:hep-ph/9909506](https://arxiv.org/abs/hep-ph/9909506),
[doi:10.1016/S0370-2693\(99\)01277-0](https://doi.org/10.1016/S0370-2693(99)01277-0)

- [28] J. Gluza *et al.*, *Comput. Phys. Commun.* **177** (2007) 879. [arXiv:0704.2423](#), [doi:10.1016/j.cpc.2007.07.001](#)
- [29] J. Gluza *et al.*, *PoS ACAT08* (2008) 124. [arXiv:0902.4830](#), [doi:10.22323/1.070.0124](#)
- [30] K. Kajda and I. Dubovyk, AMBRE 2.2 (12 Sep 2015), a Mathematica package representing Feynman integrals by Mellin–Barnes integrals, <http://prac.us.edu.pl/~gluza/ambre/>
- [31] J. Gluza *et al.*, *Nucl. Phys. Proc. Suppl.* **205–206** (2010) 147. [arXiv:1006.4728](#), [doi:10.1016/j.nuclphysbps.2010.08.034](#)
- [32] I. Dubovyk *et al.*, *J. Phys. Conf. Ser.* **608** (2015) 012070. [doi:10.1088/1742-6596/608/1/012070](#)
- [33] I. Dubovyk *et al.*, *PoS LL2016* (2016) 034. [arXiv:1607.07538](#), [doi:10.22323/1.260.0034](#)
- [34] J. Usovitsch, Ph.D. thesis, Humboldt-Universität zu Berlin, 2018. [doi:10.18452/19484](#)
- [35] I. Dubovyk, Ph.D. thesis, Universität Hamburg, 2019. <http://ediss.sub.uni-hamburg.de/volltexte/2019/10081>
- [36] N.I. Usyukina, *Theor. Math. Phys.* **22** (1975) 210. [doi:10.1007/BF01037795](#)
- [37] K. Kajda, Ph.D. thesis, University of Silesia, 2009. <http://inspirehep.net/record/1419883/files/phdKajda.pdf>
- [38] D.B. Melrose, *Nuovo Cim.* **40** (1965) 181. [doi:10.1007/BF028329](#)
- [39] E.W. Barnes, *Proc. London Math. Soc.* **s2-6** (1908) 141. [doi:10.1112/plms/s2-6.1.141](#)
- [40] E. Whittaker and G. Watson, *A Course of Modern Analysis* (Cambridge University Press, Cambridge, 1927).
- [41] K.H. Phan *et al.*, *Acta Phys. Pol.* **B48** (2017) 2313. [arXiv:1711.05510](#), [doi:10.5506/APhysPolB.48.2313](#)
- [42] T. Regge and G. Barucchi, *Nuovo Cim.* **34** (1964) 106. [doi:10.1007/BF02725874](#)
- [43] I. Bernshtein, *Funct. Anal. Appl.* **5** (1971) 89. [doi:10.1007/BF01076413](#)
- [44] V.A. Golubeva and V.Z. Énoľ'skii, *Math. Notes Acad. Sci USSR* **23** (1978) 63. [doi:10.1007/BF01104888](#)
- [45] G.N. Watson, *A Treatise on the Theory of Bessel Functions* (Cambridge University Press, Cambridge 1922). https://www.forgottenbooks.com/de/books/ATreatiseontheTheoryofBesselFunctions_10019747
- [46] J. Usovitsch *et al.*, MBnumerics: numerical integration of Mellin–Barnes integrals in physical regions, LL2018, St. Goar, Germany, 2018 2018, <https://indico.desy.de/indico/event/16613/session/4/contribution/22/material/slides/0.pdf>
- [47] J. Usovitsch *et al.*, *PoS LL2018* (2018) 046. [arXiv:1810.04580](#), [doi:10.22323/1.303.0046](#)
- [48] J. Usovitsch and T. Riemann, New approach to Mellin–Barnes integrals for massive one-loop Feynman integrals, Standard Model Theory for the FCC-ee Tera-Z Stage, (CERN-2019-003), section E.6. [arXiv:1809.01830](#), [doi:10.23731/CYRM-2019-003](#)

- [49] T. Riemann, Scalar 1-loop Feynman integrals in arbitrary space–time dimension D , 14th Workshop on Calculations for Modern and Future Colliders (CALC2018), 2018, JINR, Dubna, Russia, <https://indico.jinr.ru/conferenceOtherViews.py?showSession=all&showDate=all&view=standard&fr=no&confId=418>, <http://indico.jinr.ru/getFile.py/access?contribId=77&sessionId=5&resId=0&materialId=slides&confId=418>
- [50] A.V. Smirnov, *Comput. Phys. Commun.* **185** (2014) 2090. [arXiv:1312.3186](https://arxiv.org/abs/1312.3186), [doi:10.1016/j.cpc.2014.03.015](https://doi.org/10.1016/j.cpc.2014.03.015)
- [51] T. Hahn and M. Perez-Victoria, *Comput. Phys. Commun.* **118** (1999) 153. [arXiv:hep-ph/9807565](https://arxiv.org/abs/hep-ph/9807565), [doi:10.1016/S0010-4655\(98\)00173-8](https://doi.org/10.1016/S0010-4655(98)00173-8), <http://www.feynarts.de/looptools>
- [52] K.H. Phan *et al.*, Scalar one-loop vertex integrals as meromorphic functions of space–time dimension d , 41st International Conference of Theoretical Physics: Matter to the Deepest, Podlesice, Poland, 2017. <http://indico.if.us.edu.pl/event/4/contribution/32/material/slides/0.pdf>
- [53] J. Usovitsch, Numerical evaluation of Mellin–Barnes integrals in Minkowskian regions, FCC-ee Mini Workshop Precision EW and QCD calculations for the FCC Studies: Methods and Techniques, 2018, CERN, Geneva, Switzerland. <https://indico.cern.ch/event/669224/contributions/2805454/attachments/1581984/2500208/Usovitsch.pdf>
- [54] T. Riemann *et al.*, Scalar one-loop Feynman integrals in arbitrary space–time dimension, LL2018, St. Goar, Germany, 2018, <https://indico.desy.de/indico/event/16613/session/12/contribution/24/material/slides/0.pdf>
- [55] G. van Oldenborgh, *Comput. Phys. Commun.* **66** (1991) 1. [doi:10.1016/0010-4655\(91\)90002-3](https://doi.org/10.1016/0010-4655(91)90002-3)
- [56] J. Usovitsch *et al.*, The MBnumerics project, Standard Model Theory for the FCC-ee Tera-Z stage, (CERN-2019-003), section E.2. [arXiv:1809.01830](https://arxiv.org/abs/1809.01830), [doi:10.23731/CYRM-2019-003](https://doi.org/10.23731/CYRM-2019-003)
- [57] T. Riemann, 1-loop Feynman integrals at arbitrary space–time d , 11th FCC-ee Workshop: Theory and Experiments, CERN, Geneva, Switzerland, 2019, <https://indico.cern.ch/event/766859/contributions/3252618/attachments/1776255/2887926/riemann11FCCeeWS2019.pdf>
- [58] G. Devaraj and R.G. Stuart, *Nucl. Phys.* **B519** (1998) 483. [arXiv:hep-ph/9704308](https://arxiv.org/abs/hep-ph/9704308), [doi:10.1016/S0550-3213\(98\)00035-2](https://doi.org/10.1016/S0550-3213(98)00035-2)
- [59] K.H. Phan and D.T. Tran, *PTEP*, **2019** (2019) 063B01 [arXiv:1904.07430](https://arxiv.org/abs/1904.07430), [doi:10.1093/ptep/ptz050](https://doi.org/10.1093/ptep/ptz050)
- [60] J. Usovitsch, MBOneLoop, a Mathematica/Fortran package for the numerical calculation of multiple MB-integral representations for one-loop Feynman integrals at arbitrary kinematics, <http://prac.us.edu.pl/~gluza/ambre/>
- [61] P. Appell, Sur les fonctions hypergéométriques de plusieurs variables, les polynômes d’Hermite et autres fonctions sphériques dans l’hyperespace, *Mémorial Sci Math* **3** (1925) 82. http://www.numdam.org/item?id=MSM_1925__3__1_0
- [62] S. Saran, *Acta Math.* **93** (1955) 293. [doi:10.1007/BF02392525](https://doi.org/10.1007/BF02392525)

- [63] L. Slater, *generalised Hypergeometric Functions* (Cambridge University Press, Cambridge, 1966). doi:10.1002/zamm.19660460536
- [64] E. Picard, *Ann Sci l'É.N.S. 2* **10** (1881) 305.
http://www.numdam.org/item?id=ASENS_1881_2_10_305_0
- [65] J. Gluza *et al.*, *Eur. Phys. J.* **C71** (2011) 1516. arXiv:1010.1667,
doi:10.1140/epjc/s10052-010-1516-y

3 NNLO corrections in four dimensions

Contribution* by: R. Pittau [pittau@ugr.es]

3.1 Introduction

Currently, four-dimensional techniques applied to higher-order calculations are under active investigation [1–8]. The main motivation for this is the need to simplify perturbative calculations necessary to cope with the precision requirements of the future LHC and FCC experiments.

In this contribution, I review the four-dimensional regularisation or renormalization (FDR) approach [9] to the computation of NNLO corrections in four dimensions. In particular, I describe how fully inclusive NNLO final-state quark-pair corrections [10]

$$\sigma^{\text{NNLO}} = \sigma_{\text{B}} + \sigma_{\text{V}} + \sigma_{\text{R}} \quad \text{with} \quad \begin{cases} \sigma_{\text{B}} = \int d\Phi_n \sum_{\text{spin}} |A_n^{(0)}|^2 \\ \sigma_{\text{V}} = \int d\Phi_n \sum_{\text{spin}} \{A_n^{(2)}(A_n^{(0)})^* + A_n^{(0)}(A_n^{(2)})^*\} \\ \sigma_{\text{R}} = \int d\Phi_{n+2} \sum_{\text{spin}} \{A_{n+2}^{(0)}(A_{n+2}^{(0)})^*\} \end{cases} \quad (3.1)$$

are computed in FDR by directly enforcing gauge invariance and unitarity in the definition of the regularised UV- and IR-divergent integrals. The IR-divergent parts of the amplitudes are depicted in Fig. C.3.1 and $d\Phi_m := \delta(P - \sum_{i=1}^m p_i) \prod_{i=1}^m d^4 p_i \delta_+(p_i^2)$.

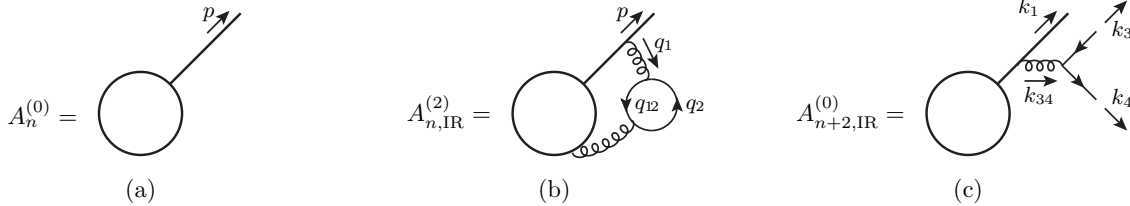


Fig. C.3.1: The lowest-order amplitude (a), the IR-divergent final-state virtual quark-pair correction (b), and the IR-divergent real component (c). The empty circle stands for the emission of $n - 1$ particles. Additional IR finite corrections are created if the gluons with momenta q_1 and k_{34} are emitted by off-shell particles contained in the empty circle.

In Section 3.2, I recall the basics of FDR. The following sections deal with its use in the context of the calculation of σ^{NNLO} in Eq. (3.1).

3.2 FDR integration and loop integrals

The main idea of FDR can be sketched out with the help of a simple one-dimensional example [11]. More details can be found in the relevant literature [9, 10, 12–16]. Let us assume that one needs to define the UV divergent integral

$$I = \lim_{\Lambda \rightarrow \infty} \int_0^\Lambda dx \frac{x}{x + M}, \quad (3.2)$$

*This contribution should be cited as:

R. Pittau, NNLO corrections in four dimensions, DOI: [10.23731/CYRM-2020-003.163](https://doi.org/10.23731/CYRM-2020-003.163), in: Theory for the FCC-ee, Eds. A. Blondel, J. Gluza, S. Jadach, P. Janot and T. Riemann, CERN Yellow Reports: Monographs, CERN-2020-003, DOI: [10.23731/CYRM-2020-003](https://doi.org/10.23731/CYRM-2020-003), p. 163. © CERN, 2020. Published by CERN under the [Creative Commons Attribution 4.0 license](https://creativecommons.org/licenses/by/4.0/).

where M stands for a physical energy scale. FDR identifies the UV divergent pieces in terms of integrands that do not depend on M , the so-called FDR vacua, and separates them by rewriting

$$\frac{x}{x+M} = 1 - \frac{M}{x} + \frac{M^2}{x(x+M)}. \quad (3.3)$$

The first term in the right-hand side of Eq. (3.3) is the vacuum responsible for the linear $\mathcal{O}(\Lambda)$ UV divergence of I and $1/x$ generates its $\ln \Lambda$ behaviour. From the *definition* of FDR integration, both divergent contributions need to be subtracted from Eq. (3.2). The subtraction of the $\mathcal{O}(\Lambda)$ part is performed over the full integration domain $[0, \Lambda]$, while the logarithmic divergence is removed over the interval $[\mu_R, \Lambda]$ only. The arbitrary separation scale $\mu_R \neq 0$ is needed to keep adimensional and finite the arguments of the logarithms appearing in the subtracted and finite parts. Thus

$$I_{\text{FDR}} := I - \lim_{\Lambda \rightarrow \infty} \left(\int_0^\Lambda dx - \int_{\mu_R}^\Lambda dx \frac{M}{x} \right) = M \ln \frac{M}{\mu_R}. \quad (3.4)$$

The advantage of the definition in Eq. (3.4) is two-fold.

- The UV cut-off Λ is traded for μ_R , which is interpreted, straight away, as the renormalization scale.
- Other than logarithmic UV divergences never contribute.

The use of Eq. (3.4) is inconvenient in practical calculations, owing to the explicit appearance of μ_R in the integration interval. An equivalent definition is obtained by adding an auxiliary unphysical scale μ to x ,

$$x \rightarrow \bar{x} := x + \mu, \quad (3.5)$$

and introducing an integral operator $\int_0^\infty [dx]$, defined in such a way that it annihilates the FDR vacua before integration. Thus

$$I_{\text{FDR}} = \int_0^\infty [dx] \frac{\bar{x}}{\bar{x}+M} = \int_0^\infty [dx] \left(1 - \frac{M}{\bar{x}} + \frac{M^2}{\bar{x}(\bar{x}+M)} \right) := M^2 \lim_{\mu \rightarrow 0} \int_0^\infty dx \frac{1}{\bar{x}(\bar{x}+M)} \Big|_{\mu=\mu_R}, \quad (3.6)$$

where $\mu \rightarrow 0$ is an asymptotic limit. Note that, in order to keep the structure of the subtracted terms as in Eq. (3.3), the replacement $x \rightarrow \bar{x}$ must be performed in *both the numerator and the denominator* of the integrated function.

This strategy can be extended to more dimensions and to integrands that are rational functions of the integration variables, as is the case of multiloop integrals. For instance, typical two-loop integrals contributing to $\sigma_V(\gamma^* \rightarrow \text{jets})$ and $\sigma_V(H \rightarrow b\bar{b} + \text{jets})$ are

$$K_1 := \int [d^4 q_1] [d^4 q_2] \frac{1}{\bar{q}_1^2 \bar{D}_1 \bar{D}_2 \bar{q}_2^2 \bar{q}_{12}^2}, \quad K_2^{\rho\sigma\alpha\beta} := \int [d^4 q_1] [d^4 q_2] \frac{q_2^\rho q_2^\sigma q_1^\alpha q_1^\beta}{\bar{q}_1^4 \bar{D}_1 \bar{D}_2 \bar{q}_2^2 \bar{q}_{12}^2}, \quad (3.7)$$

where $q_{12} := q_1 + q_2$, $\bar{D}_{1,2} = \bar{q}_1^2 + 2(q_1 \cdot p_{1,2})$, $p_{1,2}^2 = 0$, and $\bar{q}_i^2 := q_i^2 - \mu^2$ ($i = 1, 2, 12$), in the same spirit as Eq. (3.5).

FDR integration keeps shift invariance in any of the loop integration variables and the possibility of cancelling reconstructed denominators, e.g.,

$$\int [d^4 q_1] [d^4 q_2] \frac{\bar{q}_1^2}{\bar{q}_1^4 \bar{D}_1 \bar{D}_2 \bar{q}_2^2 \bar{q}_{12}^2} = K_1. \quad (3.8)$$

Since, instead,

$$\int [d^4 q_1] [d^4 q_2] \frac{q_1^2}{\bar{q}_1^4 \bar{D}_1 \bar{D}_2 \bar{q}_2^2 \bar{q}_{12}^2} \neq K_1,$$

this last property is maintained only if the replacement $q_i^2 \rightarrow \bar{q}_i^2$ is also made in the numerator of the loop integrals whenever q_i^2 is generated by Feynman rules. This is called *global prescription* (GP), often denoted $q_i^2 \xrightarrow{\text{GP}} \bar{q}_i^2$.

GP and shift invariance guarantee results that do not depend on the chosen gauge [12, 14]. Nevertheless, unitarity should also be maintained. This requires that any given UV divergent subdiagram produce the same result when computed or manipulated separately or when embedded in the full diagram. Such a requirement is called *subintegration consistency* (SIC) [15]. Enforcing SIC in the presence of IR-divergent integrals, such as those in Eq. (3.7), needs extra care. In fact, the IR treatments of σ_V and σ_R should match each other. In the next sections, I describe how this is achieved in the computation of the observable in Eq. (3.1).

3.3 Keeping unitarity in the virtual component

Any integral contributing to σ_V has the form

$$I_V = \int [d^4 q_1] [d^4 q_2] \frac{N_V}{\bar{D} \bar{q}_2^2 \bar{q}_{12}^2}, \quad (3.9)$$

where \bar{D} collects all q_2 -independent propagators and N_V is the numerator of the corresponding Feynman diagram. I_V can be subdivergent or globally divergent for large values of the integration momenta. For example, K_1 in Eq. (3.7) only diverges when $q_2 \rightarrow \infty$, while K_2 also diverges when $q_{1,2} \rightarrow \infty$. This means that FDR prescribes the subtraction of a *global vacuum* (GV) involving both integration variables in K_2 , while the *subvacuum* (SV) developed when $q_2 \rightarrow \infty$ should be removed from both K_1 and K_2 . In addition, IR infinities are generated by the on-shell conditions $p_{1,2}^2 = 0$. Even though IR divergences are automatically regulated when barring the loop denominators, a careful SIC preserving treatment is necessary in order not to spoil unitarity. Since the only possible UV subdivergence is produced by the quark loop in Fig. C.3.1(b), this is accomplished as follows [10].

- One does not apply GP to the contractions $g_{\rho\sigma} q_2^\rho q_2^\sigma$ when $g_{\rho\sigma}$ refers to indices external to the UV divergent subdiagram.
- One replaces everywhere $\bar{q}_1^2 \rightarrow q_1^2$ after GV subtraction.

The external indices entering the calculation of σ_V in Eq. (3.1) are denoted $\hat{\rho}$ and $\hat{\sigma}$ in Fig. C.3.2(a,b). Using this convention, one can rephrase the first rule as follows: $g_{\rho\sigma} q_2^\rho q_2^\sigma = q_2^2 \xrightarrow{\text{GP}} \bar{q}_2^2$, but $g_{\hat{\rho}\hat{\sigma}} q_2^\rho q_2^\sigma := \hat{q}_2^2 \xrightarrow{\text{GP}} q_2^2$, which gives, for instance,

$$\begin{aligned} g_{\rho\sigma} K_2^{\rho\sigma\alpha\beta} &\xrightarrow{\text{GP}} \bar{K}_2^{\alpha\beta} = \int [d^4 q_1] \frac{q_1^\alpha q_1^\beta}{\bar{q}_1^4 \bar{D}_1 \bar{D}_2} \int [d^4 q_2] \frac{1}{\bar{q}_{12}^2} = 0, \text{ but} \\ g_{\hat{\rho}\hat{\sigma}} K_2^{\rho\sigma\alpha\beta} &\xrightarrow{\text{GP}} \hat{K}_2^{\alpha\beta} = \int [d^4 q_1] [d^4 q_2] \frac{q_2^\alpha q_1^\alpha q_1^\beta}{\bar{q}_1^4 \bar{D}_1 \bar{D}_2 \bar{q}_2^2 \bar{q}_{12}^2} \neq 0, \end{aligned} \quad (3.10)$$

where $\bar{K}_2^{\alpha\beta}$ vanishes because the shift $q_2 \rightarrow q_2 - q_1$ makes it proportional to the subvacuum $1/\bar{q}_2^2$, which is annihilated by the $\int [d^4 q_2]$ operator. It can be shown [10, 15] that integrals such as $\hat{K}_2^{\alpha\beta}$ generate the unitarity-restoring logarithms missed by $\bar{K}_2^{\alpha\beta}$.

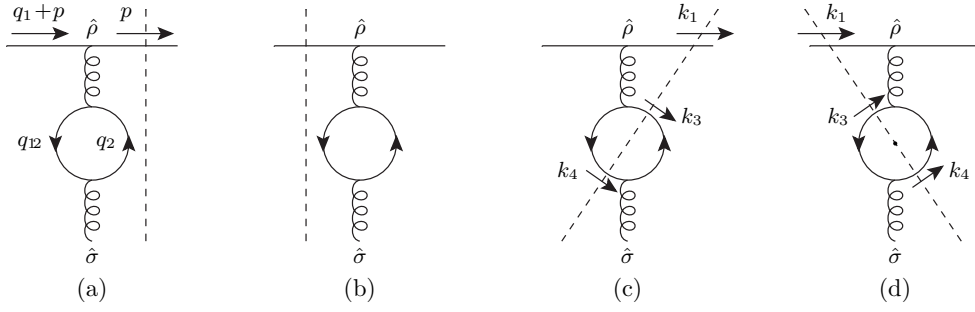


Fig. C.3.2: Virtual and real cuts contributing to the IR-divergent parts of σ_V (a,b) and σ_R (c,d).

As for the second rule, it states that a GV subtraction is needed first. In the case of $\hat{K}_2^{\alpha\beta}$, this is achieved by rewriting

$$\frac{1}{\bar{D}_1} = \frac{1}{\bar{q}_1^2} - \frac{2(q_1 \cdot p_1)}{\bar{D}_1 \bar{q}_1^2}.$$

The first term gives a scaleless integral, annihilated by $\int [d^4 q_1][d^4 q_2]$, so that

$$\hat{K}_2^{\alpha\beta} = -2 \int [d^4 q_1] [d^4 q_2] \frac{(q_1 \cdot p_1) q_2^2 q_1^\alpha q_1^\beta}{\bar{q}_1^6 \bar{D}_1 \bar{D}_2 \bar{q}_2^2 \bar{q}_{12}^2}, \quad (3.11)$$

which is now only subdivergent when $q_2 \rightarrow \infty$, as is K_1 in Eq. (3.7). After that, the replacement $\bar{q}_1^2 \rightarrow q_1^2$ produces

$$K_1 \rightarrow \tilde{K}_1 = \int d^4 q_1 [d^4 q_2] \frac{1}{q_1^2 D_1 D_2 \bar{q}_2^2 \bar{q}_{12}^2}, \quad \hat{K}_2^{\alpha\beta} \rightarrow \tilde{K}_2^{\alpha\beta} = -2 \int d^4 q_1 [d^4 q_2] \frac{(q_1 \cdot p_1) q_2^2 q_1^\alpha q_1^\beta}{q_1^6 D_1 D_2 \bar{q}_2^2 \bar{q}_{12}^2} \quad (3.12)$$

All two-loop integrals I_V in Eq. (3.9) should be treated in this way. In the case of the N_F part of $\sigma_V(\Upsilon^* \rightarrow \text{jets})$ and $\sigma_V(H \rightarrow b\bar{b} + \text{jets})$, this produces three master integrals, which can be computed as described in Appendix D of Ref. [10].

After loop integration, σ_V contains logarithms of μ^2 of both UV and IR origin. The former should be replaced by logarithms of μ_R^2 , as dictated by Eq. (3.6), while the latter compensate the IR behaviour of σ_R . To disentangle the two cases, it is convenient to renormalise σ_V first. This involves expressing the bare strong coupling constant $a^0 := \alpha_S^0/4\pi$ and the bare bottom Yukawa coupling y_b^0 in terms of $a := \alpha_S^{\overline{\text{MS}}}(s)/4\pi$ and y_b extracted from the the bottom pole mass m_b . The relevant relations in terms of $L := \ln \mu^2/(p_1 - p_2)^2$ and $L'' := \ln \mu^2/m_b^2$ are [10]

$$a^0 = a \left(1 + a \delta_a^{(1)} \right), \quad y_b^0 = y_b \left(1 + a \delta_y^{(1)} + a^2 \left(\delta_y^{(2)} + \delta_a^{(1)} \delta_y^{(1)} \right) \right), \quad (3.13)$$

with

$$\delta_a^{(1)} = \frac{2}{3} N_F L, \quad \delta_y^{(1)} = -C_F (3L'' + 5), \quad \delta_y^{(2)} = C_F N_F \left(L''^2 + \frac{13}{3} L'' + \frac{2}{3} \pi^2 + \frac{151}{18} \right). \quad (3.14)$$

After renormalization, the remaining μ^2 s are the IR ones.

3.4 Keeping unitarity in the real component

The integrands in σ_R of Eq. (3.1) are represented in Fig. C.3.2(c,d). They are of the form

$$J_R = \frac{N_R}{S s_{34}^\alpha s_{134}^\beta}, \quad s_{i\dots j} := (k_i + \dots + k_j)^2, \quad 0 \leq \alpha, \quad \beta \leq 2, \quad (3.15)$$

where N_R is the numerator of the amplitude squared and S collects the remaining propagators. Depending on the values of α and β , J_R becomes infrared divergent when integrated over Φ_{n+2} . These IR singularities must be regulated consistently with the SIC preserving treatment of σ_V described in Section 3.3.

The changes $q_2^2 \xrightarrow{\text{GF}} \bar{q}_2^2$ and $q_{12}^2 \xrightarrow{\text{GF}} \bar{q}_{12}^2$ in the virtual cuts of Fig. C.3.2(a,b) imply the Cutkosky relation

$$\frac{1}{(\bar{q}_2^2 + i0^+)(\bar{q}_{12}^2 + i0^+)} \leftrightarrow \left(\frac{2\pi}{i}\right)^2 \delta_+(\bar{k}_3^2) \delta_+(\bar{k}_4^2), \quad (3.16)$$

with $\bar{k}_{3,4}^2 := k_{3,4}^2 - \mu^2$. Hence, one replaces in Eq. (3.1) $\Phi_{n+2} \rightarrow \tilde{\Phi}_{n+2}$, where the phase space $\tilde{\Phi}_{n+2}$ is such that $k_3^2 = k_4^2 = \mu^2$ and $k_i^2 = 0$ when $i \neq 3, 4$. In Ref. [10], it is proven that SV subtraction in σ_V does not alter Eq. (3.16). Analogously, the correspondence between cuts (a) and (d)

$$\frac{1}{(q_1 + p)^2 + i0^+} \leftrightarrow \frac{2\pi}{i} \delta_+(k_1^2) \quad (3.17)$$

is not altered by GV subtraction. Finally, k_3^2 , k_4^2 , and $(k_3 + k_4)^2 = s_{34}$ in N_R of Eq. (3.15) should be treated using the same prescriptions imposed on q_2^2 , q_{12}^2 , and q_1^2 in N_V of Eq. (3.9), respectively. This means replacing

$$k_{3,4}^2 \rightarrow \bar{k}_{3,4}^2 = 0, \quad (k_3 \cdot k_4) = \frac{1}{2} (s_{34} - k_3^2 - k_4^2) \rightarrow \frac{1}{2} (s_{34} - \bar{k}_3^2 - \bar{k}_4^2) = \frac{1}{2} s_{34}, \quad (3.18)$$

where the last equalities are induced by the delta functions in Eq. (3.16). These changes should be made everywhere in N_R , except in contractions induced by the external indices $\hat{\rho}$ and $\hat{\sigma}$ in cuts (c,d). In this case

$$g_{\hat{\rho}\hat{\sigma}} k_{3,4}^\rho k_{3,4}^\sigma \rightarrow k_{3,4}^2 = \mu^2, \quad g_{\hat{\rho}\hat{\sigma}} k_3^\rho k_4^\sigma \rightarrow (k_3 \cdot k_4) = \frac{s_{34} - 2\mu^2}{2}. \quad (3.19)$$

In the case of the N_F part of $\sigma_R(\gamma^* \rightarrow \text{jets})$ and $\sigma_R(\text{H} \rightarrow \text{b}\bar{\text{b}} + \text{jets})$, integrating J_R over $\tilde{\Phi}_4$ and taking the asymptotic $\mu \rightarrow 0$ limit produces the phase space integrals reported in Appendix E of Ref. [10].

3.5 Results and conclusions

Using the approach outlined in Sections 3.3 and 3.4, one reproduces the known $\overline{\text{MS}}$ results for the N_F components of $\sigma^{\text{NNLO}}(\text{H} \rightarrow \text{b}\bar{\text{b}} + \text{jets})$ and $\sigma^{\text{NNLO}}(\gamma^* \rightarrow \text{jets})$ [10]

$$\begin{aligned} \sigma^{\text{NNLO}}(\text{H} \rightarrow \text{b}\bar{\text{b}} + \text{jets}) &= \Gamma_{\text{BORN}}(y_{\text{b}}^{\overline{\text{MS}}}(M_{\text{H}})) \left\{ 1 + a^2 C_{\text{F}} N_{\text{F}} \left(8\zeta_3 + \frac{2}{3}\pi^2 - \frac{65}{2} \right) \right\}, \\ \sigma^{\text{NNLO}}(\gamma^* \rightarrow \text{jets}) &= \sigma_{\text{BORN}} \left\{ 1 + a^2 C_{\text{F}} N_{\text{F}} (8\zeta_3 - 11) \right\}. \end{aligned} \quad (3.20)$$

This shows, for the first time, that a fully four-dimensional framework to compute NNLO quark-pair corrections can be constructed based on the requirement of preserving gauge invariance and unitarity. The basic principles leading to a consistent treatment of all the parts contributing to the NNLO results in Eq. (3.20) are also expected to remain valid when considering more complicated environments. A general four-dimensional NNLO procedure including initial-state IR singularities is currently under investigation.

References

- [1] R.A. Fazio *et al.*, *Eur. Phys. J.* **C74** (2014) 3197. [arXiv:1404.4783](#),
[doi:10.1140/epjc/s10052-014-3197-4](#)
- [2] O.A. Battistel *et al.*, *Mod. Phys. Lett.* **A13** (1998) 1597.
[doi:10.1142/S0217732398001686](#)
- [3] A.L. Cherchiglia *et al.*, *Int. J. Mod. Phys.* **A26** (2011) 2591. [arXiv:1008.1377](#),
[doi:10.1142/S0217751X11053419](#)
- [4] R.J. Hernández-Pinto *et al.*, *JHEP* **02** (2016) 044. [arXiv:1506.04617](#), [doi:10.1007/JHEP02\(2016\)044](#)
- [5] G.F.R. Sborlini *et al.*, *JHEP* **08** (2016) 160. [arXiv:1604.06699](#),
[doi:10.1007/JHEP08\(2016\)160](#)
- [6] G.F.R. Sborlini *et al.*, *JHEP* **10** (2016) 162. [arXiv:1608.01584](#), [doi:10.1007/JHEP10\(2016\)162](#)
- [7] F. Driencourt-Mangin *et al.*, *JHEP* **02** (2019) 143. [arXiv:1901.09853](#), [doi:10.1007/JHEP02\(2019\)143](#)
- [8] R. Runkel *et al.*, *Phys. Rev. Lett.* **122** (2019) 111603 [arXiv:1902.02135](#),
[doi:10.1103/PhysRevLett.122.111603](#)
- [9] R. Pittau, *JHEP* **11** (2012) 151. [arXiv:1208.5457](#),
[doi:10.1007/JHEP11\(2012\)151](#)
- [10] B. Page and R. Pittau, *Eur. Phys. J.* **C79** (2019) 361. [arXiv:1810.00234](#)
[doi:10.1140/epjc/s10052-019-6865-6](#)
- [11] R. Pittau, *Nucl. Phys.* **B950** (2020), 114835. [arXiv:1902.01767](#),
[doi:10.1016/j.nuclphysb.2019.114835](#)
- [12] A.M. Donati and R. Pittau, *JHEP* **04** (2013) 167. [arXiv:1302.5668](#), [doi:10.1007/JHEP04\(2013\)167](#)
- [13] R. Pittau, *Eur. Phys. J.* **C74** (2014) 2686. [arXiv:1307.0705](#),
[doi:10.1140/epjc/s10052-013-2686-1](#)
- [14] A.M. Donati and R. Pittau, *Eur. Phys. J.* **C74** (2014) 2864. [arXiv:1311.3551](#),
[doi:10.1140/epjc/s10052-014-2864-9](#)
- [15] B. Page and R. Pittau, *JHEP* **11** (2015) 183. [arXiv:1506.09093](#),
[doi:10.1007/JHEP11\(2015\)183](#)
- [16] A. Blondel *et al.*, Standard Model theory for the FCC-ee Tera-Z stage, (CERN-2019-003).
[arXiv:1809.01830](#), [doi:10.23731/CYRM-2019-003](#)

4 Unsubtractions at NNLO

Contribution* by: J.J. Aguilera-Verdugo, F. Driencourt-Mangin, J. Plenter, S. Ramírez-Uribe, G. Rodrigo, G.F.R. Sborlini, W.J. Torres Bobadilla, S. Tracz
Corresponding author: G. Rodrigo [german.rodrigo@csic.es]

4.1 Introduction

Computations in perturbative quantum field theory (pQFT) feature several aspects that, although intrinsically non-physical, are traditionally successfully eluded by modifying the dimensions of space–time. Closed loops in pQFT implicitly extrapolate the validity of the Standard Model (SM) to infinite energies—equivalent to zero distance—much above the Planck scale. We should expect this to be a legitimate procedure if the loop scattering amplitudes that contribute to the physical observables are either suppressed at very high energies, or if there is a way to suppress or renormalise their contribution in this limit. In gauge theories like QCD, massless particles can be emitted with zero energy, and pQFT treats the quantum state with N external partons as different from the quantum state with emission of extra massless particles at zero energy, while these two states are physically identical. In addition, partons can be emitted in exactly the same direction, or, in other words, at zero distance. All these unphysical features have a price and lead to the emergence of infinities in the four dimensions of space–time.

In dimensional regularisation (DREG) [1–5], the infinities are replaced by explicit poles in $1/\varepsilon$, with $d = 4 - 2\varepsilon$, through integration of the loop momenta and the phase space of real radiation. Then, the $1/\varepsilon$ ultraviolet (UV) singularities of the virtual contributions are removed by renormalization, and the infrared (IR) soft and collinear singularities are subtracted. The general idea of subtraction [6–18] involves introducing counterterms that mimic the local IR behaviour of the real components and that can easily be integrated analytically in d dimensions. In this way, the integrated form is combined with the virtual component, while the unintegrated counterterm cancels the IR poles originated from the phase space integration of the real-radiation contribution.

Although this procedure efficiently transforms the theory into a calculable and well-defined mathematical framework, a big effort needs to be invested in evaluating loop and phase space integrals in arbitrary space–time dimensions, which are particularly difficult at higher perturbative orders. In view of the highly challenging demands imposed by the expected accuracy attainable at the LHC and future colliders, like the FCC, there has been a recent interest in the community to define perturbative methods directly in $d = 4$ space–time dimensions in order to avoid the complexity of working in a non-physical multidimensional space [19]. Examples of these methods are the four-dimensional formulation (FDF) [20] of the four-dimensional helicity scheme, the six-dimensional formalism (SDF) [21], implicit regularisation (IREG) [22, 23], and four-dimensional regularisation or renormalization (FDR) [24, 25].[†] In this section, we review the four-dimensional unsubtraction (FDU) [26–28] method, which is based on loop-tree duality

*This contribution should be cited as:

J.J. Aguilera-Verdugo, F. Driencourt-Mangin, J. Plenter, S. Ramírez-Uribe, G. Rodrigo, G.F.R. Sborlini, W.J. Torres Bobadilla, S. Tracz, Unsubtractions at NNLO, DOI: [10.23731/CYRM-2020-003.169](https://doi.org/10.23731/CYRM-2020-003.169), in: Theory for the FCC-ee, Eds. A. Blondel, J. Gluza, S. Jadach, P. Janot and T. Riemann, CERN Yellow Reports: Monographs, CERN-2020-003, DOI: [10.23731/CYRM-2020-003](https://doi.org/10.23731/CYRM-2020-003), p. 169.

© CERN, 2020. Published by CERN under the [Creative Commons Attribution 4.0 license](https://creativecommons.org/licenses/by/4.0/).

[†]See Section C.3 in this report.

(LTD) [29–36]. The idea behind FDU is to exploit a suitable mapping of momenta between the virtual and real kinematics in such a way that the summation over the degenerate soft and collinear quantum states is performed locally at integrand level without the necessity of introducing IR subtractions, whereas the UV singularities are locally suppressed at very high energies, e.g., at two loops [35]. The method should improve the efficiency of Monte Carlo event generators because it simultaneously describes real and virtual contributions.

Finally, LTD is also a powerful framework to analyse the singular structure of scattering amplitudes directly in the loop momentum space, which is particularly interesting for characterizing unitarity thresholds and anomalous thresholds for specific kinematic configurations [36].

4.2 Loop-tree duality

The LTD representation of a one-loop scattering amplitude is given by

$$\mathcal{A}^{(1)}(\{p_n\}_N) = - \int_{\ell} \mathcal{N}(\ell, \{p_n\}_N) \otimes G_D(\alpha) , \quad (4.1)$$

where $G_D(\alpha) = \sum_{i \in \alpha} \tilde{\delta}(q_i) \prod_{j \neq i} G_D(q_i; q_j)$, and $\mathcal{N}(\ell, \{p_n\}_N)$ is the numerator of the integrand, which depends on the loop momentum ℓ and the external momenta $\{p_n\}_N$. The delta function $\tilde{\delta}(q_i) = i2\pi \theta(q_{i,0}) \delta(q_i^2 - m_i^2)$ sets on-shell the internal propagator with momentum $q_i = \ell + k_i$ and selects its positive energy mode, $q_{i,0} > 0$. At one loop, $\alpha = \{1, \dots, N\}$ labels all the internal momenta, and Eq. (4.1) is the sum of N single-cut dual amplitudes. The dual propagators,

$$G_D(q_i; q_j) = \frac{1}{q_j^2 - m_j^2 - i0 \eta \cdot k_{ji}} , \quad (4.2)$$

differ from the usual Feynman propagators only by the imaginary prescription, which now depends on $\eta \cdot k_{ji}$, with $k_{ji} = q_j - q_i$. The dual propagators are implicitly linear in the loop momentum, owing to the on-shell conditions. With $\eta = (1, \mathbf{0})$, which is equivalent to integrating out the energy component of the loop momentum, the remaining integration domain is Euclidean.

At two loops, the corresponding dual representation is [31, 35]

$$\begin{aligned} \mathcal{A}^{(2)}(\{p_n\}_N) = \int_{\ell_1} \int_{\ell_2} \mathcal{N}(\ell_1, \ell_2, \{p_n\}_N) \otimes [& G_D(\alpha_1) G_D(\alpha_2 \cup \alpha_3) + G_D(-\alpha_2 \cup \alpha_1) G_D(\alpha_3) \\ & - G_D(\alpha_1) G_D(\alpha_2) G_D(\alpha_3)] . \end{aligned} \quad (4.3)$$

Now, the internal momenta are $q_i = \ell_1 + k_i$, $q_j = \ell_2 + k_j$, and $q_k = \ell_1 + \ell_2 + k_k$, and are classified into three different sets, with $i \in \alpha_1$, $j \in \alpha_2$, and $k \in \alpha_3$ (see Fig. C.4.1). The minus sign in front of α_2 indicates that the momenta in α_2 are reversed to hold a momentum flow consistent with α_1 . The dual representation in Eq. (4.3) spans over the sum of all possible double-cut contributions, with each of the two cuts belonging to a different set. In general, at higher orders, LTD transforms any loop integral or loop scattering amplitude into a sum of tree-level-like objects that are constructed by setting on-shell a number of internal loop propagators equal to the number of loops.

Explicit LTD representations of the scattering amplitude describing the decay $H \rightarrow \gamma\gamma$ have been presented at one [34] and two loops [35].

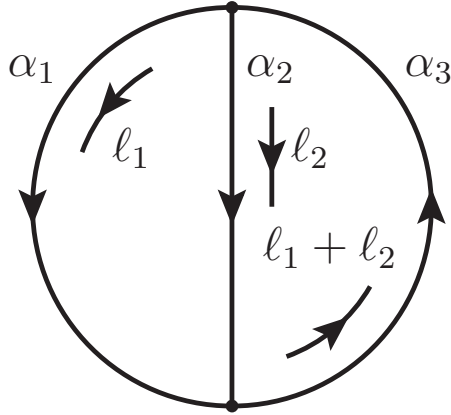


Fig. C.4.1: Momentum flow of a two-loop Feynman diagram

4.3 Four-dimensional unsubtraction

It is interesting to note that although in Eqs. (4.1) and (4.3) the on-shell loop three-momenta are unrestricted, all the IR and physical threshold singularities of the dual amplitudes are restricted to a compact region [32, 36], as discussed in Section 4.4. This is essential to define the four-dimensional unsubtraction (FDU) [26–28] algorithm, namely, to establish a mapping between the real and virtual kinematics in order to locally cancel the IR singularities without the need for subtraction counterterms.

In the FDU approach, the cross-section at next-to-leading order (NLO) is constructed, as usual, from the renormalised one-loop virtual correction with N external partons and the exclusive real cross-section with $N + 1$ partons

$$\sigma^{\text{NLO}} = \int_N d\sigma_{\text{V}}^{(1,\text{R})} + \int_{N+1} d\sigma_{\text{R}}^{(1)}, \quad (4.4)$$

integrated over the corresponding phase space, \int_N and \int_{N+1} . The virtual contribution is obtained from its LTD representation

$$\int_N d\sigma_{\text{V}}^{(1,\text{R})} = \int_{(N,\bar{\ell})} 2 \text{Re} \langle \mathcal{M}_N^{(0)} | \left(\sum_i \mathcal{M}_N^{(1)}(\tilde{\delta}(q_i)) \right) - \mathcal{M}_{\text{UV}}^{(1)}(\tilde{\delta}(q_{\text{UV}})) \rangle \hat{\mathcal{O}}(\{p_n\}_N), \quad (4.5)$$

where $\mathcal{M}_N^{(0)}$ is the N -leg scattering amplitude at leading order (LO), and $\mathcal{M}_N^{(1)}(\tilde{\delta}(q_i))$ is the dual representation of the unrenormalised one-loop scattering amplitude with the internal momentum q_i set on-shell. The integral is weighted with the explicit observable function $\hat{\mathcal{O}}(\{p_n\}_N)$. The expression includes appropriate counterterms, $\mathcal{M}_{\text{UV}}^{(1)}(\tilde{\delta}(q_{\text{UV}}))$, that implement renormalization by subtracting the UV singularities locally, as discussed in Refs. [27, 28], including UV singularities of degree higher than logarithmic that integrate to zero.

By means of an appropriate mapping between the real and virtual kinematics [27, 28],

$$\{p'_r\}_{N+1} \rightarrow (q_i, \{p_n\}_N), \quad (4.6)$$

the real phase space is rewritten in terms of the virtual phase space and the loop three-momentum

$$\int_{N+1} = \int_{(N,\bar{\ell})} \sum_i \mathcal{J}_i(q_i) \mathcal{R}_i(\{p'_r\}_{N+1}), \quad (4.7)$$

where $\mathcal{J}_i(q_i)$ is the Jacobian of the transformation with q_i on-shell, and $\mathcal{R}_i(\{p'_j\}_{N+1})$ defines a complete partition of the real phase space

$$\sum_i \mathcal{R}_i(\{p'_r\}_{N+1}) = 1 . \quad (4.8)$$

As a result, the NLO cross-section is cast into a single integral in the Born or virtual phase space and the loop three-momentum

$$\begin{aligned} \sigma^{\text{NLO}} = \int_{(N, \vec{\ell})} \left[2 \operatorname{Re} \langle \mathcal{M}_N^{(0)} | \left(\sum_i \mathcal{M}_N^{(1)}(\tilde{\delta}(q_i)) \right) - \mathcal{M}_{\text{UV}}^{(1)}(\tilde{\delta}(q_{\text{UV}})) \rangle \hat{\mathcal{O}}(\{p_n\}_N) \right. \\ \left. + \sum_i \mathcal{J}_i(q_i) \mathcal{R}_i(\{p'_r\}_{N+1}) |\mathcal{M}_{N+1}^{(0)}(\{p'_r\}_{N+1})|^2 \hat{\mathcal{O}}(\{p'_r\}_{N+1}) \right] , \quad (4.9) \end{aligned}$$

and exhibits a smooth four-dimensional limit in such a way that it can be evaluated directly in four space–time dimensions. Explicit computations are presented in Refs. [27, 28] with both massless and massive final-state quarks. More importantly, with suitable mappings in Eq. (4.6) conveniently describing the quasi-collinear configurations, the transition from the massive [28] to the massless configuration [27] is also smooth.

The extension of FDU to next-to-next-to-leading order (NNLO) is obvious; the total cross-section consists of three contributions

$$\sigma^{\text{NNLO}} = \int_N d\sigma_{\text{VV}}^{(2,\text{R})} + \int_{N+1} d\sigma_{\text{VR}}^{(2,\text{R})} + \int_{N+2} d\sigma_{\text{RR}}^{(2)} , \quad (4.10)$$

where the double virtual cross-section $d\sigma_{\text{VV}}^{(2,\text{R})}$ receives contributions from the interference of the two-loop with the Born scattering amplitudes, the square of the one-loop scattering amplitude with N external partons, the virtual-real cross-section $d\sigma_{\text{VR}}^{(2,\text{R})}$ includes the contributions from the interference of one-loop and tree-level scattering amplitudes with one extra external particle, and the double real cross-section $d\sigma_{\text{RR}}^{(2)}$ comprises tree-level contributions with the emission of two extra particles. The LTD representation of the two-loop scattering amplitude, $\langle \mathcal{M}_N^{(0)} | \mathcal{M}_N^{(2)}(\tilde{\delta}(q_i, q_j)) \rangle$, is obtained from Eq. (4.3), while the two-loop momenta of the squared one-loop amplitude are independent and generate dual contributions of the type $\langle \mathcal{M}_N^{(1)}(\tilde{\delta}(q_i)) | \mathcal{M}_N^{(1)}(\tilde{\delta}(q_j)) \rangle$. In both cases, there are two independent loop three-momenta and N external momenta with which to reconstruct the kinematics of the tree-level corrections entering $d\sigma_{\text{RR}}^{(2)}$ and the one-loop corrections in $d\sigma_{\text{VR}}^{(2,\text{R})}$:

$$\{p''_r\}_{N+2} \rightarrow (q_i, q_j, \{p_n\}_N) , \quad (q'_k, \{p'_s\}_{N+1}) \rightarrow (q_i, q_j, \{p_n\}_N) , \quad (4.11)$$

in such a way that all the contributions to the NNLO cross-section are cast into a single phase space integral

$$\sigma^{\text{NNLO}} = \int_{(N, \vec{\ell}_1, \vec{\ell}_2)} d\sigma^{\text{NNLO}} . \quad (4.12)$$

Explicit applications of FDU at NNLO are currently under investigation.

4.4 Unitarity thresholds and anomalous thresholds

An essential requirement for FDU to work is to prove that all the IR singularities of the dual amplitudes are restricted to a compact region of the loop three-momenta. This has recently

been proven at higher orders [36], thus extending the one-loop analysis of Ref. [32], as well as analysing the case of anomalous thresholds. The location of the singularities of the dual amplitudes in the loop three-momentum space are encoded at one loop through the set of conditions

$$\lambda_{ij}^{\pm\pm} = \pm q_{i,0}^{(+)} \pm q_{j,0}^{(+)} + k_{ji,0} \rightarrow 0, \quad (4.13)$$

where $q_{r,0}^{(+)} = \sqrt{\vec{q}_r^2 + m_r^2}$, with $r \in \{i, j\}$, are the on-shell loop energies. There are, indeed, only two independent solutions. The limit $\lambda_{ij}^{++} \rightarrow 0$ describes the causal unitarity threshold, and determines that $q_{r,0}^{(+)} < |k_{ji,0}|$, where $k_{ji,0}$ depends on the external momenta only and is therefore bounded. For massless partons, it also describes soft and collinear singularities. The other potential singularity occurs for $\lambda_{ij}^{+-} \rightarrow 0$, but this is a non-causal or unphysical threshold and it cancels locally in the forest defined by the sum of all the on-shell dual contributions. For this to happen, the dual prescription of the dual propagators plays a central role. Finally, anomalous thresholds are determined by overlapping causal unitarity thresholds, e.g., λ_{ij}^{++} and $\lambda_{ik}^{++} \rightarrow 0$ simultaneously.

At two loops, the location of the singularities is determined by the set of conditions

$$\lambda_{ijk}^{\pm\pm\pm} = \pm q_{i,0}^{(+)} \pm q_{j,0}^{(+)} \pm q_{k,0}^{(+)} + k_{k(ij),0} \rightarrow 0, \quad (4.14)$$

where $k_{k(ij)} = q_k - q_i - q_j$ depends on external momenta only, with $i \in \alpha_1$, $j \in \alpha_2$, and $k \in \alpha_3$. Now, the unitarity threshold is defined by the limit $\lambda_{ijk}^{+++} \rightarrow 0$ (or $\lambda_{ijk}^{---} \rightarrow 0$) with $q_{r,0}^{(+)} \leq |k_{k(ij),0}|$ and $r \in \{i, j, k\}$, and the potential singularities at $\lambda_{ijk}^{+-+} \rightarrow 0$ and $\lambda_{ijk}^{+--} \rightarrow 0$ cancel locally in the forest of all the dual contributions. Again, the anomalous thresholds are determined by the simultaneous contribution of unitarity thresholds. The generalisation of Eq. (4.14) to higher orders is straightforward.

4.5 Conclusions

The bottleneck in higher-order perturbative calculations is not only the evaluation of multiloop Feynman diagrams, but also the gathering of all the quantum corrections from different loop orders (and thus different numbers of final-state partons). To match the expected experimental accuracy at the LHC, particularly in the high-luminosity phase, and at future colliders, new theoretical efforts are still needed to overcome the current precision frontier. LTD is also a powerful framework to analyse, comprehensively, the emergence of anomalous thresholds at higher orders.

References

- [1] C.G. Bollini and J.J. Giambiagi, *Nuovo Cim.* **B12** (1972) 20. [doi:10.1007/BF02895558](https://doi.org/10.1007/BF02895558)
- [2] G. 't Hooft and M.J.G. Veltman, *Nucl. Phys.* **B44** (1972) 189. [doi:10.1016/0550-3213\(72\)90279-9](https://doi.org/10.1016/0550-3213(72)90279-9)
- [3] G.M. Cicuta and E. Montaldi, *Lett. Nuovo Cim.* **4** (1972) 329. [doi:10.1007/BF02756527](https://doi.org/10.1007/BF02756527)
- [4] J.F. Ashmore, *Lett. Nuovo Cim.* **4** (1972) 289. [doi:10.1007/BF02824407](https://doi.org/10.1007/BF02824407)
- [5] K.G. Wilson, *Phys. Rev.* **D7** (1973) 2911. [doi:10.1103/PhysRevD.7.2911](https://doi.org/10.1103/PhysRevD.7.2911)
- [6] Z. Kunszt and D.E. Soper, *Phys. Rev.* **D46** (1992) 192. [doi:10.1103/PhysRevD.46.192](https://doi.org/10.1103/PhysRevD.46.192)
- [7] S. Frixione *et al.*, *Nucl. Phys.* **B467** (1996) 399. [arXiv:hep-ph/9512328](https://arxiv.org/abs/hep-ph/9512328), [doi:10.1016/0550-3213\(96\)00110-1](https://doi.org/10.1016/0550-3213(96)00110-1)

- [8] S. Catani and M.H. Seymour, *Phys. Lett.* **B378** (1996) 287. [arXiv:hep-ph/9602277](#), [doi:10.1016/0370-2693\(96\)00425-X](#)
- [9] S. Catani and M.H. Seymour, *Nucl. Phys.* **B485** (1997) 291 [Erratum: **B510** (1998) 503]. [arXiv:hep-ph/9605323](#), [doi:10.1016/S0550-3213\(96\)00589-5](#), [doi:10.1016/S0550-3213\(98\)81022-5](#)
- [10] A. Gehrmann-De Ridder *et al.*, *JHEP* **09** (2005) 056. [arXiv:hep-ph/0505111](#), [doi:10.1088/1126-6708/2005/09/056](#)
- [11] S. Catani and M. Grazzini, *Phys. Rev. Lett.* **98** (2007) 222002. [arXiv:hep-ph/0703012](#), [doi:10.1103/PhysRevLett.98.222002](#)
- [12] M. Czakon, *Phys. Lett.* **B693** (2010) 259. [arXiv:1005.0274](#), [doi:10.1016/j.physletb.2010.08.036](#)
- [13] P. Bolzoni *et al.*, *JHEP* **01** (2011) 059. [arXiv:1011.1909](#), [doi:10.1007/JHEP01\(2011\)059](#)
- [14] R. Boughezal *et al.*, *Phys. Rev. Lett.* **115** (2015) 062002. [arXiv:1504.02131](#), [doi:10.1103/PhysRevLett.115.062002](#)
- [15] J. Gaunt *et al.*, *JHEP* **09** (2015) 058. [arXiv:1505.04794](#), [doi:10.1007/JHEP09\(2015\)058](#)
- [16] V. Del Duca *et al.*, *Phys. Rev.* **D94** (2016) 074019. [arXiv:1606.03453](#), [doi:10.1103/PhysRevD.94.074019](#)
- [17] F. Caola *et al.*, *Eur. Phys. J.* **C77** (2017) 248. [arXiv:1702.01352](#), [doi:10.1140/epjc/s10052-017-4774-0](#)
- [18] L. Magnea *et al.*, *JHEP* **12** (2018) 107. [arXiv:1806.09570](#), [doi:10.1007/JHEP12\(2018\)107](#)
- [19] C. Gnendiger *et al.*, *Eur. Phys. J.* **C77** (2017) 471. [arXiv:1705.01827](#), [doi:10.1140/epjc/s10052-017-5023-2](#)
- [20] R.A. Fazio *et al.*, *Eur. Phys. J.* **C74** (2014) 3197. [arXiv:1404.4783](#), [doi:10.1140/epjc/s10052-014-3197-4](#)
- [21] Z. Bern *et al.*, *Phys. Rev.* **D66** (2002) 085002. [arXiv:hep-ph/0202271](#), [doi:10.1103/PhysRevD.66.085002](#)
- [22] O.A. Battistel *et al.*, *Mod. Phys. Lett.* **A13** (1998) 1597. [doi:10.1142/S0217732398001686](#)
- [23] H.G. Fargnoli *et al.*, *Mod. Phys. Lett.* **A26** (2011) 289. [arXiv:1001.1543](#), [doi:10.1142/S0217732311034773](#)
- [24] A.M. Donati and R. Pittau, *Eur. Phys. J.* **C74** (2014) 2864. [arXiv:1311.3551](#), [doi:10.1140/epjc/s10052-014-2864-9](#)
- [25] B. Page and R. Pittau, *Eur. Phys. J.* **C79** (2019) 361. [arXiv:1810.00234](#), [doi:10.1140/epjc/s10052-019-6865-6](#)
- [26] R.J. Hernández-Pinto *et al.*, *JHEP* **02** (2016) 044. [arXiv:1506.04617](#), [doi:10.1007/JHEP02\(2016\)044](#)
- [27] G.F.R. Sborlini *et al.*, *JHEP* **08** (2016) 160. [arXiv:1604.06699](#), [doi:10.1007/JHEP08\(2016\)160](#)

- [28] G.F.R. Sborlini *et al.*, *JHEP* **10** (2016) 162. [arXiv:1608.01584](#), [doi:10.1007/JHEP10\(2016\)162](#)
- [29] S. Catani *et al.*, *JHEP* **09** (2008) 065. [arXiv:0804.3170](#), [doi:10.1088/1126-6708/2008/09/065](#)
- [30] I. Bierenbaum *et al.*, *JHEP* **10** (2010) 073. [arXiv:1007.0194](#), [doi:10.1007/JHEP10\(2010\)073](#)
- [31] I. Bierenbaum *et al.*, *JHEP* **03** (2013) 025. [arXiv:1211.5048](#), [doi:10.1007/JHEP03\(2013\)025](#)
- [32] S. Buchta *et al.*, *JHEP* **11** (2014) 014. [arXiv:1405.7850](#), [doi:10.1007/JHEP11\(2014\)014](#)
- [33] S. Buchta *et al.*, *Eur. Phys. J.* **C77** (2017) 274. [arXiv:1510.00187](#), [doi:10.1140/epjc/s10052-017-4833-6](#)
- [34] F. Driencourt-Mangin *et al.*, *Eur. Phys. J.* **C78** (2018) 231. [arXiv:1702.07581](#), [doi:10.1140/epjc/s10052-018-5692-5](#)
- [35] F. Driencourt-Mangin *et al.*, *JHEP* **02** (2019) 143. [arXiv:1901.09853](#), [doi:10.1007/JHEP02\(2019\)143](#)
- [36] J.J. Aguilera-Verdugo *et al.*, *JHEP* **12** (2019), 163 [arXiv:1904.08389](#), [doi:10.1007/JHEP12\(2019\)163](#)

5 Numerics for elliptic Feynman integrals

Contribution* by: C. Bogner, I. Hönemann, K. Tempest, A. Schweitzer, S. Weinzierl
Corresponding author: S. Weinzierl [weinzierl@uni-mainz.de]

The Standard Model involves several heavy particles: the Z and W bosons, the Higgs boson, and the top quark. Precision studies of these particles require, on the theoretical side, quantum corrections at the two-loop order and beyond. It is a well-known fact that, starting from two loops, Feynman integrals with massive particles can no longer be expressed in terms of multiple polylogarithms. This immediately raises the following question. What is the larger class of functions needed to express the relevant Feynman integrals? For single-scale two-loop Feynman integrals related to a single elliptic curve we now have the answer: they are expressed as iterated integrals of modular form [1]. This brings us to a second question: is there an efficient method to evaluate these functions numerically in the full kinematic range? In this contribution, we review how this can be done. This review is mainly based on Refs. [2, 3].

Efficient numerical evaluation methods rely on three ingredients: (i) an (iterated) integral representation, used to transform the arguments into the region of convergence, (ii) a (nested) sum representation, defined in the region of convergence, which can be truncated and gives a numerical approximation, and (iii) methods to accelerate the convergence of the truncated series. Let us illustrate this strategy for the numerical evaluation of the dilogarithm [4], defined by

$$\text{Li}_2(x) = \int_0^x \frac{dt_1}{t_1} \int_0^{t_1} \frac{dt_2}{1-t_2} = \sum_{n=1}^{\infty} \frac{x^n}{n^2}. \quad (5.1)$$

The power series expansion can be evaluated numerically, provided $|x| < 1$. Using the functional equations

$$\text{Li}_2(x) = -\text{Li}_2\left(\frac{1}{x}\right) - \frac{\pi^2}{6} - \frac{1}{2}(\ln(-x))^2, \quad \text{Li}_2(x) = -\text{Li}_2(1-x) + \frac{\pi^2}{6} - \ln(x)\ln(1-x),$$

any argument of the dilogarithm can be mapped into the region $|x| \leq 1$ and $-1 \leq \text{Re}(x) \leq 1/2$. The numerical computation can be accelerated by using an expansion in $z = -\ln(1-x)$ and the Bernoulli numbers B_i :

$$\text{Li}_2(x) = \sum_{i=0}^{\infty} B_i \frac{z^{i+1}}{(i+1)!}. \quad (5.2)$$

Multiple polylogarithms are defined for $z_k \neq 0$ by [5–7]

$$G(z_1, \dots, z_k; y) = \int_0^y \frac{dy_1}{y_1 - z_1} \int_0^{y_1} \frac{dy_2}{y_2 - z_2} \dots \int_0^{y_{k-1}} \frac{dy_k}{y_k - z_k}. \quad (5.3)$$

*This contribution should be cited as:

C. Bogner, I. Hönemann, K. Tempest, A. Schweitzer, S. Weinzierl, Numerics for elliptic Feynman integrals, DOI: [10.23731/CYRM-2020-003.177](https://doi.org/10.23731/CYRM-2020-003.177), in: Theory for the FCC-ee, Eds. A. Blondel, J. Gluza, S. Jadach, P. Janot and T. Riemann, CERN Yellow Reports: Monographs, CERN-2020-003, DOI: [10.23731/CYRM-2020-003](https://doi.org/10.23731/CYRM-2020-003), p. 177.
 © CERN, 2020. Published by CERN under the [Creative Commons Attribution 4.0 license](https://creativecommons.org/licenses/by/4.0/).

This represents multiple polylogarithms as iterated integrals. Alternatively, we may define multiple polylogarithms through a nested sum

$$\text{Li}_{m_1, \dots, m_k}(x_1, \dots, x_k) = \sum_{n_1 > n_2 > \dots > n_k > 0} \frac{x_1^{n_1}}{n_1^{m_1}} \dots \frac{x_k^{n_k}}{n_k^{m_k}}. \quad (5.4)$$

With the shorthand notation

$$G_{m_1, \dots, m_k}(z_1, \dots, z_k; y) = G(\underbrace{0, \dots, 0}_{m_1-1}, z_1, \dots, z_{k-1}, \underbrace{0, \dots, 0}_{m_k-1}, z_k; y), \quad (5.5)$$

where all z_j for $j = 1, \dots, k$ are assumed to be non-zero, the two notations are related by

$$\text{Li}_{m_1, \dots, m_k}(x_1, \dots, x_k) = (-1)^k G_{m_1, \dots, m_k}\left(\frac{1}{x_1}, \frac{1}{x_1 x_2}, \dots, \frac{1}{x_1 \dots x_k}; 1\right). \quad (5.6)$$

The numerical evaluation of multiple polylogarithms follows the same strategy [8]. Using the integral representation, one transforms all arguments into a region, where the sum representation gives a converging power series expansion. In addition, the Hölder convolution is used to accelerate the convergence of the series expansion. The Hölder convolution reads (with $z_1 \neq 1$ and $z_k \neq 0$)

$$G(z_1, \dots, z_k; 1) = \sum_{j=0}^k (-1)^j G\left(1 - z_j, 1 - z_{j-1}, \dots, 1 - z_1; \frac{1}{2}\right) G\left(z_{j+1}, \dots, z_k; \frac{1}{2}\right). \quad (5.7)$$

Multiple polylogarithms are a special case of iterated integrals. Let us briefly review Chen's definition of iterated integrals [9]: let M be an n -dimensional manifold and

$$\gamma : [0, 1] \rightarrow M \quad (5.8)$$

a path with start point $x_i = \gamma(0)$ and endpoint $x_f = \gamma(1)$. Suppose further that $\omega_1, \dots, \omega_k$ are differential 1-forms on M . Let us write

$$f_j(\lambda) d\lambda = \gamma^* \omega_j \quad (5.9)$$

for the pull-backs to the interval $[0, 1]$. For $\lambda \in [0, 1]$ the k -fold iterated integral of $\omega_1, \dots, \omega_k$ along the path γ is defined by

$$I_\gamma(\omega_1, \dots, \omega_k; \lambda) = \int_0^\lambda d\lambda_1 f_1(\lambda_1) \int_0^{\lambda_1} d\lambda_2 f_2(\lambda_2) \dots \int_0^{\lambda_{k-1}} d\lambda_k f_k(\lambda_k). \quad (5.10)$$

For multiple polylogarithms, we have $\omega_j = d \ln(\lambda - z_j)$. A second special case is given by iterated integrals of modular forms [10]:

$$\omega_j = 2\pi i f_j(\tau) d\tau, \quad (5.11)$$

where $f_j(\tau)$ is a modular form. This type of iterated integral occurs in physics for the equal-mass sunrise integral [1, 11–14] and the kite integral [15, 16]. A physical application is the two-loop electron self-energy in quantum electrodynamics, if the mass of the electron is not neglected [3, 17]. This is a single-scale problem and we set $x = p^2/m^2$. In all these examples, the

complication is related to the equal-mass sunrise integral, which cannot be expressed in terms of multiple polylogarithms. This is related to the fact that the system of differential equations for this Feynman integral contains an irreducible second-order differential operator [18–20]

$$L = x(x-1)(x-9) \frac{d^2}{dx^2} + (3x^2 - 20x + 9) \frac{d}{dx} + x - 3. \quad (5.12)$$

Let ψ_1 and ψ_2 be two independent solutions of the homogeneous equation

$$L \psi = 0. \quad (5.13)$$

ψ_1 and ψ_2 can be taken as the periods of the elliptic curve

$$E : w^2 - z(z+4) \left[z^2 + 2(1+x)z + (1-x)^2 \right] = 0. \quad (5.14)$$

One defines the modulus k and the complementary modulus k' by

$$k^2 = \frac{16\sqrt{x}}{(1+\sqrt{x})^3(3-\sqrt{x})}, \quad k'^2 = 1 - k^2. \quad (5.15)$$

In a neighbourhood of $x = 0$, the periods may be taken as

$$\psi_{1,0} = \frac{4K(k)}{(1+\sqrt{x})^{\frac{3}{2}}(3-\sqrt{x})^{\frac{1}{2}}}, \quad \psi_{2,0} = \frac{4iK(k')}{(1+\sqrt{x})^{\frac{3}{2}}(3-\sqrt{x})^{\frac{1}{2}}}. \quad (5.16)$$

The complete elliptic integral $K(k)$ can be computed efficiently from the arithmetic-geometric mean

$$K(k) = \frac{\pi}{2 \operatorname{agm}(k', 1)}. \quad (5.17)$$

The periods ψ_1 and ψ_2 generate a lattice. Any other basis of the lattice again gives two independent solutions of the homogeneous differential equation (Eq. (5.13)). It is a standard convention to normalise one basis vector of the lattice to one: $(\psi_2, \psi_1) \rightarrow (\tau, 1)$ where $\tau = \psi_2/\psi_1$ and $\operatorname{Im}\tau > 0$. Let us now consider a change of basis:

$$\begin{pmatrix} \psi'_2 \\ \psi'_1 \end{pmatrix} = \gamma \begin{pmatrix} \psi_2 \\ \psi_1 \end{pmatrix}, \quad \gamma = \begin{pmatrix} a & b \\ c & d \end{pmatrix}. \quad (5.18)$$

The transformation should be invertible and preserve $\operatorname{Im}(\psi'_2/\psi'_1) > 0$, therefore, $\gamma \in \operatorname{SL}_2(\mathbb{Z})$. In terms of τ and τ' , this yields

$$\tau' = \frac{a\tau + b}{c\tau + d}. \quad (5.19)$$

This is a modular transformation and we write $\tau' = \gamma(\tau)$. Let us denote the complex upper half plane by \mathbb{H} . A meromorphic function $f : \mathbb{H} \rightarrow \mathbb{C}$ is a modular form of modular weight k for $\operatorname{SL}_2(\mathbb{Z})$, if (i) f transforms under Möbius transformations as $f(\tau') = (c\tau + d)^k \cdot f(\tau)$ for all $\gamma \in \operatorname{SL}_2(\mathbb{Z})$, (ii) f is holomorphic on \mathbb{H} , and (iii) f is holomorphic at infinity. Furthermore, one defines modular forms for congruence subgroups $\Gamma \subset \operatorname{SL}_2(\mathbb{Z})$ by requiring property (i) only

for $\gamma \in \Gamma$ (plus holomorphicity on \mathbb{H} and at the cusps). Relevant to us will be the congruence subgroup $\Gamma_1(6)$, defined by

$$\Gamma_1(6) = \left\{ \begin{pmatrix} a & b \\ c & d \end{pmatrix} \in \mathrm{SL}_2(\mathbb{Z}) : a, d \equiv 1 \pmod{6}, c \equiv 0 \pmod{6} \right\}. \quad (5.20)$$

With $\psi_{1,0}$ and $\psi_{2,0}$ defined by Eq. (5.16), we set

$$\tau_0 = \frac{\psi_{2,0}}{\psi_{1,0}}, \quad q_0 = e^{2i\pi\tau_0}. \quad (5.21)$$

We then change the variable from x to τ_0 (or q_0) [12]. The differential equation for the master integrals \vec{I} relevant to the two-loop electron self-energy then reads

$$\frac{d}{d\tau_0} \vec{I} = \varepsilon A(\tau_0) \vec{I}, \quad (5.22)$$

where $A(\tau_0)$ is an ε -independent matrix whose entries are modular forms for $\Gamma_1(6)$ [1, 14]. It follows immediately that all master integrals can be expressed in terms of iterated integrals of modular forms.

Let us now discuss how to evaluate numerically iterated integrals of modular forms in an efficient way. The essential point is that modular forms have a q -expansion. Using

$$2\pi i \, d\tau_0 = \frac{dq_0}{q_0}, \quad (5.23)$$

we may integrate term-by-term and obtain the q_0 -expansion of the master integrals. Truncating the q_0 -series to the desired accuracy gives a polynomial in q_0 . This needs to be done only once. The resulting polynomial can then be evaluated for different values of q_0 (or x) numerically. Note that the conversion from x to q_0 is also fast, since the complete elliptic integrals can be computed efficiently with the help of the arithmetic-geometric mean. Let us give an example. One finds for the ε^2 -term of the sunrise integral [3]

$$I_6^{(2)} = 3\mathrm{Cl}_2\left(\frac{2\pi}{3}\right) - 3\sqrt{3} \left[q_0 - \frac{5}{4}q_0^2 + q_0^3 - \frac{11}{16}q_0^4 + \frac{24}{25}q_0^5 - \frac{5}{4}q_0^6 + \frac{50}{49}q_0^7 - \frac{53}{64}q_0^8 + q_0^9 \right] + \mathcal{O}(q_0^{10}). \quad (5.24)$$

We have $q_0 = 0$ for $x = 0$ and Eq. (5.24) gives a fast convergent series in a neighbourhood of $x = 0$. We are interested in evaluating the master integrals in the full kinematic range $x \in \mathbb{R}$. This raises the question: for which values $x \in \mathbb{R}$ do the q_0 -series for the master integrals converge? Or phrased differently, for which values $x \in \mathbb{R}$ do we have $|q_0| < 1$? It turns out that we have $|q_0| < 1$ for $x \in \mathbb{R} \setminus \{1, 9, \infty\}$, corresponding to $p^2 \in \mathbb{R} \setminus \{m^2, 9m^2, \infty\}$ [2]. Thus, the q_0 -series for the master integrals converge for all real values of x except three points. Let us stress that the q_0 -series give the correct real and imaginary part of the master integrals, as specified by Feynman's $i\delta$ prescription. To cover the three remaining points, $x \in \{1, 9, \infty\}$, we recall that the periods ψ_1 and ψ_2 are not uniquely determined. By using four different choices for the pair of periods (ψ_1, ψ_2) , we may define q_0, q_1, q_9 and q_∞ such that (i) the integration kernels are modular forms of $\Gamma_1(6)$ and (ii) $q_j = 0$ for $x = j$ [3]. This gives expansions around all singular points of the system of differential equations or—phrased differently—around all cusps of $\Gamma_1(6)$. In particular, there is always a choice such that $|q_j| \lesssim 0.163$ for all real values

of x . Truncation of the q -series to order $\mathcal{O}(q^{30})$ gives for the finite part of the two-loop electron self-energy a relative precision better than 10^{-20} for all real values p^2/m^2 .

Although we focused on the two-loop electron self-energy, we expect the methods discussed here to be applicable to any single-scale Feynman integral related to a single elliptic curve. This is a significant step beyond Feynman integrals evaluating to multiple polylogarithms and puts single-scale Feynman integrals related to a single elliptic curve on the same level of understanding as Feynman integrals evaluating to multiple polylogarithms. With the ongoing research on Feynman integrals beyond multiple polylogarithms [1, 2, 11–16, 20–50] we may expect more results—in particular, on multiscale Feynman integrals beyond multiple polylogarithms—to be coming soon.

References

- [1] L. Adams and S. Weinzierl, *Commun. Num. Theor. Phys.* **12** (2018) 193. [arXiv:1704.08895](#), [doi:10.4310/CNTP.2018.v12.n2.a1](#)
- [2] C. Bogner *et al.*, *Nucl. Phys.* **B922** (2017) 528. [arXiv:1705.08952](#), [doi:10.1016/j.nuclphysb.2017.07.008](#)
- [3] I. Hönemann *et al.*, *Phys. Rev.* **D98** (2018) 113008. [arXiv:1811.09308](#), [doi:10.1103/PhysRevD.98.113008](#)
- [4] G. 't Hooft and M.J.G. Veltman, *Nucl. Phys.* **B153** (1979) 365. [doi:10.1016/0550-3213\(79\)90605-9](#)
- [5] A. Goncharov, *Math. Res. Lett.* **5** (1998) 497. [doi:10.4310/MRL.1998.v5.n4.a7](#)
- [6] J.M. Borwein *et al.*, *Trans. Am. Math. Soc.* **353** (2001) 907. [arXiv:math.CA/9910045](#), <https://mathscinet.ams.org/mathscinet-getitem?mr=1709772>
- [7] S. Moch *et al.*, *J. Math. Phys.* **43** (2002) 3363. [arXiv:hep-ph/0110083](#)
- [8] J. Vollinga and S. Weinzierl, *Comput. Phys. Commun.* **167** (2005) 177. [arXiv:hep-ph/0410259](#)
- [9] K.-T. Chen, *Bull. Am. Math. Soc.* **83** (1977) 831. <https://projecteuclid.org/euclid.bams/1183539443>
- [10] F. Brown, Multiple modular values and the relative completion of the fundamental group of $M_{1,1}$, [arXiv:1407.5167](#).
- [11] S. Laporta and E. Remiddi, *Nucl. Phys.* **B704** (2005) 349. [arXiv:hep-ph/0406160](#), [doi:10.1016/j.nuclphysb.2004.10.044](#)
- [12] S. Bloch and P. Vanhove, *J. Number Theory* **148** (2015) 328. [arXiv:1309.5865](#), [doi:10.1016/j.jnt.2014.09.032](#)
- [13] L. Adams *et al.*, *J. Math. Phys.* **57** (2016) 032304. [arXiv:1512.05630](#), [doi:10.1063/1.4944722](#)
- [14] L. Adams and S. Weinzierl, *Phys. Lett.* **B781** (2018) 270. [arXiv:1802.05020](#), [doi:10.1016/j.physletb.2018.04.002](#)
- [15] E. Remiddi and L. Tancredi, *Nucl. Phys.* **B907** (2016) 400. [arXiv:1602.01481](#), [doi:10.1016/j.nuclphysb.2016.04.013](#)
- [16] L. Adams *et al.*, *J. Math. Phys.* **57** (2016) 122302. [arXiv:1607.01571](#), [doi:10.1063/1.4969060](#)

- [17] A. Sabry, *Nucl. Phys.* **33** (1962) 401. [doi:10.1016/0029-5582\(62\)90535-7](https://doi.org/10.1016/0029-5582(62)90535-7)
- [18] D.J. Broadhurst *et al.*, *Z. Phys.* **C60** (1993) 287. [arXiv:hep-ph/9304303](https://arxiv.org/abs/hep-ph/9304303), [doi:10.1007/BF01474625](https://doi.org/10.1007/BF01474625)
- [19] S. Müller-Stach *et al.*, *Commun. Math. Phys.* **326** (2014) 237. [arXiv:1212.4389](https://arxiv.org/abs/1212.4389), [doi:10.1007/s00220-013-1838-3](https://doi.org/10.1007/s00220-013-1838-3)
- [20] L. Adams *et al.*, *Phys. Rev. Lett.* **118** (2017) 141602. [arXiv:1702.04279](https://arxiv.org/abs/1702.04279), [doi:10.1103/PhysRevLett.118.141602](https://doi.org/10.1103/PhysRevLett.118.141602)
- [21] S. Müller-Stach *et al.*, *Commun. Num. Theor. Phys.* **6** (2012) 203. [arXiv:1112.4360](https://arxiv.org/abs/1112.4360), [doi:10.4310/CNTP.2012.v6.n1.a5](https://doi.org/10.4310/CNTP.2012.v6.n1.a5)
- [22] L. Adams *et al.*, *J. Math. Phys.* **54** (2013) 052303. [arXiv:1302.7004](https://arxiv.org/abs/1302.7004), [doi:10.1063/1.4804996](https://doi.org/10.1063/1.4804996)
- [23] E. Remiddi and L. Tancredi, *Nucl. Phys.* **B880** (2014) 343. [arXiv:1311.3342](https://arxiv.org/abs/1311.3342), [doi:10.1016/j.nuclphysb.2014.01.009](https://doi.org/10.1016/j.nuclphysb.2014.01.009)
- [24] L. Adams *et al.*, *J. Math. Phys.* **55** (2014) 102301. [arXiv:1405.5640](https://arxiv.org/abs/1405.5640), [doi:10.1063/1.4896563](https://doi.org/10.1063/1.4896563)
- [25] S. Bloch *et al.*, *Compos. Math.* **151** (2015) 2329. [arXiv:1406.2664](https://arxiv.org/abs/1406.2664), [doi:10.1112/S0010437X15007472](https://doi.org/10.1112/S0010437X15007472)
- [26] L. Adams *et al.*, *J. Math. Phys.* **56** (2015) 072303. [arXiv:1504.03255](https://arxiv.org/abs/1504.03255), [doi:10.1063/1.4926985](https://doi.org/10.1063/1.4926985)
- [27] M. Søgaard and Y. Zhang, *Phys. Rev.* **D91** (2015) 081701. [arXiv:1412.5577](https://arxiv.org/abs/1412.5577), [doi:10.1103/PhysRevD.91.081701](https://doi.org/10.1103/PhysRevD.91.081701)
- [28] S. Bloch *et al.*, *Adv. Theor. Math. Phys.* **21** (2017) 1373. [arXiv:1601.08181](https://arxiv.org/abs/1601.08181), [doi:10.4310/ATMP.2017.v21.n6.a1](https://doi.org/10.4310/ATMP.2017.v21.n6.a1)
- [29] L. Tancredi, *Nucl. Phys.* **B901** (2015) 282. [arXiv:1509.03330](https://arxiv.org/abs/1509.03330), [doi:10.1016/j.nuclphysb.2015.10.015](https://doi.org/10.1016/j.nuclphysb.2015.10.015)
- [30] A. Primo and L. Tancredi, *Nucl. Phys.* **B916** (2017) 94. [arXiv:1610.08397](https://arxiv.org/abs/1610.08397), [doi:10.1016/j.nuclphysb.2016.12.021](https://doi.org/10.1016/j.nuclphysb.2016.12.021)
- [31] R. Bonciani *et al.*, *JHEP* **12** (2016) 096. [arXiv:1609.06685](https://arxiv.org/abs/1609.06685), [doi:10.1007/JHEP12\(2016\)096](https://doi.org/10.1007/JHEP12(2016)096)
- [32] A. von Manteuffel and L. Tancredi, *JHEP* **06** (2017) 127. [arXiv:1701.05905](https://arxiv.org/abs/1701.05905), [doi:10.1007/JHEP06\(2017\)127](https://doi.org/10.1007/JHEP06(2017)127)
- [33] J. Ablinger *et al.*, *J. Math. Phys.* **59** (2018) 062305. [arXiv:1706.01299](https://arxiv.org/abs/1706.01299), [doi:10.1063/1.4986417](https://doi.org/10.1063/1.4986417)
- [34] A. Primo and L. Tancredi, *Nucl. Phys.* **B921** (2017) 316. [arXiv:1704.05465](https://arxiv.org/abs/1704.05465), [doi:10.1016/j.nuclphysb.2017.05.018](https://doi.org/10.1016/j.nuclphysb.2017.05.018)
- [35] E. Remiddi and L. Tancredi, *Nucl. Phys.* **B925** (2017) 212. [arXiv:1709.03622](https://arxiv.org/abs/1709.03622), [doi:10.1016/j.nuclphysb.2017.10.007](https://doi.org/10.1016/j.nuclphysb.2017.10.007)
- [36] J.L. Bourjaily *et al.*, *Phys. Rev. Lett.* **120** (2018) 121603. [arXiv:1712.02785](https://arxiv.org/abs/1712.02785), [doi:10.1103/PhysRevLett.120.121603](https://doi.org/10.1103/PhysRevLett.120.121603)
- [37] M. Hidding and F. Moriello, *JHEP* **01** (2019) 169. [arXiv:1712.04441](https://arxiv.org/abs/1712.04441), [doi:10.1007/JHEP01\(2019\)169](https://doi.org/10.1007/JHEP01(2019)169)

- [38] J. Broedel *et al.*, *JHEP* **05** (2018) 093. [arXiv:1712.07089](#),
[doi:10.1007/JHEP05\(2018\)093](#)
- [39] J. Broedel *et al.*, *Phys. Rev.* **D97** (2018) 116009. [arXiv:1712.07095](#),
[doi:10.1103/PhysRevD.97.116009](#)
- [40] J. Broedel *et al.*, *JHEP* **08** (2018) 014. [arXiv:1803.10256](#),
[doi:10.1007/JHEP08\(2018\)014](#)
- [41] L. Adams, *et al.*, *Phys. Rev. Lett.* **121** (2018) 142001. [arXiv:1804.11144](#),
[doi:10.1103/PhysRevLett.121.142001](#)
- [42] L. Adams *et al.*, *JHEP* **10** (2018) 206. [arXiv:1806.04981](#),
[doi:10.1007/JHEP10\(2018\)206](#)
- [43] J. Broedel *et al.*, *JHEP* **01** (2019) 023. [arXiv:1809.10698](#),
[doi:10.1007/JHEP01\(2019\)023](#)
- [44] J.L. Bourjaily *et al.*, *Phys. Rev. Lett.* **122** (2019) 031601. [arXiv:1810.07689](#),
[doi:10.1103/PhysRevLett.122.031601](#)
- [45] J.L. Bourjaily *et al.*, *JHEP* **08** (2018) 184. [arXiv:1805.10281](#),
[doi:10.1007/JHEP08\(2018\)184](#)
- [46] M. Besier *et al.*, *Commun. Num. Theor. Phys.* **13** (2019) 253. [arXiv:1809.10983](#),
[doi:10.4310/CNTP.2019.v13.n2.a1](#)
- [47] P. Mastrolia and S. Mizera, *JHEP* **02** (2019) 139. [arXiv:1810.03818](#), [doi:10.1007/JHEP02\(2019\)139](#)
- [48] J. Ablinger *et al.*, *Nucl. Phys.* **B939** (2019) 253. [arXiv:1810.12261](#),
[doi:10.1016/j.nuclphysb.2018.12.010](#)
- [49] H. Frellesvig *et al.*, *JHEP* **05** (2019) 153. [arXiv:1901.11510](#),
[doi:10.1007/JHEP05\(2019\)153](#)
- [50] J. Broedel *et al.*, *JHEP* **05** (2019) 120. [arXiv:1902.09971](#),
[doi:10.1007/JHEP05\(2019\)120](#)

6 Numerical multiloop calculations: sector decomposition and QMC integration in pySecDec

Contribution* by: S. Borowka, G. Heinrich, S. Jahn, S.P. Jones, M. Kerner, J. Schlenk
Corresponding author: S.P. Jones [s.jones@cern.ch]

The FCC-ee will allow the experimental uncertainties on several important observables, such as the electroweak precision observables (EWPOs), to be reduced by up to two orders of magnitude compared with the previous generation LEP and SLC experiments [1, 2]. To be able to best exploit this unprecedented boost in precision, it is also necessary for theoretical predictions to be known with sufficient accuracy. In practice, this means that very high-order perturbative corrections to electroweak precision observables and other processes will be required, both in the Standard Model (SM) and potentially also in BSM scenarios.

One of the key challenges for computing perturbative corrections is our ability to compute the Feynman integrals that appear in these multiloop corrections. There has been very significant progress in this direction in recent years, ranging from purely analytic approaches [3–17] to semi-analytical approaches based on expansions [18–23] and also via purely numerical methods [24–32].

So far, the method of sector decomposition has already proved to be useful for computing the complete electroweak two-loop corrections to Z boson production and decay [33], which is of direct relevance to the FCC-ee, as well as several processes of significant interest at the LHC [34–37] and also BSM corrections [38, 39]. The latter calculations were based on SECDEC 3 [40]. Another code based on sector decomposition, FIESTA [41–43], has also been used successfully in various multiloop calculations, for example for numerical checks of recent evaluations of four-loop three-point functions [13–16].

In this contribution, we will briefly describe the essential aspects of this method and provide a short update regarding some of the recent developments [26, 44] that have enabled state-of-the-art predictions to be made using this technique.

In Section 6.1, we will introduce the method of sector decomposition as we use it for computing Feynman integrals and describe how it leads to integrals that are suitable for numerical evaluation. In Section 6.2, we will discuss a particular type of quasi-Monte Carlo integration that allows us to numerically integrate the sector-decomposed loop integrals efficiently. Finally, in Section 6.3, we will give a short outlook for the field of numerical multiloop calculations.

6.1 Feynman integrals and sector decomposition

A general scalar Feynman integral I in $D = 4 - 2\epsilon$ dimensions with L loops and N propagators P_j , each raised to a power ν_j , can be written in momentum space as

$$I = \int_{-\infty}^{\infty} \prod_{l=1}^L [d^D k_l] \frac{1}{\prod_{j=1}^N P_j^{\nu_j}}, \quad \text{where} \quad [d^D k_l] = \frac{\mu^{4-D}}{i\pi^{\frac{D}{2}}} d^D k_l, \quad P_j = (q_j - m_j^2 + i\delta), \quad (6.1)$$

*This contribution should be cited as:

S. Borowka, G. Heinrich, S. Jahn, S.P. Jones, M. Kerner, J. Schlenk, Numerical multiloop calculations: sector decomposition and QMC integration in pySECDEC, DOI: [10.23731/CYRM-2020-003.185](https://doi.org/10.23731/CYRM-2020-003.185), in: Theory for the FCC-ee, Eds. A. Blondel, J. Gluza, S. Jadach, P. Janot and T. Riemann, CERN Yellow Reports: Monographs, CERN-2020-003, DOI: [10.23731/CYRM-2020-003](https://doi.org/10.23731/CYRM-2020-003), p. 185.
 © CERN, 2020. Published by CERN under the [Creative Commons Attribution 4.0 license](https://creativecommons.org/licenses/by/4.0/).

and q_j are linear combinations of external momenta p_i and loop momenta k_l . After introducing Feynman parameters, the momentum integrals can be performed straightforwardly and the integral can be recast in the form

$$I = (-1)^{N_\nu} \frac{\Gamma(N_\nu - LD/2)}{\prod_{j=1}^N \Gamma(\nu_j)} \int_0^\infty \prod_{j=1}^N dx_j x_j^{\nu_j-1} \delta\left(1 - \sum_{i=1}^N x_i\right) \frac{\mathcal{U}^{N_\nu-(L+1)D/2}(\vec{x})}{\mathcal{F}^{N_\nu-LD/2}(\vec{x}, s_{ij}, m_j^2)}, \quad (6.2)$$

where the momentum integrals have been replaced by an N -fold parameter integral. Here, \mathcal{U} and \mathcal{F} are the first and second Symanzik polynomials; they are homogeneous polynomials in the Feynman parameters of degree L and $L+1$, respectively, and $N_\nu = \sum_j \nu_j$. This procedure can be extended to support Feynman integrals with tensor numerators. There are three possibilities of poles in the dimensional regulator ϵ arising.

1. The overall $\Gamma(N_\nu - LD/2)$ can diverge, resulting in a single UV pole.
2. $\mathcal{U}(\vec{x})$ vanishes for some $x = 0$ and has a negative exponent, resulting in a UV subdivergence.
3. $\mathcal{F}(\vec{x}, s_{ij}, m_j^2)$ vanishes on the boundary and has a negative exponent, giving rise to an IR divergence.

After integrating out the δ distribution and extracting a common factor of $(-1)^{N_\nu} \Gamma(N_\nu - LD/2)$, we are faced with integrals of the form

$$I_i = \int_0^1 \prod_{j=1}^{N-1} dx_j x_j^{\nu_j-1} \frac{\mathcal{U}_i(\vec{x})^{\exp \mathcal{U}(\epsilon)}}{\mathcal{F}_i(\vec{x}, s_{ij}, m_j^2)^{\exp \mathcal{F}(\epsilon)}}. \quad (6.3)$$

The sector decomposition algorithms aim to factorise, via integral transforms, the polynomials \mathcal{U}_i and \mathcal{F}_i (or, more generally, any product of polynomials $\mathcal{P}(\{x_j\})$) as products of a monomial and a polynomial with non-zero constant term, explicitly

$$\mathcal{P}(\{x_j\}) \rightarrow \prod_j x_j^{\alpha_j} (c + p(\{x_j\})), \quad (6.4)$$

where $\{x_j\}$ is the set of Feynman parameters, c is a constant, and the polynomial p has no constant term. After this procedure, singularities in ϵ resulting from the region where one or more $x_j \rightarrow 0$ can appear only from the monomials $x_j^{\alpha_j}$. In this factorised form, the integrand can now be expanded in ϵ and the coefficients of the expansion can be numerically integrated; for an overview, see Ref. [25].

If we consider only integrals for which the Mandelstam variables and masses can be chosen such that the \mathcal{F} polynomial is positive semidefinite (i.e., with a Euclidean region), this procedure is sufficient to render the integrals numerically integrable.[†] However, not all integrals of interest have a Euclidean region in this sense. Consider, for example, the three-point function depicted in Fig. C.6.1, which appears in the two-loop electroweak corrections to the $Z\bar{b}b$ vertex [48, 49]. The \mathcal{F} polynomial is given by

$$\mathcal{F}/m_Z^2$$

[†]In the physical region, such integrals may still require the integration contour to be deformed into the complex plane, in accordance with the causal $i\delta$ Feynman prescription [45–47].

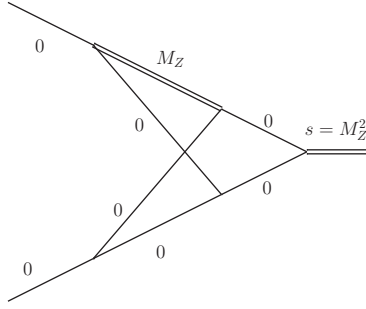


Fig. C.6.1: A $Zb\bar{b}$ vertex diagram with no Euclidean region, which can give rise to poorly convergent numerical integrals after sector decomposition. Figure taken from Ref. [49].

$$\begin{aligned}
 = & x_3^2 x_5 + x_3^2 x_4 + x_2 x_3 x_5 + x_2 x_3 x_4 + x_1 x_3 x_5 + x_1 x_3 x_4 + x_1 x_3^2 + x_1 x_2 x_3 + x_0 x_3 x_4 + x_0 x_3^2 + x_0 x_2 x_3 \\
 & - x_1 x_2 x_4 - x_0 x_1 x_5 - x_0 x_1 x_4 - x_0 x_1 x_2 - x_0 x_1 x_3, \quad (6.5)
 \end{aligned}$$

where m_Z is the Z boson mass and x_j are the Feynman parameters. Note that the massive propagator has the same mass as the external Z boson, which gives rise to terms in the \mathcal{F} polynomial of differing sign, regardless of the value chosen for m_Z .

After sector decomposition, integrals for which the \mathcal{F} polynomial is not positive semidefinite can diverge not only as some $x_j \rightarrow 0$ but also as some $x_j \rightarrow 1$. One solution for dealing with such integrals is to split the integration domain in each Feynman parameter and then map the integration boundaries back to the unit hypercube such that the divergences at $x_j \rightarrow 1$ are mapped to divergences at $x_j \rightarrow 0$. Sector decomposition can then resolve the singularities at $x_j \rightarrow 0$ as usual. Such a splitting procedure was introduced in earlier versions of SECDEC [50, 51], and also in FIESTA [42, 43].

However, prior to pySECDEC [44], integrals were always split at $x_j = 1/2$ and, as shown in Ref. [52], this can again lead to problems if the \mathcal{F} polynomial vanishes at this point (which happens to be the case for the polynomial in Eq. (6.5)). The proposed solution in Ref. [52] was therefore to split the integrals at a random point, such that, if one run produces a problematic result, it is always possible to rerun the code and avoid a problematic split.

Alternatively, it is often possible to avoid having to evaluate such problematic integrals, as well as integrals that have poor numerical convergence properties, through the use of integration by parts identities (IBPs) [53, 54]. In particular, it is usually possible to express Feynman integrals in terms of a sum of (quasi-)finite integrals[‡] with rational coefficients [55, 56]. Typically, choosing a basis of (quasi-)finite integrals leads to significantly improved numerical properties; see, for example, Ref. [57]. The choice of a quasi-finite basis proved advantageous for the numerical evaluation of the $gg \rightarrow HH$ and $gg \rightarrow Hg$ amplitudes [34–36].

6.2 Quasi-Monte Carlo integration

Numerical integration of the sector-decomposed finite integrals can be a computationally intensive process. One of the most widely used tools for numerical integration is the CUBA package [58, 59], which implements several different numerical integration routines, relying on pseudo-random sampling, quasi-random sampling, or cubature rules.

[‡]Here, quasi-finite integrals are integrals for which the overall $\Gamma(N_\nu - LD/2)$ can give rise to poles in ϵ but for which no poles arise from the integration over the \mathcal{U} and \mathcal{F} polynomials.

In the last few years, it was found that a particular type of quasi-Monte Carlo (QMC) integration based on rank-1 shifted lattice (R1SL) rules has particularly good convergence properties for the numerical integration of Feynman parametrized integrals [60–62]. An unbiased R1SL estimate $\bar{Q}_{n,m}[f]$ of the integral $I[f]$ can be obtained from the following (QMC) cubature rule [63]:

$$I[f] \approx \bar{Q}_{n,m}[f] \equiv \frac{1}{m} \sum_{k=0}^{m-1} Q_n^{(k)}[f], \quad Q_n^{(k)}[f] \equiv \frac{1}{n} \sum_{i=0}^{n-1} f\left(\left\{\frac{i\mathbf{z}}{n} + \mathbf{\Delta}_k\right\}\right). \quad (6.6)$$

Here, the estimate of the integral depends on the number of lattice points n and the number of random shifts m . The generating vector $\mathbf{z} \in \mathbb{Z}^d$ is a fixed d -dimensional vector of integers coprime to n . The shift vectors $\mathbf{\Delta}_k \in [0, 1)^d$ are d -dimensional vectors with components consisting of independent, uniformly distributed, random real numbers in the interval $[0, 1)$. Finally, the curly brackets indicate that the fractional part of each component is taken, such that all arguments of f remain in the interval $[0, 1)$. An unbiased estimate of the mean-square error due to the numerical integration can be obtained by computing the variance of the different random shifts $Q_n^{(k)}[f]$.

The latest version of pySECDEC provides a public implementation of a R1SL (QMC) integrator. The implementation is also capable of performing numerical integration on a number of CUDA-compatible graphics processing units (GPUs), which can significantly accelerate the evaluation of the integrand. The integrator, which is distributed as a header-only C++ library, can also be used as a stand-alone integration package [26]. The generating vectors distributed with the package are generated using the component-by-component construction [64].

6.3 Summary and outlook

We have presented new developments for the numerical calculation of multiloop integrals, focusing on the sector decomposition approach in combination with quasi-Monte Carlo (QMC) integration. We described a new feature present in pySECDEC, which allows integrals with special (non-Euclidean) kinematic configurations to be calculated as they occur, e.g., in electroweak two-loop corrections, which previously had shown poor convergence in SECDEC 3. We also described a QMC integrator, developed in conjunction with pySECDEC as well as for stand-alone usage, which can lead to considerably more accurate results in a given time compared with standard Monte Carlo integration. This integrator is also capable of utilising CUDA-compatible graphics processing units (GPUs).

In view of the need for high-precision calculations with many mass scales at future colliders, as they occur, for example, in electroweak corrections, numerical methods are a promising approach, and are actively being developed to best utilise recent progress in computing hardware. Several further developments towards the automation of numerical multiloop calculations, with sector decomposition as an ingredient, could be envisaged. For example, to provide boundary conditions for numerical solutions to differential equations, along the lines of Refs. [29, 65], for automated asymptotic expansions, similar to Refs. [20, 66], or aiming at fully numerical evaluations of both virtual and real corrections.

Acknowledgements

We thank Tom Zirke for his contributions to earlier versions of the code and Oliver Schulz for providing GPU computing support.

References

- [1] G.S. Abrams *et al.*, *Phys. Rev. Lett.* **63** (1989) 724. [doi:10.1103/PhysRevLett.63.724](https://doi.org/10.1103/PhysRevLett.63.724)
- [2] S. Schael *et al.*, *Phys. Rep.* **532** (2013) 119. [arXiv:1302.3415](https://arxiv.org/abs/1302.3415),
[doi:10.1016/j.physrep.2013.07.004](https://doi.org/10.1016/j.physrep.2013.07.004)
- [3] S. Badger *et al.*, *Phys. Rev. Lett.* **120** (2018) 092001. [arXiv:1712.02229](https://arxiv.org/abs/1712.02229),
[doi:10.1103/PhysRevLett.120.092001](https://doi.org/10.1103/PhysRevLett.120.092001)
- [4] S. Abreu *et al.*, *Phys. Rev.* **D97** (2018) 116014. [arXiv:1712.03946](https://arxiv.org/abs/1712.03946),
[doi:10.1103/PhysRevD.97.116014](https://doi.org/10.1103/PhysRevD.97.116014)
- [5] T. Gehrmann *et al.*, *JHEP* **10** (2018) 103. [arXiv:1807.09812](https://arxiv.org/abs/1807.09812),
[doi:10.1007/JHEP10\(2018\)103](https://doi.org/10.1007/JHEP10(2018)103)
- [6] S. Abreu *et al.*, *JHEP* **11** (2018) 116. [arXiv:1809.09067](https://arxiv.org/abs/1809.09067),
[doi:10.1007/JHEP11\(2018\)116](https://doi.org/10.1007/JHEP11(2018)116)
- [7] S. Abreu *et al.*, *Phys. Rev. Lett.* **122** (2019) 082002. [arXiv:1812.04586](https://arxiv.org/abs/1812.04586),
[doi:10.1103/PhysRevLett.122.082002](https://doi.org/10.1103/PhysRevLett.122.082002)
- [8] S. Abreu *et al.*, *Phys. Rev. Lett.* **122** (2019) 121603. [arXiv:1812.08941](https://arxiv.org/abs/1812.08941),
[doi:10.1103/PhysRevLett.122.121603](https://doi.org/10.1103/PhysRevLett.122.121603)
- [9] D. Chicherin *et al.*, *Phys. Rev. Lett.* **123** (2019) 041603 [arXiv:1812.11160](https://arxiv.org/abs/1812.11160), [doi:10.1103/PhysRevLett.123.041603](https://doi.org/10.1103/PhysRevLett.123.041603)
- [10] D. Chicherin *et al.*, *Phys. Rev. Lett.* **122** (2019) 121602. [arXiv:1812.11057](https://arxiv.org/abs/1812.11057),
[doi:10.1103/PhysRevLett.122.121602](https://doi.org/10.1103/PhysRevLett.122.121602)
- [11] J. Broedel *et al.*, *JHEP* **05** (2019) 120. [arXiv:1902.09971](https://arxiv.org/abs/1902.09971),
[doi:10.1007/JHEP05\(2019\)120](https://doi.org/10.1007/JHEP05(2019)120)
- [12] H. Frellesvig *et al.*, *JHEP* **05** (2019) 153. [arXiv:1901.11510](https://arxiv.org/abs/1901.11510),
[doi:10.1007/JHEP05\(2019\)153](https://doi.org/10.1007/JHEP05(2019)153)
- [13] R.N. Lee *et al.*, *JHEP* **02** (2019) 172. [arXiv:1901.02898](https://arxiv.org/abs/1901.02898),
[doi:10.1007/JHEP02\(2019\)172](https://doi.org/10.1007/JHEP02(2019)172)
- [14] R. Brüser *et al.*, *JHEP* **05** (2019) 186. [arXiv:1902.05076](https://arxiv.org/abs/1902.05076),
[doi:10.1007/JHEP05\(2019\)186](https://doi.org/10.1007/JHEP05(2019)186)
- [15] J.M. Henn *et al.*, *Phys. Rev. Lett.* **122** (2019) 201602. [arXiv:1901.03693](https://arxiv.org/abs/1901.03693),
[doi:10.1103/PhysRevLett.122.201602](https://doi.org/10.1103/PhysRevLett.122.201602)
- [16] A. von Manteuffel and R.M. Schabinger, *JHEP* **05** (2019) 073. [arXiv:1903.06171](https://arxiv.org/abs/1903.06171),
[doi:10.1007/JHEP05\(2019\)073](https://doi.org/10.1007/JHEP05(2019)073)
- [17] J. Blümlein and C. Schneider, *Int. J. Mod. Phys.* **A33** (2018) 1830015. [arXiv:1809.02889](https://arxiv.org/abs/1809.02889),
[doi:10.1142/S0217751X18300156](https://doi.org/10.1142/S0217751X18300156)
- [18] S. Borowka *et al.*, *JHEP* **08** (2018) 111. [arXiv:1804.06824](https://arxiv.org/abs/1804.06824),
[doi:10.1007/JHEP08\(2018\)111](https://doi.org/10.1007/JHEP08(2018)111)
- [19] J. Davies *et al.*, *JHEP* **01** (2019) 176. [arXiv:1811.05489](https://arxiv.org/abs/1811.05489),
[doi:10.1007/JHEP01\(2019\)176](https://doi.org/10.1007/JHEP01(2019)176)
- [20] G. Mishima, *JHEP* **02** (2019) 080. [arXiv:1812.04373](https://arxiv.org/abs/1812.04373), [doi:10.1007/JHEP02\(2019\)080](https://doi.org/10.1007/JHEP02(2019)080)
- [21] F. Caola *et al.*, *JHEP* **09** (2018) 035. [arXiv:1804.07632](https://arxiv.org/abs/1804.07632), [doi:10.1007/JHEP09\(2018\)035](https://doi.org/10.1007/JHEP09(2018)035)
- [22] R. Bonciani *et al.*, *Phys. Rev. Lett.* **121** (2018) 162003. [arXiv:1806.11564](https://arxiv.org/abs/1806.11564),
[doi:10.1103/PhysRevLett.121.162003](https://doi.org/10.1103/PhysRevLett.121.162003)

- [23] R. Gröber *et al.*, *JHEP* **03** (2018) 020. [arXiv:1709.07799](#),
[doi:10.1007/JHEP03\(2018\)020](#)
- [24] T. Binoth and G. Heinrich, *Nucl. Phys.* **B585** (2000) 741. [arXiv:hep-ph/0004013](#),
[doi:10.1016/S0550-3213\(00\)00429-6](#)
- [25] G. Heinrich, *Int. J. Mod. Phys.* **A23** (2008) 1457. [arXiv:0803.4177](#),
[doi:10.1142/S0217751X08040263](#)
- [26] S. Borowka *et al.*, *Comp. Phys. Comm.* **240** (2019) 120. [arXiv:1811.11720](#),
[doi:10.1016/j.cpc.2019.02.015](#)
- [27] M. Czakon, *Comput. Phys. Commun.* **175** (2006) 559. [arXiv:hep-ph/0511200](#),
[doi:10.1016/j.cpc.2006.07.002](#)
- [28] J. Usovitsch *et al.*, *PoS LL2018* (2018) 046. [arXiv:1810.04580](#)
[doi:10.22323/1.303.0046](#)
- [29] M.K. Mandal and X. Zhao, *JHEP* **03** (2019) 190. [arXiv:1812.03060](#),
[doi:10.1007/JHEP03\(2019\)190](#)
- [30] X. Liu *et al.*, *Phys. Lett.* **B779** (2018) 353. [arXiv:1711.09572](#),
[doi:10.1016/j.physletb.2018.02.026](#)
- [31] F. Driencourt-Mangin *et al.*, *JHEP* **02** (2019) 143. [arXiv:1901.09853](#),
[doi:10.1007/JHEP02\(2019\)143](#)
- [32] R. Runkel *et al.*, *Phys. Rev. Lett.* **122** (2019) 111603. [arXiv:1902.02135](#),
[doi:10.1103/PhysRevLett.122.111603](#)
- [33] I. Dubovyk *et al.*, *Phys. Lett.* **B783** (2018) 86. [arXiv:1804.10236](#),
[doi:10.1016/j.physletb.2018.06.037](#)
- [34] S. Borowka *et al.*, *Phys. Rev. Lett.* **117** (2016) 012001 [Erratum: **117** (2016) 079901].
[arXiv:1604.06447](#),
[doi:10.1103/PhysRevLett.117.012001](#), [doi:10.1103/PhysRevLett.117.079901](#)
- [35] S. Borowka *et al.*, *JHEP* **10** (2016) 107. [arXiv:1608.04798](#),
[doi:10.1007/JHEP10\(2016\)107](#)
- [36] S.P. Jones *et al.*, *Phys. Rev. Lett.* **120** (2018) 162001. [arXiv:1802.00349](#),
[doi:10.1103/PhysRevLett.120.162001](#)
- [37] G. Heinrich *et al.*, *JHEP* **06** (2019) 066. [arXiv:1903.08137](#),
[doi:10.1007/JHEP06\(2019\)066](#)
- [38] G. Buchalla *et al.*, *JHEP* **09** (2018) 057. [arXiv:1806.05162](#),
[doi:10.1007/JHEP09\(2018\)057](#)
- [39] S. Borowka *et al.*, *Eur. Phys. J.* **C74** (2014) 2994. [arXiv:1404.7074](#),
[doi:10.1140/epjc/s10052-014-2994-0](#)
- [40] S. Borowka *et al.*, *Comput. Phys. Commun.* **196** (2015) 470. [arXiv:1502.06595](#),
[doi:10.1016/j.cpc.2015.05.022](#)
- [41] A. Smirnov and M. Tentyukov, *Comput. Phys. Commun.* **180** (2009) 735.
[arXiv:0807.4129](#), [doi:10.1016/j.cpc.2008.11.006](#)
- [42] A.V. Smirnov, *Comput. Phys. Commun.* **185** (2014) 2090. [arXiv:1312.3186](#),
[doi:10.1016/j.cpc.2014.03.015](#)

- [43] A.V. Smirnov, *Comput. Phys. Commun.* **204** (2016) 189. [arXiv:1511.03614](#),
[doi:10.1016/j.cpc.2016.03.013](#)
- [44] S. Borowka *et al.*, *Comput. Phys. Commun.* **222** (2018) 313. [arXiv:1703.09692](#),
[doi:10.1016/j.cpc.2017.09.015](#)
- [45] D.E. Soper, *Phys. Rev.* **D62** (2000) 014009. [arXiv:hep-ph/9910292](#),
[doi:10.1103/PhysRevD.62.014009](#)
- [46] T. Binoth *et al.*, *JHEP* **10** (2005) 015. [arXiv:hep-ph/0504267](#),
[doi:10.1088/1126-6708/2005/10/015](#)
- [47] Z. Nagy and D.E. Soper, *Phys. Rev.* **D74** (2006) 093006. [arXiv:hep-ph/0610028](#),
[doi:10.1103/PhysRevD.74.093006](#)
- [48] J. Fleischer *et al.*, *Nucl. Phys.* **B547** (1999) 343. [arXiv:hep-ph/9808242](#),
[doi:10.1016/S0550-3213\(99\)00078-4](#)
- [49] I. Dubovyk *et al.*, *PoS* **LL2016** (2016) 075. [arXiv:1610.07059](#),
[doi:10.22323/1.260.0075](#)
- [50] J. Carter and G. Heinrich, *Comput. Phys. Commun.* **182** (2011) 1566. [arXiv:1011.5493](#),
[doi:10.1016/j.cpc.2011.03.026](#)
- [51] S. Borowka *et al.*, *Comput. Phys. Commun.* **184** (2013) 396. [arXiv:1204.4152](#),
[doi:10.1016/j.cpc.2012.09.020](#)
- [52] S. Jahn, *PoS* **LL2018** (2018) 019. [doi:10.22323/1.303.0019](#)
- [53] F.V. Tkachov, *Phys. Lett.* **100B** (1981) 65. [doi:10.1016/0370-2693\(81\)90288-4](#)
- [54] K.G. Chetyrkin and F.V. Tkachov, *Nucl. Phys.* **B192** (1981) 159.
[doi:10.1016/0550-3213\(81\)90199-1](#)
- [55] E. Panzer, Ph.D. thesis, Humboldt University, 2015.
[arXiv:1506.07243](#), [doi:10.18452/17157](#)
- [56] A. von Manteuffel *et al.*, *JHEP* **02** (2015) 120. [arXiv:1411.7392](#),
[doi:10.1007/JHEP02\(2015\)120](#)
- [57] A. von Manteuffel and R.M. Schabinger, *JHEP* **04** (2017) 129. [arXiv:1701.06583](#),
[doi:10.1007/JHEP04\(2017\)129](#)
- [58] T. Hahn, *Comput. Phys. Commun.* **168** (2005) 78. [arXiv:hep-ph/0404043](#),
[doi:10.1016/j.cpc.2005.01.010](#)
- [59] T. Hahn, *J. Phys. Conf. Ser.* **608** (2015) 012066. [arXiv:1408.6373](#),
[doi:10.1088/1742-6596/608/1/012066](#)
- [60] Z. Li *et al.*, *Chinese Phys. C* **40** (2016) 033103. [arXiv:1508.02512](#),
[doi:10.1088/1674-1137/40/3/033103](#)
- [61] E. de Doncker *et al.*, *J. Phys. Conf. Ser.* **1085** (2018) 052005.
[doi:10.1088/1742-6596/1085/5/052005](#)
- [62] E de Doncker *et al.*, *J. Phys. Conf. Ser.* **1136** (2018) 012002.
[doi:10.1088/1742-6596/1136/1/012002](#)
- [63] J. Dick *et al.*, *Acta Numer.* **22** (2013) 133. [doi:10.1017/S0962492913000044](#)
- [64] D. Nuyens and R. Cools, *Math. Comput.* **75** (2006) 903.
[doi:10.1090/S0025-5718-06-01785-6](#)

- [65] M. Czakon, *Phys. Lett.* **B664** (2008) 307. [arXiv:0803.1400](#),
[doi:10.1016/j.physletb.2008.05.028](#)
- [66] B. Jantzen *et al.*, *Eur. Phys. J.* **C72** (2012) 2139. [arXiv:1206.0546](#),
[doi:10.1140/epjc/s10052-012-2139-2](#)

7 Analytics from numerics: five-point QCD amplitudes at two loops

Contribution* by: S. Abreu, J. Dormans, F. Febres Cordero, H. Ita and B. Page
Corresponding author: B. Page [bpage@ipht.fr]

7.1 Introduction

The operation of the Large Hadron Collider (LHC) has been a great success, with Run 1 culminating in the discovery of the Higgs boson by the ATLAS and CMS experiments in 2012. In Run 2, the LHC experiments have moved towards performing high-precision measurements with uncertainties reaching below the percentage level for certain observables. Looking forward to the Future Circular Collider with electron beams (FCC-ee), which will operate in the experimentally much cleaner environment of electron–positron initial states, there will be an even more dramatic increase in experimental precision. To exploit the precision measurements, the theory community will need to provide high-precision predictions that match the experimental uncertainties. This requires the development of efficient ways to compute these corrections, breaking through the current computational bottlenecks.

In this section, we discuss the calculation of a key component in making such predictions—the loop amplitude. Specifically, we discuss the computation of an independent set of analytical two-loop five-gluon helicity amplitudes in the leading-colour approximation. These amplitudes are an ingredient for the phenomenologically relevant description of three-jet production at next-to-next-to-leading order (NNLO) for hadron colliders. Nonetheless, the methods we present are completely general and can also be applied to predictions for electron–positron collisions.

The first two-loop five-gluon amplitude to be computed was the one with all helicities positive in the leading-colour approximation, initially numerically [1] and subsequently analytically [2, 3]. In the last few years, a flurry of activity in this field led to the numerical calculation of all five-gluon [4, 5], and then all five-parton [6, 7] amplitudes in the leading-colour approximation. The combination of numerical frameworks with finite-field techniques, with a view to the reconstruction of the rational functions appearing in the final results, was first introduced to our field in Ref. [8], and an algorithm applicable to multiscale calculations was presented in Ref. [9]. Inspired by these ideas, the four-gluon amplitudes were analytically reconstructed from floating-point evaluations [10]. The first application involving multiple scales was the single-minus two-loop five-gluon amplitude [11]. In this section, we describe the calculation of the full set of independent five-gluon amplitudes in the leading-colour approximation [12]. These results were obtained using analytical reconstruction techniques, starting from numerical results obtained in the framework of two-loop numerical unitarity [5, 7, 10, 13]. Recently, the remaining five-parton amplitudes have also become available [14], and all two-loop amplitudes for three-jet production at NNLO in QCD are now known analytically in the leading-colour approximation.[†]

*This contribution should be cited as:

S. Abreu, J. Dormans, F. Febres Cordero, H. Ita, B. Page, Analytics from numerics: five-point QCD amplitudes at two loops, DOI: [10.23731/CYRM-2020-003.193](https://doi.org/10.23731/CYRM-2020-003.193), in: Theory for the FCC-ee, Eds. A. Blondel, J. Gluza, S. Jadach, P. Janot and T. Riemann, CERN Yellow Reports: Monographs, CERN-2020-003, DOI: [10.23731/CYRM-2020-003](https://doi.org/10.23731/CYRM-2020-003), p. 193.

© CERN, 2020. Published by CERN under the [Creative Commons Attribution 4.0 license](https://creativecommons.org/licenses/by/4.0/).

[†]The approach taken in Ref. [14] is very similar to that described here; we refer the reader to the results presented in Ref. [14] for a more compact expression for the five-gluon amplitudes and further improvements in

This section is organised as follows. In Section 7.2, we describe the amplitudes under consideration and the numerical unitarity framework employed for their evaluation. Section 7.3 describes the objects we will be computing and the simplifications that are made to allow for an efficient functional reconstruction. The implementation and the results are presented in Section 7.4 and we conclude in Section 7.5.

7.2 Amplitudes

We discuss the computation of the two-loop five-gluon amplitudes in QCD. The calculation is performed in the leading-colour approximation where there is a single partial amplitude. The bare amplitude can be perturbatively expanded as

$$\mathcal{A}(\{p_i, h_i\}_{i=1,\dots,5}) \Big|_{\text{leading colour}} = \sum_{\sigma \in S_5/Z_5} \text{Tr}(T^{a_{\sigma(1)}} T^{a_{\sigma(2)}} T^{a_{\sigma(3)}} T^{a_{\sigma(4)}} T^{a_{\sigma(5)}}) g_0^3 \left(\mathcal{A}^{(0)} + \lambda \mathcal{A}^{(1)} + \lambda^2 \mathcal{A}^{(2)} + \mathcal{O}(\lambda^3) \right). \quad (7.1)$$

Here, $\lambda = N_c g_0^2 / (4\pi)^2$, g_0 is the bare QCD coupling and S_5/Z_5 is the set of all non-cyclic permutations of five indices. The amplitudes $\mathcal{A}^{(k)}$ appearing in the expansion of Eq. (7.1) depend on the momenta $p_{\sigma(i)}$ and the helicities $h_{\sigma(i)}$ and these proceedings focus on the calculation of $\mathcal{A}^{(2)}$ in the 't Hooft–Veltman scheme of dimensional regularisation, with $D = 4 - 2\epsilon$.

The first step in the analytic reconstruction procedure is the numerical evaluation of the amplitude. We evaluate the amplitudes in the framework of two-loop numerical unitarity [5, 7, 10, 13]. The integrands of the amplitudes $\mathcal{A}^{(2)}$ are parametrized with a decomposition in terms of master integrands and surface terms. On integration, the former yield the master integrals, while the latter vanish. Labelling the loop momenta ℓ_l , the parametrization we use is given by

$$\mathcal{A}^{(2)}(\ell_l) = \sum_{\Gamma \in \Delta} \sum_{i \in M_\Gamma \cup S_\Gamma} c_{\Gamma,i} \frac{m_{\Gamma,i}(\ell_l)}{\prod_{j \in P_\Gamma} \rho_j}, \quad (7.2)$$

with Δ being the set of all propagator structures Γ , P_Γ the associated set of propagators, and M_Γ and S_Γ denoting the corresponding sets of master integrands and surface terms, respectively. If the master integrals are known, the evaluation of the amplitude reduces to the determination of master coefficients $c_{\Gamma,i}$ with $i \in M_\Gamma$. In numerical unitarity, this is achieved by solving a linear system, which is generated by sampling on-shell values of the loop momenta ℓ_l^Γ belonging to the algebraic variety of P_Γ . In this limit, the leading contribution to Eq. (7.1) factorises into products of tree amplitudes

$$\sum_{\text{states}} \prod_{i \in T_\Gamma} \mathcal{A}_i^{\text{tree}}(\ell_l^\Gamma) = \sum_{\substack{\Gamma' \supseteq \Gamma, \\ i \in M_{\Gamma'} \cup S_{\Gamma'}}} \frac{c_{\Gamma',i} m_{\Gamma',i}(\ell_l^\Gamma)}{\prod_{j \in (P_{\Gamma'} \setminus P_\Gamma)} \rho_j(\ell_l^\Gamma)}. \quad (7.3)$$

The tree amplitudes associated with vertices in the diagram corresponding to Γ are denoted T_Γ and the sum is over the physical states of each internal line of Γ . On the right-hand side, the sum is performed over all propagator structures Γ' , such that $P_\Gamma \subseteq P_{\Gamma'}$. At two loops, subleading contributions appear, which cannot be described by a factorisation theorem in the on-shell limit. In practice, this complication is eliminated by constructing a larger system of equations, as described, for instance, in Ref. [15]. For a given (rational) phase space point, we

the methodology.

solve the linear system in Eq. (7.3) using finite-field arithmetic. This allows us to obtain exact results for the master integral coefficients in a very efficient manner.

Once the coefficients $c_{\Gamma,i}$ are known, the amplitude can be decomposed into a linear combination of master integrals $\mathcal{I}_{\Gamma,i}$, according to

$$\mathcal{A}^{(2)} = \sum_{\Gamma \in \Delta} \sum_{i \in M_{\Gamma}} c_{\Gamma,i} \mathcal{I}_{\Gamma,i}, \quad (7.4)$$

with

$$\mathcal{I}_{\Gamma,i} = \int d^D l_l \frac{m_{\Gamma,i}(l_l)}{\prod_{j \in P_{\Gamma}} \rho_j}. \quad (7.5)$$

For planar massless five-point scattering at two loops, the basis of master integrals is known in analytical form [16, 17].

7.3 Simplifications for functional reconstruction

Functional reconstruction techniques allow one to reconstruct rational functions from numerical data, preferably in a finite field to avoid issues related to loss of precision [8, 9]. By choosing an appropriate set of variables, such as momentum twistors [18], we can guarantee that the coefficients $c_{\Gamma,i}$ in Eq. (7.4) are rational. The specific parametrization we use is [9]

$$\begin{aligned} s_{12} &= x_4, & s_{23} &= x_2 x_4, & s_{34} &= x_4 \left(\frac{(1+x_1)x_2}{x_0} + x_1(x_3-1) \right), \\ s_{45} &= x_3 x_4, & s_{51} &= x_1 x_4 (x_0 - x_2 + x_3), \\ \text{tr}_5 &= 4i \varepsilon(p_1, p_2, p_3, p_4) \\ &= x_4^2 \left(x_2(1+2x_1) + x_0 x_1 (x_3-1) - \frac{x_2(1+x_1)(x_2-x_3)}{x_0} \right), \end{aligned} \quad (7.6)$$

where $s_{ij} = (p_i + p_j)^2$, with the indices defined cyclically. One could, in principle, reconstruct the rational master integral coefficients. However, the difficulty of the reconstruction is governed by the complexity of the function under consideration. The amplitude $\mathcal{A}^{(2)}$ of Eq. (7.4) contains a lot of redundant information; to improve the efficiency of the reconstruction, it is thus beneficial to remove this redundancy. Furthermore, while Eq. (7.4) provides a decomposition in terms of master integrals in dimensional regularisation, after expanding the master integrals in ϵ there can be new linear relations between the different terms in the Laurent expansion in ϵ . We thus expect cancellations between the different coefficients $c_{\Gamma,i}$. In this section, we discuss how we address these issues and define the object we reconstruct.

We start by expressing the Laurent expansion of the master integrals in Eq. (7.5) in terms of a basis B of so-called pentagon functions $h_i \in B$ [17]. That is, we rewrite the amplitudes as

$$\mathcal{A}^{(2)} = \sum_{i \in B} \sum_{k=-4}^0 \epsilon^k \tilde{c}_{k,i}(\vec{x}) h_i(\vec{x}) + \mathcal{O}(\epsilon), \quad (7.7)$$

where $\vec{x} = \{x_0, x_1, x_2, x_3, x_4\}$ and the $\tilde{c}_{k,i}(\vec{x})$ are rational functions of the twistor variables. All linear relations between master integrals that appear after expansion in ϵ are resolved in such a decomposition.

Next, we recall that the singularity structure of two-loop amplitudes is governed by lower-loop amplitudes [19–22]. One can thus exploit this knowledge to subtract the pole structure from the amplitudes in order to obtain a finite remainder that contains the new two-loop information. There is freedom in how to define the remainders, as they are only constrained by removing the poles of the amplitudes. For helicity amplitudes that vanish at tree level, $\mathcal{A}_{\pm++++}^{(k)}$, we use

$$\mathcal{R}_{\pm++++}^{(2)} = \bar{\mathcal{A}}_{\pm++++}^{(2)} + S_\epsilon \bar{\mathcal{A}}_{\pm++++}^{(1)} \sum_{i=1}^5 \frac{(-s_{i,i+1})^{-\epsilon}}{\epsilon^2} + \mathcal{O}(\epsilon), \quad (7.8)$$

where $S_\epsilon = (4\pi)^\epsilon e^{-\epsilon\gamma_E}$. The $\bar{\mathcal{A}}^{(k)}$ denote amplitudes normalised to remove any ambiguity related to overall phases. In the case of amplitudes that vanish at tree level, we normalise to the leading order in ϵ of the (finite) one-loop amplitude. For the maximally helicity violating (MHV) amplitudes, $\mathcal{A}_{-\mp\pm\pm\pm}^{(k)}$, which we normalise to the corresponding tree amplitude, we define

$$\mathcal{R}_{-\mp\pm\pm\pm}^{(2)} = \bar{\mathcal{A}}_{-\mp\pm\pm\pm}^{(2)} - \left(\frac{5\tilde{\beta}_0}{2\epsilon} + \mathbf{I}^{(1)} \right) S_\epsilon \bar{\mathcal{A}}_{-\mp\pm\pm\pm}^{(1)} + \left(\frac{15\tilde{\beta}_0^2}{8\epsilon^2} + \frac{3}{2\epsilon} (\tilde{\beta}_0 \mathbf{I}^{(1)} - \tilde{\beta}_1) - \mathbf{I}^{(2)} \right) S_\epsilon^2 + \mathcal{O}(\epsilon), \quad (7.9)$$

where $\tilde{\beta}_i$ are the coefficients of the QCD β function divided by N_c^{i+1} and $\mathbf{I}^{(1)}$ and $\mathbf{I}^{(2)}$ are the standard Catani operators at leading colour. Precise expressions for the operators in our conventions can be found in Appendix B of Ref. [7]. We note that for both Eq. (7.8) and Eq. (7.9) we require one-loop amplitudes expanded up to order ϵ^2 . By expressing the one-loop amplitudes and the Catani operators in the basis of pentagon functions, the remainder can be expressed in the same way,

$$\mathcal{R}^{(2)} = \sum_{i \in \mathcal{B}} r_i(\vec{x}) h_i(\vec{x}). \quad (7.10)$$

We observe that the coefficients $r_i(\vec{x})$ are rational functions of lower total degree than the $\tilde{c}_{k,i}(\vec{x})$ of Eq. (7.7).

As a further simplification, we investigate the pole structure of the coefficients $r_i(\vec{x})$. The alphabet determines the points in phase space where the pentagon functions have logarithmic singularities, and as such provides a natural candidate to describe the pole structure of the coefficients. We use the alphabet A determined in Ref. [17] to build an ansatz for the denominator structure of the $r_i(\vec{x})$,

$$r_i(\vec{x}) = \frac{n_i(\vec{x})}{\prod_{j \in A} w_j(\vec{x})^{q_{ij}}}. \quad (7.11)$$

We then reconstruct the remainder on a slice $\vec{x}(t) = \vec{a} \cdot t + \vec{b}$, where all the twistor variables depend on a single parameter t and \vec{a} and \vec{b} are random vectors of finite-field values. This reconstruction in one variable is drastically simpler than the full multivariate reconstruction. In addition, the maximal degree in t on the slice corresponds to the total degree in \vec{x} . We determine the exponents q_{ij} by matching the ansatz on the univariate slice and check its validity on a second slice. Having determined the denominators of the rational coefficients r_i , the reconstruction reduces to the much simpler polynomial reconstruction of the numerators $n_i(\vec{x})$.

The last simplification we implement is a change of basis in the space of pentagon functions. Amplitudes are expected to simplify in specific kinematic configurations where the pentagon functions degenerate into a smaller basis, which requires relations between the different coefficients. This motivates the search for (helicity-dependent) bases with coefficients of lower

Table C.7.1: Each t^n/t^d denotes the total degree of numerator (n) and denominator (d) of the most complex coefficient for each helicity amplitude in the decomposition of Eq. (7.7) (second column) or Eq. (7.10) (third column). The fourth column lists the highest polynomial we reconstruct. The final column lists the number of letters $w_j(\vec{x})$ that contribute in the denominator of Eq. (7.11).

Helicity	$\tilde{c}_{k,i}(t)$	$r_i(t)$	$n'_i(t)$	w_j s in denominator
+++++	t^{34}/t^{28}	t^{10}/t^4	t^{10}	3
-++++	t^{50}/t^{42}	t^{35}/t^{28}	t^{35}	14
--+++	t^{70}/t^{65}	t^{50}/t^{45}	t^{40}	17
-+-++	t^{84}/t^{82}	t^{68}/t^{66}	t^{53}	20

total degree. To find them, we construct linear combinations of coefficients

$$\sum_{i \in B} a_{i,k} r_i(\vec{x}) = \frac{N_k(\vec{x}, a_{i,k})}{\prod_{j \in A} w_j(\vec{x})^{q_{kj}}}, \quad (7.12)$$

and solve for phase space independent $a_{i,k}$ such that the numerators $N_k(\vec{x}, a_{i,k})$ factorise a subset of the $w_j \in A$. This can be performed on univariate slices by only accepting solutions that are invariant over a number of slices. The matrix $a_{i,k}$ allows us to change to a new basis B' in the space of special functions, in which remainders can be decomposed as in Eq. (7.10), with coefficients $r'_i(\vec{x})$ whose numerators $n'_i(\vec{x})$ are polynomials of lower total degree than those of Eq. (7.11).

7.4 Implementation and results

The master integral coefficients of the one- and two-loop amplitudes are computed using numerical unitarity in a finite field. They are combined with the corresponding master integrals, expressed in terms of pentagon functions, and the known pole structure is subtracted to obtain the finite remainders as a linear combination of pentagon functions. After a rotation in the space of pentagon functions and multiplication by the predetermined denominator factors, we obtain numerical samples for the numerators $n'_i(\vec{x})$ in a finite field. These samples are used to analytically reconstruct the $n'_i(\vec{x})$ with the algorithm of Ref. [9], which we slightly modified to allow a more efficient parallelization. These steps were implemented in a flexible C++ framework, which was used to reconstruct the analytical form of the two-loop remainders of a basis of five-gluon helicity amplitudes (the other helicities can be obtained by parity and charge conjugation). Two finite fields of cardinality $O(2^{31})$ were necessary for the rational reconstruction by means of the Chinese remainder theorem.

Table C.7.1 shows the impact of the simplifications discussed in the previous section for each helicity. In the most complicated case, the $g^-g^+g^-g^+g^+$ helicity amplitude, we must reconstruct a polynomial of degree 53. This required 250 000 numerical evaluations, with 4.5 min per evaluation.

The results that we provide contain the one-loop amplitudes in terms of master integrals and the two-loop remainders in terms of pentagon functions. The one-loop master integrals are provided in terms of pentagon functions up to order ϵ^2 . The combined size of the expressions amounts to 45 MB without attempting any simplification (we refer the reader to Ref. [14]

for more compact expressions). These expressions can be combined to construct the full analytical expression for the two-loop five-gluon leading-colour amplitudes in the Euclidean region. We validated our expressions by reproducing all the target benchmark values available in the literature [1–5, 7, 11].

7.5 Conclusion

In this section, we have presented the recent computation of the analytical form of the leading-colour contributions to the two-loop five-gluon scattering amplitudes in pure Yang–Mills theory. This computation was undertaken in a novel way, made possible by a collection of mature tools. The amplitude is first numerically reduced to a basis of master integrals with the two-loop numerical unitarity approach, where the coefficients take finite-field values [5, 7, 10, 13]. This allows us to numerically calculate a finite remainder, expressed in terms of pentagon functions [17]. The generation of these numerical samples is driven by a functional reconstruction algorithm [9], which determines the analytical form of the pentagon-function coefficients from a series of evaluations. A key step in efficiently implementing this strategy was to utilise physical information to simplify the analytical form of the objects we reconstruct, and hence reduce the required number of evaluations. First, we reconstruct the finite remainder, which removes redundant information related to lower-loop contributions. Second, we decompose the remainder in terms of pentagon functions to account for relations between different master integrals after expansion in the dimensional regulator. Next, we exploit the knowledge of the singularity structure of the pentagon functions to efficiently establish the denominators of the coefficient functions. Finally, we find a basis of pentagon functions with coefficients of lower degree by exploiting their reconstruction on a univariate slice.

These techniques show a great deal of potential for future calculations. Indeed, they have very recently been used to obtain the full set of leading-colour contributions to the five-parton scattering amplitudes [14]. We foresee further applications to processes with a higher number of scales and loops, such as those required for a future lepton collider in the near future.

References

- [1] S. Badger *et al.*, *JHEP* **12** (2013) 045. [arXiv:1310.1051](#), [doi:10.1007/JHEP12\(2013\)045](#)
- [2] T. Gehrmann *et al.*, *Phys. Rev. Lett.* **116** (2016) 062001 [Erratum: **116** (2016) 189903]. [arXiv:1511.05409](#), [doi:10.1103/PhysRevLett.116.062001](#), [doi:10.1103/PhysRevLett.116.189903](#)
- [3] D.C. Dunbar and W.B. Perkins, *Phys. Rev.* **D93** (2016) 085029. [arXiv:1603.07514](#), [doi:10.1103/PhysRevD.93.085029](#)
- [4] S. Badger *et al.*, *Phys. Rev. Lett.* **120** (2018) 092001. [arXiv:1712.02229](#), [doi:10.1103/PhysRevLett.120.092001](#)
- [5] S. Abreu *et al.*, *Phys. Rev.* **D97** (2018) 116014. [arXiv:1712.03946](#), [doi:10.1103/PhysRevD.97.116014](#)
- [6] S. Badger *et al.*, *PoS LL2018* (2018) 006. [arXiv:1807.09709](#), [doi:10.22323/1.303.0006](#)
- [7] S. Abreu *et al.*, *JHEP* **11** (2018) 116. [arXiv:1809.09067](#), [doi:10.1007/JHEP11\(2018\)116](#)
- [8] A. von Manteuffel and R.M. Schabinger, *Phys. Lett.* **B744** (2015) 101. [arXiv:1406.4513](#), [doi:10.1016/j.physletb.2015.03.029](#)

- [9] T. Peraro, *JHEP* **12** (2016) 030. [arXiv:1608.01902](#), [doi:10.1007/JHEP12\(2016\)030](#)
- [10] S. Abreu *et al.*, *Phys. Rev. Lett.* **119** (2017) 142001. [arXiv:1703.05273](#),
[doi:10.1103/PhysRevLett.119.142001](#)
- [11] S. Badger *et al.*, *JHEP* **01** (2019) 186. [arXiv:1811.11699](#),
[doi:10.1007/JHEP01\(2019\)186](#)
- [12] S. Abreu *et al.*, *Phys. Rev. Lett.* **122** (2019) 082002. [arXiv:1812.04586](#),
[doi:10.1103/PhysRevLett.122.082002](#)
- [13] H. Ita, *PoS LL2016* (2016) 080. [arXiv:1607.00705](#), [doi:10.22323/1.260.0080](#)
- [14] S. Abreu *et al.*, *JHEP* **05** (2019) 084. [arXiv:1904.00945](#), [doi:10.1007/JHEP05\(2019\)084](#)
- [15] S. Abreu *et al.*, *Phys. Rev.* **D95** (2017) 096011. [arXiv:1703.05255](#),
[doi:10.1103/PhysRevD.95.096011](#)
- [16] C.G. Papadopoulos *et al.*, *JHEP* **04** (2016) 078. [arXiv:1511.09404](#),
[doi:10.1007/JHEP04\(2016\)078](#)
- [17] T. Gehrmann *et al.*, *JHEP* **10** (2018) 103. [arXiv:1807.09812](#),
[doi:10.1007/JHEP10\(2018\)103](#)
- [18] A. Hodges, *JHEP* **05** (2013) 135. [arXiv:0905.1473](#), [doi:10.1007/JHEP05\(2013\)135](#)
- [19] S. Catani, *Phys. Lett.* **B427** (1998) 161. [arXiv:hep-ph/9802439](#),
[doi:10.1016/S0370-2693\(98\)00332-3](#)
- [20] G.F. Sterman and M.E. Tejeda-Yeomans, *Phys. Lett.* **B552** (2003) 48.
[arXiv:hep-ph/0210130](#), [doi:10.1016/S0370-2693\(02\)03100-3](#)
- [21] T. Becher and M. Neubert, *Phys. Rev. Lett.* **102** (2009) 162001 [Erratum: **111** (2013) 199905]. [arXiv:0901.0722](#),
[doi:10.1103/PhysRevLett.102.162001](#), [doi:10.1103/PhysRevLett.111.199905](#)
- [22] E. Gardi and L. Magnea, *JHEP* **03** (2009) 079. [arXiv:0901.1091](#),
[doi:10.1088/1126-6708/2009/03/079](#)

8 Recent developments in Kira

Contribution* by: P. Maierhöfer, J. Usovitsch

Corresponding author: J. Usovitsch [usovitsj@maths.tcd.ie]

In this section, we report on the recent progress made in the development of the Feynman integral reduction program **Kira**. The development is focused on algorithmic improvements that are essential to extend the range of feasible high-precision calculations for present and future colliders like the FCC-ee.

8.1 Introduction

Kira [1] implements Laporta’s algorithm [2] to reduce Feynman integrals to a basis of master integrals. In this approach, large systems of integration by parts [3] and Lorentz invariance [4] identities, as well as symmetry relations, are generated and solved by a variant of Gaussian elimination, systematically expressing complicated integrals in terms of simpler integrals with respect to a given complexity criterion. Though alternative reduction techniques have been proposed and applied to specific problems, see, e.g., Refs. [5–8], to date programs based on Laporta’s algorithm [9–11] pose the only general-purpose tools suited for large-scale applications. Since these reduction programs constitute one of the bottlenecks of high-precision predictions, their continuous improvement is crucial to meet the increasing demand for such calculations.

A key element of **Kira** is its equation selector to extract a linearly independent system of equations, discarding equations that are not required to fully reduce all integrals requested by the user. The selector is based on Gaussian elimination using modular arithmetic on the coefficients.

8.2 Improved symmetrization

The detection of symmetry relations between sectors within and across topologies received a performance boost as a result of the implementation of the algorithm described in Ref. [12]. In this approach, a canonical form of the integrand of each sector is constructed, so that a one-to-one comparison of the representations can be made. Additionally, the combinatorial complexity of the loop momentum shift finder to determine the mapping prescriptions of equivalent sectors has been reduced. Furthermore, the detection of trivial sectors received a significant speed-up by employing **Kira**’s IBP solver instead of the less optimised previous linear solver.

As an example, the ‘cube topology’ shown in Fig. C.8.1, i.e., the five-loop vacuum bubble with 12 propagators of equal mass and the symmetry of a cube, can now be analysed in less than 10 min on a state-of-the-art desktop computer.

8.3 Parallel simplification algorithms for coefficients

8.3.1 Algebraic simplifications with Fermat

To simplify multivariate rational functions in masses and kinematic quantities, which appear as coefficients in the Gaussian elimination steps, **Kira** relies on the program **Fermat** [13]. In

*This contribution should be cited as:

P. Maierhöfer, J. Usovitsch, Recent developments in Kira, DOI: [10.23731/CYRM-2020-003.201](https://doi.org/10.23731/CYRM-2020-003.201), in: Theory for the FCC-ee, Eds. A. Blondel, J. Gluza, S. Jadach, P. Janot and T. Riemann, CERN Yellow Reports: Monographs, CERN-2020-003, DOI: [10.23731/CYRM-2020-003](https://doi.org/10.23731/CYRM-2020-003), p. 201. © CERN, 2020. Published by CERN under the [Creative Commons Attribution 4.0 license](https://creativecommons.org/licenses/by/4.0/).

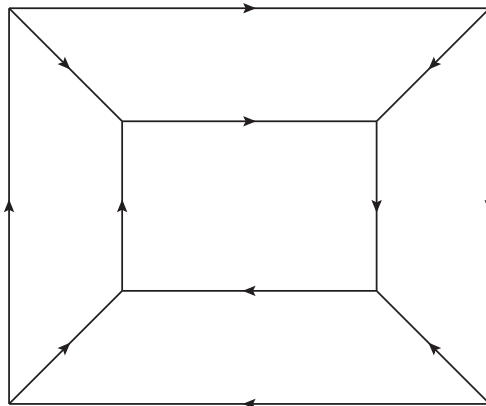


Fig. C.8.1: The cube topology is the five-loop vacuum bubble with 12 propagators of equal mass and octahedral symmetry. The high symmetry of 48 equivalent propagator permutations in the top-level sector makes this topology an ideal candidate for symmetrization benchmarks.

almost all cases, the run time for the reduction is dominated by those algebraic simplifications. It turns out that, when a new coefficient is constructed from several (often thousands of) known coefficients, combining them naïvely and simplifying them in one step results in an avoidable performance penalty. Instead, *Kira* recursively combines coefficients pairwise, choosing the pairs based on the size of their string representations. Besides the improved performance, this strategy also offers new possibilities for the parallelization, since the pairwise combinations can be evaluated by different *Fermat* instances.

In the Gaussian back substitution, one can restrict a solver to calculate only the coefficients of a specific master integral. This allows the user to parallelize the reduction across several machines and merge the results in a final step.

8.3.2 Algebraic reconstruction over integers

An alternative algorithm to simplify the coefficients is given by algebraic reconstruction over integers, introduced in Refs. [7, 14, 15]. This strategy is based on sampling the rational functions by setting kinematic invariants and masses to integer values repeatedly. Each sample can be evaluated rather quickly, but the number of samples required to reconstruct the simplified result increases with the degree of the numerator and denominator of the rational function, the number of invariants involved, and the number of invariants over which it is sampled. Of course, the sample can again be evaluated in parallel, leading to the potential for massive parallelization on dozens of CPU cores. An implementation of this algorithm is available in *Kira* 1.2 and is continuously being improved and extended. Furthermore, *Kira* automatically decides which simplification strategy, i.e., algebraic reconstruction or *Fermat*, is expected to be more efficient in each case. The criteria for these decisions are subject to investigation and offer room for future improvements.

8.3.3 Algebraic reconstruction over finite integer fields

Instead of sampling rational functions over integers, it is also possible to reconstruct them from samples over finite integer fields. Mapping coefficients to a finite field limits the size of each coefficient and, with that, the complexity of each operation. Choosing the module as a word-size prime, numerical operations on coefficients correspond to the native arithmetic

capabilities of the employed CPU, allowing for high performance sampling of the coefficients. A reconstruction algorithm for multivariate rational functions was first presented in Ref. [16]. Recently, the library `FireFly` [17] became available, implementing a similar algorithm. `FireFly` has been combined with `Kira` to use it for Feynman integral reduction, calculating the samples with `Kira`'s finite integer Gaussian elimination. An independent implementation is available in `FIRE 6` [11].

In the sampling over (arbitrary-size) integers described here, whenever a coefficient is required to proceed with the reduction, the solver needs to wait until that coefficient has been reconstructed. Using finite integers, the entire solver can be parallelized, opening the possibility of distributing solvers over different machines. The reconstructor can then collect the samples from the solvers and finish the calculation when a sufficient number of samples is available. The finite integer reconstruction is expected to become publicly available in a future `Kira` release in combination with `FireFly`.

8.4 Basis choice

It is well-known that the reduction time strongly depends on the choice of the master integrals. In a convenient basis, the reduction coefficients tend to become much simpler than, e.g., in the basis that follows directly from the integral ordering. In this respect, uniformly transcendental bases [18], finite bases [19], or finite uniformly transcendental bases [20] present interesting candidates to study the impact of the basis choice on the reduction performance. These special choices involve linear combinations of integrals as basis elements that we call ‘master equations’.

In `Kira`, integrals are represented by integer ‘weights’ in such a way that they obey the imposed integral ordering. Choosing a specific basis of master integrals is already possible. To this end, the weights are modified so that the preferred basis integrals are regarded as simpler than all other integrals. In the presence of master equations, a new kind of object must be introduced, representing the master equation instead of a particular integral. With appropriate bookkeeping, the implementation becomes straightforward and will soon be available in a `Kira` release.

8.5 Conclusions

The complexity of precision calculations needed to match the accuracy of the FCC-ee experiment demands for integral reduction tools beyond the state-of-the-art capabilities. For example, the computation of pseudo-observables at the Z boson resonance, involving reductions of three-loop Feynman diagrams with up to five scales, will be necessary to reach the accuracy that may be achieved with the FCC-ee [21]. We expect that Feynman integral reduction programs based on Laporta’s algorithm will continue to play a key role in such calculations; e.g., by harnessing the potential of rational reconstruction, basis choices, and large-scale parallelization, we are convinced that `Kira` will keep up with the arising technical challenges.

References

- [1] P. Maierhöfer *et al.*, *Comput. Phys. Commun.* **230** (2018) 99. [arXiv:1705.05610](https://arxiv.org/abs/1705.05610), [doi:10.1016/j.cpc.2018.04.012](https://doi.org/10.1016/j.cpc.2018.04.012)
- [2] S. Laporta, *Int. J. Mod. Phys.* **A15** (2000) 5087. [arXiv:hep-ph/0102033](https://arxiv.org/abs/hep-ph/0102033), [doi:10.1016/S0217-751X\(00\)00215-7](https://doi.org/10.1016/S0217-751X(00)00215-7)

-
- [3] K.G. Chetyrkin and F.V. Tkachov, *Nucl. Phys.* **B192** (1981) 159. [doi:10.1016/0550-3213\(81\)90199-1](https://doi.org/10.1016/0550-3213(81)90199-1)
- [4] T. Gehrmann and E. Remiddi, *Nucl. Phys.* **B580** (2000) 485. [arXiv:hep-ph/9912329](https://arxiv.org/abs/hep-ph/9912329), [doi:10.1016/S0550-3213\(00\)00223-6](https://doi.org/10.1016/S0550-3213(00)00223-6)
- [5] A.V. Smirnov and V.A. Smirnov, *JHEP* **01** (2006) 001. [arXiv:hep-lat/0509187](https://arxiv.org/abs/hep-lat/0509187), [doi:10.1088/1126-6708/2006/01/001](https://doi.org/10.1088/1126-6708/2006/01/001)
- [6] R.N. Lee, *J. Phys. Conf. Ser.* **523** (2014) 012059. [arXiv:1310.1145](https://arxiv.org/abs/1310.1145), [doi:10.1088/1742-6596/523/1/012059](https://doi.org/10.1088/1742-6596/523/1/012059)
- [7] K.J. Larsen and Y. Zhang, *Phys. Rev.* **D93** (2016) 041701. [arXiv:1511.01071](https://arxiv.org/abs/1511.01071), [doi:10.1103/PhysRevD.93.041701](https://doi.org/10.1103/PhysRevD.93.041701)
- [8] D.A. Kosower, *Phys. Rev.* **D98** (2018) 025008. [arXiv:1804.00131](https://arxiv.org/abs/1804.00131), [doi:10.1103/PhysRevD.98.025008](https://doi.org/10.1103/PhysRevD.98.025008)
- [9] C. Anastasiou and A. Lazopoulos, *JHEP* **07** (2004) 046. [arXiv:hep-ph/0404258](https://arxiv.org/abs/hep-ph/0404258), [doi:10.1088/1126-6708/2004/07/046](https://doi.org/10.1088/1126-6708/2004/07/046)
- [10] A. von Manteuffel and C. Studerus, Reduze 2—distributed Feynman integral reduction, [arXiv:1201.4330](https://arxiv.org/abs/1201.4330)
- [11] A.V. Smirnov and F.S. Chuharev, *Comput. Phys. Commun.* **247** 106877. [arXiv:1901.07808](https://arxiv.org/abs/1901.07808), [doi:10.1016/j.cpc.2019.106877](https://doi.org/10.1016/j.cpc.2019.106877)
- [12] A. Pak, *J. Phys. Conf. Ser.* **368** (2012) 012049. [arXiv:1111.0868](https://arxiv.org/abs/1111.0868), [doi:10.1088/1742-6596/368/1/012049](https://doi.org/10.1088/1742-6596/368/1/012049)
- [13] R.H. Lewis, Computer algebra system Fermat, https://www.academia.edu/677352/Computer_algebra_system_Fermat
- [14] J. Böhm *et al.* *Phys. Rev.* **D98** (2018) 025023. [arXiv:1712.09737](https://arxiv.org/abs/1712.09737), [doi:10.1103/PhysRevD.98.025023](https://doi.org/10.1103/PhysRevD.98.025023)
- [15] J. Böhm *et al.* *JHEP* **09** (2018) 024. [arXiv:1805.01873](https://arxiv.org/abs/1805.01873), [doi:10.1007/JHEP09\(2018\)024](https://doi.org/10.1007/JHEP09(2018)024)
- [16] T. Peraro, *JHEP* **12** (2016) 030. [arXiv:1608.01902](https://arxiv.org/abs/1608.01902), [doi:10.1007/JHEP12\(2016\)030](https://doi.org/10.1007/JHEP12(2016)030)
- [17] J. Klappert and F. Lange, *Comput. Phys. Commun.* **247** (2020) 106951. [arXiv:1904.00009](https://arxiv.org/abs/1904.00009), [doi:10.1016/j.cpc.2019.106951](https://doi.org/10.1016/j.cpc.2019.106951)
- [18] J.M. Henn, *Phys. Rev. Lett.* **110** (2013) 251601. [arXiv:1304.1806](https://arxiv.org/abs/1304.1806), [doi:10.1103/PhysRevLett.110.251601](https://doi.org/10.1103/PhysRevLett.110.251601)
- [19] E. Panzer, Ph.D. thesis, Humboldt University, 2015. [arXiv:1506.07243](https://arxiv.org/abs/1506.07243), [doi:10.18452/17157](https://doi.org/10.18452/17157)
- [20] R.M. Schabinger, *Phys. Rev.* **D99** (2019) 105010. [arXiv:1806.05682](https://arxiv.org/abs/1806.05682), [doi:10.1103/PhysRevD.99.105010](https://doi.org/10.1103/PhysRevD.99.105010)
- [21] A. Blondel *et al.*, Standard Model theory for the FCC-ee Tera-Z stage, (CERN-2019-003), [arXiv:1809.01830](https://arxiv.org/abs/1809.01830), [doi:10.23731/CYRM-2019-003](https://doi.org/10.23731/CYRM-2019-003)

9 Precision Monte Carlo simulations with WHIZARD

Contribution* by: S. Braß, W. Kilian, T. Ohl, J. Reuter, V. Rothe, P. Stienemeier
Corresponding author: J. Reuter [juergen.reuter@desy.de]

The precision physics programmes of the FCC-ee demand for a precise simulation of all Standard Model (SM) processes and possible beyond-the-SM (BSM) signals in a state-of-the-art way by means of Monte Carlo (MC) techniques. As a standard tool for e^+e^- simulations, the multi-purpose event generator WHIZARD [1,2] has been used: this generator was originally developed for the TESLA project, and was later used, e.g., for the ILC Technical Design Report [3,4]. The WHIZARD package has a modular structure, which serves a modern unit-test driven software development and guarantees a high level of maintainability and extendability. WHIZARD comes with its own fully general tree-level matrix element generator for the hard process, O'Mega [5]. It generates amplitudes in a recursive way, based on the graph-theoretical concepts of directed acyclical graphs, thereby avoiding all redundancies. The matrix elements are generated either as compilable modern Fortran code or as byte-code instructions interpreted by a virtual machine [6]. For QCD, WHIZARD uses the colour flow formalism [7]. Matrix elements support all kinds of particles and interactions up to spin-2. A large number of BSM models are hard-coded, particularly the minimal supersymmetric Standard Model (MSSM) and next-to-MSSM (NMSSM) [8,9]. General BSM models can be loaded from a Lagrangian level tool, using the interface to FeynRules [10]; from version 2.8.0 of WHIZARD on (early summer 2019) a fully fledged interface to the general UFO format is available. One of the biggest assets of WHIZARD is its general phase space parametrization, which uses a heuristic based on the dominating sub-processes, which allows integration and simulation of processes with up to ten fermions in the final state. The integration is based on an adaptive multichannel algorithm, called VAMP [11]. Recently, this multichannel adaptive integration has been enhanced to a parallelized version using the MPI3 protocol, showing speed-ups of up to 100 [12], while a first physics study using this MPI parallelized integration and event generation has been published [13].

WHIZARD allows all the necessary ingredients for a high-precision e^+e^- event simulation to be described: the CIRCE1/CIRCE2 modules [14] simulate the spectrum of beamstrahlung (including beam energy spectra) that comes from classical electromagnetic radiation, owing to extreme space charge densities of highly collimated bunches for high-luminosity running. This takes care of a precise description of the peaks of the luminosity spectra and a smooth mapping of the tail that does not lead to artificial spikes and kinks in differential distributions. For the beam set-up, WHIZARD furthermore allows polarised beams to be correctly described, with arbitrary polarisation settings and fractions, asymmetric beams, and crossing angles. QED initial-state radiation (ISR) is convoluted in a collinear approximation according to a resummation of soft photons to all orders and hard-collinear photons up to third order [15]. While this will give a correct normalization of the cross-section to the given QED order, one explicit ISR photon per beam will be inserted into the event record. A special handler generates transverse momentum according to a physical p_T distribution and boosts the complete events

*This contribution should be cited as:

S. Braß, W. Kilian, T. Ohl, J. Reuter, V. Rothe, P. Stienemeier, Precision Monte Carlo simulations with WHIZARD, DOI: [10.23731/CYRM-2020-003.205](https://doi.org/10.23731/CYRM-2020-003.205), in: Theory for the FCC-ee, Eds. A. Blondel, J. Gluza, S. Jadach, P. Janot and T. Riemann, CERN Yellow Reports: Monographs, CERN-2020-003, DOI: [10.23731/CYRM-2020-003](https://doi.org/10.23731/CYRM-2020-003), p. 205.
© CERN, 2020. Published by CERN under the [Creative Commons Attribution 4.0 license](https://creativecommons.org/licenses/by/4.0/).

accordingly. This treatment is also available for the photon beam components, according to the Weizsäcker–Williams spectrum (equivalent photon approximation, EPA).

The MC generator WHIZARD offers a vast functionality, which cannot be given full justice here, e.g., automatic generation of decays, factorised processes, including full spin correlations (which can also be switched off for case studies), specification of the helicity of decaying resonances, preset branching ratios, etc. WHIZARD supports all used HEP event formats, such as StdHEP, LHE, HepMC, LCIO, and various ASCII formats. It allows easy reweighting of event samples. WHIZARD has its own two QCD parton shower algorithms, a k_T -ordered shower and an analytic parton shower [16], and ships with the final version of PYTHIA6 [17] for showering and hadronization. The event records are directly interfaced and exchanged, and the framework has been validated with the full LEP dataset by the Linear Collider Generator Group in a set-up similar to the FCC-ee. Recently, we added a corresponding interface for an externally linked PYTHIA8 [18], which, again, allows direct communication between the event records of WHIZARD and PYTHIA. This offers the ability to use all the machinery for QCD jet matching and merging from PYTHIA inside WHIZARD. WHIZARD also directly interfaces Fastjet [19] for jet clustering. One important feature of WHIZARD is the proper resonance matching of hadronically decaying resonances, e.g., in the process $e^+e^- \rightarrow jjjj$. This is predominantly WW production ($\sim 80\%$), followed by ZZ production ($\lesssim 20\%$) and the QCD four-jet continuum. When simulating full quantum theoretical amplitudes for four-jet production, the parton shower does not know intermediate resonances because of the full coherence of the process, and hence does not preserve the resonance mass of the hadronic Ws. WHIZARD allows one to automatically determine underlying resonance histories, evaluates their approximate rates, and inserts resonance histories for final-state jets according to these rates. Figure C.9.1 shows, for the process $e^+e^- \rightarrow jjjj$, the photon energy distribution after hadronization and hadronic decays. The central line in the inset (red) shows the full process, which disagrees with LEP data, while the blue line shows the factorised process $e^+e^- \rightarrow W^+W^- \rightarrow (jj)(jj)$ (where the shower program knows the resonance history) and the resonance-matched processes (green and orange). These correctly reproduce the data using full matrix elements, thereby allowing different handles on how far to take Breit–Wigner tails of resonances into account. This type of matching has now been validated for six-jet processes, including $H \rightarrow b\bar{b}$.

Finally, we comment on the NLO QCD capabilities of WHIZARD: WHIZARD has completed its final validation phase for lepton collider QCD NLO corrections, and version 3.0.0 will be released (approximately at the end of 2019) when proton collider processes are also completely validated. For NLO QCD corrections, WHIZARD uses the Frixione–Kunszt–Signer subtraction (FKS) formalism [20], where real and integrated subtraction terms are automatically generated for all processes. WHIZARD also implements the resonance-aware variant [21]. Virtual multileg one-loop matrix elements are included from one-loop providers, such as GoSam [22], OpenLoops [23, 24], and RECOLA [25, 26]. First proof-of-principle NLO calculations have been made for electroweak corrections [27, 28] in lepton collisions, while NLO QCD has been implemented for LHC processes first [29, 30]. The automated FKS subtraction has been tested and reported in a study of off-shell $t\bar{t}$ and $t\bar{t}H$ processes in lepton collisions [31]. The complete validation of the automated NLO QCD set-up will be available after the version 3.0.0 release of WHIZARD (S. Braß *et al.*, in preparation). WHIZARD allows fixed-order NLO events for differential distributions to be generated at NLO QCD using weighted events, as well as automatically POWHEG-matched and damped events [32, 33]. Decays at NLO QCD are treated in the same set-up as scattering processes.

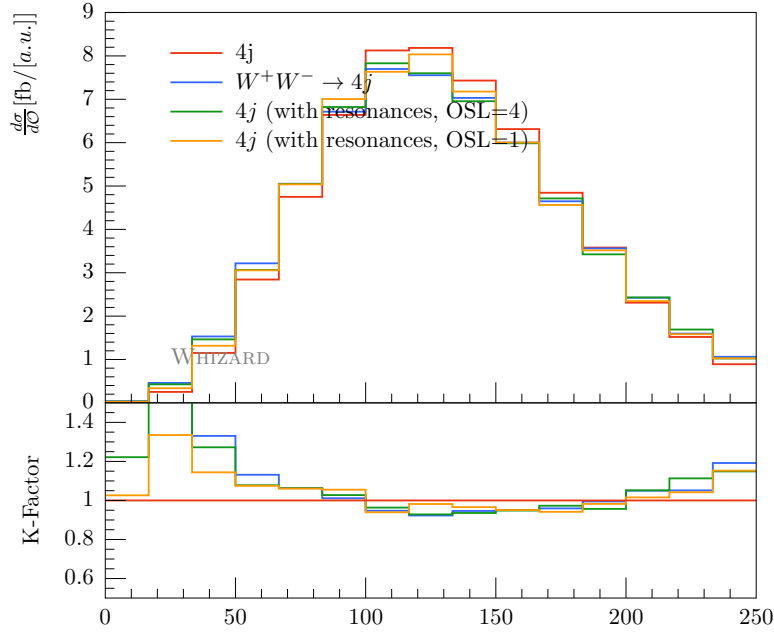


Fig. C.9.1: Energy distribution of photons in $e^+e^- \rightarrow jjjj$ after parton shower and hadronization. Full amplitudes without resonance histories (red), factorised process $e^+e^- \rightarrow W^+W^- \rightarrow (jj)(jj)$ (blue), and full process with resonance histories and different Breit–Wigner settings (green and orange, respectively).

The scan of the top threshold is a crucial component of the FCC-ee physics programme. To determine systematic uncertainties from, e.g., event selection, WHIZARD allows simulation at the completely exclusive final-state $e^+e^- \rightarrow W^+bW^-\bar{b}$, matching the continuum NLO QCD calculation to the NRQCD threshold NLL resummation [34]. This simulation is available via a specific top threshold model inside WHIZARD.

References

- [1] W. Kilian *et al.*, *Eur. Phys. J.* **C71** (2011) 1742. [arXiv:0708.4233](#), [doi:10.1140/epjc/s10052-011-1742-y](#)
- [2] <http://whizard.hepforge.org>, last accessed 24 January 2020.
- [3] H. Baer *et al.*, The international linear collider technical design report, vol. 2: physics (2013), [arXiv:1306.6352](#)
- [4] H. Abramowicz *et al.*, The international linear collider technical design report, vol. 4: detectors, [arXiv:1306.6329](#)
- [5] M. Moretti *et al.*, O’Mega: an optimising matrix element generator, 2001, [arXiv:hep-ph/0102195](#)
- [6] B. Chokoufe Nejad *et al.*, *Comput. Phys. Commun.* **196** (2015) 58. [arXiv:1411.3834](#), [doi:10.1016/j.cpc.2015.05.015](#)
- [7] W. Kilian *et al.*, *JHEP* **10** (2012) 022. [arXiv:1206.3700](#), [doi:10.1007/JHEP10\(2012\)022](#)
- [8] T. Ohl and J. Reuter, *Eur. Phys. J.* **C30** (2003) 525. [arXiv:hep-th/0212224](#), [doi:10.1140/epjc/s2003-01301-7](#)

- [9] K. Hagiwara *et al.*, *Phys. Rev.* **D73** (2006) 055005. [arXiv:hep-ph/0512260](#), [doi:10.1103/PhysRevD.73.055005](#)
- [10] N.D. Christensen *et al.*, *Eur. Phys. J.* **C72** (2012) 1990. [arXiv:1010.3251](#), [doi:10.1140/epjc/s10052-012-1990-5](#)
- [11] T. Ohl, *Comput. Phys. Commun.* **120** (1999) 13. [arXiv:hep-ph/9806432](#), [doi:10.1016/S0010-4655\(99\)00209-X](#)
- [12] S. Brass *et al.*, *Eur. Phys. J.* **C79** (2019) 344. [arXiv:1811.09711](#), [doi:10.1140/epjc/s10052-019-6840-2](#)
- [13] A. Ballestrero *et al.*, *Eur. Phys. J.* **C78** (2018) 671. [arXiv:1803.07943](#), [doi:10.1140/epjc/s10052-018-6136-y](#)
- [14] T. Ohl, *Comput. Phys. Commun.* **101** (1997) 269. [arXiv:hep-ph/9607454](#), [doi:10.1016/S0010-4655\(96\)00167-1](#)
- [15] M. Skrzypek and S. Jadach, *Z. Phys.* **C49** (1991) 577. [doi:10.1007/BF01483573](#)
- [16] W. Kilian *et al.*, *JHEP* **04** (2012) 013. [arXiv:1112.1039](#), [doi:10.1007/JHEP04\(2012\)013](#)
- [17] T. Sjöstrand *et al.*, *JHEP* **05** (2006) 026. [arXiv:hep-ph/0603175](#), [doi:10.1088/1126-6708/2006/05/026](#)
- [18] T. Sjöstrand *et al.*, *Comput. Phys. Commun.* **178** (2008) 852. [arXiv:0710.3820](#), [doi:10.1016/j.cpc.2008.01.036](#)
- [19] M. Cacciari *et al.*, *Eur. Phys. J.* **C72** (2012) 1896. [arXiv:1111.6097](#), [doi:10.1140/epjc/s10052-012-1896-2](#)
- [20] S. Frixione *et al.*, *Nucl. Phys.* **B467** (1996) 399. [arXiv:hep-ph/9512328](#), [doi:10.1016/0550-3213\(96\)00110-1](#)
- [21] T. Jezo and P. Nason, *JHEP* **12** (2015) 065. [arXiv:1509.09071](#), [doi:10.1007/JHEP12\(2015\)065](#)
- [22] G. Cullen *et al.*, *Eur. Phys. J.* **C74** (2014) 3001. [arXiv:1404.7096](#), [doi:10.1140/epjc/s10052-014-3001-5](#)
- [23] F. Cascioli *et al.*, *Phys. Rev. Lett.* **108** (2012) 111601. [arXiv:1111.5206](#), [doi:10.1103/PhysRevLett.108.111601](#)
- [24] F. Buccioni *et al.*, *Eur. Phys. J.* **C78** (2018) 70. [arXiv:1710.11452](#), [doi:10.1140/epjc/s10052-018-5562-1](#)
- [25] S. Actis *et al.*, *Comput. Phys. Commun.* **214** (2017) 140. [arXiv:1605.01090](#), [doi:10.1016/j.cpc.2017.01.004](#)
- [26] A. Denner *et al.*, *Comput. Phys. Commun.* **224** (2018) 346. [arXiv:1711.07388](#), [doi:10.1016/j.cpc.2017.11.013](#)
- [27] W. Kilian *et al.*, *Eur. Phys. J.* **C48** (2006) 389. [arXiv:hep-ph/0607127](#), [doi:10.1140/epjc/s10052-006-0048-y](#)
- [28] T. Robens *et al.*, *Acta Phys. Pol.* **B39** (2008) 1705. [arXiv:0803.4161](#)
- [29] T. Binoth *et al.*, *Phys. Lett.* **B685** (2010) 293. [arXiv:0910.4379](#), [doi:10.1016/j.physletb.2010.02.010](#)
- [30] N. Greiner *et al.*, *Phys. Rev. Lett.* **107** (2011) 102002. [arXiv:1105.3624](#), [doi:10.1103/PhysRevLett.107.102002](#)

- [31] B. Chokoufe Nejad *et al.*, *JHEP* **12** (2016) 075. [arXiv:1609.03390](#),
[doi:10.1007/JHEP12\(2016\)075](#)
- [32] B. Chokoufe Nejad *et al.*, *PoS EPS-HEP2015* (2015) 317. [arXiv:1510.02739](#), [doi:10.22323/1.234.0317](#)
- [33] J. Reuter *et al.*, *J. Phys. Conf. Ser.* **762** (2016) 012059. [arXiv:1602.06270](#),
[doi:10.1088/1742-6596/762/1/012059](#)
- [34] F. Bach *et al.*, *JHEP* **03** (2018) 184. [arXiv:1712.02220](#), [doi:10.1007/JHEP03\(2018\)184](#)

10 FCC tau polarisation

Contribution* by: **S. Banerjee, Z. Was**

Corresponding author: **Z. Was** [z.was@cern.ch]

SM parameters, such as the τ polarisation can be measured very precisely in τ decays. The phenomenology is quite similar to that of measurement of the A_{FB} parameter of the SM [1]. Details of the τ decay spectrum, as well as a good understanding of associated uncertainty, play an important role in this measurement of polarisation, because the spin of the τ lepton is not measured directly.

The distribution of hadronic final-state products in decays of a τ lepton needs to be evaluated to understand the substructure of the vertex. An important effect is related to bremsstrahlung, because the signature of every decay mode needs to take into account the final-state configurations with accompanying photons. Corresponding virtual corrections cancel the bulk of these effects and specialised programs, such as PHOTOS [2, 3], are useful.

Corresponding effects can be sizeable; even during the early stages of LEP preparations, it was found [4] that the corresponding corrections affect the slope of the π spectrum in $\tau^- \rightarrow \pi^- \nu$, for example. This translates to a 0.013 effect on τ idealised observable A_{pol} . For more discussion and essential experimental context, see Ref. [5].

However, not all of the final-state photons can be associated with bremsstrahlung. For example, in the cascade decay $\tau^- \rightarrow \pi^- \omega \nu$, a subsequent decay of $\omega \rightarrow \pi^0 \gamma$ contributes to the final state $\tau^- \rightarrow \pi^- \pi^0 \gamma \nu$, coinciding with the radiative corrections to the final state of the $\tau^- \rightarrow \rho^- \nu$ decay channel. In this case, the photon originates from the $\omega \rightarrow \pi^0 \gamma$ decay and is of non-QED bremsstrahlung origin.

The branching fractions for the $\tau^- \rightarrow \pi^- \omega \nu$ decay and for the $\omega \rightarrow \pi^0 \gamma$ decay are 0.02 and 0.08, respectively [6]. Thus, the resulting decay channel $\tau^- \rightarrow \pi^- \pi^0 \gamma \nu$ contributes 0.0015 of all τ decays.

Such contributions and subsequent changes of the hadronic decay energy spectrum in τ decays need to be understood for each spin-sensitive channel. Resulting deformation of $\tau^- \rightarrow \rho^- \nu$ decay spectra may mimic the contribution of the τ polarisation that can be obtained from future high-precision data analysis at the Belle II experiment.

This is the case when one of the τ decay channels mimics bremsstrahlung correction for the other one. The dynamics of the low-energy strong interactions are difficult to obtain from a perturbative calculation.

Another hint of the non-point-like nature of the τ vertex was explained in the corrections to the π energy spectra in the $\tau^- \rightarrow \pi^- \nu$ decay channel [7, 8]. Although at the lowest order, the spectrum is fully determined by the Lorentz structure of the vertex, and the real and virtual photonic corrections play an important role in the level of precision under discussion. The dominant part of the effects of the QED bremsstrahlung from point-like sources can be seen in Fig. 3 of Ref. [8], where the effects induced by hadronic resonances also play an important role.

The Belle II experiment is expected to collect 10^{11} τ lepton decays with 50 ab^{-1} of data,

*This contribution should be cited as:

S. Banerjee, Z. Was, FCC tau polarisation, DOI: [10.23731/CYRM-2020-003.211](https://doi.org/10.23731/CYRM-2020-003.211), in: Theory for the FCC-ee, Eds. A. Blondel, J. Gluza, S. Jadach, P. Janot and T. Riemann, CERN Yellow Reports: Monographs, CERN-2020-003, DOI: [10.23731/CYRM-2020-003](https://doi.org/10.23731/CYRM-2020-003), p. 211.
 © CERN, 2020. Published by CERN under the [Creative Commons Attribution 4.0 license](https://creativecommons.org/licenses/by/4.0/).

and the detector is extremely well-suited to study τ lepton physics. The backgrounds can be well-controlled in an electron–positron collider environment. We can expect that the τ decay spectra can be measured without large degradation, owing to a highly granular electromagnetic calorimeter with large fiducial coverage, as explained in the Belle II technical design report [9].

References

- [1] A. Blondel *et al.*, Standard Model theory for the FCC-ee Tera-Z stage, (CERN-2019-003), [arXiv:1809.01830](#), [doi:10.23731/CYRM-2019-003](#)
- [2] E. Barberio and Z. Was, *Comput. Phys. Commun.* **79** (1994) 291. [doi:10.1016/0010-4655\(94\)90074-4](#)
- [3] N. Davidson *et al.*, *Comput. Phys. Commun.* **199** (2016) 86. [arXiv:1011.0937](#), [doi:10.1016/j.cpc.2015.09.013](#)
- [4] F. Boillot and Z. Was, *Z. Phys.* **C43** (1989) 109. [doi:10.1007/BF02430616](#)
- [5] LEP Electroweak Working Group, Precision electroweak measurements and constraints on the Standard Model, [arXiv:1012.2367](#)
- [6] M. Tanabashi *et al.*, *Phys. Rev.* **D98** (2018) 030001. [doi:10.1103/PhysRevD.98.030001](#)
- [7] R. Decker and M. Finkemeier, *Phys. Lett.* **B316** (1993) 403. [arXiv:hep-ph/9307372](#), [doi:10.1016/0370-2693\(93\)90345-I](#)
- [8] R. Decker and M. Finkemeier, *Nucl. Phys. Proc. Suppl.* **40** (1995) 453. [arXiv:hep-ph/9411316](#), [doi:10.1016/0920-5632\(95\)00170-E](#)
- [9] T. Abe *et al.*, Belle II technical design report, [arXiv:1011.0352](#)

11 Electron–positron annihilation processes in MCSAN_{Cee}

Contribution* by: A. Arbuzov, S. Bondarenko, Y. Dydyshka, L. Kalinovskaya, L. Rumyantsev, R. Sadykov, V. Yermolchyk

Corresponding author: A. Arbuzov [arbuzov@theor.jinr.ru]

The Monte Carlo event generator MCSAN_{Cee} is used to estimate the significance of polarisation effects in one-loop electroweak radiative corrections. The electron–positron annihilation processes $e^+e^- \rightarrow \mu^-\mu^+$ ($\tau^-\tau^+$, ZH) are considered, taking into account conditions of future colliders.

11.1 Introduction

Radiative corrections with effects due to polarisation of the initial particles will play an important role in the high-precision programme at the FCC-ee. MCSAN_{Cee} is a Monte Carlo generator of unweighted events for polarised e^+e^- scattering and annihilation processes with complete one-loop electroweak (EW) corrections. The generator uses the adaptive Monte Carlo algorithm mFOAM [1], which is a part of the ROOT [2] framework.

The SANC computer system is capable of calculating cross-sections of general Standard Model (SM) processes with up to three final-state particles [3, 4]. Using the SANC system, we calculated electroweak radiative corrections at the one-loop level to the polarised Bhabha scattering [5, 6], which is the basic normalization process at e^+e^- colliders. For processes

$$e^+e^- \rightarrow \mu^-\mu^+ (\tau^-\tau^+, ZH), \quad (11.1)$$

we made a few upgrades of the standard procedures in the SANC system. We investigated the effect of the polarisation degrees of initial particles on the differential cross-sections. We found that the EW corrections to the total cross-section range from -18% to $+69\%$, when the centre-of-mass energy \sqrt{s} varies in the set 250 GeV, 500 GeV, and 1 TeV.

11.2 Cross-section structure

The cross-section of a generic $2 \rightarrow 2(\gamma)$ process $e^+e^- \rightarrow X_3X_4(\gamma)$ ($X_3X_4 = \mu^-\mu^+, \tau^-\tau^+, ZH$) reads

$$\sigma_{P_{e^-}P_{e^+}} = \frac{1}{4} \sum_{\chi_1, \chi_2} (1 + \chi_1 P_{e^-})(1 + \chi_2 P_{e^+}) \sigma_{\chi_1 \chi_2},$$

where $\chi_i = -1(+1)$ corresponds to a lepton with left (right) helicity state.

The cross-section at the one-loop level can be divided into four parts:

$$\sigma^{1\text{-loop}} = \sigma^{\text{Born}} + \sigma^{\text{virt}}(\lambda) + \sigma^{\text{soft}}(\lambda, \omega) + \sigma^{\text{hard}}(\omega),$$

where σ^{Born} is the Born level cross-section, σ^{virt} is the virtual (loop) contribution, σ^{soft} is the contribution due to soft-photon emission, and σ^{hard} is the contribution due to hard photon

*This contribution should be cited as:

A. Arbuzov, S. Bondarenko, Y. Dydyshka, L. Kalinovskaya, L. Rumyantsev, R. Sadykov, V. Yermolchyk, Electron–positron annihilation processes in MCSAN_{Cee}, DOI: [10.23731/CYRM-2020-003.213](https://doi.org/10.23731/CYRM-2020-003.213), in: Theory for the FCC-ee, Eds. A. Blondel, J. Gluza, S. Jadach, P. Janot and T. Riemann, CERN Yellow Reports: Monographs, CERN-2020-003, DOI: [10.23731/CYRM-2020-003](https://doi.org/10.23731/CYRM-2020-003), p. 213. © CERN, 2020. Published by CERN under the [Creative Commons Attribution 4.0 license](https://creativecommons.org/licenses/by/4.0/).

emission (with energy $E_\gamma > \omega$). Auxiliary parameters λ ('photon mass') and ω cancel out after summation.

We treat all contributions using the helicity amplitudes approach:

$$\sigma_{\chi_1\chi_2}^{\text{Part}} = \frac{1}{2s} \sum_{\chi_i, i \geq 3} \left| \mathcal{H}_{\chi_1\chi_2\chi_3, \dots}^{\text{Part}} \right|^2 d\text{LIPS}, \quad (11.2)$$

where $\text{Part} \in \{\text{Born}, \text{virt}, \text{hard}\}$, and $d\text{LIPS}$ is a volume element of the Lorentz-invariant phase space.

The soft-photon contribution is factorised in front of the Born level cross-section:

$$d\sigma_{\chi_1\chi_2}^{\text{soft}} = d\sigma_{\chi_1\chi_2}^{\text{Born}} \cdot \frac{\alpha}{2\pi} K^{\text{soft}}(\omega, \lambda).$$

11.3 Numerical results and comparison

The following input parameters are used for numerical estimates and comparisons:

$$\begin{aligned} \alpha^{-1}(0) &= 137.035\,999\,76, \\ M_W &= 80.451\,495\,8 \text{ GeV}, & M_Z &= 91.1876 \text{ GeV}, & \Gamma_Z &= 2.499\,77 \text{ GeV}, \\ m_e &= 0.510\,999\,07 \text{ MeV}, & m_\mu &= 0.105\,658\,389 \text{ GeV}, & m_\tau &= 1.777\,05 \text{ GeV}, \\ m_d &= 0.083 \text{ GeV}, & m_s &= 0.215 \text{ GeV}, & m_b &= 4.7 \text{ GeV}, \\ m_u &= 0.062 \text{ GeV}, & m_c &= 1.5 \text{ GeV}, & m_t &= 173.8 \text{ GeV}. \end{aligned}$$

The following simple cuts are imposed:

$$\begin{aligned} |\cos\theta| &< 0.9, \\ E_\gamma &> 1 \text{ GeV} \quad (\text{for comparison of hard bremsstrahlung}). \end{aligned}$$

Tuned comparison of our results for polarised Born and hard bremsstrahlung with the results of the `WHIZARD` [7] and `CalCHEP` [8] programs shows an agreement within statistical errors. The unpolarised *soft + virtual* contribution agrees with the results of Ref. [9] for $e^+e^- \rightarrow \mu^+\mu^-(\tau^+\tau^-)$ and with the ones of the `GRACE` system [10]. For $e^+e^- \rightarrow \text{ZH}$, we found an agreement with the results of the `GRACE` system [10] and with those given in Ref. [11].

The integrated cross-sections of Eq. (11.1) and the relative corrections δ are given in Tables C.11.1 [12] and C.11.2 [13] for various energies and beam polarisation degrees.

In these tables, we summarise the estimates of the Born and one-loop cross-sections and the relative corrections δ of the processes $e^+e^- \rightarrow \mu^+\mu^-, (\tau^+\tau^-, \text{ZH})$ for the set $(0, 0; -0.8, 0; -0.8, -0.6; -0.8, +0.6)$ of longitudinal polarisations P_{e^+} and P_{e^-} of the positron and electron beams, respectively. Values of energy 250, 500, and 1000 GeV were taken. The relative correction δ is defined as

$$\delta = \frac{\sigma^{\text{1-loop}} - \sigma^{\text{Born}}}{\sigma^{\text{Born}}} \cdot 100\%. \quad (11.3)$$

11.4 Conclusion

As can be seen from Tables C.11.1 and C.11.2, the difference between values of δ for polarisation degrees of initial particles $(0, 0)$ and $(-0.8, 0; -0.8, -0.6; -0.8, +0.6)$ amounts to a significant value: 6–20%.

Table C.11.1: Processes $e^+e^- \rightarrow \mu^+\mu^-$ and $e^+e^- \rightarrow \tau^+\tau^-$: Born vs one loop

P_{e^-}, P_{e^+}	$\sigma_{\mu^+\mu^-}^{\text{Born}}$ (pb)	$\sigma_{\mu^+\mu^-}^{1\text{-loop}}$ (pb)	δ (%)	$\sigma_{\tau^+\tau^-}^{\text{Born}}$ (pb)	$\sigma_{\tau^+\tau^-}^{1\text{-loop}}$ (pb)	δ (%)
$\sqrt{s} = 250 \text{ GeV}$						
0, 0	1.417(1)	2.397(1)	69.1(1)	1.417(1)	2.360(1)	66.5(1)
-0.8, 0	1.546(1)	2.614(1)	69.1(1)	1.546(1)	2.575(1)	66.5(1)
-0.8, -0.6	0.7690(2)	1.301(1)	69.2(1)	0.7692(1)	1.298(1)	68.8(1)
-0.8, +0.6	2.323(1)	3.927(1)	69.1(1)	2.324(1)	3.850(1)	65.7(1)
$\sqrt{s} = 500 \text{ GeV}$						
0, 0	0.3436(1)	0.4696(1)	36.7(1)	0.3436(1)	0.4606(1)	34.0(3)
-0.8, 0	0.3716(1)	0.4953(1)	33.3(1)	0.3715(1)	0.4861(1)	30.8(1)
-0.8, -0.6	0.1857(1)	0.2506(1)	35.0(1)	0.1857(1)	0.2466(1)	32.8(1)
-0.8, +0.6	0.5575(1)	0.7399(1)	32.7(1)	0.5575(1)	0.7257(1)	30.1(1)
$\sqrt{s} = 1000 \text{ GeV}$						
0, 0	0.08535(1)	0.1163(1)	36.2(1)	0.08534(2)	0.1134(1)	33.6(1)
-0.8, 0	0.09213(1)	0.1212(1)	31.6(1)	0.09213(1)	0.11885(2)	29.0(1)
-0.8, -0.6	0.04608(1)	0.06169(1)	33.9(1)	0.04608(1)	0.06067(1)	31.7(1)
-0.8, +0.6	0.1382(1)	0.1807(1)	30.8(1)	0.1382(1)	0.1770(1)	28.1(1)

 Table C.11.2: Process $e^+e^- \rightarrow ZH$: Born vs one loop

P_{e^-}, P_{e^+}	$\sigma_{ZH}^{\text{Born}}$ (pb)	$\sigma_{ZH}^{1\text{-loop}}$ (pb)	δ (%)
$\sqrt{s} = 250 \text{ GeV}$			
0, 0	205.64(1)	186.6(1)	-9.24(1)
-0.8, 0	242.55(1)	201.5(1)	-16.94(1)
-0.8, -0.6	116.16(1)	100.8(1)	-13.25(1)
-0.8, +0.6	368.93(1)	302.2(1)	-18.10(1)
$\sqrt{s} = 500 \text{ GeV}$			
0, 0	51.447(1)	57.44(1)	11.65(1)
-0.8, 0	60.680(1)	62.71(1)	3.35(2)
-0.8, -0.6	29.061(1)	31.25(1)	7.54(1)
-0.8, +0.6	92.299(1)	94.17(2)	2.03(2)
$\sqrt{s} = 1000 \text{ GeV}$			
0, 0	11.783(1)	12.92(1)	9.68(1)
-0.8, 0	13.898(1)	13.91(1)	0.10(2)
-0.8, -0.6	6.6559(1)	6.995(1)	5.09(2)
-0.8, +0.6	21.140(1)	20.83(1)	-1.47(2)

In assessing theoretical uncertainties for future e^+e^- colliders, it is necessary to achieve an accuracy of approximately 10^{-4} for many observables. Estimating the value of δ at different degrees of polarisation of the initial states, we see that taking beam polarisation into account is crucial.

Further development of the process library of the Monte Carlo generator MCSAN_{Cee} involves $e^+e^- \rightarrow \gamma\gamma$ (plus cross-symmetric processes) and ('W fusion') $e^+e^- \rightarrow \nu_e\nu_e H$. We have started work on the introduction of higher-order corrections, as well as on the implementation of multiphoton emission contributions.

References

- [1] S. Jadach and P. Sawicki, *Comput. Phys. Commun.* **177** (2007) 441. [arXiv:physics/0506084](#), [doi:10.1016/j.cpc.2007.02.112](#)
- [2] <https://root.cern.ch>, last accessed 27 January 2020.
- [3] A. Andonov *et al.*, *Comput. Phys. Commun.* **174** (2006) 481 [Erratum: **177** (2007) 623]. [arXiv:hep-ph/0411186](#), [doi:10.1016/j.cpc.2005.12.006](#), [doi:10.1016/j.cpc.2007.06.010](#)
- [4] A. Arbuzov *et al.*, *JETP Lett.* **103** (2016) 131. [arXiv:1509.03052](#), [doi:10.1134/S0021364016020041](#)
- [5] D. Bardin *et al.*, *Phys. Rev.* **D98** (2018) 013001. [arXiv:1801.00125](#), [doi:10.1103/PhysRevD.98.013001](#)
- [6] A. Blondel *et al.*, Standard Model theory for the FCC-ee Tera-Z stage, (CERN-2019-003), [arXiv:1809.01830](#), [doi:10.23731/CYRM-2019-003](#)
- [7] W. Kilian *et al.*, *Eur. Phys. J.* **C71** (2011) 1742. [arXiv:0708.4233](#), [doi:10.1140/epjc/s10052-011-1742-y](#)
- [8] A. Belyaev *et al.*, *Comput. Phys. Commun.* **184** (2013) 1729. [arXiv:1207.6082](#), [doi:10.1016/j.cpc.2013.01.014](#)
- [9] A. Lorca and T. Riemann, *Comput. Phys. Commun.* **174** (2006) 71. [arXiv:hep-ph/0412047](#), [doi:10.1016/j.cpc.2005.09.003](#)
- [10] G. Belanger *et al.*, *Phys. Rep.* **430** (2006) 117. [arXiv:hep-ph/0308080](#), [doi:10.1016/j.physrep.2006.02.001](#)
- [11] A. Denner and S. Dittmaier, *Nucl. Phys.* **B398** (1993) 265. [doi:10.1016/0550-3213\(93\)90109-3](#)
- [12] R. Sadykov, MCSAN_{Cee} generator with one-loop electroweak corrections for processes with polarised e^+e^- beams, aCAT, Saas Fee, Switzerland, 2019, https://indico.cern.ch/event/708041/contributions/3266626/attachments/1810462/2956579/ACAT19_Sadykov.pdf
- [13] S. Bondarenko *et al.*, *Phys. Rev.* **D100** (2019) 073002. [arXiv:1812.10965](#), [doi:10.1103/PhysRevD.100.073002](#)

12 Global electroweak fit in the FCC-ee era

Contribution* by: J. Erler, M. Schott

Corresponding author: J. Erler [erler@fisica.unam.mx]

The top quark and Higgs boson masses have been predicted before their respective discoveries by the global fit of the Standard Model to electroweak precision data. With the Higgs boson discovery and the measurement of its mass, the last missing parameter of the Standard Model has been fixed and thus the internal consistency of the Standard Model can be probed at a new level by comparing direct measurements with the indirect predictions of the global electroweak fit. In this section, we discuss the expected precisions in the most important indirect predictions that are expected in the FCC-ee era and compare them with the state of the art.

Global electroweak analyses and fits have a long history in particle physics, starting before the discovery of the W and Z bosons. The basic idea of the global electroweak fit is the comparison of the state-of-the-art calculations of the electroweak precision observables with the most recent experimental data to constrain the free parameters of the fit and to test the goodness of fit. The free parameters of the SM relevant for the global electroweak analysis are the coupling constant of the electromagnetic, weak, and strong interactions, as well as the masses of the elementary fermions and bosons. This number can be reduced by fixing parameters with insignificant uncertainties compared with the sensitivity of the fit, as well as imposing the relations of the electroweak unification. The typical floating parameters chosen in the fit are the masses of the Z and the Higgs boson, the top, the bottom, and charm quark masses, and the coupling parameters $\Delta\alpha_5$ and $\alpha_S(m_Z)$. An introduction and a review of the current status of the global electroweak fit can be found in Ref. [1].

Besides a global analysis of the consistency between observables and their relations, the global electroweak fit can be used to indirectly determine and hence predict the expected values of observables. Technically, this indirect parameter determination is performed by scanning the parameter in a chosen range and calculating the corresponding χ^2 values. It should be noted that the value of χ_{\min}^2 is not relevant for the uncertainty estimation, only its difference relative to the global minimum, $\Delta\chi^2 := \chi^2 - \chi_{\min}^2$.

These indirect determinations have been recently performed with the latest measured values of electroweak precision observables in Ref. [1] and the state-of-the-art fitting frameworks GAPP and Gfitter. While GAPP (Global Analysis of Particle Properties) [2] is a Fortran library for the evaluations of pseudo-observables, Gfitter consist of independent object-oriented C++ code [3]. Both frameworks yield consistent results. Selected input parameters of the fit, including their current experimental uncertainty, are summarised in Table C.12.1, while the $\Delta\chi^2$ distributions for the indirect determinations of M_H , M_W , and m_{top} are summarised in Figure C.12.1.

We repeat the indirect fit of these observables using the GAPP program, mainly by assuming the FCC-ee projections and target uncertainties from Refs. [4, 5], as well as non-dominant theory uncertainties from unknown higher orders. It should be noted that the uncer-

*This contribution should be cited as:

J. Erler, M. Schott, Global electroweak fit in the FCC-ee era, DOI: [10.23731/CYRM-2020-003.217](https://doi.org/10.23731/CYRM-2020-003.217), in: Theory for the FCC-ee, Eds. A. Blondel, J. Gluza, S. Jadach, P. Janot and T. Riemann, CERN Yellow Reports: Monographs, CERN-2020-003, DOI: [10.23731/CYRM-2020-003](https://doi.org/10.23731/CYRM-2020-003), p. 217.
 © CERN, 2020. Published by CERN under the [Creative Commons Attribution 4.0 license](https://creativecommons.org/licenses/by/4.0/).

Table C.12.1: Overview of selected observables, their values, and current uncertainties, which are used or determined within the global electroweak fit [1]. The future expected FCC-ee uncertainties are also shown [4, 5].

Parameter	Current value	FCC-ee unc.-target	Parameter	Current value	FCC-ee unc.-target
M_H	125.09 ± 0.15 GeV	± 0.01 GeV	M_Z	91.1875 ± 0.0021 GeV	< 0.1 MeV
M_W	80.380 ± 0.013 GeV	± 0.6 MeV	Γ_Z	2.4952 ± 0.0023 GeV	25 keV
Γ_W	2.085 ± 0.042 GeV	± 1.0 MeV	σ_{had}^0	41.540 ± 0.037 nb	0.004 nb
m_{top}	172.90 ± 0.47 GeV	± 15 MeV	R_b	0.21629 ± 0.00066	< 0.00006
$\Delta\alpha_{\text{had}} [\times 10^{-5}]$	2758 ± 10	± 3	$A_{\text{LR}}^{\text{FB}}(b)$	0.0992 ± 0.0016	± 0.0001

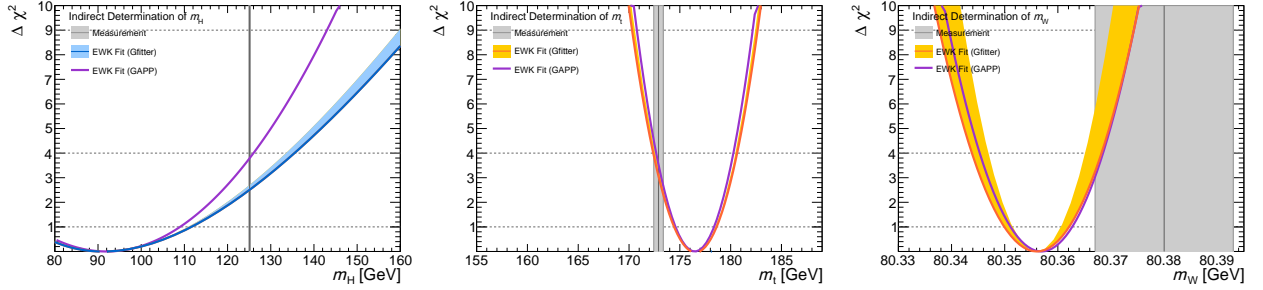


Fig. C.12.1: Comparisons of χ^2 distributions for scanning different observables using the Gitter and the GAPP, using the current experimental values and uncertainties. Theoretical uncertainties are indicated by the filled blue and yellow areas, respectively.

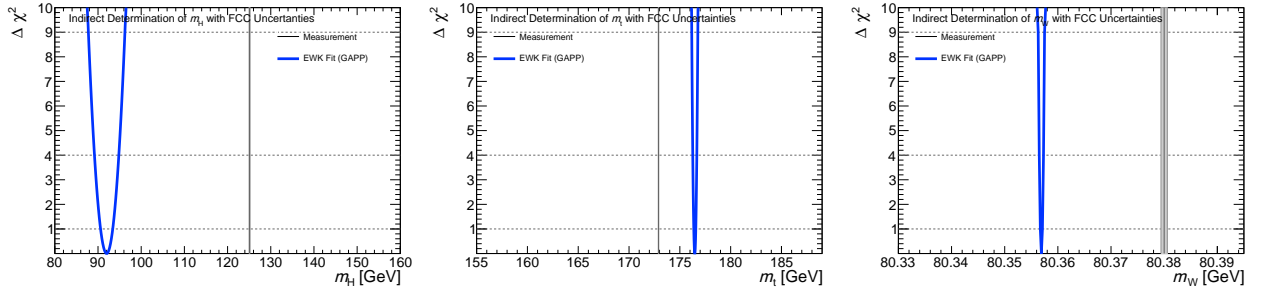


Fig. C.12.2: Comparisons of χ^2 distributions for scanning different observables using GAPP with the current experimental values but the expected uncertainties from FCC.

tainty in the weak mixing angle is assumed to be $\pm 5 \times 10^{-6}$ during the fit.[†]

Similar studies have been previously performed [6, 7]. Of special importance are the significantly lower uncertainties in m_Z , m_W , and m_{top} (Table C.12.1), which could be reduced by an order of magnitude. The $\Delta\chi^2$ distributions for M_H , M_W , and m_{top} are summarised in Figure C.12.2, yielding precisions of the indirect determinations of $\Delta M_H = \pm 1.4$ GeV, $\Delta M_W = \pm 0.2$ MeV, and $\Delta m_{\text{top}} = \pm 0.1$ GeV. Thus, the indirect test of the internal consistency of the electroweak sector would be brought to a new level. The uncertainty in m_H increases from ± 1.4 GeV to ± 5.7 GeV, if no advances are made on the theory side. Likewise, the expected uncertainty in the indirectly determined value of $\Delta\alpha_{\text{had}}$ increases from 0.05% to 0.1%. Last but

[†]This uncertainty combines the expected measurement precision of the asymmetry observables, i.e., it can be seen as a combination of $A^{\text{FB}}(\mu)$, $A^{\text{FB}}(b)$ and the τ polarisation measurements.

not least, the number of active neutrinos N_ν can be constrained at FCC-ee within ± 0.0006 , compared with the current result $N_\nu = 2.992 \pm 0.007$.

References

- [1] J. Erler and M. Schott, *Prog. Part. Nucl. Phys.* **106** (2019) 68. [arXiv:1902.05142](#), [doi:10.1016/j.pnpnp.2019.02.007](#)
- [2] J. Erler, Global fits to electroweak data using GAPP, QCD and Weak Boson Physics in Run II. Proc., Batavia, USA, 1999, [arXiv:hep-ph/0005084](#)
- [3] J. Haller *et al.*, *Eur. Phys. J.* **C78** (2018) 675. [arXiv:1803.01853](#), [doi:10.1140/epjc/s10052-018-6131-3](#)
- [4] M. Bicer *et al.*, *JHEP* **01** (2014) 164. [arXiv:1308.6176](#), [doi:10.1007/JHEP01\(2014\)164](#)
- [5] A. Abada *et al.*, *Eur. Phys. J. Spec. Top.* **228** (2019) 261. [doi:10.1140/epjst/e2019-900045-4](#)
- [6] M. Baak *et al.*, *Eur. Phys. J.* **C74** (2014) 3046. [arXiv:1407.3792](#), [doi:10.1140/epjc/s10052-014-3046-5](#)
- [7] P. Azzurri *et al.*, Physics behind precision, [arXiv:1703.01626](#)

Chapter D

SMEFT

1 CoDEx: BSM physics being realised as SMEFT

Contribution* by: S.D. Bakshi, J. Chakraborty, S.K. Patra
Corresponding author: S.D. Bakshi [sdbakshi13@gmail.com]

Program summary

Program title: CoDEx

Version: 1.0.0

Licensing provisions: CC By 4.0

Programming language: Wolfram Language®

Mathematica® Version: 10+

URL: <https://effexteam.github.io/CoDEx>

Send BUG reports and questions: effex.package@gmail.com

1.1 Introduction

In spite of the non-observation of any new resonances after the discovery of the Standard Model (SM) Higgs-like particle, which announces the success of the SM, we have enough reason to believe the existence of theories beyond it (BSM), with the SM as a part. As any such theory will affect the electroweak and the Higgs sector, and the sensitivity of these precision observables is bound to increase in the near future, indirect estimation of the allowed room left for BSM using Standard Model effective field theory (SMEFT) is well motivated.

Provided that the S-matrix can be expanded perturbatively in the inverse powers of the ultraviolet scale (Λ^{-1}), and the resultant series is convergent, we can integrate out heavy degrees of freedom and the higher mass dimensional operators capture their impact through $-\sum_i (1/\Lambda^{d_i-4}) C_i \mathcal{O}_i$, where d_i is the operator mass dimension (>5), and C_i , a function of BSM parameters, is the corresponding Wilson coefficient. Among different choices of operator base, we restrict ourselves to ‘**SILH**’ [1, 2] and ‘**Warsaw**’ [3–6] bases. All WCs are computed at the cut-off scale Λ , usually identified as the mass of the heavy field. The truncation the $1/\Lambda$ series depends on the experimental precision of the observables [7]. Already, there has been quite good progress in building packages and libraries [8–13].

One can justifiably question the validity of choosing to use SMEFT over the full BSM Lagrangian; the answer lies in the trade-off between the computational challenge of the full BSM and the precision of the observables. The choice of Λ ensures the convergence of the M_Z/Λ series. Using the anomalous dimension matrix (γ) (which is basis dependent), the SMEFT WCs

*This contribution should be cited as:

S.D. Bakshi, J. Chakraborty, S.K. Patra, CoDEx: BSM physics being realised as SMEFT, DOI: [10.23731/CYRM-2020-003.221](https://doi.org/10.23731/CYRM-2020-003.221), in: Theory for the FCC-ee, Eds. A. Blondel, J. Gluza, S. Jadach, P. Janot and T. Riemann, CERN Yellow Reports: Monographs, CERN-2020-003, DOI: [10.23731/CYRM-2020-003](https://doi.org/10.23731/CYRM-2020-003), p. 221.
© CERN, 2020. Published by CERN under the [Creative Commons Attribution 4.0 license](https://creativecommons.org/licenses/by/4.0/).

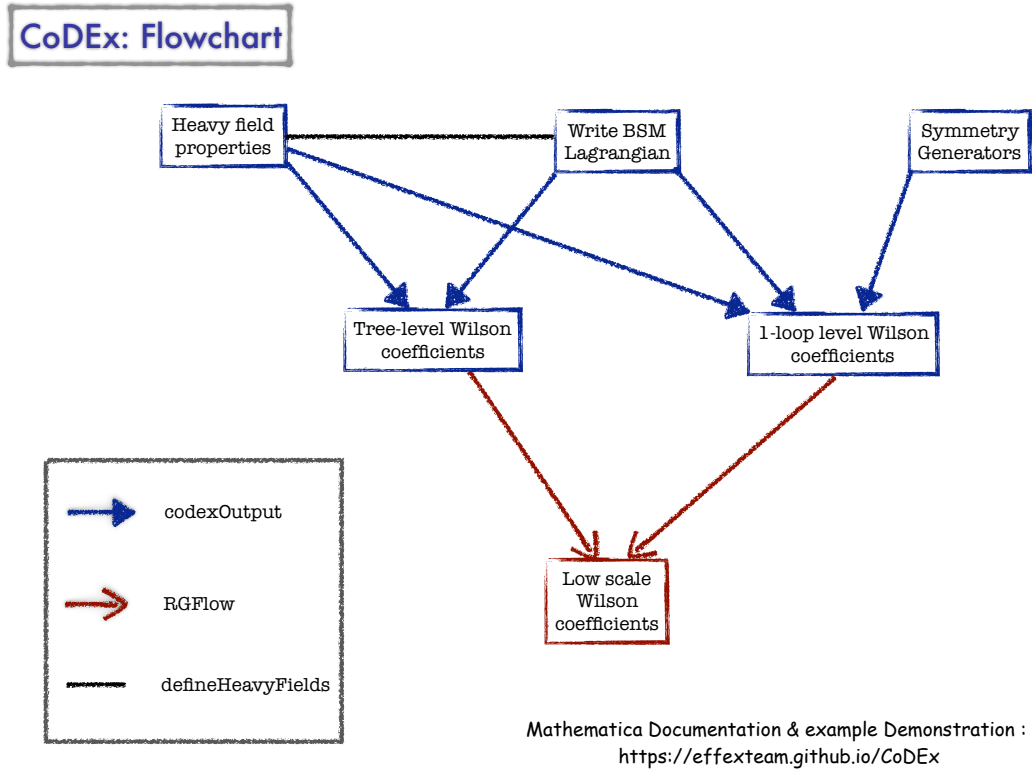


Fig. D.1.1: Flow-chart demonstrating the working principle of CoDEx

$C_i(\Lambda)$ (computed at Λ) are evolved to $C_i(M_Z)$, some of which are absent at the Λ scale, as the matrix γ contains non-zero off-diagonal elements. See Refs. [4–6, 14] regarding the running of the SMEFT operators. We need to choose only those ‘complete’ bases in which the precision observables are defined.

CoDEx, a *Mathematica*[®] package [15], in addition to integrating out the heavy field propagators from tree and one-loop processes and generating SMEFT operators up to dimension-6, provides the WCs as a function of BSM parameters (Fig. D.1.1). In this draft, we briefly discuss the underlying principle of **CoDEx**, and give one illustrative example of the workflow. Details about downloading, installation, and detailed documentation of the functions are available at the website [16].

1.2 The package in detail

CoDEx is a Wilson coefficient calculator, developed in the Mathematica environment. The algorithm of this code is based on the ‘covariant derivative expansion’ method discussed in Refs. [17–31]. Each and every detail of this package can be found in Ref. [16]. The main functions provided by this program are given in Table D.1.1. Here we have demonstrated the working methodology of **CoDEx** with an explicit example.

Table D.1.1: Main functions provided by CoDEx

Function	Details
<code>CoDExHelp</code>	Opens the CoDEx guide, with all help files listed
<code>treeOutput</code>	Calculates WCs generated from tree-level processes
<code>loopOutput</code>	Calculates WCs generated from one-loop processes
<code>codexOutput</code>	Generic function for WC calculation with choices for level, bases, etc., given with OptionValues
<code>defineHeavyFields</code>	Creates representation of heavy fields
<code>texTable</code>	Use the output to construct BSM Lagrangian Given a List , returns the L ^A T _E X output of a tabular environment, displayed or copied to clipboard*
<code>formPick</code>	Applied on a list of WCs from a specific operator basis, reformats the output in the specified style
<code>RGFlow</code>	RG Flow of WCs of dim. 6 operators in ‘ Warsaw ’ basis, from matching scale to a lower (arbitrary) scale
<code>initializeLoop</code>	Prepares the Isospin and colour symmetry generators for a specific model with a specific heavy field content: <code>loopOutput</code> can only be run after this step is completed

*This is a simplified version of the package titled `TeXTableForm` [32].

1.2.1 Detailed example: electroweak $SU(2)_L$ triplet scalar with hypercharge $Y = 1$

Here, we have demonstrated the workflow of **CoDEx** with the help of a complete analysis of a representative model.

$$\mathcal{L}_{\text{BSM}} = \mathcal{L}_{\text{SM}} + \text{Tr}[(\mathcal{D}_\mu \Delta)^\dagger (\mathcal{D}^\mu \Delta)] - m_\Delta^2 \text{Tr}[\Delta^\dagger \Delta] + \mathcal{L}_Y - V(H, \Delta), \quad (1.1)$$

where

$$V(H, \Delta) = \zeta_1 (H^\dagger H) \text{Tr}[\Delta^\dagger \Delta] + \zeta_2 (H^\dagger \tau^i H) \text{Tr}[\Delta^\dagger \tau^i \Delta] + [\mu (H^T i \sigma^2 \Delta^\dagger H) + \text{h.c.}], \quad (1.2)$$

$$\text{and } \mathcal{L}_Y = y_\Delta L^T C i \tau^2 \Delta L + \text{h.c.} \quad (1.3)$$

Here, the heavy field is Δ . Once this heavy field, Δ , is integrated out using **CoDEx**, the effective operators up to dimension-6 for both bases are generated. The effective operators and their respective Wilson coefficients are listed in Tables D.1.2 to D.1.4. Next, we give the exact steps that must be followed to run the code and compute the desired results.

1. First, load the package:

```
In[1]:= Needs["CoDEx"]
```

2. We have to define the field Δ as:

```
fields =
{
{fieldName, components, colorDim, isoDim,
hyperCharge, spin, mass}
};
```

Table D.1.2: Effective operators and Wilson coefficients in ‘SILH’ basis for complex triplet scalar ($Y = 1$) model.

O_{2B}	$\frac{g_Y^2}{160\pi^2 m_\Delta^2}$
O_{2W}	$\frac{g_W^2}{240\pi^2 m_\Delta^2}$
O_{3W}	$\frac{g_W^2}{240\pi^2 m_\Delta^2}$
O_6	$-\frac{\zeta_1 \mu^2}{m_\Delta^4} - \frac{\zeta_2 \mu^2}{4m_\Delta^4} - \frac{\zeta_1^3}{4\pi^2 m_\Delta^2} - \frac{\zeta_2^2 \zeta_1}{32\pi^2 m_\Delta^2}$
O_{BB}	$\frac{\zeta_1}{32\pi^2 m_\Delta^2}$
O_H	$\frac{\zeta_1^2}{8\pi^2 m_\Delta^2} + \frac{\mu^2}{2m_\Delta^4}$
O_R	$\frac{\zeta_2^2}{96\pi^2 m_\Delta^2} + \frac{\mu^2}{m_\Delta^4}$
O_T	$\frac{\zeta_2^2}{192\pi^2 m_\Delta^2} - \frac{\mu^2}{2m_\Delta^4}$
O_{WB}	$-\frac{\zeta_2}{96\pi^2 m_\Delta^2}$
O_{WW}	$\frac{\zeta_1}{48\pi^2 m_\Delta^2}$

Table D.1.3: Effective operators and Wilson coefficients in ‘Warsaw’ basis for complex triplet scalar ($Y = 1$) model.

Q_H	$-\frac{\zeta_1 \mu^2}{m_\Delta^4} - \frac{\zeta_2 \mu^2}{4m_\Delta^4} - \frac{\zeta_1^3}{4\pi^2 m_\Delta^2} - \frac{\zeta_2^2 \zeta_1}{32\pi^2 m_\Delta^2}$
$Q_{H\Box}$	$\frac{\zeta_2^2}{192\pi^2 m_\Delta^2} + \frac{\mu^2}{2m_\Delta^4}$
Q_{HD}	$\frac{\zeta_1^2}{4\pi^2 m_\Delta^2} + \frac{\zeta_2^2}{96\pi^2 m_\Delta^2} - \frac{2\mu^2}{m_\Delta^4}$
Q_{HW}	$\frac{\zeta_1 g_W^2}{48\pi^2 m_\Delta^2}$
Q_{HWB}	$-\frac{\zeta_2 g_W g_Y}{48\pi^2 m_\Delta^2}$
Q_{ll}	$\frac{y_\Delta^2}{4m_\Delta^2}$
Q_W	$\frac{g_W^3}{1440\pi^2 m_\Delta^2}$

Table D.1.4: Mass dimension-5 effective operators and Wilson coefficients for complex triplet scalar ($Y = 1$) model.

Dimension-5 operator	Wilson coefficient
llHH	$\frac{y_\Delta^2}{m_\Delta}$

We follow the convention in this line.

```

In[2]:= fieldewcts=
{
{hf,3,1,3,1,0,m $\Delta$ }
};

In[3]:= hfvecst2ss=defineHeavyFields[fieldewcts];

In[4]:=  $\delta$ =hfvecst2ss[[1,1]]

Out[4]= {hf[1,1]+i ihf[1,1],hf[1,2]+i ihf[1,2],hf[1,3]+i ihf[1,3]}

```

- Now, we will build the Lagrangian after defining the heavy field. We need to provide only those terms that contain the heavy fields. The kinetic terms (covariant derivative and mass terms) of the heavy field will not play any role in this construction, and thus can be ignored. The Lagrangian is written in the following way:

```

In[5]:=  $\Delta$ = $\sum_i^3 \delta[[i]]$  PauliMatrix[i];

In[6]:=  $\Delta$ c =i tau[2]. $\Delta$ ;

In[7]:= V= $\zeta$ 1 dag[H].H Tr[dag[ $\Delta$ ]. $\Delta$ ]
+ $\zeta$ 2  $\sum_i^3$  dag[H].tau[i].H Tr[dag[ $\Delta$ ].tau[i]. $\Delta$ ]
+ $\mu$  H.(i tau[2].dag[ $\Delta$ ]).H
+ $\mu$  dag[H].(-i  $\Delta$ .tau[2]).hermitianConjugate[H];

In[8]:= lyukawa=Expand[y $\Sigma$   $\sum_i^2 \sum_j^2$  hermitianConjugate[lep[1][[i]]].
gamma[0].chargeC.( $\Delta$ c[[i,j]] lep[1][[j]])
+y $\Sigma$   $\sum_i^2 \sum_j^2$  lep[1][[i]].gamma[0].
(dag[ $\Delta$ c][[i,j]] dag[chargeC].lep[1][[j]])];

In[9]:= Lpotent2ss=Expand[lyukawa-V];

In[10]:= initializeLoop["t2ss",fieldt2ss]

Out[10]= Check the documentation page CoDExParaferalia for details.

```

- » Isospin Symmetry Generators for the field ‘hf’ are
isot2ss[1,a] = tauadj[a]
- » colour Symmetry Generators for the field ‘hf’ are colt2ss[1,a] = 0

(See the documentation of [initializeLoop](#) for details.)

```
In[13]:= wcT2SSwar=codexOutput[Lpotent2ss,fielddt2ss,model->"t2ss"];
formPick["Warsaw","Detailed2",wcT2SSwar,FontSize->Medium,
FontFamily->"Times New Roman",Frame->All]
```

4. The operators can be generated in both ‘SILH’ and ‘Warsaw’ bases along with their respective Wilson coefficients. This output can be exported into a L^AT_EX format as well; see Table [D.1.3](#).

```
In[14]:= wcT2SSsilh=codexOutput[Lpotent2ss,fielddt2ss,model->"t2ss",
operBasis->"SILH"];
formPick["SILH","Detailed2",wcT2SSsilh,FontSize->Medium,
FontFamily->"Times New Roman",Frame->All]
```

The output of this is given in Table [D.1.2](#).

```
In[15]:= wcT2SSdim5=codexOutput[Lpotent2ss,fielddt2ss,model->"t2ss",
operBasis->"Dim5"];
formPick["Dim5","Detailed2",wcT2SSdim5,FontSize->Medium,
FontFamily->"Times New Roman",Frame->All]
```

The output of this is given in Table [D.1.4](#).

5. The RG evolution of these WCs can be performed only in the ‘Warsaw’ basis, as this is the complete one using [RGFlow](#):

```
In[16]:= RGFlow[wcT2SSwar,m,μ]
```

Let us consider that the CoDEx output, which is the WCs at the high scale, is generated, and saved as:

```
In[17]:= wcT2SSwar={{"qH",-frac{ζ1^3}{4 mΔ^2 π^2}-frac{ζ1 ζ2^2}{32 mΔ^2 π^2}-frac{ζ1 μ^2}{mΔ^4}-frac{ζ2 μ^2}{4 mΔ^4}},
{"qHbox",frac{ζ2^2}{192 mΔ^2 π^2}+frac{μ^2}{2 mΔ^4}},
{"qHD",frac{ζ1^2}{4 mΔ^2 π^2}+frac{ζ2^2}{96 mΔ^2 π^2}-frac{2 μ^2}{mΔ^4}},{"qHW",frac{gW^2 ζ1}{48 mΔ^2 π^2}},
{"qHWB",-frac{gW gY ζ2}{48 mΔ^2 π^2}},{"qll[1,1,1,1]",frac{yΣ^2}{4 mΔ^2}},{"qW",frac{gW^3}{1440 mΔ^2 π^2}}}
```

Once we declare the matching scale (high scale) as the mass of the heavy particle (‘m’), we need to recall the function [RGFlow](#) to generate the WCs at low scale, as:

```
In[18]:= floRes1 = RGFlow[wcT2SSwar,m,μ]
```

Out[18]=

$$\begin{aligned}
 & \left\{ \left\{ qW, \frac{gW^3}{1440 m_\Delta^2 \pi^2} + \frac{29 gW^5 \text{Log}[\frac{\mu}{m}]}{46080 m_\Delta^2 \pi^4}, \{qH, -\frac{\zeta_1^3}{4 m_\Delta^2 \pi^2} - \frac{\zeta_1 \zeta_2^2}{32 m_\Delta^2 \pi^2} - \frac{\zeta_1 \mu^2}{m_\Delta^4} - \frac{\zeta_2 \mu^2}{4 m_\Delta^4} - \frac{3 gW^6 \zeta_1 \text{Log}[\frac{\mu}{m}]}{256 m_\Delta^2 \pi^4} \right. \right. \\
 & \left. \frac{gW^4 gY^2 \zeta_1 \text{Log}[\frac{\mu}{m}]}{256 m_\Delta^2 \pi^4} - \frac{3 gW^2 \zeta_1^2 \text{Log}[\frac{\mu}{m}]}{32 m_\Delta^2 \pi^4} - \frac{3 gW^4 \zeta_1^2 \text{Log}[\frac{\mu}{m}]}{256 m_\Delta^2 \pi^4} - \frac{3 gY^2 \zeta_1^2 \text{Log}[\frac{\mu}{m}]}{32 m_\Delta^2 \pi^4} \right. \\
 & \left. \frac{3 gW^2 gY^2 \zeta_1^2 \text{Log}[\frac{\mu}{m}]}{3 gY^4 \zeta_1^2 \text{Log}[\frac{\mu}{m}]} + \frac{27 gW^2 \zeta_1^3 \text{Log}[\frac{\mu}{m}]}{27 gW^2 \zeta_1^3 \text{Log}[\frac{\mu}{m}]} + \frac{9 gY^2 \zeta_1^3 \text{Log}[\frac{\mu}{m}]}{9 gY^2 \zeta_1^3 \text{Log}[\frac{\mu}{m}]} \right. \\
 & \left. \frac{128 m_\Delta^2 \pi^4}{gW^4 gY^2 \zeta_2 \text{Log}[\frac{\mu}{m}]} + \frac{256 m_\Delta^2 \pi^4}{gW^2 gY^4 \zeta_2 \text{Log}[\frac{\mu}{m}]} - \frac{128 m_\Delta^2 \pi^4}{gW^2 \zeta_2^2 \text{Log}[\frac{\mu}{m}]} - \frac{128 m_\Delta^2 \pi^4}{gW^4 \zeta_2^2 \text{Log}[\frac{\mu}{m}]} + \frac{gY^2 \zeta_2^2 \text{Log}[\frac{\mu}{m}]}{gY^2 \zeta_2^2 \text{Log}[\frac{\mu}{m}]} \right. \\
 & \left. \frac{256 m_\Delta^2 \pi^4}{gW^2 gY^2 \zeta_2^2 \text{Log}[\frac{\mu}{m}]} - \frac{256 m_\Delta^2 \pi^4}{gY^4 \zeta_2^2 \text{Log}[\frac{\mu}{m}]} - \frac{256 m_\Delta^2 \pi^4}{27 gW^2 \zeta_1 \zeta_2^2 \text{Log}[\frac{\mu}{m}]} - \frac{2048 m_\Delta^2 \pi^4}{256 m_\Delta^2 \pi^4} + \frac{2048 m_\Delta^2 \pi^4}{256 m_\Delta^2 \pi^4} \right. \\
 & \left. \frac{1024 m_\Delta^2 \pi^4}{9 gY^2 \zeta_1 \zeta_2^2 \text{Log}[\frac{\mu}{m}]} - \frac{2048 m_\Delta^2 \pi^4}{3 gW^4 \zeta_1 \lambda \text{Log}[\frac{\mu}{m}]} - \frac{1024 m_\Delta^2 \pi^4}{gW^2 gY^2 \zeta_2 \lambda \text{Log}[\frac{\mu}{m}]} + \frac{5 gW^2 \zeta_2^2 \lambda \text{Log}[\frac{\mu}{m}]}{5 gW^2 \zeta_2^2 \lambda \text{Log}[\frac{\mu}{m}]} \right. \\
 & \left. \frac{1024 m_\Delta^2 \pi^4}{3 gW^2 \mu^2 \text{Log}[\frac{\mu}{m}]} + \frac{64 m_\Delta^2 \pi^4}{3 gW^4 \mu^2 \text{Log}[\frac{\mu}{m}]} - \frac{64 m_\Delta^2 \pi^4}{3 gY^2 \mu^2 \text{Log}[\frac{\mu}{m}]} + \frac{1152 m_\Delta^2 \pi^4}{1152 m_\Delta^2 \pi^4} \right. \\
 & \left. \frac{4 m_\Delta^4 \pi^2}{3 gW^2 gY^2 \mu^2 \text{Log}[\frac{\mu}{m}]} + \frac{32 m_\Delta^4 \pi^2}{3 gY^4 \mu^2 \text{Log}[\frac{\mu}{m}]} - \frac{4 m_\Delta^4 \pi^2}{27 gW^2 \zeta_1 \mu^2 \text{Log}[\frac{\mu}{m}]} \right. \\
 & \left. \frac{16 m_\Delta^4 \pi^2}{9 gY^2 \zeta_1 \mu^2 \text{Log}[\frac{\mu}{m}]} + \frac{32 m_\Delta^4 \pi^2}{27 gW^2 \zeta_2 \mu^2 \text{Log}[\frac{\mu}{m}]} + \frac{32 m_\Delta^4 \pi^2}{9 gY^2 \zeta_2 \mu^2 \text{Log}[\frac{\mu}{m}]} + \frac{5 gW^2 \lambda \mu^2 \text{Log}[\frac{\mu}{m}]}{12 m_\Delta^4 \pi^2} \right\}, \\
 & \left\{ qHbox, \frac{gW^2 \zeta_2^2 \text{Log}[\frac{\mu}{m}]}{1536 m_\Delta^2 \pi^4} + \frac{\mu^2}{8 m_\Delta^4 \pi^2} + \frac{5 gY^2 \zeta_1^2 \text{Log}[\frac{\mu}{m}]}{5 gY^2 \zeta_1^2 \text{Log}[\frac{\mu}{m}]} - \frac{gW^2 \zeta_2^2 \text{Log}[\frac{\mu}{m}]}{768 m_\Delta^2 \pi^4} \right\}, \\
 & \left\{ qHD, \frac{192 m_\Delta^2 \pi^2}{gY^2 \zeta_2^2 \text{Log}[\frac{\mu}{m}]} + \frac{2 m_\Delta^4}{gW^2 \mu^2 \text{Log}[\frac{\mu}{m}]} + \frac{192 m_\Delta^2 \pi^4}{gY^2 \mu^2 \text{Log}[\frac{\mu}{m}]} - \frac{768 m_\Delta^2 \pi^4}{768 m_\Delta^2 \pi^4} \right\}, \\
 & \left\{ qHW, \frac{4 m_\Delta^4 \pi^2}{3 gW^2 \zeta_2^2 \text{Log}[\frac{\mu}{m}]} + \frac{96 m_\Delta^2 \pi^2}{5 gY^2 \zeta_2^2 \text{Log}[\frac{\mu}{m}]} - \frac{m_\Delta^4}{9 gW^2 \mu^2 \text{Log}[\frac{\mu}{m}]} + \frac{128 m_\Delta^2 \pi^4}{5 gY^2 \mu^2 \text{Log}[\frac{\mu}{m}]} - \frac{384 m_\Delta^2 \pi^4}{5 gY^2 \mu^2 \text{Log}[\frac{\mu}{m}]} \right. \\
 & \left. \frac{1024 m_\Delta^2 \pi^4}{1024 m_\Delta^2 \pi^4} + \frac{3072 m_\Delta^2 \pi^4}{3072 m_\Delta^2 \pi^4} - \frac{16 m_\Delta^4 \pi^2}{16 m_\Delta^4 \pi^2} + \frac{16 m_\Delta^4 \pi^2}{16 m_\Delta^4 \pi^2} \right\}, \\
 & \left\{ qHW, \frac{gW^2 \zeta_1 \text{Log}[\frac{\mu}{m}]}{48 m_\Delta^2 \pi^2} - \frac{1536 m_\Delta^2 \pi^4}{768 m_\Delta^2 \pi^4} - \frac{4608 m_\Delta^2 \pi^4}{4608 m_\Delta^2 \pi^4} \right\}, \\
 & \left\{ qHWB, -\frac{gW gY \zeta_2}{48 m_\Delta^2 \pi^2} + \frac{gW^5 gY \text{Log}[\frac{\mu}{m}]}{7680 m_\Delta^2 \pi^4} + \frac{gW^3 gY \zeta_1 \text{Log}[\frac{\mu}{m}]}{384 m_\Delta^2 \pi^4} - \frac{gW^3 gY \zeta_2 \text{Log}[\frac{\mu}{m}]}{576 m_\Delta^2 \pi^4} - \frac{19 gW gY^3 \zeta_2 \text{Log}[\frac{\mu}{m}]}{2304 m_\Delta^2 \pi^4} \right\}, \\
 & \left\{ qeH[1,1], \frac{3 gW^4 \zeta_1 \text{Log}[\frac{\mu}{m}] \text{Yu}^\dagger[e]}{256 m_\Delta^2 \pi^4} - \frac{3 gW^2 \zeta_1^2 \text{Log}[\frac{\mu}{m}] \text{Yu}^\dagger[e]}{128 m_\Delta^2 \pi^4} \right. \\
 & \left. \frac{3 gY^2 \zeta_1^2 \text{Log}[\frac{\mu}{m}] \text{Yu}^\dagger[e]}{3 gY^2 \zeta_1^2 \text{Log}[\frac{\mu}{m}] \text{Yu}^\dagger[e]} + \frac{gW^2 gY^2 \zeta_2 \text{Log}[\frac{\mu}{m}] \text{Yu}^\dagger[e]}{256 m_\Delta^2 \pi^4} \right. \\
 & \left. \frac{128 m_\Delta^2 \pi^4}{9216 m_\Delta^2 \pi^4} + \frac{256 m_\Delta^2 \pi^4}{1024 m_\Delta^2 \pi^4} + \frac{7 gW^2 \mu^2 \text{Log}[\frac{\mu}{m}] \text{Yu}^\dagger[e]}{24 m_\Delta^4 \pi^2} - \frac{3 gY^2 \mu^2 \text{Log}[\frac{\mu}{m}] \text{Yu}^\dagger[e]}{16 m_\Delta^4 \pi^2} \right\}, \\
 & \left\{ quH[1,1], \frac{3 gW^4 \zeta_1 \text{Log}[\frac{\mu}{m}] \text{Yu}^\dagger[u]}{512 m_\Delta^2 \pi^4} - \frac{3 gW^2 \zeta_1^2 \text{Log}[\frac{\mu}{m}] \text{Yu}^\dagger[u]}{128 m_\Delta^2 \pi^4} \right. \\
 & \left. \frac{3 gY^2 \zeta_1^2 \text{Log}[\frac{\mu}{m}] \text{Yu}^\dagger[u]}{3 gY^2 \zeta_1^2 \text{Log}[\frac{\mu}{m}] \text{Yu}^\dagger[u]} + \frac{gW^2 gY^2 \zeta_2 \text{Log}[\frac{\mu}{m}] \text{Yu}^\dagger[u]}{768 m_\Delta^2 \pi^4} + \frac{gW^2 \zeta_2^2 \text{Log}[\frac{\mu}{m}] \text{Yu}^\dagger[u]}{9216 m_\Delta^2 \pi^4} \right. \\
 & \left. \frac{128 m_\Delta^2 \pi^4}{9216 m_\Delta^2 \pi^4} + \frac{256 m_\Delta^2 \pi^4}{768 m_\Delta^2 \pi^4} + \frac{7 gW^2 \mu^2 \text{Log}[\frac{\mu}{m}] \text{Yu}^\dagger[u]}{24 m_\Delta^4 \pi^2} - \frac{3 gY^2 \mu^2 \text{Log}[\frac{\mu}{m}] \text{Yu}^\dagger[u]}{16 m_\Delta^4 \pi^2} \right\}, \\
 & \left\{ qdH[1,1], \frac{3 gW^4 \zeta_1 \text{Log}[\frac{\mu}{m}] \text{Yu}^\dagger[d]}{512 m_\Delta^2 \pi^4} - \frac{3 gW^2 \zeta_1^2 \text{Log}[\frac{\mu}{m}] \text{Yu}^\dagger[d]}{128 m_\Delta^2 \pi^4} \right. \\
 & \left. \frac{3 gY^2 \zeta_1^2 \text{Log}[\frac{\mu}{m}] \text{Yu}^\dagger[d]}{3 gY^2 \zeta_1^2 \text{Log}[\frac{\mu}{m}] \text{Yu}^\dagger[d]} + \frac{gW^2 gY^2 \zeta_2 \text{Log}[\frac{\mu}{m}] \text{Yu}^\dagger[d]}{768 m_\Delta^2 \pi^4} + \frac{gW^2 \zeta_2^2 \text{Log}[\frac{\mu}{m}] \text{Yu}^\dagger[d]}{9216 m_\Delta^2 \pi^4} \right. \\
 & \left. \frac{128 m_\Delta^2 \pi^4}{9216 m_\Delta^2 \pi^4} + \frac{256 m_\Delta^2 \pi^4}{768 m_\Delta^2 \pi^4} + \frac{7 gW^2 \mu^2 \text{Log}[\frac{\mu}{m}] \text{Yu}^\dagger[d]}{24 m_\Delta^4 \pi^2} - \frac{3 gY^2 \mu^2 \text{Log}[\frac{\mu}{m}] \text{Yu}^\dagger[d]}{16 m_\Delta^4 \pi^2} \right\}, \\
 & \left\{ qeW[1,1], -\frac{gW^3 \zeta_1 \text{Log}[\frac{\mu}{m}] \text{Yu}^\dagger[e]}{768 m_\Delta^2 \pi^4} - \frac{gW gY^2 \zeta_2 \text{Log}[\frac{\mu}{m}] \text{Yu}^\dagger[e]}{512 m_\Delta^2 \pi^4} \right\}, \\
 & \left\{ qeB[1,1], \frac{gW^2 gY \zeta_2 \text{Log}[\frac{\mu}{m}] \text{Yu}^\dagger[e]}{512 m_\Delta^2 \pi^4} \right\}, \\
 & \left\{ quW[1,1], -\frac{gW^3 \zeta_1 \text{Log}[\frac{\mu}{m}] \text{Yu}^\dagger[u]}{768 m_\Delta^2 \pi^4} - \frac{5 gW gY^2 \zeta_2 \text{Log}[\frac{\mu}{m}] \text{Yu}^\dagger[u]}{4608 m_\Delta^2 \pi^4} \right\}, \\
 & \left\{ quB[1,1], -\frac{gW^2 gY \zeta_2 \text{Log}[\frac{\mu}{m}] \text{Yu}^\dagger[u]}{512 m_\Delta^2 \pi^4} \right\}, \\
 & \left\{ qdW[1,1], -\frac{gW^3 \zeta_1 \text{Log}[\frac{\mu}{m}] \text{Yu}^\dagger[d]}{768 m_\Delta^2 \pi^4} - \frac{gW gY^2 \zeta_2 \text{Log}[\frac{\mu}{m}] \text{Yu}^\dagger[d]}{4608 m_\Delta^2 \pi^4} \right\}, \\
 & \left\{ qdB[1,1], \frac{gW^2 gY \zeta_2 \text{Log}[\frac{\mu}{m}] \text{Yu}^\dagger[u]}{512 m_\Delta^2 \pi^4} \right\}, \\
 & \left\{ q1Hl[1,1], -\frac{gY^2 y \Sigma^2 \text{Log}[\frac{\mu}{m}]}{96 m_\Delta^2 \pi^2} - \frac{gY^2 \zeta_1^2 \text{Log}[\frac{\mu}{m}]}{384 m_\Delta^2 \pi^4} - \frac{gY^2 \zeta_2^2 \text{Log}[\frac{\mu}{m}]}{6144 m_\Delta^2 \pi^4} + \frac{gY^2 \mu^2 \text{Log}[\frac{\mu}{m}]}{64 m_\Delta^4 \pi^2} \right\}, \\
 & \left\{ q3Hl[1,1], \frac{gW^2 y \Sigma^2 \text{Log}[\frac{\mu}{m}]}{96 m_\Delta^2 \pi^2} + \frac{gW^2 \zeta_2^2 \text{Log}[\frac{\mu}{m}]}{18432 m_\Delta^2 \pi^4} + \frac{gW^2 \mu^2 \text{Log}[\frac{\mu}{m}]}{192 m_\Delta^4 \pi^2} \right\}, \\
 & \left\{ qHe[1,1], -\frac{gY^2 \zeta_1^2 \text{Log}[\frac{\mu}{m}]}{192 m_\Delta^2 \pi^4} - \frac{gY^2 \zeta_2^2 \text{Log}[\frac{\mu}{m}]}{3072 m_\Delta^2 \pi^4} + \frac{gY^2 \mu^2 \text{Log}[\frac{\mu}{m}]}{32 m_\Delta^4 \pi^2} \right\}, \\
 & \left\{ q1Hq[1,1], \frac{gY^2 \zeta_1^2 \text{Log}[\frac{\mu}{m}]}{1152 m_\Delta^2 \pi^4} + \frac{gY^2 \zeta_2^2 \text{Log}[\frac{\mu}{m}]}{18432 m_\Delta^2 \pi^4} - \frac{gY^2 \mu^2 \text{Log}[\frac{\mu}{m}]}{192 m_\Delta^4 \pi^2} \right\}, \\
 & \left\{ q3Hq[1,1], \frac{gW^2 \zeta_2^2 \text{Log}[\frac{\mu}{m}]}{18432 m_\Delta^2 \pi^4} + \frac{gW^2 \mu^2 \text{Log}[\frac{\mu}{m}]}{192 m_\Delta^4 \pi^2} \right\},
 \end{aligned}$$

$$\begin{aligned}
 & \{qHu[1,1], \frac{gY^2 \zeta^2 \text{Log}[\frac{\mu}{m}]}{288 m_\Delta^2 \pi^4} + \frac{gY^2 \zeta^2 \text{Log}[\frac{\mu}{m}]}{4608 m_\Delta^2 \pi^4} - \frac{gY^2 \mu^2 \text{Log}[\frac{\mu}{m}]}{48 m_\Delta^4 \pi^2}\}, \\
 & \{qHd[1,1], -\frac{gY^2 \zeta^2 \text{Log}[\frac{\mu}{m}]}{576 m_\Delta^2 \pi^4} - \frac{gY^2 \zeta^2 \text{Log}[\frac{\mu}{m}]}{9216 m_\Delta^2 \pi^4} + \frac{gY^2 \mu^2 \text{Log}[\frac{\mu}{m}]}{96 m_\Delta^4 \pi^2}\}, \\
 & \{qll[1,1,1,1], \frac{y\Sigma^2}{4 m_\Delta^2} + \frac{11 gW^2 y\Sigma^2 \text{Log}[\frac{\mu}{m}]}{192 m_\Delta^2 \pi^2} + \frac{5 gY^2 y\Sigma^2 \text{Log}[\frac{\mu}{m}]}{64 m_\Delta^2 \pi^2}\}, \{qllq[1,1,1,1], -\frac{gY^2 y\Sigma^2 \text{Log}[\frac{\mu}{m}]}{96 m_\Delta^2 \pi^2}\}, \\
 & \{q3lq[1,1,1,1], \frac{gW^2 y\Sigma^2 \text{Log}[\frac{\mu}{m}]}{96 m_\Delta^2 \pi^2}\}, \{qle[1,1,1,1], \frac{gY^2 y\Sigma^2 \text{Log}[\frac{\mu}{m}]}{16 m_\Delta^2 \pi^2}\}, \\
 & \{q1u[1,1,1,1], -\frac{gY^2 y\Sigma^2 \text{Log}[\frac{\mu}{m}]}{24 m_\Delta^2 \pi^2}\}, \{qld[1,1,1,1], \frac{gY^2 y\Sigma^2 \text{Log}[\frac{\mu}{m}]}{48 m_\Delta^2 \pi^2}\}
 \end{aligned}$$

We have provided the flexibility to users to reformat, save, or export all these WCs corresponding to the effective operators at the electroweak scale (μ) to \LaTeX , using `formPick`. We have also provided an illustrative example:

```
In[19]:= formPick["Warsaw", "Detailed2", floRes1, Frame→All,
                FontSize→Medium, FontFamily→"Times New Roman"]
```

```
Out[19]=
```

Q_W	$\epsilon^{abc} W_\rho^{a,\mu} W_\mu^{b,\nu} W_\nu^{c,\rho}$	$\frac{29 g_W^5 \log\left(\frac{\mu}{m_\Delta}\right)}{46080 \pi^4 m_\Delta^2} + \frac{g_W^3}{1440 \pi^2 m_\Delta^2}$
\vdots	\vdots	\vdots
Q_{ld}	$(\bar{l}\gamma_\mu l)(\bar{d}\gamma_\mu d)$	$\frac{g_Y^2 y_\Sigma^2 \log\left(\frac{\mu}{m_\Delta}\right)}{48 \pi^2 m_\Delta^2}$

Acknowledgement

S.D. Bakshi thanks the organisers of the 11th FCC-ee workshop: Theory and Experiments, CERN for the invitation and providing the opportunity to present this work.

References

- [1] G.F. Giudice *et al.*, *JHEP* **06** (2007) 045. [arXiv:hep-ph/0703164](#), [doi:10.1088/1126-6708/2007/06/045](#)
- [2] R. Contino *et al.*, *JHEP* **07** (2013) 035. [arXiv:1303.3876](#), [doi:10.1007/JHEP07\(2013\)035](#)
- [3] B. Grzadkowski *et al.*, *JHEP* **10** (2010) 085. [arXiv:1008.4884](#), [doi:10.1007/JHEP10\(2010\)085](#)
- [4] E.E. Jenkins *et al.*, *JHEP* **10** (2013) 087. [arXiv:1308.2627](#), [doi:10.1007/JHEP10\(2013\)087](#)
- [5] E.E. Jenkins *et al.*, *JHEP* **01** (2014) 035. [arXiv:1310.4838](#), [doi:10.1007/JHEP01\(2014\)035](#)
- [6] R. Alonso *et al.*, *JHEP* **04** (2014) 159. [arXiv:1312.2014](#), [doi:10.1007/JHEP04\(2014\)159](#)
- [7] R.J. Furnstahl *et al.*, *Phys. Rev.* **C92** (2015) 024005. [arXiv:1506.01343](#), [doi:10.1103/PhysRevC.92.024005](#)
- [8] B. Gripaios and D. Sutherland, *JHEP* **01** (2019) 128. [arXiv:1807.07546](#), [doi:10.1007/JHEP01\(2019\)128](#)
- [9] A. Falkowski *et al.*, *Eur. Phys. J.* **C75** (2015) 583. [arXiv:1508.05895](#), [doi:10.1140/epjc/s10052-015-3806-x](#)

- [10] A. Celis *et al.*, *Eur. Phys. J.* **C77** (2017) 405. [arXiv:1704.04504](#),
[doi:10.1140/epjc/s10052-017-4967-6](#)
- [11] J.C. Criado, *Comput. Phys. Commun.* **227** (2018) 42. [arXiv:1710.06445](#),
[doi:10.1016/j.cpc.2018.02.016](#)
- [12] J. Aebischer *et al.*, *Eur. Phys. J.* **C78** (2018) 1026. [arXiv:1804.05033](#),
[doi:10.1140/epjc/s10052-018-6492-7](#)
- [13] J. Aebischer *et al.*, *Comput. Phys. Commun.* **232** (2018) 71. [arXiv:1712.05298](#),
[doi:10.1016/j.cpc.2018.05.022](#)
- [14] J.D. Wells and Z. Zhang, *JHEP* **06** (2016) 122. [arXiv:1512.03056](#),
[doi:10.1007/JHEP06\(2016\)122](#)
- [15] S.D. Bakshi *et al.*, *Eur. Phys. J.* **C79** (2019) 21. [arXiv:1808.04403](#),
[doi:10.1140/epjc/s10052-018-6444-2](#)
- [16] <https://effexteam.github.io/CoDEX>, last accessed 27 January 2020.
- [17] M.K. Gaillard, *Nucl. Phys.* **B268** (1986) 669. [doi:10.1016/0550-3213\(86\)90264-6](#)
- [18] O. Cheyette, *Phys. Rev. Lett.* **55** (1985) 2394. [doi:10.1103/PhysRevLett.55.2394](#)
- [19] B. Henning *et al.*, *JHEP* **01** (2016) 023. [arXiv:1412.1837](#),
[doi:10.1007/JHEP01\(2016\)023](#)
- [20] B. Henning *et al.*, *JHEP* **01** (2018) 123. [arXiv:1604.01019](#),
[doi:10.1007/JHEP01\(2018\)123](#)
- [21] S.A.R. Ellis *et al.*, *Phys. Lett.* **B762** (2016) 166. [arXiv:1604.02445](#),
[doi:10.1016/j.physletb.2016.09.016](#)
- [22] J. Fuentes-Martin *et al.*, *JHEP* **09** (2016) 156. [arXiv:1607.02142](#),
[doi:10.1007/JHEP09\(2016\)156](#)
- [23] F. del Aguila *et al.*, *Eur. Phys. J.* **C76** (2016) 244. [arXiv:1602.00126](#),
[doi:10.1140/epjc/s10052-016-4081-1](#)
- [24] B. Henning *et al.*, *JHEP* **08** (2017) 016. [arXiv:1512.03433](#),
[doi:10.1007/JHEP08\(2017\)016](#)
- [25] A. Drozd *et al.*, *JHEP* **03** (2016) 180. [arXiv:1512.03003](#),
[doi:10.1007/JHEP03\(2016\)180](#)
- [26] J.D. Wells and Z. Zhang, *JHEP* **01** (2016) 123. [arXiv:1510.08462](#),
[doi:10.1007/JHEP01\(2016\)123](#)
- [27] L. Lehman and, A. Martin, *JHEP* **02** (2016) 081. [arXiv:1510.00372](#),
[doi:10.1007/JHEP02\(2016\)081](#)
- [28] R. Huo, *Phys. Rev.* **D97** (2018) 075013. [arXiv:1509.05942](#),
[doi:10.1103/PhysRevD.97.075013](#)
- [29] R. Huo, *JHEP* **09** (2015) 037. [arXiv:1506.00840](#),
[doi:10.1007/JHEP09\(2015\)037](#)
- [30] C.-W. Chiang and R. Huo, *JHEP* **09** (2015) 152. [arXiv:1505.06334](#), [doi:10.1007/JHEP09\(2015\)152](#)
- [31] L. Lehman and A. Martin, *Phys. Rev.* **D91** (2015) 105014. [arXiv:1503.07537](#),
[doi:10.1103/PhysRevD.91.105014](#)

- [32] <http://library.wolfram.com/infocenter/MathSource/2720/>,
last accessed 27 January 2020.

Chapter E

Beyond the Standard Model (BSM)

1 (Triple) Higgs coupling imprints at future lepton colliders

Contribution* by: J. Baglio, C. Weiland

Corresponding author: J. Baglio [julien.baglio@uni-tuebingen.de]

1.1 Triple Higgs coupling studies in an EFT framework

The measurement of the triple Higgs coupling is one of the major goals of the future colliders. The direct measurement at lepton colliders relies on the production of Higgs boson pairs in two main channels: $e^+e^- \rightarrow ZHH$, which is dominant at centre-of-mass energies below 1 TeV and maximal at around 500 GeV, and $e^+e^- \rightarrow HH\nu_e\bar{\nu}_e$, which becomes dominant for high-energy colliders. This direct measurement is required to be at least at a centre-of-mass energy of 500 GeV, and is hence only possible at future linear colliders, such as the International Linear Collider (ILC), operating at 500 GeV or 1 TeV [1], or the Compact Linear Collider (CLIC), operating at 1.4 TeV (stage 2) or 3 TeV (stage 3) [2]. The SM triple Higgs coupling sensitivity is estimated to be $\delta\kappa_\lambda = (\lambda_{HHH}/\lambda_{HHH}^{\text{SM}} - 1) \sim 28\%$ at the 500 GeV ILC, with a luminosity of 4 ab^{-1} [3, 4], and $\delta\kappa_\lambda \sim 13\%$ at the CLIC, when combining the 1.4 TeV run, with 2.5 ab^{-1} of data, and the 3 TeV run, with 5 ab^{-1} of data [5].

Still, circular lepton collider projects, such as the Circular Electron–Positron Collider (CEPC) [6] or the FCC-ee [7, 8], which run at energies below 500 GeV (not to mention the ILC or the CLIC running at lower energies), can provide a way to constrain the triple Higgs coupling [9]. Since Ref. [10], in which it was first proposed to use precision measurements to constrain the triple Higgs coupling, in particular, the measurements in single Higgs production at lepton colliders, there have been studies of the combination of single and double Higgs production observables, not only at lepton but also at hadron colliders [11–14]. The analyses use the framework of Standard Model effective field theory (SMEFT). According to the latest ECFA report [15], the combination of HL-LHC projections [16] with ILC exclusive single Higgs data gives $\delta\kappa_\lambda = 26\%$ at 68% CL, while with the FCC-ee (at 250 or 365 GeV) this goes down to $\delta\kappa_\lambda = 19\%$, and with CEPC we get $\delta\kappa_\lambda = 17\%$. We will present in more detail the results of Refs. [12, 13], which demonstrate how important the combination of the LHC results with an analysis at lepton colliders is, and show the potential of the FCC-ee.†

Figure E.1.1 (left) displays the latest experimental results available at the 13 TeV LHC for the search of non-resonance Higgs pair production and the 95% CL limits on the triple Higgs coupling, which have been presented in Ref. [17]. The results constrain $\delta\kappa_\lambda$ in the range

*This contribution should be cited as:

J. Baglio, C. Weiland, (Triple) Higgs coupling imprints at future lepton colliders, DOI: [10.23731/CYRM-2020-003.231](https://doi.org/10.23731/CYRM-2020-003.231), in: Theory for the FCC-ee, Eds. A. Blondel, J. Gluza, S. Jadach, P. Janot and T. Riemann, CERN Yellow Reports: Monographs, CERN-2020-003, DOI: [10.23731/CYRM-2020-003](https://doi.org/10.23731/CYRM-2020-003), p. 231.

© CERN, 2020. Published by CERN under the [Creative Commons Attribution 4.0 license](https://creativecommons.org/licenses/by/4.0/).

†Julien Baglio thanks Christophe Grojean for his very useful input to this subsection.

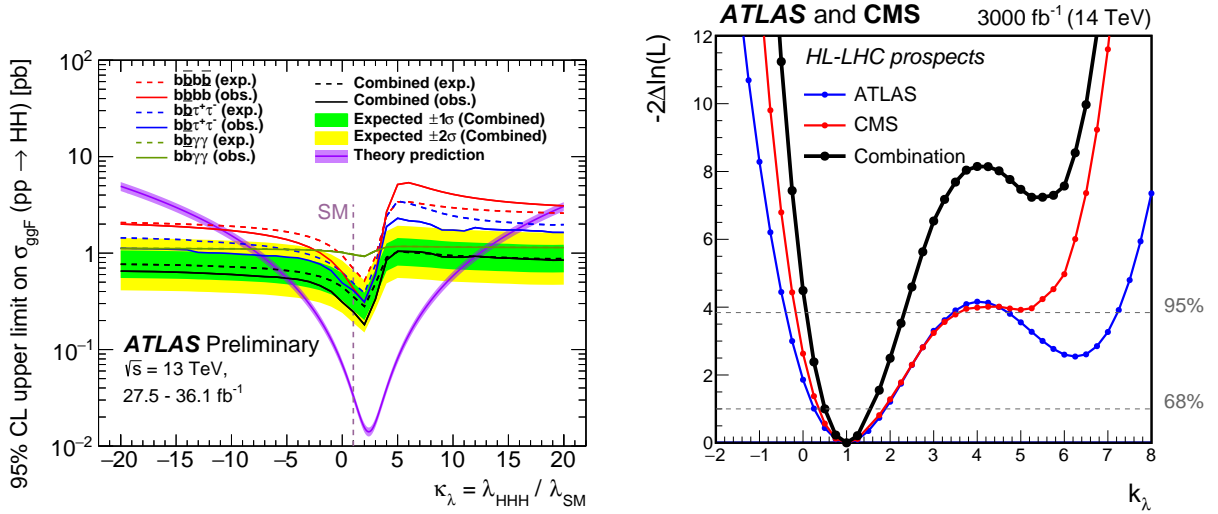


Fig. E.1.1: Left: Latest experimental bounds on the triple Higgs coupling from the ATLAS collaboration at the 13 TeV LHC, combining $b\bar{b}b\bar{b}$, $b\bar{b}\tau^+\tau^-$, and $b\bar{b}\gamma\gamma$ final states. Taken from Ref. [17]. Right: Minimum negative-log-likelihood distribution of κ_λ at the HL-LHC with 3 ab^{-1} of data, including differential observables in Higgs pair production, with ATLAS (blue), CMS (red), and ATLAS+CMS (black) projected results. Figure taken from Ref. [16].

$[-6.0 : 11.1]$. We can compare them with the projections at the HL-LHC with 3 ab^{-1} presented in the HL-HE LHC report [16] in an SMEFT framework, using a differential analysis in the channel $pp \rightarrow HH$. Compared with the projection in Ref. [12], which also included single Higgs data in the channels $pp \rightarrow W^\pm H, ZH, t\bar{t}H$, there is a substantial improvement, thanks to the experimental differential analysis. We have $-0.5 \leq \delta\kappa_\lambda \leq 0.5$ at 68% CL and $-0.9 \leq \delta\kappa_\lambda \leq 1.3$ at 95% CL. The degeneracy observed in Ref. [12] with a second minimum at $\delta\kappa_\lambda \sim 5$ is now excluded at 4σ .

The combination with data from lepton colliders removes the second minimum even more drastically and only the SM minimum is left at $\delta\kappa_\lambda = 0$ [13], in particular when data from 250 GeV and 350–365 GeV centre-of-mass energies are combined [13]. This is shown in Fig. E.1.2, where two set-ups are compared, the combination of HL-LHC data with circular lepton colliders (FCC-ee or CEPC) data on the left-hand side, and the combination of HL-LHC data with the ILC data on the right-hand side. In both cases, the lepton collider data consist of measurements in the channels $e^+e^- \rightarrow W^+W^-, ZH, \nu_e\bar{\nu}_e H$. The second minimum disappears completely even with a relatively low integrated luminosity of $\mathcal{L} = 200\text{ fb}^{-1}$ at 350 GeV, when combined with the data at 250 GeV. Note that the FCC-ee (or CEPC), thanks to its much higher luminosity in the 250 GeV run, is doing significantly better than the ILC.

1.2 Probing heavy neutral leptons via Higgs couplings

Since the confirmation of neutrino oscillations in 1998 by the Super-Kamiokande experiment [18], it has been established that at least two neutrinos have a non-zero mass [19]. This experimental fact cannot be accounted for in the SM and requires new physics. One of the simplest extensions is the addition of new heavy neutral leptons that are gauge singlets and mix with the active neutrinos to generate the light neutrino masses. An appealing model, allowing for these new fermionic states to be in the range of gigaelectronvolts to a few teraelectronvolts

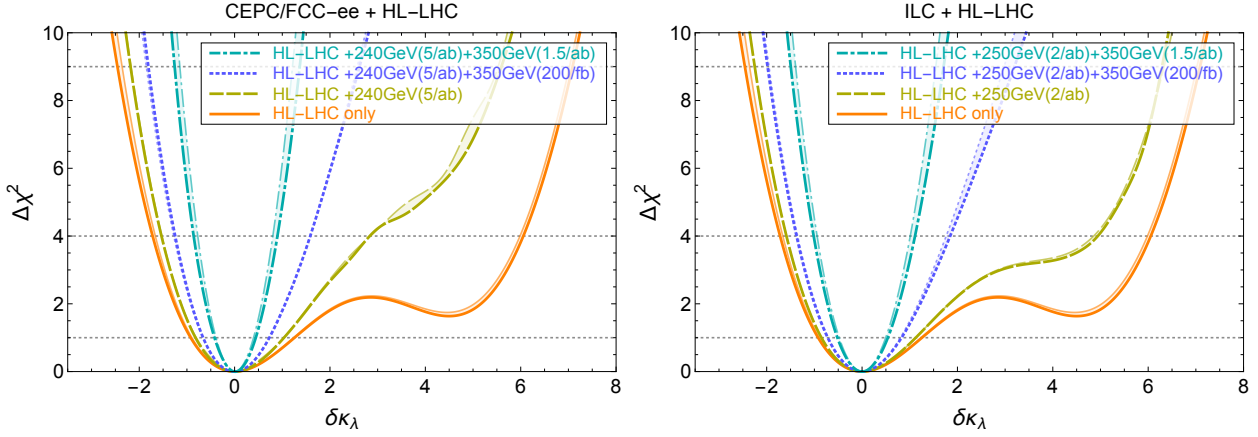


Fig. E.1.2: $\Delta\chi^2$ distributions for a global fit of the parameter $\delta\kappa_\lambda$ at circular lepton colliders (left) or at the ILC (right), combined with HL-LHC data. The different lines compare the different centre-of-mass energies and luminosity scenarios. Figures taken from Ref. [13].

while having Yukawa couplings of order one, is the inverse see-saw (ISS) model [20–22], in which a nearly conserved lepton-number symmetry [23, 24] is introduced, naturally explaining the smallness of the mass of the lightest neutrino states while allowing for large couplings between the heavy neutrinos and the Higgs boson, leading to a rich phenomenology. In this view, the very precise study of the Higgs sector at lepton colliders can offer a unique opportunity to test low-scale see-saw mechanisms, such as the ISS.

1.2.1 Heavy neutral leptons in the gigaelectronvolt regime

We begin with the gigaelectronvolt regime. In these low-scale see-saw models, the mixing between the active and the sterile neutrinos leads to modified couplings of neutrinos to the W, Z, and Higgs bosons. This naturally leads to the idea of using precision measurements of the Higgs boson branching fractions into gauge bosons in order to test the mass range $M_N < M_H$, where M_N is the mass of the heavy neutrino states and M_H is the mass of the Higgs boson. As $H \rightarrow NN$ is allowed, the invisible Higgs decay width is modified and hence the branching fraction $\text{BR}(H \rightarrow W^+W^-)$ is modified via the modified total decay width Γ_H . According to an analysis of 2015 [25], the FCC-ee could be the most competitive lepton collider to test this option, as demonstrated in Fig. E.1.3. In particular, the experimental sensitivity to $\text{BR}(H \rightarrow W^+W^-)$ is expected to be 0.9% at the FCC-ee, compared with 1.3% at the CEPC, operating at 240 GeV [26], and 6.4% at the ILC, operating at 250 GeV [1].[‡]

1.2.2 Probing heavy neutral leptons in the multi-teraelectronvolt regime

Since the coupling of the heavy neutral leptons to the Higgs boson can be quite large in low-scale see-saw models for masses M_N of a few teraelectronvolts, it is also very appealing to use, again, Higgs properties to probe a mass regime of $M_N \sim \mathcal{O}(1 - 10 \text{ TeV})$.

Off-diagonal couplings of the Higgs boson to heavy neutral leptons will induce charged-lepton-flavour-violating (cLFV) decays [28]. In particular, simplified formulae were provided in Ref. [29], showing that cLFV Higgs decays exhibit a different functional dependence on see-

[‡]The latest analysis at the ILC, using a luminosity of 500 fb^{-1} , states that a precision of 4.1% can be achieved [27].

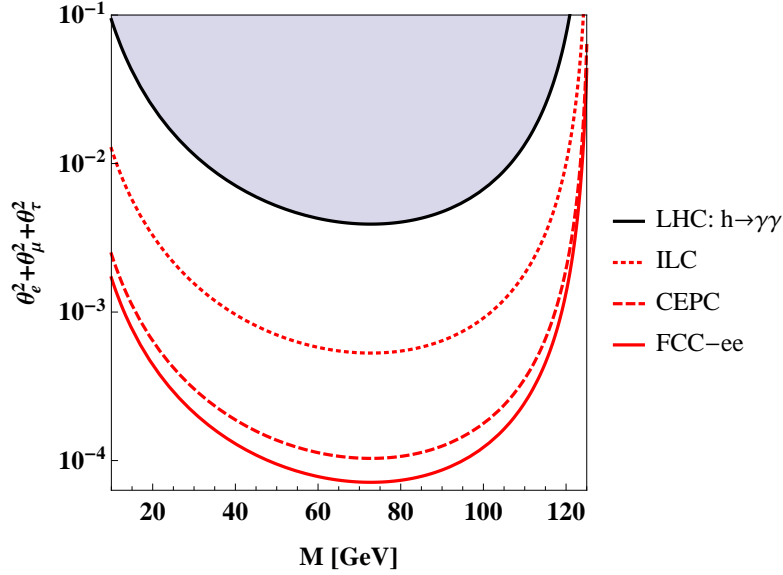


Fig. E.1.3: Estimated sensitivities on the heavy sterile neutrino properties from the decay $H \rightarrow W^+W^-$, assuming 10 years of data collection. The black line denotes the bound from the LHC coming from $H \rightarrow \gamma\gamma$ with up to 2015 data. Taken from Ref. [25].

saw parameters than cLFV radiative decays. They thus provide complementary observables to search for heavy neutral leptons. In a typical low-scale see-saw model like the ISS, the predicted branching fraction can be as large as $\text{BR}(H \rightarrow \tau\mu) \sim 10^{-5}$ and could even reach $\text{BR}(H \rightarrow \tau\mu) \sim 10^{-2}$ in a supersymmetric model [30], thus being well within the reach of a Higgs factory like the FCC-ee. However, Higgs observables are also uniquely sensitive to diagonal couplings and this was discussed in particular in Refs. [31, 32], using the triple Higgs coupling, and in Ref. [33], using a direct physical observable, the production cross-section $\sigma(e^+e^- \rightarrow W^+W^-H)$. Taking into account all theoretical and experimental constraints that were available, the three studies have found sizeable effects.

In the triple Higgs coupling studies, the one-loop corrections to λ_{HHH} , defined as the physical triple Higgs coupling after electroweak symmetry breaking, are studied. The calculation is performed in the on-shell scheme and compares the SM prediction with the prediction in low-scale see-saw models (specifically the ISS presented in Ref. [32]). Representative one-loop diagrams involving the new heavy neutral leptons are given in Fig. E.1.4 and details of the calculation and analytical formulae can be found in the original articles. The results are given in terms of deviations with respect to the tree-level value λ_{HHH}^0 and to the renormalised one-loop value in the SM $\lambda_{\text{HHH}}^{1,\text{SM}}$ of the triple Higgs coupling,

$$\begin{aligned} \Delta^{(1)}\lambda_{\text{HHH}} &= \frac{1}{\lambda^0} (\lambda_{\text{HHH}}^1 - \lambda^0), \\ \Delta^{\text{BSM}} &= \frac{1}{\lambda_{\text{HHH}}^{1,\text{SM}}} (\lambda_{\text{HHH}}^1 - \lambda_{\text{HHH}}^{1,\text{SM}}), \end{aligned} \quad (1.1)$$

with λ_{HHH}^1 being the one-loop renormalised triple Higgs coupling in the low-scale see-saw model considered. The constraints from low-energy neutrino observables are implemented via the μ_X parametrization; see Ref. [29] for more details and Appendix A of Ref. [32] for terms beyond the lowest order in the see-saw expansion. All relevant theoretical and experimental bounds

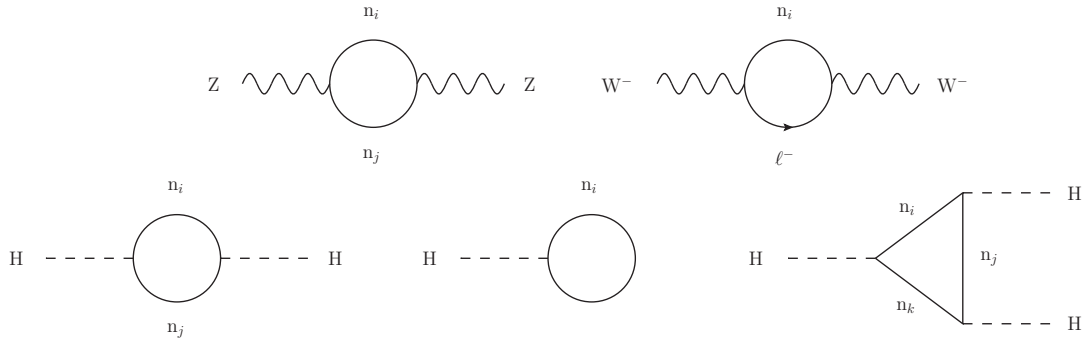


Fig. E.1.4: Representative Feynman diagrams for the one-loop corrections to λ_{HHH} involving the neutrinos in the ISS model.

are taken into account. The most stringent constraint comes from the global fit to electroweak precision observables and lepton universality tests [34].

Figure E.1.5 displays the results of the analysis in the plane $M_R - |Y_\nu|$ where M_R is the see-saw scale and $|Y_\nu|$ is the magnitude of the Yukawa coupling between the heavy neutral leptons and the Higgs boson. For an off-shell Higgs momentum of $q_{H^*} = 500$ GeV splitting into two on-shell Higgs bosons, sizeable deviations can be obtained, up to $\Delta^{\text{BSM}} \simeq -8\%$. Compared with the expected sensitivity of $\sim 10\%$ at the ILC at 1 TeV with 5 ab^{-1} [35] or the FCC-hh sensitivity of $\sim 5\%$ when two experiments were to be combined [36], the deviation can be probed and hence test masses of order $\mathcal{O}(10 \text{ TeV})$. In the case of the FCC-hh, as the hadronic centre-of-mass energy is large, the case $q_{H^*} = 2500$ GeV is even more interesting, with a deviation up to $\Delta^{\text{BSM}} \simeq +35\%$, leading to a larger coverage of the parameter space and the possibility of testing the model at the 3 TeV CLIC, where the sensitivity to λ_{HHH} is expected to be of the order of 13% [5]. The triple Higgs coupling λ_{HHH} is a viable new (pseudo-)observable for the neutrino sector in order to constrain mass models, and might also be used in the context of the FCC-ee in an indirect way in $e^+e^- \rightarrow ZH$ at the two-loop order, given the expected sensitivity the FCC-ee is supposed to reach in this channel. Studies remain to be done in this context.

The study presented in Ref. [33] considered a more direct observable, the production cross-section $\sigma(e^+e^- \rightarrow W^+W^-H)$ at lepton colliders. The set-up is the same as in Ref. [32], albeit with an updated global fit using NuFIT 3.0 [37] to explain neutrino oscillations. The representative diagrams in the Feynman-'t Hooft gauge are displayed in Fig. E.1.6, with the contributions of the heavy neutral leptons in the t channel.

The deviation Δ^{BSM} now stands for the comparison between the total cross-section $\sigma(e^+e^- \rightarrow W^+W^-H)$ calculated in the ISS model and in the SM, $\Delta^{\text{BSM}} = (\sigma^{\text{ISS}} - \sigma^{\text{SM}})/\sigma^{\text{SM}}$. Using the CLIC baseline for the polarisation of the beams [2] with an unpolarised positron beam, $P_{e^+} = 0$, and a polarised electron beam, $P_{e^-} = -80\%$, the contour map at 3 TeV in the same $M_R - |Y_\nu|$ plane is presented in the left-hand side of Fig. E.1.7. Again, the grey area is excluded by the constraints that mostly originate from the global fit [34]. The process $e^+e^- \rightarrow W^+W^-H$ exhibits sizeable negative deviations, of at least -20% . Note that the full results can be approximated within 1% for $M_R > 3 \text{ TeV}$ by the simple formulae presented in Ref. [33]. Compared with the left-hand side of Fig. E.1.5, the coverage of the parameter space is here much larger. Optimised cuts can also be chosen to enhance the deviation, such as the cuts $|\eta_{H/W^\pm}| < 1$ and $E_H > 1 \text{ TeV}$ (see the right-hand side of Fig. E.1.7 for the η distributions),

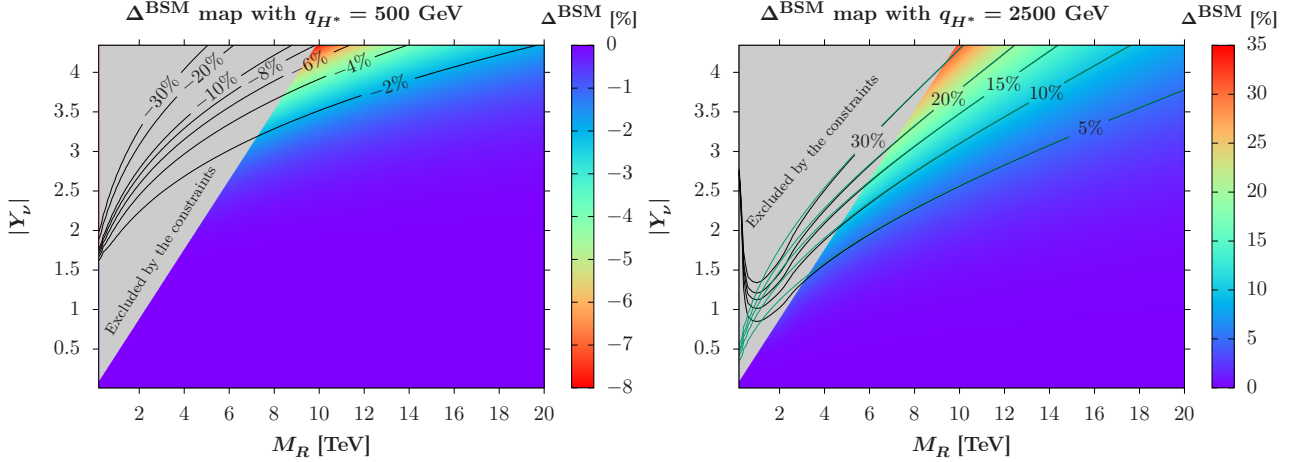


Fig. E.1.5: Contour maps of the heavy neutral lepton correction Δ^{BSM} to the triple Higgs coupling λ_{HHH} (in %) as a function of the heavy neutral lepton parameters M_R (in teraelectronvolts) and $|Y_\nu|$ at a fixed off-shell Higgs momentum $q_{H^*} = 500$ GeV (left) and $q_{H^*} = 2500$ GeV (right). The details of the spectrum are given in Ref. [32]. The grey area is excluded by the constraints on the model and the green lines on the right figure are contour lines that correspond to our approximate formula, while the black lines correspond to the full calculation.

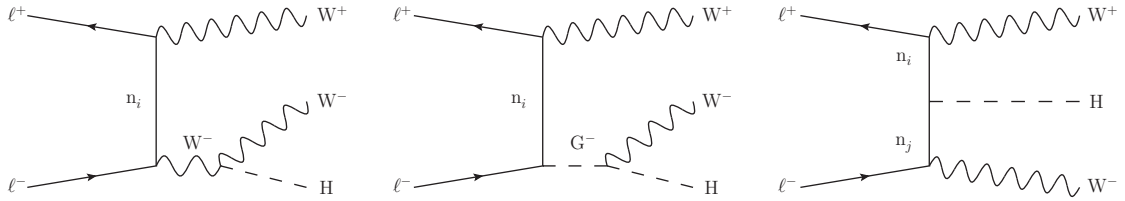


Fig. E.1.6: ISS neutrino contributions to the process $\ell^+\ell^- \rightarrow W^+W^-H$ in the Feynman-'t Hooft gauge. Mirror diagrams can be obtained by flipping all the electric charges; the indices i, j run from 1 to 9.

which push the corrections down to -66% while keeping an ISS cross-section at a reasonable level: 0.14 fb, as compared with 1.23 fb before cuts. This has been studied for a benchmark scenario with $|Y_\nu| = 1$ and heavy neutrinos in the range 2.4–8.6 TeV. The results means that this observable has a great potential that needs to be checked in a detailed sensitivity analysis. In the context of the FCC-ee, a similar observable could be chosen to test the effects of heavy neutral leptons in the same mass range, albeit at the one-loop level, namely the production cross-section $\sigma(e^+e^- \rightarrow ZH)$.

1.3 Conclusions

This contribution has presented the current status of the triple Higgs coupling measurements at the LHC and the prospects for future lepton colliders. As combined studies in an EFT framework using precision measurements in single Higgs observables, as well as direct Higgs pair production, have shown, lepton colliders are able to completely remove the degeneracy in the measurement of the triple Higgs coupling beyond the 4σ level, and the combination of data collected at a centre-of-mass energy of 250 GeV with data collected at energies of at least 350 GeV is of crucial importance for very-high-precision measurements in single Higgs

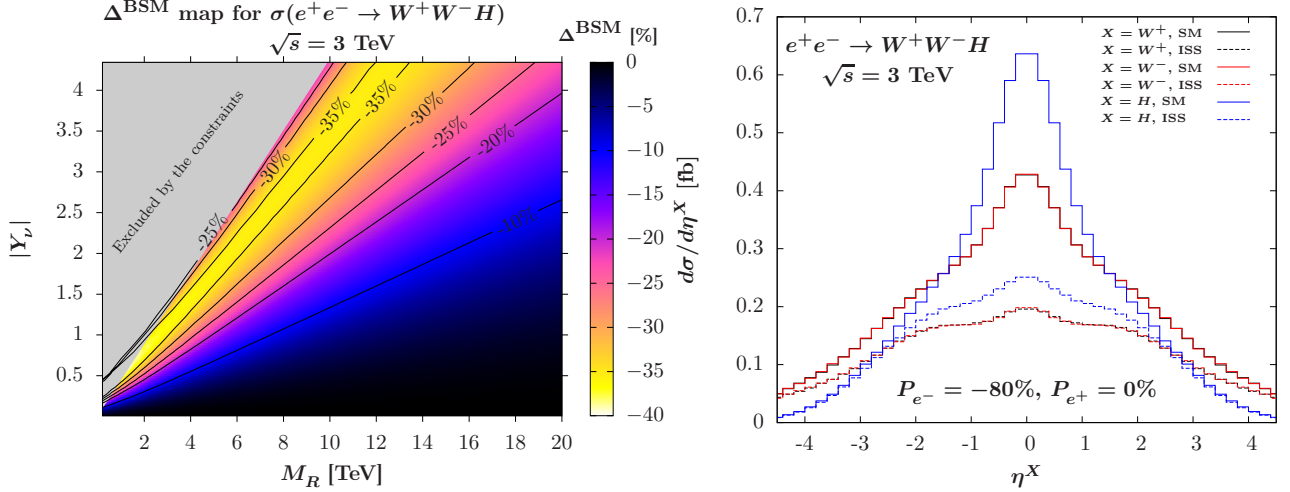


Fig. E.1.7: Left: Contour map of the neutrino corrections Δ^{BSM} at the 3 TeV CLIC, using a -80% polarised electron beam, as a function of the see-saw scale M_R and $|Y_\nu|$. Right: Pseudo-rapidity distributions of the W^+ (black), W^- (red), and Higgs (blue) bosons. The solid curves stand for the SM predictions while the dashed curves stand for the ISS predictions, for the benchmark scenario described in the text. Figures taken from Ref. [33].

physics. Opportunities offered by the Higgs sector to test neutrino mass models at future lepton colliders have also been presented. The FCC-ee is very competitive to test the heavy sterile neutrino option in the gigaelectronvolt regime. As far as the teraelectronvolt regime for the heavy neutrino scale is concerned, studies reported in the literature have shown that the CLIC and ILC at high energies could offer new avenues in the Higgs sector via precision measurements of the triple Higgs coupling, as well as of the production cross-section of a pair of W bosons in association with a Higgs boson. In the same spirit, the FCC-ee may well offer new opportunities in the same mass regime via precision calculations at one and two loops for the ZH production cross-section, which remain to be studied.

References

- [1] H. Baer *et al.*, The international linear collider technical design report, vol. 2: physics (2013), [arXiv:1306.6352](https://arxiv.org/abs/1306.6352)
- [2] M.J. Boland *et al.*, Updated baseline for a staged compact linear collider, [arXiv:1608.07537](https://arxiv.org/abs/1608.07537), [doi:10.5170/CERN-2016-004](https://doi.org/10.5170/CERN-2016-004).
- [3] C.F. Dürig, Ph.D. thesis, Hamburg University, 2016. http://inspirehep.net/record/1493742/files/phd_thesis_duerig.pdf
- [4] T. Barklow *et al.*, *Phys. Rev.* **D97** (2018) 053004. [arXiv:1708.09079](https://arxiv.org/abs/1708.09079), [doi:10.1103/PhysRevD.97.053004](https://doi.org/10.1103/PhysRevD.97.053004)
- [5] H. Abramowicz *et al.*, *Eur. Phys. J.* **C77** (2017) 475. [arXiv:1608.07538](https://arxiv.org/abs/1608.07538), [doi:10.1140/epjc/s10052-017-4968-5](https://doi.org/10.1140/epjc/s10052-017-4968-5)
- [6] M. Dong and G. Li, CEPC conceptual design report, vol. 2: physics & detector (2018), [arXiv:1811.10545](https://arxiv.org/abs/1811.10545)
- [7] A. Abada *et al.*, *Eur. Phys. J.* **C79** (2019) 474. [doi:10.1140/epjc/s10052-019-6904-3](https://doi.org/10.1140/epjc/s10052-019-6904-3)

- [8] A. Abada *et al.*, *Eur. Phys. J. Spec. Top.* **228** (2019) 261.
[doi:10.1140/epjst/e2019-900045-4](https://doi.org/10.1140/epjst/e2019-900045-4)
- [9] A. Blondel and P. Janot, Future strategies for the discovery and the precise measurement of the Higgs self coupling, [arXiv:1809.10041](https://arxiv.org/abs/1809.10041)
- [10] M. McCullough, *Phys. Rev.* **D90** (2014) 015001 [Erratum: **D92** (2015) 039903].
[arXiv:1312.3322](https://arxiv.org/abs/1312.3322),
[doi:10.1103/PhysRevD.90.015001](https://doi.org/10.1103/PhysRevD.90.015001), [doi:10.1103/PhysRevD.92.039903](https://doi.org/10.1103/PhysRevD.92.039903)
- [11] G. Degrossi *et al.*, *JHEP* **04** (2017) 155. [arXiv:1702.01737](https://arxiv.org/abs/1702.01737),
[doi:10.1007/JHEP04\(2017\)155](https://doi.org/10.1007/JHEP04(2017)155)
- [12] S. Di Vita *et al.*, *JHEP* **09** (2017) 069. [arXiv:1704.01953](https://arxiv.org/abs/1704.01953),
[doi:10.1007/JHEP09\(2017\)069](https://doi.org/10.1007/JHEP09(2017)069)
- [13] S. Di Vita *et al.*, *JHEP* **02** (2018) 178. [arXiv:1711.03978](https://arxiv.org/abs/1711.03978),
[doi:10.1007/JHEP02\(2018\)178](https://doi.org/10.1007/JHEP02(2018)178)
- [14] F. Maltoni *et al.*, *JHEP* **07** (2018) 087. [arXiv:1802.07616](https://arxiv.org/abs/1802.07616),
[doi:10.1007/JHEP07\(2018\)087](https://doi.org/10.1007/JHEP07(2018)087)
- [15] J. de Blas *et al.*, *JHEP* **01** (2020) 139. [arXiv:1905.03764](https://arxiv.org/abs/1905.03764),
[doi:10.1007/JHEP01\(2020\)139](https://doi.org/10.1007/JHEP01(2020)139)
- [16] M. Cepeda *et al.*, *CERN Yellow Rep. Monogr.* **7** (2019) 221. [arXiv:1902.00134](https://arxiv.org/abs/1902.00134),
[doi:10.23731/CYRM-2019-007.221](https://doi.org/10.23731/CYRM-2019-007.221)
- [17] The ATLAS collaboration, Combination of searches for Higgs boson pairs in pp collisions at 13 TeV with the ATLAS experiment, ATLAS-CONF-2018-043.
<https://inspirehep.net/literature/1694007>
- [18] Y. Fukuda *et al.*, *Phys. Rev. Lett.* **81** (1998) 1562. [arXiv:hep-ex/9807003](https://arxiv.org/abs/hep-ex/9807003),
[doi:10.1103/PhysRevLett.81.1562](https://doi.org/10.1103/PhysRevLett.81.1562)
- [19] I. Esteban *et al.*, *JHEP* **01** (2019) 106. [arXiv:1811.05487](https://arxiv.org/abs/1811.05487),
[doi:10.1007/JHEP01\(2019\)106](https://doi.org/10.1007/JHEP01(2019)106)
- [20] R.N. Mohapatra, *Phys. Rev. Lett.* **56** (1986) 561. [doi:10.1103/PhysRevLett.56.561](https://doi.org/10.1103/PhysRevLett.56.561)
- [21] R.N. Mohapatra and J.W.F. Valle, *Phys. Rev.* **D34** (1986) 1642.
[doi:10.1103/PhysRevD.34.1642](https://doi.org/10.1103/PhysRevD.34.1642)
- [22] J. Bernabeu *et al.*, *Phys. Lett.* **B187** (1987) 303. [doi:10.1016/0370-2693\(87\)91100-2](https://doi.org/10.1016/0370-2693(87)91100-2)
- [23] J. Kersten and A. Y. Smirnov, *Phys. Rev.* **D76** (2007) 073005. [arXiv:0705.3221](https://arxiv.org/abs/0705.3221),
[doi:10.1103/PhysRevD.76.073005](https://doi.org/10.1103/PhysRevD.76.073005)
- [24] K. Moffat *et al.*, Equivalence between massless neutrinos and lepton number conservation in fermionic singlet extensions of the Standard Model, [arXiv:1712.07611](https://arxiv.org/abs/1712.07611)
- [25] S. Antusch and O. Fischer, *JHEP* **05** (2015) 053. [arXiv:1502.05915](https://arxiv.org/abs/1502.05915),
[doi:10.1007/JHEP05\(2015\)053](https://doi.org/10.1007/JHEP05(2015)053)
- [26] M. Ruan, *Nucl. Part. Phys. Proc.* **273–275** (2016) 857. [arXiv:1411.5606](https://arxiv.org/abs/1411.5606),
[doi:10.1016/j.nuclphysbps.2015.09.132](https://doi.org/10.1016/j.nuclphysbps.2015.09.132)
- [27] M. Pandurović, Physics potential for the measurement of $\sigma(\text{HZ}) \times \text{BR}(\text{H} \rightarrow \text{WW}^*)$ at the 250 GeV ILC, Int. Workshop on Future Linear Colliders (LCWS 2018), Arlington, TZ, USA, 2018, [arXiv:1902.08032](https://arxiv.org/abs/1902.08032)
- [28] A. Pilaftsis, *Phys. Lett.* **B285** (1992) 68. [doi:10.1016/0370-2693\(92\)91301-0](https://doi.org/10.1016/0370-2693(92)91301-0)

- [29] E. Arganda *et al.*, *Phys. Rev.* **D91** (2015) 015001. [arXiv:1405.4300](#),
[doi:10.1103/PhysRevD.91.015001](#)
- [30] E. Arganda *et al.*, *Phys. Rev.* **D93** (2016) 055010. [arXiv:1508.04623](#),
[doi:10.1103/PhysRevD.93.055010](#)
- [31] J. Baglio and C. Weiland, *Phys. Rev.* **D94** (2016) 013002. [arXiv:1603.00879](#),
[doi:10.1103/PhysRevD.94.013002](#)
- [32] J. Baglio and C. Weiland, *JHEP* **04** (2017) 038. [arXiv:1612.06403](#),
[doi:10.1007/JHEP04\(2017\)038](#)
- [33] J. Baglio *et al.*, *Eur. Phys. J.* **C78** (2018) 795. [arXiv:1712.07621](#),
[doi:10.1140/epjc/s10052-018-6279-x](#)
- [34] E. Fernandez-Martinez *et al.*, *JHEP* **08** (2016) 033. [arXiv:1605.08774](#),
[doi:10.1007/JHEP08\(2016\)033](#)
- [35] K. Fujii *et al.*, Physics case for the International Linear Collider, [arXiv:1506.05992](#)
- [36] H.-J. He *et al.*, *Phys. Rev.* **D93** (2016) 015003. [arXiv:1506.03302](#),
[doi:10.1103/PhysRevD.93.015003](#)
- [37] I. Esteban *et al.*, *JHEP* **01** (2017) 087. [arXiv:1611.01514](#),
[doi:10.1007/JHEP01\(2017\)087](#)

2 Exotic Higgs decays (and long-lived particles) at future colliders

Contribution* by: J.F. Zurita [jose.zurita@kit.edu]

2.1 Exotic Higgs decays: motivations and signatures

The theoretical motivations and the large breadth of signatures for exotic Higgs decays have been thoroughly reviewed in Ref. [1]. They were first considered as a discovery mode of new physics in the context of a hidden valley scenario [2–4]. In the last few years, exotic Higgs decays have been revisited, as they arise ubiquitously in models of neutral naturalness, such as twin Higgs [5], folded supersymmetry [6], fraternal twin Higgs [7], hyperbolic Higgs [8], and singlet scalar top partners [9].

A simple proxy model for hidden valleys is obtained via a Higgs portal set-up,

$$\mathcal{L} \supset \frac{1}{2}(\partial_\mu\phi)^2 - \frac{1}{2}M^2\phi^2 - A|H|^2\phi - \frac{1}{2}\kappa|H|^2\phi^2 - \frac{1}{6}\mu\phi^3 - \frac{1}{24}\phi^4 - \frac{1}{2}\lambda_H|H|^4. \quad (2.1)$$

The fields H and ϕ mix, depending on κ and A , giving rise to physical states $h(125)$ and $X(m_X)$. Note that the phenomenology is fully encapsulated by three free parameters: m_X , $c\tau(X) \equiv c\tau$, and $\text{Br}(h \rightarrow XX)$. We will assume that the $h \rightarrow XX$ is always kinematically open. Existing constraints on the $h(125)$ properties imply that currently the room for an exotic Higgs branching ratio, $\text{Br}(h \rightarrow XX)$ is below about 10%. Since the mixing controls the X decay widths, a small mixing naturally gives rise to particles that travel a macroscopic distance $c\tau \gtrsim \text{mm}$ before decaying. Exotic Higgs decays are then encompassed within the larger class of ‘long-lived particles’ (LLP) signatures. For concreteness, we review LLPs in the next subsection.

It is worth stressing that the HL-LHC will produce about 10^8 Higgs bosons, while the CEPC and FCC-ee (240) will only give about 10^6 . Hence, there is a trade-off between the clean environment provided by the collider and the corresponding production cross-section. This already tells us that future electron–positron colliders might probe exotic Higgs branching fractions down to 10^{-5} , while at the HL-LHC one could, in principle, go down to 10^{-6} or even 10^{-7} , depending on the visibility of the target final state.

2.2 Long-lived particles (LLPs)

Long-lived particles are Beyond Standard Model states with macroscopic lifetimes (\gtrsim nanoseconds). These are theoretically well motivated in extensions of the SM trying to solve fundamental problems of the SM, such as dark matter or neutrino masses. A comprehensive overview of the theoretical motivations for LLPs can be found in Ref. [10], while a signature-driven document was put forward by the LLP@LHC community in Ref [11].

In a nutshell, to obtain a macroscopic lifetime (or a very narrow width), one is led to one of three choices: a large mass hierarchy (e.g., muon decay), a compressed spectrum (e.g., neutron lifetime), and feeble interactions. The latter is the one that concerns exotic Higgs decays.

*This contribution should be cited as:

J.F. Zurita, Exotic Higgs decays (and long-lived particles) at future colliders, DOI: [10.23731/CYRM-2020-003.241](https://doi.org/10.23731/CYRM-2020-003.241), in: Theory for the FCC-ee, Eds. A. Blondel, J. Gluza, S. Jadach, P. Janot and T. Riemann, CERN Yellow Reports: Monographs, CERN-2020-003, DOI: [10.23731/CYRM-2020-003](https://doi.org/10.23731/CYRM-2020-003), p. 241.
© CERN, 2020. Published by CERN under the [Creative Commons Attribution 4.0 license](https://creativecommons.org/licenses/by/4.0/).

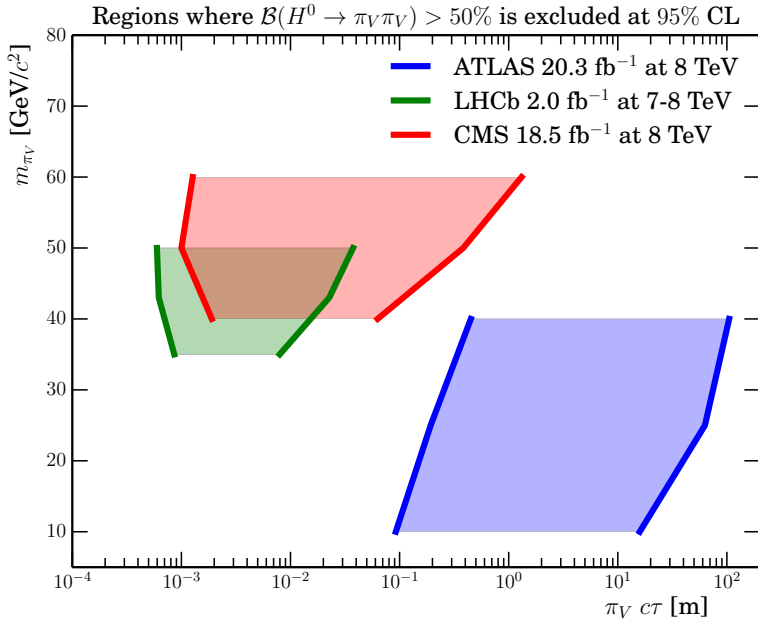


Fig. E.2.1: Reach of the ATLAS [16], CMS [17], and LHCb [18] studies for $X \rightarrow jj$, where X is taken to be a dark pion π_V of the hidden valley scenario. This model is in one-to-one correspondence with that described in Section 2.1. The shaded regions show where $\text{Br}(H \rightarrow XX) > 50\%$ is excluded. Note that the area to the lower left cannot be probed by current searches. Plot taken from the supplementary material of Ref. [18].

In the last few years, there several proposed detectors have been targeting neutral LLPs, such as MATHUSLA [12], FASER [13], CODEX-b [14], and AL3X [15]. Exotic Higgs decays constitute a major theoretical motivation in the design of such experiments, which can probe the difficult phase space regions where the standard triggers and object reconstruction became inefficient. These shortcomings will be detailed in the next subsection.

2.3 Exotic Higgs decays vis-à-vis current LHC data

Since, in the simplest scenarios, the X particle decays like a SM Higgs boson of m_X , what occurs is that the predominant decays are into $b\bar{b}$ pairs, if the channel is open. In that case, the existing programme of LHC searches for displaced hadronic vertexes (see, e.g., Refs. [16–18]) can cover part of the parameter space. We display the current coverage in the $c\tau$ – m_X plane in Fig. E.2.1. We immediately see that the current LHC data are not able to cover the region of short lifetimes ($c\tau \lesssim 10$ cm) and low masses ($m_X < 35$ GeV). Low masses for X imply lower boosts, so the soft jets of the event will not pass the typical H_T or $p_T(j)$ trigger thresholds used by ATLAS and CMS.[†] As a sample, the reported trigger efficiency of CMS for $m_X = 50$ GeV and $c\tau = 30$ mm is about 2%. The other limitation corresponds to short lifetimes, which is limited by the vertex resolution. Hence, the shortcomings of pp machines can be targeted, instead, with a collider providing better angular resolution, lower p_T thresholds, and more accurate vertexing, which happens at both e^-p and e^+e^- machines. We stress that additional data will not alter this picture, and the low $c\tau$ and low m_X region would continue to be extremely hard to probe.

[†]It is worth noting that LHCb has the capability to trigger directly on displaced vertexes.

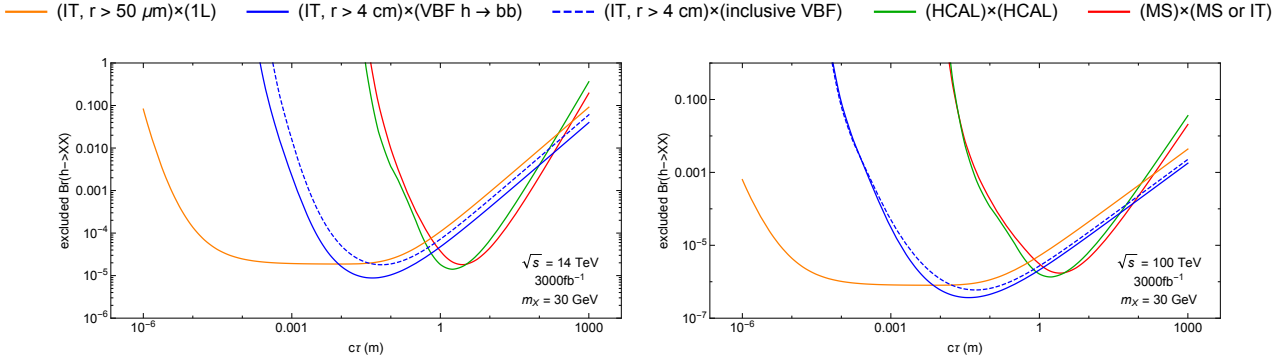


Fig. E.2.2: Sensitivities of the displaced searches for exotic Higgs decays at the HL-LHC (left) and FCC-hh (right), in the $c\tau$ - $\text{Br}(h \rightarrow XX)$ plane, for $m_X = 30$ GeV. The curves correspond to the use of different triggers and different assumptions about the reconstruction of the displaced vertexes. Plot taken from Ref [19].

2.4 Future experiments: HL-LHC, FCC, CEPC, LHeC

2.4.1 Proton–proton colliders

We show in Fig. E.2.2 (taken from Ref. [19]) the expected reach at the HL-LHC ($\sqrt{s} = 14$ TeV and total integrated luminosity of 3 ab^{-1}) and at the FCC-hh ($\sqrt{s} = 100$ TeV and total integrated luminosity of 3 ab^{-1}) for a scalar mass of $m_X = 30$ GeV. The curves indicate different choices of trigger and of reconstruction capabilities of the displaced vertex. In particular, the orange curve corresponds to one displaced vertex in the inner tracker with an impact parameter of $50 \mu\text{m}$, which poses an interesting experimental challenge and thus should be regarded as an optimistic case. The blue curve corresponds to the realistic case of using VBF, $h \rightarrow b\bar{b}$ triggers down to an impact parameter of 4 cm.

We see that one can cover lifetimes as short as a millimetre (or even one micrometre for the optimistic scenario), while the probed exotic branching ratios can reach down to 10^{-5} (10^{-6}) for the HL-LHC (FCC-hh), for the benchmark case of $m_X = 30$ GeV. As discussed before, lower masses would suffer from a poor trigger efficiency, which opens a window of opportunity for both electron–proton and electron–positron colliders.

2.4.2 Electron–proton colliders

The reach on exotic Higgs decays for future electron–proton colliders is displayed in Fig. E.2.3. We see that the electron–proton colliders, owing to their better resolution, can test masses down to 5 GeV for exotic branching fractions of about 10^{-4} . This mass range is almost impossible to probe at the LHC, because of the overwhelming multijet background. We also note that electron–proton colliders provide a smaller luminosity.[‡] Hence, electron–proton colliders provide a window of opportunity to overcome the gaps in coverage discussed for proton–proton colliders.

[‡]During a 25 year run period of the Future Circular Collider (FCC), the proton–proton incarnation (FCC-hh) is expected to collect $15\text{--}30 \text{ ab}^{-1}$ while the electron–proton version will collect only 1 ab^{-1} [20].

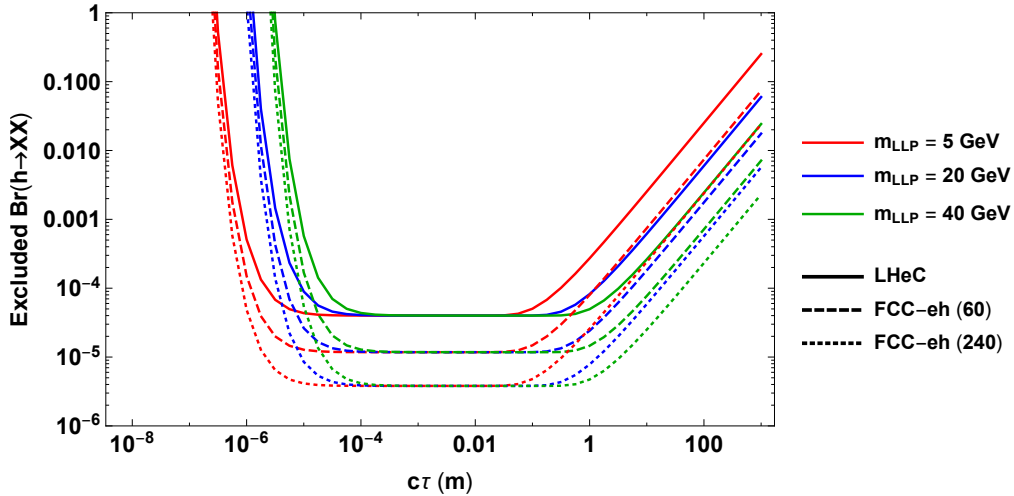


Fig. E.2.3: Reach of the future electron–proton colliders: LHeC (solid), FCC-eh (60), and FCC-eh (240). The LHeC would collide a 7 TeV proton from the LHC against a 50 GeV electron beam, while for the FCC-eh a 50 TeV proton beam will collide against a 60 GeV (design case) or 240 GeV beam (optimistic scenario). Taken from Refs. [21, 22].

2.4.3 Electron–positron colliders

Finally, we take a look at the e^+e^- case. A detailed analysis is reported in Ref [23]; here, we briefly summarise the most salient points. This study considers the Higgs-strahlung process $e^+e^- \rightarrow hZ$ with leptonic decays of the Z boson for both the FCC-ee [24] and the CEPC [25, 26]. A set of basic selection cuts allows us to achieve a zero-background regime for the irreducible SM processes.[§] Two different strategies are pursued: the large mass and the long-lifetime regime. The main difference between the two is in the requirements on the minimal distance between the displaced vertexes. The results are shown in Fig. E.2.4.

One immediately sees that the e^+e^- colliders can test exotic branching fractions down to 5×10^{-5} . Moreover, they can go low in mass, down to a few gigaelectronvolts, and they can also probe decay lengths down to micrometres, where the proton–proton colliders would be ineffective.

2.5 Conclusions

In this contribution, I have summarised the existing studies on exotic Higgs decays at current and future colliders. While the proton–proton machines would, in principle, be the best option, owing to their larger energies and luminosities, we have also seen that the phase space regions where the LHC and FCC-hh lose steam, namely, low X masses and short lifetimes provide a unique window of opportunity for both e^-p and e^+e^- colliders. The latter two types of machine have only recently been studied, and thus there is naturally much room for improvement. It should also be stressed that these kinds of study can help to optimise the detector design of future colliders.

[§]Backgrounds from particles originating away from the interaction point (e.g., beam halo, cosmic muons, cavern radiation) are not considered.

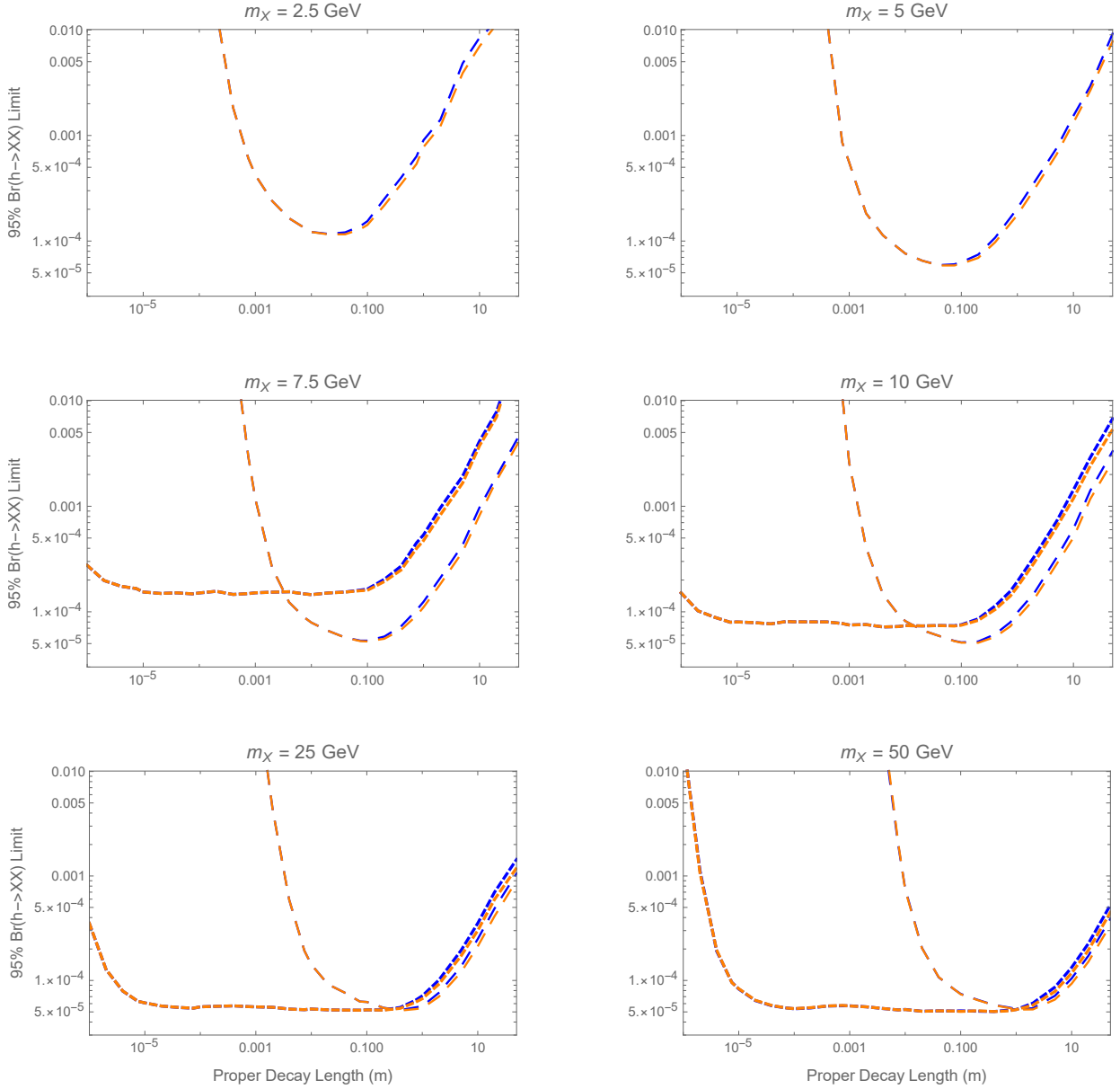


Fig. E.2.4: FCC-ee (blue) and CEPC (orange) limits on the exotic branching ratio $h \rightarrow XX$ at the 95% CL. The ‘long-lifetime’ analysis is shown with larger dashes, while smaller dashes correspond to the ‘large-mass’ study. Taken from Ref. [23].

References

- [1] D. Curtin *et al.*, *Phys. Rev.* **D90** (2014) 075004. [arXiv:1312.4992](https://arxiv.org/abs/1312.4992), [doi:10.1103/PhysRevD.90.075004](https://doi.org/10.1103/PhysRevD.90.075004)
- [2] M.J. Strassler and K.M. Zurek, *Phys. Lett.* **B651** (2007) 374. [arXiv:hep-ph/0604261](https://arxiv.org/abs/hep-ph/0604261), [doi:10.1016/j.physletb.2007.06.055](https://doi.org/10.1016/j.physletb.2007.06.055)
- [3] M.J. Strassler and K.M. Zurek, *Phys. Lett.* **B661** (2008) 263. [arXiv:hep-ph/0605193](https://arxiv.org/abs/hep-ph/0605193), [doi:10.1016/j.physletb.2008.02.008](https://doi.org/10.1016/j.physletb.2008.02.008)
- [4] M.J. Strassler, Possible effects of a hidden valley on supersymmetric phenomenology, [arXiv:hep-ph/0607160](https://arxiv.org/abs/hep-ph/0607160)

-
- [5] Z. Chacko *et al.*, *Phys. Rev. Lett.* **96** (2006) 231802. [arXiv:hep-ph/0506256](#), [doi:10.1103/PhysRevLett.96.231802](#)
- [6] G. Burdman *et al.*, *JHEP* **02** (2007) 009. [arXiv:hep-ph/0609152](#), [doi:10.1088/1126-6708/2007/02/009](#)
- [7] N. Craig *et al.*, *JHEP* **07** (2015) 105. [arXiv:1501.05310](#), [doi:10.1007/JHEP07\(2015\)105](#)
- [8] T. Cohen *et al.*, *JHEP* **05** (2018) 091. [arXiv:1803.03647](#), [doi:10.1007/JHEP05\(2018\)091](#)
- [9] H.-C. Cheng *et al.*, *JHEP* **05** (2018) 057. [arXiv:1803.03651](#), [doi:10.1007/JHEP05\(2018\)057](#)
- [10] D. Curtin *et al.*, *Rept. Prog. Phys.* **82** (2019) 116201. [arXiv:1806.07396](#), [doi:10.1088/1361-6633/ab28d6](#)
- [11] J. Alimena *et al.*, Searching for long-lived particles beyond the Standard Model at the Large Hadron Collider, [arXiv:1903.04497](#)
- [12] J.P. Chou *et al.*, *Phys. Lett.* **B767** (2017) 29. [arXiv:1606.06298](#), [doi:10.1016/j.physletb.2017.01.043](#)
- [13] J.L. Feng *et al.*, *Phys. Rev.* **D97** (2018) 035001. [arXiv:1708.09389](#), [doi:10.1103/PhysRevD.97.035001](#)
- [14] V.V. Gligorov *et al.*, *Phys. Rev.* **D97** (2018) 015023. [arXiv:1708.09395](#), [doi:10.1103/PhysRevD.97.015023](#)
- [15] V.V. Gligorov *et al.*, *Phys. Rev.* **D99** (2019) 015023. [arXiv:1810.03636](#), [doi:10.1103/PhysRevD.99.015023](#)
- [16] G. Aad *et al.*, *Phys. Rev.* **D92** (2015) 072004. [arXiv:1504.05162](#), [doi:10.1103/PhysRevD.92.072004](#)
- [17] V. Khachatryan *et al.*, *Phys. Rev.* **D91** (2015) 012007. [arXiv:1411.6530](#), [doi:10.1103/PhysRevD.91.012007](#)
- [18] R. Aaij *et al.*, *Eur. Phys. J.* **C77** (2017) 812. [arXiv:1705.07332](#), [doi:10.1140/epjc/s10052-017-5178-x](#)
- [19] D. Curtin and C.B. Verhaaren, *JHEP* **12** (2015) 072. [arXiv:1506.06141](#), [doi:10.1007/JHEP12\(2015\)072](#)
- [20] M. Mangano *et al.*, *Eur. Phys. J.* **C79** (2019) 474. [doi:10.1140/epjc/s10052-019-6904-3](#)
- [21] D. Curtin *et al.*, *JHEP* **07** (2018) 024. [arXiv:1712.07135](#), [doi:10.1007/JHEP07\(2018\)024](#)
- [22] D. Curtin *et al.*, *PoS DIS2018* (2018) 090. [arXiv:1805.12533](#), [doi:10.22323/1.316.0090](#)
- [23] S. Alipour-Fard *et al.*, *Chin. Phys.* **C43** (2019) 053101. [arXiv:1812.05588](#), [doi:10.1088/1674-1137/43/5/053101](#)
- [24] M. Bicer *et al.*, *JHEP* **01** (2014) 164. [arXiv:1308.6176](#), [doi:10.1007/JHEP01\(2014\)164](#)
- [25] M. Dong and G. Li, CEPC conceptual design report, vol. 2: physics & detector (2018), [arXiv:1811.10545](#)
- [26] C.S. Group, CEPC conceptual design report: vol. 1: accelerator, [arXiv:1809.00285](#)

3 Precision predictions for Higgs decays in the (N)MSSM

Contribution* by: F. Domingo, S. Heinemeyer, S. Paßehr, G. Weiglein
Corresponding author: S. Heinemeyer [Sven.Heinemeyer@cern.ch]

3.1 Introduction

The signal that was discovered in the Higgs searches at ATLAS and CMS at a mass of ~ 125 GeV [1–3] is, within current theoretical and experimental uncertainties, compatible with the properties of the Higgs boson predicted within the Standard Model (SM) of particle physics. No conclusive signs of physics beyond the SM have been reported so far. However, the measurements of Higgs signal strengths for the various channels leave considerable room for Beyond Standard Model (BSM) interpretations. Consequently, the investigation of the precise properties of the discovered Higgs boson will be one of the prime goals at the LHC and beyond. While the mass of the observed particle is already known with excellent accuracy [4, 5], significant improvements of the information about the couplings of the observed state are expected from the upcoming runs of the LHC [3, 6–9] and even more so from the high-precision measurements at a future e^+e^- collider [10–18]. For the accurate study of the properties of the Higgs boson, precise predictions for the various partial decay widths, the branching ratios (BRs), and the Higgs boson production cross-sections, along with their theoretical uncertainties, are indispensable.

Motivated by the ‘hierarchy problem’, supersymmetry (SUSY) inspired extensions of the SM play a prominent role in the investigations of possible new physics. As such, the minimal supersymmetric Standard Model (MSSM) [19, 20] or its singlet extension, the next-to-MSSM (NMSSM) [21, 22], have been the object of many studies in the last decades. Despite this attention, these models are not yet prepared for an era of precision tests, as the uncertainties at the level of the Higgs mass calculation [23–25] are about one order of magnitude larger than the experimental uncertainty. At the level of the decays, the theoretical uncertainty arising from unknown higher-order corrections has been estimated for the case of the Higgs boson of the SM (where the Higgs mass is treated as a free input parameter) in Refs. [26, 27] and updated in Ref. [28]: depending on the channel and the Higgs mass, it typically falls in the range of ~ 0.5 –5%. To our knowledge, no similar analysis has been performed in SUSY-inspired models (or other BSM models), but one can expect the uncertainties from missing higher-order corrections to be larger in general—with many nuances, depending on the characteristics of the Higgs state and the considered point in parameter space: we provide some discussion of this issue at the end of this section. In addition, parametric uncertainties that are induced by the experimental errors of the input parameters should be taken into account. For the case of the SM decays, those parametric uncertainties have been discussed in the references cited. In the SUSY case, the parametric uncertainties induced by the (known) SM input parameters can be determined in the same way as for the SM, while the dependence on unknown SUSY parameters can be utilised in setting constraints on those parameters. While still competitive

*This contribution should be cited as:

F. Domingo, S. Heinemeyer, S. Paßehr, G. Weiglein, Precision predictions for Higgs decays in the (N)MSSM, DOI: [10.23731/CYRM-2020-003.247](https://doi.org/10.23731/CYRM-2020-003.247), in: Theory for the FCC-ee, Eds. A. Blondel, J. Gluza, S. Jadach, P. Janot and T. Riemann,

CERN Yellow Reports: Monographs, CERN-2020-003, DOI: [10.23731/CYRM-2020-003](https://doi.org/10.23731/CYRM-2020-003), p. 247.

© CERN, 2020. Published by CERN under the [Creative Commons Attribution 4.0 license](https://creativecommons.org/licenses/by/4.0/).

today, the level of accuracy of the theoretical predictions of Higgs boson decays in SUSY models should soon become outclassed by the achieved experimental precision (in particular at future e^+e^- colliders) on the decays of the observed Higgs signal. Without comparable accuracy of the theoretical predictions, the impact of the exploitation of the precision data will be diminished—either in terms of further constraining the parameter space or of interpreting deviations from the SM results. Further efforts towards improving the theoretical accuracy are therefore necessary in order to enable a thorough investigation of the phenomenology of these models. Besides the decays of the SM-like state at 125 GeV of a SUSY model—where the goal is clearly to reach an accuracy that is comparable to the case of the SM—it is also of interest to obtain reliable and accurate predictions for the decays of the other Higgs bosons in the spectrum. The decays of the non-SM-like Higgs bosons can be affected by large higher-order corrections as a consequence of either large enhancement factors or a suppression of the lowest-order contribution. Confronting accurate predictions with the available search limits yields important constraints on the parameter space. Here, we review the evaluation of the decays of the neutral Higgs bosons of the \mathbb{Z}_3 -conserving NMSSM into SM particles, as presented in Ref. [29].

Current work focusing on NMSSM Higgs decays is part of the effort for developing a version of `FeynHiggs` [23, 30–37] dedicated to the NMSSM [38, 39]. The general methodology relies on a Feynman-diagrammatic calculation of radiative corrections, which employs `FeynArts` [40, 41], `FormCalc` [42], and `LoopTools` [42]. The renormalization scheme has been implemented within the NMSSM [39] in such a way that the result in the MSSM limit of the NMSSM exactly coincides with the MSSM result obtained from `FeynHiggs` without any further adjustments of parameters.

3.2 Higgs decays to SM particles in the \mathcal{CP} -violating NMSSM

In this section, we review the technical aspects of our calculation of the Higgs decays. Our notation and the renormalization scheme that we employ for the \mathbb{Z}_3 -conserving NMSSM in the general case of complex parameters are presented in Section 2 of Ref. [39], and we refer the reader to that article for further details.

3.2.1 Decay amplitudes for a physical (on-shell) Higgs state—generalities

3.2.1.1 On-shell external Higgs leg

In this section, we consider the decays of a physical Higgs state, i.e., an eigenstate of the inverse propagator matrix for the Higgs fields, evaluated at the corresponding pole eigenvalue. The connection between such a physical state and the tree-level Higgs fields entering the Feynman diagrams is non-trivial in general since the higher-order contributions induce mixing among the Higgs states and between the Higgs states and the gauge bosons (as well as the associated Goldstone bosons). The LSZ reduction fully determines the (non-unitary) transition matrix \mathbf{Z}^{mix} between the loop-corrected mass eigenstates and the lowest-order states. Then, the amplitude describing the decay of the physical state h_i^{phys} (we shall omit the superscript ‘phys’ later on), into e.g., a fermion pair $f\bar{f}$, relates to the amplitudes in terms of the tree-level states h_j^0 according to (see the following for the mixing with gauge bosons and Goldstone bosons):

$$\mathcal{A}[h_i^{\text{phys}} \rightarrow f\bar{f}] = Z_{ij}^{\text{mix}} \mathcal{A}[h_j^0 \rightarrow f\bar{f}]. \quad (3.1)$$

Here, we characterize the physical Higgs states according to the procedure outlined in Ref. [39] (see also Refs. [32, 43, 44]).

1. The Higgs self-energies include full one-loop and leading $\mathcal{O}(\alpha_t\alpha_s, \alpha_t^2)$ two-loop corrections (with two-loop effects obtained in the MSSM approximation via the publicly available code `FeynHiggs`[†]).
2. The pole masses correspond to the zeros of the determinant of the inverse propagator matrix.
3. The (5×5) matrix \mathbf{Z}^{mix} is obtained in terms of the solutions of the eigenvector equation for the effective mass matrix evaluated at the poles, and satisfying the appropriate normalization conditions (see Section 2.6 of Ref., [39]).

In correcting the external Higgs legs by the full matrix \mathbf{Z}^{mix} —instead of employing a simple diagrammatic expansion—we resum contributions to the transition amplitudes that are formally of higher-loop order. This resummation is convenient for taking into account numerically relevant leading higher-order contributions. It can, in fact, be crucial for the frequent case where radiative corrections mix states that are almost mass-degenerate in order to properly describe the resonance-type effects that are induced by the mixing. Conversely, care needs to be taken to avoid the occurrence of non-decoupling terms when Higgs states are well-separated in mass, since higher-order effects can spoil the order-by-order cancellations with vertex corrections.

We stress that all public tools, with the exception of `FeynHiggs`, neglect the full effect of the transition to the physical Higgs states encoded within \mathbf{Z}^{mix} , and instead employ the unitary approximation \mathbf{U}^0 neglecting external momenta (which is in accordance with leading-order or QCD-improved leading-order predictions). We refer the reader to Refs. [32, 39, 44] for the details of the definition of \mathbf{U}^0 or \mathbf{U}^m (another unitary approximation), as well as a discussion of their impact at the level of Higgs decay widths.

3.2.1.2 Higgs–electroweak mixing

For the mass determination, we do not take into account contributions arising from the mixing of the Higgs fields with the neutral Goldstone or Z bosons, since these corrections enter at the subdominant two-loop level (contributions of this kind can also be compensated by appropriate field-renormalization conditions [47]). We note that, in the \mathcal{CP} -conserving case, only external \mathcal{CP} -odd Higgs components are affected by such a mixing. Yet, at the level of the decay amplitudes, the Higgs mixing with the Goldstone and Z bosons already enters at the one-loop order (even if the corresponding self-energies are cancelled by an appropriate field-renormalization condition, this procedure will still provide a contribution to the $h_i\bar{f}f$ counterterm). Therefore, for a complete one-loop result of the decay amplitudes, it is, in general, necessary to incorporate Higgs–Goldstone and Higgs–Z self-energy transition diagrams [43, 48, 49]. In the following, we evaluate such contributions to the decay amplitudes in the usual diagrammatic fashion (as prescribed by the LSZ reduction), with the help of the `FeynArts` model file for the \mathcal{CP} -violating NMSSM [39]. The corresponding one-loop amplitudes (including the associated counterterms) will be symbolically denoted as $\mathcal{A}_{G/Z}^{\text{1L}}$. These amplitudes can be written in terms of the self-energies $\Sigma_{h_i G/Z}$ with Higgs and Goldstone or Z bosons in the external legs. In turn, these self-energies are connected by a Slavnov–Taylor identity (see e.g., Appendix A of

[†]The Higgs masses in `FeynHiggs` could be computed with additional improvements, such as additional fixed-order results [45, 46] or the resummation of large logarithms for very heavy SUSY particles [33–35]; for simplicity, we do not take such refinements into account in this section.

Ref. [50]):[‡]

$$0 = M_Z \Sigma_{h_i G}(p^2) + i p^2 \Sigma_{h_i Z}(p^2) + M_Z (p^2 - m_{h_i}^2) f(p^2) - \frac{e}{2 s_w c_w} \sum_j [(U_n)_{i1}(U_n)_{j4} - (U_n)_{i2}(U_n)_{j5} - (U_n)_{j1}(U_n)_{i4} + (U_n)_{j2}(U_n)_{i5}] T_{h_j}, \quad (3.2a)$$

$$f(p^2) \equiv -\frac{\alpha}{16 \pi s_w c_w} \sum_j [(U_n)_{i1}(U_n)_{j4} - (U_n)_{i2}(U_n)_{j5} - (U_n)_{j1}(U_n)_{i4} + (U_n)_{j2}(U_n)_{i5}] \times [c_\beta (U_n)_{j1} + s_\beta (U_n)_{j2}] B_0(p^2, m_{h_j}^2, M_Z^2), \quad (3.2b)$$

where the T_{h_i} correspond to the tadpole terms of the Higgs potential and $(U_n)_{ij}$ are the elements of the transition matrix between the gauge- and tree-level mass-eigenstate bases of the Higgs bosons—the notation is introduced in Section 2.1 of Ref. [39]. Similar relations in the MSSM are also provided in Eq. (127) of Ref. [43]. We checked this identity at the numerical level.

3.2.1.3 Inclusion of one-loop contributions

The wave function normalization factors contained in \mathbf{Z}^{mix} , together with the described treatment of the mixing with the Goldstone and Z bosons, ensure the correct on-shell properties of the external Higgs leg in the decay amplitude, so that no further diagrams correcting this external leg are needed. Moreover, the SM fermions and gauge bosons are also treated as on-shell particles in our renormalization scheme. Beyond the transition to the loop-corrected states incorporated by \mathbf{Z}^{mix} , we thus compute the decay amplitudes at the one-loop order as the sum of the tree-level contribution $\mathcal{A}^{\text{tree}}$ (possibly equal to zero), the Higgs–electroweak one-loop mixing $\mathcal{A}_{G/Z}^{\text{1L}}$ and the (renormalised) one-loop vertex corrections $\mathcal{A}_{\text{vert}}^{\text{1L}}$ (including counterterm contributions)—we note that each of these pieces of the full amplitude is separately ultraviolet-finite. In the example of the $f\bar{f}$ decay, the amplitudes with a tree-level external Higgs field h_j^0 —on the right-hand side of Eq. (3.1)—thus symbolically read

$$\mathcal{A}[h_j^0 \rightarrow f\bar{f}] = \mathcal{A}^{\text{tree}}[h_j^0 \rightarrow f\bar{f}] + \mathcal{A}_{G/Z}^{\text{1L}}[h_j^0 \rightarrow f\bar{f}] + \mathcal{A}_{\text{vert}}^{\text{1L}}[h_j^0 \rightarrow f\bar{f}]. \quad (3.3)$$

All the pieces on the right-hand side of this equation are computed with the help of **FeynArts** [40, 41], **FormCalc** [42], and **LoopTools** [42], according to the prescriptions that are encoded in the model file for the \mathcal{CP} -violating NMSSM. However, we use a specific treatment for some of the contributions, such as QED and QCD one-loop corrections to Higgs decays into final-state particles that are electrically or colour charged, or include certain higher-order corrections. We describe these channel-specific modifications in the following subsections.

3.2.1.4 Goldstone-boson couplings

The cubic Higgs–Goldstone-boson vertices can be expressed as

$$\mathcal{L} \ni -\frac{1}{\sqrt{2}v} \left\{ \sum_j m_{h_j}^2 [\cos \beta (U_n)_{j1} + \sin \beta (U_n)_{j2}] h_j^0 \left[G^+ G^- + \frac{1}{2} (G^0)^2 \right] + \left[\sum_j (m_{H^\pm}^2 - m_{h_j}^2) (\sin \beta [(U_n)_{j1} + i (U_n)_{j4}] - \cos \beta [(U_n)_{j2} - i (U_n)_{j5}]) h_j^0 H^+ G^- + \text{h. c.} \right] \right\}$$

[‡]We denote the imaginary unit by i .

$$+ \frac{1}{2} \sum_{j,k} (m_{h_k}^2 - m_{h_j}^2) [(U_n)_{j1}(U_n)_{k4} - (U_n)_{j2}(U_n)_{k5} - (j \leftrightarrow k)] h_j^0 h_k^0 G^0 \Big\}. \quad (3.4)$$

The doublet vacuum expectation value (VEV), $v = M_W s_w / \sqrt{2\pi\alpha}$, is expressed in terms of the gauge-boson masses M_W and M_Z ($s_w = \sqrt{1 - M_W^2/M_Z^2}$), as well as the electromagnetic coupling α . The symbol $m_{h_j}^2$, ($j = 1, \dots, 5$), represents the tree-level mass squared of the neutral Higgs state h_j^0 , and $m_{H^\pm}^2$ represents the mass squared of the charged Higgs state.

The use of the tree-level couplings of Eq. (3.4), together with a physical (loop-corrected) external Higgs leg $h_i = \sum_j Z_{ij}^{\text{mix}} h_j^0$, is potentially problematic regarding the gauge properties of the matrix elements. The structure of the gauge theory and its renormalization indeed guarantee that the gauge identities are observed at the order of the calculation (one loop). However, the evaluation of Feynman amplitudes is not protected against a violation of the gauge identities at the (incomplete) two-loop order. We detected such gauge-violating effects of two-loop order at several points in our calculation of the neutral Higgs decays.

1. The Ward identity in $h_i \rightarrow \gamma\gamma$ is not satisfied (see also Ref. [51]).
2. Infrared (IR) divergences of the virtual corrections in $h_i \rightarrow W^+W^-$ do not cancel their counterparts in the bremsstrahlung process $h_i \rightarrow W^+W^-\gamma$ (see also Ref. [52]).
3. Computing $h_i \rightarrow f\bar{f}$ in an R_ξ gauge entails non-vanishing dependence of the amplitudes on the electroweak gauge-fixing parameters ξ_Z and ξ_W .

As these gauge-breaking effects could intervene with sizeable and uncontrolled numerical impact, it is desirable to add two-loop order terms, restoring the gauge identities at the level of the matrix elements. Technically, there are different possible procedures to achieve this: one would amount to replacing the kinematic Higgs masses that appear in Higgs–gauge-boson couplings with tree-level Higgs masses; we prefer the alternative procedure, which involves changing the Higgs–Goldstone-boson couplings of Eq. (3.4): for the Higgs mass associated to the external Higgs leg, the loop-corrected Higgs mass M_{h_i} is used instead of the tree-level one. This is actually the form of the Higgs–Goldstone-boson coupling that would be expected in an effective field theory of the physical Higgs boson h_i . Using the definition of Z_{ij}^{mix} as an eigenvector of the loop-corrected mass matrix for the eigenvalue $M_{h_i}^2$ —see Section 2.6 of Ref. [39]—one can verify that the effective Higgs–Goldstone-boson vertices employing the physical Higgs mass differ from their tree-level counterparts by a term of one-loop order (proportional to the Higgs self-energies) so that the alteration of the one-loop amplitudes is indeed of two-loop order. Employing this shift of the Higgs–Goldstone couplings cures the gauge-related issues that we mentioned earlier.

Another issue with gauge invariance appears in connection with the amplitudes $\mathcal{A}_{G/Z}^{\text{1L}}$. The Goldstone and Z boson propagators generate denominators with pole M_Z^2 (or $\xi_Z M_Z^2$ in an R_ξ gauge): in virtue of the Slavnov–Taylor identity of Eq. (3.2a), these terms should cancel one another in the total amplitude at the one-loop order—we refer the reader to Section 4.3 of Ref. [43] for a detailed discussion. However, the term $(p^2 - M_Z^2)^{-1}$ multiplying $f(p^2)$ of Eq. (3.2a) only vanishes if $p^2 = m_{h_i}^2$: if we employ $p^2 = M_{h_i}^2$ (the loop-corrected Higgs mass), the cancellation is spoiled by a term of two-loop order. To address this problem, we redefine

$\mathcal{A}_{G/Z}^{1L}$ by adding a two-loop term:

$$\tilde{\mathcal{A}}_{G/Z}^{1L}[h_i \rightarrow f\bar{f}] \equiv Z_{ij}^{\text{mix}} \cdot \mathcal{A}_{G/Z}^{1L}[h_j^0 \rightarrow f\bar{f}] + \frac{\Gamma_{Gff}^{\text{tree}}}{M_{h_i}^2} \sum_{j,k} \hat{\Sigma}_{h_j h_k}(M_{h_i}^2) \cdot Z_{ik}^{\text{mix}} \frac{f(M_{h_i}^2) \xi_Z M_Z^2}{M_{h_i}^2 - \xi_Z M_Z^2}, \quad (3.5)$$

where $\Gamma_{Gff}^{\text{tree}}$ represents the tree-level vertex of the neutral Goldstone boson with the fermion f (in the particular example of a Higgs decay into $f\bar{f}$). Then it is straightforward to check that $\tilde{\mathcal{A}}_{G/Z}^{1L}$ is gauge-invariant. The transformation of Eq. (3.5) can also be interpreted as a two-loop shift redefining $\Sigma_{h_i Z}$, so that it satisfies a generalised Slavnov–Taylor identity of the form of Eq. (3.2a), but applied to a physical (loop-corrected) Higgs field, with the term $(p^2 - m_{h_i}^2) f(p^2)$ of Eq. (3.2a) replaced with $(p^2 - M_{h_i}^2) f(p^2)$.

3.2.1.5 Numerical input in the one-loop corrections

As usual, the numerical values of the input parameters need to reflect the adopted renormalization scheme, and the input parameters corresponding to different schemes differ from each other by shifts of the appropriate loop order (at the loop level, there exists some freedom to use a numerical value of an input parameter that differs from the tree-level value by a one-loop shift, since the difference induced in this way is of higher order). Concerning the input values of the relevant light quark masses, we follow in our evaluation the choice of `FeynHiggs` and employ $\overline{\text{MS}}$ quark masses with three-loop QCD corrections evaluated at the scale of the mass of the decaying Higgs, $m_q^{\overline{\text{MS}}}(M_{h_i})$, in the loop functions and the definition of the Yukawa couplings. In addition, the input value for the pole top mass is converted to $m_t^{\overline{\text{MS}}}(m_t)$ using up to two-loop QCD and one-loop top Yukawa or electroweak corrections (corresponding to the higher-order corrections included in the Higgs boson mass calculation). Furthermore, the $\tan\beta$ -enhanced contributions are always included in the defining relation between the bottom Yukawa coupling and the bottom mass (and similarly for all other down-type quarks). Concerning the Higgs VEV appearing in the relation between the Yukawa couplings and the fermion masses, we parametrize it in terms of $\alpha(M_Z)$. Finally, the strong coupling constant employed in SUSY-QCD diagrams is set to the scale of the supersymmetric particles entering the loop. We will comment on deviations from these settings if needed.[§]

3.2.2 Higgs decays into SM fermions

Our calculation of the Higgs decay amplitudes into SM fermions closely follows the procedure outlined in the previous subsection. However, we include the QCD and QED corrections separately, making use of analytical formulae that are well-documented in the literature [54, 55]. We also employ an effective description of the Higgs– $b\bar{b}$ interactions in order to resum potentially large effects for large values of $\tan\beta$. Next, we comment on these two issues and discuss further the derivation of the decay widths for this class of channel.

[§]Possibly large contributions by electroweak double-logarithms of the Sudakov type as well as the corresponding counterparts in fermionic Higgs decays with additional real radiation of gauge bosons are investigated in a separate article [53].

3.2.2.1 Tree-level amplitude

At the tree level, the decay $h_j^0 \rightarrow \bar{f}f$ is determined by the Yukawa coupling Y_f and the decomposition of the tree-level state h_j^0 in terms of the Higgs-doublet components:

$$\mathcal{A}^{\text{tree}}[h_j^0 \rightarrow \bar{f}f] = -i \frac{Y_f}{\sqrt{2}} \bar{u}_f(p_f) \left\{ \delta_{f,d_k/e_k}(U_n)_{j1} + \delta_{f,u_k}(U_n)_{j2} - i\gamma_5 \left[\delta_{f,d_k/e_k}(U_n)_{j4} + \delta_{f,u_k}(U_n)_{j5} \right] \right\} v_f(p_{\bar{f}}) \quad (3.6)$$

$$\equiv -i \bar{u}_f(p_f) \left\{ g_{h_j \bar{f} f}^S - \gamma_5 g_{h_j \bar{f} f}^P \right\} v_f(p_{\bar{f}}). \quad (3.7)$$

The δ s are Kronecker symbols selecting the appropriate Higgs matrix element for the fermionic final state, $u_k = u, c, t$, $d_k = d, s, b$, or $e_k = e, \mu, \tau$. We have written the amplitude in the Dirac-fermion convention, separating the scalar part $g_{h_j \bar{f} f}^S$ (first two terms between curly brackets in the first line) from the pseudo-scalar one $g_{h_j \bar{f} f}^P$ (last two terms). The fermion and antifermion spinors are denoted $\bar{u}_f(p_f)$ and $v_f(p_{\bar{f}})$, respectively.

3.2.2.2 Case of the $b\bar{b}$ final state: $\tan\beta$ -enhanced corrections

In the case of a decay to $b\bar{b}$ (and analogously for down-type quarks of first and second generation, but with smaller numerical impact), the loop contributions that receive a $\tan\beta$ enhancement may have a sizeable impact, thus justifying an effective description of the Higgs– $b\bar{b}$ vertex that provides a resummation of large contributions [43, 56–62]. We denote the neutral components of \mathcal{H}_1 and \mathcal{H}_2 from Eq. (2.2) of Ref. [39] by H_d^0 and H_u^0 , respectively. The large $\tan\beta$ -enhanced effects arise from contributions to the $(H_u^0)^* \bar{b} P_L b$ operator— $P_{L,R}$ are the left- and right-handed projectors in the Dirac description of the b spinors—and can be parametrized in the following fashion:

$$\mathcal{L}^{\text{eff}} = -Y_b \bar{b} \left[H_d^0 + \frac{\Delta_b}{\tan\beta} \left(\frac{\lambda}{\mu_{\text{eff}}} S H_u^0 \right)^* \right] P_L b + \text{h.c.} \equiv - \sum_j g_{h_j b\bar{b}}^{L\text{eff}} h_j^0 \bar{b} P_L b + \text{h.c.} \quad (3.8)$$

Here, Δ_b is a coefficient that is determined via the calculation of the relevant ($\tan\beta$ -enhanced) one-loop diagrams to the Higgs– $b\bar{b}$ vertex, involving gluino–sbottom, chargino–stop, and neutralino–sbottom loops.[¶] The symbol μ_{eff} represents the effective μ term that is generated when the singlet field acquires a VEV. The specific form of the operator, $(S H_u^0)^* \bar{b} P_L b$, is designed so as to preserve the \mathbb{Z}_3 symmetry, and it can be shown that this operator is the one that gives rise to leading contributions to the $\tan\beta$ -enhanced effects. We evaluate Δ_b at a scale corresponding to the arithmetic mean of the masses of the contributing SUSY particles: this choice is consistent with the definition of Δ_b employed for the Higgs mass calculation.

From the parametrization of Eq. (3.8), one can derive the non-trivial relation between the ‘genuine’ Yukawa coupling Y_b and the effective bottom mass m_b : $Y_b = m_b/(v_1(1 + \Delta_b))$. Then, the effective couplings of the neutral Higgs fields to $b\bar{b}$ read:

$$g_{h_j b\bar{b}}^{L\text{eff}} = \frac{m_b}{\sqrt{2} v_1 (1 + \Delta_b)} \left\{ (U_n)_{j1} + i(U_n)_{j4} + \frac{\Delta_b}{\tan\beta} \left((U_n)_{j2} - i(U_n)_{j5} + \frac{\lambda^* v_2}{\mu_{\text{eff}}^*} [(U_n)_{j3} - i(U_n)_{j6}] \right) \right\}. \quad (3.9)$$

This can be used to substitute $\mathcal{A}^{\text{tree}}[h_j^0 \rightarrow b\bar{b}]$ in Eq. (3.3) for:

$$\mathcal{A}^{\text{eff}}[h_j^0 \rightarrow b\bar{b}] = -i \bar{u}_b(p_b) \left[g_{h_j b\bar{b}}^{L\text{eff}} P_L + g_{h_j b\bar{b}}^{L\text{eff}*} P_R \right] v_b(p_{\bar{b}}), \quad (3.10)$$

[¶]Two-loop corrections to Δ_b have also been reported in Refs. [63, 64].

where this expression resums the effect of $\tan\beta$ -enhanced corrections to the $h_j^0\bar{b}b$ vertex. However, if one now adds the one-loop amplitude $\mathcal{A}_{\text{vert}}^{\text{1L}}$, the one-loop effects associated with the $\tan\beta$ -enhanced contributions would be included twice. To avoid this double counting, the terms that are linear in Δ_b in Eq. (3.9) need to be subtracted. Employing the ‘subtraction’ couplings

$$g_{h_j\bar{b}b}^{L\text{sub}} = \frac{m_b \Delta_b}{\sqrt{2} v_1} \left\{ (U_n)_{j1} + i(U_n)_{j4} - \frac{1}{\tan\beta} \left((U_n)_{j2} - i(U_n)_{j5} + \frac{\lambda^* v_u}{\mu_{\text{eff}}^*} [(U_n)_{j3} - i(U_n)_{j6}] \right) \right\}, \quad (3.11)$$

we define the following ‘tree-level’ amplitude for the Higgs decays into bottom quarks:

$$\mathcal{A}^{\text{tree}}[h_j^0 \rightarrow b\bar{b}] = \mathcal{A}^{\text{eff}}[h_j^0 \rightarrow b\bar{b}] + \mathcal{A}^{\text{sub}}[h_j^0 \rightarrow b\bar{b}], \quad (3.12a)$$

$$\mathcal{A}^{\text{sub}}[h_j^0 \rightarrow b\bar{b}] \equiv -i \bar{u}_b(p_b) \left[g_{h_j\bar{b}b}^{L\text{sub}} P_L + g_{h_j\bar{b}b}^{L\text{sub}*} P_R \right] v_b(p_{\bar{b}}). \quad (3.12b)$$

3.2.2.3 QCD and QED corrections

The inclusion of QCD and QED corrections requires a proper treatment of IR effects in the decay amplitudes. The IR-divergent parts of the virtual contributions by gluons or photons in $\mathcal{A}_{\text{vert}}^{\text{1L}}$ are cancelled by their counterparts in processes with radiated photons or gluons. We directly employ the QCD and QED correction factors that are well-known analytically (see next) and therefore omit the Feynman diagrams involving a photon or gluon propagator when computing, with `FeynArts` and `FormCalc`, the one-loop corrections to the $h_j^0\bar{f}f$ vertex and to the fermion mass and wave function counterterms. The QCD and QED correction factors applying to the fermionic decays of a \mathcal{CP} -even Higgs state are given in Ref. [54]. The \mathcal{CP} -odd case was addressed later in Ref. [55]. In the \mathcal{CP} -violating case, it is useful to observe that the $h_j\bar{f}f$ scalar and pseudo-scalar operators do not interfere, so that the \mathcal{CP} -even and \mathcal{CP} -odd correction factors can be applied directly at the level of the amplitudes—although they were obtained at the level of the squared amplitudes:

$$\mathcal{A}^{\text{tree+QCD/QED}}[h_j^0 \rightarrow f\bar{f}] = -i \frac{m_f^{\overline{\text{MS}}}(M_{h_i})}{m_f} \bar{u}_f(p_f) \left\{ g_{h_j\bar{f}f}^S c_S - \gamma_5 g_{h_j\bar{f}f}^P c_P \right\} v_f(p_{\bar{f}}), \quad (3.13a)$$

$$c_{S,P} = \sqrt{1 + c_{S,P}^{\text{QED}} + c_{S,P}^{\text{QCD}}}, \quad (3.13b)$$

$$c_{S,P}^{\text{QED}} \equiv \frac{\alpha}{\pi} Q_f^2 \Delta_{S,P} \left(\sqrt{1 - \frac{4m_f^2}{M_{h_i}^2}} \right), \quad (3.13c)$$

$$c_{S,P}^{\text{QCD}} \equiv \frac{\alpha_s(M_{h_i})}{\pi} C_2(f) \left[\Delta_{S,P} \left(\sqrt{1 - \frac{4m_f^2}{M_{h_i}^2}} \right) + 2 + 3 \log \left(\frac{M_{h_i}}{m_f} \right) \right]. \quad (3.13d)$$

Here, Q_f is the electric charge of the fermion f , $C_2(f)$ is equal to 4/3 for quarks and equal to 0 for leptons, M_{h_i} corresponds to the kinematic (pole) mass in the Higgs decay under consideration and the functions $\Delta_{S,P}$ are explicated in e.g., Section 4 of Ref. [65]. In the limit of $M_{h_i} \gg m_f$, both $\Delta_{S,P}$ reduce to $\left[-3 \log(M_{h_i}/m_f) + \frac{9}{4} \right]$. As noted in Ref. [54], the leading logarithm in the QCD correction factor can be absorbed by the introduction of a running $\overline{\text{MS}}$ fermion mass in the definition of the Yukawa coupling Y_f . Therefore, it is motivated to factorise $m_f^{\overline{\text{MS}}}(M_{h_i})$, with higher orders included in the definition of the QCD beta function.

The QCD (and QED) correction factors generally induce a sizeable shift of the tree-level width of as much as $\sim 50\%$. While these effects were formally derived at the one-loop order, we apply them over the full amplitudes (without the QCD and QED corrections), i.e., we include

the one-loop vertex amplitude without QCD/QED corrections $\mathcal{A}_{\text{vert}}^{\text{1Lwo. QCD/QED}}$ and $\mathcal{A}_{\text{G/Z}}^{\text{1L}}$ in the definitions of the couplings $g_{h_j\text{ff}}^{S,P}$ that are employed in Eq. (3.13)—we will use the notation $g_{h_j\text{ff}}^{S,P\text{1L}}$ in the following. The adopted factorisation corresponds to a particular choice of the higher-order contributions beyond the ones that have been explicitly calculated.

3.2.2.4 Decay width

Putting together the various pieces discussed before, we can express the decay amplitude at the one-loop order as

$$\mathcal{A}[h_i \rightarrow \text{ff}] = -i \frac{m_{\text{f}}^{\overline{\text{MS}}}(M_{h_i})}{m_{\text{f}}} Z_{ij}^{\text{mix}} \bar{u}_{\text{f}}(p_{\text{f}}) \left\{ g_{h_j\text{ff}}^{S\text{1L}} c_S - \gamma_5 g_{h_j\text{ff}}^{P\text{1L}} c_P \right\} v_{\text{f}}(p_{\text{f}}), \quad (3.14a)$$

$$-i \bar{u}_{\text{f}}(p_{\text{f}}) \left\{ g_{h_j\text{ff}}^{S\text{1L}} - \gamma_5 g_{h_j\text{ff}}^{P\text{1L}} \right\} v_{\text{f}}(p_{\text{f}}) \equiv \left(\mathcal{A}^{\text{tree}} + \mathcal{A}_{\text{vert}}^{\text{1Lwo. QCD/QED}} + \mathcal{A}_{\text{G/Z}}^{\text{1L}} \right) [h_j \rightarrow \text{ff}]. \quad (3.14b)$$

Summing over spinor and colour degrees of freedom, the decay width is then obtained as

$$\Gamma[h_i \rightarrow \text{ff}] = \frac{1}{16\pi M_{h_i}} \sqrt{1 - \frac{4m_{\text{f}}^2}{M_{h_i}^2}} \sum_{\text{polarisation, colour}} \left| \mathcal{A}[h_i^{\text{phys.}} \rightarrow \text{ff}] \right|^2. \quad (3.15)$$

At the considered order, we could dismiss the one-loop squared terms in $|\mathcal{A}[h_i \rightarrow \text{ff}]|^2$. However, to tackle the case where the contributions from irreducible one-loop diagrams are numerically larger than the tree-level amplitude, we keep the corresponding squared terms in the expression (it should be noted that the QCD and QED corrections have been stripped off from the one-loop amplitude, which gets squared). The approach of incorporating the squared terms should give a reliable result in a situation where the tree-level result is significantly suppressed, since the other missing contribution at this order, consisting of the tree-level amplitude times the two-loop amplitude, would be suppressed, owing to the small tree-level result. In such a case, however, the higher-order uncertainties are expected to be comparatively larger than in the case where one-loop effects are subdominant to the tree level.

The kinematic masses of the fermions are easily identified in the leptonic case. For decays into top quarks, the ‘pole’ mass m_{t} is used, while for all other decays into quarks we employ the $\overline{\text{MS}}$ masses evaluated at the scale of the Higgs mass $m_{\text{q}}^{\overline{\text{MS}}}(M_{h_i})$. We note that these kinematic masses have little impact on the decay widths, as long as the Higgs state is much heavier. In the NMSSM, however, singlet-like Higgs states can be very light, in which case the choice of an $\overline{\text{MS}}$ mass is problematic. Yet, in this case, the Higgs state is typically near threshold so that the free-parton approximation in the final state is not expected to be reliable. Our current code is not properly equipped to address decays directly at threshold independently of the issue of running kinematic masses. Improved descriptions of the hadronic decays of Higgs states close to the bb threshold or in the chiral limit have been presented in, e.g., Refs. [66–71].

3.2.3 Decays into SM gauge bosons

Now we consider Higgs decays into the gauge bosons of the SM. Almost each of these channels requires a specific processing in order to include higher-order corrections consistently or to deal with off-shell effects.

3.2.3.1 Decays into electroweak gauge bosons

Higgs decays into on-shell Ws and Zs can easily be included at the one-loop order in comparable fashion to the fermionic decays. However, the notion of WW or ZZ final states usually includes contributions from off-shell gauge bosons as well, encompassing a wide range of four-fermion final states. Such off-shell effects mostly impact the decays of Higgs bosons with a mass below the WW or ZZ thresholds. Instead of a full processing of the off-shell decays at one-loop order, we pursue two distinct evaluations of the decay widths in these channels.

Our first approach is that already employed in `FeynHiggs` for the corresponding decays in the MSSM. It involves exploiting the precise one-loop results of `Prophecy4f` for the SM Higgs decays into four fermions [72–74]. For an (N)MSSM Higgs boson h_i , the SM decay width is thus evaluated at the mass M_{h_i} and then rescaled by the squared ratio of the tree-level couplings to gauge bosons for h_i and an SM Higgs boson H_{SM} ($V = W, Z$):

$$\Gamma[h_i \rightarrow VV] = \Gamma^{\text{SM}}[H_{\text{SM}}(M_{h_i}) \rightarrow VV] \left| \mathcal{R}_{ij} \cdot \frac{g_{h_j VV}^{\text{NMSSM}}}{g_{H_{\text{SM}} VV}^{\text{SM}}} \right|^2, \quad (3.16a)$$

$$\frac{g_{h_j VV}^{\text{NMSSM}}}{g_{H_{\text{SM}} VV}^{\text{SM}}} \equiv \cos \beta (U_n)_{j1} + \sin \beta (U_n)_{j2}, \quad (3.16b)$$

where $\Gamma[h_i \rightarrow VV]$ represents the decay width of the physical Higgs state h_i in the NMSSM, while $\Gamma^{\text{SM}}[H_{\text{SM}}(M_{h_i}) \rightarrow VV]$ denotes the decay width of an SM Higgs boson with mass M_{h_i} . The matrix elements \mathcal{R}_{ij} reflect the connection between the tree-level Higgs states and the physical states. This role is similar to \mathbf{Z}^{mix} . However, decoupling in the SM limit of the model yields the additional condition that the ratio in Eq. (3.16a) reduces to 1 in this limit for the SM-like Higgs boson of the NMSSM. For this reason, `FeynHiggs` employs the matrix \mathbf{U}^m (or \mathbf{U}^0) as a unitary approximation of \mathbf{Z}^{mix} —see Section 2.6 of Ref. [39]. An alternative choice involves using $X_{ij} \equiv Z_{ij}^{\text{mix}} / \sqrt{\sum_k |Z_{ik}^{\text{mix}}|^2}$. However, the difference of the widths when employing \mathbf{U}^0 , \mathbf{U}^m , \mathbf{Z}^{mix} , or $\mathbf{X} \equiv (X_{ij})$ corresponds to effects of higher order, which should be regarded as part of the higher-order uncertainty. The rescaling of the one-loop SM width should only be applied for the SM-like Higgs of the NMSSM, where this implementation of the $h_i \rightarrow VV$ widths is expected to provide an approximation that is relatively close to a full one-loop result incorporating all NMSSM contributions. However, for the other Higgs states of the NMSSM, one-loop contributions beyond the SM may well be dominant. Actually, the farther the quantity $[\mathcal{R}_{ij} \cdot (U_n)_{j2}] / [\mathcal{R}_{ij} \cdot (U_n)_{j1}]$ departs from $\tan \beta$, the more inaccurate the prediction based on SM-like radiative corrections becomes.

Our second approach involves a one-loop calculation of the Higgs decay widths into on-shell gauge bosons (see Ref. [52] for the MSSM case), including tree-level off-shell effects. This evaluation is meant to address the case of heavy Higgs bosons at the full one-loop order. The restriction to on-shell kinematics is justified above the threshold for electroweak gauge-boson production (off-shell effects at the one-loop level could be included via a numerical integration over the squared momenta of the gauge bosons in the final state—see Refs. [75, 76] for a discussion in the MSSM). For details of our implementation, see Ref. [29], with the noteworthy feature that contributions from Higgs–electroweak mixing $\mathcal{A}_{G/Z}^{\text{H}}$ vanish. In the case of the W^+W^- final state, the QED IR divergences are regularised with a photon mass and cancel with bremsstrahlung corrections: soft and hard bremsstrahlung are included according to Refs. [77, 78] (see also Ref. [52]). We stress that the exact cancellation of the IR divergences is only achieved through the replacement of the $h_i G^+ G^-$ coupling with the expression in terms of the kinematic Higgs

mass (see Ref. [29] for more details). This fact had already been observed in Ref. [52]. To extend the validity of the calculation below the threshold, we process the Born-order term separately, applying an off-shell kinematic integration over the squared external momentum of the gauge bosons—see, e.g., Eq. (37) in Ref. [79]. Thus, this evaluation is performed at tree level below threshold and at full one-loop order (for the on-shell case) above threshold. The vanishing on-shell kinematic factor multiplying the contributions of one-loop order ensures the continuity of the prediction at threshold. Finally, we include the one-loop squared term in the calculation. Indeed, as we will discuss later, the tree-level contribution vanishes for a decoupling doublet, meaning that the Higgs decays to WW/ZZ can be dominated by one-loop effects. To this end, the infrared divergences of two-loop order are regularised in an ad-hoc fashion—which appears compulsory as long as the two-loop order is incomplete—making use of the one-loop real radiation and estimating the logarithmic term in the imaginary part of the one-loop amplitude.

3.2.3.2 Radiative decays into gauge bosons

Higgs decays into photon pairs, gluon pairs, or γZ appear at the one-loop level—i.e., $\mathcal{A}^{\text{tree}} = 0$ for all these channels. We compute the one-loop order using the `FeynArts` model file, although the results are well-known analytically in the literature—see, e.g., Ref. [51] or Section III of Ref. [80] (Ref. [79] for the MSSM). The electromagnetic coupling in these channels is set to the value $\alpha(0)$, corresponding to the Thomson limit.

The use of tree-level Higgs–Goldstone couplings together with loop-corrected kinematic Higgs masses M_{h_i} in our calculation would induce an effective violation of Ward identities by two-loop order terms in the amplitude: we choose to restore the proper gauge structure by redefining the Higgs–Goldstone couplings in terms of the kinematic Higgs mass M_{h_i} (see Ref. [29] for more details). Since our calculation is restricted to the leading—here, one-loop—order, the transition of the amplitude from tree-level to physical Higgs states is performed via \mathbf{U}^m or \mathbf{X} instead of \mathbf{Z}^{mix} in order to ensure the appropriate behaviour in the decoupling limit.

Leading QCD corrections to the diphoton Higgs decays have received substantial attention in the literature. A frequently used approximation for this channel involves multiplying the amplitudes driven by quark and squark loops by the factors $[1 - \alpha_s(M_{h_i})/\pi]$ and $[1 + 8\alpha_s(M_{h_i})/(3\pi)]$, respectively—see, e.g., Ref. [81]. However, these simple factors are only valid in the limit of heavy quarks and squarks (compared with the mass of the decaying Higgs boson). More general analytical expressions can be found in, e.g., Ref. [82]. In our calculation, we apply the correction factors $[1 + C^S(\tau_q)\alpha_s(M_{h_i})/\pi]$ and $[1 + C^P(\tau_q)\alpha_s(M_{h_i})/\pi]$ to the contributions of the quark q to the \mathcal{CP} -even and the \mathcal{CP} -odd $h_i\gamma\gamma$ operators, respectively, and $[1 + C(\tau_{\tilde{Q}})\alpha_s(M_{h_i})/\pi]$ to the contributions of the squark \tilde{Q} (to the \mathcal{CP} -even operator). Here, τ_X denotes the ratio $[4m_X^2(M_{h_i}/2)/M_{h_i}^2]$. The coefficients $C^{S,P}$ and C are extracted from Refs. [83] and [84]. To obtain a consistent inclusion of the $\mathcal{O}(\alpha_s)$ corrections, the quark and squark masses m_X entering the one-loop amplitudes or the correction factors are chosen as defined in Eq. (5) of Ref. [83] and Eq. (12) of Ref. [84] (rather than $\overline{\text{MS}}$ running masses).

The QCD corrections to the digluon decays include virtual corrections but also gluon and light quark radiation. They are thus technically defined at the level of the squared amplitudes. In the limit of heavy quarks and squarks, the corrections are known beyond NLO—see the discussion in Ref. [79] for a list of references. The full dependence in mass was derived at NLO in Refs. [83, 84], for both quark and squark loops. In our implementation, we follow the prescriptions of Eqs. (51), (63), and (67) of Ref. [79] in the limit of light radiated quarks

and heavy particles in the loop. For consistency, the masses of the particles in the one-loop amplitude are taken as pole masses. Effects beyond this approximation can be sizeable, as evidenced by Fig. 20 of Ref. [83] and Fig. 12 of Ref. [84]. As the \mathcal{CP} -even and \mathcal{CP} -odd Higgs– gg operators do not interfere, it is straightforward to include both correction factors in the \mathcal{CP} -violating case. Finally, we note that parts of the leading QCD corrections to $h_i \rightarrow gg$ are induced by the real radiation of quark–antiquark pairs. In the case of the heavier quark flavours (top, bottom, and possibly charm), the channels are experimentally easily distinguishable from gluonic decays. Therefore, the partial widths related to these corrections could be attached to the Higgs decays into quarks instead [85]. The resolution of this ambiguity would involve a dedicated experimental analysis of the kinematics of the gluon radiation in $h_i \rightarrow gq\bar{q}$ (collinear or back-to-back emission).

The QCD corrections to the quark loops of an SM Higgs decay into γZ have been studied in Refs. [86–88], but we do not consider them here.

3.3 Discussion concerning the remaining theoretical uncertainties

Next, we provide a summary of the main sources of theoretical uncertainties from unknown higher-order corrections applying to our calculation of the NMSSM Higgs decays. We do not discuss here the parametric theoretical uncertainties arising from the experimental errors of the input parameters. For the experimentally known SM-type parameters, the induced uncertainties can be determined in the same way as for the SM case (see, e.g., Ref. [26]). The dependence on the unknown SUSY parameters, however, is usually not treated as a theoretical uncertainty but rather exploited for setting indirect constraints on those parameters.

3.3.1 Higgs decays into quarks ($h_i \rightarrow q\bar{q}$, $q = c, b, t$)

In our evaluation, these decays have been implemented at full one-loop order, i.e., at QCD, electroweak, and SUSY next-to-leading order (NLO). In addition, leading QCD logarithmic effects have been resummed within the parametrization of the Yukawa couplings in terms of a running quark mass at the scale of the Higgs mass. The Higgs propagator-type corrections determining the mass of the considered Higgs particle, as well as the wave function normalization at the external Higgs leg of the process, contain full one-loop and dominant two-loop contributions.

For an estimate of the remaining theoretical uncertainties, several higher-order effects should be taken into account.

1. First, we should assess the magnitude of the missing QCD NNLO (two-loop) effects. We stress that there should be no large logarithms associated with these corrections, since these are already resummed through the choice of running parameters and the renormalization scale. For the remaining QCD pieces, we can directly consider the situation in the SM. In the case of the light quarks, the QCD contributions of higher order have been evaluated and amount to $\sim 4\%$ at $m_H = 120$ GeV (see, e.g., Ref. [89]). For the top quark, the uncertainty due to missing QCD NNLO effects was estimated at 5% [26].
2. Concerning the electroweak corrections, the numerical analysis in Ref. [29] suggests that the one-loop contribution is small—at the percentage level—for an SM-like Higgs, which is consistent with earlier estimates in the SM [26]. For the heavy Higgs states, the numerical analysis in Ref. [29] indicates a larger impact of such effects—at the level of $\sim 10\%$ in the

considered scenario. Assuming that the electroweak NNLO corrections are comparable to the squared one-loop effects, our estimate for pure electroweak higher orders in decays of heavy Higgs states reaches the percentage level. In fact, for multiteraelectronvolt Higgs bosons, the electroweak Sudakov logarithms may require a resummation (see Ref. [53]). Furthermore, mixed electroweak–QCD contributions are expected to be larger than the pure electroweak NNLO corrections, adding a few more percent to the uncertainty budget. For light Higgs states, the electroweak effects are much smaller, since the Sudakov logarithms remain of comparatively modest size.

3. Finally, the variations with the squark masses in the numerical analysis in Ref. [29] for the heavy doublet states show that the one-loop SUSY effects could amount to 5–10% for a subteraelectronvolt stop or sbottom spectrum. In such a case, the two-loop SUSY and the mixed QCD or electroweak–SUSY corrections may reach the percentage level. Conversely, for very heavy squark spectra, we expect to recover an effective singlet-extended two-Higgs-doublet model (an effective SM if the heavy doublet and singlet states also decouple) at low energy. However, all the parameters of this low-energy effective field theory implicitly depend on the SUSY radiative effects, since unsuppressed logarithms of SUSY origin generate terms of dimension ≤ 4 —e.g., in the Higgs potential or the Higgs couplings to SM fermions. Conversely, the explicit dependence of the Higgs decay widths on SUSY higher-order corrections is suppressed for a large SUSY scale. In this case, the uncertainty from SUSY corrections reduces to a parametric effect, that of the matching between the NMSSM and the low-energy Lagrangian—e.g., in the SM limit, the uncertainty on the mass prediction for the SM-like Higgs continues to depend on SUSY logarithms and would indirectly affect the uncertainty on the decay widths.

Considering all these higher-order effects together, we conclude that the decay widths of the SM-like Higgs should be relatively well-controlled (up to $\sim 5\%$), while those of a heavy Higgs state could receive sizeable higher-order contributions, possibly adding up to the level of $\sim 10\%$.

3.3.2 Higgs decays into leptons

Here, QCD corrections appear only at two-loop order in the Higgs propagator-type corrections, as well as in the counterterms of the electroweak parameters, and only from three-loop order onwards in the genuine vertex corrections. Thus, the theory uncertainty is expected to be substantially smaller than in the case of quark final states. For an SM-like Higgs, associated uncertainties were estimated to be below the percentage level [28]. For heavy Higgs states, however, electroweak one-loop corrections are enhanced by Sudakov logarithms (see Ref. [53]) and reach the $\sim 10\%$ level for Higgs masses of the order of 1 TeV, so that the two-loop effects could amount to a few percent. In addition, light staus may generate a sizeable contribution of SUSY origin, where the unknown corrections are of two-loop electroweak order.

3.3.3 Higgs decays into WW/ZZ

The complexity of these channels is illustrated by our presentation of two separate estimates, expected to perform differently in various regimes.

1. In the SM, the uncertainty of `Prophecy4f` in the evaluation of these channels was assessed at the subpercentage level below 500 GeV, but up to $\sim 15\%$ at 1 TeV [26]. For an SM-like Higgs, our numerical analysis in Ref. [29] shows that the one-loop electroweak

corrections are somewhat below 10%, making plausible a subpercentage uncertainty in the results employing `Prophecy4f`. Conversely, the assumption that the decay widths for an NMSSM Higgs boson can be obtained through a simple rescaling of the result for the width in the SM by tree-level couplings is, in itself, a source of uncertainties. We expect this approximation to be accurate only in the limit of a decoupling SM-like composition of the NMSSM Higgs boson. If these SM-like characteristics are altered through radiative corrections of SUSY origins or NMSSM Higgs mixing effects—both of which may still reach the level of several percentage in a phenomenologically realistic set-up—the uncertainty in the rescaling procedure for the decay widths should be of corresponding magnitude.

2. In the case of heavier states, our numerical analysis in Ref. [29] indicates that the previous procedure is unreliable in the mass range $\gtrsim 500$ GeV. In particular, for heavy doublets in the decoupling limit, radiative corrections dominate over the—then vanishing—tree-level amplitude, shifting the widths by orders of magnitude. In such a case, our one-loop calculation captures only the leading order and one can expect sizeable contributions at the two-loop level: as discussed in the numerical analysis in Ref. [29], shifting the quark masses between pole and $\overline{\text{MS}}$ values—two legitimate choices at the one-loop order that differ in the treatment of QCD two-loop contributions—results in modifications of the widths of order $\sim 50\%$. Conversely, one expects the decays of a decoupling heavy doublet into electroweak gauge bosons to remain a subdominant channel, so that a less accurate prediction may be tolerable. It should be noted, however, that the magnitude of the corresponding widths is sizeably enhanced by the effects of one-loop order; this may be of interest regarding their phenomenological impact.

3.3.4 Radiative decays into gauge bosons

As these channels appear at the one-loop order, our (QCD-corrected) results represent (only) an improved leading-order evaluation. Yet the situation is contrasted.

1. In the SM, the uncertainty for a Higgs decay into $\gamma\gamma$ was estimated at the level of 1% in Ref. [26]; however, the corresponding calculation includes both QCD NLO and electroweak NLO corrections. In our case, only QCD NLO corrections (with full mass dependence) are taken into account. The comparison with `NMSSMCALC` in Ref. [29] provides us with a lower bound on the magnitude of electroweak NLO and QCD NNLO effects: both evaluations are of the same order but differ by a few percent. The uncertainty in the SUSY contribution should be considered separately, as light charginos or sfermions could have a sizeable impact. In any case, we expect the accuracy of our calculation to perform at the level of $\gtrsim 4\%$.
2. In the case of the Higgs decays into gluons, for the SM prediction—including QCD corrections with full mass dependence and electroweak two-loop effects—an uncertainty of 3% from QCD effects and 1% from electroweak effects was estimated in Ref. [26]. In our case, the QCD corrections are only included in the heavy-loop approximation, and NLO electroweak contributions have not been considered. Consequently, the uncertainty budget should settle above the corresponding estimate for the SM quoted here. In the case of heavy Higgs bosons, the squark spectrum could have a significant impact on the QCD two-loop corrections, as exemplified in Fig. 5 of Ref. [84].

3. For $h_i \rightarrow \gamma Z$, QCD corrections are not yet available, so the uncertainty should be above the $\sim 5\%$ estimated in the SM [26].

3.3.5 Additional sources of uncertainty from higher orders

For an uncertainty estimate, the following effects apply to essentially all channels and should be considered as well.

1. The mixing in the Higgs sector plays a central role in the determination of the decay widths. Following the treatment in `FeynHiggs`, we have considered \mathbf{Z}^{mix} in all our one-loop evaluations, as prescribed by the LSZ reduction. Most public codes consider a unitary approximation in the limit of the effective scalar potential (\mathbf{U}^0 , in our notation). The analysis of Ref. [39] and our most recent analysis in Ref. [29]—employing \mathbf{U}^m , a more reliable unitary approximation than \mathbf{U}^0 —indicate that the different choices of mixing matrices may affect the Higgs decays by a few percent (and far more in contrived cases). However, even the use of \mathbf{Z}^{mix} is, of course, subject to uncertainties from unknown higher-order corrections. While the Higgs propagator-type corrections determining the mass of the considered Higgs boson and the wave function normalization contain corrections up to the two-loop order, the corresponding prediction for the mass of the SM-like Higgs still has an uncertainty at the level of about 2%, depending on the SUSY spectrum.
2. In this section, we confined ourselves to the evaluation of the Higgs decay widths into SM particles and did not consider the branching ratios. For the latter, an implementation at the full one-loop order of many other two-body decays, relevant, in particular, for the heavy Higgs states, would be desirable, but goes beyond the scope of the present analysis. Furthermore, to consider the Higgs branching ratios at the one-loop order, we would have to consider three-body widths at the tree level, for instance $h_i \rightarrow b\bar{b}Z$, since these are formally of the same magnitude as the one-loop effects for two-body decays [53]. In addition, these three-body decays—typically real radiation of electroweak and Higgs bosons—exhibit Sudakov logarithms that would require resummation in the limit of heavy Higgs states [53].
3. At decay thresholds, the approximation of free particles in the final state is not sufficient, and a more accurate treatment would require the evaluation of final-state interactions. Several cases have been discussed in, e.g., Refs. [69, 71, 90].

In this discussion, we did not attempt to provide a quantitative estimate of the remaining theoretical uncertainties from unknown higher-order corrections, as such an estimate would, in any case, sensitively depend on the considered region in parameter space. Instead, we have pointed out the various sources of higher-order uncertainties remaining at the level of our state-of-the-art evaluation of the Higgs decays into SM particles in the NMSSM. For a decoupling SM-like Higgs boson, one would ideally expect that the level of accuracy of the predictions approaches that achieved in the SM. However, even in this limit, missing NNLO pieces—which are known for the SM, but not for the NMSSM—give rise to a somewhat larger theoretical uncertainty in the NMSSM. Furthermore, uncertainties of parametric nature (for instance, from the theoretical prediction of the Higgs boson mass) need to be taken into account as well. For heavy Higgs states, the impact of electroweak Sudakov logarithms and SUSY corrections add to the theoretical uncertainty to an extent that is strongly dependent on the details of the

spectrum and the characteristics of the Higgs state (see Ref. [53]). For a decoupling doublet at ~ 1 TeV, an uncertainty of $\sim 5\text{--}15\%$ may be used as a guideline for the fermionic and radiative decays, while the uncertainty may be as large as $\sim 50\%$ in $h_i \rightarrow WW/ZZ$.

References

- [1] G. Aad *et al.*, *Phys. Lett.* **B716** (2012) 1. [arXiv:1207.7214](#),
[doi:10.1016/j.physletb.2012.08.020](#)
- [2] S. Chatrchyan *et al.*, *Phys. Lett.* **B716** (2012) 30. [arXiv:1207.7235](#),
[doi:10.1016/j.physletb.2012.08.021](#)
- [3] G. Aad *et al.*, *JHEP* **08** (2016) 045. [arXiv:1606.02266](#), [doi:10.1007/JHEP08\(2016\)045](#)
- [4] G. Aad *et al.*, *Phys. Rev. Lett.* **114** (2015) 191803. [arXiv:1503.07589](#),
[doi:10.1103/PhysRevLett.114.191803](#)
- [5] A.M. Sirunyan *et al.*, *JHEP* **11** (2017) 047. [arXiv:1706.09936](#),
[doi:10.1007/JHEP11\(2017\)047](#)
- [6] CMS Collaboration, The CMS phase II upgrade scope document, CERN-LHCC-2015-019, (CERN, Geneva, 2015), <https://cds.cern.ch/record/2055167>
- [7] ATLAS Collaboration, ATLAS phase-II upgrade scoping document, CERN-LHCC-2015-020, (CERN, Geneva, 2015), <https://cds.cern.ch/record/2055248>
- [8] M. Testa, Prospects on Higgs physics at the HL-LHC for ATLAS, ATLAS Higgs HL-LHC, https://indico.cern.ch/event/647676/contributions/2721145/subcontributions/241006/attachments/1549120/2433004/testa_HLLHC_v5.pdf
- [9] M. Cepeda, HIGGS @ HL-LHC, CMS Higgs HL-LHC, 2017,
https://indico.cern.ch/event/647676/contributions/2721145/subcontributions/241007/attachments/1549081/2433323/CMS_LHCB_HIGGS_HLLHC.pdf
- [10] H. Baer *et al.*, The international linear collider technical design report, vol. 2: physics (2013), [arXiv:1306.6352](#)
- [11] K. Fujii *et al.*, Physics case for the International Linear Collider, [arXiv:1506.05992](#)
- [12] K. Fujii *et al.*, The potential of the ILC for discovering new particles, [arXiv:1702.05333](#)
- [13] A. Arbey *et al.*, *Eur. Phys. J.* **C75** (2015) 371. [arXiv:1504.01726](#),
[doi:10.1140/epjc/s10052-015-3511-9](#)
- [14] M. Bicer *et al.*, *JHEP* **01** (2014) 164. [arXiv:1308.6176](#),
[doi:10.1007/JHEP01\(2014\)164](#)
- [15] F. An *et al.*, *Chin. Phys.* **C43** (2019) 043002. [arXiv:1810.09037](#),
[doi:10.1088/1674-1137/43/4/043002](#)
- [16] A. Abada *et al.*, *Eur. Phys. J. Spec. Top.* **228** (2019) 261.
[doi:10.1140/epjst/e2019-900045-4](#)
- [17] A. Abada *et al.*, *Eur. Phys. J.* **C79** (2019) 474. [doi:10.1140/epjc/s10052-019-6904-3](#)
- [18] <https://fcc-cdr.web.cern.ch/>, last accessed 15 January 2020.
- [19] H.-P. Nilles, *Phys. Rep.* **110** (1984) 1.
[doi:10.1016/0370-1573\(84\)90008-5](#)

- [20] H.E. Haber and G.L. Kane, *Phys. Rep.* **117** (1985) 75.
[doi:10.1016/0370-1573\(85\)90051-1](https://doi.org/10.1016/0370-1573(85)90051-1)
- [21] U. Ellwanger *et al.*, *Phys. Rep.* **496** (2010) 1. [arXiv:0910.1785](https://arxiv.org/abs/0910.1785),
[doi:10.1016/j.physrep.2010.07.001](https://doi.org/10.1016/j.physrep.2010.07.001)
- [22] M. Maniatis, *Int. J. Mod. Phys. A* **25** (2010) 3505. [arXiv:0906.0777](https://arxiv.org/abs/0906.0777),
[doi:10.1142/S0217751X10049827](https://doi.org/10.1142/S0217751X10049827)
- [23] G. Degrandi *et al.*, *Eur. Phys. J.* **C28** (2003) 133. [arXiv:hep-ph/0212020](https://arxiv.org/abs/hep-ph/0212020),
[doi:10.1140/epjc/s2003-01152-2](https://doi.org/10.1140/epjc/s2003-01152-2)
- [24] F. Staub *et al.*, *Comput. Phys. Commun.* **202** (2016) 113. [arXiv:1507.05093](https://arxiv.org/abs/1507.05093),
[doi:10.1016/j.cpc.2016.01.005](https://doi.org/10.1016/j.cpc.2016.01.005)
- [25] P. Drechsel *et al.*, *Eur. Phys. J.* **C77** (2017) 366. [arXiv:1612.07681](https://arxiv.org/abs/1612.07681),
[doi:10.1140/epjc/s10052-017-4932-4](https://doi.org/10.1140/epjc/s10052-017-4932-4)
- [26] A. Denner *et al.*, *Eur. Phys. J.* **C71** (2011) 1753. [arXiv:1107.5909](https://arxiv.org/abs/1107.5909),
[doi:10.1140/epjc/s10052-011-1753-8](https://doi.org/10.1140/epjc/s10052-011-1753-8)
- [27] J.R. Andersen *et al.*, Handbook of LHC Higgs cross sections: 3. Higgs properties,
[arXiv:1307.1347](https://arxiv.org/abs/1307.1347), [doi:10.5170/CERN-2013-004](https://doi.org/10.5170/CERN-2013-004)
- [28] D. de Florian *et al.*, Handbook of LHC Higgs cross sections: 4. Deciphering the nature of
the Higgs sector, [arXiv:1610.07922](https://arxiv.org/abs/1610.07922), [doi:10.23731/CYRM-2017-002](https://doi.org/10.23731/CYRM-2017-002)
- [29] F. Domingo *et al.*, *Eur. Phys. J.* **C78** (2018) 942. [arXiv:1807.06322](https://arxiv.org/abs/1807.06322),
[doi:10.1140/epjc/s10052-018-6400-1](https://doi.org/10.1140/epjc/s10052-018-6400-1)
- [30] S. Heinemeyer *et al.*, *Eur. Phys. J.* **C9** (1999) 343. [arXiv:hep-ph/9812472](https://arxiv.org/abs/hep-ph/9812472), [doi:10.1007/s100529900006](https://doi.org/10.1007/s100529900006)
- [31] S. Heinemeyer *et al.*, *Comput. Phys. Commun.* **124** (2000) 76. [arXiv:hep-ph/9812320](https://arxiv.org/abs/hep-ph/9812320),
[doi:10.1016/S0010-4655\(99\)00364-1](https://doi.org/10.1016/S0010-4655(99)00364-1)
- [32] M. Frank *et al.*, *JHEP* **02** (2007) 047. [arXiv:hep-ph/0611326](https://arxiv.org/abs/hep-ph/0611326),
[doi:10.1088/1126-6708/2007/02/047](https://doi.org/10.1088/1126-6708/2007/02/047)
- [33] T. Hahn *et al.*, *Phys. Rev. Lett.* **112** (2014) 141801. [arXiv:1312.4937](https://arxiv.org/abs/1312.4937),
[doi:10.1103/PhysRevLett.112.141801](https://doi.org/10.1103/PhysRevLett.112.141801)
- [34] H. Bahl and W. Hollik, *Eur. Phys. J.* **C76** (2016) 499. [arXiv:1608.01880](https://arxiv.org/abs/1608.01880),
[doi:10.1140/epjc/s10052-016-4354-8](https://doi.org/10.1140/epjc/s10052-016-4354-8)
- [35] H. Bahl *et al.*, *Eur. Phys. J.* **C78** (2018) 57. [arXiv:1706.00346](https://arxiv.org/abs/1706.00346),
[doi:10.1140/epjc/s10052-018-5544-3](https://doi.org/10.1140/epjc/s10052-018-5544-3)
- [36] H. Bahl *et al.*, *Comput. Phys. Commun.* **249** (2020) 107099. [arXiv:1811.09073](https://arxiv.org/abs/1811.09073),
[doi:10.1016/j.cpc.2019.107099](https://doi.org/10.1016/j.cpc.2019.107099)
- [37] www.feynhiggs.de, last accessed 28 January 2020.
- [38] P. Drechsel *et al.*, *Eur. Phys. J.* **C77** (2017) 42. [arXiv:1601.08100](https://arxiv.org/abs/1601.08100),
[doi:10.1140/epjc/s10052-017-4595-1](https://doi.org/10.1140/epjc/s10052-017-4595-1)
- [39] F. Domingo *et al.*, *Eur. Phys. J.* **C77** (2017) 562. [arXiv:1706.00437](https://arxiv.org/abs/1706.00437),
[doi:10.1140/epjc/s10052-017-5104-2](https://doi.org/10.1140/epjc/s10052-017-5104-2)
- [40] J. Kublbeck *et al.*, *Comput. Phys. Commun.* **60** (1990) 165.
[doi:10.1016/0010-4655\(90\)90001-H](https://doi.org/10.1016/0010-4655(90)90001-H)

- [41] T. Hahn, *Comput. Phys. Commun.* **140** (2001) 418. [arXiv:hep-ph/0012260](#), [doi:10.1016/S0010-4655\(01\)00290-9](#)
- [42] T. Hahn and M. Perez-Victoria, *Comput. Phys. Commun.* **118** (1999) 153. [arXiv:hep-ph/9807565](#), [doi:10.1016/S0010-4655\(98\)00173-8](#)
- [43] K.E. Williams *et al.*, *Eur. Phys. J.* **C71** (2011) 1669. [arXiv:1103.1335](#), [doi:10.1140/epjc/s10052-011-1669-3](#)
- [44] E. Fuchs and G. Weiglein, *JHEP* **09** (2017) 079. [arXiv:1610.06193](#), [doi:10.1007/JHEP09\(2017\)079](#)
- [45] S. Paßehr and G. Weiglein, *Eur. Phys. J.* **C78** (2018) 222. [arXiv:1705.07909](#), [doi:10.1140/epjc/s10052-018-5665-8](#)
- [46] S. Borowka *et al.*, *Eur. Phys. J.* **C78** (2018) 576. [arXiv:1802.09886](#), [doi:10.1140/epjc/s10052-018-6055-y](#)
- [47] W. Hollik *et al.*, *Nucl. Phys.* **B639** (2002) 3. [arXiv:hep-ph/0204350](#), [doi:10.1016/S0550-3213\(02\)00538-2](#)
- [48] K.E. Williams and G. Weiglein, *Phys. Lett.* **B660** (2008) 217. [arXiv:0710.5320](#), [doi:10.1016/j.physletb.2007.12.049](#)
- [49] A.C. Fowler and G. Weiglein, *JHEP* **01** (2010) 108. [arXiv:0909.5165](#), [doi:10.1007/JHEP01\(2010\)108](#)
- [50] N. Baro *et al.*, *Phys. Rev.* **D78** (2008) 115003. [arXiv:0807.4668](#), [doi:10.1103/PhysRevD.78.115003](#)
- [51] R. Benbrik *et al.*, *Eur. Phys. J.* **C72** (2012) 2171. [arXiv:1207.1096](#), [doi:10.1140/epjc/s10052-012-2171-2](#)
- [52] P. González *et al.*, *Eur. Phys. J.* **C73** (2013) 2367. [arXiv:1211.3079](#), [doi:10.1140/epjc/s10052-013-2367-0](#)
- [53] F. Domingo and S. Paßehr, *Eur. Phys. J.* **C79** (2019) 905. [doi:10.1140/epjc/s10052-019-7415-y](#)
- [54] E. Braaten and J.P. Leveille, *Phys. Rev.* **D22** (1980) 715. [doi:10.1103/PhysRevD.22.715](#)
- [55] M. Drees and K.-I. Hikasa, *Phys. Lett.* **B240** (1990) 455 [Erratum: **B262** (1991) 497]. [doi:10.1016/0370-2693\(90\)91130-4](#), [doi:10.1016/0370-2693\(91\)90629-5](#)
- [56] T. Banks, *Nucl. Phys.* **B303** (1988) 172. [doi:10.1016/0550-3213\(88\)90222-2](#)
- [57] L.J. Hall *et al.*, *Phys. Rev.* **D50** (1994) 7048. [arXiv:hep-ph/9306309](#), [doi:10.1103/PhysRevD.50.7048](#)
- [58] R. Hempfling, *Phys. Rev.* **D49** (1994) 6168. [doi:10.1103/PhysRevD.49.6168](#)
- [59] M. Carena *et al.*, *Nucl. Phys.* **B426** (1994) 269. [arXiv:hep-ph/9402253](#), [doi:10.1016/0550-3213\(94\)90313-1](#)
- [60] M. Carena *et al.*, *Nucl. Phys.* **B577** (2000) 88. [arXiv:hep-ph/9912516](#), [doi:10.1016/S0550-3213\(00\)00146-2](#)
- [61] H. Eberl *et al.*, *Phys. Rev.* **D62** (2000) 055006. [arXiv:hep-ph/9912463](#), [doi:10.1103/PhysRevD.62.055006](#)
- [62] J. Baglio *et al.*, *Comput. Phys. Commun.* **185** (2014) 3372. [arXiv:1312.4788](#), [doi:10.1016/j.cpc.2014.08.005](#)

- [63] D. Noth and M. Spira, *Phys. Rev. Lett.* **101** (2008) 181801. [arXiv:0808.0087](#), [doi:10.1103/PhysRevLett.101.181801](#)
- [64] D. Noth and M. Spira, *JHEP* **06** (2011) 084. [arXiv:1001.1935](#), [doi:10.1007/JHEP06\(2011\)084](#)
- [65] A. Dabelstein, *Nucl. Phys.* **B456** (1995) 25. [arXiv:hep-ph/9503443](#), [doi:10.1016/0550-3213\(95\)00523-2](#)
- [66] M. Drees and K.-I. Hikasa, *Phys. Rev.* **D41** (1990) 1547. [doi:10.1103/PhysRevD.41.1547](#)
- [67] E. Fullana and M.-A. Sanchis-Lozano, *Phys. Lett.* **B653** (2007) 67. [arXiv:hep-ph/0702190](#), [doi:10.1016/j.physletb.2007.06.078](#)
- [68] D. McKeen, *Phys. Rev.* **D79** (2009) 015007. [arXiv:0809.4787](#), [doi:10.1103/PhysRevD.79.015007](#)
- [69] F. Domingo and U. Ellwanger, *JHEP* **06** (2011) 067. [arXiv:1105.1722](#), [doi:10.1007/JHEP06\(2011\)067](#)
- [70] M.J. Dolan *et al.*, *JHEP* **03** (2015) 171 [Erratum: **07** (2015) 103]. [arXiv:1412.5174](#), [doi:10.1007/JHEP03\(2015\)171](#), [doi:10.1007/JHEP07\(2015\)103](#)
- [71] F. Domingo, *JHEP* **03** (2017) 052. [arXiv:1612.06538](#), [doi:10.1007/JHEP03\(2017\)052](#)
- [72] A. Bredenstein *et al.*, *Phys. Rev.* **D74** (2006) 013004. [arXiv:hep-ph/0604011](#), [doi:10.1103/PhysRevD.74.013004](#)
- [73] A. Bredenstein *et al.*, *Nucl. Phys. Proc. Suppl.* **160** (2006) 131. [arXiv:hep-ph/0607060](#), [doi:10.1016/j.nuclphysbps.2006.09.104](#)
- [74] A. Bredenstein *et al.*, *JHEP* **02** (2007) 080. [arXiv:hep-ph/0611234](#), [doi:10.1088/1126-6708/2007/02/080](#)
- [75] W. Hollik and J.-H. Zhang, Radiative corrections to $h^0 \rightarrow WW^*/ZZ^* \rightarrow 4$ leptons in the MSSM, [arXiv:1011.6537](#)
- [76] W. Hollik and J.-H. Zhang, *Phys. Rev.* **D84** (2011) 055022. [arXiv:1109.4781](#), [doi:10.1103/PhysRevD.84.055022](#)
- [77] B.A. Kniehl, *Nucl. Phys.* **B357** (1991) 439. [doi:10.1016/0550-3213\(91\)90476-E](#)
- [78] B.A. Kniehl, *Phys. Rep.* **240** (1994) 211. [doi:10.1016/0370-1573\(94\)90037-X](#)
- [79] M. Spira, *Prog. Part. Nucl. Phys.* **95** (2017) 98. [arXiv:1612.07651](#), [doi:10.1016/j.pnpnp.2017.04.001](#)
- [80] G. Belanger *et al.*, *Phys. Rev.* **D89** (9) (2014) 095023. [arXiv:1402.3522](#), [doi:10.1103/PhysRevD.89.095023](#)
- [81] J.S. Lee *et al.*, *Comput. Phys. Commun.* **156** (2004) 283. [arXiv:hep-ph/0307377](#), [doi:10.1016/S0010-4655\(03\)00463-6](#)
- [82] U. Aglietti *et al.*, *JHEP* **01** (2007) 021. [arXiv:hep-ph/0611266](#), [doi:10.1088/1126-6708/2007/01/021](#)
- [83] M. Spira *et al.*, *Nucl. Phys.* **B453** (1995) 17. [arXiv:hep-ph/9504378](#), [doi:10.1016/0550-3213\(95\)00379-7](#)
- [84] M. Muhlleitner and M. Spira, *Nucl. Phys.* **B790** (2008) 1. [arXiv:hep-ph/0612254](#), [doi:10.1016/j.nuclphysb.2007.08.011](#)

- [85] A. Djouadi *et al.*, *Z. Phys.* **C70** (1996) 427. [arXiv:hep-ph/9511344](#),
[doi:10.1007/s002880050120](#)
- [86] M. Spira *et al.*, *Phys. Lett.* **B276** (1992) 350. [doi:10.1016/0370-2693\(92\)90331-W](#)
- [87] R. Bonciani *et al.*, *JHEP* **08** (2015) 108. [arXiv:1505.00567](#),
[doi:10.1007/JHEP08\(2015\)108](#)
- [88] T. Gehrmann *et al.*, *JHEP* **09** (2015) 038. [arXiv:1505.00561](#),
[doi:10.1007/JHEP09\(2015\)038](#)
- [89] P.A. Baikov *et al.*, *Phys. Rev. Lett.* **96** (2006) 012003. [arXiv:hep-ph/0511063](#),
[doi:10.1103/PhysRevLett.96.012003](#)
- [90] U. Haisch *et al.*, *JHEP* **03** (2018) 178. [arXiv:1802.02156](#),
[doi:10.1007/JHEP03\(2018\)178](#)

Acknowledgements

The work of *J.J. Aguilera-Verdugo*, *F. Driencourt-Mangin*, *J. Plenter*, *S. Ramírez-Uribe*, *G. Rodrigo*, *G.F.R. Sborlini*, *W.J. Torres Bobadilla*, and *S. Tracz* was supported by the Spanish Government (Agencia Estatal de Investigación) and ERDF funds from European Commission (grant numbers FPA2017-84445-P and SEV-2014-0398), by Generalitat Valenciana (grant number PROMETEO/2017/ 053), and by Consejo Superior de Investigaciones Científicas (grant number PIE-201750E021).

J.J. Aguilera-Verdugo acknowledges support from Generalitat Valenciana (GRISOLIAP/2018/101). Results by *A. Arbuzov*, *S. Bondarenko*, *Y. Dydyshka*, *L. Kalinovskaya*, *L. Rumyantsev*, *R. Sadykov*, and *V. Yermolchik* are obtained in the framework of state's task N 3.9696.2017/8.9 of the Ministry of Education and Science of Russia.

The work of *J. Baglio* is supported by the Institutional Strategy of the University of Tübingen (DFG, ZUK 63) and the Carl-Zeiss foundation.

S.D. Bakshi acknowledges the financial support of IIT Kanpur and an Arepalli-Karumuri travel grant for attending this conference at CERN.

The work of *M. Beneke*, *C. Bobeth*, and *R. Szafron* was supported by the DFG Sonderforschungsbereich/Transregio 110 'Symmetries and the Emergence of Structure in QCD'.

S. Borowka gratefully acknowledges the financial support of the ERC Starting Grant 'MathAm' (39568).

The work of *J. Chakraborty* is supported by the Department of Science and Technology, Government of India, under grant number IFA12/PH/34 (INSPIRE Faculty Award), the Science and Engineering Research Board, Government of India, under agreement number SERB-PHY/2016348 (Early Career Research Award), and an Initiation Research Grant, agreement number IITK/PHY/2015077, of IIT Kanpur.

The work of *M. Chruszcz*, *Z. Was*, and *J. Zaremba* is partly supported by the Polish National Science Center, grant number 2016/23/B/ST2/03927, and the CERN FCC Design Study Programme.

The work of *J. Gluza* is supported in part by the Polish National Science Centre, grant number 2017/25/B/ST2/01987 and by international mobilities for research activities of the University of Hradec Králové, CZ.02.2.69/0.0/0.0/16_027/0008487.

The work of *J.A. Gracey* was supported by a DFG Mercator Fellowship.

The work of *S. Heinemeyer* is supported in part by the MEINCOP Spain under contract FPA2016-78022-P, in part by the Spanish Agencia Estatal de Investigación (AEI) and the EU Fondo Europeo de Desarrollo Regional (FEDER) through the project FPA2016-78645-P, in part by the AEI through the grant IFT Centro de Excelencia Severo Ochoa SEV-2016-0597, and by the 'Spanish Red Consolider Multidark' FPA2017-90566-REDC.

The work of *S. Jadach*, *M. Skrzypek*, and *Z. Was* is partly supported by the Polish National Science Center, grant number 2016/23/B/ST2/03927, and the CERN FCC Design Study Programme.

A. Kardos acknowledges financial support from the Premium Postdoctoral Fellowship programme of the Hungarian Academy of Sciences. This work was supported by grant K 125105 of the National Research, Development and Innovation Fund in Hungary.

M. Kerner acknowledges supported by the Swiss National Science Foundation (SNF) under grant number 200020-175595.

P. Maierhöfer acknowledges support by the state of Baden-Württemberg through bwHPC and

the German Research Foundation (DFG) through grant number INST 39/963-1 FUGG.

The work of *R. Pittau* was supported by the MECD project FPA2016-78220-C3-3-P.

J. Plenter acknowledges support from the ‘la Caixa’ Foundation (grant numbers ID 100010434 and LCF/BQ/IN17/11620037) and from the European Union’s H2020-MSCA Grant (agreement number 713673).

S. Ramírez-Uribe acknowledges support from CONACYT.

The work of *T. Riemann* is funded by Deutsche Rentenversicherung Bund. He is supported in part by a 2015 Alexander von Humboldt Honorary Research Scholarship of the Foundation for Polish Sciences (FNP) and by the Polish National Science Centre (NCN) under grant agreement 2017/25/B/ST2/01987. Support of participation at the workshop from the FCC group is acknowledged.

The research of *J. Schlenk* was supported by the European Union through the ERC Advanced Grant MC@NNLO (340983).

C. Schwinn acknowledges support by the Heisenberg Programme of the DFG and a fellowship of the Collaborative Research Centre SFB 676 ‘Particles, Strings, and the Early Universe’ at Hamburg University.

W.J. Torres Bobadilla acknowledges support from the Spanish Government (grant number FJCI-2017-32128).

J. Usovitsch has received funding from the European Research Council (ERC) under the European Union’s Horizon 2020 research and innovation programme (grant agreement 647356, CutLoops).

C. Weiland received financial support from the European Research Council under the European Union’s Seventh Framework Programme (FP/2007-2013)/ERC Grant NuMass, agreement number 617143, and is also supported in part by the US Department of Energy under contract DE-FG02-95ER40896 and in part by the PITT PACC. His work was done in collaboration with S. Pascoli.

This report was partly supported by COST (European Cooperation in Science and Technology) Action CA16201 PARTICLEFACE and the CERN FCC design study programme.

